SCIENCE WITH A NEXT-GENERATION VERY LARGE ARRAY

COVER ILLUSTRATION:

Front cover caption and credit.

ASTRONOMICAL SOCIETY OF THE PACIFIC
CONFERENCE SERIES

A SERIES OF BOOKS ON RECENT DEVELOPMENTS IN ASTRONOMY AND ASTROPHYSICS

Monograph 7

ASPCS volumes may be found online with color images at http://www.aspbooks.org.
ASP Monographs may be found online at http://www.aspmonographs.org.

For a complete list of ASPCS Volumes, ASP Monographs, and
other ASP publications see http://www.astrosociety.org/pubs.html.

All book order and subscription inquiries should be directed to the ASP at
800-335-2626 (toll-free within the USA) or 415-337-2126,
or email service@astrosociety.org

ASTRONOMICAL SOCIETY OF THE PACIFIC
CONFERENCE SERIES

Monograph 7

SCIENCE WITH A NEXT-GENERATION VERY LARGE ARRAY

A collection of White Papers prepared by the radio astronomy community and compiled by the National Radio Astronomy Observatory in preparation for the U.S. 2020 Astronomy and Astrophysics Decadal Survey conducted by the National Research Council of the National Academy of Sciences.

Edited by

Eric Murphy
National Radio Astronomy Observatory, Charlottesville, Virginia, USA

and

the Next-Generation Very Large Array Science Advisory Council

SAN FRANCISCO

ASTRONOMICAL SOCIETY OF THE PACIFIC

390 Ashton Avenue
San Francisco, California, 94112-1722, USA

Phone: 415-337-1100
Fax: 415-337-5205
E-mail: service@astrosociety.org
Web site: www.astrosociety.org
E-books: www.aspbooks.org

First Edition

ASP Conference Series

ISBN:
e-book ISBN:

Library of Congress (LOC) Cataloging in Publication (CIP) Data:
Main entry under title
Library of Congress Control Number (LCCN):

Printed in the United States of America by Sheridan Books, Ann Arbor, Michigan.
This book is printed on acid-free paper.

Contents

Part X. Cosmology:

Part I

A Current Summary of the Project:

Science with a Next-Generation Very Large Array
ASP Conference Series, Monograph 7
Eric J. Murphy, ed.

DRAFT EDITION

The ngVLA Science Case and Associated Science Requirements

Eric J. Murphy,[1] Alberto Bolatto,[2] Shami Chatterjee,[3] Caitlin M. Casey,[4] Laura Chomiuk,[5] Daniel Dale,[6] Imke de Pater,[7] Mark Dickinson,[8] James Di Francesco,[9,10] Gregg Hallinan,[11] Andrea Isella,[12] Kotaro Kohno,[13] S. R. Kulkarni,[11] Cornelia Lang,[14] T. Joseph W. Lazio,[15] Adam K. Leroy,[16] Laurent Loinard,[17,18] Thomas J. Maccarone,[19] Brenda C. Matthews,[9,10] Rachel A. Osten,[20] Mark J. Reid,[21] Dominik Riechers,[3] Nami Sakai,[22] Fabian Walter,[23] & David Wilner[21]

Abstract. The science case and associated science requirements for a next-generation Very Large Array (ngVLA) are described, highlighting the five key science goals developed out of a community-driven vision of the highest scientific priorities in the next decade. Building on the superb cm observing conditions and existing infrastructure of the VLA site in the U.S. Southwest, the ngVLA is envisaged to be an interferometric array with more than 10 times the sensitivity and spatial resolution of the current VLA and the ALMA, operating at frequencies spanning $\sim 1.2-116$ GHz. The ngVLA will be optimized for observations at wavelengths between the exquisite performance of ALMA at submm wavelengths, and the future SKA-1 at decimeter to meter wavelengths, thus lending itself to be highly complementary with these facilities. The ngVLA will be the only facility in the world that can tackle a broad range of outstanding scientific questions in modern astronomy by simultaneously delivering the capability to: unveil the formation of Solar System analogues; probe the initial conditions for planetary systems and life with astrochemistry; characterize the assembly, structure, and evolution of galaxies from the first billion years to the present; use pulsars in the Galactic center as fundamental tests of gravity; and understand the formation and evolution of stellar and supermassive blackholes in the era of multi-messenger astronomy.

1. Introduction

The Very Large Array (VLA) has had a major impact on nearly every branch of astronomy, and the results of its research are abundant in the pages of scientific journals and textbooks. Five years after the completion of the Expanded Very Large Array (EVLA) Project, and more than 40 years since the first VLA antenna was commissioned, the VLA has strengthened its position as the most versatile, widely-used radio telescope in the world. Rededicated as the Karl G. Jansky VLA in March 2012, the array continues to make cutting-edge discoveries across a broad range of disciplines including exoplanet formation, galaxy formation in the nearby and distant Universe, and the rapidly growing field of time-domain astronomy. More than 3,000 researchers from around the world have used the VLA for more than 11,000 observing projects.

Inspired by the VLA's ability to perennially deliver high-impact scientific results, and to prepare for the changing landscape in science priorities and capabilities of facilities at other wavelengths, the National Radio Astronomy Observatory (NRAO) recently started to consider ways to continue the legacy of the VLA as one of the most powerful radio telescopes to be included in the next generation of the world's suite of cutting edge astronomical observatories. By teaming with the greater astronomical community in an exercise to develop a cogent science case requiring observations at cm–mm wavelengths, NRAO is now currently pursuing a large collecting area radio interferometer that will open new discovery space by delivering an angular resolution and sensitivity that is each an order of magnitude larger than that of the VLA and the Atacama Large Millimeter Array (ALMA), allowing it to address fundamental questions in all major areas of astrophysics.

This documents describes the community response following a solicitation from the NRAO to develop key science cases for a future U.S.-led radio telescope, the next generation Very Large Array (ngVLA). The resulting list of more than 80 science use cases received by NRAO represent some of the fundamental astrophysical problems that require observing capabilities at millimeter and centimeter wavelengths well beyond those of existing, or already planned, telescopes. The summary of this exercise has resulted in a transformative radio facility having roughly 10 times the sensitivity of the VLA and ALMA, frequency coverage from $\sim 1.2 - 116$ GHz with up to 20 GHz of instantaneous sampled bandwidth, a compact core for good sensitivity to low surface-brightness emission, and extended baselines of at least hundreds of kilometers and ultimately across the continent to provide high-resolution imaging. The ngVLA is being built on the scientific and technical legacies of the VLA and ALMA, and is being designed to provide the next major leap forward in our understanding of planets, galaxies, black holes, and the dynamic sky. As such, the ngVLA will open a new window on the universe through ultra-sensitive imaging of thermal line and continuum emission down to milliarcecond resolution, as well as deliver unprecedented broad band continuum polarimetric imaging of non-thermal processes.

2. Developing the ngVLA Key Science Goals

The ngVLA Science Advisory Committee (SAC)[1], a group of experts appointed by NRAO, in collaboration with the broader international astronomical community, recently developed a series of than 80 compelling science cases requiring ≈200 unique observations between $\sim 1.2-116$ GHz with sensitivity, angular resolution, and mapping capabilities far beyond those provided by the VLA, ALMA, and the Square Kilometre Array Phase 1 (SKA-1). The science cases submitted spanned a broad range of topics in the fields of planetary science, Galactic and extragalactic astronomy, as well as fundamental physics, and formed the basis for developing the ngVLA Key Science Goals (KSGs).

Given the overwhelmingly large spread of compelling science cases generated by the community, it is clear that the primary science requirement for the ngVLA is to be flexible enough to support the wide breadth of scientific investigations that will be proposed by its highly creative user base over the full lifetime of the instrument. This mandate is also made obvious given the breadth of scientific endeavors included in this Volume, ranging from studies of planet formation and understanding the conditions for habitability in other star systems to rigorous testing of the theory of gravity using pulsars immersed in the space-time potential of the Galaxy's supermassive black hole.

[1]http://ngvla.nrao.edu/page/sciencecouncil

This in turn makes the ngVLA a different style of instrument than many other facilities on the horizon (e.g., SKA-1, LSST, etc.), which are heavily focused on carrying out large surveys.

In the next stage of the process, each of the individual science cases were objectively reviewed and thoroughly discussed by the different Science Working Groups within the ngVLA-SAC. The ultimate goal of this exercise was to distill the top scientific goals for a future radio/mm telescope. The resulting initial KSGs, along with the results from the entire list of over 80 science use cases (Selina, Murphy & Erickson 2017) were then presented and discussed with the broader community at the ngVLA Science and Technology Workshop June 26 – 29, 2017 in Socorro NM in an attempt to build consensus around a single vision for the key science missions of the ngVLA. Here we describe the five KSGs to come out of this community-driven science use case capture process along with their corresponding requirements that in turn drive the Reference Design described by Selina et al., (this volume, p. **??**).

3. The ngVLA Key Science Goals and Associated Requirements

In this section we briefly describe each of the five highest-priority ngVLA KSGs that are expected to be carried out during the lifetime of the ngVLA. We also provide a brief description of their basic requirements that in turn form the foundation used to construct the ngVLA Reference Design described in Selina et al., (this volume, p. **??**). A more detailed description of the ngVLA KSGs can be found in (Bolatto et al. 2017), and the corresponding full description of the ngVLA Level 0 Science Requirements can be found in Murphy et al. (2017).

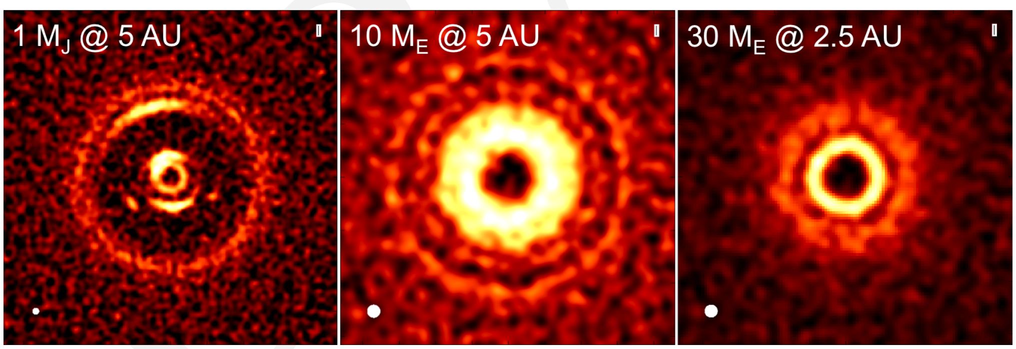

Figure 1. Simulated ngVLA observations of protoplanetary disk continuum emission perturbed by a Jupiter mass planet at 5 AU (left), a 10 Earth mass planet at 5 AU (center), and a 30 Earth mass planet at 2.5 AU (right). The ngVLA observations at 100 GHz were simulated with 5 mas angular resolution and 0.5 μJy/bm rms (Ricci et al. 2018).

3.1. KSG1: Unveiling the Formation of Solar System Analogs on Terrestrial Scales

Planets are thought to be assembled in disks around pre-main sequence stars, but the physical processes responsible for their formation are poorly understood. Only recently, optical, infrared, and (sub-) millimeter telescopes have achieved the angular resolution required to spatially resolve the innermost regions of nearby protoplanetary disks, unveiling morphological features with characteristic sizes of >20 AU suggestive of gravitational perturbations of yet unseen giant planets. This in turn provides a powerful tool to measure planet masses, orbital radii, study the circumplanetary environment, and investigate how forming planets interact with the circumstellar material. The angular resolution, frequency coverage, and sensitivity of current disk imagery is limited to probing for the presence of planets more massive than Neptune at orbital radii larger than 20 – 30 AU. The next step forward in the study of planet formation is the ability to image the formation of super-Earths and giant planets across the entire disk, particularly within 10 AU from the central star.

To achieve this science goal requires that the ngVLA have the frequency coverage, sensitivity, and angular resolution to be able to measure the planet initial mass function down to a mass of 5 – 10 Earth masses. This capability will unveil the formation of planetary systems similar to our own Solar System by probing the presence of planets on orbital radii as small as 0.5 AU at the distance of ≈140 pc. The ngVLA shall also be able to reveal circumplanetary disks and sub-structures in the distribution of mm-size dust particles created by close-in planets and measure the orbital motion of these features on monthly timescales.

To achieve this science goal requires continuum observations for center frequencies between 20 – 110 GHz with angular resolution better than 5 mas. This requirement will enable studies on the formation of planets in the innermost 10 AU of nearby ($\lesssim$140 pc) proto-planetary disks. Extensive simulations of the disks perturbed by planets (see Figure 1; Ricci et al. 2018), suggest that a sensitivity of 0.2 μJy/bm in the continuum at 100 GHz is required to map structures in the dust distribution created by planets of mass down to 10 Earth-masses and orbital radius of 2.5 AU. Matching resolution (i.e., 5 mas) and achieving a continuum sensitivity of order 0.02 μJy/bm at 30 GHz will map the planet-disk interactions where the disk emission is expected to be optically thin.

3.2. KSG2: Probing the Initial Conditions for Planetary Systems and Life with Astrochemistry

One of the most challenging aspects in understanding the origin and evolution of planets and planetary systems is tracing the influence of chemistry on the physical evolution of a system from a molecular cloud to a solar system, while also trying to determine the potential for habitability. To make significant progress in this area requires that the ngVLA has the frequency coverage and sensitivity to be able to detect predicted, but as yet unobserved, complex prebiotic species that are the basis of our understanding of chemical evolution toward amino acids and other biogenic molecules. In doing so, the ngVLA will also allow us to detect and study chiral molecules, testing ideas on the origins of homochirality in biological systems. The detection of such complex organic molecules will provide the chemical initial conditions of forming solar systems and individual planets.

Presently, current observations of complex organic (prebiotic) molecules using ALMA and the Great Bank Telescope (GBT) are hitting the limit of what can be achieved due to a combination of achievable sensitivity and line confusion at higher frequencies. Both problems can be solved by sensitive observations in the cm-wave regime with the ngVLA. State-of-the-art models predict these molecules will display emission lines with intensities that are easily detectable with the ngVLA, but well below the cur-

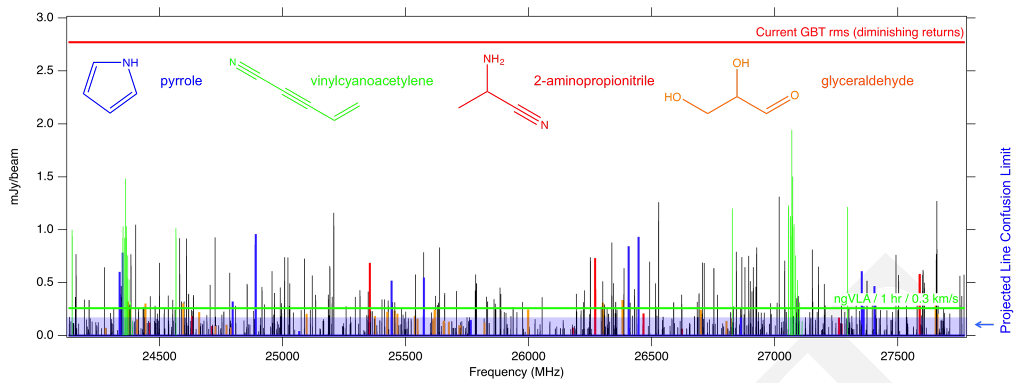

Figure 2. A conservative simulation of 30 as-yet-undetected complex interstellar molecules (black) likely to be observed by the ngVLA above the confusion limit around hot cores with typical sizes of $\sim 1 - 4''$. Key molecules are highlighted in color. (Credit: B. McGuire)

rent detectability thresholds of existing telescopes including ALMA, GBT, and IRAM. Figure 2 shows simulations of a representative set of the types of molecules whose discovery will be enabled by the ngVLA: N, O, and S-bearing small aromatic molecules, direct amino acid precursors, biogenic species such as sugars, chiral molecules, and, possibly amino acids themselves. The simulation assumes column densities of $10^{12} - 10^{14}\,\mathrm{cm}^{-2}$ (with more complex molecules being assigned lower column densities), a temperature of 200 K, and 3 km/s linewidth.

To achieve this science goal requires an angular resolution on the order of 50 mas at 50 GHz along with an rms sensitivity of $30\,\mu$Jy/bm/km/s for frequencies between 16 – 50 GHz. Further, spectral resolution of 0.1 km/s is required, preferably concurrent with broadband (4+ GHz) observations.

3.3. KSG3: Charting the Assembly, Structure, and Evolution of Galaxies from the First Billion Years to the Present

To make substantial progress in the field of galaxy formation and evolution requires that the ngVLA have the sensitivity to survey cold gas in thousands of galaxies back to early cosmic epochs, while simultaneously enabling routine sub-kiloparsec scale resolution imaging of their gas reservoirs. In doing so, the ngVLA will afford a unique view into how galaxies accrete, process, and expel their gas through detailed imaging of their extended atomic reservoirs and circumgalactic regions. To reveal the detailed physical conditions for galaxy assembly and evolution throughout the history of the universe requires that the ngVLA also have enough sensitivity to map the physical and chemical properties of molecular gas over the entire local galaxy population.

To carry out detailed studies of CO kinematics of high-z galaxies and blind CO searches of > 1000 galaxies requires a line sensitivity of $\sim 46\,\mu$Jy/bm/km/s at $0\farcs1$ and $1''$angular resolution between 10 – 50 GHz with a spectral resolution of 5 km/s. This is illustrated by a simulation of M 51 (the Whirlpool galaxy) shown in the top three panels of Figure 3 (see Carilli & Shao 2017). The spatial and kinematic information recovered by the ngVLA allows for the measurement of a precise rotation curve, which would only be possible to obtain from ALMA with an extraordinarily large ($\sim$ 1000 hr) time investment. Furthermore, a large instantaneous bandwidth (i.e., a minimum 1.6:1

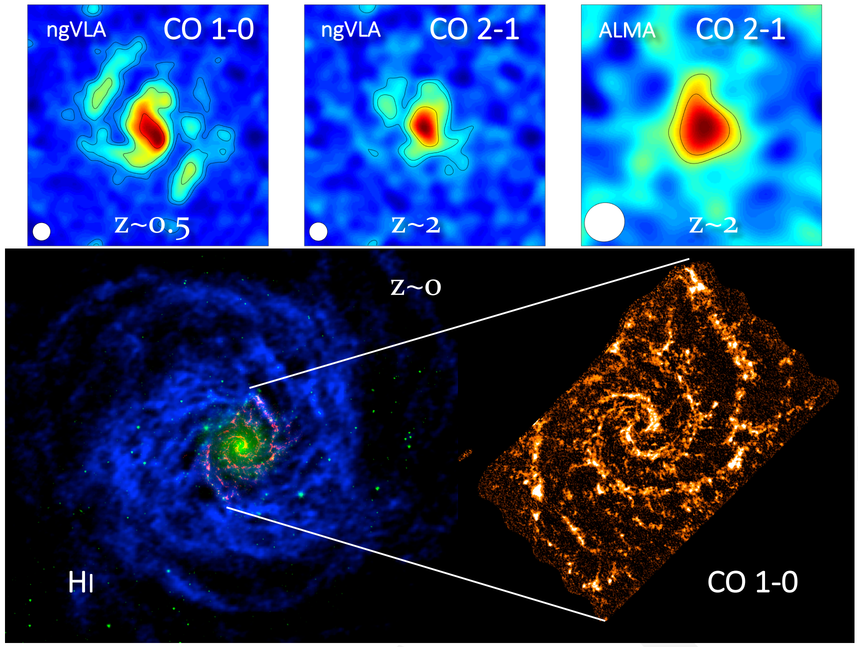

Figure 3. *Top Panels:* Simulations based on M 51 with molecular mass scaled by 1.4× (z = 0.5) and 3.5× (z = 2) to match the lowest molecular mass galaxies observable by ALMA and the NOEMA (Carilli & Shao 2017). The synthesized beam shown in the bottom left corner is (left to right) θ_s = 0.″19, 0.″20, and 0.″43 corresponding to linear scales L = 1.2, 1.7, and 3.7 kpc, respectively. Integration times are 30 hr. *Bottom Panels:* The spiral galaxy M 74 illustrating the CO molecular disk imaged by ALMA (red; Schinnerer in prep.), the stellar disk at 4.5 μm imaged by *Spitzer* (green; Kennicutt et al. 2003), and the atomic disk imaged in HI by the VLA (blue; Walter et al. 2008), showing the gas phases to which the ngVLA will be sensitive. *Right Panel:* The CO $J = 2 \rightarrow 1$ map at 1″ resolution.

BW ratio, up to 20 GHz instantaneous bandwidth) is required to conduct wide band observations at 5 km/s resolution to efficiently perform blind surveys of large cosmic volumes in a single observation and provide routine access molecular species in addition to CO (e.g., HCN, HCO^+, or N_2H^+).

Thermal imaging of 0.1 – 0.2 K sensitivity of CO (115 GHz) at 0.″1 angular resolution and 1 km/s spectral resolution is required for detailed studies of molecular gas in the nearby universe (see bottom panels of Figure 3). Thermal imaging of 1 – 5 mK sensitivity between 70 and 116 GHz at 1 – 5″ angular resolution and 1 – 5 km/s spectral resolution is required to support studies of gas density across the local universe.

Full 1.2 – 116 GHz frequency coverage is required to obtain accurate, simultaneous measurements of star formation rates from free-free continuum and radio recombination line (RRL) emission. Angular resolutions of 0.″1 – 1″ for continuum imaging at all available frequencies are required. A continuum sensitivity of 0.15 μJy/bm at 33 GHz for a 1″ synthesized beam is required to robustly study star formation within large samples of nearby galaxies. For studies of galaxies in the local universe, accurate recovery of flux density for extended objects on arcminute scales at all frequencies is required.

The ability to make large mosaics or conduct on-the-fly line and/or continuum mappings of galaxies that extend beyond the area of a single primary beam.

Finally, a brightness dynamic range of $\approx$50 and 40 db is required at 10 GHz for deep field continuum studies of MW-like galaxies at Cosmic Noon to not be dynamic range limited in total and polarized intensity, respectively. Such deep field observations will be sensitive to $\gtrsim$90% of all stars formed since $z \lesssim 3$.

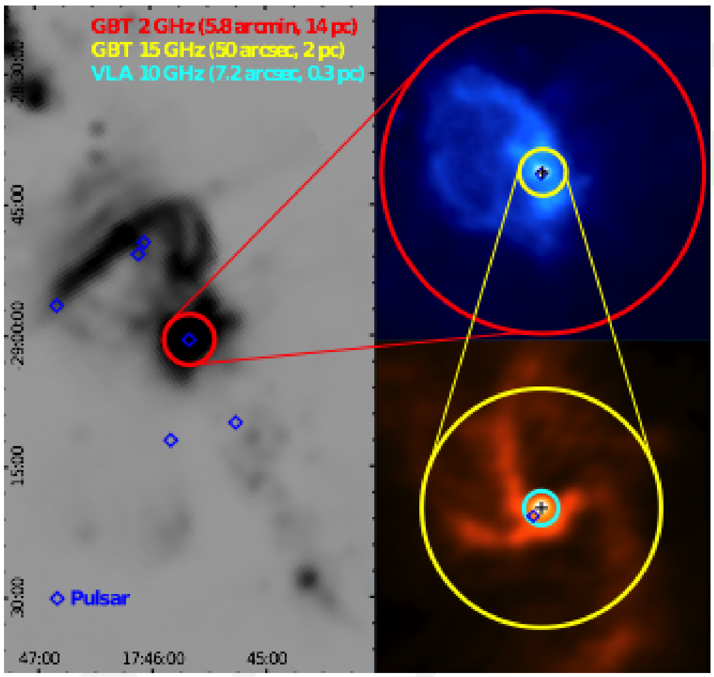

Figure 4. The pulsar distribution near the Galactic Center. Despite being the highest density in the Galaxy and multiple searches at sensitivities comparable to the VLA, only a few pulsars are known though $\sim$ 1000 are predicted. (Credit: R. Wharton)

3.4. KSG4: Using Pulsars in the Galactic Center to Make a Fundamental Test of Gravity

Testing theories of gravity requires probing as close as possible to the strong field regime, for which pulsars near the Galactic Center offer a powerful path forward. However, only a handful of pulsars in the central half-degree of the Galaxy are currently known (see Figure 4), which may be the result of enhanced radio-wave scattering toward the inner Galaxy that further decreases the effective sensitivity of searches, by increasing both the dispersion measure smearing and pulse broadening. Observing at higher frequencies than currently planned for the SKA can mitigate radio-wave scattering, but by itself the benefits are limited because of the generally steep radio spectra of pulsars. Thus, to achieve this goal, the ngVLA must deliver a combination of sensitivity and frequency range, enabling it to probe much deeper into the likely Galactic Center pulsar population to address fundamental questions in relativity and stellar evolution. The ability to address these questions is afforded by the fact that pulsars in the Galactic Center represent clocks moving in the space-time potential of a super-massive black hole and allow for qualitatively new tests of theories of gravity. More generally, they offer the opportunity to constrain the history of star formation, stellar dynamics, stellar evolution, and the magneto-ionic medium in the Galactic Center.

To carryout this science requires that the ngVLA be able to support pulsar search and timing observations from $\sim 1-30$ GHz for Galactic Center pulsars. Pulsar searching requires the ability to search on $100\,\mu$s scales ($20\,\mu$s scales desired), while timing requires $20\,\mu$s resolution. Continuum sensitivity of order 50 nJy/bm is desired at 20 GHz, which is a significant improvement compared to existing 100 m-class radio telescopes that have found few pulsars, indicating that substantial additional sensitivity is necessary. The system timing accuracy also must be better than 10 ns (1 ns desired) over periods correctable to a known standard from 30 min to 10 yr. To efficiently time time multiple pulsars, the array must have the ability to make multiple (minimum 10) beams (i.e., phase centers within the primary beam) within a single subarray, or distributed amongst multiple subarrays. Timing multiple pulsars within a single primary beam is desirable. Support for 5 or more independent de-dispersion and folding threads is desired.

3.5. KSG5: Understanding the Formation and Evolution of Stellar and Supermassive Black Holes in the Era of Multi-Messenger Astronomy

While we now know that black holes exist on practically all mass scales, the astrophysics of how these objects form and grow remains a mystery. The Laser Interferometer Gravitational-wave Observatory (LIGO) is now detecting black holes that are substantially more massive than previously known stellar mass black holes, and observing black hole-black hole mergers, although we do not know how black hole binaries form. While supermassive black holes (SMBHs) are thought to be widespread in galaxy centers, we do not understand how their growth was seeded or how (and how often) these extreme objects merge. To address these questions requires that the ngVLA have the combination of sensitivity and angular resolution to be able to survey everything from the remnants of massive stars to the supermassive black holes that lurk in the centers of galaxies, making it the ultimate black hole hunting machine. High-resolution imaging abilities are required to separate low-luminosity black hole systems in our local Universe from background sources, thereby providing critical constraints on the formation and growth of black holes of all sizes and mergers of black hole-black hole binaries.

To become the ultimate black-hole survey instrument requires that the ngVLA have high angular resolution (mas – μas) imaging with relative astrometric accuracy that is $< 1\%$ of the synthesized beam FWHM or equal to the positional uncertainty in the reference frame, for a bright ($SNR \gtrsim 100$) point source. Such high-resolution imaging will enable proper motion separation of local black holes (both Galactic and in nearby galaxies, out to 15 Mpc) from background sources. Long baselines are required to enable the ngVLA to image the SMBH binaries that will be detected in gravitational waves by LISA and pulsar timing arrays. These astrometric science goals benefit from the implementation of very long baselines ($\gtrsim 1000$ km for mas – μas accuracy). Associated VLBI recording capabilities shall be available for 3 or more beams (for 2 calibrators and the science target).

The field of multi-messenger astronomy continues to mature as we continue to open new astronomical windows through gravitational waves and neutrino observations. However, to progress further in our understanding of the physics associated with these phenomena requires the ability to localize and characterize the sources. Only the

Figure 5. Two tiny, but very dense neutron stars merge and explode as a kilonova. Such a very rare event produces gravitational waves and electromagnetic radiation, as observed on 17 August 2017. The ngVLA will play a pivotal role in characterizing the physics of such events in the era of multi-messenger astronomy. (Artist's impression, Credit: ESO/L. CalÇada/M. Kornmesser).

detection of the electromagnetic radiation associated with these energetic, and often cataclysmic events, can provide precise localization, establish energetics and allow us to understand how such events interact with their surrounding environments. Thus, to have a transformational impact in the growing era of multi-messenger astronomy, the ngVLA must also be able to identify the radio counterparts to transient sources discovered by gravitational wave, neutrino, and optical observatories (see Figure 5). This requires high-resolution, fast-mapping capabilities to make it the preferred instrument to pinpoint transients associated with violent phenomena such as supermassive black hole mergers and blast waves.

Specifically, mapping a $\sim$10 square degree region (i.e., the localization uncertainty expected by gravitational wave detectors when ngVLA is operational) to a depth of $\sim 1\,\mu$Jy/bm at 2.5 GHz for detection of NS-NS and NS-BH mergers is required. Completing the on-the-fly mapping of each epoch within $\sim$ 10 hr is desirable. Similarly, mapping a $\sim$ 10 square degree region at 28 GHz to a depth of $\sim 10\,\mu$Jy/bm with on-the-fly mapping is required for localization of LISA-detected SMBH mergers. Completing the on-the-fly mapping of each epoch within $\sim$ 10 hr is desirable.

Furthermore, the ability to receive and respond to external triggers rapidly is also an essential requirement to enable multi-messenger science. Triggered response times not to exceed 10 minutes is required, while response times of better than 3 minutes is desired. The ability to perform time-domain transient searchers (e.g., for Fast Radio Bursts) requires a search capability on $100\,\mu$s scales, with 20 s scales desired.

4. Summary

The ngVLA is being designed to tap into the astronomical community's intellectual curiosity by providing them with a world-class instrument that will enable a broad range of scientific discoveries (e.g., planet formation, signatures of pre-biotic molecules, cosmic cycling of cool gas in galaxies, test of gravity, characterizing the energetics of gravitational wave counterparts, etc.). Based on community input to date, the ngVLA is the obvious next step to build on the VLA's legacy and continue the U.S.'s place as a world leader in radio astronomy. The ultimate goal of the ngVLA is to give the U.S. and international communities a highly capable and flexible instrument to pursue their science in critical, yet complementary ways, with the large range of multi-wavelength facilities that are on a similar horizon. Presently, there have been no major technological risks identified. However, the project is continually looking to take advantage of major engineering advancements seeking performance and operations optimizations. As the project continues to move forward and mature, the project will continue to work with the community to refine the ngVLA science mission and instrument specifications/performance. This science book acts as a major milestones in this effort.

Acknowledgments. The authors thank the 100's of community members that have contributed to the definition of the ngVLA science mission and corresponding science requirements. The National Radio Astronomy Observatory is a facility of the National Science Foundation operated under cooperative agreement by Associated Universities, Inc. Part of this work was carried out at the Jet Propulsion Laboratory, California Institute of Technology, under contract with the National Aeronautics and Space Administration.

References

Bolatto, A. D., Chatterjee, S., Casey, C. M., et al. 2017, arXiv:1711.09960

Carilli C. L. & Shao, Y. "Image Capabilities: High redshift CO' Next Generation VLA Memo. No. 13. (2017).

Kennicutt, R. C., Jr., Armus, L., Bendo, G., et al. 2003, PASP, 115, 928

Murphy, E. et. al., "ngVLA Science Requirements" Next Generation VLA Document No. 020.10.15.00-0001-REQ. (2017)

Ricci, L., Liu, S.-F., Isella, A., & Li, H. 2018, ApJ, 853, 110

Selina, R. et al. 2018, ASP Monograph 7, Title of the Book, ed. E. Murphy (San Francisco, CA: ASP)

Selina, R. & Murphy E. "ngVLA Reference Design Development & Performance Estimates" Next Generation VLA Memo. No. 17. (2017).

Selina, R., Murphy, E., Erickson, A. "Summary of the Science Use Case Analysis", Next Generation VLA Memo. No. 18. (2017).

Walter, F., Brinks, E., de Blok, W. J. G., et al. 2008, AJ, 136, 2563

[1]*NRAO, Charlottesville, VA, 22903, USA;* emurphy@nrao.edu

[2]*Univ. of Maryland, Dept. of Astronomy, College Park, MD 20742, USA*

[3]*Dept. of Astronomy, Cornell University, Ithaca, NY 14853, USA*

[4]*Astronomy, UT Austin, 2515 Speedway Blvd Stop C1400, Austin, TX 78712*

[5]*Dept. of Physics & Astronomy, MSU, East Lansing, MI 48824, USA*

[6]*Dept. of Physics & Astronomy, University of Wyoming, Laramie WY, USA*

[7]*Dept. of Astronomy and Earth & Planetary Sciences, UCB, Berkeley, CA, USA*

[8]*NOAO, 950 N Cherry Avenue, Tucson, AZ 85719, USA*

[9]*NRC Herzberg, 5071 W. Saanich Rd., Victoria, BC, V9E 2E7, Canada*

[10]*Univ. of Victoria, 3800 Finnerty Road, Victoria, BC, V8P 5C2, Canada*

[11]*Cahill Center for Astronomy & Astrophysics, Caltech, Pasadena CA, USA*

[12]*Physics & Astronomy, Rice 6100 Main Street, MS-108, Houston, Texas 77005*

[13]*Inst. of Astronomy, Univ. of Tokyo, Osawa, Mitaka, Tokyo 181-0015, Japan*

[14]*Physics & Astr., 703 Van Allen Hall, U. Iowa, Iowa City, IA 52242, USA*

[15]*JPL, Caltech, Pasadena, CA 91109, USA*

[16]*Dept. of Astronomy, OSU, 140 West 18th Avenue, Columbus, OH 43210*

[17]*Instituto de Radioastronomía y Astrofísica, Universidad Nacional Autónoma de México, Morelia 58089, Mexico*

[18]*Univ. Nacional Autónoma de México, Apartado Postal 70-264, 04510 Ciudad de México, México*

[19]*Dept. of Physics, Box 41051, Sci. Building, TTU, Lubbock TX, 79409, USA*

[20]*STScI 3700 San Martin Drive, Baltimore, MD 21218, USA*

[21] *Harvard-Smithsonian CfA 60 Garden Street, Cambridge MA 02138, USA*

[22]*RIKEN, 2-1 Hirosawa, Wako-shi, Saitama 351-0198, Japan*

[23]*MPIfA, Königstuhl 17, Heidelberg D-69117, Germany*

Science with a Next-Generation Very Large Array
ASP Conference Series, Monograph 7
Eric J. Murphy, ed.

DRAFT EDITION

The ngVLA Reference Design

Robert J. Selina,[1] Eric J. Murphy,[2] Mark McKinnon,[1] Anthony Beasley,[2] Bryan Butler,[1] Chris Carilli,[1] Barry Clark,[1] Alan Erickson,[1] Wes Grammer,[1] James Jackson,[1] Brian Kent,[2] Brian Mason,[2] Matthew Morgan,[2] Omar Ojeda,[2] William Shillue,[2] Silver Sturgis,[1] and Denis Urbain.[1]

[1]*National Radio Astronomy Observatory, Socorro, NM, USA*

[2]*National Radio Astronomy Observatory, Charlottesville, VA, Country*

Abstract. The next-generation Very Large Array (ngVLA) is an astronomical observatory planned to operate at centimeter wavelengths (25 to 0.26 centimeters, corresponding to a frequency range extending from 1.2 GHz to 116 GHz). The observatory will be a synthesis radio telescope constituted of approximately 214 reflector antennas each of 18 meters diameter, operating in a phased or interferometric mode.

We provide a technical overview of the reference design of the ngVLA. The concepts for major system elements such as the antenna, receiving electronics, and central signal processing are presented. We also describe the major development activities that are presently underway to advance the design.

1. Introduction

As part of its mandate as a national observatory, the National Science Foundation's (NSF) National Radio Astronomy Observatory (NRAO) is looking toward the long-range future of radio astronomy and fostering the long-term growth of the U.S. and global astronomical community. With NSF support, NRAO has sponsored a series of science and technical community meetings to define the science mission and concept for a next-generation Very Large Array (ngVLA; McKinnon 2016), building on the legacies of the Atacama Large Millimeter/submillimeter Array (ALMA) and the Jansky Very Large Array (VLA).

Based on input solicited from the astronomical community, the ngVLA is planned as an astronomical observatory that will operate at centimeter wavelengths (25 to 0.26 centimeters, corresponding to a frequency range extending from 1.2 GHz to 116 GHz). The observatory will be a synthesis radio telescope with a main array constituted of approximately 214 reflector antennas each of 18 meters diameter, operating in a phased or interferometric mode. A dense core short baseline array (SBA) of 19 reflector antennas of 6 m aperture will be sensitive to a portion of the larger angular scales undetected by the main array. The SBA may be combined with 4 18 m (main-array) antennas used in total power mode to completely fill in the central hole in the (u, v)-plane left by the 6 m dishes.

The ngVLA will have approximately ten times the sensitivity of the VLA and ALMA, with more than thirty times longer baselines (∼1000 km) providing milliarcsecond resolution, plus a dense core on km-scales for high surface brightness sensitivity. Such an array bridges the gap between ALMA, a superb sub-mm array, and the future SKA1, optimized for longer wavelengths.

The dense core and the signal processing center of the array will be located at the Very Large Array site, on the plains of San Agustin, New Mexico. The array will include stations in other locations throughout the state of New Mexico, Arizona, west Texas, and northern Mexico. The high desert plains of the Southwest U.S., at over 2000 m elevation, provide excellent observing conditions for the frequencies under consideration, including reasonable phase stability and opacity at 3 mm wavelength over a substantial fraction of the year.

Operations will be conducted from both the VLA site facilities and the Array Operations Center in Socorro, NM. Additional operations centers may be incorporated into the design.

The facility will be operated as a proposal-driven instrument. The fundamental data products for ngVLA users will be science-ready data products (i.e., images and cubes) generated using calibration and imaging pipelines created and maintained by the project. Both the pipeline products and the "raw" visibilities and calibration tables will be archived, retaining the option of future re-processing and archival science projects.

The ngVLA project is developing a Reference Design for the array that will form a baseline for construction and operation costing, and future design trade-off decisions. This Reference Design is intended to be low technical risk in order to provide a degree of conservativism in the estimates. However, leading-edge concepts and techniques that may help improve the performance and/or reduce cost are being developed in parallel, and will be evaluated in the conceptual design phase of the facility.

2. Key Science & Technical Requirements

The Key Science Goals and all other science use cases were parameterized and analyzed (Selina, Murphy & Erickson 2017) to determine the science requirements for the ngVLA (Murphy 2017). While this aspect of the requirements definition is top-down and mission-driven, some judicious adjustment of the requirements is still appropriate. A primary science requirement for the ngVLA is to be flexible enough to support the breadth of scientific investigations that will be proposed by its creative scientist-users over the decades-long lifetime of the instrument. The requirements have therefore been adjusted to provide a balanced, flexible, and coherent complement of capabilities. The primary requirements that drive the design are described below:

- **Frequency Coverage:** The ngVLA should be able to observe in all atmospheric windows between 1.2 and 116 GHz. These frequency limits are bracketed by spectral line emission from HI and CO respectively.

- **Continuum Sensitivity:** A continuum sensitivity of better than 0.02 μJy/bm at 30 GHz and 0.2 μJy/bm 100 GHz is required for studying protoplanetary disks. This requires a combination of large collecting area and wide system bandwidth.

- **Line Sensitivity:** A line sensitivity of 30 μJy/bm/km/s for frequencies between 10 and 50 GHz is simultaneously required to support both astrochemistry studies and deep/blind spectral line surveys. A line sensitivity of $1-100$ mK at $0''.1-5''$ angular resolution and $1-5$ km/s spectral resolution between 70 and 116 GHz is required to simultaneously support detailed studies of CO and variations in gas density across the local universe. The spectral line cases push the system design towards quantum-limited noise performance at the expense of bandwidth above 10 GHz.

- **Angular Resolution:** A synthesized beam having a FWHM better than 5 mas with uniform weights is required at both 30 and 100 GHz, while meeting the continuum sensitivity targets.
- **Largest Recoverable Scale:** Angular scales of $> 20'' \times (100\,\mathrm{GHz}/\nu)$ must be recovered at frequencies $\nu < 100$ GHz. A more stringent desire is accurate flux recovery on arcminute scales at all frequencies. These scales approach the size of the primary beam of an 18 m dish, so both shorter baselines and a total power capability are necessary to completely fill in the central hole in the (u, v)-plane.
- **Surface Brightness Sensitivity:** The array shall provide high-surface brightness sensitivity over the full range of angular scales recoverable with the instrument. This leads to a centrally condensed distribution of antennas.
- **Brightness Dynamic Range:** The system brightness dynamic range shall be better than 50 dB for deep field studies. This requirement pushes a number of systematic requirements including pointing, gain, and phase stability.
- **Survey Speed:** The array shall be able to map a ~10 square degree region to a depth of $\sim 1\,\mu$Jy/bm at 2.5 GHz and a depth of $\sim 10\,\mu$Jy/bm at 28 GHz within a 10 hr epoch for localization of transient phenomena identified with other instruments. Holding collecting area and receiver noise constant, this favors smaller apertures.
- **Beamforming for Pulsar Search, Pulsar Timing and VLBI:** The array shall support no less than 10 beams spread over 1 to 10 subarrays that are transmitted, over the full available bandwidth, to a VLBI recorder/correlator, pulsar search engine or pulsar timing engine. The pulsar search and timing engine must be integral to the baseline design.
- **Science Ready Data Products:** The primary data product delivered to users shall be calibrated images and cubes. Uncalibrated, "raw" visibilities shall be archived to permit reprocessing. Producing these higher-level data products requires some standardization of the initial modes/configurations that the system is used in (e.g., limited tuning options), and repeatability/predictability from the analog system to reduce the calibration overheads.
- **Cost (Construction & Operations):** The construction cost of the array shall not exceed $1.5B USD (2016) and the annual operation cost of the array shall not exceed $75M USD (2016). The operations cap favors designs with less elements (i.e., small N, large D), which is in conflict with a number of performance metrics.

3. Site Selection & Performance

Decades of data on the quality of the VLA site as an observing location are available, including extensive studies of opacity and phase stability, establishing the Plains of San

Agustin as a good site for millimeter-wavelength interferometry (Carilli 2015). The VLA site was used for acceptance testing of the original ALMA antennas, including observations up to 230 GHz, and the experience was that the VLA site, at 2124 m elevation is a high-quality 90 GHz site - comparable to the Plateau de Bure site in overall performance (Thompson, Moran & Swenson 2004).

Analysis of data from the VLA site atmospheric phase monitor shows that fast switching phase calibration at 3 mm should be viable, day or night, for most of the year with a 30 s total calibration cycle. There should be a 25 mJy calibrator source within 2° in 98% of observed fields, ensuring short slews. Such a calibrator is adequate to ensure that the residual rms phase noise due to the signal-to-noise ratio on the phase calibrator is much less than that due to the troposphere, even for a 30 s cycle time with only 3 s on the calibrator each visit (Carilli 2015; Clark 2015). The project is also investigating radiometric phase correction techniques as part of the ngVLA project to increase the total phase calibration cycle time.

In addition, the VLA is remote enough that Radio Frequency Interference (RFI) is not a particular problem, in comparison to other sites, so it will also be possible to observe at lower frequencies (Stewart 2005). The degree of characterization of the site reduces the risk in site selection, and leveraging existing infrastructure could create significant cost savings for both the construction and operation of the array.

Because of the quality of the site for both low- and high-frequency observing, and the existing infrastructure, we choose to center the ngVLA near the current VLA.

4. Array Configuration

The main array configuration will consist of 214 18 m antennas at the approximate locations shown in Figure Figure 7. The array collecting area is distributed to provide high surface brightness sensitivity on a range of angular scales spanning from approximately 1000 to 10 mas (see Table 1). In practice, this means a core with a large fraction of the collecting area in a randomized distribution to provide high snapshot imaging fidelity, and arms extending asymmetrically out to ~1000 km baselines, filling out the (u, v)-plane with Earth rotation and frequency synthesis.

The array configuration is practical, accounting for logistical limitations such as topography and utility availability. Investigations are underway to improve the imaging sensitivity and fidelity while accounting for additional limitations such as local RFI sources and land management/availability.

Radius	Collecting Area Fraction	Quantity
0 km< R < 1.3 km	$\approx$ 44%	94
1.3 km< R < 36 km	$\approx$ 35%	74
36 km< R <1000 km	$\approx$ 21%	46

Table 1. Radial distribution of collecting area.

The configuration will be a primary area for investigation in the coming years. We have investigated different Briggs weighting schemes for specific science applications (Carilli 2017), and find that the current configuration provides a reasonable compromise and baseline for further iteration.

The design has been extended from the main interferometric array to include both a short spacing array and total power dishes (Mason 2018b). This is necessary after

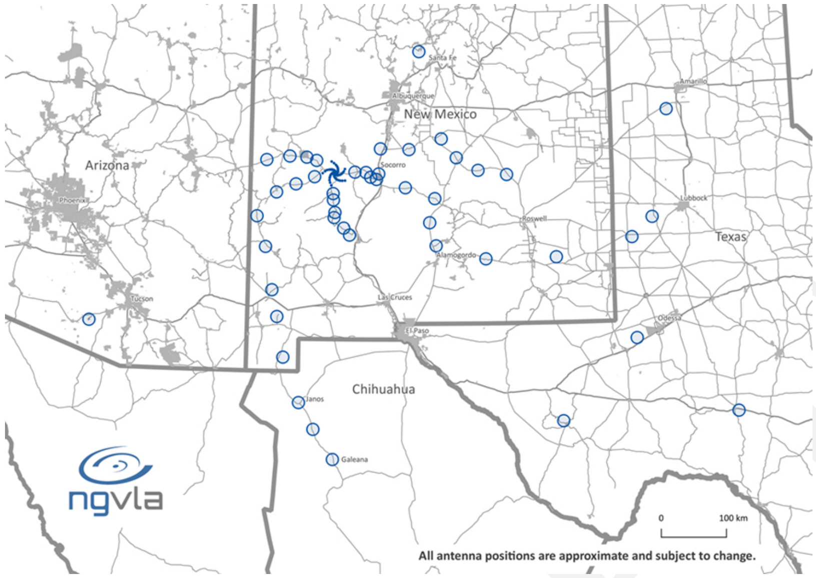

Figure 1. ngVLA Array Configuration Rev. B (Spiral-214). Antenna positions are still notional, but are representative for performance quantification.

a review of the key science cases, as these are dependent on the recovery of large scale structure that approaches the size of the antenna primary beam. A cumulative histogram of the minimum baseline required to recover the largest angular scale of interest is shown in Figure 3.

An auxiliary short baseline array (SBA) of 19 reflector antennas of 6 m aperture will be sensitive to a portion of the larger angular scales undetected by the main array. The SBA will provide spacings from 11 m to 60 m, providing comparable surface brightness sensitivity to the main array, in equal observing time, when the main array is (u, v)-tapered to the natural resolution of the SBA. This allows for commensal observing, and more importantly, full cross-correlation and cross-calibration of the SBA and main array. The array distribution is semi-randomized to improve the point spread function (Mason et al. 2018a).

The SBA will be combined with 4 18 m (main-array) antennas used in total power (TP) mode to completely fill in the central hole in the (u, v)-plane left by the 6 m dishes. It is a design goal to share the mount design of the 18 m interferometric array antennas and the TP antennas, but this will require further study. The array configuration elements are summarized in Table 2.

5. Array Calibration

The calibration strategy for ngVLA is being developed early in the design so that it may guide the design of the hardware elements. The size and complexity of the calibration and imaging pipeline requires that the system design be responsive to its needs, and it should drive the design where possible.

A secondary concern is the efficiency of the calibration process. Algorithms used must be suitable for parallel processing, antennas must not require much individual

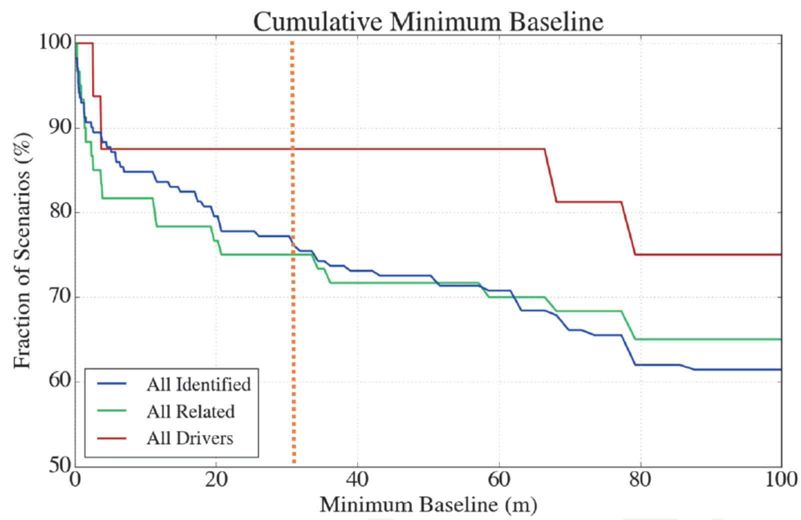

Figure 2. Cumulative histogram of the minimum baseline required to recover the largest angular scale of interest. Approximately 75% of cases can be supported by a 1.65**D* spacing between 18 m diameter dishes, shown as a dashed vertical line. The remaining 25% of cases require a large single dish, or short baseline array and total power antennas. (Selina, Murphy & Erickson 2017).

Array Element	Aperture Diameter	Quantity	B_{MIN}	B_{MAX}	ν_{MIN}	ν_{MAX}
Main Interferometric Array	18 m	214	30 m	1005 km	1.2 GHz	116 GHz
Short Baseline Array	6 m	19	11 m	56 m	1.2 GHz	116 GHz
Total Power / Single Dish	18 m	4	-	-	1.2 GHz	116 GHz

Table 2. Elements within the ngVLA configuration.

attention, and minimal human intervention should be generally required. The calibration overheads applied will vary with the science requirements of a given observation, and less rigorous (and computationally or time efficient) calibration approaches will be applied when possible.

The general calibration strategies under consideration for the reference design are summarized below.

- **Fast Atmospheric Phase Calibration:** Rapid atmospheric phase fluctuations will be mitigated by a combination of relative water vapor radiometry (WVR) and antenna switching cycles to astronomical phase calibrators. The switching cycle time will depend on empirical validation of the strategy, but is expected to be necessary on one to ten minute scales. The antenna will be designed to both house the WVR and move 4° on sky and settle to within the pointing specification with 10 seconds for elevation angles $< 70^\circ$ (Selina 2017).
- **Slow Atmospheric & Electronic Phase Calibration:** Slow atmospheric and electronic phase calibration will be achieved by traditional approaches, with astronomical phase calibrator observations bracketing all observations. Several astronomical calibrators may be used to map the slow varying terms, including ionospheric fluctuations.
- **Amplitude Calibration:** A list of known astronomical amplitude calibrators will be used to correct for system gain fluctuations within an observation and between observations taken over an extended period of time. The calibration pipeline will maintain a history of recent solutions to enable look-up of prior values.
- **Bandpass Calibration:** At a minimum, the system would first correct for digital effects, given the predictable bandpass ripple from finite impulse response filters. The number of setups in the analog portions of the system will be limited, so typical calibration can correct for analog bandpass effects based on historical lookup tables that are updated as the configuration of the system changes (when an antenna is serviced).
- **Polarization Calibration:** The use of linear feeds will require polarization calibration for most observations. Feeds will be placed at different (but known) position angles in the various antennas, so a single observation of a point source can solve simultaneously for the polarization leakage terms and the source polarization. Calibration for polarization as a function of position within the antenna beam will be assumed to be time invariant and corrected based on look-up tables.
- **Relative Flux Calibration:** This calibration is used to tie together observations of a source taken over an extended period. The system will model opacity based on barometric pressure and temperature monitored at the array core and each outlying station. A temperature stabilized noise diode will provide a reference, and when combined with corrections for modeled atmospheric opacity, we can assume a constant ratio in power from the switched noise calibrator and the source.
- **Absolute Flux Calibration:** Absolute flux scale calibration will employ similar methods to relative calibration, with two notable changes. First, atmospheric tipping scans will be used to empirically determine atmospheric opacity. Second, observations of astronomical flux calibrators will be used, along with the switched power system, to determine the absolute flux of the source.

The ngVLA will need to maintain multiple lists of calibrators by calibration intent. The flux calibrator list can be relatively small and based on the one built and maintained by the VLA. An extensive grid of sources will be required for phase and amplitude calibration. The large range of baselines present on the ngVLA means that it cannot be assumed that the source is unresolved, and these calibrators themselves must be imaged before use in the calibration process.

6. Antenna

The antenna concept strikes a balance between competing science and the programmatic targets for life cycle cost. Sensitivity goals will be met by the total effective collecting area of the array. The reference design includes 214 antennas of 18 m aperture (main array) and 19 antennas of 6 m aperture (short baseline array) using an offset Gregorian optical design.

The inclusion of frequencies down to 1.2 GHz when combined with the operational cost targets significantly constrain the optical configuration. The use of feeds with wide illumination angles decreases their size such that they can be mounted within shared cryostats. This choice constrains the secondary angle of illumination to a degree that only Gregorian optical designs are practical. However, with a science priority of high imaging dynamic range in the 10 – 50 GHz frequency range, an offset Gregorian is near optimal. The unblocked aperture will minimize scattering, spillover and sidelobe pickup. Both performance and maintenance requirements favor antenna optical configurations where the feed support arm is on the "low side" of the reflector.

The optimization for operations and construction cost suggests that a smaller number of larger apertures is preferable to larger numbers of small apertures. Survey speed requirements push the opposite direction, and a compromise value of 18 m diameter is adopted for the reference design. The design aims for Ruze performance to 116 GHz, with a surface accuracy of 160 μm RMS ($\lambda/16$ @ 116 GHz) for the primary and subreflector combined under precision environmental conditions. The antenna optics are optimized for performance above 5 GHz with some degradation in performance accepted at the lowest frequencies due to diffraction, in exchange for more stiffness in the feed arm to improve pointing performance.

Since the ngVLA is envisioned as a general purpose, proposal-driven, pointed instrument (rather than a dedicated survey telescope), the optics will be shaped to optimize the illumination pattern of single pixel feeds, increasing antenna gain while minimizing spillover. High pointing accuracy will also be necessary to provide the required system imaging dynamic range. With an unblocked aperture, variations in the antenna gain pattern are expected to be dominated by pointing errors. Preliminary requirements are for absolute pointing accuracy of 18 arc-seconds RMS, with referenced pointing of 3 arc-seconds RMS, during the most favorable environmental conditions (Mason 2018b).

The mechanical and servo design is a typical altitude-azimuth design, Figure 3. Initial studies suggest pedestal designs are expected to have lower life-cycle cost while meeting pointing specifications. The antenna mechanical and servo design will need to be optimized for rapid acceleration and a fast settling time, in order to manage the switching overhead associated with short slews.

The project is presently pursuing a reference design to specifications for the 18 m antenna with General Dynamics Mission Systems (GDMS). A parallel study into a composite design concept with the National Research Council of Canada (NRCC) is also underway, and NRCC are also preparing a reference design for the 6 m short baseline array antenna. All three costed designs will be delivered in the fall of 2018.

The short baseline array 6 m aperture design shares the majority of its specifications with the main antenna, including the interfaces with the front end equipment such that feeds, receivers and other antenna electronics are interchangeable between the two arrays. The design employs a composite reflector and backup structure on a steel pedestal mount. The mount includes space to house the digital electronics, power supplies and servo system, Figure 3.

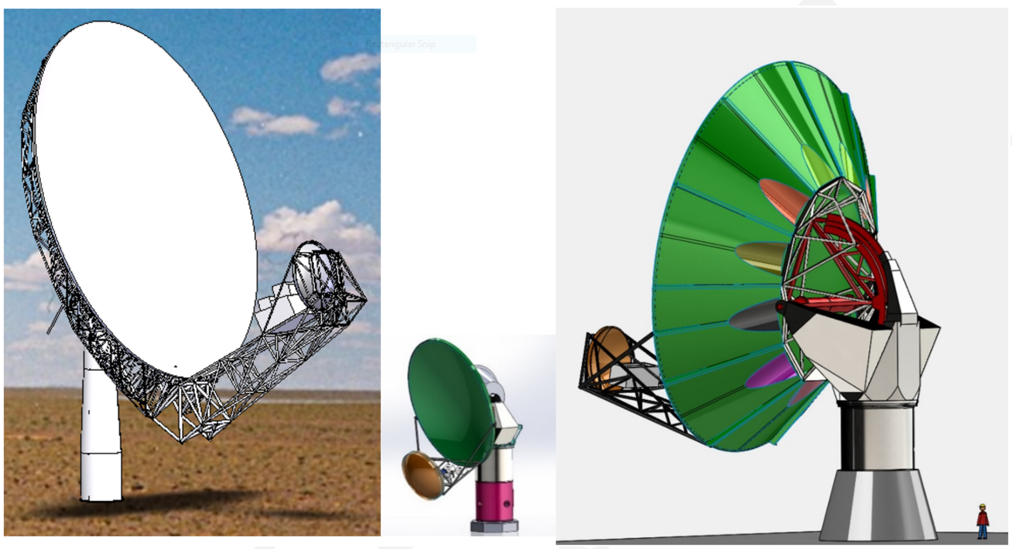

Figure 3. Left: ngVLA 18 m antenna reference design concept prepared by GDMS. Center: 6 m short spacing array antenna concept prepared by NRCC. Right: ngVLA 18 m antenna composite design concept prepared by NRCC.

7. Receiver Configuration

The ngVLA will provide continuous frequency coverage from 1.2 - 50.5 GHz and 70 - 116 GHz in multiple bands. Receivers will be cryogenically-cooled, with the receiver cryostats designed to integrate multiple receiver bands to the extent possible. Limiting the number of cryostats will reduce both maintenance and electrical power costs. The total number of bands required strongly depends on their fractional bandwidths: maximizing bandwidths will reduce the number of cryostats, with a possible penalty in sensitivity. Feeds for all receiver bands are cooled, and fully contained within the cryostat(s).

The baseline ngVLA receiver configuration consists of the low-frequency receiver (1.2 - 3.5 GHz) in one cryostat, and receivers spanning from 3.5 to 116 GHz in a second cryostat.

Bands 1 and 2 employ wideband feed horns and LNAs, each covering L+S bands, and C+X bands. Quad-ridged feed horns (QRFHs) are used, having dual coaxial outputs. Due to improved optical performance (reducing T_{spill}), cooled feeds, and the

Band #	f_L (GHz)	f_M (GHz)	f_H (GHz)	BW (GHz)	Aptr. Eff., ηA @f_L	@f_M	@f_H
1	1.2	2.0	3.5	2	0.78	0.79	0.74
2	3.5	6.6	12.3	8.8	0.78	0.79	0.70
3	12.3	15.9	20.5	8.2	0.84	0.87	0.86
4	20.5	26.4	34	13.5	0.83	0.86	0.83
5	30.5	39.2	50.5	20	0.81	0.82	0.78
6	70	90.1	116	46	0.68	0.61	0.48

Table 3. Band definitions and aperture efficiency of the baseline receiver concept.

simplified RF design sensing linear polarization, the T_{sys} is lower than current VLA L, S bands and comparable for C and X bands. Overall aperture efficiency and T_{sys} are slightly degraded from optimal due to the wider bandwidths spanned, but permits a compact package that can be affordably constructed and operated.

The four high-frequency bands (12.3 - 116 GHz) employ waveguide-bandwidth (~1.67:1) feeds & LNAs, for optimum noise performance. Axially corrugated feed horns with circular waveguide output ensure even illumination over frequency and minimal loss.

Band #	T_{spill} (K) @f_L	@f_M	@f_H	T_{RX} (K) @f_L	@f_M	@f_H	T_{sys} (K) @f_L	@f_M	@f_H
1	10	7	5	9	10	10.5	25	23	22
2	10	6	4	11	12	15	28	25	26
3	4	4	4	9	10	11	20	22	31
4	4	4	4	11	13	18	32	33	38
5	4	4	4	17	21	27	36	45	105
6	4	4	4	39	41	60	116	65	181

Table 4. Noise performance of the baseline receiver concept. Assumes 1 mm PWV for band 6, 6 mm PWV for others; 45° elev. on sky for all.

The electronics concept relies on integrated receiver packages (Morgan & Wunduke 2017) to further amplify the signals provided by the cryogenic stage, down convert them if necessary, digitize them, and deliver the resultant data streams by optical fiber to a moderately remote collection point (typically the antenna pedestal) where they can be launched onto a conventional network for transmission back to the array central processing facility. Interfaces are provided for synchronization of local oscillators (LO's) and sampler clocks, power leveling, command and control, health and performance monitoring, and diagnostics for troubleshooting in the event of component failure.

The integrated receiver concept is central to the antenna electronics concept for the ngVLA. Compact, fully-integrated, field-replaceable, warm electronic modules support single-stage, direct-to-baseband downconversion (when needed), followed by a very low-power, low-overhead digitization scheme and an industry-standard fiber optic interface carrying unformatted serial data. The frequency plan is shown in Figure 4 (Morgan & Wunduke 2017).

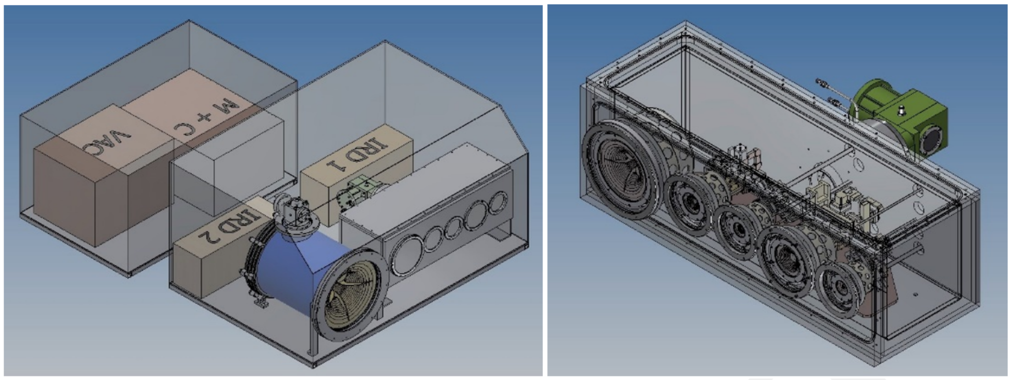

Figure 4. Front end component packaging at the secondary focus of the antenna. Band selection and focus are achieved with a dual-axis translation stage.The integrated receiver packages (labeled IRD 1 and IRD 2) are located in close proximity to the cryostats. Bands 2 – 6 are housed within in single cryostat.

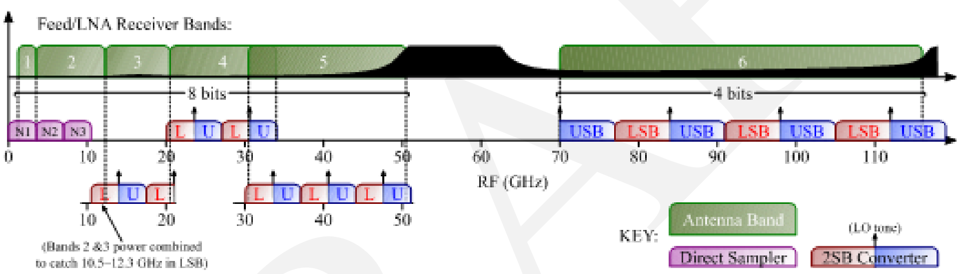

Figure 5. Present sampling concept employing integrated receiver technology for both direct and dual sideband converter/samplers.

8. Reference Distribution & Data Transmission

Given the large extent of the array, multiple time and frequency reference distribution concepts will likely be required to optimize for cost and performance. The array will likely be built as a combination of two different design methodologies.

A large number of antennas located on the Plains of San Agustin, would be part of a compact core, and each antenna in the core would be connected directly to a central processing facility by fiber optics. Roughly 80% of the ngVLA antennas will be within this region. Clocks and local oscillator signals may be generated locally at the antenna and locked to a central reference with round trip phase correction, possibly sharing a DTS transceiver (Figure 6).

The remainder of the antennas, the long baseline antennas, would fall into a VLBI station model with a number of local oscillator (LO) and data transmission stations located beyond the central core. These stations will be linked to the central timing system, correlator, and monitor and control system via long haul fiber optics. Several options will be explored for precision timing and references at these stations, including local GPS-disciplined masers, fiber optic connections to the central site, and satellite-based timing.

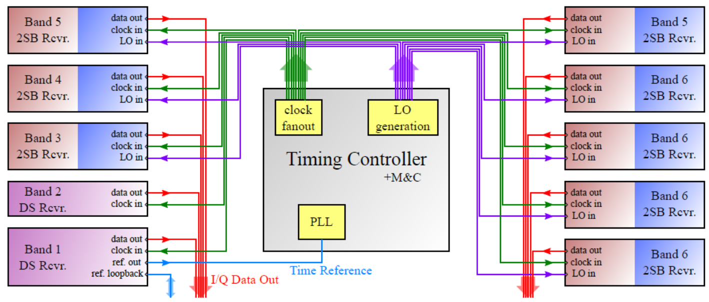

Figure 6. Schematic of clock and LO distribution inside the antenna.

9. Central Signal Processor

The Central Signal Processor (CSP) ingests the voltage streams recorded and packetized by the antennas and transmitted via the data transmission system, and produces a number of low-level data products to be ingested by the archive. In addition to synthesis imaging, the CSP will support other capabilities required of modern telescopes to enable VLBI and time-domain science. The functional capabilities of the CSP include:

- Auto-correlation
- Cross-correlation
- Beamforming
- Pulsar Timing
- Pulsar Search
- VLBI Recording

The CSP data products will vary by operation mode. The most common will be raw/uncalibrated visibilities, recorded in a common data model. The CSP will include all necessary "back end" infrastructure to average visibilities and package them for the archive, where they will be recorded to disk in a standard format. Calibration of these data products will be the responsibility of asynchronous data post-processing pipelines that are outside the scope of the CSP element. The CSP will support multiple sub-arrays. A key requirement for the system is the degree of commensality supported both within a sub-array and by commensal sub-arrays. The following commensal modes will be supported:

- Cross-correlation and Auto-correlation (Commensal within a sub-array)
- Cross-correlation & Pulsar Timing (Commensal sub-arrays)
- Cross-correlation & Pulsar Search (Commensal sub-arrays)
- Cross-correlation & VLBI Recording (Commensal sub-arrays)

Providing correlation and beamforming products simultaneously within a subarray is also under evaluation. Such a mode would aid calibration of the beamformer, and provide for localization/imaging concurrent with time-domain observations. The degree of commensality is expected to be a cost/complexity driver in the system and will be optimized on a best value basis.

The ngVLA correlator will employ an FX architecture, and will process an instantaneous bandwidth of up to 20 GHz per polarization. The correlator-beamformer Frequency Slice Architecture (Rupen 2017) developed by NRC Canada for the SKA Phase 1 CSP Mid Telescope is well suited to ngVLA demands and is under evaluation for the reference design. This architecture will scale to the additional ngVLA apertures, bandwidth, and commensal mode requirements. Adopting this architecture will significantly reduce the non-recurring engineering costs during the design phase, while additional improvements in electrical efficiency can be expected from one additional FPGA manufacturing process improvement cycle due to ngVLA's later construction start date. Key performance requirements for the correlator are summarized in Table 5.

Requirement Description	**Specification**
Number of Connected Antennas	256 total, composed of 214 18 m elements, 19 6 m elements, 12 VLBI stations (TBC), and 11 spare inputs
Maximum Baseline Length	1,000 km
Maximum Instantaneous Bandwidth	20 GHz
Maximum Number of Channels	300,000 channels
Highest Frequency Resolution	400 Hz, corresponding to 0.1 km/s resolution at 1.2 GHz.
Pulsar Search Beamforming	$\geq$ 91 beams, 60 km diameter sub-array, $1''$ coverage
Pulsar Timing Beamforming	$\geq$ 10 independent sub-arrays, 50 beams total

Table 5. Correlator-beamformer key specifications.

10. Post Processing System

The software architecture for ngVLA will leverage NRAO's existing algorithm development in reducing VLA and ALMA data and the CASA software infrastructure. The array will have a progressive series of data products suitable to different users groups. The data products may also change based on how well supported a mode is - common modes should have higher level data products that add value to the user, while clearly not all permutations can benefit from such a degree of automation. As with the VLA, the fundamental data product that will be archived are uncalibrated visibilities. The online software system will also produce flags to be applied to the visibilities that would identify known system problems such as antennas being late on source, or the presence of RFI.

Automated post-processing pipelines will calibrate the raw data and create higher-level data products (typically image cubes) that will be delivered to users via the central archive. Calibration tables that compensate for large-scale instrumental and atmospheric effects in phase, gain, and bandpass shapes will be provided. Data analysis tools will allow users to analyze the data directly from the archive, reducing the need for data transmission and reprocessing at the user's institution.

The VLA and ALMA "Science Ready Data Products" project will be an ngVLA pathfinder to identify common high-level data products that will be delivered to the Principal Investigator and to the data archive to facilitate data reuse. This will also enable the facility to support a broader user base, possibly catering to astronomers who are not intimately aware of the nuances of radio interferometry, thereby facilitating multi-wavelength science.

11. Overall System Performance

The predicted performance of the array is summarized in Table 6. This is an update to the performance estimates originally documented in Selina & Murphy (2017)[1].

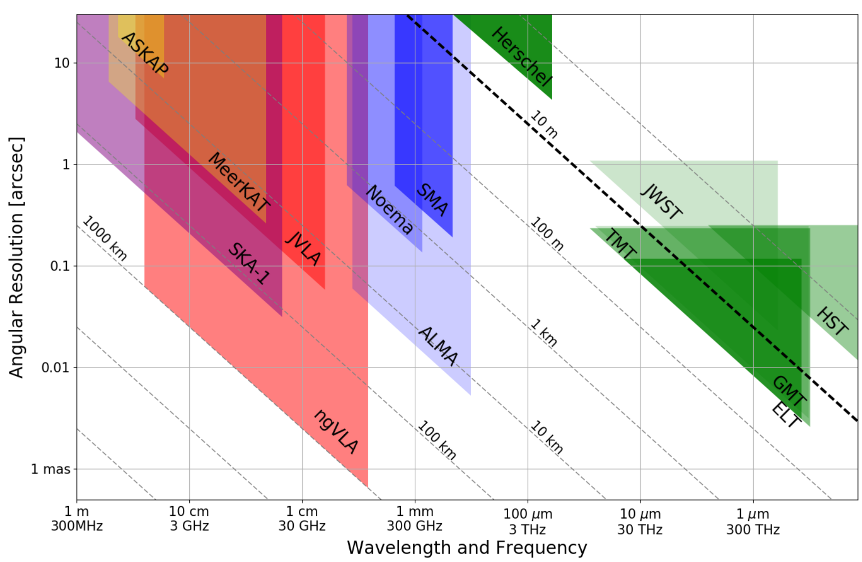

Figure 7. Spatial resolution versus frequency set by the maximum baselines of the ngVLA as compared to that of other existing and planned facilities.

The continuum and line rms values in Table 1 are for point source sensitivity with a naturally weighted beam. Imaging sensitivity is estimated based on Carilli (2017) and provided as a function of angular resolution in Table 7. The table is by necessity a simplification and the imaging sensitivity will vary from these reported values depending on the quality (defined as the ratio of the power in the main beam attenuation pattern to the power in the entire beam attenuation pattern as a function of the FWHM

[1] http://ngvla.nrao.edu/page/refdesign

Center Frequency [GHz]	2.4	8	16	27	41	93	Notes
Band Lower Frequency [GHz]	1.2	3.5	12.3	20.5	30.5	70.0	a
Band Upper Frequency [GHz]	3.5	12.3	20.5	34.0	50.5	116.0	a
Field of View FWHM [arcmin]	24.4	7.3	3.7	2.2	1.4	0.6	b
Aperture Efficiency	0.78	0.77	0.86	0.85	0.81	0.60	b
Effective Area, A_{eff}, x 10^3 [m^2]	42.2	41.7	46.8	46.0	44.0	32.4	b
System Temp, T_{sys} [K]	23	25	22	33	45	62	a, e
Max Inst. Bandwidth [GHz]	2.3	8.8	8.2	13.5	20.0	20.0	a
Sampler Resolution [Bits]	8	8	8	8	8	4	
Antenna SEFD [Jy]	329	362	283	432	617	1154	a, b
Resolution of Max. Baseline [mas]	26	8	4	2.3	1.5	0.7	c
Resolution FWHM @ Natural Weighting [mas]	163	49	24	14	10	4	c, d
Continuum rms, 1 hr [μJy/beam]	0.41	0.23	0.19	0.22	0.26	0.48	d
Line Width, 10 km/s [kHz]	80.0	266.7	533.3	900.0	1367	3100	
Line rms, 1 hr, 10 km/s [μJy/beam]	69.0	41.6	23.0	27.1	31.3	38.9	d

Table 6. ngVLA Key Performance Metrics. Notes: (a) 6-band 'baseline' receiver configuration. (b) Reference design concept of 214 18 m aperture antennas. Unblocked aperture with 160um surface. (c) Rev. B 2018 Configuration. Resolution in EW axis. (d) Point source sensitivity using natural weights, dual pol, and all baselines. (e) At the nominal mid-band frequency shown. Assumes 1 mm PWV for W-band, 6 mm PWV for others, 45° elevation on sky for all.

of the synthesized beam (Murphy 2017) of the (sculpted) synthesized beam required to support the science use case.

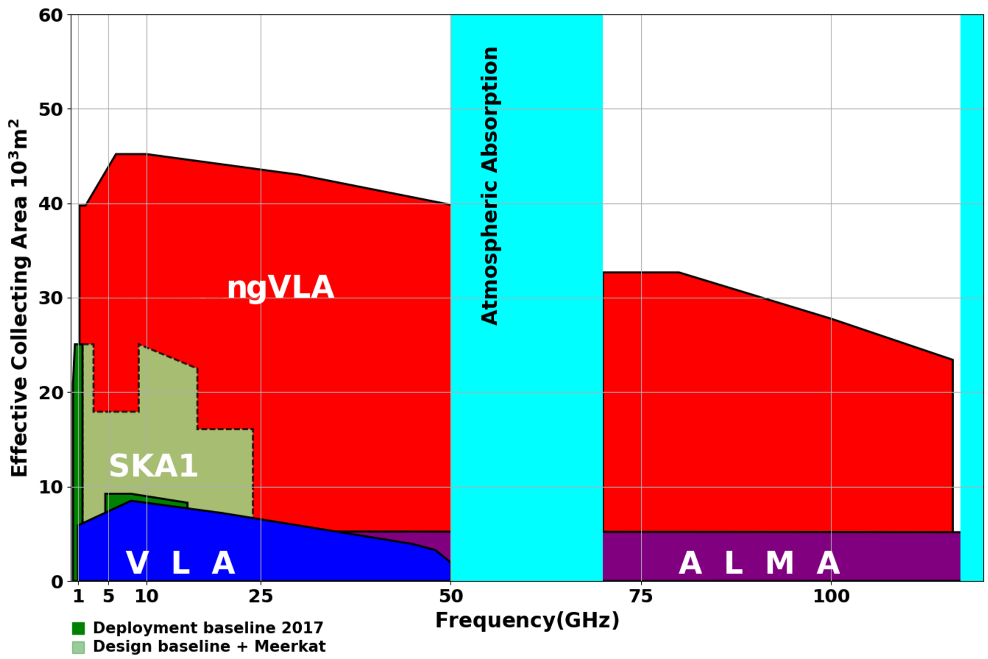

Figure 8. Effective collecting area versus frequency for the ngVLA as compared to that for other existing or planned facilities. Note that lower and higher frequencies are not shown (e.g. SKA-1 will extend to below 100 MHz and ALMA extends up to about a THz). Both the SKA1 'deployment baseline' (dark green) and 'design baseline' (light green) are shown, inclusive of the MeerKAT array (Dewdney 2013).

The brightness sensitivity of an array is critically dependent on the array configuration. The ngVLA has the competing desires of both good point source sensitivity at full resolution, and good surface brightness sensitivity on scales similar to the primary beam size. Different array configurations that might provide a reasonable compromise through judicious weighting of the visibilities for a given application have been explored (Clark & Brisken 2015) – see Lal (2011) for similar studies for the SKA. It is important to recognize the fact that for any given observation, from full resolution imaging of small fields, to imaging structure on scales approaching that of the primary beam, some compromise will have to be accepted.

Figure 7 shows a slice through the parameter space, resolution versus frequency, covered by the ngVLA along with other existing and planned facilities that are expected in the 2030s at all wavelengths. The maximum baselines of the ngVLA imply a resolution of better than 3 mas at 1 cm. Coupled with the high sensitivity of the array, this resolution provides a unique window into the formation of planets in disks on scales of our own Solar system at the distance of the nearest active star forming regions.

Figure 8 shows a second slice through parameter space: effective collecting area versus frequency. A linear-linear plot highlights the parameter space opened by the ngVLA. Note that the SKA-1 will extend to below 100 MHz while ALMA extends up to almost a THz. We note that there are other aspects of telescope phase space that are

Center Frequency [GHz]	2.4	8	16	27	41	93
Resolution [mas] : 1000						
Continuum rms, 1 hr, Robust [μJy/beam]	0.80	0.50	0.43	0.53	0.64	1.28
Line rms 1 hr, 10 km/s Robust [μJy/beam]	135.6	91.0	53.3	65.2	77.9	102.6
Brightness Temp. (T_B) rms continuum, 1 hr, Robust [K]	0.1688	0.0095	0.002	0.0009	0.0005	0.0002
T_B rms line, 1 hr, 10 km/s, Robust [K]	28.62	1.73	0.25	0.11	0.06	0.01
Resolution [mas] : 100						
Continuum rms, 1 hr, Robust [μJy/beam]	0.63	0.40	0.35	0.44	0.53	1.07
Line rms 1 hr, 10 km/s Robust [μJy/beam]	106.4	73.4	43.5	53.8	64.7	86.1
Brightness Temp. (T_B) rms continuum, 1 hr, Robust [K]	13.246	0.767	0.167	0.073	0.039	0.015
T_B rms line, 1 hr, 10 km/s, Robust [K]	2245.9	139.4	20.7	9.0	4.7	1.2
Resolution [mas] : 10						
Continuum rms, 1 hr, Robust [μJy/beam]	-	0.31	0.27	0.35	0.43	0.87
Line rms 1 hr, 10 km/s Robust [μJy/beam]	-	55.8	33.8	42.3	51.4	69.7
Brightness Temp. (T_B) rms continuum, 1 hr, Robust [K]	-	58.3	12.9	5.8	3.1	1.2
T_B rms line, 1 hr, 10 km/s, Robust [K]	-	10596	1605	706	372	98

Table 7. Projected imaging sensitivity as a function of angular resolution.

relevant, including field of view, mapping speed, surface brightness sensitivity, bandwidth, system temperature, dynamic range, etc. We have presented the two principle and simplest design goals, namely, maximum spatial resolution and total effective collecting area (as a gross measure of system sensitivity).

Acknowledgments. The ngVLA is a project of the National Science Foundation's National Radio Astronomy Observatory which is operated under cooperative agreement by Associated Universities, Inc.

References

Akiyama, K. et al., "230 GHz VLBI Observations of M87: Event-Horizon-Scale Structure During an Enhanced Very-High-Energy-Ray State in 2012" ApJ, 807, 150 (2015).

Bolatto, et. al. "Key Science Goals for the Next Generation Very Large Array (ngVLA): Report from the ngVLA Science Advisory Council", Next Generation VLA Memo. No. 19 (2017).

Brisken, W. "Major Option: Continent-scale baselines" U.S. RMS Futures III Conference (2017).

Carilli, C. "Fast Switching Phase Calibration at 3 mm at the VLA site", ngVLA Memo Series No. 1, (2015).

Carilli, C., "More on Synthesized Beams and Sensitivity" Next Generation VLA Memo. No. 16. (2017).

Clark, B. & Brisken, W, "Possible Configurations for the ngVLA" Next Generation VLA Memo. No. 3. (2015).

Clark, B. "Calibration Strategies for the Next Generation VLA", ngVLA Memo Series No. 2, (2015).

Dewdney, P. "SKA1 System Baseline Design" SKA Doc No. SKA-TEL-SKO-DD-001 (2013).

McKinnon, M., "The Next Generation Very Large Array", Proc. SPIE 9906, 10.1117/12.2234941 (2016)

Lal, D., Lobanov, A., Jimenez-Monferrer, S., SKA Design Studies Technical Memo 107. (2011)

Mason, B. S., Cotton, W., Condon, J., et al. 2018a, American Astronomical Society Meeting Abstracts #231, 231, #342.11

Mason, B. et al. "The ngVLA Short Baseline Array", ngVLA Memo No. 43 (2018b).

McLaughlin, M. A., "The North American Nanohertz Observatory for Gravitational Waves", Classical and Quantum Gravity, 30(22):224008 (2013).

Morgan, M. & Wunduke, S. "An Integrated Receiver Concept for the ngVLA", Next Generation VLA Memo. No. 29. (2017).

Murphy, E. et. al., "ngVLA Science Requirements" Next Generation VLA Document No. 020.10.15.00-0001-REQ. (2017)

Rupen, M. "TMâĂŹs View of the Mid.CBF Frequency Slice Approach".

Selina, R. "ngVLA Antenna: Preliminary Technical Specifications" Next Generation VLA Document No. 020.25.00.00.00-0001-SPE. Version B. (2017)

Selina, R. and Demorest P. "A Dedicated Pulsar Timing Array Telescope", ngVLA Memo Series, (In Prep.)

Selina, R. & Murphy E. "ngVLA Reference Design Development & Performance Estimates" Next Generation VLA Memo. No. 17. (2017).

Selina, R., Murphy, E., Erickson, A. "Summary of the Science Use Case Analysis", Next Generation VLA Memo. No. 18. (2017).

Stewart, K. P. et al. "An RFI Survey at the Site of the Long Wavelength Demonstration Array (LWDA)", BAAS 37, 1389 (2005).

Taylor, G. et. al. "A Next Generation Low Band Observatory: A Community Study Exploring Low Frequency Options for ngVLA" (2017), arXiv:1708.00090.

[22] Thompson A., Moran, J. & Swenson, G. Interferometry and Synthesis in Radio Astronomy. Wiley-VCH, (2004)

Science with a Next-Generation Very Large Array
ASP Conference Series, Monograph 7
Eric J. Murphy, ed.

DRAFT EDITION

Reaching Communities and Creating New Opportunities with the ngVLA

Lyndele von Schill,[1] Suzanne Gurton,[1]

[1]*National Radio Astronomy Observatory, Charlottesville, VA, USA;*
`lvonschi@nrao.edu`, `sgurton@nrao.edu`

Abstract. The Office of Diversity and Inclusion (ODI) and the Education and Public Outreach (EPO) Department serve the strategic goal of the National Radio Astronomy Observatory (NRAO) to broaden public awareness of and participation in Science, Technology, Engineering, and Mathematics (STEM). ODI has a suite of programs for undergraduate students through early career professionals, ensuring a diverse workforce. EPO highlights the discoveries, technologies, and careers pioneered and exemplified by the NRAO via multipurpose engagement strategies that include face-to-face and standalone learning programs, products, and public services for the general public and K-12 students. These established and diverse programs are described along with the unique opportunities enabled by the realization of a next-generation Very Large Array (ngVLA).

1. Broadening Participation

As a facility under the management of the National Radio Astronomy Observatory (NRAO), the next-generation Very Large Array (ngVLA) has full access to NRAO's suite of widely well-regarded Broadening Participation programs. NRAO's programs address the key priorities identified by the National Science Foundation (NSF) that include:

- Preparing a diverse, globally engaged science, technology, engineering, and mathematics (STEM) workforce;
- Integrating research with education, and building capacity;
- Expanding efforts to broaden participation from underrepresented groups and diverse institutions across all geographical regions in all NSF activities; and
- Improving processes to recruit and select highly qualified reviewers and panelists.

The NRAO has adopted a comprehensive, observatory-wide, "pipeline" approach to the development of STEM capacity, with particular emphasis on broadening participation of underrepresented groups and diverse institutions. This approach begins with engaging k-12 students in STEM activities that relate to the full spectrum of fields associated with radio astronomy, and continues through providing undergraduate, graduate, and post-doctoral research, training, education, and mentoring programs (described below). The ngVLA will vastly increase the opportunities that the NRAO can offer to the U.S. and international communities.

Figure 1. The NRAO's Broadening Participation "Pipeline".

In addition to its "outward-facing" broadening participation efforts, the NRAO has developed a set of policies and practices that are designed to recruit and select highly qualified, and diverse, reviewers, panelists, and search committees, with the goal of ensuring that selections are fair and equitable across all populations.

Examples of the NRAO's significant investment in broadening participation efforts that will continue under ngVLA include:

K-12 Education Programs: The NRAO's education programs are designed to introduce the hidden universe revealed by radio astronomy by engaging their participants in age appropriate inquiry based activities and research. Examples of K-12 education programs aimed at broadening participation include:

- **Radio Astronomy and Physics in New Mexico (RAP-NM):** a one-week residential summer camp experience on the NM Tech campus for rising 9^{th} graders from around the state of New Mexico. Student mentors are first recruited from the National Astronomy Consortium (NAC) program (see below).

- **Sister Cities and Observatories** is a 10-day international exchange recruiting from high school youth in communities near the Atacama Large Millimeter / submillimeter Array (ALMA) and VLA introducing them to the world class observatories and the diverse range of careers possible at each. This program will continue under ngVLA.

National Astronomy Consortium (NAC) Program: Opportunities for undergraduate research will be coordinated through the NRAO's NAC program, which is designed to provide research opportunities to underrepresented minority students. Students are recruited for participation in this program from an established network of Historically Black Colleges and Universities (HBCUs) and Hispanic-serving Institutions (HSIs).

The ngVLA will open more opportunities for traditionally underrepresented students to participate in cutting-edge research which, in turn, increases opportunities for the students to attend graduate school and/or begin careers in radio astronomy.

National and International Non-Traditional Exchange (NINE) Program: Collaborative opportunities also exist with the NRAO NINE, which trains the next generation of scientists and engineers from countries in which radio astronomy expertise is limited, but needed. The NINE program focuses on training traditionally underrepresented populations in skills that result in meaningful contributions to the astronomical science body of knowledge. The NINE program includes a network of ever-growing national and international "Hubs" where regional populations learn state-of-the art science and technology relevant to astronomy. The ngVLA will provide cutting edge research opportunities to the NINE program, while benefiting from access to skilled scientists and technicians from the broad network of NINE Hub communities.

2. Public Engagement

Public Website: In addition to programs designed with face-to-face interactions, the ngVLA will have a strong presence on the NRAO website which will serve as a portal for the public to explore the engineering advances and astronomical discoveries made possible by ngVLA. Clear information for visitors wishing to visit the site will be on the website, as well as opportunities to explore the site virtually. An ngVLA Explorer[1], combining video and augmented reality, will be created to give those who cannot visit the facility a virtual tour. The Role Model[2] series will be expanded to include ngVLA staff. It currently reflects the diversity of jobs and experiences that are needed to run a national observatory.

Visitor Center: The planned upgrade of the VLA Visitor Center (VC) reflects modern interpretive methods to explore the intersection of three realms: The stories arising from the resource, visitors' intrinsic interests, and the mission and goals of NRAO. The goals for the ngVLA VC will echo those for the VLA VC, with a substantial update to be inclusive of the international collaborations that will help make the ngVLA possible. These interpretive goals will be expressed through an overarching theme that the ngVLA serves humanity's deep curiosity and drive to explore the universe and our relationship to it:

- Interpretation will make information understandable and relevant for non-scientists as well as scientists.
  - Non-scientist visitors will understand in general terms the basics of radio astronomy and the ngVLA - and feel happily surprised that they can.
  - Scientists will appreciate the clarity of the message, without over-simplification to the point of introducing inaccuracies.

---

[1] e.g., `https://public.nrao.edu/special-features/vla-explorer/`

[2] `https://public.nrao.edu/special-features/role-models/`

- People of diverse backgrounds will feel welcome and actively included as the VC will actively:
  - Provide a venue for diverse cultural voices.
  - Include women, persons of color.
  - Encourage Navajo and Puebloans to share their stories.
- Educators will value and use the ngVLA as a resource
- Visitors and residents will understand how natural conditions here support the VLA, and will feel inspired to help maintain those conditions
- Visitors will understand why the ngVLA exists, and feel the program is useful, relevant and worth supporting.
  - People will understand how the ngVLA fits into the bigger picture of astronomy and human discovery.
  - Users will feel they are an integral part of the universe, not separate from it.
  - Local residents and visitors will feel pride and ownership in the ngVLA's role in unlocking the secretes of the universe.
- Visitors will share their positive experiences with others back home.

Media Relations NRAO's EPO department includes a full media relations team with public information officers, artists and graphic designers to best represent the discoveries made possible by ngVLA observations in the popular science media. News and information about ngVLA will be featured in such national outreach venues as the U.S.A. Science and Engineering Festival and National Astronomy Night on the Mall.

3. Broader Impacts: Training the Next Generation

In addition to the NAC and NINE programs that focus on providing research, engineering, and other "full spectrum" astronomy fields, to underrepresented students, the NRAO has provided substantial internship opportunities for undergraduate and graduate students through its REU, graduate research, and NM Ops undergraduate internship programs. The NM Ops internship program, for example, has provided engineering students will experience working in the Observatory's electronics lab. The ngVLA will provide an opportunity to significantly increase the number of students with access to state-of-the-art research and engineering projects.

For the last 2 years EPO has funded a media intern at NRAO headquarters each summer, with the inauguration of ngVLA a media intern will also be stationed at the ngVLA to supplement the efforts of the PIO and assist with major media efforts.

4. Summary

The ngVLA will build on NRAO's existing, well-designed, and implemented, suite of Education and Public Outreach (EPO) programs, including the creation of new opportunities to educate the general public about the exciting science resulting from ngVLA observations. The ngVLA will make use of, and significantly enhance, the Observatory's flagship National Astronomy Consortium (NAC) and National and International Non-traditional Exchange (NINE) programs, by providing cutting-edge research and engineering opportunities for a new generation of astronomers, engineers, and technicians. Importantly, the ngVLA will embrace the NRAO's commitment to providing these opportunities to populations that are unrepresented in STEM fields, and in the field of astronomy in particular.

Part II

The Solar System:

Science with a Next-Generation Very Large Array
ASP Conference Series, Monograph 7
Eric J. Murphy, ed.

DRAFT EDITION

High-resolution imaging of comets

M. A. Cordiner[1,2] and C. Qi[3]
[1]*NASA Goddard Space Flight Center, 8800 Greenbelt Road, MD 20771, USA.*
`martin.cordiner@nasa.gov`

[2]*Institute for Astrophysics and Computational Sciences, The Catholic University of America, Washington, DC 20064, USA.*

[3]*Harvard-Smithsonian Center for Astrophysics, 60 Garden Street, MS 42, Cambridge, MA 02138, USA* `cqi@cfa.harvard.edu`

1. Comets: messengers from the birth of the Solar System

Comets are thought to have accreted in the Solar System at around the same time as the planets. Depending on the degree of subsequent thermal and radiative processing, cometary nuclei may contain pristine material from the proto-Solar disk or prior interstellar cloud. Studies of cometary ices therefore provide unique information on the physical and chemical properties of the early Solar System and pre-solar Nebula (Mumma & Charnley 2011). By virtue of their organic-rich composition, cometary impacts could have been important for initiating prebiotic chemistry on the early Earth, and examining their molecular content provides crucial details on the relationship between interstellar and planetary material (Ehrenfreund & Charnley 2000; Alexander et al. 2018).

To a first-order approximation, the structure of cometary comae can be interpreted using a uniform, spherically-symmetric outflow model, which defines volatile molecules as either 'primary' (parent) species, sublimated directly from the nucleus or photo-chemical 'product' (daughter) species produced in the coma (Haser 1957). Molecules commonly detected in the coma using ground-based telescopes include H_2O, CO, CH_4, CH_3OH, NH_3, HCN, C_2H_2, C_2H_6, H_2S and CS but detections of more complex molecules such as HC_3N, as well as above-average abundances of HNC, H_2CO, CN, C_2 and C_3 in some comets imply that other organic parents are likely present (Crovisier et al. 2004; Cottin & Fray 2008; Lis et al. 2008), probably in the form of organic polymers or macro-molecules. Distributed coma sources are known or suspected for several commonly-observed species (including CN, HNC and H_2CO), originating from presently unknown precursor material(s) at distances up to $\sim 10^5$ km from the nucleus (Biver et al. 1999; Cordiner et al. 2014, 2017). The clearest measure of release from the nucleus (*vs.* production in the coma) requires measurement of the detailed spatial distribution of a species, especially its variation with nucleocentric distance in the innermost coma, within a few hundred to a few thousand km of the nucleus.

2. Elucidating the origins of cometary gases through radio interferometry

A fundamental goal of cometary investigations is to understand the origin and nature of cometary nuclei, in order to explore the chemical link between mature planetary systems and the material present in the accretion disk from which they formed. Of particular interest are the primary volatiles, as measurement of their production can reveal relative abundances of species originally incorporated into a particular cometary nucleus, and therefore information about the conditions under which the comet formed.

The Rosetta mission to comet 67P demonstrated unequivocally the complex nature of cometary outgassing and activity. Strong chemical differentiation was observed for outgassing from different parts of the nucleus (Bockelée-Morvan et al. 2016), and narrow, highly directional jets were observed during outburst events as the comet approached perihelion (see Figure 1). Such features typically span kilometer (milliarcsecond) scales, which can only be resolved from the ground using the high-sensitivity, long-baseline interferometry.

Figure 1. Optical images of comet 67P/Churyumov-Gerasimenko from Rosetta's OSIRIS camera, obtained near perihelion on 12 August 2015, showing strong, narrow jets of gas and dust. Credit: ESA/Rosetta/MPS for OSIRIS Team MPS/UPD/LAM/IAA/SSO/INTA/UPM/DASP/IDA

Radio interferometers can map the spatial distributions of multiple primordial molecules released directly from the interior of the nucleus. Heterodyne receiver technology enables the derivation of high-resolution line-of-sight velocity information, from which 3-D structures can be obtained for the observed species, assisting in investigations of the chemical heterogeneity and true composition of the nucleus (Qi et al. 2015). The first reported interferometric observation of a comet was of the 18 cm OH line in 1P/Halley, detected and mapped using the VLA by de Pater et al. (1986). Formaldehyde (H_2CO) was then detected with the VLA by Snyder et al. (1990) in comet Machholz, and subsequently mapped in comet Hale-Bopp by Milam et al. (2006) using the BIMA interferometer. Figure 2 shows OVRO observations of molecular emission from the inner coma of comet Hale-Bopp (Blake et al. 1999), in which the HNC, DCN, and HDO are seen to lie in arcs or partial shells, offset from the nucleus of the comet. This was likely caused by asymmetric outgassing/jet activity, which lifted a population of icy grains from the nucleus that sublimated to release the observed gases. Interferometric mapping is thus required to properly elucidate the production mechanisms of cometary species, to enable the derivation of accurate mixing ratios.

The importance of radio interferometry to distinguish between molecules arising from different parts of the nucleus and coma was confirmed by Cordiner et al. (2014,

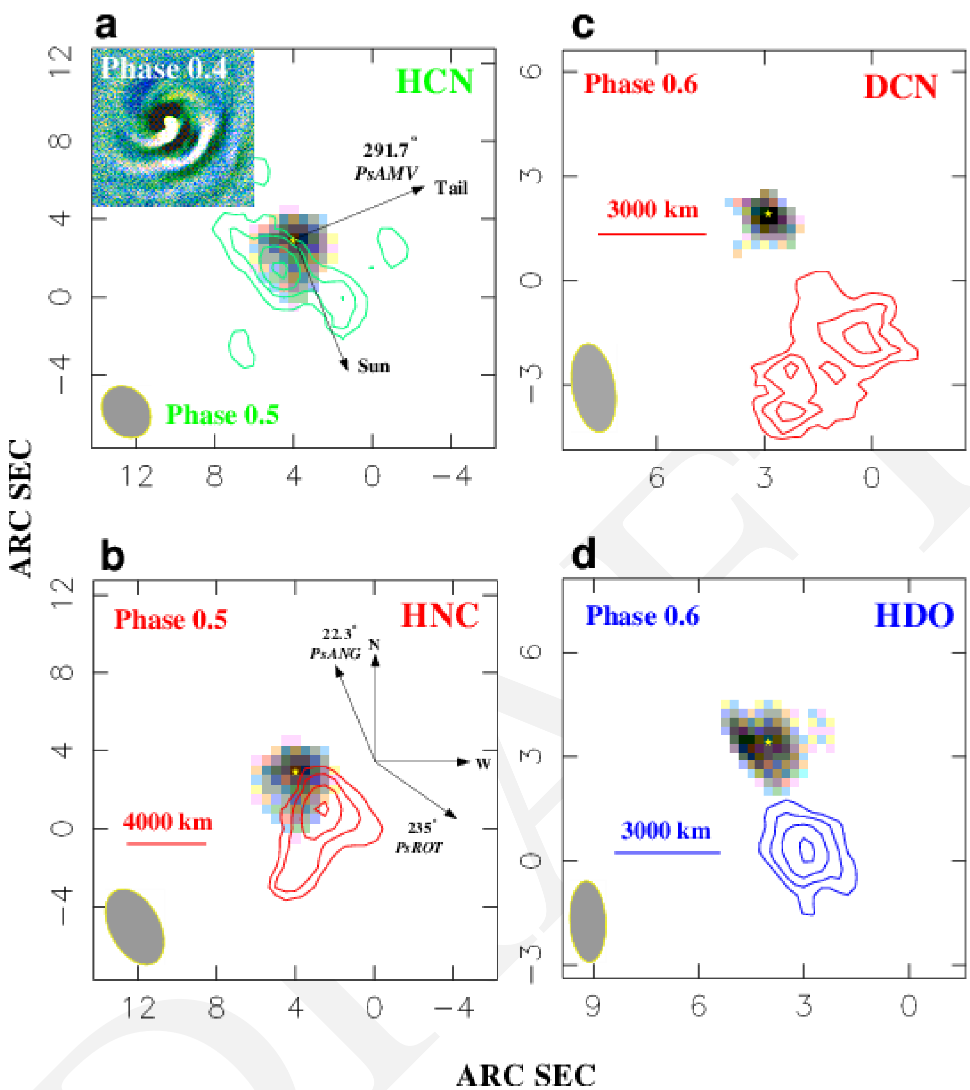

Figure 2. OVRO 3 mm observations of molecular emission from the inner coma of comet Hale-Bopp (Blake et al. 1999). The scattered light optical image (upper left) is dominated by a precessing nuclear dust jet. The star marks the position of the nucleus, and the grey scale presents the continuum emission. Contours in the various panels depict molecular emission from the species listed in the upper right corner. Arrows show the direction of the sun, the cometary rotation axis, and the motion of the comet on the sky. Note that the HCN and DCN emissions were observed on different days but are compared at the same rotational phase.

2017). Observations of two comets (C/2012 S1 (ISON) and C/2012 F6 (Lemmon)) were made using the Atacama Large Millimeter/submillimeter Array (ALMA) at frequencies 339-365 GHz (0.82-0.89 mm) with baselines 15-2700 m, resulting in an angular resolution of approximately 0.5″. Figure 3 shows spectrally-integrated maps for three different molecules (HCN, HNC and H_2CO) in these two comets, and dramatic differences between their spatial distributions are evident.

Modeling of the interferometric visibility amplitudes (*e.g.* Boissier et al. 2007) enables the coma origins of the observed species to be derived. In both ISON and Lemmon, HCN was found to originate from (or very close to) the nucleus, with a spatial distribution largely consistent with spherically-symmetric, uniform outflow. The HNC and H_2CO distributions, on the other hand, were found to be consistent with release as products of coma chemistry — *i.e.* they do not originate directly from the nucleus, but most likely arise from the breakdown of large organic molecules/polymers in the coma. The observed molecular distributions were found to be variable on a timescale of days to minutes (Cordiner et al. 2017). Thus, the importance of 'snapshot' interferometry of cometary comae is demonstrated.

The proposed ngVLA concept will provide important improvements for cometary studies compared with currently available facilities. In particular, the unique centimeter-wave capabilities will open up the possibility of high-resolution OH and NH_3 mapping for the first time. The exceptional *uv* coverage and surface brightness sensitivity of ngVLA will provide an order of magnitude improvement in signal-to-noise for mapping these species compared with existing state-of-the-art interferometers such as the JVLA.

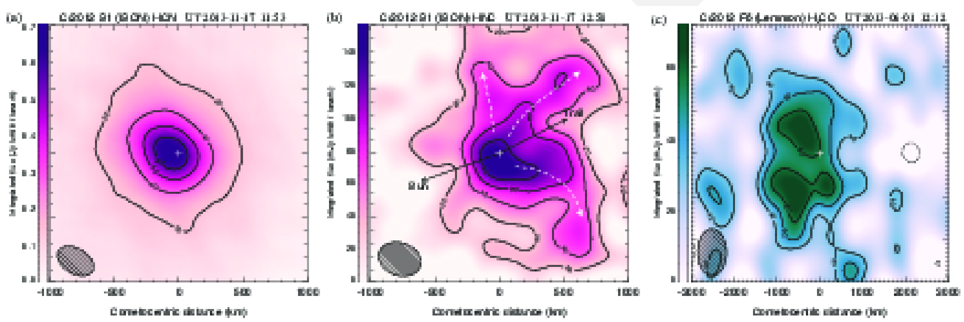

Figure 3. Contour maps of spectrally-integrated molecular line flux observed in comets S1/ISON and F6/Lemmon using ALMA. Contour intervals in each map are 20% of the peak flux (the 20% contour has been omitted from panel (c) for clarity). On panel (b), white dashed arrows indicate HNC streams/jets. The peak position of the (simultaneously observed) 0.9 mm continuum is indicated with a white '+'. See Cordiner et al. (2014) for further details.

3. Measuring the chemical composition of the nucleus

While the chemistry of interstellar clouds and collapsing protostellar envelopes is known from radio and IR spectroscopy (Herbst & van Dishoeck 2009), our knowledge of protoplanetary disk compositions is comparatively sparse (Walsh et al. 2016). Theoretical models show that disk chemistry is very sensitive to the thermal, radiative and dynamical history (Drozdovskaya et al. 2016), which are not well constrained for the protosolar nebula. Understanding the chemical evolution of matter as it passes from interstellar to planetary phases is crucial for theories concerning the accretion and composition of planetary bodies and their atmospheres, but this work is hindered by the extreme difficulty of disk mid-plane ice (and gas) observations. Measurements of cometary compositions provide a unique method for probing the chemistry of the protosolar disk mid-plane, and may be used to test theories regarding the chemical evolution of the early solar system.

To determine the capabilities of the proposed ngVLA concept with regard to cometary composition studies, we generated spectral line flux simulations for a range of commonly-observed coma molecules. These simulations are based on a spherically-symmetric (Haser-type) outflow model in LTE at 75 K, for a typical (moderately bright) comet at 1 au from Earth, with a water production rate $Q(\mathrm{H_2O}) = 2 \times 10^{29}$ s^{-1} and outflow velocity 0.8 km s^{-1}. Assumed abundances (with respect to the dominant volatile H_2O) are based on typically-observed values (Mumma & Charnley 2011). The coma morphology is dominated by a $1/\rho$ brightness distribution (where ρ is the sky-projected distance), and our calculated fluxes are for a nucleus-centered ngVLA beam, tapered to a resolution of 1″.

Results of these calculations are given for the strongest line of each species (in the nominal ngVLA frequency range 1.2-116 GHz) in Table 1; for many species, additional lines will be observable. We have only included molecules for which detections will be readily achievable based on current estimates for the ngVLA sensitivity (with line fluxes $\gtrsim$ 1 mJy per 1″ beam per 1.6 km s^{-1} unit bandwidth), assuming 1 hour on-source. Accurate, instantaneous OH and NH_3 abundance measurements will thus be possible at spectral line sensitivities 50-100 μJy, which are expected to be achievable using ngVLA, but would take weeks of integration with the JVLA. In addition to these fundamental cometary species, other species such as sulphur-bearing molecules and more complex organics may also be detectable, permitting detailed studies of cometary compositions beyond what is possible using currently-available instruments.

Table 1. Calculated fluxes for representative cometary lines using ngVLA concept (1″ beam)

Species	Transition	Frequency (MHz)	Abund. (%)	Flux (mJy)
OH	$J = 3/2, F = 2 - 2$	1667	86	1.7
NH_3	$J_K = 3_3 - 3_{-3}$	23870	1.0	1.0
H_2CO	$J_{K_aK_c} = 1_{01} - 0_{00}$	72838	0.5	1.7
HCN	$J = 1 - 0$	88632	0.2	13.9
HNC	$J = 1 - 0$	90664	0.02	2.7
HC_3N	$J = 10 - 9$	90979	0.02	3.0
CS	$J = 2 - 1$	97981	0.1	7.2
CH_3OH	$J_K = 3_1 - 4_0\, A^+$	107014	2.0	4.9
CH_3CN	$J_K = 6_0 - 5_0$	110383	0.02	1.5
CO	$J = 1 - 0$	115271	5.0	2.3

Flux calculations are based on a Haser parent model for a typical comet at 1 au (see text). For OH, the predicted flux was scaled from the VLA observation of comet Wilson by Palmer et al. (1989), with a representative inversion parameter of 0.4.

4. Revealing the coma structure through high-resolution molecular imaging

Cometary activity occurs as a result of solar radiation that heats the volatile ices in the nucleus as the comet approaches the inner solar system. Despite decades of remote and in-situ studies, the physical outgassing mechanisms and primary drivers of cometary activity remain to be fully understood (Gundlach et al. 2015).

The unique capability of ngVLA to map OH and NH_3 at high spatial resolution (see Section 2), will allow a leap forward in our ability to probe the detailed outgassing behaviour of comets. Hydroxyl (OH) and ammonia (NH_3) are among the most abundant cometary molecules, but their centimeter-wave transitions have never before been mapped in a cometary coma at high ($\sim 1''$) resolution. The spatial distribution of NH_3 in the coma is largely unknown, so detailed mapping is expected to reveal important new insights into the nature of the main reservoir of cometary nitrogen. Ammonia will be detectable in the proposed ngVLA receiver band 4 through its inversion transitions around 23.7-23.9 GHz, whereas OH has strong fine structure transitions around 1.7 GHz. Release of NH_3 from the nucleus may be mapped in active comets within a few astronomical units of Earth, allowing the detailed structure of the inner coma to be measured on scales $\sim 1''$ ($\sim$ 1000 km). This will reveal jets and other outgassing features, similar to those detectable by ALMA in other molecules (Figure 3). By contrast, OH is produced further from the nucleus as a result of H_2O photolysis, and can be used to map the larger-scale coma structure (*e.g.* de Pater et al. 1986). To fully capitalize on the unique sensitivity and mapping capability of ngVLA for comets, the need for long ($\sim$ 100 km) as well as short ($\sim$ 50 m) baselines is emphasized, to allow measurement of the coma structure on (milli-)arcsecond to arcminute scales. Cometary comae tend to be centrally peaked (with a $\sim 1/\rho$ brightness distribution), but can extend to over $100''$, so our science case would also benefit from high-sensitivity, simultaneous single-dish observations to fill in lost flux from the largest coma scales.

Resolved spectral line profiles for the observed gases (at ~ 0.1 km s^{-1} resolution) will reveal the detailed coma kinematics, and the gas temperatures may be obtained by measuring multiple NH_3 lines from the different fine structure levels of this molecule. This will enable new tests for our understanding of coma physics.

5. Resolving the nucleus using long-baseline interferometry

Cometary nuclei are among the most difficult objects of the solar system to detect and characterize (Lamy et al. 2004). Rendezvous missions such as Giotto, Deep Impact and Rosetta have provided our only close-up views of a handful cometary nuclei, revealing diverse morphologies and surface properties that provide information on their origins as well as thermal and collisional histories. Direct imaging of cometary nuclei using traditional ground-based observing strategies is extremely difficult due to their faintness and small sizes (typically $\lesssim$ 10 km, or 14 mas at 1 au). In addition, dust emission (and reflected sunlight) tends to swamp the weak signal from the nucleus in the optical and infrared. Although thermal emission from large dust grains in the coma contributes significantly to the cometary continuum signal in the centimeter and millimeter bands, the much broader extent of the coma dust emission allows it to be identified and separated from the compact nucleus contribution.

Detections of nucleus thermal emission have previously been possible only in the case of rare, extremely favourable cometary apparitions (*e.g.* Boissier et al. 2014). The ngVLA will provide, for the first time, the ability to routinely observe the nuclei of comets and other near-Earth objects. Assuming an albedo of 0.05, the (black body) continuum flux from a 5 km-diameter comet within 0.5 au of Earth will be easily detectable at around 0.4 mJy. Observed with ngVLA at an angular resolution of 2 mas at 115 GHz (assuming 300 km baselines), the nucleus of such a comet would be well-resolved (with 7 resolution elements across), allowing accurate size and shape measurements.

6. Conclusion

Due to their relatively low surface brightness, cometary comae are extremely challenging to image at radio wavelengths. Only since the advent of ALMA has spectral mapping of moderately bright comets become routine, resulting in a paradigm shift in our understanding of the chemistry and physics of the molecular coma. However, the limited frequency coverage of ALMA prohibits the study of fundamental cometary molecules such as OH and NH_3, which will be uniquely accessible for high resolution mapping by ngVLA. Furthermore, in this article we have demonstrated the possible power of ngVLA for detecting and mapping a range of key coma species in the 1.2-116 GHz range, as well as the possibility of detecting dust, and thermal emission from the nucleus itself. Interferometry of comets with sub-millijansky sensitivity for narrow lines in the centimeter-millimeter spectral region will enable new insights into the composition of the nucleus, and consequently, the early history of our Solar System.

Acknowledgments. This work was supported by the National Science Foundation under Grant No. AST-1614471.

References

Alexander, C. M., McKeegan, K. D., Altwegg, K. 2018, Space Sci. Rev. 214, 36
Biver, N., Bockelée-Morvan, D., Crovisier, J. et al. 1999, AJ, 118, 1850
Blake, G. A., Qi, C., Hogerheijde, M. R., Gurwell, M. A., Muhleman, D. O. 1999, Nature, 398, 213
Bockelée-Morvan, D., Crovisier, J., Erard, S. et al. 2016, MNRAS, 426, 170
Boissier, J., Bockelée-Morvan, D., Biver, N. et al. 2007, A&A, 475, 1131
Boissier, J., Bockelée-Morvan, D., Biver, N. et al. 2014, Icarus, 228, 197
Cordiner, M. A., Remijan, A. J., Boissier, J. et al. 2014, ApJ, 792, L2
Cordiner, M. A.; Boissier, J.; Charnley, S. B. et al. 2017, ApJ, 838, 147
Cottin, H., Fray, N. 2008, Space Sci. Rev. 138, 179
Crovisier, J., Bockelée-Morvan, D., Colom, P. et al. 2004, A&A, 418, 1141
de Pater, I., Palmer, P., Snyder, L. E. 1986, ApJ, 304, 33
Drozdovskaya, M. N., Walsh, C., van Dishoeck, E. F. et al. 2016, MNRAS, 462, 977
Ehrenfreund, P., Charnley, S. B. 2000, ARA&A, 38, 427
Gundlach, B., Blum, J., Keller, H. U., Skorov, Y. V. 2015, A&A, 583, 12
Haser, L. 1957, Bulletin de la Societe Royale des Sciences de Liege, 43, 740
Herbst, E. & van Dishoeck, E. 2009, ARA&A, 47, 427
Lamy, P. L., Toth, I., Fernandez, Y. R., Weaver, H. A. 2004, Comets II, Eds. M. C. Festou, H. U. Keller, and H. A. Weaver, University of Arizona Press, Tucson, 223
Lis, D. C., Bockelée-Morvan, D., Boissier, J. et al. 2008, ApJ, 675, 931
Milam, S. N., Remijan, A. J., Womack, M. et al. 2006, ApJ, 649, 1169
Mumma, M. J., Charnley, S. B. 2011, ARA&A, 49, 471
Palmer, P., de Pater, I., Snyder, L. E. 1989, AJ, 97, 1791
Qi, C., Hogerheijde, M. R., Jewitt, D., Gurwell, M. A., Wilner, D. J., ApJ, 799, 110

Snyder, L., Palmer, P., de Pater, I. 1990, Icarus, 86, 289
Walsh, C., Loomis, R. A., Öberg, K. I. et al. 2016, ApJ, 823, L10

Science with a Next-Generation Very Large Array
ASP Conference Series, Monograph 7
Eric J. Murphy, ed.

DRAFT EDITION

Spacecraft Telecommunications

T. Joseph W. Lazio[1] and Sami Asmar[1]
[1]*Jet Propulsion Laboratory, California Institute of Technology, Pasadena, CA, USA;* `Joseph.Lazio@jpl.nasa.gov`

Abstract. There is a long history of radio telescopes being used to augment the radio antennas regularly used to conduct telemetry, tracking, and command of deep space spacecraft. Radio telescopes are particularly valuable during short-duration mission critical events, such as planetary landings, or when a mission lifetime itself is short, such as a probe into a giant planet's atmosphere. By virtue of its high sensitivity and frequency coverage, the next-generation Very Large Array would be a powerful addition to regular spacecraft ground systems. Further, the science focus of many of these deep-space missions provides a "ground truth" in the solar system that complements other aspects of the ngVLA's science case, such as the formation of planets in proto-planetary disks.

1. Introduction

In addition to the multitude of astronomical applications described elsewhere in this volume, the next generation Very Large Array (ngVLA) could provide valuable benefits in other fields such as the telecommunications with robotic spacecraft on scientific missions throughout the Solar System. There have been many cases of radio astronomical telescopes participating in and enabling planetary missions by augmenting the receiving capabilities of traditional spacecraft tracking facilities, with notable examples including the VLA's participation in Voyager 2's flyby of the planet Neptune (Figure 1, Layland & Brown 1985) and the use of the Green Bank Telescope to track the descent of the Huygens probe to the surface of Titan and enabling the Doppler Wind Experiment (Folkner et al. 2006). The sensitivity and frequency coverage of the ngVLA has the potential to exceed considerably that of any existing or planned dedicated spacecraft radio tracking facility. This contribution is focused on the relevance of the ngVLA for potential NASA missions, but, with the increasing number of space agencies conducting deep space missions,[1] the ngVLA could be of benefit to many space agencies for increasing the science return from their space missions.

[1] In addition to NASA, the European Space Agency (ESA), the Japanese Aerospace Exploration Agency (JAXA), the Indian Space Research Organization (ISRO), and the Roscosmos State Corporation for Space Activities (Roscosmos) send robotic spacecraft into deep space, and potentially Korean and United Arab Emirates will do so in the future.

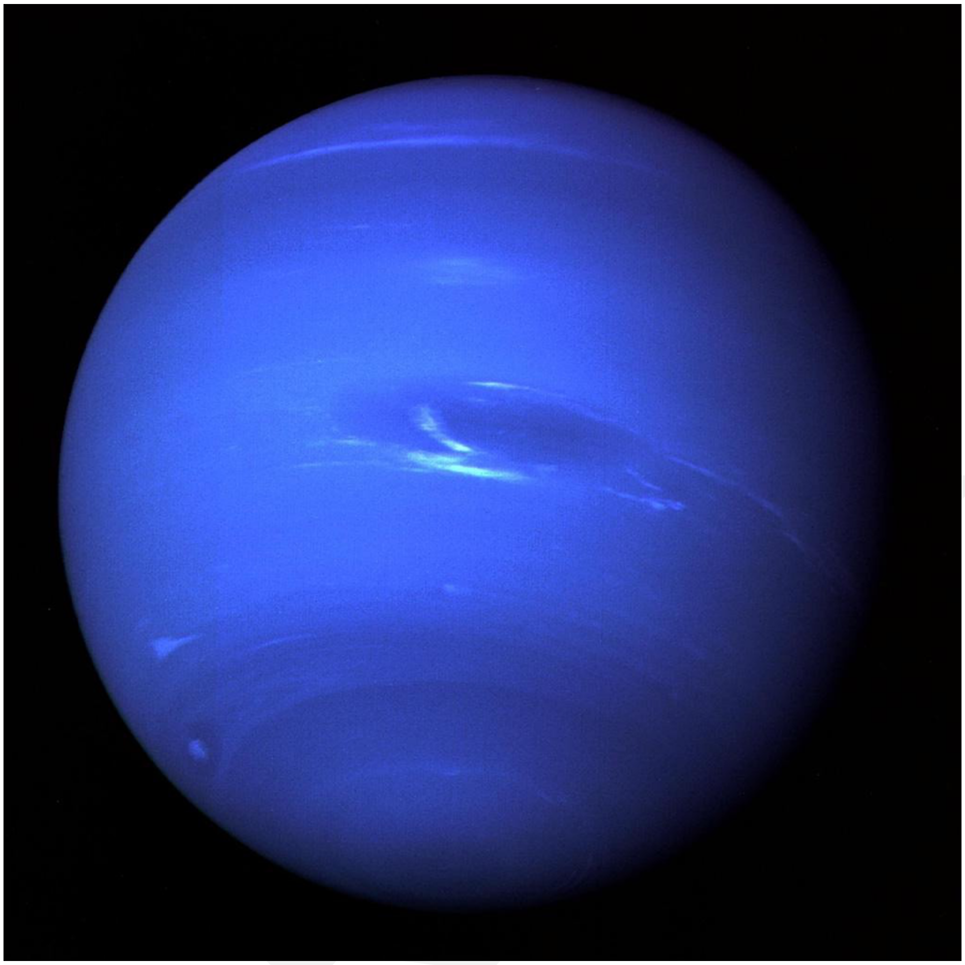

Figure 1. Neptune as viewed by Voyager 2 during its encounter in 1989. This image is a combination of images acquired with the green and orange filters from the narrow angle camera, acquired on 1989 August 20, just under five days from closest approach. Clearly visible is the Great Dark Spot. These images were likely downloaded via a combination of telemetry downlinks from the Very Large Array (VLA) and NASA's Deep Space Network. In a similar manner, the ngVLA could enable future mission critical events by robotic spacecraft throughout the solar system.

2. Scientific Context

Historically, NASA's most demanding application for highly sensitive ground receiving stations has been planetary science missions, in which spacecraft have been sent to other bodies in the solar system, often at distances of multiple astronomical units from the Earth. Increasingly, however, heliophysics and astrophysics missions have begun to demand similarly sensitive ground receiving stations. For instance, the Solar TErrestrial RElations Observatory (STEREO) mission has two spacecraft, one in an Earth-leading orbit and one in an Earth-trailing orbit, that are approximately 1 au distant[2] and the Parker Solar Probe[3] will dip to within a few solar radii of the Sun (i.e., travel to approximately 1 au from the Earth). In order to reduce interference from the Earth and operate in a stable environment, many astrophysics missions (e.g., Planck, *Spitzer* Space Telescope, *Kepler*, *James Webb Space Telescope*) are being launched into orbits such as Earth-trailing orbits or Earth-Sun Lagrange 2 point halo orbits.

In this landscape, the ngVLA would complement NASA and ESA's network of deep space antennas by providing additional sensitivity for short-duration, high priority events. NASA's Deep Space Network (DSN) is a network of 34 m and 70 m diameter antennas at three longitudes around the world that provides routine collection of telemetry data (a.k.a. "downlink") from spacecraft beyond geosynchronous orbit; ESA has three 35 m antennas at similar longitudes with similar functionality. However, it is standard practice to consider augmenting these antennas during mission critical events, such as the entry, descent, and landing of a spacecraft on another planet. Such augmentation provides resiliency for the mission; for instance, for the Doppler wind experiment on the Huygens probe to Titan, the receiver on-board the *Cassini* spacecraft was not configured correctly and only the data from Earth-based radio telescopes assured the success of that experiment (Folkner et al. 2006). In addition, with its higher sensitivity, the ngVLA may enable the collection of additional data.

Table 1 compares the relative performance of the current DSN antennas (DSN 810-005 Modules 101, 104) with that potentially achievable with a fraction of the ngVLA, using the antenna gain at two standard deep space communications bands, X band (receiving at 8.24 GHz) and Ka band (receiving at 32 GHz); a 34 m antenna operating at X band is taken to be the reference. For the ngVLA, only the Core Array (Carilli 2018), consisting of 94 antennas of 18 m diameter, is considered; the antennas are assumed to have an efficiency of 65%. While the actual performance of the ngVLA may differ from that shown in Table 1, it is clear that even a fraction of the full ngVLA offers substantial improvements. All other things being equal, the relative performance of Table 1 is equivalent to the signal-to-noise ratio achieved on the downlink signal, as the DSN antennas have system temperatures of approximately 20 K and we assume similar values for the ngVLA antennas. In turn, signal-to-noise ratio translates approximately linearly to downlink data rate; alternately, the higher sensitivity can be considered additional margin against unexpected events. We now discuss a few examples of mission concepts that could benefit from having extremely high sensitivity ground receiving stations.

The *Visions and Voyages for Planetary Science in the Decade 2013–2022* Decadal Survey describes two New Frontier[4] mission concepts that would necessarily be short-lived. The Saturn Probe concept would deploy a probe into Saturn's atmosphere to measure its structure and composition. While the materials used to construct such a probe may have improved since the construction of the Galileo probe (Young et al. 1996, and references within), the Saturn probe would suffer the same eventual fate, crushed under the rising pressures as it descends. The Venus In Situ Explorer concept would land on the surface of Venus in order to sample the composition of the crust.

[2]At the time of writing, the STEREO-B spacecraft is not operational.

[3]At the time of writing, scheduled for launch in 2018 August.

[4]NASA's medium-class missions, with a cost cap of approximately $1 billion.

Table 1. DSN and ngVLA Receiving Antenna Relative Performance

System	**Relative Performance** X band	Ka band
DSN 34 m	1.0	11.7
DSN 70 m	4.3	...
DSN 4 × 34 m	3.7	46.8
ngVLA Core Array (94 antennas, 18 m diameter)	17.1	248

Again, while material properties and thermal control systems have improved since the construction Soviet Venera landers, the surface of Venus is such a harsh environment that a lander will have a necessarily finite lifetime.

The *Ice Giants Pre-Decadal Survey Mission Study Report* considers flagship-class mission concepts to Uranus, Neptune, or both. Four mission architectures were studied in detail, with three of the four including an atmospheric probe. (Two architectures involved an atmospheric probe for Uranus, one for Neptune.) The expected lifetime of such a probe in the atmosphere of either planet is approximately 1 hr.

During the last perihelion passage of Comet 1/P Halley, a figurative armada of spacecraft were sent to conduct close fly-bys of its nucleus. Because of the high relative velocities between the Earth and a long-period comet such as Halley, the durations of the fly-bys were short. Inspired by both the success of the spacecraft that flew by Halley and the recent discovery of the first interstellar object (1I/2017 U1 'Oumuamua, Meech et al. 2017), there is active consideration of what kind of mission concept or concepts might be possible to enable a similar encounter. While the relative velocities could be even higher than in the case of the Halley encounters, the potential science return from a close encounter with an interstellar object would likely be significant.

These mission concepts are intended to be illustrative only, and specific instruments have not been selected. Nonetheless, the higher data rates enabled by the use of the ngVLA could enable more capable instruments (e.g., higher resolution mass spectrometers). Further, these example mission concepts are certainly not an exhaustive list of all possible short-lived mission concepts, but they illustrate how high-priority missions might nonetheless be short-lived and benefit greatly from additional sensitivity such as could be provided by the ngVLA.

An additional benefit of the ngVLA may be for use during spacecraft emergencies. It is standard practice to include low-gain antennas on deep space spacecraft for the purposes of enabling communications even if the spacecraft's attitude is unknown or uncontrolled. Low-gain antennas have the obvious benefit of a wide field of view at the cost of sensitivity. The received signal from a spacecraft in "safe mode" would most likely be (much) weaker than planned from its high-gain antenna, for which the ngVLA's high sensitivity could be of benefit in capturing engineering data and understanding the problem with the spacecraft.

3. Design Considerations

The primary requirement for the ngVLA to receive spacecraft telemetry is for it to have frequency coverage of the allocated space-to-Earth downlink bands (Table 2). The relevance of the ngVLA is immediately obvious, as its planned frequency coverage encompasses all of the frequency allocations.

Table 2. Frequency Bands for Deep-Space Spacecraft Telemetry

Name	**Telemetry (Downlink)** (space-Earth) (GHz)
S band	2.29–2.30
X band	8.40–8.45
Ka band	31.8–32.3

Two additional bands warrant comment. There is a space-to-Earth allocation in the K band (25.5 GHz–27.0 GHz). This band is allocated for spacecraft with orbits that take them no farther than 2×10^6 km from Earth. This distance includes the Earth-Sun L2 point, which is used increasingly by astrophysics missions such as the *James Webb Space Telescope*. While such missions would also benefit from high sensitivity, they have regular telemetry requirements, which are more likely to be met by NASA's DSN (or ESA's Deep Space Antennas). However, should such a spacecraft enter "safe mode," the ngVLA could assist with the recovery of the spacecraft.

There is also an allocation in the ultra-high frequency (UHF) portion of the radio spectrum used for spacecraft-to-spacecraft communications ("proximity links"). This band is not within the ngVLA's frequency coverage, and the SKA1-Mid or a similar facility would be more appropriate.

Like pulsars, spacecraft are point sources, and full field interferometric synthesis is not required. Beamforming suffices. In general, the requirements for pulsar beam-formed observations would be sufficient for spacecraft telemetry reception, with the added benefit that spacecraft signals are typically quite narrow band relative to astronomical sources. A specific concern with the legacy VLA for both pulsar observations and spacecraft telemetry was the "waveguide switch cycle," which resulted in a 1.5 ms data gap every 50 ms (Deutsch 1982; Hankins 1999); modern digital electronics and fiber optic transmission should obviate this particular concern.

4. Conclusion

In conclusion, the ngVLA would be well suited for occasional use of high priority space missions, particularly those with intrinsically short lifetimes. Not only can these missions be considerable investments by a space agencies (with costs in excess of $1 billion), the science motivations for them often complement the larger ngVLA science case. Most notably, the planets in our solar system form the end states of the protoplanetary disks that the ngVLA will image and only by studying both will we understand planet formation and evolution.

Acknowledgments. We thank D. Jones, L. Deutsch, and R. Preston for helpful discussions and guidance on this topic. Some of the information presented is pre-decisional and is intended for informational purposes only. Part of this work was carried out at the Jet Propulsion Laboratory, California Institute of Technology, under contract with the National Aeronautics and Space Administration.

References

Carilli, C. L. 2018, “Next Generation Very Large Array Memo No. 47: Resolution and Sensitivity of ngvla-revB,” `http://library.nrao.edu/public/memos/ngvla/NGVLA_47.pdf`

Deutsch, L. J. 1982, “The Performance of VLA as a Telemetry Receiver for Voyager Planetary Encounters,” Telecommunications and Data Acquisition Prog. Report, TDA PR 42-71, 1982 July–September (Jet Propulsion Laboratory, California Institute of Technology: Pasadena, CA) pp. 27–39

Deep Space Network Telecommunications Link Design Handbook, DSN No. 810-005, Module 104, Rev. J, 2018 January 12, JPL D-19379 (Jet Propulsion Laboratory, California Institute of Technology: Pasadena, CA) `https://deepspace.jpl.nasa.gov/dsndocs/810-005/`

Deep Space Network Telecommunications Link Design Handbook, DSN No. 810-005, Module 101, Rev. F, 2015 August 5, JPL D-19379 (Jet Propulsion Laboratory, California Institute of Technology: Pasadena, CA) `https://deepspace.jpl.nasa.gov/dsndocs/810-005/`

Folkner, W. M., Asmar, S. W. Border, J. S., Franklin, G. W., Finley, S. G., Gorelik, J., Johnston, D. V., Kerzhanovich, V. V., Lowe, S. T., Preston, R. A., Bird, M. K., Dutta-Roy, R., Allison, M., Atkinson, D. H., Edenhofer, P., Plettemeier, D., & Tyler, G. L. 2006, “Winds on Titan from ground-based tracking of the Huygens probe,” J. Geophys. Res., 111, E07S02; doi: 10.1029/2005JE002649

Hankins, T. H. 1999, “Pulsar Observing at the VLA,” in *Synthesis Imaging in Radio Astronomy II, A Collection of Lectures from the Sixth NRAO/NMIMT Synthesis Imaging Summer School*, eds. G. B. Taylor, C. L. Carilli, & R. A. Perley, Astronomical Society of the Pacific Conference Series, Vol. 180 (Astronomical Society of the Pacific: San Francisco, CA) p. 613

Ice Giants Pre-Decadal Study Final Report, Solar System Exploration Directorate, Jet Propulsion Laboratory for Planetary Science Division, Science Mission Directorate, National Aeronautices and Space Administration, June 2017, JPL D-100520

Layland, J. W., & Brown, D. W. 1985, “Planning for VLA/DSN Arrayed Support to the Voyager at Neptune,” Telecommunications and Data Acquisition Report 42-82, Jet Propulsion Laboratory, California Institute of Technology

Meech, K. J., Weryk, R., Micheli, M., et al. 2017, “A brief visit from a red and extremely elongated interstellar asteroid,” Nature, 552, 378; doi: 10.1038/nature25020

Vision and Voyages for Planetary Science in the Decade 2013–2022, Committee on the Planetary Science Decadal Survey, National Research Council (National Academies Press: Washington, DC) ISBN: 0-309-20955-2

Young, R. E., Smith, M. A., & Sobeck, C. K. 1996, “Galileo Probe: In situ Observations of Jupiter’s Atmosphere,” Science, 272, 837; doi: 10.1126/science.272.5263.837

Part III

Planet Formation:

Science with a Next-Generation Very Large Array
ASP Conference Series, Monograph 7
Eric J. Murphy, ed.

DRAFT EDITION

Resolved Substructures in Protoplanetary Disks with the ngVLA

Sean M. Andrews, David J. Wilner,

Harvard-Smithsonian Center for Astrophysics, Cambridge, MA, USA 02138; `sandrews@cfa.harvard.edu` , `dwilner@cfa.harvard.edu`

Enrique Macías,

Department of Astronomy, Boston University, Boston, MA, USA 02215; `emacias@bu.edu`

Carlos Carrasco-González,

Instituto de Radioastronomía y Astrofísica (IRyA-UNAM), 58089, Morelia, México; `c.carrasco@irya.unam.mx`

and Andrea Isella

Department of Physics and Astronomy, Rice University, Houston, TX, USA 77005; `isella@rice.edu`

1. Introduction

In the "core accretion" paradigm for planet formation, terrestrial planets and giant planet cores are created by the sequential collisional agglomeration of solids over ~20 orders of magnitude in size within a few million years (e.g., Pollack et al. 1996; Raymond et al. 2014). Early in that process, the standard theoretical assumptions introduce two fundamental obstacles to that growth. The first is related to the migration of "pebbles" (~mm/cm-sized particles): as these solids decouple from the gas disk, they migrate faster than they can collide and grow (Takeuchi & Lin 2002; Brauer et al. 2007). The second is that the timescales for assembling (~km-scale) "planetesimals" is too long, given the migration and destructive impacts of their precursors (e.g., Johansen et al. 2014). The potential solution to both issues is to locally concentrate pebbles in the disk (Whipple 1972; Pinilla et al. 2012), halting their migration and slowing their relative velocities to promote rapid growth (e.g., Chiang & Youdin 2010). The requirement to facilitate such concentrations is a gas pressure profile that is not smooth or monotonic, but rather has local maxima induced by abrupt variations in disk properties (e.g., Dzyurkevich et al. 2010; Stammler et al. 2017), dynamical effects (e.g., Baruteau et al. 2014), or fluid instabilities (e.g., Zhu et al. 2014; Flock et al. 2015).

The optimal way to directly test this hypothesis is to search for and characterize local concentrations of pebbles in protoplanetary disks. These particles emit a thermal continuum at wavelengths roughly comparable to their sizes (i.e., radio to microwave frequencies, ~10–1000 GHz); the detailed spatial distribution of this continuum emission in nearby disks can be resolved with an interferometer. If the optical depth of this emission is low, the spectrum provides constraints on the temperatures, densities, and size distribution of the constituent solids in any accessible disk region. Variations in

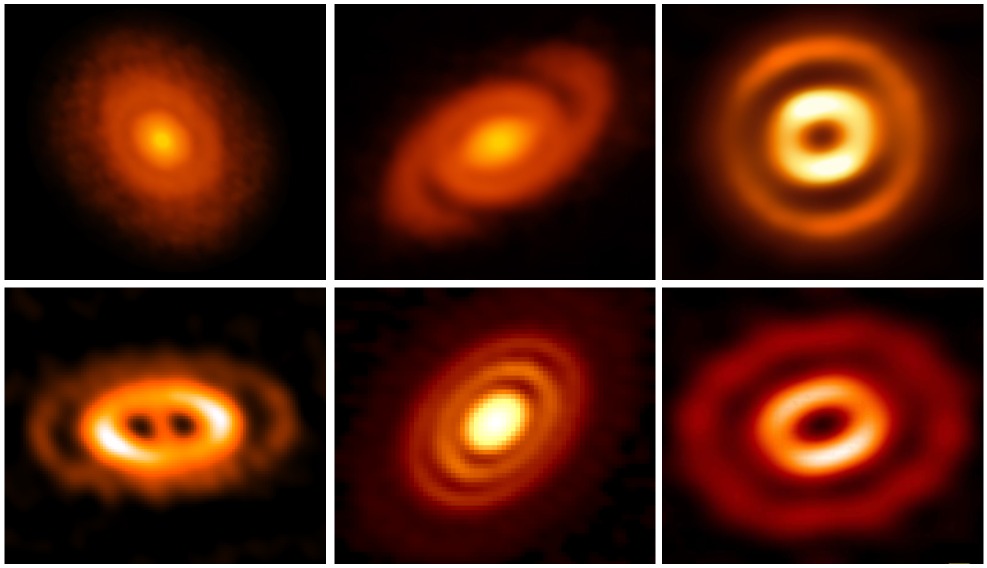

Figure 1. Examples of substructures in the ~1 mm continuum emission from nearby protoplanetary disks at scales of ~10–20 au, from the ALMA interferometer. Clockwise from top left: the V883 Ori (Cieza et al. 2016), Elias 27 (Pérez et al. 2016), HD 169142 (Fedele et al. 2017), HD 97804 (van der Plas et al. 2017), HD 163296 (Isella et al. 2016), and AA Tau (Loomis et al. 2017) disks.

the particle concentrations on small spatial scales would be manifested as *substructures* in the microwave continuum surface brightness morphology. The properties of those substructures provide crucial information on the mechanisms that create them and their potential for driving rapid, localized planetesimal formation.

In the past few years, the ALMA interferometer has found that such substructures on scales of $\lesssim$10–20 au (70–150 mas) are common, and perhaps ubiquitous (e.g., Zhang et al. 2016). Usually they are manifested as concentric bands or narrow rings of emission separated by pronounced depletions, or “gaps" (Isella et al. 2016; Cieza et al. 2016, 2017; Loomis et al. 2017; van der Plas et al. 2017; Cox et al. 2017; Fedele et al. 2017, 2018; Dipierro et al. 2018), although at least one disk has a spiral emission pattern (Pérez et al. 2016). Figure 1 shows a gallery of representative ALMA continuum images of disk substructures. In the two specific cases of the HL Tau and TW Hya disks, ALMA data reveal ring+gap features at even finer scales, down to (and presumably beyond) the ~20 mas (3 and 1 au, respectively) resolution limit of the longest ALMA baseline configuration (ALMA Partnership et al. 2015; Andrews et al. 2016).

2. The Role of the ngVLA

While these ALMA discoveries have rightly ushered in a major shift in the field, they also reveal two crucial, but subtle, problems related to the interpretation of disk substructures. First, the emission substructures that have so far been observed at very high resolution appear to be largely optically thick at frequencies higher than ~200 GHz. And second, the ring or gap features often remain unresolved (or nearly so) even for

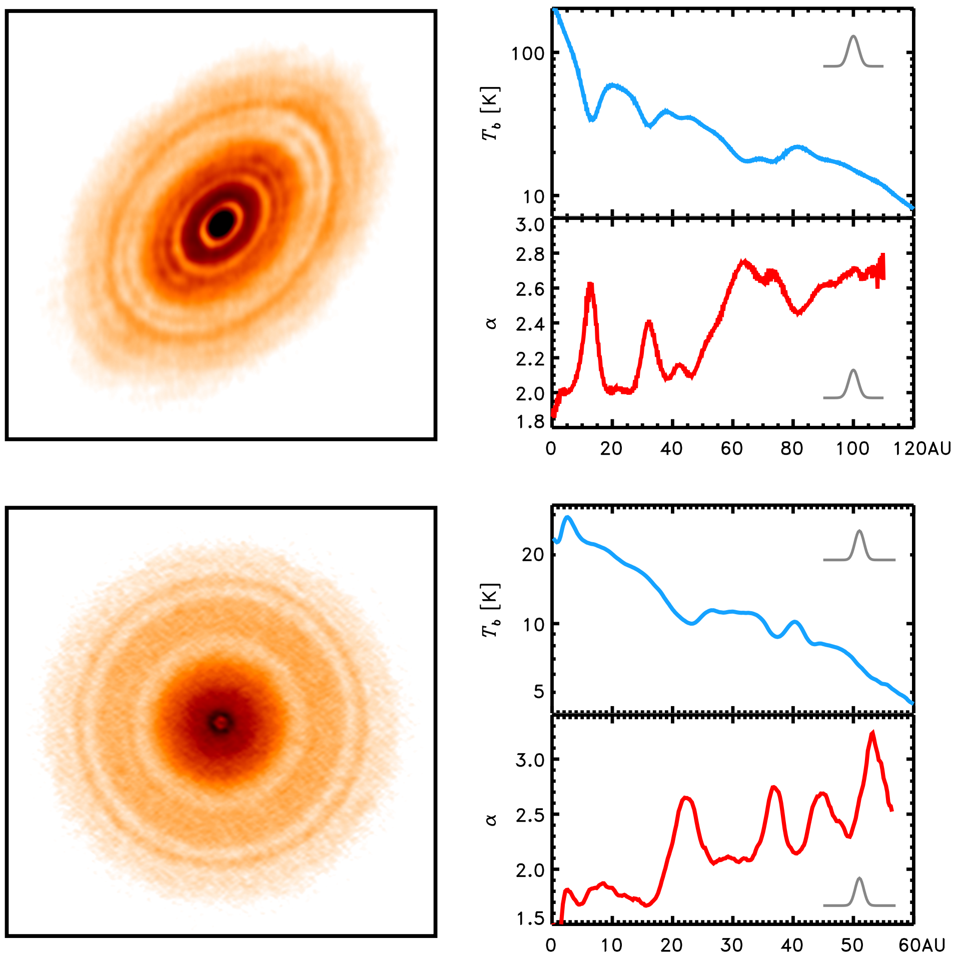

Figure 2. A more detailed look at ALMA observations of the HL Tau (*top*) and TW Hya (*bottom*) disks, based on the analyses of ALMA Partnership et al. (2015) and Huang et al. (2018). The left panels show 290 GHz continuum images. The right panels feature the azimuthally-average radial T_b (*top*) and α (340–230 GHz) profiles. The corresponding beam profiles are shown in gray. Local T_b depletions are accompanied by α enhancements. The high T_b values and low α values in the emission bands / rings are suggestive of high optical depths at these frequencies.

the longest ALMA baselines (scales $\lesssim$20 mas). Both of these issues are illustrated in Figure 2, which shows synthesized images along with azimuthally-averaged brightness temperature (T_b) and spectral index (α) profiles for the HL Tau (*top*) and TW Hya (*bottom*) disks for the continuum emission around 290 GHz (ALMA Partnership et al. 2015; Huang et al. 2018; see also Tsukagoshi et al. 2016). Note that the scales of the substructures are comparable to the resolutions in the T_b profiles, and also that the T_b values are similar to the expected dust temperatures at the locations where the spectral indices are near the Rayleigh-Jeans value, as would be expected for high optical depths ($\alpha \approx 2$). If this behavior ends up being common in the broader disk population, then high frequency continuum measurements will only be able to offer relatively weak lim-

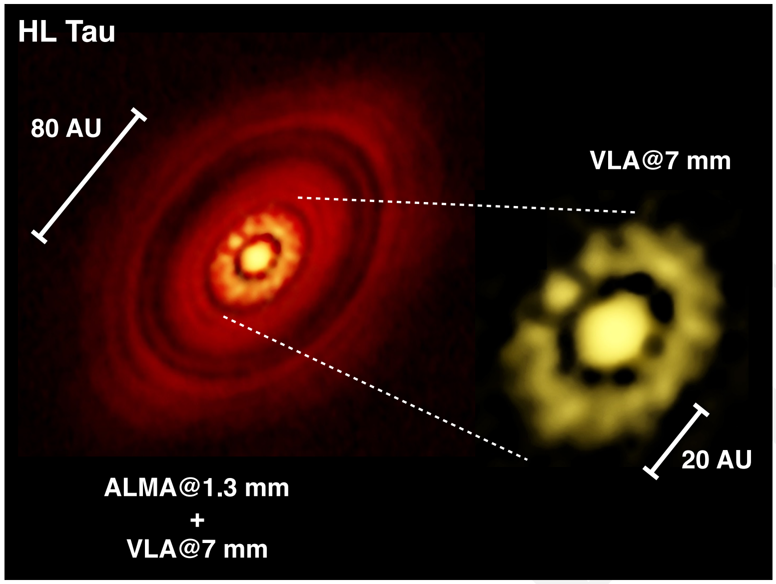

Figure 3. A comparison of the ALMA 230 GHz (*left*; ALMA Partnership et al. 2015) and VLA 43 GHz (*right*; Carrasco-González et al. 2016) continuum images for the HL Tau disk. At the lower frequency of the VLA data, the emission preferentially tracers structures in the inner disk but the observations are very expensive and only possible for the very brightest targets (and are still limited in resolution). The ngVLA will make substantially improved measurements for a large population of disks routine. (*credit: C. Carrasco-Gonzalez / Bill Saxton / NRAO / AUI / NSF*)

its on the densities and particle size distributions in these substructures. Moreover, all but the strongest features in the innermost disk ($\lesssim$10 au) will be inaccessible at ALMA frequencies, due to both very high optical depths and limited angular resolution.

The solution to these potential problems is to instead probe these continuum substructures at lower frequencies ($\lesssim$100 GHz), where the optical depths are correspondingly lower (a linear frequency scaling for the optical depth, $\tau_\nu \propto \nu$, is reasonable; e.g., see Ricci et al. 2010). The current VLA is too limited in sensitivity and angular resolution to optimally perform in this area, but nevertheless has produced some early results that demonstrate feasibility for the brightest available targets (e.g., Isella et al. 2014; Marino et al. 2015; Macías et al. 2016, 2017). Figure 3 illustrates perhaps the best example, for the HL Tau disk (Carrasco-González et al. 2016). Perhaps the most compelling result from these forays are the hints of substructure asymmetries that are not visible at higher frequencies due to their high optical depths.

Real progress in this line of inquiry into planetesimal formation will require the sensitivity and resolution capabilities only available with the proposed ngVLA facility. The ideal tracer of the solids concentrated in protoplanetary disk substructures is the 30–100 GHz continuum, which strikes the best balance in sensitivity (emission still bright), optical depth (low enough to reliably estimate densities), and angular resolution (high enough to resolve fine-scale features at disk radii as small as $\sim$1 au). A modest survey could be used to understand the underlying physical mechanisms that control the prevalence, forms, scales, amplitudes, spacings, and symmetry of disk substructures and their presumably crucial roles in the planet formation process.

3. Benchmarks for Measuring Disk Substructures

The experiment design principle most relevant for probing disk substructures is ultimately related to the feasibility of detecting a microwave continuum brightness temperature contrast for a given perturbation in the local surface density of solids (or, more precisely, the associated optical depth). There is a bewildering array of potential *forms* for such perturbations – ranging from simple rings and gaps, to spirals, to azimuthally asymmetric features like vortices, and perhaps even stochastically-distributed pockets of material – depending on the various physical mechanism(s) responsible for modifying the gas pressure gradient. Aside from theoretical ideas and the preliminary work being done with ALMA, we simply do not yet know the diversity of these forms in the general disk population. So, to simplify a discussion of the tractability of studying these features, specifying the morphology is less important than the locations, spatial scales, and amplitudes of the associated particle concentrations.

The baseline temperatures T_d and optical depths τ_ν, and thereby brightness temperatures $T_b(\nu)$, should typically be higher in the inner disk (closer to the host star). As some fiducial reference points to illustrate feasibility, we consider hypothetical substructures at radii of 5 and 40 au in a disk model orbiting a $\sim 1\,M_\odot$ host star at an age of 1 Myr (with a corresponding $L_* \approx 2\,L_\odot$). We assume that the baseline 230 GHz continuum optical depths are 10 and 1 at these locations, based roughly on models of the HL Tau and TW Hya ALMA studies referenced in the previous section, and that the optical depth spectra vary like $\tau_\nu \propto \nu^\beta$ with $\beta \approx 1$. Given a simple model of the stellar irradiation, we expect temperatures of $T_d \approx 75$ and 25 K at 5 and 40 au, respectively. These basic properties also set the expected scale of local perturbations, thought to be tied to the gas pressure scale height $H_p = c_s/\Omega$, the ratio of the sound speed to the Keplerian orbital frequency. At 5 and 40 au in this reference model, $H_p \approx 0.3$ and 2.5 au (i.e., the aspect ratio is $H_p/r \approx 0.06$). Presuming a Gaussian perturbation and a typical distance for nearby protoplanetary disks of 140 pc, we will consider substructures with FWHM sizes of $3H_p$ at 5 au ($\sim$10 mas), and $\sim H_p$ at 40 au ($\sim$40 mas), respectively.

With these assumptions and some measured or expected sensitivity and resolution metrics, we can then calculate the minimum detectable (at a given signal-to-noise ratio, SNR) fractional optical depth perturbation for a given integration time ($t_{\rm int}$). Presuming the local particle opacity does not also change (which is not necessarily the case), there is a one-to-one correspondance between optical depth and surface density perturbations. Because the base optical depths at these locations and frequencies span around unity, there is some nuance in the meaning of 'fractional optical depth perturbation' depending on whether we are considering an enhancement, $\tau'_\nu = \tau_\nu(1 + \Delta\tau_\nu)$, or a depletion, $\tau'_\nu = \tau_\nu(1 - \Delta\tau_\nu)$: we will illustrate both scenarios for clarity. However, in either case, we can quantify the sensitivity by first calculating a generic

$$\mathrm{SNR}_\nu = \frac{1}{\sigma_\nu} \left(\frac{t_{\rm int}}{2}\right)^{1/2} \left| T_d\,(1 - e^{-\tau_\nu}) - T_d\,(1 - e^{-\tau'_\nu}) \right|, \tag{1}$$

where σ_ν is the RMS noise level for a given beam area (in T_b units), as a function of $\Delta\tau_\nu$ and t. From that, we can then identify the smallest fractional optical depth contrast (i.e., the minimum $\Delta\tau_\nu$) that could be detected with a specific SNR threshold for a given

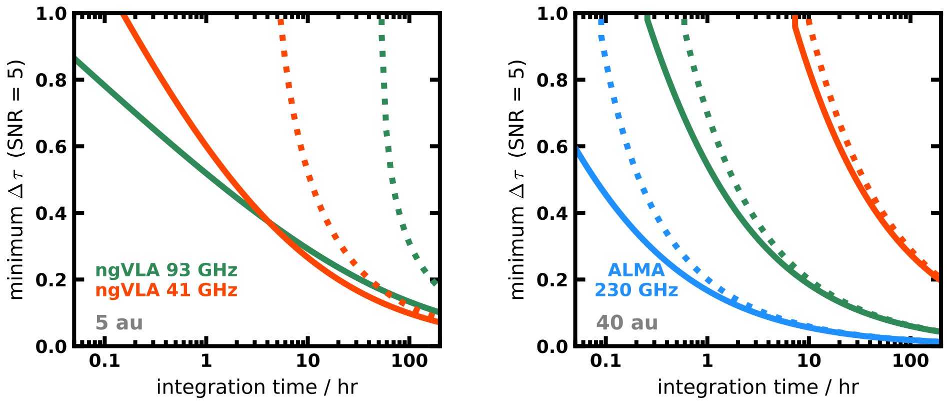

Figure 4. Illustrative examples of the minimum optical depth (fractional) contrast that can be detected at 5 σ in a given integration time, for fiducial disk substructures at 5 (*left*) and 40 au (*right*). Solid curves are for τ_ν depletions; dotted curves are for enhancements. The blue, green, and red curves are for ALMA 230 GHz, ngVLA 93 GHz, and ngVLA 41 GHz, respectively. See the text for a detailed discussion.

integration time $t_{\rm int}$. Considering ALMA observations at 230 GHz (Band 6) and ngVLA measurements at 93 (W-band) and 41 GHz (Q/Ka-band), we collect estimates of σ_ν for FWHM beam diameters of 10 and 40 mas from the ALMA sensitivity calculator[1] and the metrics discussion in ngVLA Memo 17[2]. Figure 3 shows the 5 σ (SNR = 5) optical depth “contrast curves" for the 5 and 40 au reference substructures. The solid and dotted curves show the cases of optical depth depletion and enhancement, respectively.

These contrast curves in Figure 3 are only illustrative examples, but they demonstrate the general feasibility of ngVLA observations that should play substantial roles in the study of protoplanetary disk substructures. As an approximate point of reference, gas density (thereby pressure) perturbations of ~20% induced by interactions with a ~0.1 $M_{\rm jup}$ planet (Fung et al. 2014), MHD zonal flows (Simon & Armitage 2014), or weak vortices (Goodman et al. 1987) are expected to be sufficient to trap particles in a nominal disk. Moreover, the corresponding perturbations in the local surface density of disk solids could be considerably amplified relative to the modulations in the gas densities (e.g., Paardekooper & Mellema 2006; Pinilla et al. 2012).

At intermediate disk radii (~tens of au; e.g., the right panel of Fig. 3), where optical depths and temperatures are low but substructures should be relatively larger, there are opportunities for synergy with high frequency measurements from ALMA at matching angular resolution. For substructures at these distances from the host star, even relatively modest optical depth contrasts could be detected and resolved in a reasonable ngVLA observing time down to frequencies of ~30 GHz. For optically thicker (or warmer) cases, it would be possible to push down to 10 GHz, and thereby more directly probe concentrations of the largest accesible particle sizes (~few cm).

The real benefit of the ngVLA is more apparent at small disk radii (inside ~10 au; e.g., the left panel of Fig. 3), where optical depths and temperatures are higher and

[1] `https://almascience.eso.org/proposing/sensitivity-calculator`

[2] `http://library.nrao.edu/public/memos/ngvla/NGVLA_17.pdf`

substructures should be smaller. There, the combination of long baselines and low frequencies offered by the ngVLA provide *unique* access to inner disk substructures on the smallest spatial scales. For example, ~20% density depletions at 5 au are accessible at ~30–100 GHz in ~10–30 hours of ngVLA integration, suitable for detecting the gaps in the local distribution of solids that are dynamically carved by young, super-Earth planets (e.g., Ricci et al. 2018). At the higher frequencies probed by ALMA, even relatively large density contrasts could remain hidden for even large integration times if the background optical depths are too high. Moreover, beam dilution due to limited baseline lengths creates an additional ALMA barrier; in short, there is good reason that no 230 GHz contrast curve is shown in the left panel of Figure 3.

4. Quantifying Substructures

The detectability of disk substructures is obviously fundamental, but it is not the sole value of ngVLA in this scientific context. Resolved wideband continuum measurements in the 30–100 GHz range permit more robust estimates of small-scale spatial variations in the continuum optical depth and spectral morphology (e.g., within and between the ~20 GHz-wide high-frequency ngVLA receiver bands), which in turn can provide strong constraints on the amplitude and shape of the particle size distribution and density perturbation of individual substructures. The spatial morphology of the spectrum across such a feature could reveal new insights on the hydrodynamical nature of particle traps: for example, various vortex models make different predictions about where and how strongly particles of different sizes are concentrated with respect to the local gas pressure maximum (e.g., Baruteau & Zhu 2016; Sierra et al. 2017). The spectral dependence of the brightness temperature perturbation from a substructure is itself sensitive to the underlying particle density contrast: if high concentrations of "pebbles" can be inferred, we could rule on the likelihood that fast-acting mechanisms (e.g., the streaming instability; Youdin & Goodman 2005) are indeed the dominant pathways for the formation of planetesimals. In all of these aspects, the ngVLA will be an indispensable and ground-breaking tool for these lines of work.

Finally, the unique ability of the ngVLA to probe substructure asymmetries at small disk radii creates some new opportunities in the time-domain. Long-term monitoring observations would be of extraordinarily high value for any inner disk substructures with a clear azimuthal asymmetry. The motions of such features compared to their expected Keplerian orbital rates can help illuminate the natures of the underlying source of the pressure maximum responsible for the particle trap. As a reference point, a Keplerian orbital displacement of a full 10 mas beam would take ~6 months for a structure at a radius of 5 au in a disk orbiting a solar-mass host.

5. Conclusions

The characterization of small-scale substructures in the spatial distributions of protoplanetary disk solids is the most pressing issue at the forefront of observational planet formation research. The new capabilities in high resolution wideband radio continuum imaging promised by the ngVLA will enable rapid progress in the field, delivering new insights on the particle size distributions in local concentrations of solids and offering unique access to the smallest substructure features at the locations where terrestrial planets (and most giant planets) are expected to form. In doing so, the ngVLA measurements have some natural synergy with ALMA data at higher frequencies, facilitating more robust constraints on particle size distributions and better links with resolved tracers of the molecular gas. Moreover, ngVLA observations of inner disk substructures will prove to be an important complement for tracers of inner disk material probed with the *JWST*, offering a structural template upon which to interpret those spatially unresolved infrared continuum and molecular spectra data. Overall, the ngVLA should prove to be a crucial tool for better understanding the complex metamorphosis of circumstellar disks into young planetary systems.

References

ALMA Partnership, et al. 2015, ApJ, 808, L3
Andrews, S. M., et al. 2016, ApJ, 820, L40
Baruteau, C., et al. 2014, in Protostars and Planets VI, eds. H. Beuther, R. S. Klessen, C. P. Dullemond, & Th. Henning (Univ. Arizona Press: Tucson), 667
Baruteau, C., & Zhu, Z. 2016, MNRAS, 458, 3927
Brauer, F., Dullemond, C. P., Johansen, A., Henning, Th., Klahr, H., & Natta, A. 2007, A&A, 469, 1169
Carrasco-González, C., et al. 2016, ApJ, 821, L16
Chiang, E., & Youdin, A. N. 2010, AREPS, 38, 493
Cieza, L. A., et al. 2016, Nature, 535, 258
Cieza, L. A., et al. 2017, ApJ, 851, L23
Cox., E. G., et al. 2017, ApJ, 851, 83
Dipierro, G., et al. 2018, MNRAS, 475, 5296
Dzyurkevich, N., Flock, M., Turner, N., Klahr, H., & Henning, Th. 2010, A&A, 515, 70
Fedele, D., et al. 2017, A&A, 600, 72
Fedele, D., et al. 2018, A&A, 610, 24
Flock, M., Ruge, J. P., Dzyurkevich, N., Henning, Th., Klahr, H., & Wolf, S. 2015, A&A, 574, 68
Fung, J., Shi, J.-M., & Chiang, E. 2014, ApJ, 782, 88
Goodman, J., Narayan, R., & Goldreich, P. 1987, MNRAS, 225, 695
Huang, J., et al. 2018, ApJ, 852, 122
Isella, A., Chandler, C. J., Carpenter, J. M., Pérez, L. M., & Ricci, L. 2014, ApJ, 788, 129
Isella, A., et al. 2016, Phys. Rev. Lett., 117, 251101
Johansen, A., Blum, J., Tanaka, H., Ormel, C. W., Bizarro, M., & Rickman, H. 2014, in Protostars and Planets VI, eds. H. Beuther, R. S. Klessen, C. P. Dullemond, & Th. Henning (Univ. Arizona Press: Tucson), 547
Loomis, R. A., Öberg, K. I., Andrews, S. M., & MacGregor, M. A. 2017, ApJ, 840, 23
Macías, E., et al. 2016, ApJ, 829, 1
Macías, E., et al. 2017, ApJ, 838, 97
Marino, S., et al. 2015, ApJ, 813, 76
Paardekooper, S.-J., & Mellema, G. 2006, A&A, 453, 1159
Pérez, L. M., et al. 2016, Science, 353, 1519
Pinilla, P., Birnstiel, T., Ricci, L., Dullemond, C. P., Uribe, A. L., Testi, L., & Natta, A. 2012, 538, 114
Pollack, J. B., Hubickyj, O., Bodenheimer, P., Lissauer, J. J., Podolak, M., & Greenzweig, Y. 1996, Icarus, 124, 62
Raymond, S. N., Kokubo, E., Morbidelli, A., Morishima, R., & Walsh, K. J. 2014, in Protostars and Planets VI, eds. H. Beuther, R. S. Klessen, C. P. Dullemond, & Th. Henning (Univ. Arizona Press: Tucson), 595
Ricci, L., Testi, L., Natta, A., Neri, R., Cabrit, S. & Herczeg, G. J. 2010, A&A, 512, 15
Ricci, L., Liu, S.-F., Isella, A., & Li, H. 2018, ApJ, 853, 110

Sierra, A., Lizano, S., & Barge, P. 2017, ApJ, 850, 115
Simon, J. B., & Armitage, P. J. 2014, ApJ, 784, 15
Stammler, S. M., Birnstiel, T., Panić, O., Dullemond, C. P., & Dominik, C. 2017, A&A, 600, 140
Takeuchi, T., & Lin, D. N. C. 2002, ApJ, 581, 1344
Tsukagoshi, T., et al. 2016, ApJ, 829, L35
van der Plas, G., et al. 2017, A&A, 597, 32
Whipple, F. L. 1972, in From Plasma to Planet, ed. A. Elvius, 211
Youdin, A. N., & Goodman, J. 2005, ApJ, 620, 459
Zhang, K., et al. 2016, ApJ, 818, L16
Zhu, Z., Stone, J. M., Rafikov, R. R., & Bai, X. 2014, ApJ, 785, 122

Science with a Next-Generation Very Large Array
ASP Conference Series, Monograph 7
Eric J. Murphy, ed.

DRAFT EDITION

Disk Winds and the Evolution of Planet-Forming Disks

I. Pascucci,[1] S. Andrews,[2] C. Chandler,[3] and A. Isella[4]
[1]*Lunar and Planetary Laboratory, Tucson, AZ, USA;*
`pascucci@lpl.arizona.edu`

[2]*Harvard-Smithsonian Center for Astrophysics, Cambridge, MA, USA;*
`sandrews@cfa.harvard.edu`

[3]*National Radio Astronomy Observatory, Socorro, NM, USA;*
`cchandle@nrao.edu`

[4]*Rice University, Houston, TX, USA;* `isella@rice.edu`

1. Introduction

Disks of gas and dust around young ($\sim$ 1 − 10 Myr) stars are active sites of planet formation. Hence, their evolution and dispersal directly impact which type of planetary systems can form. Accretion through the circumstellar disk is a ubiquitous phenomenon (see Hartmann et al. 2016 for a recent review) and thought to dominate disk evolution at early times (e.g., Alexander et al. 2014). However, the physical mechanism enabling accretion, and therefore global disk evolution, is as yet unclear (e.g., Turner et al. 2014).

The prevailing view for the past 40 years has been that accretion occurs because disks are viscous and transport angular momentum outward via correlated turbulent fluctuations. Magneto-rotational instability (MIR, Balbus & Hawley 1998) would produce the necessary turbulence. In this picture, viscous-dominated evolution lasts for the first few Myr of disk evolution until accretion drops below the mass loss rate from thermal disk winds driven by high-energy stellar photons, also known as photoevaporative winds. At that point photoevaporation limits the supply of gas to the inner ($\sim$ 1 au) disk which drains onto the star on the local viscous timescale, of order 100,000 years (e.g., Gorti et al. 2016). Recently, simulations including non-ideal MHD effects have shown that most of the disk is not MRI active, hence not accreting onto the star (e.g., Bai & Stone 2013). Instead, these simulations develop vigorous magneto-thermal MHD winds that extract angular momentum from the disk surface and hence enable accretion (e.g., Gressel et al. 2015). In this scenario, wind mass loss rates are comparable to mass accretion rates even at early times and disk dispersal can be rapid if the disk retains most of its magnetic flux during evolution (Bai 2016 but see also Zhu & Stone 2017). As the surface density evolution of a viscous disk is very different from that of a disk where accretion is driven by MHD winds, and surface density directly impacts planet formation, it is important to understand which physical process dominates. Detecting disk winds, spatially resolving them, and measuring wind mass loss rates is crucial to make progress in this field.

2. Disk wind diagnostics - the role of cm observations

Identifying disk winds and understanding their origin requires detecting gravitationally unbound/outflowing disk gas within a ~30 au radius from the star (e.g., Simon et al. 2017). Given the typical distance of star-forming regions (~140 pc), this requirement translates into a spatial resolution better than ~100 mas. This is why most direct evidence for disk winds relies on spatially unresolved/high-resolution (Δv ~10 km/s) optical and infrared spectroscopy of gaseous species probing the disk surface (see Ercolano & Pascucci 2017 for a recent review). Kinematic separation of different components in optical forbidden lines has demonstrated that MHD disk winds are present in the inner ~0.5 au for the majority of accreting stars while line ratios constrain the range of temperature-electron densities for the emitting gas (e.g., Simon et al. 2016). Infrared forbidden line profiles hinting to more radially extended disk winds that could be photoevaporative in nature have been also detected toward a dozen disks (e.g., Pascucci & Sterzik 2009, Sacco et al. 2012). *The missing critical parameter for a reliable computation of wind mass loss rates is a measurement of the spatial extent of the wind emitting region.*

As a fully or partially ionized disk surface emits free-free continuum radiation and H recombination lines, long mm and cm-wavelength observations can be also used to detect disk winds (Pascucci et al. 2012; Owen et al. 2013). Current radio facilities have identified candidate disk wind emission from the presence of emission in excess of the thermal dust emission and, when available, multi-wavelength cm observations have been used to exclude other possible sources of excess emission, such as gyro synchrotron non-thermal radiation and emission from very large cm-size grains or very small nanometer-size grains (e.g., Pascucci et al. 2014, Gálvan-Madrid et al. 2014). Even in these multi-wavelength studies, it remains difficult to properly separate free-free emission from a collimated fast (~100 km/s) jet (e.g., Anglada et al. 1998) and from the ionized disk surface, which hampers measuring the disk ionization fraction and the wind mass loss rate. This is illustrated in the left panel of Figure 1 which reports the 3.3 cm VLA image of GM Aur (Macías et al. 2016), a star surrounded by a disk with a dust cavity (e.g., Andrews et al. 2011; Oh et al. 2016) . With a spatial resolution of $0.5''$, ~ 70 au at the distance of Taurus-Auriga, an elongation perpendicular to the disk emission is barely detected. This elongation strongly suggests that a jet contributes to the excess cm emission even in disks that are thought to be substantially evolved. *Higher spatial resolution and sensitivity are necessary to separate the jet and disk wind contributions.*

3. Connection to the unique ngVLA capabilities

Spatially resolving disk winds requires deep, multi-frequency radio continuum imaging at high angular resolution, and supplementary spectral imaging of H recombination lines. The continuum measurements target free-free emission from an ionized wind (and potentially jet). As dust thermal emission dominates at frequencies higher than 30 GHz, modest spectral coverage ($\Delta\nu/\nu \sim 0.8$) in the 5-30 GHz range is essential. For a photoevaporative wind heated and ionized solely by stellar X-rays and typical star/disk parameters the expected integrated flux density at 8 GHz is ~3μJy (eq. 3 in

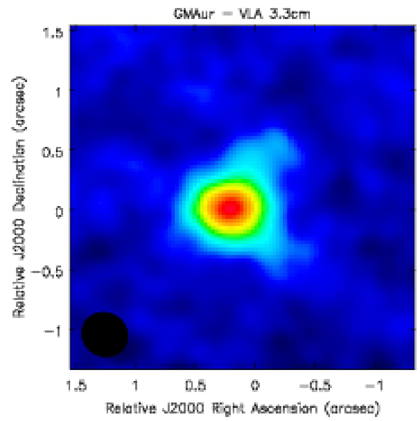

Figure 1. **This is a placeholder as we plan to have a two panel figure. Left panel: VLA 3.3 cm image of GM Aur by Macias et al. Right panel: a simulated ngVLA image of the same disk at higher spatial resolution and sensitivity.**

Pascucci et al. 2012)[1] and should arise within a ~10 au radius (Fig. 4 in Owen et al. 2013). Spatially resolving the emission in two beams and requiring a S/N of at least 5 means reaching an RMS noise level of 0.3μJy/beam. Theoretical estimates for the free-free continuum (and H recombination line emission) from MHD winds have not yet been reported in the literature. However, observations tracing the jet and MHD wind of DG TauA hint at higher flux densities (~300μJy) distributed over the $\sim 0.1''$ beam of e-MERLIN (upper panel of Fig. 1 in Ainsworth et al. 2013).

In a fully or partially ionized optically thin region, such as a photoevaporative wind, the H line to free-free continuum ratios increase with frequency but so does the thermal dust emission. Unless the thermal continuum and H lines can be spatially separated, the best frequency to detect H lines is around 30 GHz (lower panel of Fig. 2 in Pascucci et al. 2012). At these frequencies, the integrated line flux densities from a photoevaporative wind are comparable to the free-free continuum emission ($\sim 3\mu$Jy) and a few percent of the total continuum (free-free + thermal dust), middle and lower panels of Fig. 2 in Pascucci et al. (2012). Line widths and blueshifts with respect to the stellar velocity depend on disk inclination but typical values are $\sim$ 10 km/s (e.g., Alexander 2008; Ercolano & Owen 2010)[2]. Such line emission is probably too weak to detect even with the ngVLA. However, if the line emission from the jet has a similar flux density as the continuum it would detectable, and be particularly important for tracing the accretion and mass-loss in embedded protostars that are obscured at optical and infrared wavelengths. With 300μJy distributed over 10 ngVLA beams obtaining a 5-sigma detection in a 5 km/s channel (to provide kinematic information) would take a

---

[1] An EUV ionized layer would produce more free-free emission (eq. 2 in Pascucci et al. 2012) but observations suggest that the disk receives only a small fraction of the stellar EUV luminosity (Pascucci et al. 2014).

[2] If H recombination lines would trace an MHD wind launched inside ~1 au line widths and blueshifts would be substantially larger (e.g., Romanova et al. 2009).

few 10s of hours with the ngVLA; stacking multiple lines (all available in the 30 GHz band) would bring the time required down by a factor of the number of lines stacked.

4. Conclusions

In this contribution we have illustrated that the sensitivity and spatial resolution of the ngVLA can bring the study of disk winds to the next level. Although H recombination lines will remain challenging to detect, the free-free continuum emission of even a partially ionized disk surface can be separated by that of a jet and, for the first time, imaged.

The combination of collecting area and sensitivity at 30 GHz needed for this science is best matched by the ngVLA and will not be available with any other facility in the world. Although ALMA is expected to add Band-1, and perhaps array receivers, it will have the same sensitivity as the current VLA for point-source observations and the best resolution will be just over 100 mas. SKA is not currently expected to operate at frequencies as high as 30 GHz.

References

Ainsworth, R. E., Ray, T. P., Scaife, A. M. M., Greaves, J. S., Beswick, R. J. 2013, MNRAS, 436L, 64

Alexander, R. D. 2008, MNRAS, 391L, 64

Alexander, R., Pascucci, I., Andrews, S., Armitage, P., Cieza, L. 2014, in Protostars and Planets VI, 914, 475

Andrews, S. M., Wilner, D. J., Espaillat, C., Hughes, A. M., Dullemond, C. P., McClure, M. K., Qi, C., Brown, J. M. 2011, ApJ, 732, 42

Anglada, G., Villuendas, E., Estalella, R., Beltrán, M. T., Rodríguez, L. F., Torrelles, José M., Curiel, S. 1998, AJ, 116, 2953

Bai, Xue-Ning & Stone, J. M. 2013, ApJ, 769, 76

Bai, Xue-Ning 2016, ApJ, 821, 80

Balbus, S. A. & Hawley, J. F. 1998, in Reviews of Modern Physics, Volume 70, Issue 1, 1-53

Ercolano, B. & Owen, J. E. 2010, MNRAS, 406, 1553

Ercolano, B. & Pascucci, I. 2017, in Royal Society Open Science, Volume 4, Issue 4

Gálvan-Madrid, R., Liu, H. B., Manara, C. F., Forbrich, J., Pascucci, I., Carrasco-Gonzalez, C., Goddi, C., Hasegawa, Y., Takami, M., Testi, L. 2014, A&A, 570L, 9

Gorti, U., Liseau, R., Sandor, Z., Clarke, C. 2016, in Space Science Reviews, Volume 205, Issue 1-4, 125-152

Gressel, O., Turner, N. J., Nelson, R. P., McNally, C. P. 2015, ApJ, 801, 84

Hartmann, L., Herczeg, G., Calvet, N. 2016, ARA&A, 54, 135

Macías, E., Anglada, G., Osorio, M., Calvet, N., Torrelles, J. M., Gómez, J. F., Espaillat, C., Lizano, S., Rodríguez, L. F., Carrasco-González, C., Zapata, L. 2016, ApJ, 829, 1

Oh, D., Hashimoto, J., Carson, J. C. et al. 2016, ApJ, 831L, 7

Owen, J. E., Scaife, A. M. M., Ercolano, B. 2013, MNRAS, 434, 3378

Pascucci, I. & Sterzik, M. 2009, ApJ, 702, 724

Pascucci, I., Gorti, U., Hollenbach, D. 2012, ApJ, 751L, 42

Pascucci, I., Ricci, L., Gorti, U., Hollenbach, D., Hendler, N. P., Brooks, K. J., Contreras, Y. 2014, ApJ, 795, 1

Romanova, M. M., Ustyugova, G. V., Koldoba, A. V., Lovelace, R. V. E. 2009, MNRAS, 399, 1802

Simon, M. N., Pascucci, I., Edwards, S., Feng, W., Gorti, U., Hollenbach, D., Rigliaco, E., Keane, J. T. 2016, ApJ, 831, 169

Sacco, G. G., Flaccomio, E., Pascucci, I., Lahuis, F., Ercolano, B., Kastner, J. H., Micela, G., Stelzer, B., Sterzik, M. 2012, ApJ, 747, 142
Simon, J. B., Bai, Xue-Ning, Flaherty, K. M., Hughes, A. M. 2017, ApJL, submitted (arXiv:1711.04770)
Turner, N. J., Fromang, S., Gammie, C., Klahr, H., Lesur, G., Wardle, M., Bai, X.-N. 2014, in Protostars and Planets VI, 914, 411
Zhu, Z. & Stone, J. M. 2017, Submitted to the AAS Journals (arXiv:1701.04627)

Part IV

Planetary Systems and Life:

Science with a Next-Generation Very Large Array
ASP Conference Series, Monograph 7
Eric J. Murphy, ed.

DRAFT EDITION

SETI Searches for Evidence of Intelligent Life in the Galaxy

Steve Croft,[1] Andrew P. V. Siemion,[1,2,3] James M. Cordes,[4] Ian Morrison,[5] Zsolt Paragi,[6] Jill Tarter[3]

[1]*Department of Astronomy, University of California, Berkeley, 501 Campbell Hall #3411, Berkeley, CA, 94720, USA*

[2]*Department of Astrophysics/IMAPP, Radboud University, P.O. Box 9010, NL-6500 GL Nijmegen, The Netherlands*

[3]*SETI Institute, Mountain View, CA 94043, USA*

[4]*Cornell Center for Astrophysics and Planetary Science and Department of Astronomy, Cornell University, Ithaca, NY 14853, USA*

[5]*Curtin Institute of Radio Astronomy, Curtin University, Perth, Australia*

[6]*Joint Institute for VLBI ERIC (JIVE), Postbus 2, NL-7990 AA Dwingeloo, The Netherlands*

Abstract. Radio SETI experiments aim to test the hypothesis that extraterrestrial civilizations emit detectable signals from communication, propulsion, or other technologies. The unprecedented capabilities of next generation radio telescopes, including ngVLA, will allow us to probe hitherto unexplored regions of parameter space, thereby placing meaningful limits on the prevalence of technological civilizations in the Universe (or, if we are fortunate, making one of the most significant discoveries in the history of science). ngVLA provides critical capabilities in the 10 – 100 GHz range, and will be a valuable complement to SKA in the southern hemisphere, as well as surveying the sky at frequencies underexplored by previous SETI experiments.

1. Description of the problem

Almost all stars are now thought to have planets, and a substantial fraction (Kasting et al. 2014; Dressing & Charbonneau 2015) have a planet in the "habitable zone" where liquid water may exist on the surface. The local Universe is thus a target-rich environment to search for signs that life may have taken hold elsewhere in our Galaxy. This can be accomplished either by looking for atmospheric biosignatures (using the next generation of space-based or extremely large ground-based optical telescopes), or by looking for advanced life by searching for signatures of technology (Tarter 2001). The latter will be an area in which ngVLA will excel. The search for extraterrestrial intelligence (SETI) is also complementary to other proposed "cradle of life" studies to be undertaken by ngVLA, including studying star and planet formation, and the formation of complex molecules (Isella et al. 2015).

The frequency coverage of ngVLA is very complementary to the bands to be covered by SKA (Siemion et al. 2013), allowing a comprehensive SETI search to be undertaken over three decades of radio frequency. These new instruments will also provide the sensitivity required to detect analogs of Earthbound transmitters such as aircraft radar from the distance of several nearby stars, in addition to more powerful (or directional) transmitters from across the Galaxy.

2. Scientific importance

"Are we alone?" is one of the most profound human questions. Yet at the turn of the seventh decade (Cocconi & Morrison 1959; Drake 1961) of SETI searches, there is, as yet, no evidence that intelligent life has arisen elsewhere in our Universe. One might infer that technological life beyond Earth is rare, or even non-existent, but in reality such a small volume of parameter space has been explored to date that this conclusion would be premature. The search for extrasolar planets provides an instructive example. As late as the 1980s, searching for planets orbiting other stars was a fruitless task, but as new techniques and powerful new instruments became available, the field has exploded (e.g., Borucki et al. 2010). We now understand that the Galaxy is replete with planets of a huge variety of sizes, temperatures, and compositions, including many similar in character to our own.

3. Astronomical impact

The detection of the first exoplanets opened an entirely new field of research. Aside from the cultural impact of a SETI detection, the dawning of the age of observational astrobiology will mark one of the most significant milestones in the history of astronomy. Even the detection of a simple beacon, indicative of the presence of another technological civilization in our Galaxy, would enable us to begin to understand the processes by which the Universe gives rise to life, and intelligence, launching a new Copernican Revolution by which we more fully understand our place in the cosmos. Were a signal to contain information that we were able to comprehend, we could potentially understand what awaits us as a species, or begin to investigate "the archaeology of the future" (Morrison 1997).

4. Anticipated results

Radio SETI experiments aim to test the hypothesis that extraterrestrial civilizations emit detectable signals from communication, propulsion, or other technologies. SETI attempts to constrain the terms in the Drake Equation (Drake 1961; Worden et al. 2017); in particular, given that we now know that habitable planets are common, can we attempt to constrain the fraction of such planets that develop life, intelligence, and technology, and the lifetime over which signs of such technology are detectable? We do not know, a priori, the frequency spectrum, luminosity function, duty cycle, or antenna gain and beaming fraction of ETI transmissions. To have the best chance of success, therefore, a SETI survey must attempt to explore a large region of parameter space in frequency (coverage and resolution), time (resolution, cadence, and duration), and sensitivity. While it is challenging to qualitatively compare one SETI survey to another, increases in computational power and survey speed are enabling modern SETI searches that far exceed the capabilities of their predecessors (Enriquez et al. 2017).

As a fast survey instrument with high sensitivity and wide frequency coverage, ngVLA will provide powerful constraints on the space density of technologically advanced civilizations employing transmission technologies over a wide swath of the radio spectrum, if not actually directly detecting such civilizations' existence.

5. Limitations of current astronomical instrumentation

Although the power of extraterrestrial transmissions may be considerably higher than those possible with human technologies, it is nevertheless useful to use our own transmission capabilities as a guide. Our most powerful beamed transmitter, the Arecibo telescope when used as a planetary radar, has an equivalent isotropic radiated power (EIRP) of 2×10^{20} erg/s, and would be detectable by ngVLA at distances of kiloparsecs. ETI signals comparable to our most powerful wide-angle transmitters, such as airport radars (EIRP $\sim 10^{17}$ erg/s) would be detectable from planets orbiting the nearest few thousand stars to the Sun. ngVLA will complement SKA1-LOW and SKA1-MID as the only facilities with the capability to detect "leakage" transmissions from omnidirectional transmitters with power close to the brightest transmitters on Earth.

6. Connection to unique ngVLA capabilities

The unprecedented capabilities of next generation radio telescopes, including ngVLA, will allow us to probe hitherto unexplored regions of parameter space (Ekers et al. 2002), thereby placing meaningful limits on the prevalence of technological civilizations in the Universe (or, if we are fortunate, making one of the most significant discoveries in the history of science).

ngVLA provides critical capabilities in the 10 – 100 GHz range, a region of the spectrum used by many human technologies, to survey the sky at sensitivities unmatched by other facilities, and underexplored by previous SETI experiments. At frequencies where ngVLA and SKA overlap, ngVLA will primarily see the northern hemisphere and SKA the southern.

Additionally, ngVLA combines high sensitivity with very high resolution (of order 10 mas). With such high resolution, the motion of a putative transmitter on a planet or spacecraft, orbiting its star at a distance of ~AU, could be discerned astrometrically even for stars at distances of $\sim$ 100 pc. Measuring the motion of such a transmitter would be a powerful additional tool for distinguishing artificial transmitters in orbit around nearby stars.

7. Experimental layout

SETI searches have two key goals:

1. Find signals that appear artificial (e.g. narrow band, modulated, pulsed, or otherwise obviously "unnatural")

2. Localize such signals at a specific right ascension and declination (to eliminate the possibility that they are radio frequency interference (RFI) from transmitters close to the telescope or from Earth-orbiting satellites)

Searches can either be performed using baseband voltage data, or, after an FFT operation, spectrograms or "waterfall plots" of intensity as a function of frequency and time. Classical SETI algorithms have typically focused on the search for narrow-band signals, but increased computing power and more sophisticated algorithms (including machine learning approaches) will enable the search for increasingly complex signals, as well as better classification of confounding RFI.

We envisage an ngVLA SETI search operating commensally with most primary science users of the array, but in addition a smaller amount (tens to hundreds of hours per year) of TAC-allocated time for pointed observations in support of time-critical or other targets of interest. Any star within the instantaneous field of view of the ngVLA is a potential SETI target, and as such a commensal search with ngVLA would enable stringent limits on ETI transmissions for millions of stars, in addition to limits at higher EIRP for more distant targets such as galaxies. In addition to stars and galaxies, solar system objects have in the past also been targets for SETI searches (e.g., Freitas & Valdes 1980; Enriquez et al. 2018; Tingay et al. 2018); commensal or targeted searches of such objects with ngVLA could easily detect transmitters with EIRPs measured in milliwatts.

The proposed observations require that the ngVLA have the capability to deliver time domain voltage data from every antenna to dedicated signal processing hardware to be installed as either a user or facility instrument at ngVLA. Similar to user instruments operating at Arecibo, Green Bank, and Parkes, such a system would run in a commensal mode, capturing or processing voltage data alongside non-SETI observations, in addition to standalone observations of SETI targets. Such equipment would consist of $\sim$ 100 PB storage and 10 PFLOPS compute (assuming Moore's Law extrapolation from current equipment) enabling digitization of the entire ngVLA bandwidth and be capable of forming and searching both incoherent and coherent (phased) beams.

As well as operating commensally with primary science programs, flexible subarraying capabilities would allow some of the antennas to undertake a dedicated SETI search simultaneously with other users of the array (albeit at reduced sensitivity). When operating in a commensal or survey mode, the primary metric of interest is survey speed, which favors an LNSD (large number of small diameter dishes) design.

8. Complementarity

The ability to access baseband data is an important capability not just for SETI, but for fast transient applications such as pulsar and FRB studies. Baseband products can also be used for spectral line or other studies, even regenerating higher-level data products to custom specifications from archival data long after the observations are taken (assuming these data are stored).

The proposed search will also provide a superb dynamic catalog of RFI, classified using machine learning algorithms, publicly accessible to other science users. To avoid inadvertent flagging of signals of interest to SETI, the ability to bypass any automatic RFI excision built in to the system is important.

By 2025, Breakthrough Listen (Worden et al. 2017) will have completed an unprecedented 10-year SETI survey. Even if Listen, or other surveys such as those that are ongoing at the Allen Telescope Array (Harp et al. 2016), do not confirm the existence of technological civilizations beyond Earth, they will constrain the parameter space in which such civilizations may exist, motivating a push to higher sensitivities and different frequencies. In the event of an ETI detection, or of the detection of biosignatures or other contingent results from JWST (Greene et al. 2016), TESS (Ricker et al. 2015), or other planet finding and characterization experiments, ngVLA will provide critical capabilities for follow-up observations.

Acknowledgments. Funding for Breakthrough Listen research is provided by the Breakthrough Prize Foundation.

References

Borucki, W. J., Koch, D., Basri, G., Batalha, N., Brown, T., Caldwell, D., Caldwell, J., Christensen-Dalsgaard, J., Cochran, W. D., DeVore, E., Dunham, E. W., Dupree, A. K., Gautier, T. N., Geary, J. C., Gilliland, R., Gould, A., Howell, S. B., Jenkins, J. M., Kondo, Y., Latham, D. W., Marcy, G. W., Meibom, S., Kjeldsen, H., Lissauer, J. J., Monet, D. G., Morrison, D., Sasselov, D., Tarter, J., Boss, A., Brownlee, D., Owen, T., Buzasi, D., Charbonneau, D., Doyle, L., Fortney, J., Ford, E. B., Holman, M. J., Seager, S., Steffen, J. H., Welsh, W. F., Rowe, J., Anderson, H., Buchhave, L., Ciardi, D., Walkowicz, L., Sherry, W., Horch, E., Isaacson, H., Everett, M. E., Fischer, D., Torres, G., Johnson, J. A., Endl, M., MacQueen, P., Bryson, S. T., Dotson, J., Haas, M., Kolodziejczak, J., Van Cleve, J., Chandrasekaran, H., Twicken, J. D., Quintana, E. V., Clarke, B. D., Allen, C., Li, J., Wu, H., Tenenbaum, P., Verner, E., Bruhweiler, F., Barnes, J., & Prsa, A. 2010, Science, 327, 977

Cocconi, G., & Morrison, P. 1959, Nat, 184, 844

Drake, F. D. 1961, Physics Today, 14

Dressing, C. D., & Charbonneau, D. 2015, ApJ, 807, 45. `1501.01623`

Ekers, R., Morrison, P., Group, S. S. . T. W., & Institute, S. 2002, SETI 2020: A Roadmap for the Search for Extraterrestrial Intelligence (SETI Press). URL `https://books.google.com/books?id=eFTOOAAACAAJ`

Enriquez, J. E., Siemion, A., Lazio, T. J. W., Lebofsky, M., MacMahon, D. H. E., Park, R. S., Croft, S., DeBoer, D., Gizani, N., Gajjar, V., Hellbourg, G., Isaacson, H., & Price, D. C. 2018, Research Notes of the American Astronomical Society, 2, 9. `1801.02814`

Enriquez, J. E., Siemion, A., Price, D. C., MacMahon, D., Lebofsky, M., Isaacson, H., Hellbourg, G., Gajjar, V., & Croft, S. 2017, ApJ, submitted

Freitas, R. A., & Valdes, F. 1980, Icarus, 42, 442 . URL `http://www.sciencedirect.com/science/article/pii/0019103580901062`

Greene, T. P., Line, M. R., Montero, C., Fortney, J. J., Lustig-Yaeger, J., & Luther, K. 2016, ApJ, 817, 17. `1511.05528`

Harp, G. R., Richards, J., Tarter, J. C., Dreher, J., Jordan, J., Shostak, S., Smolek, K., Kilsdonk, T., Wilcox, B. R., Wimberly, M. K. R., Ross, J., Barott, W. C., Ackermann, R. F., & Blair, S. 2016, AJ, 152, 181. `1607.04207`

Isella, A., Hull, C. L. H., Moullet, A., Galván-Madrid, R., Johnstone, D., Ricci, L., Tobin, J., Testi, L., Beltran, M., Lazio, J., Siemion, A., Liu, H. B., Du, F., Öberg, K. I., Bergin, T., Caselli, P., Bourke, T., Carilli, C., Perez, L., Butler, B., de Pater, I., Qi, C., Hofstadter, M., Moreno, R., Alexander, D., Williams, J., Goldsmith, P., Wyatt, M., Loinard, L., Di Francesco, J., Wilner, D., Schilke, P., Ginsburg, A., Sánchez-Monge, Á., Zhang, Q., & Beuther, H. 2015, ArXiv e-prints. `1510.06444`

Kasting, J., Kopparapu, R., Ramirez, R., & Harman, C. 2014, Proceedings of the National Academy of Sciences of the United States of America, 111, 12641. Cited By 32, URL `https://www.scopus.com/inward/record.uri?eid=2-s2.0-84907227871&doi=10.1073%2fpnas.1309107110&partnerID=40&md5=9e4f2b02aafaf018fb99a407ce6b484c`

Morrison, P. 1997, Nothing Is Too Wonderful to Be True, Masters of Modern Physics (American Inst. of Physics). URL `https://books.google.com/books?id=UeXw59mRY-sC`

Ricker, G. R., Winn, J. N., Vanderspek, R., Latham, D. W., Bakos, G. Á., Bean, J. L., Berta-Thompson, Z. K., Brown, T. M., Buchhave, L., Butler, N. R., Butler, R. P., Chaplin, W. J., Charbonneau, D., Christensen-Dalsgaard, J., Clampin, M., Deming, D., Doty, J., De Lee, N., Dressing, C., Dunham, E. W., Endl, M., Fressin, F., Ge, J., Henning, T., Holman, M. J., Howard, A. W., Ida, S., Jenkins, J. M., Jernigan, G., Johnson, J. A., Kaltenegger, L., Kawai, N., Kjeldsen, H., Laughlin, G., Levine, A. M., Lin, D., Lissauer, J. J., MacQueen, P., Marcy, G., McCullough, P. R., Morton, T. D., Narita, N., Paegert, M., Palle, E., Pepe, F., Pepper, J., Quirrenbach, A., Rinehart, S. A., Sasselov, D., Sato, B., Seager, S., Sozzetti, A., Stassun, K. G., Sullivan, P., Szentgyorgyi, A., Torres, G., Udry, S., & Villasenor, J. 2015, Journal of Astronomical Telescopes, Instruments, and Systems, 1, 014003

Siemion, A. P. V., Demorest, P., Korpela, E., Maddalena, R. J., Werthimer, D., Cobb, J., Howard, A. W., Langston, G., Lebofsky, M., Marcy, G. W., & Tarter, J. 2013, ApJ, 767, 94. 1302.0845

Tarter, J. 2001, ARA&A, 39, 511

Tingay, S. J., Kaplan, D. L., Lenc, E., Croft, S., McKinley, B., Beardsley, A., Crosse, B., Emrich, D., Franzen, T. M. O., Gaensler, B. M., Horsley, L., Johnston-Hollitt, M., Kenney, D., Morales, M. F., Pallot, D., Steele, K., Trott, C. M., Walker, M., Wayth, R. B., Williams, A., & Wu, C. 2018, ApJ, submitted

Worden, S. P., Drew, J., Siemion, A., Werthimer, D., DeBoer, D., Croft, S., MacMahon, D., Lebofsky, M., Isaacson, H., Hickish, J., Price, D., Gajjar, V., & Wright, J. T. 2017, Acta Astronautica, 139, 98 . URL http://www.sciencedirect.com/science/article/pii/S0094576517303144

Science with a Next-Generation Very Large Array
ASP Conference Series, Monograph 7
Eric J. Murphy, ed.

DRAFT EDITION

Exo-space Weather in the Era of the ngVLA[1]

Rachel A. Osten,[1,2] Michael K. Crosley,[3] and Gregg Hallinan[4]

[1]*Space Telescope Science Institute, Baltimore, MD, USA;* osten@stsci.edu

[2]*Center for Astrophysical Sciences, Johns Hopkins University, Baltimore, MD, USA*

[3]*Physics & Astronomy Dept., Johns Hopkins University, Baltimore, MD, USA*

[4]*California Institute of Technology, Pasadena, CA, USA*

1. Introduction

With the announcement by the Kepler mission of more than two thousand confirmed transiting exoplanets, population statistics (Dressing & Charbonneau 2015) suggesting that the nearest non-transiting exoplanet in the habitable zone of its star is at a distance of 2.6±0.4 pc, with the nearest transiting exoplanet in the habitable zone at a distance of $10.6^{+1.6}_{-1.8}$ pc, and recent confirmation via radial velocity techniques of a planet in the habitable zone of our nearest star (Anglada-Escudé et al. 2016), astronomy is firmly in the age of exoplanets. This is an area which grabs the public's attention as well as unites professional astronomers, planetary scientists, and astrobiologists, in the search for life. Ground- (MEarth project) and space-based (TESS, PLATO) projects have as their primary goal the discovery of even more, closer transiting exoplanets, and large ground- and space-based projects like the James Webb Space Telescope and giant segmented mirror telescopes (E-ELT, TMT, GSMT) will characterize their atmospheres. Characterizing the atmospheres and environments of potentially habitable exoplanets will be a major focus of the astronomical community in the next ten to twenty years. During that time, we can expect that the phase space for exoplanet demographics will be fleshed out, with major inroads into understanding the interrelationship between planet properties and stellar properties. There will be many potentially habitable worlds, and one major question will be how to move beyond that potentiality into a more informed assessment of the likelihood of seeing an *inhabited* world.

Planetary habitability is a multi-faceted issue and depends not just on the planetary parameters, but is strongly influenced by the environment set by the host star. Space weather is an important factor to consider in assessing the type of environment which may exist on a distant exoplanet. Space weather broadly posed is the impact of the star's magnetic activity: the structure of the magnetosphere itself and its interplay with close-in planetary orbits; the nonradiative heating and enhanced levels of ultraviolet-extreme ultraviolet-X-ray (UV-XEUV) radiation; a steady stellar wind; and flares, energetic particles and coronal mass ejections produced during magnetic eruptions. For close-in planets, orbits crossing the Alfvén surface of the stellar magnetosphere would experience severe space weather (Garaffo et al. 2016, 2017). Space weather has potentially played a role in defining habitability within our own solar system. The long-term impact of such activity was recently established in dramatic fashion by the Mars Atmosphere and Volatile EvolutioN (MAVEN) mission, which confirmed that ion loss due to solar CMEs early in Mars history likely severely depleted its atmosphere (Jakosky et al. 2015). The nonlinear dependence of a star's XEUV radiation with time will impact planetary atmospheric loss processes (Johnstone et al. 2015), and stellar activity can create false positive signatures in biomarkers (Tian et al. 2014). The star can influence the planetary environment through radiation and particles. Stellar flaring and associated coronal mass ejections, a steady stellar wind, and star-planet magnetospheric interactions are all important factors in the space weather environments of these exoplanets. Radio emission is the only wavelength regime capable of placing direct constraints on the particle environment that stars produce, and adds significant information on the steady mass loss of nearby stars.

2. Mass Loss on the Lower Half of the Main Sequence

Stellar winds affect the migration and/or evaporation of exoplanets (Lovelace et al. 2008), and are important not only for understanding stellar rotational evolution, but it also their influence on planetary dynamos (Heyner et al. 2012). At present only indirect measures of cool stellar mass loss inform these topics. Mass loss in the cool half of the HR diagram, along/near the main sequence, has been notoriously difficult to detect directly, due in part to the much lower values of mass loss here compared to other stellar environments ($\dot{M}$ of 2× 10^{-14} solar masses per year for the Sun). Detection of Lyman α astrospheric absorption (Wood et al. 2004) does not detect the wind directly, but rather the bow shock created when the wind interacts with the local interstellar medium. This can only be done with high-resolution ultraviolet spectrographs in space; currently the Space Telescope Imaging Spectrograph on the Hubble Space Telescope, installed in 1997, is the only instrument capable of making such measurements. Non-detections of this feature do not provide upper limits to the stellar mass loss.

Cool stellar mass loss is characterized by an ionized stellar wind, whose radio flux can have a $\nu^{0.6}$ or $\nu^{-0.1}$ dependence if in the optically thick or thin regime, respectively. A direct measurement of stellar mass loss through its radio signature would be a significant leap forward not only for understanding the plasma physics of the stars themselves, but also for understanding what kind of environment those stars create. Previous attempts at a direct detection of cool stellar mass loss via radio emission have led to upper limits typically three to four orders of magnitude higher than the Sun's present-day mass loss, while indirect methods find evidence for mass loss rates comparable to or slightly higher than the Sun's present day mass loss rate (up to ~80 times solar $\dot{M}$; Fichtinger et al. 2017)

Initial work assessing the feasibility of the ngVLA's ability to detect directly the stellar winds of nearby cool, main sequence stars was done as part of the Bower et al. (2015) report of ngVLA Working Group 4. This brief work used analytic formulae in Drake et al. (1987), based on the expected optically thick and thin radio emission from an ionized stellar wind presented in Wright & Barlow (1975), and Panagia & Felli (1975); optically thick emission from an ionized stellar wind is expressed as

$$S_\nu = 1.6 \times 10^{11} \left(\frac{\dot{M}}{v_w}\right)^{1.33} \frac{\nu_5^{0.6} T_4^{0.1}}{d_{kpc}^2} \tag{1}$$

where S_ν is the predicted radio flux in mJy per beam, $\dot{M}$ is the mass loss rate in solar masses per year, v_w is the velocity of the stellar wind, ν_5 is the frequency normalized to 5 GHz, T_4 indicates the temperature of the solar wind in units of 10^4K, and d_{kpc} is the distance in kpc. As winds from late-type stars are presumed to originate in the open field lines of the outer corona, a coronal wind temperature of 10^6 or T_4=100 is used. We expand on these calculations to different frequencies in the expected ngVLA range, and incorporate demographics of the nearest stars using catalogues of nearby stars. We use the recent continuum sensitivities quoted for the ngVLA at a variety of frequencies as posted at `http://science.nrao.edu/futures/ngvla/concepts`, extended for a 12 hour integration. The stellar escape velocity is ~600 km s^{-1} for main sequence solar-like stars and cooler, and the minimum constrainable mass loss rate for this velocity is quoted in this memo. However, we note that recent results from studies of exoplanets (Vidotto et al. 2015 and others) have found evidence for hot Jupiters embedded in slower stellar winds than would be expected based on solar scalings, with expectations of a denser stellar wind than experienced by solar system planets. With this in mind, we explore a range of assumed wind speeds, from 100 to 1200 km s^{-1}.

2.1. Increasing the Look-back Time for Studying the Young Sun

Table 1 lists nearby commonly used solar analogs within 15 pc from the Sun, and their ages. Results from high spectral resolution UV data of nearby stars where astrospheric absorption is seen suggest that there is a power-law relationship between inferred mass loss and surface X-ray flux, with a limit in surface X-ray flux of about 10^6 erg cm^{-2} s^{-1}, above which no or significantly reduced mass loss is inferred (Wood et al. 2004). This limits the ability to constrain the mass-loss history of the Sun, using analogues. In particular, the lack of detection of this feature does not provide any quantitative constraints on the mass-loss of that star. Based on this work, the most active stars appear not to have strong winds; there is evidence via astrospheric detection towards the nearby young solar analog π^1UMa (Wood et al. 2014), with age estimates between 300 and 500 million years, of a weak wind from the young Sun.

There is tension between the results returned from the astrospheric detection method and the mass loss expected from stellar rotational evolution models. Stars are expected to lose angular momentum in a wind as their rotation decreases with time; the rate of rotation period decrease can be determined from distributions of rotation periods in clusters of known ages, while MHD wind models are required to interpret the implied mass loss rates which should accompany this. Johnstone et al. (2015) performed such calculations, suggesting that the stellar mass-loss rate can be parameterized as

$$\dot{M}_\star \propto R_\star \Omega_\star^{1.33} M_\star^{-3.36} \quad . \tag{2}$$

The results suggest that the Sun at young ages should have had a mass loss rate roughly an order of magnitude higher than it does today. Fichtinger et al. (2017) presented recent results obtained from the JVLA and ALMA for a sample of nearby stars. Results are shown in Figure 1. They expanded upon the earlier spherically symmetric wind models, and showed that a conical opening angle for the wind can reduce the mass loss rate implied from a given radio flux density by about a factor of two compared to the spherically symmetric case. Their upper limits for implied mass loss are still two to three orders of magnitude above the levels of mass loss implied from the rotational evolution models, which themselves are about an order of magnitude above the mass loss rate implied by the detection of astrospheric absorption from the nearby solar analogue

π^1 UMa. Results from the ngVLA will be able to make a significant leap in understanding the mass loss history of the Sun through its two order of magnitude improvement over what can be achieved at present with the JVLA. The strength of the ngVLA observations lie in the ability to provide direct constraints (either detections or upper limits) on the stellar wind mass loss; non-detections provide quantitative constraints on the mass loss rate, a marked difference from the astrospheric absorption method.

Table 1. Commonly used Solar Analogs and Potential ngVLA Mass-Loss Constraints

Name	Age (MY)	Distance (pc)	$\dot{M}$ constraint[1,2] ($\dot{M}_\odot$)
EK Dra	100	34	425
χ^1 Ori	300	8.7	55
π^1 UMa	500	14.3	116
κ^1Cet	650	9.2	60

[1] Using ngVLA sensitivity at 17 GHz, extrapolated for a 12 hour integration
[2] For $\dot{M}_\odot$=2×10^{-14} M$_\odot$ yr^{-1} and wind speed equal to escape speed

2.2. M Dwarfs in the Solar Neighborhood

After initial skepticism about the possibility of M dwarfs hosting exoplanets, attention is fully fixed on these cool dim stars. M dwarfs are the most common type of star in our galaxy, and recent results have shown a high occurrence rate of planets around M dwarfs. This makes planets around M dwarfs one of most common modes of planet formation in our galaxy. The magnetic activity of M dwarfs can have significant influence on the chemistry and dynamics of these planets' atmospheres due to the planets' close proximity to the star, and these effects may be observable with JWST (Venot et al. 2016). Recent results (Garaffo et al. 2016, 2017) have shown that the stellar magnetosphere influences the inner edge of the traditional habitable zone. In the case of the iconic TRAPPIST-1 system of seven planets, magnetospheric models suggest that all but two of these planets would have orbits crossing the Alfvén surface and thus would experience severe space weather. Thus consideration of the steady stellar wind as well as time-varying flares and coronal mass ejections from M dwarfs are vital components to understanding the complex intertwining that may or may not turn a potentially habitable planet into an inhabited planet. Current studies suggest that there are about 270 M dwarfs within 10 pc (Figure 2). Several of these are already known to host exoplanets; by the time that the ngVLA is operational, at the end of the 2020s, all of these will have have been surveyed for both close-in exoplanets (via the transit and radial velocity methods), and those in more distant orbits (by coronography). Radio observations to constrain the mass loss from a steady stellar wind will be crucial measurements to add to the mix to understand the impact the star may have on exoplanet companions.

Very little is known observationally about the mass-loss of nearby M dwarfs. The nearby, magnetically active M dwarf EV Lac is one exception, having had an astrospheric detections from Lyman α absorption. The inference is for a mass loss rate of only 0.7 times the solar mass loss rate, after correcting the results of Wood et al. (2004)

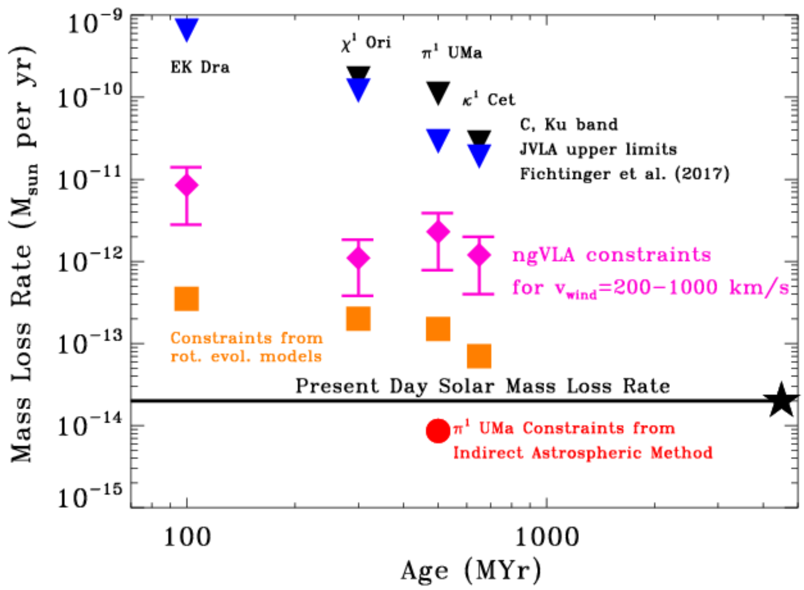

Figure 1. Summary of current mass loss constraints for nearby solar analogs, along with prospects achievable with the ngVLA. Black and blue triangles indicate upper limits from C and Ka bands obtained with the JVLA (Fichtinger et al. 2017) for spherically symmetric winds; orange squares show mass loss constraints from the rotational evolution models of Johnstone et al. (2015); and red circle shows detection from the indirect method of inferring mass loss via astrospheric absorption (Wood et al. 2014). Magenta diamonds and error bars display the grasp of the ngVLA, for wind velocities spanning 200-1000 km s^{-1}. The present-day solar mass loss rate is 2×10^{-14} $\dot{M}$ yr^{-1}.

for the much smaller surface area of EV Lac. Wargelin & Drake (2001) presented a different method for detecting stellar winds, which makes use of an X-ray charge exchange halo which should exist between the highly charged ions in the stellar wind and the surrounding ISM. This method is promising; they were able to provide an upper limit to the mass loss rate of Proxima at 3×10^{-13} $M_\odot$ yr^{-1}, with approximately a factor of three uncertainty in their model. This requires the use of a space-based X-ray observatory with sufficient sensitivity and spatial resolution to resolve this emission from the stellar coronal emission, expected to be thousands of times stronger (the spatial resolution is required to discern this signature in the wings of the coronal PSF). This may be a complementary approach to the detection of radio emission of an ionized stellar wind, possible with the Lynx mission concept under study by NASA with 50 times Chandra's sensitivity and Chandra-like angular resolution. Because of the angular resolution requirement, it is most competitive for stars within about 5 pc.

The method of detecting radio emission from nearby M dwarfs will be an important contributor to understanding how the wind environment of nearby M dwarfs contributes to the habitability of orbiting exoplanets. Figure 3 shows the sensitivity of the ngVLA to detecting radio emission from an ionized stellar wind for M dwarfs within 10 pc, using similar methods as described in the above section for the mass loss history of the Sun. The green triangle depicts the constraint on mass loss rate for the nearest M dwarf, Proxima, described above, along with the estimated uncertainty in the

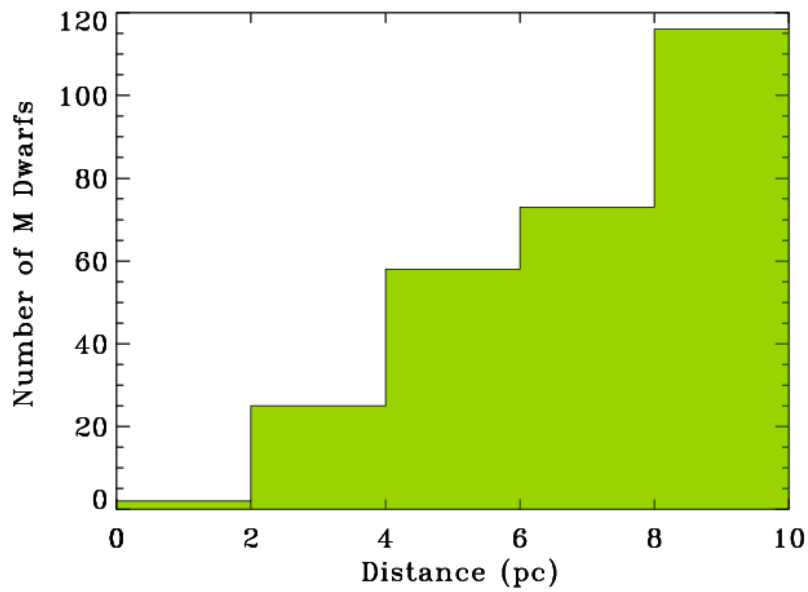

Figure 2. Number of M dwarfs as a function of distance, from the REsearch COnsortium of Nearby Stars (RECONS). There are more than about 270 M dwarfs within 10 pc; several of these are known to host exoplanets and by the time of the late 2020s all of these will have been surveyed for close-in exoplanets. An important constraint for further characterization of these exoplanets will be the extent to which the star makes its proximate environment helpful or harmful for habitability.

model. The red circle shows the mass loss rate in solar masses per year for the nearby M dwarf EV Lac, as obtained from the detection of astrospheric absorption.

Sensitive, broadband observations of a small sample of the highest priority stellar systems, hosting terrestrial planets in the habitable zone, could potentially detect discrete mass ejection events. The most likely scenario is for an inactive mid-M dwarf at a distance of ~3 pc. The expected rate of large flares (radiated energy 5×10^{29} - 5×10^{32} erg) is one per week, with an estimated associated CME mass loss of 10^{-18} – $-10^{-15}M_{\odot}$/year (Osten & Wolk 2015). This will result in an increased flux of bremsstrahlung emission (optically thick in ngVLA bands) with flux densities at 30 and 80 GHz that range from 0.05-50 μJy and 0.2-200 μJy respectively, assuming equipartition between flare bolometric energy and CME kinetic energy. Large bandwidth ($\nu/\Delta\nu \sim 1$), either instantaneously or via rapid transition between observing bands, is essential to separate the CME-produced bremsstrahlung from other components of the stellar emission, such as coronal gyrosynchrotron emission. This is also aided by observations at the higher frequencies (> 50 GHz) where the bremsstrahlung will dominate over gyrosynchrotron. Observations in Stokes V can also be used to separate contaminating components from the signal. ngVLA observations will be most efficient if observing only the largest CME events (few per year per star). Such observations can be scheduled via external triggers from telescopes monitoring the stellar sample for large flares. Rapid response (< 15 minutes) is essential to this scheme.

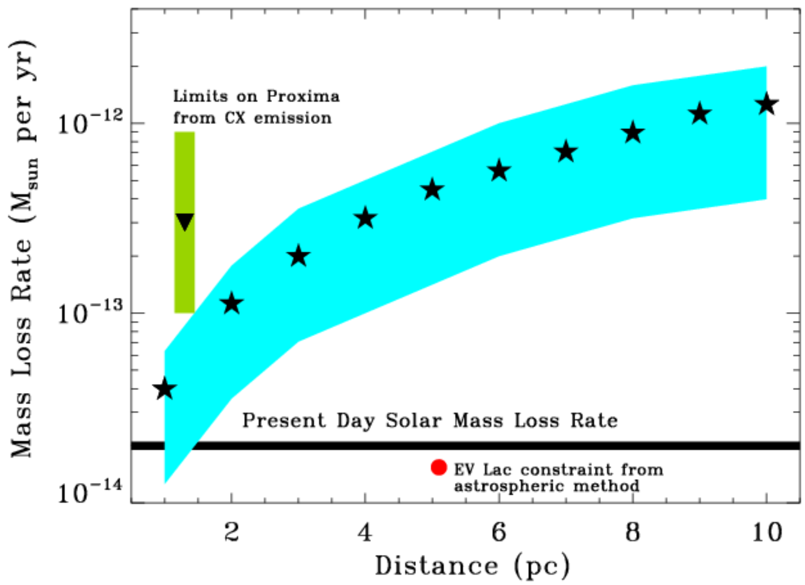

Figure 3. Regions of stellar mass loss rate which can be constrained by a 12 hour ngVLA integration for studies of radio emission from an ionized stellar wind, for M dwarfs at a range of distances from 1-10 pc. Stars indicate expected amount of optically thick emission at 28 GHz from a spherically symmetric wind with wind velocity equal to the escape velocity, and cyan shaded region gives area encompassed by a range of assumed wind velocities, from 200 - 1000 km^{-1}. Current observational limits on M dwarf wind mass loss are indicated at the distance of the objects: the green triangle indicates the upper limit for Proxima based on limits from charge exchange emission (Wargelin & Drake 2001), along with the uncertainty in their model. The stellar wind mass loss rate implied by the detection of Lyman α astrospheric absorption towards the M dwarf EV Lac at 5.1 pc is also indicated.

2.3. Interpretation of Radio Emission

While measurements of radio emission from point sources are easy to undertake, their interpretation is complicated. The calculations in the above sub-sections have been performed under the assumption of optically thick emission, in which case the emission increases as $\nu^{0.6}$. The commonly observed gyrosynchrotron emission from radio active stars typically has a peak frequency near 10 GHz, with flat or slightly negative spectrum at higher frequencies. Indeed, the upper limits returned by Fichtinger et al. (2017) were obtained after careful removal of observed variable emission attributed to gyrosynchrotron emission. The peak frequency is a function of activity, so observations at higher frequencies are necessary to separate any wind emission from these other sources. At even higher frequencies such as those probed by ALMA, stellar chromospheric emission is detected. Thus the region between 10 and 100 GHz is ideal for searching for wind emission from nearby stars.

The stellar wind must be optically thin to nonthermal radio emission originating closer to the stellar surface. The time-averaged mass-loss from coronal mass ejections, considered a component of a stellar wind, can not be higher than a steady spherically symmetric stellar wind. Both Drake et al. (2013) and Osten & Wolk (2015) have argued for a high flare-associated transient mass loss from active stars; for the young solar analog EK Dra flare-associated CME-induced mass-loss rate of 4×10^{-11} $M_\odot$ yr^{-1}. The mass loss rate of M dwarfs is expected to vary widely as a function of magnetic activity, with flare-associated mass loss rates of 10^{-12} and 10^{-11} $M_\odot$ yr^{-1} for the active M dwarfs AD Leo and EV Lac, respectively, both at distances of about 5 pc. Constraints from ngVLA measurements would be below both of these numbers, and would provide a robust constraint on the breakdown of flare-CME connections, as implied in Crosley et al. (2018ab). Instrument requirements are a large enough bandwidth to disentangle different contributions to the spectral energy distribution and mitigate variability expected to dominate in the lower frequency bands, and circular polarization for additional constraints on ruling out nonthermal emission.

3. Particles and Fields: Contribution to Exo-Space Weather

Habitability studies are interested in the flux of accelerated particles directed outward from the stellar surface; the most energetic ones are the most impactful to an exoplanetary atmosphere. Studying the population of accelerated particles near the stellar surface can provide details of the particle spectrum. Comparison to well-studied solar events enables systematics with respect to scalings or extrapolations used for stellar space weather calculations to be investigated. Segura et al. (2010) investigated the impact on the ozone layer of a superflare from an M dwarf. The energetic particles can deplete the ozone layer of a planet in the habitable zone of an Earthlike planet around an M dwarf experiencing a superflare.

Radio observations provide the clearest signature of accelerated particles and shocks in stars arising from transient magnetic reconnection, and provide more realistic constraints on these factors than scaling by solar values (Osten & Wolk 2017). Optically thin gyrosynchrotron emission constrains the index of the accelerated particles, and also enables a constraint on magnetic field strengths in the radio-emitting source (Smith et al. 2005, Osten et al. 2016). The peak frequency is about 10 GHz, so observations at higher frequencies are necessary to disentangle optical depth effects from the interpretation.

3.1. Radio-Active Cool Stars

Variable stellar radio emission in the cool half of the HR diagram is more typical than steady flux levels, at least at microwave frequencies. This is a consequence of the dominance of emission from accelerated particles, and an indicator of the nonsteady levels of particle acceleration, varying as a function of position on the stellar disk and time. While previous studies estimating the contribution of stellar magnetic reconnection flaring from different types of active stars have used average or “typical" flux densities, the existence of extreme levels of variability (up to 1-2 orders of magnitude) make this approach susceptible to biases. The timescales for stellar flares can vary from milliseconds, in the case of some highly circularly polarized radio bursts (Osten & Bastian 2006, 2008), to minutes to many hours or days for the most dramatic examples (Richards et al. 2003).

We examined objects characteristic of their class for several types of radio-active cool stars illustrating a large amount of variability. This included Algol, RS CVn, and BY Dra active binaries, and nearby magnetically active mid-M and late-M dwarf stars. We used a radio luminosity distribution which gives the range of radio emission expected to be observed for each type of object, under the assumption that the flux variation seen in one object is typical of the class. Figure 4 shows this time-domain information recast as a cumulative probability distribution for each object. The time-domain information for Algol, HR 1099, σ^2CrB, and UX Ari is taken from multi-year monitoring with the Green Bank Interferometer (Richards et al. 2003). The M dwarf distribution comes from extensive 8 GHz light curves of the nearby M dwarf EV Lac (Osten et al. 2005, Osten et al. in prep.), while the ultracool dwarf LP349-25 was used for the distribution of radio luminosities for ultracool dwarfs (Ngoc et al. 2007, Osten et al. 2009). For young stellar objects, the radio luminosity distribution was obtained from the 556 sources detected in the deep centimeter wavelength catalog of the Orion Nebula Cluster (Forbrich et al. 2016). For this sample, objects with negative spectral index were removed as potential contaminating extragalactic sources, and the distribution of radio luminosities for the remaining 478 sources was computed.

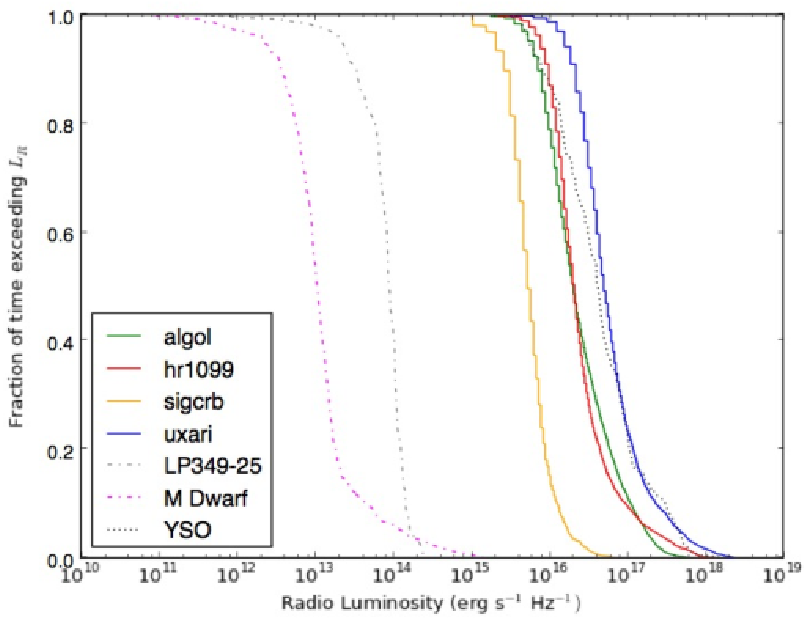

Figure 4. Cumulative distributions of 8 GHz cm radio luminosities for different categories of variable cool stellar objects: red, blue, yellow, and green histograms are active binary systems (Algol and RS CVn-type systems); the purple dashed histogram is the result of several multi-wavelength campaigns of the M dwarf flare star EV Lac (Osten et al. 2005, Osten et al. in prep.); grey red dotted histogram is the result of several monitoring observations of the ultracool dwarf LP349-25 (Ngoc et al. 2007, Osten et al. 2009); gray dotted histogram is the results of a deep centimeter-wavelength catalog of the Orion Nebula Cluster (Forbrich et al. 2016). Converting these to probability distributions enables a more realistic assessment of the likelihood of observing a given radio luminosity, and hence detectability of these types of radio sources, than averages or maximum luminosities.

We used demographic information and space densities (listed in Table 2) to come up with a likelihood of observing a given radio luminosity level for types of stars at a given distance. This is more probabilistic and represents reality better than taking the largest radio luminosity of a given type, assuming that that is characteristic level of radio emission, and projecting that to find the farthest distance to which the system is sensible, to arrive at source numbers. An rms for given frequency and integration time determines the distance to which an observation is sensitive, for a source of a particular radio luminosity,

$$L_R = F_{3\sigma} 4\pi d_{\rm sens}^2 \tag{3}$$

with L_R the radio luminosity, $F_{3\sigma}$ the flux density density sensitivity, and $d_{\rm sens}$ the resulting sensitivity distance. Then, the number of stars is

$$\#Stars = \left(\frac{f_{\rm sky}}{4\pi}\right)\frac{4\pi n_{\rm obj}}{3}\left(\frac{L_R}{4\pi F_{3\sigma}}\right)^{3/2} P(L_R) \tag{4}$$

where $f_{\rm sky}$ is the fraction of the sky visible from the ngVLA site, ≈ 10.3 steradian (Condon et al. 1998), $n_{\rm obj}$ is the space density of the type of star, L_R the radio luminosity, $F_{3\sigma}$ the sensitivity threshold, and $P(L_R)$ the probability of the stellar object having that luminosity. We realize that the assumption of spherical geometry will break down at the scale of the Milky Way thick disk, or 1 kpc, but this treatment gives a simplified approach to the maximum distance detectable. Figure 5 plots the number of stars detectable with the ngVLA as a function of radio luminosity, using the radio luminosity distributions shown in Figure 4. Only luminosity ranges available from the data shown in Figure 4 are used, and inflections in the radio luminosity distribution show up as departures from the $\propto L_R^{3/2}$ trend of number of stars as a function of radio luminosity in Figure 5. The active binary systems have larger intrinsic radio luminosities than the M dwarf classes.

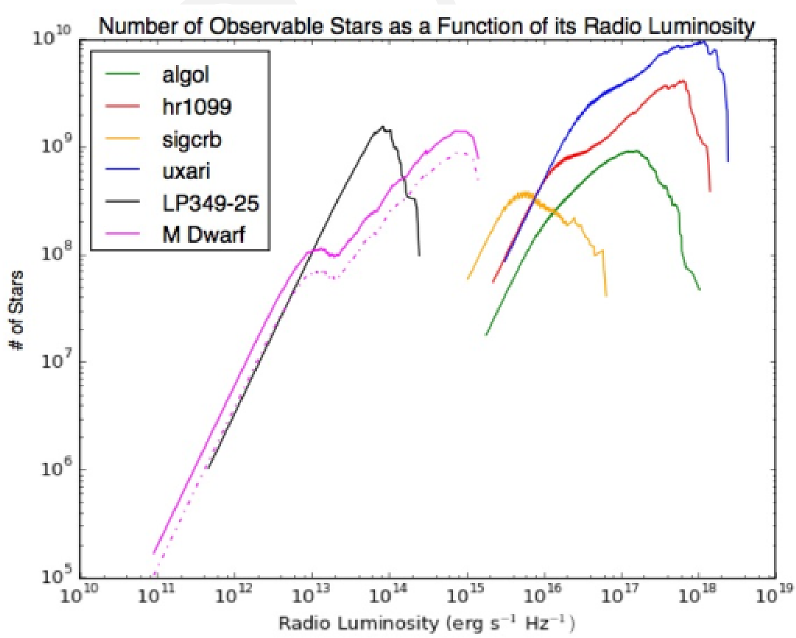

Figure 5. Number of stars detectable with the ngVLA as a function of radio luminosity, using the radio luminosity distributions shown in Fig. 4, for a . five minute integration at a frequency of 10 GHz.

Figure 6 shows the number of stars detectable as a function of distance. Here the distance at which the trend for each type of star flattens indicates the distance at which the smallest radio luminosity present in Figure 4 is no longer detected. All stars are detectable at small distances, and the number scales as distance^3. Eventually only the brighter stars are able to be detected at farther distances, so the rate of additional star counts decreases until no more stars would be detected at the largest distances. The calculation for M dwarfs used two different space density values as listed in Table 2.

Table 2. Categories of radio-active cool stars and references to their space densities.

Category	Space Density stars pc^{-3}	Reference
active binaries	3.7×10^{-5}	Favata et al. (1995)
early-mid M dwarfs	0.08	Reid et al. (2007)
	0.05	Reid et al. (2008)
ultracool dwarfs	0.013	Reid et al. (2008)

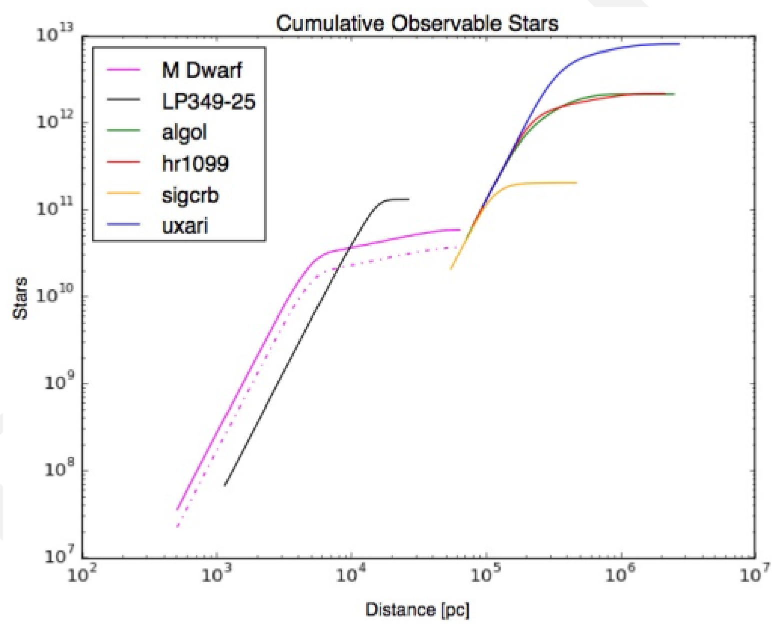

Figure 6. Cumulative number of stars observable as a function of distance.

Our approach for YSOs differed slightly. Since YSOs are found in clusters at discrete distances, for this population, we estimated the fraction of sources which would be detectable in a cluster similar to the ONC but placed further away. For these purposes we used the ngVLA's continuum rms in one hour at 8 GHz to set the percent of sources detected for a 3σ detection. Figure 7 displays the result of this calculation, and demonstrates that 100% of the sources could be recovered in clusters at 2 kpc distance, sufficient to characterize many of the typical radio-emitting sources in star forming regions located in the nearest parts of the Sagittarius and Perseus arms of our galaxy.

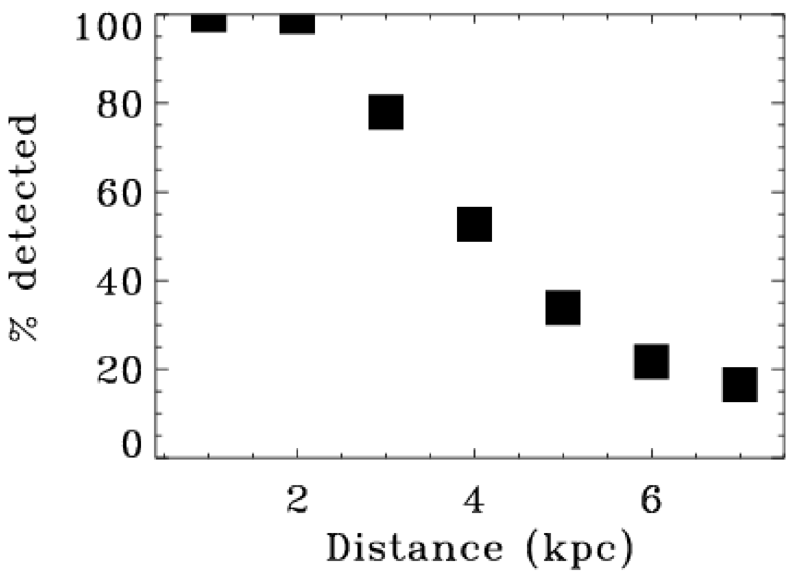

Figure 7. Percentage of the 478 radio sources detected in the deep exposure of the Orion Nebula Cluster reported by Forbrich et al. (2016), for clusters at various distances. Sensitivities appropriate to a one hour 8 GHz observation with the ngVLA are used.

3.2. Constraining Particle Distributions and Magnetic Fields in Magnetic Reconnection Flares

Radio observations provide a unique way to characterize the nature of the accelerated electron population near the star. This is important for understanding the radiation and particle environment in which close-in exoplanets are situated.

An aspect of star-planet interactions which can be probed with radio observations is the magnetospheric interactions of a magnetized close-in planet with its host star. Similar to the idea that the proximity of two stellar magnetospheres due to close passage can cause periodic episodes of magnetic reconnection (as in Massi et al. 2006), recent results (Pilliterri et al. 2014) have suggested a triggering mechanism for regularly recurring stellar flares on stars hosting close-in exoplanets (hot Jupiters). For radio wavelength observations, the time-dependent response of radio emission reveals the changing nature of the magnetic field strength and number and distribution of accelerated particles. As stellar radio emission typically has a peak frequency near 10 GHz, a wide bandwidth system spanning this range can probe the optically thick and thin conditions, diagnose the changing conditions during the course of a magnetic reconnection flare associated with close passage of an exoplanet, and deduce the nature of the accelerated particle population through measurements of spectral indices from confirmed optically thin emission. This would provide constrains on the accelerated particle population of close-in exoplanets unavailable from any other observational method; such a constraint is necessary to perform detailed modeling of the atmospheres of such exoplanets, due to the influence of accelerated particles in affecting the chemical reactions in terrestrial planet atmospheres (Jackman et al. 1990).

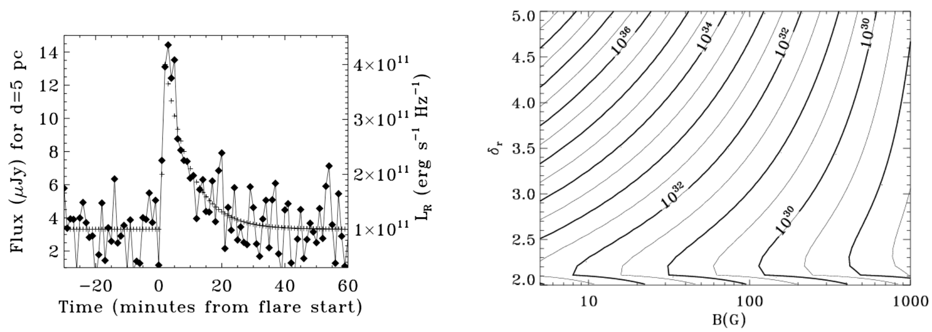

Figure 8. (*left*) Light curve of a short duration (lasting 5 minutes), small enhancement (factor of three increase above quiescence) flare on a nearby (5 pc) star. Right yaxis gives intrinsic radio luminosity, left axis gives the estimated radio flux density at 17 GHz. Noise is estimated in each 1 minute bin by offsetting the flux by a random number times the expected rms values. (*right*) Contour plot of δ_r, the index of accelerated particles, and B, the magnetic field strength in the radio-emitting source, for the radio flare seen above.

Smith et al. (2005) and Osten et al. (2016) laid out the basic framework for such a measurement, which requires multi-wavelength observations of the radio flare and its counterpart at higher energies. The uniqueness of the measurement lies in the difficulty in determining the characteristics of accelerated particles in nondegenerate environments in the cool half of the HR diagram. The usual technique for solar physicists is to deconvolve hard X-ray spectra exhibiting optically thin measurements of nonthermal bremsstrahlung emission to determine the power-law index of the accelerated electrons and source size. Because of astrophysical detector sensitivity coupled with typically hot thermal flaring plasma, this observational method has not yielded results in stellar cases. Radio constraints on accelerated particle characteristics are therefore the only measurement technique that will yield results for planet-hosting stars in the solar neighborhood.

The integrated radio flare energy provides a constraint on the accelerated particle kinetic energy, under the assumption of optically thin emission. The radio light curve provides constraints on both the index of the distribution of accelerated particles, as well as the magnetic field strength in the radio-emitting source. The contour plot of δ_r, the index of accelerated particles, versus the magnetic field strength in the radio-emitting source as a function of kinetic energy in the accelerated particles in a stellar superflare reported in Osten et al. (2016) was for an event with a peak radio luminosity at 15 GHz of $5{\times}10^{16}$ erg s^{-1} Hz^{-1}. Based on Figure 5, there are numerous M dwarfs detectable with the ngVLA at the lower radio luminosity end, near 10^{11-12} erg s^{-1} Hz^{-1} for which similar analyses could be performed. Using the same methodology, we worked out the sensitivity to a radio flare with a peak flare enhancement of only 3 times this base level, for a flare lasting only 5 minutes total duration. Such an example is shown in the top part of Figure 8. These types of observations would be most sensitive to the nearest M dwarfs, in order to study time-variable emission over very short timescales (minutes). Quiescent radio luminosities as low as 10^{11} erg s^{-1} Hz^{-1} (at the limit of current detection capabilities; Osten et al. 2015) would be detectable in short integrations, allowing for study of small enhancement events only factors of a few larger. The kinetic energies probed here are moderate to large sized solar flares, and probe magnetic field strengths in the tens to hundreds of Gauss level.

A wide bandwidth system spanning the 10-20 GHz range can probe the optically thick and thin conditions, diagnose the changing conditions during the course of a magnetic reconnection flare associated with the close passage of an exoplanet, and deduce the nature of the accelerated particle population through measurements of spectral indices from confirmed optically thin emission. Operation of multiple subarrays would enable the frequency coverage available simultaneously to be significantly expanded. This would provide constraints on the accelerated particle population of close-in exoplanets unavailable from any other observational method; such a constraint is necessary to perform detailed modeling of the atmospheres of such exoplanets, due to the influence of accelerated particles in affecting the chemical reactions in terrestrial planet atmospheres.

4. Summary

The influence that stars have on their near environments is a timely research topic now, and is expected only to grow in the future as exoplanet discoveries grow. While we expect that new discoveries in this area in the next decade will fill in some areas where we currently lack insight, there will remain gaps in our knowledge which can only be filled by a next generation sensitive radio telescope operating in the deka-GHz range. Observations with the SKA at lower frequencies will be sensitive to magnetic and plasma emissions from stars, and will be able to study magnetic reconnection flaring and associated radio emission variability. The emphasis on lower frequencies with the SKA, however, means that the studies discussed here will not be possible to undertake with SKA observations due to optical depth effects and frequency dependence of the emission.

References

Anglada-Escudé, G. et al. 2016 Nature, 536, 437
Bower, G. et al. 2015 arXiv 1510.06432
Condon, J. et al. 1998 AJ 115, 1693
Crosley, M. K. & Osten, R. A. 2018a ApJ 856, 39
Crosley, M. K. & Osten, R. A. 2018b ApJ, submitted
Drake, S. A. et al. 1987 AJ 94, 1280
Drake, J. et al. 2013 ApJ 764, 170
Dressing, C. & Charbonneau, D. 2015 ApJ 807, 45
Favata, F. et al. 1995 A&A 298, 482
Fichtinger, B. et al. 2017 A&A 599, 127
Forbrich, J. et al. 2016 ApJ 822, 93
Garraffo, C. et al. 2016 ApJ 833, L4
Garraffo, C. et al. 2017 ApJ 843, L33
Heyner, D. et al. 2012 ApJ 750, 133
Jackman, C. H. et al. 1990 JGR 95, 7417
Jakosky, B. et al. 2015 Science 350, 0210
Johnstone, C. P. et al. 2015 A&A 577, 28
Lovelace, R. et al. 2008 MNRAS 389, 1233
Massi, M. et al. 2006 A&A 453, 959
Ngoc, P. et al. 2007 ApJ 658, 553

Osten, R. A. & Bastian, T. 2006 ApJ 637, 1016
Osten, R. A. & Bastian, T. 2008 ApJ 674, 1078
Osten, R. A. et al. 2005 ApJ 621, 398
Osten, R. A. et al. 2009 ApJ 700, 1750
Osten, R. A. et al. 2016 ApJ 832, 174
Osten, R. A. & Wolk, S. J. 2015 ApJ 809, 79
Osten, R. A. & Wolk, S. J. 2017 IAUS 328, 243
Panagia, N. & Felli, M. 1975 A&A 39, 1
Pilliterri, I. et al. 2014, ApJ 785, 145
Reid, I. N. et al. 2007AJ 133, 2825
Reid, I. N. et al. 2008 AJ 136, 1290
Richards, M. et al. 2003 ApJS 147, 337
Segura, A. et al. 2010 AsBio 10, 751
Smith, K. et al. 2005 A&A 436, 241
Tian, F. et al. 2014 E&PSL 385, 22
Venot, O. et al. 2016 ApJ 830, 77
Vidotto, A. et al. 2015 MNRAS 449, 4117
Wargelin, B. J. & Drake, J. 2001 ApJ 546, L57
Wood, B. E. et al. 2004 AdSpR 34, 66
Wood, B. E. et al. 2014 ApJ 781, L33
Wright, A. E. & Barlow, M. J. 1975 MNRAS 170, 41

Science with a Next-Generation Very Large Array
ASP Conference Series, Monograph 7
Eric J. Murphy, ed.

DRAFT EDITION

Prebiotic Molecules

Brett A. McGuire,[1] P. Brandon Carroll,[2] and Robin T. Garrod[3]
[1]*National Radio Astronomy Observatory, Charlottesville, VA, 22903;* `bmcguire@nrao.edu`

[2]*Harvard-Smithsonian Center for Astrophysics, Cambridge, MA, 02138;* `paul.carroll@cfa.harvard.edu`

[3]*University of Virginia, Charlottesville, VA, 22904;* `rgarrod@virginia.edu`

Abstract. We aim to greatly expand our understanding of the molecular inventory of prebiotic molecules and their chemical evolution by leveraging the ngVLA?s unique capabil ities to detect new complex organic molecules. Informed by state-of-the-art chemical models, we will search for N, O, and S-bearing small aromatic molecules, direct amino acid precursors, biogenic species such as sugars, and chiral molecules well beyond the reach of modern facilities.

1. Introduction

Extraterrestrial amino acids, the chemical building blocks of the biopolymers that comprise life as we know it on Earth are present in meteoritic samples. More recently, glycine (NH_2CH_2COOH), the simplest amino acid, was detected by the Rosetta mission in comet 67P. Despite these exciting discoveries, our understanding of the chemical and physical pathways to the formation of (pre)biotic molecules is woefully incomplete. This is largely because our knowledge of chemical inventories during the different stages of star and planet formation is incomplete. It is therefore imperative to solidify our accounting of the chemical inventories, especially of critical yet low-abundance species, in key regions and to use this knowledge to inform, expand, and constrain chemical models of these reactions. This is followed naturally by a requirement to understand the spatial distribution and temporal evolution of this inventory. Here, we briefly outline a handful of particularly-impactful use cases in which the ngVLA will drive the field forward.

2. Expanding Chemical Inventories: Pushing cm-wave Chemical Complexity to the Confusion Limit

Existing facilities in the (sub-)millimeter regime, particularly ALMA, are capable of reaching the line-confusion limit in molecular line surveys of the richest interstellar sources in a matter of hours. That is, the density of molecular lines in the resulting spectra is such that there is at least one spectral line every FWHM; there are no line-free channels. When line-confusion is reached, no additional information can be gained

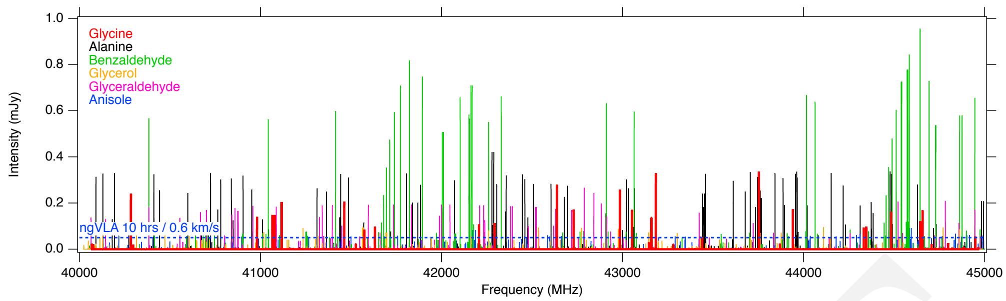

Figure 1. Simulation of six complex organic molecules in a 5″ source at $T_{\mathrm{ex}} = 100$ K, $\Delta V = 3$ km s^{-1}, and $N_T = 5 \times 10^{13}$ cm $^{-2}$. The simulation assumes the source completely fills the beam. Glycine transitions have been shown in **bold red** for emphasis. The approximate noise level of a 10 hour ngVLA integration with 0.6 km s^{-1} resolution is shown as a dashed blue line.

from longer integration times at the same spatial resolution. We are rapidly approaching the point at which deep drill observations with ALMA and the GBT will no longer produce new spectral lines in the richest sources.

In the cm-wave regime, however, the most sensitive survey (PRIMOS) with the most sensitive facility (the GBT) toward the most line-rich source (Sgr B2) has lines in only ∼10-20% of its channels. Diminishing returns on sensitivity for this survey have already set in with an RMS of ∼2.75 mJy/beam (in ∼0.2 km/s channels) - to increase the sensitivity substantially would require hundreds of hours of dedicated observations for every ∼2 GHz window. With the higher sensitivity of the ngVLA, at interferometric resolutions better matched to the size of the cores in this source (∼1–5″), we can reach the line-confusion limit in this survey, which we project will set in around 100 μJy/beam RMS. These RMS values are reachable with the ngVLA, on appropriate spatial scales, in 4-10 hours.

Observation of a substantial number of predicted, but as yet undetected, complex prebiotic species are needed to truly understand chemical evolution toward glycine and other biogenic molecules. State-of-the-art models predict these molecules will display emission lines with intensities that are easily detectable with the ngVLA, but well below the current detectability thresholds of ALMA, GBT, IRAM, etc. Figure 1 below shows simulations of a representative set of the types of molecules whose discovery will be enabled by the ngVLA: N, O, and S-bearing small aromatic molecules, direct amino acid precursors, biogenic species such as sugars, and chiral molecules.

3. Grasping for Truly Biogenic Species: Glycine and Glyceraldehyde

The detection and characterization of glycine and glyceraldehyde (the simplest sugar) would be transformational for the field. Using state-of-the-art chemical models combined with observationally-constrained physical conditions and temperature-density profiles, we have simulated the expected intensity of the rotational transitions of these molecules toward two high-profile targets: Sgr B2(N) and IRAS 16293.

For glyceraldehyde, we predict intensities of 100–200 μJy/beam toward Sgr B2(N), which puts it within reach for the ngVLA with a dedicated observing session, although many lines will be at or around the confusion limit. By contrast, we expect that the emission in IRAS 16293 is likely to be too weak. For glycine, intensities at the lower end of the ngVLA frequency range (<10 GHz) are unlikely to be sufficient for detection, even with the ngVLA, while intensities at mm-wave frequencies are at or below the current line-confusion limit. In the heart of the ngVLA range (10 – 50 GHz), however, our models predict line intensities of order ~500 μJy/beam in Sgr B2(N). This offers substantial room for variance in the actual abundance while still remaining detectable, but only with the sensitivity and spatial resolution of the ngVLA.

In IRAS 16293, a population of glycine at the abundances predicted by our chemical model is likely beyond the reach of even the ngVLA. However, the cold chemistry in this region is not as well-matched to the hot core model of Garrod (2013) used here, and a more optimistic abundance estimate, based on the detected abundance of glycine in comet 67P by Altwegg et al. (2016), indicates transitions of up to ~1 mJy/beam (at 0.2″ resolution) are possible. These values are only realistically achievable with the ngVLA.

4. Explorations of Interstellar Chirality

Chiral molecules, that is, molecules whose mirror image is not identical to the original, are central to biological function. Molecular chirality has a profound effect on the structure and function of biological molecules, as a result of nature's use of only one of the mirror images in biological processes (a concept known as homochirality). There is no energetic basis for the dominance in life of one handedness of a chiral molecule over another. Rather, a plausible explanation is that the slight primordial excess of one handedness was inherited from the nascent molecular inventory and subsequently enhanced and enriched catalytically by life. Material in molecular clouds from which planetary systems form is processed through circumstellar disks, and can subsequently be incorporated into planet(esimal)s. Thus, a primordial excess found in the parent molecular cloud may be inherited by the fledgling system. The detection of chiral molecules toward molecular clouds is therefore key to advancing our understanding of this process. Chiral molecules, like other complex species detected earlier, are necessarily large, with propylene oxide, the only detected chiral species to date (McGuire & Carroll et al. 2016), being perhaps the only example simple enough for detection with existing facilities. The ngVLA will provide the sensitivity and angular resolution required to detect additional, biologically-relevant chiral species, such as glyceraldehyde.

Indeed, one possible route to generate a chiral excess is through UV-driven photodissociation of chiral molecules by an excess of left or right circularly polarized light. The ability not only to detect, but to image the abundance of chiral species at spatial scales commensurate with observations of circularly polarized light toward star-forming regions would be an immense leap forward. Using known, polarization-dependent photodissociation cross sections from laboratory studies, these observations would enable quantitative estimates of potential UV-driven excess. While such studies are well beyond the capability of existing observatories, they would be achievable with the ngVLA.

5. Uniqueness to ngVLA Capabilities

As discussed above, the cm-wave regime is an under-explored, but extraordinarily-rich wavelength regime for prebiotic chemical studies. Existing facilities in this wavelength range, particularly the GBT and VLA, have produced stunning scientific results, but they have nearly reached the limits of their capabilities in this area, particularly in their sensitivity. The GBT beam is poorly matched to compact sources and suffers incredibly from beam dilution, while the VLA lacks the raw collecting area. Finally, the Band 1 receivers at ALMA will cover only a portion of the critical 10–50 GHz range necessary to enable this science, and at far worse brightness sensitivity. The ngVLA is the only facility, extant or planned, that can unlock the specific science goals outlined above at these frequencies.

6. Synergies at Other Wavelengths

The complex chemistry described here, which is detected and probed through gas-phase observations, has its genesis in the icy mantles of dust grains. As a protostar turns on and warms the surrounding medium, or through the passage of shocks, these ices and the complex molecules that formed within them, are liberated into the gas phase where they are detected. Observational studies of these ices are extraordinarily limited, and no species more complex than methanol (CH_3OH) has been detected. This will change with the launch of the JWST, which will enable the study of a far larger sample of molecular ices, with far greater complexity than is currently possible. The interpretation of these observations, and their synergy with gas-phase molecular inventories and observations, will rely upon the types of ngVLA observations outlined here.

References

Altwegg, K, Balsiger, H., Bar-Nun, A., Bertheller, J.J., Bieler, A. et al. 2016 Science Advances 2, e1600285

Garrod, R. T. 2013 ApJ 765, 60

McGuire, B.A. & Carroll, P.B. et al. 2016 Science 352, 1449.

Part V

Stellar Systems and Formation:

Science with a Next-Generation Very Large Array
ASP Conference Series, Monograph 7
Eric J. Murphy, ed.

DRAFT EDITION

Stellar Activity on Red Giant and Supergiant Stars: Mass Loss and the Evolution of the Stellar Dynamo.

Graham M. Harper,[1]
[1]*Center for Astrophysics and Space Astronomy, University of Colorado Boulder, CO, USA;* graham.harper@colorado.edu

1. Context

Cool stars have vigorous sub-photospheric convection zones that lead to turbulent motions in their photospheres, and in the layers above. The interaction of surface magnetic fields (e.g., Auriére et al. 2015) and dynamic ionized plasma leads to complex phenomena including starspots, active regions, chromospheres, and stellar outflows. These manifestations of *Stellar Activity* (Schrijver & Zwaan 2000) are not well understood but have important astrophysical consequences, ranging from the effects of mass loss on galactic structure and chemical evolution, the nature of space-weather for exo-planets orbiting red giants, to the effects of cool supergiant mass-loss history on the interpretation of early-time supernovae spectra (e.g., Dessart et al. 2017). Theoretical models have not been able to reproduce observational signatures of stellar activity, and progress is being led by state-of-the-art observations made at the highest spatial resolution and with the greatest sensitivity.

Thermal radio continuum observations are powerful diagnostics in this context because the atomic cross-sections are very accurately known (Hummer 1988) and the emission source term is the Planck function, which is linear in electron temperature. For example, resolved VLA images provided a ground breaking discovery and new insights into red supergiant (RSG) outflows with the finding by Lim et al. (1998) that Betelgeuse's extended atmosphere is cooler and much less ionized than predicted by leading theoretical and semi-empirical models of the time (see Hartmann & Avrett 1984; Harper et al. 2001).

However, red giants and supergiants are not strong radio emitters and have relatively small angular sizes so that future progress requires greater sensitivity *and* higher spatial resolution. The ngVLA will be able to provide both of these.

2. Mass Loss

Red giants and RSGs return mass that is enriched by nuclear processing back into the interstellar medium, supplying giant molecular clouds that may host the next generation of star formation, and leading to new stars and their exo-planets. The rate at which mass is returned by cool stars is, to a first approximation, proportional to a star's surface area and the inverse cube of the surface escape speed (Holzer et al. 1983). So low surface-gravity cool evolved stars with radii $10-10^3 R_\odot$ currently inject more processed material than their main-sequence progenitors. However, the mechanisms that drive mass-loss for K through mid-M giants and the yellow and RSGs are very poorly understood:

They have too little dust or molecules in their outflows for radiation driven winds; they have too little photospheric variability or pulsation to have acoustic and shock driven winds (e.g., Arroyo-Torres et al. 2015), and they are too cool for a Parker-like thermal winds. Some form of magnetic activity, or a combination of processes, is likely to be the cause of these ubiquitous mass outflows (Lamers & Cassinelli 1999). Clearly a quantitative physical model for mass loss is lacking for these stars, and even for the later spectral-type pulsating asymptotic giant branch (AGB) stars the role of magnetic fields in driving and shaping the outflows is not understood.

2.1. What empirical data do we need to make progress?

Outflows from cool evolved stars have terminal wind speeds, v_∞, that are typically a small fraction of the surface escape speed, v_{esc}. This means that **most** of the energy that goes into driving the outflows, proportional to $\mathsf{v}_{esc}^2 + \mathsf{v}_\infty^2$, goes into overcoming the star's gravitational potential, i.e., $\propto \mathsf{v}_{esc}^2$. Therefore, *the optimum region to study mass loss mechanisms is within the first few stellar radii where most of the energy goes into the wind and the thermodynamic signatures of the outflow driving mechanisms will be most apparent*.

Nearby red giants have photospheric angular diameters, θ_*, of 10-20 mas, and the two nearest RSGs (Betelgeuse: M2 Iab, and Antares: M1.5 Iab) have $\theta_* \simeq 42 - 44$ mas (Ohnaka et al. 2013; Montargès et al. 2016). The luminous Herschel's Garnet Star (μ Cep: M2 Ia) has $\theta_* = 14.1$ mas (Perrin et al. 2005), the next nearest luminosity class Iab-Ib RSG (CE Tau) has $\theta_* \simeq 10$ mas (Cruzalèbes et al. 2013), and α^1 Her (M5 Ib-II) has $\theta_* = 33$ mas (Benson et al. 1993). Importantly, at 50 GHz, the atmospheres of RSGs have angular extents about twice that of their photospheres, and the ngVLA, with baselines of 200 km, would provide a resolution of better than 10 mas. This would match the highest ALMA spatial resolutions, for example, as shown in Fig. 1.

This figure shows the 338 GHz (0.89 mm) thermal continuum image of the RSG Betelgeuse obtained with ALMA with the longest (16 km) baselines, providing a spatial resolution of 15 mas (O'Gorman et al. 2017). At this wavelength the atmosphere of the star has an angular diameter of ~ 55 mas, and this image shows the non-uniform heating in the atmosphere that might be related to giant convection cells or regions of enhanced magnetic fields. The thermal cm-continuum opacity $\kappa_\lambda \propto \lambda^{2.1}$, so observations at multiple wavelengths map out the temperature and ion density distribution as a function of radius, providing vital clues to the processes levitating and heating the stellar outflow. This requires that the ngVLA 200 km baselines support a range of observing frequencies.

3. Dynamos in Cool Evolved Stars

Most studies of solar-type $\alpha\Omega$ dynamos have focused on main-sequence stars that explore a relatively small parameter space of radius and mass, with a wide range of rotation rates (e.g., Brun & Browning 2017). Red giants, however, provide a different challenge for dynamo theories because they typically have low rotation rates but a much greater range of radii and convection zone depths. It is an open question as to whether an $\alpha\Omega$ dynamo is maintained on the red giant branch or whether a turbulent dynamo (e.g., Durney et al. 1993) is responsible for the generation of magnetic fields that power the ultraviolet (UV) and X-ray emission, and drive stellar outflows. Another important application for the long baselines of the ngVLA is to measure the extent of the mag-

Figure 1. 338 GHz ALMA map of Betelgeuse with a half-power beam width of $\simeq 15$ mas (shown lower left), from O'Gorman et al. (2017). The yellow circle is the photospheric angular diameter measured with VLTI-PIONIER in H-band ($\simeq 1.6\,\mu$m) by Montargès et al. (2016). The larger angular extent seen at ALMA frequencies reveals the lower chromosphere and temperature minimum region. In contrast, the frequencies probed by the VLA sample the more extended chromosphere and wind acceleration region. In this image localized excess emission is marked with crosses. The ngVLA would be able to image the extended regions with the same spatial resolution as ALMA, allowing us to build a tomographic map from the upper-photosphere out into the region where the outflow is initiated. Credit: O'Gorman et al., A&A, Vol. 602, p. L11, 2017, reproduced with permission © ESO.

netically heated chromosphere of red giant stars. Spatial resolution breaks the *spatial impasse* that limits what can be learned from disk integrated flux diagnostics alone (e.g., Harper et al. 2013). There are some recent clues that red giants show signs of magnetic cycles (Sennhauser & Berdyugina 2011) and non-uniform optical brightness distributions (Richichi et al. 2018), indications that magnetic phenomena might be important in creating starspots and active regions. High spatial resolution ngVLA observations would reveal the radio size and uniformity of the chromosphere for the nearest red giant stars. This information would help constrain the nature of stellar dynamos, and thus the shape of magnetic fields that drive outflows from red giants. Such radio observations might also help determine whether low-activity red giants, so called basal-flux stars, are heated by acoustic shocks (Pérez Martínez et al. 2014). These would have compact chromospheres, but if they too are heated by magnetic fields (Judge & Carpenter 1998) they may have more extended atmospheres. There are 12 K and M non-Mira red giants with limb-darkened angular diameters >10 mas obtained with the Mark III Stellar Optical Interferometer (Mozurkewich et al. 2003) that would be resolved at 50 GHz with 200 km baselines. These stars are given in Table 1 along with the MK spectral-types from Keenan & McNeil (1989). The atmospheric electron density scale-heights are expected to be small compared to the stellar radii, so that the radio specific intensity distribution is, to first order, a top-hat and thus relatively easy to interpret. A sweep through radio continuum frequencies provides an opportunity to build a tomographic map of the mean atmospheric temperature profile: ngVLA observations would sample the key chromosphere and wind regions, while synergistic ALMA observations would probe the temperature minimum and upper photosphere (see Figs. 1 and 2 of O'Gorman et al. 2013).

Table 1. Stellar properties for red giants with θ_* >10 mas (Mozurkewich et al. 2003).

HR	Name	Spectral-Type	Ang. Diam. (mas)	T_{eff} (K)
5340	α Boo	K1.5 III	21.37 ± 0.25	4226 ± 53
5563	β Umi	K4- III	10.30 ± 0.10	3849 ± 47
1457	α Tau	K5+ III	21.10 ± 0.21	3871 ± 48
337	β And	M0+ IIIa	13.75 ± 0.14	3763 ± 46
6056	δ Oph	M0.5 III	10.47 ± 0.12	3721 ± 47
911	α Cet	M1.5 IIIa	13.24 ± 0.26	3578 ± 53
2216	η Gem	M2 IIIa	11.79 ± 0.12	3462 ± 43
8775	β Peg	M2.5 II-III	17.98 ± 0.18	3448 ± 42
2286	μ Gem	M3 IIIab	15.12 ± 0.15	3483 ± 43
4910	δ Vir	M3+ III	10.71 ± 0.11	3602 ± 44
921	ρ Per	M4+ IIIa	16.56 ± 0.17	3281 ± 40
6146	g Her	M6- III	19.09 ± 0.19	3008 ± 37

4. Synergies with other Observatories

Free-free radio continuum diagnostics *directly* relate to the thermodynamic state of the atmospheres, and spatially-resolved multi-wavelength observations provide measures of the temperature and electron (ion) density scale-heights. The radio therefore provides the physical context with which to interpret optical and IR images made a similar high spatial resolutions. The 10 mas spatial resolution obtainable with the ngVLA complements the spectro-interferometry and imaging currently being made with the *Very Large Telescope*, e.g., Kervella et al. (2016) and Montargès et al. (2017).

Another ngVLA synergy is that with UV spectroscopy. UV emission line fluxes and radio optical depths are proportional to the emission measure, i.e.,

$$F_{UV} \propto \int n_e n_H \, dR \, dA \qquad \tau_{radio} \propto \int n_e^2 \, dR$$

where n_e and n_H are the electron and hydrogen densities, respectively. dR and dA are the radial and area integral elements, respectively. Since $n_e \propto n_H$, then

$$F_{UV} \propto \tau_{radio} \, dA.$$

The combination of radio and UV flux data, especially when spatially resolved, i.e., when dA is measured, provides very powerful constraints on inhomogeneous atmospheric structures because of the very different temperature sensitivities of radio and collisionally excited UV line emission.

5. Astrophysical Impact

One of the major goals of this research is to be able to build a quantitative predictive model of atmospheric structure and mass loss based on underlying physical principles. Such a model could be used to improve stellar and galactic chemical evolution calculations, and predict the mass-loss histories of RSG which would in turn help to interpret early-time supernova spectra (Moriya et al. 2017). Today we are very far from such a model. The observational constraints that the ngVLA will provide on red giant and RSG extended atmospheres, where the winds accelerate, would be a major step forward. ngVLA would provide the basic measurements of size, electron density scale-height, and degree of uniformity that any theoretical model must satisfy.

6. Uniqueness of the ngVLA Capabilities

The power of the ngVLA lies in its high-spatial resolution *and* high sensitivity which, when combined, provide the ability to probe the spatial scales of the extended near-star atmospheres of evolved stars. This is the zone where the physics that controls different aspects of stellar activity will reveal itself.

Acknowledgments. GMH thanks CU-CASA for infrastructure resources to support ongoing stellar astrophysics radio research. This research has made use of NASA's Astrophysics Data System Bibliographic Services and the VizieR catalogue access tool, CDS, Strasbourg, France (Ochsenbein et al. 2000).

References

Arroyo-Torres, B., Wittkowski, M., Chiavassa, A., et al. 2015, A&A, 575, 50
Auriére, M., Konstantinova-Antova, R., Charbonnel, C., et al. 2015, A&A, 574, 90

Benson, J. A., Dyck, H. M., Ridgway, S. T., Dixon, D. J., Mason, W. L., & Howell, R. R. 1993, AJ, 105, 736
Brun, A. S. & Browning, M. K. 2017, Living Reviews in Solar Physics, 14, 4
Cruzalèbes, P., Jorrisen, A., Rabbia, Y. et al. 2012, MNRAS, 434, 437
Dessart, L., Hillier, D. J., & Audit, E. 2017, A&A, 605, A83
Durney, B. R., De Young, D. S., & Roxburgh, I. W. 1993, Solar Phys., 145, 207
Harper, G. M., Brown, A., & Lim, J. 2001, ApJ, 551, 1073
Harper, G. M., O'Riain, N., & Ayres, T. R. 2013, MNRAS, 428, 2064
Hartmann, L. & Avrett, E. 1984, ApJ, 284, 238
Holzer, T. E., Flå, T., & Leer, E. 1983, ApJ, 275, 808
Hummer, D. G. 1988, ApJ, 327, 477
Judge, P. G. & Carpenter, K. G. 1998, ApJ, 494, 828
Keenan, P. C. & McNeil, R. C. 1989, ApJS, 71, 245
Kervella, P., Lagadec, E., Montargès, M., et al. 2016, A&A, 585, A28
Lamers, H. J. G. L. M. & Cassinelli, J. 1999, *Introduction to Stellar Winds*, CUP, Cambridge UK
Lim, J., Carili, C. L., White, S. M., Beasley, A. J., & Marson, R. G. 1998, Nat, 392, 575
Moriya, T. J., Yoon, S.-C., Graäfener, G., & Blinnikov, S. I. 2017, MNRAS, 469, L108
Pérez Martínez, M. I., Schröder, K.-P., & Hauschidlt, P. 2014, MNRAS, 445, 270
Montargès, M., Kervella, P., Perrin, G., et al. 2016, A&A, 588, A130
Montargès, M., Chiavassa, A., Kervella, P., Ridway, S. T., Perrin, G., Le Bouquin, J.-B., & Lacour, S. 2017, A&A, 605, 108
Mozurkewich, D., Armstrong, J. T., Hindsley, R. B. et al. 2003, AJ, 126, 2502
Ochsenbein, F., Bauer, P., & Marcout, J. 2000, A&AS, 143, 23
Ohnaka, K., Hofmann, K.-H., Schertl, D., et al. 2013, A&A, 555, 183
O'Gorman, E., Harper, G. M., Brown, A., Drake, S., & Richards, A. M. S. 2013, AJ, 146, 98
O'Gorman, E., Kervella, P., Harper, G. M., Richards, A. M. S., Decin, L., Montargès, M., & McDonald, I. 2017, A&A, 602, L10
Perrin, G., Ridgway, S. T., Verhoelst, T., et al. 2005, A&A, 436, 317
Richichi, A., Sharma, S., Pandey, A. K., Sinha, T., & Norharizan, M. D. 2018, New Astronomy, 59, 28
Schrijver, C. J. & Zwaan, C. 2000, *Solar and Stellar Magnetic Activity*, CUP, New York USA
Sennhauser, C. & Berdyugina, S. V. 2011, A&A, 529, 100

Science with a Next-Generation Very Large Array
ASP Conference Series, Monograph 7
Eric J. Murphy, ed.

DRAFT EDITION

ngVLA Studies of Classical Novae

Justin D. Linford[1], Laura Chomiuk,[2], and Michael P. Rupen[3]
[1]*The George Washington University, Washington, DC, USA;* `jlinford@gwu.edu`

[2]*Michigan State University, East Lansing, MI, USA;* `chomiuk@pa.msu.edu`

[3]*Herzberg Institute of Astrophysics, Penticton, BC, Canada;* `michael.rupen@nrc-cnrc.gc.ca`

Abstract. Observations with modern radio telescopes have revealed that classical novae are far from the simple, spherically symmetric events they were once assumed to be. It is now understood that novae provide excellent laboratories to study several astrophysical properties including binary interactions, stellar outflows, and shock physics. The ngVLA will provide unprecedented opportunities to study these events. It will enable us to observe more distant and fainter novae than we can today. It will allow us to simultaneously resolve both the thermal and non-thermal components in the ejecta. Finally, monitoring novae with the ngVLA will reveal the evolution of the ejecta in better detail than is possible with any current instrument.

1. Introduction

A nova outburst results when sufficient mass accretes onto the surface of a white dwarf from a companion star, triggering a thermonuclear explosion. In classical novae the bulk of the emission comes from the warm, expanding ejecta—10^{-7} – 10^{-3} $M_\odot$ expanding at a few thousand km/s. The prevailing theories assume that the explosion occurs as a single, spherically symmetric ejection event and predict a simple relationship between the white dwarf mass, the accretion rate, and the ejecta mass and energetics of the explosion (e.g., Yaron et al. 2005). However, observations with modern instruments indicate that nova eruptions are far from simple. There is now evidence for multiple ejection events (e.g., Nelson et al. 2014), common envelopes (e.g., Chomiuk et al. 2014), non-spherical geometry (e.g., Slavin et al. 1995; Linford et al. 2015), and even jet-like structures in the ejecta (e.g., Rupen et al. 2008).

One of the most surprising discoveries of the *Fermi Gamma-ray Space Telescope* was that novae produce GeV γ-ray emission. While MeV emission from novae was predicted (and yet never observed; Hernanz 2013), GeV emission requires a population of accelerated particles that was not expected to be present in nova explosions. The first nova detected by *Fermi*/LAT was V407 Cyg, which had a Mira giant companion (Abdo et al. 2010). The nova was therefore embedded in the dense wind of its companion star, providing an ideal environment for producing strong shocks when the fast nova ejecta slammed into the slow wind material. However, even novae with main sequence companions are capable of producing detectable γ-rays (e.g., Ackermann et al. 2014; Cheung et al. 2016), which is surprising given the negligible stellar winds

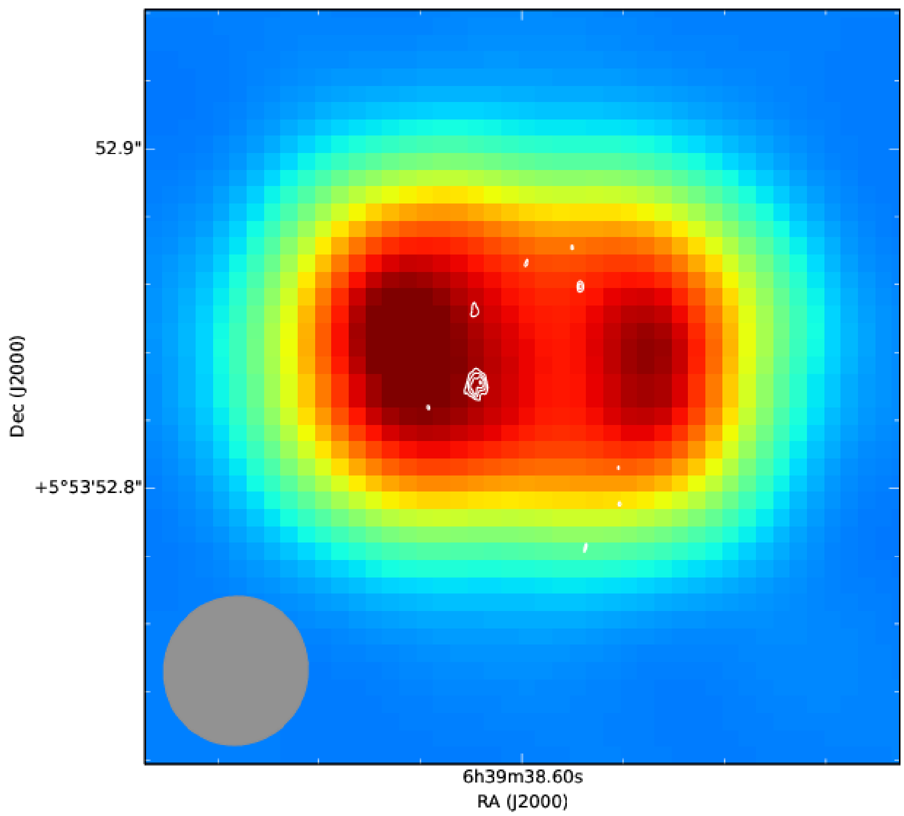

Figure 1. *Imaging of the gamma-ray detected nova V959 Mon (2012), with compact regions of synchrotron emission (white contours) superimposed on the thermal ejecta (color scale). The synchrotron contours were imaged by the VLBA at 5 GHz 106 days after discovery, while the morphology of the thermal ejecta was revealed by the Jansky VLA at 36.5 GHz, 126 days after discovery. The gray ellipse in the lower left corner represents the 36.5 GHz VLA restoring beam. Adapted from Chomiuk et al. 2014.*

leading to low density circumstellar material surrounding these binaries. Recent results from studies at radio wavelengths demonstrate of the importance of shocks in novae, including detection of γ-ray producing shocks in several sources (e.g., Chomiuk et al. 2014; Weston et al. 2016a,b), and the realization that multiple, long-lived outflows are much more common than previously assumed in these explosions (e.g., Nelson et al. 2014). Here we illustrate how the next generation Very Large Array will contribute to the study of classical novae, with an emphasis on characterizing the shocks that develop early in the evolution of these complex explosions.

2. The Case of V959 Mon

The 2012 nova V959 Mon was one of the first classical novae with a main sequence companion detected by *Fermi*. In fact, the nova was discovered by Fermi as it was too close to the Sun for optical observations. Chomiuk et al. (2014) were able to directly image the shocked regions with the Very Long Baseline Array (VLBA) and European

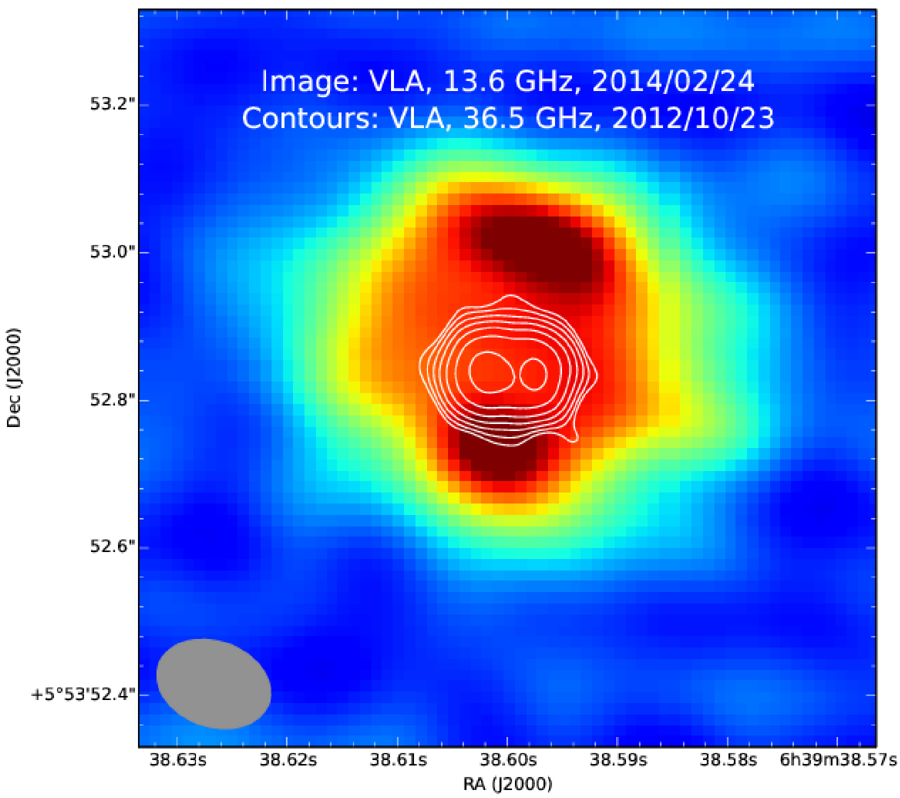

Figure 2. *The evolution of V959 Mon over the two years following nova explosion, as imaged by the Jansky VLA which is sensitive to the thermal ejecta. The plane of the binary system is oriented in the N-S (up-down) direction.* ***White Contours*** *show the 36.5 GHz image of V959 Mon 126 days after discovery, which is dominated by a fast bipolar outflow perpendicular to the orbital plane.* ***Color*** *shows the 13.6 GHz image of V959 Mon 615 days after discovery, which is dominated by the slowly expanding torus oriented along the orbital plane. The Gray ellipse in the lower left represents the 13.6 GHz VLA restoring beam. Adapted from Chomiuk et al. 2014.*

VLBI Network (EVN). As shown in Figure 1, the synchrotron-emitting compact regions did not align with the bipolar structure of the expanding thermal gas, as imaged by the Karl G. Jansky Very Large Array (VLA). Instead, the combined VLBA, EVN, and VLA observations revealed that the compact components were moving on a path roughly 45° to the VLA structure. High-resolution observations with the VLA separated by more than a year also revealed an apparent 90° flip in the orientation of the bipolar outflow (Figure 2). Chomiuk et al. (2014) concluded that the nova ejecta had two distinct components: a slow flow in the equatorial plane of the binary with a velocity of $\sim$ 480 km s^{-1}, and a faster flow in the polar direction with a velocity of $\sim$ 1200 km s^{-1}. Analysis of high-resolution VLA images of these two outflows led to a distance estimate of 1.4 $\pm$ 0.4 kpc (Linford et al. 2015). The interaction between these flows led to the shocks seen in the VLBI observations, and inferred from the γ-ray detections.

In our model (Figure 3), the initial ejection of material from the nova is relatively slow (a few hundred km s^{-1}). This slow ejecta forms a common envelope around the binary and angular momentum is transferred such that a dense torus forms in the orbital plane (Porter et al. 1998). Later, a fast wind develops and is confined by the torus to be ejected perpendicular to the orbital plane. This fast flow dominated the VLA images during the first year of observing. The slow equatorial flow in the torus remained optically thick much longer, and dominated the VLA images at late times. The collision of the fast flow with the slower torus leads to shocks, creating a population of accelerated particles (Chomiuk et al. 2014). In V959 Mon, these accelerated particles were detected via radio synchrotron emission (Chomiuk et al. 2014). There is new evidence that the shocks are also at least partially responsible for the optical emission. Li et al. (2017) found a correlation between the optical and γ-ray light curves for V5856 Sgr that indicated the optical emission could be reprocessed shock emission.

In addition to uncovering the shocks, observations of V959 Mon in both the radio (Linford et al. 2015) and X-rays (Nelson et al., in prep.) suggest that the initial expansion stalled during the first month after eruption. In the radio, the measured angular expansion rate of the bipolar material is inconsistent with expansion starting at the time of eruption. Instead, the expanding material appears to have been ejected $\sim$ 25 days after the initial eruption. In the X-rays, there is an observed drop in column density towards the X-ray emitting region that is best described by a shell of material that was ejected $\sim$ 30 days after the nova was initially detected.

3. Impact of the ngVLA: Sensitivity

The radio emission from classical novae provides information on the amount of mass ejected from the surface of the white dwarf. Because thermal bremsstrahlung dominates the radio emission from the ejecta, radio observations trace the bulk of the ejecta more simply and more accurately than observations at other wavelengths (Seaquist & Bode 2008). For the first 100–200 days after eruption, the ejecta are optically thick at radio frequencies and the flux density is proportional to the electron temperature and the projected area. This means that the sample of radio-detected novae is biased, since novae with small ejecta masses can only be detected if they are nearby (i.e., within a few kpc). The increased sensitivity of the ngVLA will remove this bias by allowing the study of the full range of novae, with observations of even low-luminosity sources out to the Galactic Center.

The recent discovery of γ-ray emission from classical novae renewed interest in understanding the causes and physics of shocks in classical novae. One of the best tracers of shocks is synchrotron emission, which results in both steeply-falling radio spectra and high radio brightness temperatures ($\gtrsim 10^5$ K). Spectral index measurements with the VLA have been moderately successful in identifying synchrotron emission early in a nova's evolution (e.g., Linford et al. 2017). Another, more subtle indicator of shocks is the presence of strong radio emission at early times. The source size may be inferred from its age and optical expansion velocities; if the radio flux density corresponds to brightness temperatures above 10^5 K, there must be at least some contribution from synchrotron emission (e.g., Weston et al. 2016a,b). This analysis rests on deep low-frequency (<7 GHz) observations early in the outburst, which have been rather sparse. Even where there are such observations, one cannot tell how long the synchrotron (shock) emission persists, without more direct indicators, since the increasing size of the remnant makes lower brightness limits from the radio flux density less constraining as the source expands.

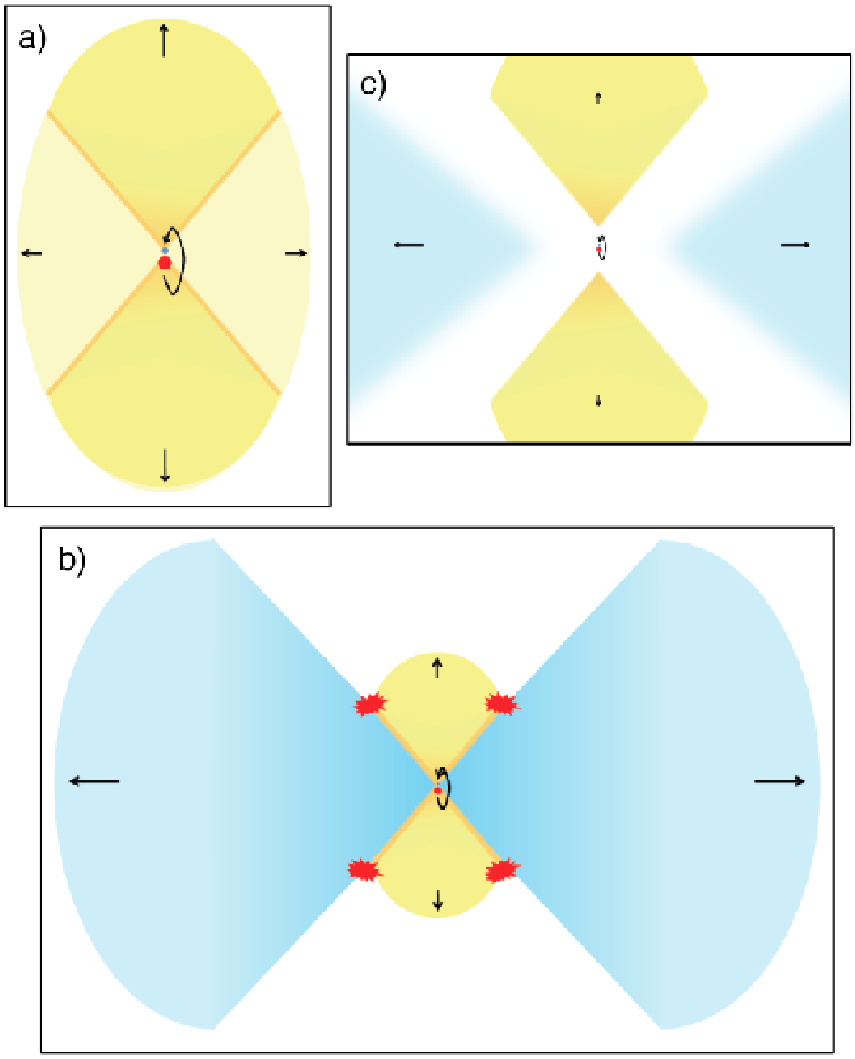

Figure 3. *A cartoon picture to explain the evolution of V959 Mon. A) At early times, the ejecta interacts with the binary and a dense torus is formed (darker yellow, oriented vertically). B) Later, a fast wind (blue) shocks against the torus leading to synchrotron and γ-ray emission (red regions). This phase corresponds to the image of V959 Mon in Figure 1. C) At late times, the wind material is too diffuse to detect and the dense torus dominates the radio emission. Adapted from Chomiuk et al. 2014.*

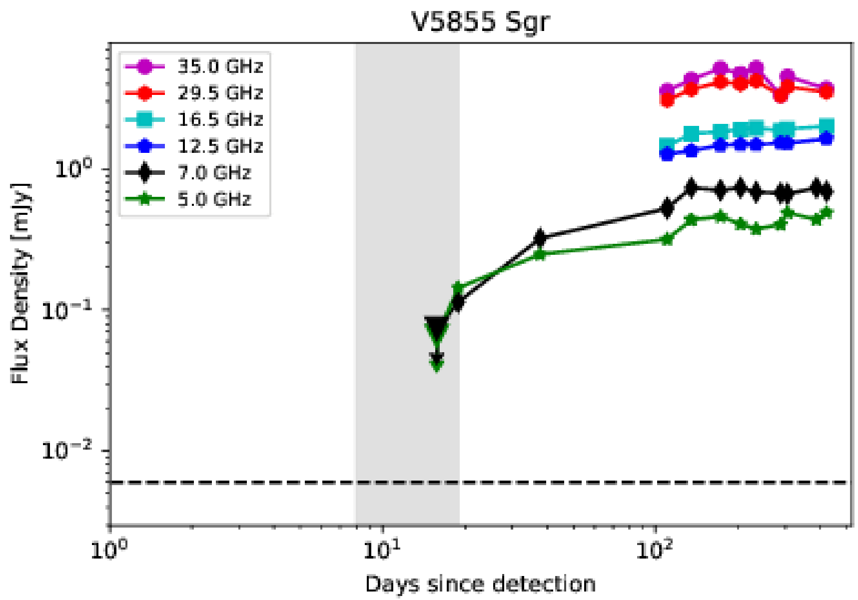

Figure 4. *The early radio light curve of V5855 Sgr. Note the sudden transition from non-detection to detection at C-band (4-8 GHz). Also, note that for the first detection, the 5 GHz flux density is higher than the 7 GHz flux density, which is opposite of what is expected for a source emitting via thermal bremsstrahlung. The gray region indicates the time range while the nova was detected by the Fermi Gamma-ray Space Telescope. The dashed line indicates the expected 3σ RMS noise level of ~6 μJy/beam for 10 minute observations with 2 GHz of bandwidth centered between 4 and 12 GHz on the Next Generation VLA.*

The 2016 eruption of nova V5855 Sgr (TCP J18102829-2929590; CBET 4332) provided an intriguing test case. The first observation was a non-detection, while observations three days later showed strong emission. Moreover, the spectral index in the second epoch was characteristic of optically thin synchrotron emission, with $S_\nu \propto \nu^{-0.7}$. This shows that early synchrotron emission can appear quite suddenly. By the third observation, 19 days after the second epoch, the nova appeared to be emitting via optically thick thermal bremsstrahlung and no clear evidence for synchrotron emission remained. Due to the sparse sampling of the light curve, it is not known how long the synchrotron emission persisted or if it showed any correlation with the γ-ray or X-ray emission.

With its high sensitivity, the ngVLA will be capable of uncovering synchrotron emission from less luminous and more distant novae. Shorter snapshot observations could be used to monitor novae at a high cadence (perhaps even daily) to look for the emergence and disappearance of synchrotron emission early in their evolution. This will provide detailed information about the development and evolution of shocks in the nova ejecta, and allow direct comparison with high-cadence observations with X-ray and γ-ray instruments.

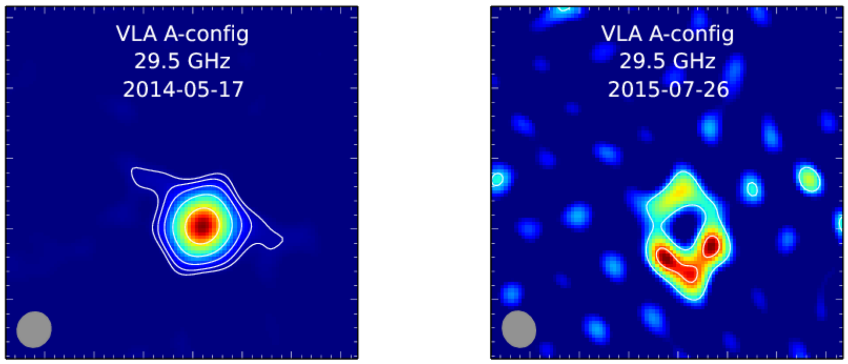

Figure 5. *(Left) VLA A configuration image of V339 Del taken 2014-05-17.; (Right) VLA A configuration image of V339 Del taken 2015-07-26. Note the appearance of a circular structure in the later image. Due to the VLA configuration schedule, there was no way of resolving the the ejecta in between the A configurations. Over a year's worth of evolution must therefore be inferred from 2 snapshots. The Next Generation VLA, with high angular resolution year-round, will for the first time allow imaging of the entire evolution of a nova.*

4. Impact of the ngVLA: Imaging

High resolution ngVLA images will allow us to answer fundamental questions about novae. With a diversity of baseline lengths extending to 1000 km, every ngVLA observation of a nova has the potential to reveal structure like that imaged in Figure 1 — simultaneously tracing both $\sim 10^4$ K thermal ejecta and compact synchrotron structure.

What are the shapes of the expanding ejecta and how do they evolve?

It is still unclear whether nova ejecta are dominated by a spherical shell, a ring, or a bipolar structure (e.g., Slavin et al. 1995; Sokoloski et al. 2013). It is also unclear if nova explosions share a common ejecta morphology and shaping physics, or if their structures are shaped by a diversity of processes. ngVLA imaging will enable the search for evidence of a dense equatorial torus which could lead to the bipolar structure seen in V959 Mon (e.g., Ribeiro et al. 2009). It is unknown exactly when this torus forms (or if it is already present prior to the eruption), so early images with higher angular resolution than the VLA allows are vital. Understanding the evolving shape of a nova remnant is essential to interpreting observations at all wavelengths, from radio to γ-rays, and to testing the two-flow model.

The transition from the radio emission being dominated by the fast wind to being dominated by the slowly expanding torus has yet to be definitively captured, although Healy et al. (2017) reported a possible example in eMERLIN observations of V959 Mon. In many novae the observations constrain only one of these phases. In the Fermi-detected nova V339 Del, for example, there is evidence for the torus at late times, but no strong imaging evidence for the faster bipolar outflow (see Figure 5). This is due in large part to the VLA only being in A configuration for roughly one quarter of the time. Even in A configuration, the VLA only has sufficient angular resolution to resolve the ejecta in the nearest novae. Having high sensitivity and high angular resolution of the ngVLA for every observation will capture the evolution from one phase to the other in detail, in a single source, and show directly whether our hypothesized ejecta morphology is universal.

Does the ejecta begin to expand immediately after eruption, or does the initial expansion stall?

As discussed in Section 2, V959 Mon showed evidence for a stall in the expansion of the ejecta during the first month after eruption. With current radio instruments, it is only possible to detect such a stall phase several months after the eruption and only for relatively nearby novae (within ~ 4 kpc). The ngVLA will have an order-of-magnitude better resolution and higher sensitivity than the VLA, and the resulting imaging should show both whether this such stalls are universal, and when and how the expansion resumes. The exact timing of this apparent stall can differentiate between a common envelope and a confinement phase (in which the nova ejecta are inhibited by external material present prior to the eruption).

What is the energy budget of novae?

Combining ngVLA images of the expanding ejecta with velocity measurements from optical spectroscopy will allow for the application of expansion parallax techniques similar to those used for V959 Mon (Linford et al. 2015). Knowing the distances to the novae will help determine whether only nearby novae are detected by *Fermi* (e.g., Morris et al. 2017; Franckowiak et al. 2018), or if there is a large range in their γ-ray luminosities. The γ-ray luminosities are also extremely valuable for understanding the energetics of these sources and determining whether the γ-ray production mechanism is leptonic or hadronic (e.g., Metzger et al. 2015; Vlasov et al. 2016).

Where is the early synchrotron radiation?

In addition to the expanding thermal ejecta, there has been evidence for early synchrotron emission in novae (e.g, Taylor et al. 1982; Weston et al. 2016a,b; Linford et al. 2017). Presumably, this early non-thermal emission is related to the shocks that produce the γ-ray emission, but the relation is not clear (e.g., Vlasov et al. 2016). For V959 Mon, For V959 Mon, observing both thermal and non-thermal components required a complicated campaign with multiple telescopes (VLA, EVN, VLBA, & eMERLIN). The higher sensitivity and longer baselines of the ngVLA will enable detection of synchrotron emission with higher confidence and earlier in the evolution of the nova than current capabilities allow. The wide frequency range of the ngVLA will also allowing both the thermal and non-thermal components, simultaneously, and with a single telescope!

5. Conclusions

The ngVLA will be an amazing instrument for studying classical novae. The increased sensitivity will enable detection of dimmer and more distant novae. Fast wideband monitoring will allow probes of synchrotron emission from shocks at early times. The large range in baselines will enable simultaneous imaging of both the diffuse thermal ejecta and the regions of shock emission. Finally, with high angular resolution at all times, every radio light curve data point will also be a frame in a movie tracing the evolution of the ejecta from shortly after the explosion to its final dispersal into the interstellar medium. These movies will provide unprecedented opportunities to study these dynamic and enigmatic sources.

Acknowledgments. We are grateful for the pioneering work of R. M. Hjellming using the original VLA.

References

Abdo, A. A., Ackermann, M., Ajello, M., et al. 2010, Science, 329, 817
Ackermann, M., Ajello, M., Albert, A., et al. 2014, Science, 345, 554
Cheung, C. C., Jeanm P., Shore, S. N., et al. 2016, ApJ, 761, 173
Chomiuk, L., Krauss, M. I., Rupen, M. P., et al. 2012, ApJ, 761, 173
Chomiuk, L., Linford, J. D., Yang, J., et al. 2014, Nature, 514, 339
Franckowiak, A., Jean, P., Wood, M., Cheung, C. C., & Buson, S. 2018, A&A, 609, 120
Healy, F., O'Brien, T. J., Breswick, R., Avison, A., & Argo, M. K. 2017, MNRAS, 469, 3976
Hernanz, M. 2013, arXiv:1301.1660
Li, K.-L., Metzger, D. D., Chomiuk, L., et al. 2017, Nature Astronomy, 1, 697
Linford, J. D., Ribeiro, V. A. R. M., Chomiuk, L., et al. 2015, ApJ, 805, 136
Linford, J. D., Chomiuk, L., Nelson, T., et al. 2017, ApJ, 842, 73
Metzger, B. D., Finzell, T., Vurn, I., Hascoët, R., Beloborodov, A. M., & Chomiuk, L. 2015, MNRAS, 450, 2739
Morris, P. J., Cotter, G., Browm, A. M., & Chadwick, P. M. 2017, MNRAS, 465, 1218
Mukai, K. 2017, PASP, 129, 2001
Nelson, T., Chomiuk, L., Roy, N., et al. 2014, ApJ, 785, 78
Porter, J. M., O'Brien, T, J., &Bode, M. F. 1998, MNRAS, 296, 943
Ribeiro, V. A. R. M, Bode, M. F., Darnley, M. J., et al. 2009, ApJ, 703, 1955
Rupen, M. P., Mioduszewski, A. J., & Sokoloski, J. L. 2008, ApJ, 688, 559
Seaquist, E. R., & Bode, M. F. 2008 in Classical Novae, 2nd Edition. Cambridge Astrophysics Series, No. 43, Cambridge: Cambridge University Press, Ed. M. F. Bode & A. Evans, 141
Slavin, A. J., O'Brien, T. J., & Dunlop, J. S. 1995, MNRAS, 276, 353
Sokoloski, J. L., Rupen, M. P., & Mioduszewski, A. J. 2008, ApJ, 685, L137
Sokoloski, J. L., Cortts, A. P. S., Lawrence, S., & Uthas, H. 2013, ApJ, 770, L33
Sokoloski, J. L., Lawrence, S., Crotts, A. P. S., & Mukai, K. 2017, APCS2016, arXiv:1702.05898
Taylor, A. R., Seaquist, E. R., Hollis, J. M., & Pottasch, S. R. 1987, A&A, 183, 38
Vlasov, A., Vurm, I., & Metzger, B. D. 2016, MNRAS, 463, 394
Weston, J. H. S., Sokoloski, J. L., Metzger, B. D., et al. 2016a, MNRAS, 457, 887
Weston, J. H. S., Sokoloski, J. L., Chomiuk, L., et al. 2016b, MNRAS, 460, 2687
Yaron, O., Prialnik, D., Shara, M. M., & Kovetz, A. 2005, ApJ, 623, 398

Science with a Next-Generation Very Large Array
ASP Conference Series, Monograph 7
Eric J. Murphy, ed.

DRAFT EDITION

Evolved Stars

Lynn D. Matthews[1] and Mark J Claussen[2]
[1]*Massachusetts Institute of Technology Haystack Observatory, Westford, MA, 01886 USA;* `lmatthew@mit.edu`

[2]*National Radio Astronomy Observatory, P.O. Box O, Socorro, NM, 87801 USA;* `mclaussen@nrao.edu`

Abstract. This chapter reviews some of the expected contributions of the ngVLA to the understanding of the late evolutionary stages of low-to-intermediate mass stars, including asymptotic giant branch (AGB) stars, post-AGB stars, and pre-planetary nebulae. Such objects represent the ultimate fate of stars like the Sun, and the stellar matter they lose to their immediate vicinity contributes significantly to the chemical enrichment of galaxies. Topics addressed in this chapter include continuum imaging of radio photospheres, studies of circumstellar envelopes in both thermal and nonthermal lines, and the investigation of the transition stages from the AGB to planetary nebulae using radio wavelength diagnostics. The authors gratefully acknowledge contributions to the content of this chapter from members of the evolved star community.

1. Introduction

Evolution onto the asymptotic giant branch (AGB) marks the final thermonuclear burning stage in the lives of low-to-intermediate mass stars ($0.8 \lesssim M_* \lesssim 8\ M_\odot$). The AGB is characterized by a dramatic increase in luminosity (factors of 10^4 or more) and significant mass-loss ($\dot{M} \sim 10^{-8}$ to $10^{-4} M_\odot$ yr^{-1}) through cool, low-velocity ($\sim$10 km s^{-1}) winds. Over the course of roughly one million years, this mass loss leads to the formation of extensive circumstellar envelopes (CSEs) of gas and dust that may span more than a parsec in size.

Knowledge of the mass-loss histories of AGB stars is fundamental to understanding the complete life-cycle of our Galaxy. The winds of AGB stars are rich in heavy elements and molecules, sowing the seeds for future generations of star and planet formation. Indeed, mass loss during the AGB is believed to be responsible for ∼50% of the chemical enrichment in the Galaxy (e.g., Van Eck et al. 2001). However, many aspects of the lives of AGB stars remain poorly understood, including the wind driving mechanisms, the geometry of AGB mass loss, and the evolutionary paths for stars of different initial masses (see Höfner & Olofsson 2018).

Radio observations play a crucial role in understanding stellar evolution on the AGB and beyond. Continuum radiation is emitted from the optically thick radio photospheres of AGB stars, as well as from the jets and torii that may appear during subsequent evolution to the post-AGB and pre-planetary nebula (pPN) stages. The cool, extended atmospheres and CSEs of evolved stars also give rise to numerous spectral lines at cm and mm wavelengths, offering powerful diagnostics of the chemistry, temperature, and density structure of the CSE, as well as wind outflow speeds and other kinematic information. Studies of radio lines supply crucial insight into the stellar mass-loss history and probe how evolved, mass-losing stars interact with their interstellar environments and shape the composition and small-scale structure of the ISM. The specific properties of CSEs gleaned from radio observations also supply insight into their role in the subsequent evolution into planetary nebulae (PNe) and Type Ia supernovae.

The ngVLA will provide enormous gains in our understanding of the end stages of the lives of Sun-like stars. Its exquisite sensitivity will permit imaging observations of large numbers of spectral lines with high angular and spectral resolution, yielding the most detailed and comprehensive maps to date of CSEs from the smallest to the largest scales. The ultrawide bandwidths will make it possible to observe simultaneously both lines and the (relatively weak) stellar continuum emission, providing precise astrometric registration required for the testing of sophisticated radiative transfer and hydrodynamical modeling of AGB star atmospheres and envelopes.

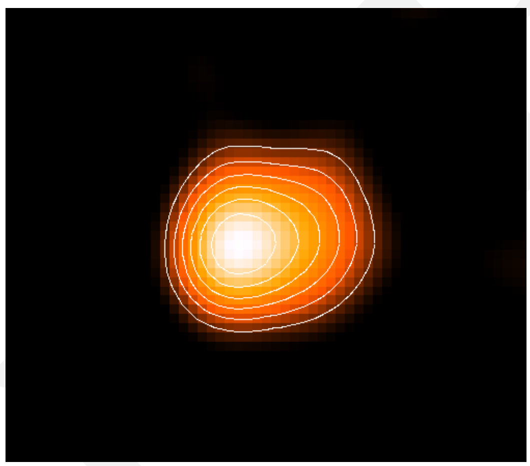

Figure 1. The radio photosphere of R Leo imaged with the VLA at 7 mm (Matthews et al. 2018). The star shows a non-spherical shape and evidence for a non-uniform surface. The image was produced using a sparse model reconstruction algorithm, enabling super-resolution of ~0.75 times the dirty beam FWHM of ~38 mas. The peak flux density is ~4 mJy beam^{-1} and the image is ~150 mas on a side. The ngVLA will enable comparable resolution on AGB stars at distances of up to 1 kpc as well as the resolution of finer surface details on nearby stars.

2. Continuum Observations of Radio Photospheres

AGB stars emit optically thick continuum radiation at cm and (sub)mm wavelengths from a region at $\sim 2R_\star$ known as the "radio photosphere" (Reid & Menten 1997; see also Harper, this volume). In a typical oxygen-rich AGB star, the radio photosphere has a diameter of ~4 AU and lies near the outskirts of the so-called molecular layer or "MOLsphere" (Tsuji 2000, 2001), but interior to the dust-formation zone and maser-emitting regions (see Section 3.2). Thus the radio photosphere samples an atmospheric region impacted by pulsation, convection, shocks, and other key processes responsible for the transport of material from the stellar surface to the outflowing wind.

Presently it is possible to resolve the radio surfaces of the nearest AGB stars ($d \lesssim 150$ pc) at $\lambda \lesssim 1$ cm using the VLA and ALMA in their most extended configurations. Such observations have led to tantalizing evidence for non-uniform radio surfaces and non-spherical photospheric shapes that evolve over time, most likely as a result of pulsation and convective effects (Reid & Menten 2007; Matthews et al. 2015b, 2018; Vlemmings et al. 2017; Figure 1). The ngVLA is expected to provide an angular resolution of ∼26 mas at 8 GHz and ∼2 mas at 93 GHz[1]; thus at shorter wavelengths, the ngVLA will be able to resolve the surfaces of AGB stars to distances beyond a kpc, making it possible to assess the ubiquity of spots and other surface features and measure their brightness temperatures and temporal evolution. For nearby stars ($d \lesssim 150$ pc), it will be possible to resolve radio photospheres over nearly two decades in frequency, effectively providing "tomography" of the atmosphere (see Lim et al. 1998; O'Gorman et al. 2015; Matthews et al. 2015b). The ngVLA will be complementary to ALMA for such work, as cm bands probe higher layers of the atmosphere than can be studied with ALMA and also suffer negligible contamination from line emission and dust. The further addition of contemporaneous imaging with optical/infrared interferometers such as the Center for High Angular Resolution Astronomy (CHARA) Array and Very Large Telescope Interferometer (VLTI) would enable the most stringent tests to date of sophisticated 3D models of AGB star atmospheres (e.g., Freytag et al. 2017).

Sensitivities of $\sim 0.4\mu$Jy beam^{-1} in one hour at $\lambda \approx 7$ mm will also permit the 5σ detection of unresolved radio photospheres to distances of at least 5 kpc. Over the course of roughly a year, the radio light curve observations of Reid & Menten (1997) found levels of variability in a small sample of AGB stars at 8 GHz to be $\lesssim 15\%$, implying that shock speeds within the radio photosphere are limited to $\lesssim 5$ km s^{-1}. But at 7 mm, evidence is now seen for larger flux density changes in data taken several years apart (Matthews et al. 2015b, 2018). The ngVLA will enable for the first time studies of the variability of radio photospheres over both short (intra-pulsation cycle) and long (several years) timescales for a statistical samples of stars. Such data will be extremely powerful for understanding the roles of shocks in governing the physics of AGB star atmospheres, as well as for gathering for the first time statistics on the frequency of possible eruptive or flaring activity in AGB stars. Evidence for the latter phenomena has already been seen at other wavelengths, including the ultraviolet (Sahai et al. 2011b, 2015) and in X-rays (Karovska et al. 2005). Such events may be triggered by accretion activity linked with a companion, chromospheric-like activity, or other still unknown mechanisms.

3. Spectral Line Studies of the CSEs of AGB Stars

3.1. Molecular Lines (Thermal)

The rich chemistry and cool temperatures of the extended atmospheres and CSEs of AGB stars give rise to emission from a multitude of molecular lines at cm and mm wavelengths, predominantly through rotational transitions (e.g., Turner & Ziurys 1988).

---

[1]Throughout this chapter we assume a maximum baseline length of ∼300 km (Selina & Murphy 2017).

Together these various line transitions provide important diagnostic information about the range of temperature and density of the CSE and its kinematics. However, with the exception of masing lines (see Section 3.2), the bulk of these lines are quite weak, requiring excellent sensitivity for their identification and mapping, particularly at the high angular resolutions needed to spatially resolve their distribution and kinematics within the CSE.

3.1.1. Astrochemistry and Searches for New Circumstellar Molecules

The leap in sensitivity of the ngVLA is expected to lead to the discovery of numerous additional molecular species in the envelopes of AGB stars. These are likely to include pre-biotic molecules, carbon chains, and other complex molecules suspected of having their origin in AGB star winds (e.g., Ziurys 2006). The frequency range covered by the ngVLA will have advantages over ALMA for searching for many complex molecules in CSEs, both because heavier molecules have lower frequency rotational transitions, and because line blending below ~100 GHz is much less severe than at higher frequencies. Even for commonly observed molecular transitions such as the CO $J = 1 - 0$ line, the ngVLA will provide important new statistics by enabling detection of late-type stars to distances of up to ~10 kpc, including within the Galactic Center Region.

3.1.2. Spiral Patterns in the Mass Ejecta of AGB Stars

Binary motion can generate spiral patterns in the CSEs of AGB stars, and modeling of the spiral pattern can be used to set constraints on orbital parameters (e.g., period, eccentricity, and inclination; see Mastrodemos & Morris 1999; Kim & Taam 2012a, b, c). Interferometric molecular-line imaging of CO lines has detected such patterns in a small number of objects (e.g., Maercker et al. 2012, Kim et al. 2017). For the carbon star CIT 6, the spiral pattern was found via VLA imaging of the HC_3N(4-3) at 36.3 GHz (Claussen et al. 2011). However, the unprecedented sensitivity of ngVLA will enable searches for such patterns in a statistical sample of AGB stars.

3.2. Non-Thermal Lines (Masers)

Molecular maser emission is frequently detected in the CSEs of AGB stars (and in young PNe; see below). The most widely observed masers in circumstellar environments include transitions of OH (1.6 GHz), H_2O (22 GHz), SiO v=0,1,2,3, J=1−0 (43 GHz), and SiO v=1, J=2−1 (86 GHz) (e.g., Alcolea 2004). These various transitions require different combinations of temperature and density to excite, hence observations of multiple transitions within a single star can be used to probe material from different regions in the CSE, ranging from a few AU from the star for SiO masers to r ~1000 AU for OH lines.

The strongest circumstellar masers show brightness temperatures of many millions of K, and the intensity and high excitation of some of these lines have enabled exquisitely high resolution mapping of CSEs using Very Long Baseline Interferometry (VLBI; e.g., Cotton et al. 2004; Gonidakis et al. 2013; Desmurs et al. 2014; Figure 2). However, there are various limitations of VLBI studies, including losses of up to ~50% of the flux density (e.g., Desmurs et al. 2017) and the difficulty of phase referencing (and thus, astrometry) at frequencies above ~20 GHz (Beasley & Conway 1995). The ngVLA will be able to systematically observe circumstellar masers with excellent angular resolutions (~10 mas at 22 GHz). But in contrast to current VLBI arrays, it will have much higher sensitivity, negligible flux loss, and excellent instantaneous *u*-*v*-coverage. The high signal-to-noise ratios (SNR) that will be achieved will additionally enable highly accurate positioning of maser lines (in principle, the achievable astrometric precision is approximately the angular resolution divided by the SNR). And crucially, the ultra-wide bandwidths of the ngVLA will permit the routine simultaneous detection of multiple maser transitions, along with the stellar photosphere in the continuum, allowing placement of the distributions of the different masers in the context of the inner circumstellar layers. In nearby stars, it will also be possible to study in detail the movements of maser spots and the relation between the structure of different maser species during the course of the stellar pulsation. These types of data will be vital for identifying the maser pumping mechanisms and providing quantitative constraints on models of AGB star atmospheres (e.g, Gray et al. 2009, 2016).

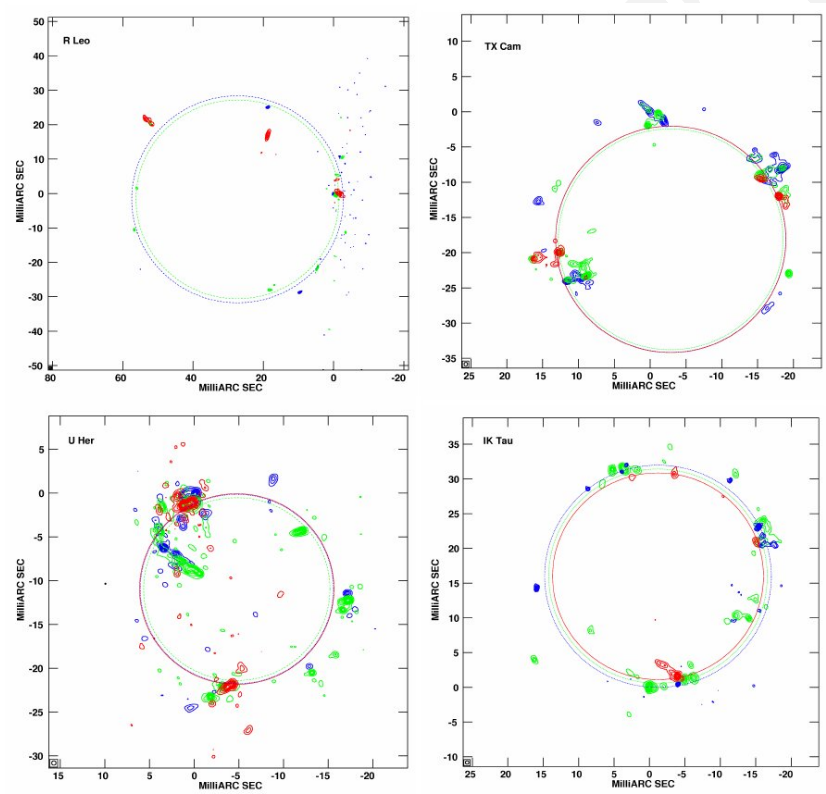

Figure 2. Very Long Baseline Array (VLBA) maps of SiO v = 1 (in blue), v=2 (in green), and v=3 (in red), J=1−0 maser lines from R Leo, TX Cam, U Her, and IK Tau (Desmurs et al. 2014). The relative positions of the maser spots of the different lines should provide clues to understanding the SiO pumping, but presently the relative astrometry is very uncertain.

The ngVLA performance will also enable systematic high-resolution mapping of relatively weak maser lines ($T_b \lesssim 10^4$ K), whose properties are not yet well understood and for which very little observational information is currently available. Examples include the SiO v=0 masers (useful to study intermediate shells of CSEs; Bolboltz & Claussen 2004); ^{29}SiO v=0,1, ^{28}SiO v=2, J=2−1, and ^{28}SiO v=3 masers (which are important for the study of SiO maser pumping; Soria-Ruiz et al. 2005, Desmurs et al. 2014), and HCN J=1−0 masers at 88.6 GHz (which may be the best way to probe the very inner regions in C-rich CSEs; Lucas et al. 1988, Menten et al. 2018).

The study of circumstellar OH masers will benefit from the ngVLA's excellent angular resolution even at longer wavelengths (18 cm), along with a factor of several gain in line sensitivity over the present VLA. This will make OH masers around late-type stars accessible throughout the Galaxy and enable new constraints on brightness temperature and maser gain models. In addition to surveys, follow-up imaging studies with a combination of high sensitivity, high angular resolution, high spectral resolution ($\leq$0.07 km s^{-1}), and full Stokes parameters will enable separation of individual maser components and detection of the often present signatures of strong linear or circular polarization that are otherwise washed out by insufficient spatial and velocity resolution (e.g., Wolak et al. 2012, 2013).

A special category of OH maser sources is the OH/IR stars, a subclass of evolved stars believed to be in the final stages of their evolution on the AGB. Their dusty winds and exceptionally high mass-loss rates (up to a few times 10^{-4} $M_{\odot}$ yr^{-1}) render them optically thick at visible wavelengths, and they generally emit a strong characteristic "doubled-peaked" 1612 MHz OH maser emission profile (e.g., Engels 1985). To test the predictions of evolutionary models, in particular the role of metallicity, observational properties of OH/IR stars during their obscured phase *and* reliable distances are needed. For OH/IR stars, the latter can be derived via the so-called "phase-lag" method (Engels et al. 2015; Etoka et al. 2017), using a combination of: (i) the linear diameter of the shell as obtained from the light curve of the varying OH maser peaks; and (ii) an angular diameter obtained from an interferometric map of the OH emission. In order to get a precise angular diameter determination it is vital to map the faint "inter-peak" emission from which the full extent of the shell and its geometry can be inferred. While challenging with current instruments, the enhanced sensitivity and resolution of the ngVLA will facilitate such measurements for larger samples of OH/IR stars. For the nearest stars ($d \lesssim$200 pc) it should become possible to do direct comparisons of such distances with OH maser parallax measurements.

3.3. The H I 21-cm Line

The CSEs surrounding AGB stars can become enormously extended, in some cases spanning more than a parsec (e.g., Villaver et al. 2012). As densities drop with increasing distance from the star, molecules, including CO, become dissociated by the interstellar radiation field. Molecular lines therefore cannot probe the outer regions of the CSE. However, neutral atomic hydrogen (H I) persists in this environment, and recent studies have demonstrated that its 21 cm line emission provides a powerful probe of outer CSE (representing $\gtrsim 10^5$ yr of mass loss history), as well as the interfaces between AGB stars and their environments (e.g., Figure 3). While FIR and/or far-ultraviolet emission can sometimes supply complementary information on the CSE outskirts, only H I studies supply *kinematic* information on the extended gas (e.g., Matthews et al. 2008).

Surveys carried out with the Nançay Radio Telescope have now identified dozens of candidate H I shells around nearby AGB stars (Gérard & Le Bertre 2006; Gérard et al. 2011 and in prep.). However, follow-up interferometric observations are critical for studying the detailed spatial and kinematic structure of the H I envelopes and for disentangling possible contamination from line-of-sight emission. Only a handful of

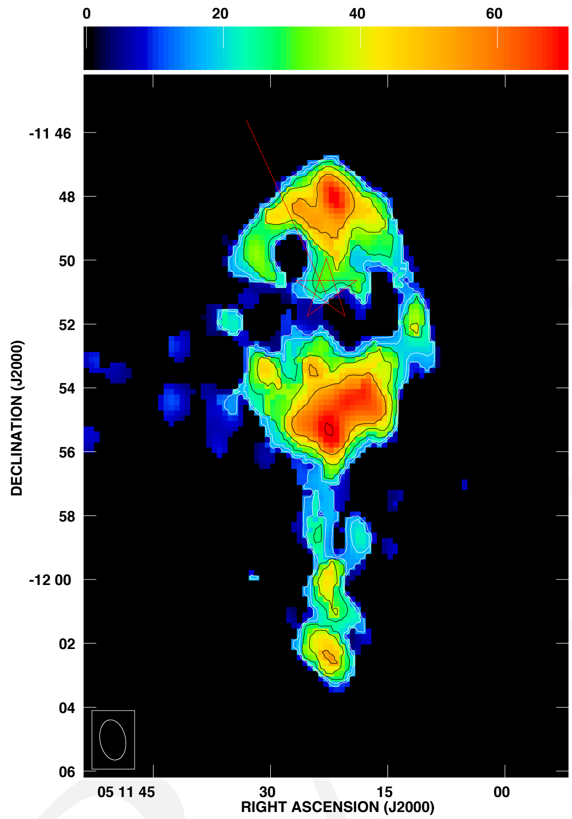

Figure 3. VLA H I total intensity image of the AGB star RX Lep (Matthews et al. 2013). The intensity scale units are Jy beam^{-1} m s^{-1}. A star symbol denotes the stellar position and the direction of space motion is shown by a red line. The projected extent of the H I shell and tail in the north-south direction is ~0.7 pc.

AGB stars have been imaged in the H I line with the VLA to date, owing to the challenging and time-consuming nature of these observations (e.g., Matthews & Reid 2007; Matthews et al. 2008, 2013). However, the ngVLA will provide substantial gains in sensitivity, survey speed, and in the mitigation of background confusion for circumstellar H I observations.

The quasi-random distribution of the individual antennas in the ngVLA core will considerably improve the *u-v* coverage compared with the existing VLA and reduce the periodic sidelobe effects caused by regularly spaced antennas, thereby helping to mitigate the problems of contamination from interstellar H I emission along the line-of-sight. (cf. Matthews et al. 2011, 2013). The addition of a large ($\gtrsim$45 m) single-dish antenna to the array core (Frayer 2017) would also significantly enhance the ability to subtract off line-of-sight emission and to image extremely low surface brightness H I emission from H I shells, tails, and other structures spanning tens of arcminutes (see e.g., Matthews et al. 2013, 2015a).

Even in the nearest AGB stars, circumstellar H I emission is typically weak with narrow linewidths (~10 km s^{-1}), requiring good spectral resolution ($\lesssim$1 km s^{-1}) to measure velocity gradients and other kinematic features (e.g., Matthews et al. 2008, 2011, 2013). For sightlines or velocity ranges that are not confusion limited, the sensitivity gained by the factor of ~4 increase in collecting area of the ngVLA will enable expansion of the study of circumstellar H I to significantly larger samples of stars, Finally, the ngVLA core configuration is expected to have baselines up to 1.55 km, which will provide ~50% higher spatial resolution than the current VLA D configuration for mapping the complex kinematics of the emission, including cases where the H I emission may trace the extension of axisymmetric outflow structures seen at smaller radii in molecular lines (Hoai et al. 2014).

4. Evolution Past the AGB

4.1. Understanding the AGB→PN Transition

The mass loss characteristic of evolved stars increases with evolutionary stage (Balick & Frank 2002, Bujarrabal et al. 2001). During the pPN stage, the star ejects a significant fraction of its initial mass (~ 1 $M_{\odot}$) via a "superwind" within only a few thousand years (e.g., Lewis 2001). During this phase, the core of the star becomes visible and illuminates (and will later ionize) a very massive nebula, forming a PN, whose central stellar core will then evolve into a white dwarf (WD). However, very few details are known about how these events unfold.

Observations of molecular lines at cm and mm wavelengths are a powerful tool for studying the AGB/PN transition, including the disks, torii, and outflows that commonly appear during this stage—as well as the central stars themselves (e.g., Alcolea et al. 2007; Bujarrabal et al. 2013; Sahai et al. 2017). The ngVLA will complement studies performed with ALMA by extending the range of molecular transitions that can be observed with exquisite sensitivity and spatial resolution to include such lines as ^{12}CO & ^{13}CO J=1−0 (110-115 GHz), HCN J=1−0 (89 GHz), SiO v=1, J=1−0 & J=2−1 (43 and 87 GHz), CS $J = 1-0$ & $2-1$ (49 and 98 GHz). At these frequencies, the ngVLA is expected to achieve angular resolutions of ~2–5 mas—of order ten times better than present ALMA resolutions. At the same time, the ngVLA's continuum sensitivity will allow probing the dust component of the central torii in a statistical sample of post-AGB objects, determine their cm-mm spectral energy distributions, and constrain the grain sizes and dust masses. Combined, this information will address key questions about the geometry and origin of these structures (e.g., Bondi-Hoyle accretion vs. common-envelope ejection).

Even at very high spatial and spectral resolutions, the impressive sensitivity of the ngVLA will allow maps of lines arising from hot inner regions, where brightness temperatures of several hundred K are expected. The innermost layers of pPNe also develop very compact H II regions, resulting from the evolution of the central star to a WD and the ensuing ionization of the surrounding material. Therefore, those regions trace the last phases of the nebular ejection. Their continuum emission is opaque or nearly opaque and very intense at most ngVLA frequencies (T_b>1000 K); recombination lines with T_b ~10% of the continuum (i.e., >100 K) are also expected (e.g., Kwok & Bignell 1984; Sánchez Contreras et al. 2017). The ngVLA will therefore enable studies with high accuracy of both the neutral and the ionized gas from very inner regions of pPNe,

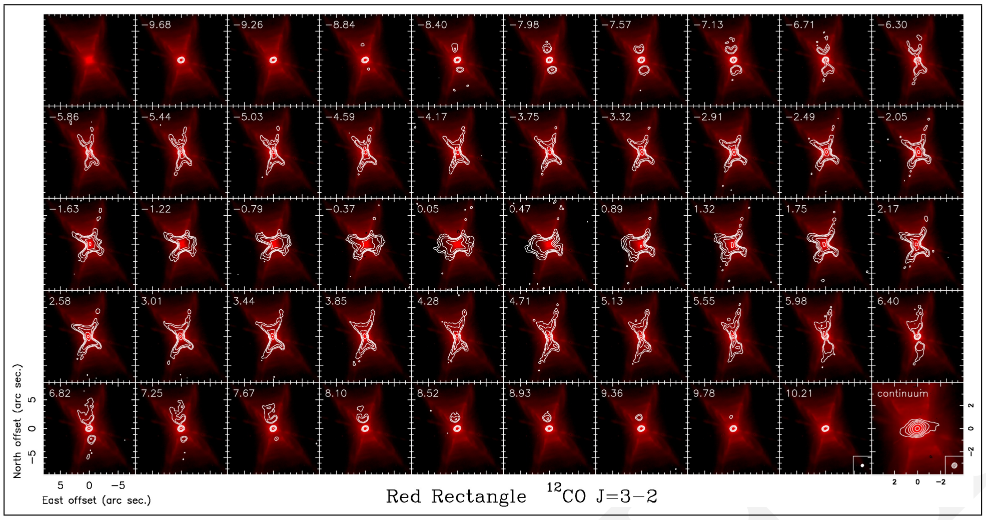

Figure 4. ALMA observations of ^{12}CO J=3−2 emission from the pPN object the Red Rectangle (Bujarrabal et al. 2013; contours). A *Hubble Space Telescope* optical image is also shown in color. The equatorial feature at the central velocities is a rotating disk; the X-shaped features come from more diffuse gas in expansion. It is thought that rotating disks in the centers of pPNe can account for their characteristic bipolar shapes, but only very high angular resolution allows mapping the relevant components.

where vital clues to understand the late evolutionary phases of stars are most likely hidden.

4.2. The Role of Binarity in Post-AGB Evolution

Binary companions are thought to play a significant role in the late evolutionary stages of Sun-like stars. For example, binary interactions are widely believed to underlie the formation of most PNe and may hold the key to the resolution of a long-standing puzzle, namely that although PNe evolve from AGB stars, whose CSEs typically appear spherical with relatively, slow, isotropic expansion ($V_{\rm exp} \sim$ 5-15 km s^{-1}), the vast majority of PNe and pPNe exhibit axisymmetric structures, with a variety of elliptical, bipolar, and multipolar morphologies, as well as fast, collimated outflows ($V_{\rm exp} \gtrsim$ 50-100 km s^{-1}; e.g., Figure 4).

About half of post-AGB objects are known or likely binaries and show prominant disks with little or no extended nebulosity. These have been dubbed "dpAGB" objects, and their dusty disks are remarkably similar to those of pPNe in harboring substantial masses of very large (mm-sized) dust grains (e.g., Sahai et al. 2011a). This supports the idea that the formation of dense "waists" in post-AGB objects is intimately linked to binarity. Surveys of dpAGBs and pPNe with the ngVLA to measure the cm-wavelength SEDs of a large population of these targets will allow the characterization of the dust disks in both classes of objects and new insights into the role of binarity.

4.3. Water Fountain Sources

Water fountain sources (WFs) are thought to be one of the first manifestations of highly collimated outflows in the very short transition from the AGB to PNe (see, e.g., Claussen et al. 2007). Simultaneous ngVLA observations of the continuum and maser emission from WFs in full polarization mode at frequencies of 1.6 GHz (OH masers), 22 GHz (H_2O masers), and 43 GHz (SiO masers) are expected to significantly advance our understanding of these sources and hence this important but short-lived evolutionary stage of Sun-like stars. Observations with the ngVLA of optically thin thermal lines such as HCN, $H^{13}CN$ $J = 1 - 0$, CS $J = 1 - 0$ & $2 - 1$, and SO $3, 2 - 2, 1$ are also expected to provide unique insights (Sahai et al. 2017).

Studies of cm wavelength continuum from WFs will enable the detection and study of the expected thermal radio jets and their powering sources. Even though thermal free-free emission produced by photoionization of the gas in the parental CSE is not expected to be significant [the central star(s) are too cold], thermal free-free emission from shock-ionized gas could be present. A similiar phenomenon is observed in low-mass young stellar objects, where ionization of the gas in the local environment may occur through strong shocks of the wind against the ambient gas (e.g., Rodríguez et al. 1999). Radio jets have been detected towards the objects in the pPNe stage, but it will be crucial to explore of the youngest phase of these jets (i.e., during the WF phase) in order to fully understand their underlying driving mechanism.

From the formulation given in Torrelles et al. (1985) and Curiel et al. (1989), it is estimated that a wind with a mass-loss rate of 10^{-7} $M_\odot$ yr^{-1} and a velocity of 500 km s^{-1} can produce via shocks thermal free-free emission at a level of ~ 1 μJy at $\lambda \sim$1 cm for a source at $d \approx$10 kpc. This emission can be detected with the ngVLA with SNR$\approx$10 for an unresolved source (assuming rms noise 0.1 μJy beam^{-1} after 10 hours of integration). By studying the radio continuum emission at different frequencies with the ngVLA, together with the kinematics of masers in the outflow, it will be possible to obtain basic parameters of the central source of the WFs (e.g., mass-loss rate and wind velocity) and to understand the physical relationship between the masers and the continuum.

Observations of the maser emission from WFs with the ngVLA over multiple epochs will also enable measurements of proper motions and enable the derivation of 3D space velocities. In particular, this will be possible for 22 GHz H_2O masers, where individual maser clumps have been observed to be moving at velocities of $\sim$100 km s^{-1} on time scales of months for sources at 10 kpc distance. Because the continuum emission will be observed simultaneously, it will be possible to derive relative positions of the masers with respect to the central source with high precision. This is mandatory to enable detailed modeling of the motions of the gas, from which one may then extract information on the physical properties of the envelope created during the AGB phase (e.g., its gas density and mass; Orosz et al. 2018). As the mass-loss rate climbs to $\sim 10^{-5} - 10^{-4} M_\odot$ yr^{-1} during the superwind phase, it will also be possible to test WF models by searching for evidence of deceleration of the jets using the spatio-kinematics of the masers (Imai et al. 2005).

Finally, in addition to allowing measurements of proper motions, observations of H_2O masers in WFs with the ngVLA will provide new information on the relationship between the magnetic field and velocity vectors through polarization measurements of the masers and their 3D velocities. Similar techniques have already been applied to the studies of YSOs (e.g., Goddi et al. 2017; see also Hunter et al., this volume). This will be invaluable for testing the role of magnetic fields in jet launching.

Acknowledgments. The authors gratefully acknowledge contributions to this Chapter from the following individuals: Javier Alcolea; Valentín Bujarrabal; Dieter Engels; Sandra Etoka; Eric Gérard; José-Francisco Gomez; Hiroshi Imai; Thibaut Le Bertre; Anita M. S. Richards; Raghvendra Sahai; José-Maria Torrelles.

References

Alcolea, J. 2004, in Proceedings of the 7th Symposium of the European VLBI Network, ed. by R. Bachiller, F. Colomer, J.-F. Desmurs, and P. de Vicente, Observatorio Astronomico Nacional of Spain, 169

Alcolea, J., Neri, R., & Bujarrabal, V. 2007, A&A, 468, L41

Balick, B., & Frank, A. 2002, ARA&A, 40, 439

Beasley, A. J. & Conway, J. E. 1995, in Very Long Baseline Interferometry and the VLBA, ASP Conf. Series, Vol. 82, ed. by J. A. Zensus, P. J. Diamond, and P. J. Napier, (San Francisco: ASP), 327

Boboltz, D. A., & Claussen, M. J. 2004, ApJ, 608, 480

Bujarrabal, V., Castro-Carrizo, A., Alcolea, J., & Sánchez Contreras, C. 2001, A&A, 377, 868

Bujarrabal, V., Castro-Carrizo, A., Alcolea, J., Van Winckel, H., & Sánchez Contreras, C., Santander-García, M., Neri, R. & Lucas, R. 2013, A&A, 557, L11

Claussen, M. J, Sahai, R., & Morris, M. 2007, Asymmetrical Planetary Nebulae IV, `http://www.iac.es/proyect/apn4`

Claussen, M. J., Sjouwerman, L. O., Rupen, M. P., Olofsson, H., Schöier, F. L., Bergman, P., & Knapp, G. R. 2011, ApJ, 739, 5

Cotton, W. D, Mennesson, B., Diamond, P. J., et al. 2004, A&A, 414, 275

Curiel, S., Rodríguez, L. F., Bohigas, J., Roth, M., Canto, J., & Torrelles, J. M. 1989, ApL&C, 27, 299

Desmurs, J.-F., Bujarrabal, V., Lindqvist, M., et al. 2014, A&A, 565, A127

Desmurs, J.-F., Alcolea, J., Bujarrabal, V., Colomer, F., & Soria-Ruiz, R. 2017, in Astrophysical Masers: Unlocking the Mysteries of the Universe, ed. by A. Tarchi, M. J. Reid, & P. Castangia, IAU Symp. 336, in press (arXiv:1712.07380)

Engels, D. 1985, in The Milky Way Galaxy, IAU Symposium No. 106, ed. by H. van Woerden, R. J. Allen, and W. B. Burton (Dordrecht: Reidel), 131

Engels, D., Etoka, S., Gérard, E., & Richards, A. 2015, in Why Galaxies Care about AGB Stars III: A CLoser Look in Space and Time, ASP Conf. Series, Vol. 497, ed. by F. Kerschbaum, R. F. Wing, and J. Hron (San Francisco: ASP), 473

Etoka, S., Engels, D., Gérard, E., & Richards, A. M. S. 2017, in Astrophysical Masers: Unlocking the Mysteries of the Universe, IAU Symposium No. 336, ed. by A. Tarchi, M. J. Reid, & P. Castangia, in press (arXiv:1711.09694)

Frayer, D. T. 2017, ngVLA Memo #14

Freytag, B., Liljegren, S., & Höfner, S. 2017, A&A, 600, A137

Gérard, E. & Le Bertre, T. 2006, AJ, 132, 2566

Gérard, E., Le Bertre, T., & Libert, Y. 2011, SF2A-2011, ed. by G. Alecian et al., 419

Goddi, C., Surcis, G., Moscadelli, L., Imai, H., Vlemmings, W. H. T., van Langevelde, H. J., & Sanna, A. 2017, A&A, 597, A43

Gonidakis, I., Diamond, P. J., & Kemball, A. J. 2013, MNRAS, 433, 3133

Gray, M., Baudry, A., Richards, A. M. S., Humphreys, E. M. L., Sobolev, A. M., & Yates, J. A. 2016, MNRAS, 456, 374

Gray, M., Wittkowski, M., Scholz, M., Humphreys, E. M. L., Ohnaka, K., & Boboltz, D. 2009, MNRAS, 394, 51

Hoai, D. T., Matthews, L. D., Winters, J. M., Nhung, P. T., Gérard, E., Libert, Y., & Le Bertre, T. 2014, A&A, 565, 54

Höfner, S. & Olofsson, H. 2018, A&ARv, 26, 1
Imai, H., Nakashima, J.-i., Diamond, P. J., Miyazaki, A., & Deguchi, S. 2005, ApJL, 622, L125
Karovska, M., Schlegel, E., Hack, W., Raymond, J. C., & Wood, B. E. 2005, ApJL, 623, L137
Kim, H. & Taam, R. E. 2012a, ApJ, 744, 136
Kim, H. & Taam, R. E. 2012b, ApJ, 759, 59
Kim, H. & Taam, R. E. 2012c, ApJL, 759, L22
Kim, H., Trejo, A., Liu, S.-Y., et al. 2017, NatAs, 1, 60
Kwok, S. & Bignell, R. C. 1984, ApJ, 276, 544
Lewis, B. M. 2001, AJ, 121, 426
Lim, J., Carilli, C. L., White, S. M., Beasley, A. J., & Marson, R. G. 1998, Nature, 392, 575
Lucas, R., Omont, A., & Guilloteau, S. 1988, A&A, 194, 230
Maercker, M., Mohamed, S., Vlemmings, W. H. T., et al. 2012, Nature, 490, 232
Mastrodemos, N. & Morris, M. 1999, ApJ 523, 357
Matthews, L. D., Gérard, E., & Le Bertre, T. 2015a, MNRAS, 449, 220
Matthews, L. D., Le Bertre, T., Gérard, E., & Johnson, M. C. 2013, AJ 145, 97
Matthews, L. D., Libert, Y., Gérard, E., Le Bertre, T., & Reid, M. J. 2008, ApJ, 684, 603
Matthews, L. D., Libert, Y., Gérard, E., Johnson, M. C., & Dame, T. M. 2011, AJ, 141, 60
Matthews, L. D. & Reid, M. J. 2007, AJ, 133, 2291
Matthews, L. D., Reid, M. J., & Menten, K. M. 2015b, ApJ, 808, 36
Matthews, L. D., Reid, M. J., Menten, K. M., & Akiyama, K. 2018, AJ, in press (arXiv:1805.05428)
Menten, K. M., Wyrowski, F., Keller, D., & Kamiński, T. 2018, A&A, in press (arXiv:1803.00943)
O'Gorman, E., Harper, G. M., Guinan, E. F., Richards, A. M. S., Vlemmings, W., & Wasatonic, R. 2015, A&A, 580, A101
Orosz, G., Gomez, J. F., Imai, H., et al. 2018, in preparation
Reid, M. J. & Menten, K. M. 1997, ApJ, 476, 327
Reid, M. J. & Menten, K. M. 2007, ApJ, 671, 2068
Rodríguez, L., F., Anglada, G., & Curiel, S. 1999, ApJS, 125, 427
Sahai, R., Claussen, M. J, Schnee, S., Morris, M. R., & Sánchez Contreras, C. 2011a, ApJL, 739, L3
Sahai, R., Neill, J. D., Gil de Paz, A., & Sánchez Contreras, C. 2011b, ApJL, 740, L39
Sahai, R., Sanz-Forcada, J., Sánchez Contreras, C., & Stute, M. 2015, ApJ, 810, 77
Sahai, R., Vlemmings, W. H. T., Gledhill, T., et al. 2017, ApJL, 835, L13
Sánchez Contreras, C., Báez-Rubio, A., Alcolea, J., Bujarrabal, V., & Martín-Pintado, J. 2017, A&A, 603, A67
Selina, R. & Murphy, E. 2017, ngVLA Memo #17
Soria-Ruiz, R., Colomer, F., Alcolea, J., et al. 2005, A&A, 432, L39
Torrelles, J. M., Ho, P. T. P., Rodríguez, L. F., & Canto, J. 1985, ApJ, 288, 595
Tsuji, T. 2000, ApJ, 540, L99
Tsuji, T. 2001, in Galaxies and their Constituents at the Highest Angular Resolutions, IAU Symposium 205, ed. by R. T. Schilizzi, (San Francisco: ASP), 316
Turner, B. E. & Ziurys, L. M. 1988, in Galactic and Extragalactic Radio Astronomy, 2nd Edition, ed. by G. L. Verschuur and K. I. Kellermann, (Berlin: Springer-Verlag), 200
Van Eck, S., Goriely, S., Jorissen, A., & Plez, B. 2001, Nature, 412, 793
Villaver, E., Manchado, A., & García-Segura, G. 2012, ApJ, 748, 94
Vlemmings, W., Khouri, T., O'Gorman, E., et al. 2017, NatAs, 1, 848
Wolak, P., Szymczak, M., & Gérard, E. 2013, MNRAS 430, 2499
Wolak, P., Szymczak, M., & Gérard, E. 2012, A&A 537, A5
Ziurys, L. M. 2006, PNAS, 103, 122274

Science with a Next-Generation Very Large Array
ASP Conference Series, Monograph 7
Eric J. Murphy, ed.

DRAFT EDITION

Complex Organic Molecules in Hot Molecular Cores/Corinos: Physics and Chemistry

Maria T. Beltrán and Víctor M. Rivilla
INAF-Osservatorio Astrofisico di Arcetri, Largo E. Fermi 5, I-50125 Firenze, Italy; mbeltran@arcetri.astro.it,rivilla@arcetri.astro.it

1. Introduction

Hot molecular cores (HMCs), the cradles of massive stars, are the most chemically rich sources in the Galaxy (Bisschop et al. 2007; Belloche et al. 2013; Rivilla et al. 2017). The typical masses of these cores (few hundreds of $M_\odot$) make them the most important reservoirs of complex organic molecules (COMs), including key species for prebiotic processes. This rich chemistry is thought to be the result of the evaporation of dust grain mantles by the strong radiation of the deeply embedded early-type star(s). Our own Sun may have been born in a high-mass star-forming region (Adams 2010), so our Earth may have inherited the primordial chemical composition of its parental hot core region, as suggested by recent studies of oxygen and sulfur chemistry in comets (Taquet et al. 2016; Drozdovskaya et al. 2018).

The immediate surroundings of high-mass protostars are not the only regions rich in COMs. In recent years, the environments of some low-mass protostars have also revealed a very complex chemistry, with the presence of large molecules with abundances similar to those found towards high-mass protostars. These low-mass cores have been called hot corinos (Bottinelli et al. 2004). Although the mechanism responsible for the emission of COMs would be the increase of temperature in the inner envelope, like for the high-mass hot cores, it is not clear what is producing such an enhancement: shocks associated with infall or with outflows (Ceccarelli et al. 1996; Charnley & Rodgers 2005). The fact that hot corinos are associated with low-mass young stellar objects allows us to study directly the environment where solar-analogs are now forming.

In this chapter, we discuss how the ngVLA can help us to study the emission of heavy COMs in both low- and high-mass star-forming regions. The emission of COMs is important not only because it allows us to understand how chemistry may have developed to eventually form life in our Earth, but also because COMs are a powerful tool for studying the physical properties and kinematics of the dense regions very close to the central protostars.

2. COMs at centimeter wavelengths

COMs in high- and low-mass star-forming regions can be observed at (sub)millimeter wavelengths but are severely affected by line blending, especially in turbulent regions where the line widths are broad. In fact, many ALMA observations of the most chemically rich regions are essentially at the line confusion limit (Fig. 1) – that is, no additional molecules can be detected that emit below that threshold regardless of the

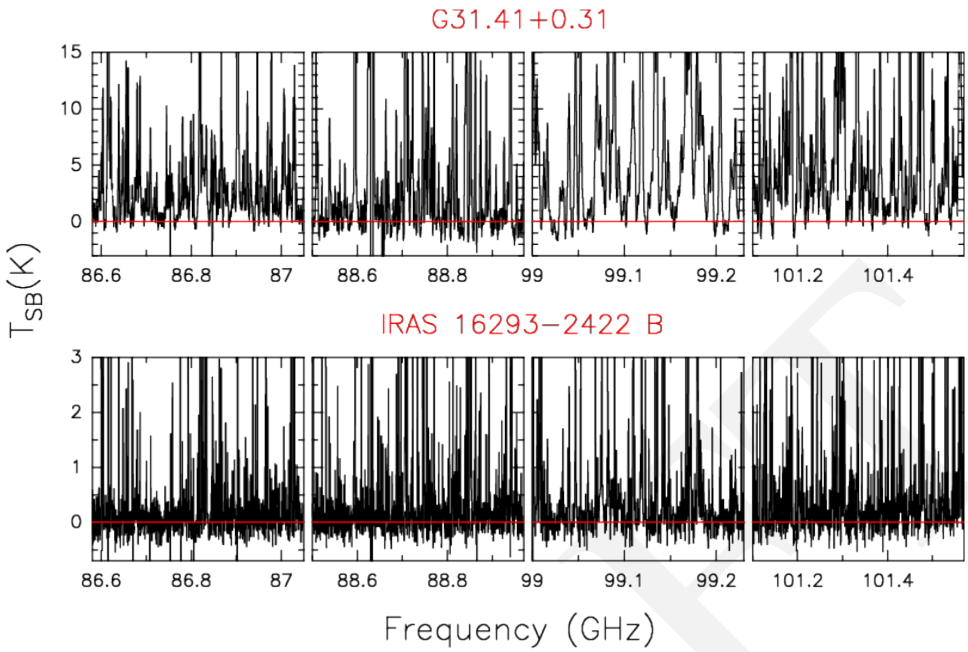

Figure 1. ALMA 3 mm spectra at ∼1″ angular resolution of the hot molecular core G31.41+0.31 (*upper panels*) and the hot corino IRAS 16293-2422 B (*lower panels*) (V. M. Rivilla, private communication). Red lines indicate T_{SB}=0 K. The 3-σ noise level at each panel falls inside the red line. The (sub)millimeter spectra of chemically rich hot cores/corinos like these two examples are full of molecular lines, which complicates the detection of very complex molecules with weak emission due to line confusion limit and blending problems.

sensitivity (rms) of the spectrum. Moving to the centimeter-wavelength window, the number of spectral lines in a selected spectral portion is significantly lower (see Fig. 2) with respect to the millimeter window, and hence, the lines are less blended. Moreover, at millimeter wavelengths, the dust opacity is commonly very high, and may produce strong line absorption, preventing in some cases the detection of the line emission itself, while at centimeter wavelengths the dust emission is usually optically thin.

The study of COMs at centimeter wavelengths is suited:

- **To detect heavy complex organic molecules in star forming-regions**. The PRIMOS survey, the GBT Legacy Survey of Prebiotic Molecules Toward Sgr B2N (Neill et al. 2012; Loomis et al. 2013; Zaleski et al. 2013), has detected in the last few years many COMs in this range in the massive HMC Sgr B2N, which is located in the Galactic Center. Some examples are: propenal (CH_2CHCHO), propanal (CH_3CH_2CHO), simple aldehyde sugars like glycolaldehyde (CH_2OHCHO), the first keto ring molecule detected in a interstellar cloud, cyclopropenone ($c{-}H_2C_3O$), ketenimine (CH_2CNH), ethanimine (CH_3CHNH), cyanomethanimine (HNCHCN) (see Fig. 3), and acetamide (CH_3CONH_2), the largest interstellar molecule detected with a peptide bond, key for prebiotic chemistry. Some of these species are, in fact, not suitable for observations at higher frequencies (millimeter and sub-millimeter regime). In general, the heavier the molecule, the more shifted to

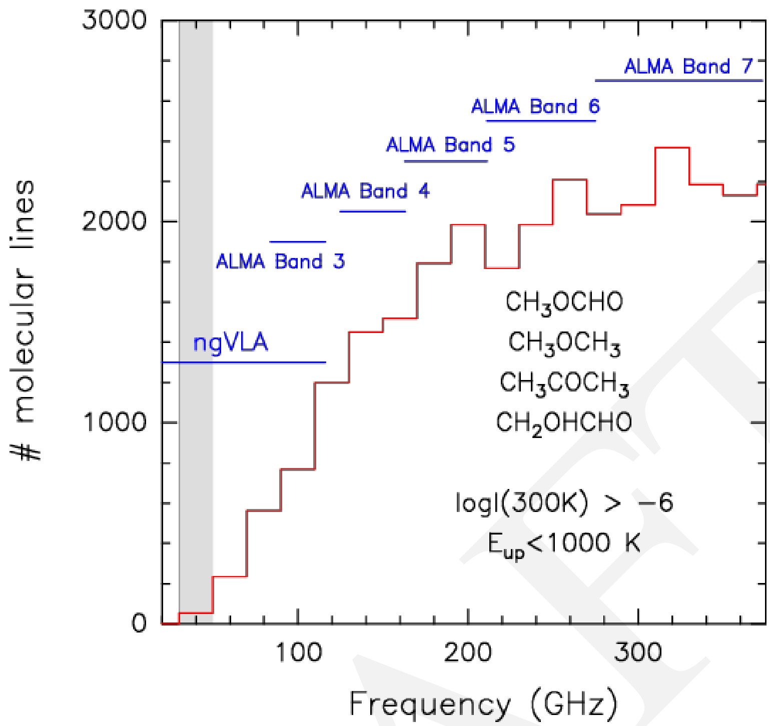

Figure 2. Distribution of the number of molecular lines as a function of frequency of four O-bearing COMs that are abundant in hot cores/corinos: methyl formate (CH_3OCHO), dimethyl ether (CH_3OCH_3), acetone (CH_3COCH_3), and glycolaldehyde (CH_2OHCHO). We have selected molecular transitions with log I (300K)> −6 and E_{up} < 1000 K from the JPL molecular catalogue. The frequency range shown in Figs. 3 and 4, 30–50 GHz, is indicated with a grey band. The spectral coverage of the ngVLA and ALMA bands 3, 4, 5, 6 and 7 is shown.

centimeter wavelengths its rotational spectrum is. In fact, these large molecules, with more than 8 atoms, have a considerable number of transitions at frequencies < 50 GHz.

- **To study circumstellar disks surrounding the protostars**. Heavy COMs are in general less abundant than typical HMC tracers, such as methyl cyanide, and therefore, their emission is expected to be optically thinner. The combination of low dust opacity at centimeter wavelengths and of low line opacity of these large and low abundant COMs, makes these species suitable to study the kinematics of high-mass star-forming regions – in particular of possible accretion disks – in a very pristine way. This probe is very important to understand better the formation of OB-type stars, for which the existence of true accretion disks is still under debate (e.g., Beltrán & de Wit 2016). The kinematics of the gas close to the central protostar should tell us whether high-mass stars have Keplerian circumstellar disks, like those observed towards lower-mass counterparts (.g., L1527 IRS: Tobin et al. 2012; Ohashi et al. 2014; HD 163296: de Gregorio-Monsalvo et al. 2013), or whether they are surrounded by rotating structures undergoing solid-body rotation.

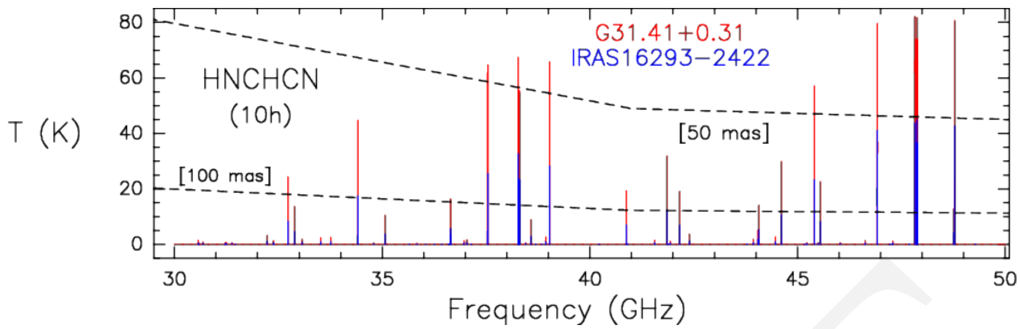

Figure 3. Synthetic spectra obtained with MADCUBA of cyanomethanimine, HNCHCN, for G31.41+0.31 hot molecular core (red) and IRAS16293-2422 B hot corino (blue). We have assumed an excitation temperature of 100 K, and column densities of 3×10^{17} cm^{-2} and 3×10^{16} cm^{-2} for G31.41+0.31 and IRAS 16293−2422, respectively. The line widths considered are 5.0 km s^{-1} and 1.5 km s^{-1} for G31.41+0.31 and IRAS 16293−2422, respectively, consistent with those found at milllimeter wavelengths (Rivilla et al. 2017; Jørgensen et al. 2016). We have overplotted with dashed lines the 3-σ noise level for an integration time of 10 hr with two different angular resolutions, assuming a spectral resolution of 1 km s^{-1}, according to the specifications of the ngVLA.

3. Measurements required

The ngVLA will provide an unprecedented sensitivity and spatial resolution in the centimeter wavelength range that will allow us to detect new complex species and spatially resolve the emission of heavy COMs, e.g., those previously detected with the GBT (resolution > 16″). By targeting two of the most chemically rich star-forming regions, a high-mass hot molecular core (G31.41+0.31: Beltrán et al. 2009; Rivilla et al. 2017) and a low-mass hot corino (IRAS 16293-2422: Jørgensen et al. 2016; Martín-Doménech et al. 2017), it will be possible to detect prebiotic species, such as HNCHCN (see Fig. 3), for the first time outside the Galactic Center. In addition, the high-angular resolution provided by the ngVLA will allow us to map the distribution of heavy COMs from the envelope down to the accretion disks embedded in the hot core and hot corino, respectively, and characterize the region where the emission originates. It is important to understand whether the emission comes from the inner circumstellar disk where planets could form, or whether it originates in an outer region of the disk/envelope, where comets reside.

In particular, the ngVLA capabilities would allow us to:

- **Detect heavy (prebiotic) COMs, for the first time outside the Galactic Center**. First detections of new species in HMCs have been carried out mainly towards Sgr B2 (see Belloche et al. 2008; Zaleski et al. 2013). This complex, located in the Central Molecular Zone, has been observed at different wavelengths and as a result, the first detections of heavy COMs in the Galaxy, such as ethylene glycol or ethyl formate (10 and 11 atoms, respectively), have been obtained there (e.g., Hollis et al. 2000, 2002). The cores in Sgr B2, however, are not typical HMCs. The current star formation rate of Sgr B2 qualifies it as a mini-starburst region and its location close to the Galactic Center makes the physical conditions in that environment quite extreme, which could have significant consequences on the chemistry. Therefore, the chemistry in Sgr B2 might not be representative of that typical of HMCs in the disk of the Galaxy. In addition, the presence of several velocity components along the line of sight makes line identification more difficult. Therefore, to study the chemistry of COMs and the environments where they form, it is important to detect heavy COMs around more typical star-forming regions. The two star-forming cores G31.41+0.31 and IRAS 16293−2422 are among the best candidates to detect new molecular species in high- and low-mass star-forming regions, respectively, outside the Galactic Center because of their chemical richness (see Fig. 1). They, thus, will serve as templates for future observations of a range of sources with different stellar masses. In particular, large molecules with > 9 atoms have been already detected in both regions (Jørgensen et al. 2016; Rivilla et al. 2017). However, these two sources are not the only ones showing a chemically rich spectrum. HMCs are the cradles of OB stars, and it is therefore expected all high-mass (proto) stars to be associated with them (Beltrán 2010). Regarding the low-mass regime, with the advent of ALMA, the number of known hot corinos is increasing

To detect new species, high sensitivity is more important than high-angular resolution. In principle, it would not even be necessary to resolve the emission. In practice, however, it is important to resolve it, at least slightly, to study the spatial distribution of the COMs and check whether the emission of different species is spatially correlated, i. e., coming from the same region.

We have used the example of the prebiotic species cyanomethanimine (HNCHCN, see Fig. 3), only detected so far by the GBT in Sgr B2N within the PRIMOS Project (Zaleski et al. 2013). To estimate the sensitivity (rms) required to detect emission from HNCHCN, we have modelled its emission assuming LTE conditions, an excitation of 100 K, typical of hot cores and hot corinos, and column densities of 3×10^{17} cm^{-2} and 3×10^{16} cm^{-2} for G31.41+0.31 and IRAS 16293−2422, respectively (see caption of Fig. 3). In this figure, we have plotted the 3-σ noise level for an angular resolution of 50 mas and 100 mas and an integration time of 10 hr. As seen in the figure, at 50 mas angular resolution, only emission from the high-mass hot molecular core G31.41+0.31 would be detectable. Since IRAS 16293−2422 is located at only 120 pc, however, the spatial resolution achieved even with 100 mas (∼12 au), is already very high.

- **Study of the physical properties and kinematics of the circumstellar disks.** The distance to the solar-type protostar IRAS 16293-2422 is 120 pc. Therefore, with a spatial resolution of ∼5–10 au, achieved with an angular resolution of 50–100 mas, we should be able to study the kinematics and the chemistry of the inner disk region where planets could form. On the other hand, the O-type (proto)star G31.41+0.31 is located much farther away, at 7.9 kpc. By observing the core with an angular resolution of 35 mas (a good compromise between angular resolution and sensitivity), the spatial scales achieved would be ∼280 au, typical of disks around intermediate-mass protostars (e.g., Beltrán & de Wit 2016). Therefore, if a circumstellar disk is surrounding this massive star, the ngVLA should be able to detect it. Note that circumstellar disks have been detected up to late O-type stars (e.g., Johnston et al. 2015), but the luminosity of G31.41+0.31 ($3\times10^5\,L_\odot$) indicates that this HMC is hosting O6–O7 (proto)stars. Therefore, detecting such

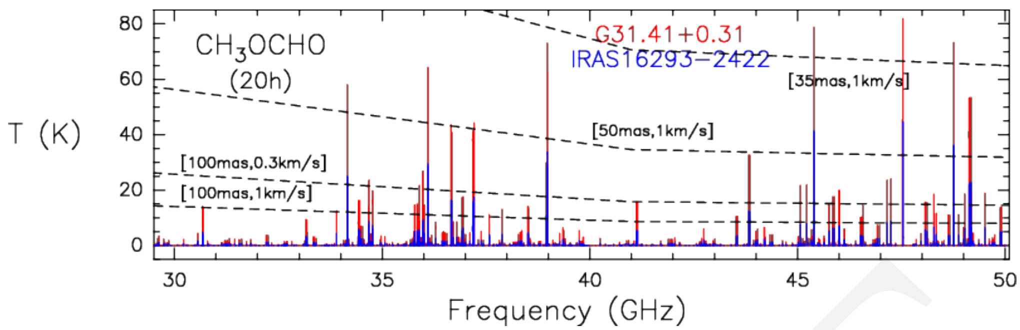

Figure 4. Synthetic spectra obtained with MADCUBA of methyl formate, CH_3OCHO, for G31.41+0.31 hot molecular core (red) and IRAS16293-2422 B hot corino (blue). We have assumed an excitation temperature of 100 K. The column densities for G31.41+0.31 and IRAS 16293−2422 are 5×10^{18} cm^{-2} and 5×10^{17} cm^{-2}, respectively, from Rivilla et al. (2017a) and Jorgensen et al. (2012). The linewidths considered are 5.0 km s^{-1} and 1.5 km s^{-1} for G31.41+0.31 and IRAS 16293−2422, respectively. We have overplotted with dashed lines the 3-σ noise level of an integration time of 20 hr with different combinations of angular and spectral resolutions, indicated with labels, according to the specifications of the ngVLA.

a disk would be crucial to confirm that stars of all masses form by disk-mediated accretion.

To study the physics and kinematics of the disks, we have chosen the well-known high-density tracer methyl formate (CH_3OCHO, see Fig. 4). Methyl formate is a complex (8 atoms) molecule, which is a good thermometer and has been clearly detected in both regions with observations at much lower angular resolution (Jørgensen et al. 2012; Beltrán et al. 2018). To estimate the required sensitivity, we have modelled the methyl formate emission assuming LTE conditions, an excitation of 100 K, typical of hot cores and hot corinos, and a column density of 5×10^{18} cm^{-2} and 5×10^{17} cm^{-2} for G31.41+0.31 and IRAS 16293−2422, respectively (see caption of Fig. 4), consistent with what found at millimeter wavelengths in the inner regions of hot cores/corinos (Jørgensen et al. 2012; Rivilla et al. 2017), and line widths of 5 km s^{-1} and 1.5 km s^{-1}. The rms noise has been estimated for different angular and spectral resolutions. As seen in Fig. 4, the methyl formate emission can be observed at high enough spatial resolution to study properly the kinematics of the circumstellar disks: up to ~5 au for IRAS 16293−2422 and up to ~280 au for G31.41+0.31.

4. Synergy with other instruments

Complex organic molecules can be observed from centimeter to millimeter wavelengths. As mentioned before, to detect new species, high sensitivity is more important than high-angular resolution. Therefore, it is not surprising that some of the most recent detections have been done with a single-dish telescope, the GBT, within the PRIMOS Project (Zaleski et al. 2013). However, although single-dish observations are a good starting point to detect new species, high-sensitivity interferometric observations are absolutely needed. On the other hand, because the emission of heavy COMs can be very weak and compact, it is not unusual that species previously not detected with a single dish, because of beam dilution, and easily detected with an interferometer. On the other hand, it is important to resolve the emission of COMs to study the spatial distribution of the COMs and check whether the emission of different species is spatially correlated, i. e., coming from the same region. This can help to constrain better the formation routes of different species and to distinguish between different chemical models (e.g., gas phase formation vs. grain surface).

Regarding the millimeter regime, COMs have been detected with facilities such as IRAM NOEMA and ALMA, although as explain before, for chemically rich sources, the millimeter observations can suffer from line confusion limit and line blending, which might difficult the identification of new species. In any case, millimeter and centimeter observations are complementary. By observing COMs at millimeter wavelengths with ALMA or NOEMA, we should be able to trace high-energy transitions of the same molecules and obtain a complete picture of the emission of such heavy species. This synergy will be very important to constrain better the formation routes of heavy COMs.

Acknowledgments. V.M.R. is funded by the European Union's Horizon 2020 research and innovation programme under the Marie Skłodowska-Curie grant agreement No 664931.

References

Adams, F. C. 2010, ARA&A, 48, 47
Belloche, A., Menten, K. M., Comito, C. et al. 2008, A&A, 482, 179
Belloche, A., Müller, H. S. P., Menten, K. M. et al. 2013, A&A, 559, A47
Beltrán, M. T. in Computational Star Formation, Proceedings of the International Astronomical Union, IAU Symp. 270, 33
Beltrán, M. T., Codella, C., Viti, S. et al. 2009, ApJ, 690, L93
Beltrán, M. T., Cesaroni, R., Rivilla, V. M. et al. 2018, A&A, arXiv:1803.05300
Beltrán, M. T., & de Wit, W. J. 2016, A&ARv, 24, 6
Bisschop, S. E., Jørgensen, J. K., van Dishoeck, E. F. et al. 2007, A&A, 465, 913
Bottinelli, S., Ceccarelli, C., Neri, R. 2004, ApJ, 617, L69
Ceccarelli, C., Hollenbach, D. J., Tielens, A. G. G. M. 1996, ApJ, 471, 400
Charnley, S., & Rodgers, S. D. 2005, Highlights of Astronomy, 13, 511
de Gregorio-Monsalvo, I., Ménard, F., Dent, W. et al. 2013, A&A, 557, A133
Drozdovskaya, M. N., van Dishoeck, E. F., Jørgensen, J. K. et al. 2018, MNRAS, 476, 4949
Hollis, J. M., Lovas, F. J., Jewell, P. R. 2000, ApJ, 540, L107
Hollis , J. M., Lovas, F. J., Jewell, P. R., Coudert, L. H. 2002, ApJ, 571, L59
Johnston, K. G., Robitaille, T. P., Beuther, H. et al. 2015, ApJ, 813, L19
Jørgensen, J. K., Favre, C., Bisschop, S. E. 2012, ApJ, 757, L4
Jørgensen, J. K., van der Wiel, M. H. D. Coutens, A. et al. 2016, A&A, 595, A117
Loomis, R. A., Zaleski, D.łP., Steber, A. L. et al. 2013, ApJ, 765, L9
Martín-Doménech, R., Rivilla, V. M., Jiménez-Serra, I. et al. 2017, MNRAS, 469, 2230
Neill, J. L., Muckle, M. T., Zaleski, D. P. et al. 2017, ApJ, 755, 153
Ohashi, N., Saigo, K., Aso, Y. et al. 2014, ApJ, 796, 131
Rivilla, V. M., Beltrán, M. T., Cesaroni, R. et al. 2017, A&A, 598, A59
Taquet, V., Furuya, K., Walsh, C., van Dishoeck, E. F. 216, MNRAS, 462, 99
Tobin, J. J., Hartmann, L., Chiang, H.-F. et al. 2012, Nature, 492, 83
Zaleski, D. P., Seifert, N. A., Steber, A. L. et al. 2013, ApJ, 765, L10

Science with a Next-Generation Very Large Array
ASP Conference Series, Monograph 7
Eric J. Murphy, ed.

DRAFT EDITION

Detecting Infall in High-Mass Protostellar Objects

Maria T. Beltrán[1], Qizhou Zhang[2], and Víctor M. Rivilla[1]
[1]*INAF-Osservatorio Astrofisico di Arcetri, Largo E. Fermi 5, I-50125 Firenze, Italy;* mbeltran@arcetri.astro.it,rivilla@arcetri.astro.it

[2]*Harvard-Smithsonian Center for Astrophysics, 60 Garden St. Cambridge, MA 02138, USA;* qzhang@cfa.harvard.edu

1. Introduction: the formation of high-mass stars

The role of accretion disks in the formation of low-mass stars has been well assessed by means of high angular resolution observations at various wavelengths. These findings confirm the prediction that conservation of angular momentum during the collapse leading to the formation of a star is bound to produce flattening and rotation of the collapsing core. Therefore, the existence of such disks around low-mass young stellar objects (YSOs) strongly supports the scenario where the formation of *low-mass* stars proceeds through contraction of a dense molecular clump and subsequent inside-out collapse with accretion onto a protostellar core. In synthesis, one can say that *low-mass stars form through accretion*.

What about *high-mass* stars? The formation process of high-mass stars has puzzled the astrophysical community for decades because of the apparent stellar mass limit for spherical accretion. Beyond this limit, theory predicted that it is impossible to continue accreting material because the stellar wind and the radiation pressure from the newly-formed early-type star would stop the infall (e.g., Kahn 1974; Yorke & Krügel 1977; Wolfire & Casinelli 1987). In the 1990s, different theoretical scenarios proposed non-spherical accretion as a possible solution for the formation of OB-type stars (Nakano 1989; Jijina & Adams 1996), and in recent years, theoretical ideas and simulations appear to have converged to a disk-mediated accretion scenario (e.g., Krumholz et al. 2009; Kuiper et al. 2010; Klassen et al. 2016). In fact, competing theories that propose very different high-mass star-formation mechanisms, such as models suggesting that massive star-formation is initiated by the monolithic collapse of a turbulent molecular core (McKee & Tan 2002), or those based on competitive accretion (Bonnell & Bate 2006), all predict the existence of circumstellar accretion disks through which the material is channeled onto the forming star. With this in mind, it is clear that the detection of infall in circumstellar disks represents a crucial test to prove the accretion scenario also applies in the case of high-mass stars.

At present, several authors have reported on detections of disks around high-mass YSOs (see Beltrán & de Wit 2016, for a review). In most cases, the existence of such a disk is also supported by the detection of a bipolar jet/outflow along the apparent rotational axis of the disk. It must be noted that some of these disks resemble massive toroids rotating about a cluster of high-mass stars, rather than geometrically thin circumstellar disks. In any case, no matter whether the disk is circumstellar or "circumcluster", these findings strongly support the accretion scenario also for the high-mass regime.

Notwithstanding these important results, the presence of disks rotating about high-mass stars is not sufficient by itself to prove unambiguously the accretion model: what is needed is iron-clad evidence of *infall*. Such evidence is very difficult to find, as the free-fall velocity becomes significant only very close to the accreting star, i.e., over a region of a few 0.01 pc (~2000 au), which is very difficult to access and disentangle from the surrounding quiescent or rotating material. In this chapter we discuss how to characterize the infall of material in a sample of 36 high-mass accretion disk candidates covering a broad range of luminosities, from $10^3\,L_\odot$ to $10^6\,L_\odot$, compiled by Beltrán & de Wit (2016) with the ngVLA.

2. Tracing infall

Red-shifted molecular absorption against a bright background continuum source is possibly the clearest way of diagnosing infall and accretion. For this, it is necessary to observe high-density tracers with excitation energies below the brightness temperature of the central continuum source, and observe them especially with interferometers (because the emission does not suffer from beam dilution). The first studies using this technique were conducted at centimeter wavelengths with the VLA by observing NH_3 in absorption against the bright ultracompact (UC) HII region G10.62−0.4 (Ho & Haschick 1986; Keto et al. 1988). Later one, infall has been detected toward other ultracompact/hypercompact (UC/HC) HII regions: e.g., W51 (Zhang & Ho 1997), G24.78+0.08 (Beltrán et al. 2006a), NGC 7538 IRS1 (Goddi et al. 2015), also observed in NH_3 with the VLA or the upgraded Jansky VLA. Ammonia is the best species to study infall in dense cores because it is possible to trace excitation up to temperatures of ~2000 K by observing its inversion transitions within a relatively narrow frequency range at centimeter wavelengths, 20–40 GHz, which cannot be observed with (sub)millimeter interferometers such as SMA, IRAM NOEMA, or ALMA. This allows us to conduct the tomography of the infall in the core. In addition, in case the main line is optically thick, one can always use the hyperfine satellite lines, which are usually optically thin, to study the absorption.

Red-shifted absorption at high-angular resolution has also been observed against bright dust continuum sources at millimeter wavelengths (e.g., Zapata et al. 2008; Girart et al. 2009; Beltrán et al. 2018). For high-mass protostars, however, dust emission from envelopes and disks becomes so optically thick that deep probes of infall motion are prevented. In addition, the brightness temperatures of the UC/HC HII regions are typically 10^3–10^4 K, much higher than those of the dust continuum sources (a few hundreds of K). This bright background enables detection of line absorption with much higher signal-to-noise ratio, as well as probing infall closer to the central protostar with higher energy molecular line transitions.

What can we learn from the gravitational collapse by observing red-shifted absorption? We can estimate the infall rate $\dot{M}_{\rm inf}$ of material in the core. Note that red-shifted absorption profiles trace infalling material in the inner part of the core or in the disk, but not actual accretion onto the central star. Following (Beltrán et al. 2006a), the infall rate in a solid angle Ω can be estimated from the expression $\dot{M}_{\rm inf} = (\Omega/4\,\pi)\,2\,\pi\,m_{\rm H_2}\,N\,R_0^{1/2}\,R^{1/2}\,V_{\rm inf}$, where N is the gas column density, R_0 is the radius of the continuum source, $V_{\rm inf}$ is the infall velocity, and R is the radius at which

$V_{\rm inf}$ is measured. The main caveat of this method is the uncertainty on R. In fact, the radius at which $V_{\rm inf}$ is associated is not known, and usually the size of the infalling core is given as an upper limit. Red-shifted absorption can also help us to constrain star-formation theories by studying whether infall spins down or spins up. In fact, the advantage of tracing a wide range of excitation temperatures (~20 K to 2000 K) with several transitions of NH_3 is that by measuring the velocity of the absorption feature for each transition it is possible to study whether the infall velocity (assumed to be the difference between the velocity of the red-shifted absorption dip and the systemic LSR velocity) changes with the energy of the line. If the infall velocity increases with the energy of the transition (spins up), this would suggest that the infall is accelerating towards the center of the core, consistent with gravitational collapse (Beltrán et al. 2018). One the other hand, if the infall velocity decreases (spins down), it could suggest that magnetic braking is acting and removing angular momentum (Basu & Mouschovias 1994). This would suggest that the gravitational collapse of the core is controlled by magnetic fields (Girart et al. 2009). In addition, a detailed modeling of the NH_3 line emission and of the spectral energy distribution with an infalling envelope model can give us information on the mass of the central star, its age and luminosity, and the mass accretion rate, similar to what Osorio et al. (2009) have done for the hot molecular core G31.41+0.31.

3. Uniqueness to ngVLA capabilities

Up to now, red-shifted absorption at centimeter wavelengths has been only detected toward the brightest UC/HC H II regions and with limited angular resolution and sensitivity using the VLA. These limits mean that, in many cases, the absorption has not been spatially resolved and only the lower excitation energy transitions, which are probably tracing the outer regions of the massive envelope, have been observed. Therefore, to trace infall in high-mass cores, with luminosities ranging from $10^3\,L_\odot$ up to $10^6\,L_\odot$, high sensitivity and high-angular resolution are essential. High sensitivity is needed to trace high-excitation transitions of high-density tracers, which are those tracing the material closest to the protostar. On the other hand, high-angular resolution would allow us to resolve spatially the absorption, even for distant objects. A good tracer of infall is NH_3 because, as already mentioned, multi transitions at different energies can be observed in red-shifted absorption against bright ionized sources.

The high sensitivity of the ngVLA will allow us to detect NH_3 inversion transitions in red-shifted absorption toward all the sources of the sample of high-mass accretion disk candidates with luminosities ranging from $10^3\,L_\odot$ up to $10^6\,L_\odot$ compiled by Beltrán & de Wit (2016), including the faintest ionized ones. In particular, the ngVLA will detect infall toward massive stars shortly after the onset of an H II region, and at a maximum angular resolution of 20 mas. Figure 1 shows the synthetic spectrum of NH_3, from the (3,3) inversion transition to the (14,14) one, obtained with MADCUBA (Madrid Data Cube Analysis on ImageJ), which is a software developed in the Center of Astrobiology (Madrid, INTA-CSIC) to visualize and analyze single spectra and datacubes (Rivilla et al. 2016; Martín et al., in prep.). The spectra have been modeled for two different angular resolutions, 20 mas and 50 mas with different column densities of NH_3, $10^{18}\,{\rm cm}^{-2}$ and $10^{17}\,{\rm cm}^{-2}$, respectively. As seen in the figure, an rms of ~45 μJy/beam, achievable after a 10 hr integration per source, would allow us to detect the main lines of the weakest inversion transitions of ammonia, up to the NH_3 (14, 14)

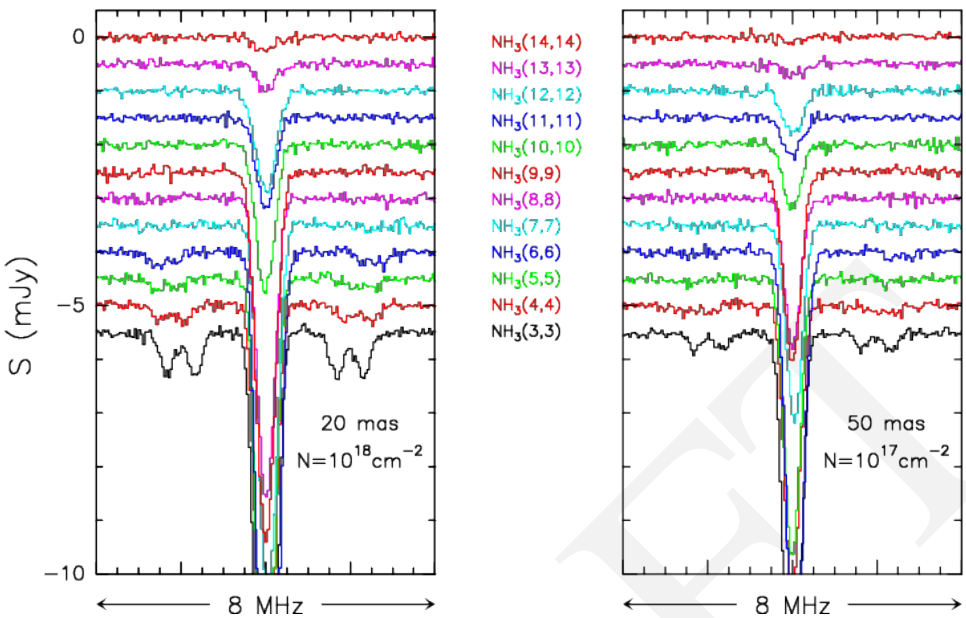

Figure 1. Synthetic spectrum of NH_3 obtained with MADCUBA, assuming LTE conditions. Different transitions, from the (3,3) inversion transition to the (14,14) one, are shown with different colors. For display purposes, the transitions have been shifted by 0.5 mJy in the y-axis. The left and right panels show two cases for different angular resolutions and column densities of NH_3: 20 mas and 10^{18} cm^{-2}, and 50 mas and 10^{17} cm^{-2}, respectively. The linewidth considered is 5 km s^{-1}. The brightness temperature of the UC/HC HII region is 10^4 K. We have considered a noise level of 45 μJy, which is the rms achieved for an integration time of 10 hr and a spectral resolution of 1 km s^{-1}, according to the specifications of the ngVLA.

transition, and the satellite lines of the strongest ones, for NH_3 column densities consistent with (or even lower than) those found around high-mass young stellar cores (e.g., Beltrán et al. 2006a; Goddi et al. 2015). Spectral resolution should not be a problem for the ngVLA, considering that a modest channel spacing of ~1 km/s is less than the typical line widths of high-mass protostellar cores of a few km/s. Regarding the angular resolution, 20 mas corresponds to 100 au at a distance of 5 kpc, which is the typical distance of O-type young stars (e.g., Beltrán et al. 2006b). Typical sizes of accretion disks around low-mass stars are of the same order, ~100 au. Note that the highest angular resolution provided by VLA at the NH_3 transition frequencies is about 50 mas. Given the high mass of these cores, they often fragment and form multiple protostars. Therefore, the high-angular resolution of ngVLA will resolve the emission and trace the accretion flows around individual protostars.

The milli-arcsecond angular resolution achieved with the ngVLA and the wide range of excitation energies covered by the NH_3 inversion transitions (from ~20 K to 2000 K) will allow us to trace the kinematics of circumstellar gas from the envelope down to the circumstellar disk, and infer the properties of the accretion to better constrain theories of massive star formation. In fact, although the two competing theories on massive star-formation propose a disk-mediated accretion scenario, the properties of such disks are expected to be different. In fact, while in the turbulent core collapse case one would expect the material to be incorporated onto the central protostar though a true accretion disk in Keplerian motion with a size of a few hundreds of au, in the competitive accretion, the disks could be asymetric, truncated and very small (< 100 au) due to tidal interactions (Cesaroni et al. 2006) in the crowded star-forming cores (according to this model, high-mass stars always form in clusters). Alternatively, accretion could proceed to the central protostar through filaments rather than through a disk (Goddi et al. 2018).

4. Synergy at other wavelengths

The study of infall at centimeter wavelengths complements: *i)* ALMA or NOEMA observations of molecular outflows aimed at estimating the mass outflow rate, which is related to the mass accretion rate onto the protostar as $\dot{M}_{\rm acc} = \dot{M}_{\rm out}/6$ (Tomisaka 1998; Shu et al. 1999), and *ii)* JWST observations of Brγ lines aimed at determining the mass accretion rate in the disk. By comparing the mass infall rate obtained at centimeter wavelengths to the mass accretion rate one could determine concretely whether the former are much higher than the latter, as suggested by recent studies (Beltrán & de Wit 2016). Such a mismatch which could indicate pile-up of material in the disk and the existence of episodic accretion, for example as recently observed in the high-mass stellar object S255IR (Caratti o Garatti et al. 2017).

5. Conclusions

The superb sensitivity and angular resolution provided by the ngVLA will allow us to study the gravitational collapse in high-mass star-forming sources of all luminosities (from $10^3\,L_\odot$ to $10^6\,L_\odot$). The detection of red-shifted absorption in several inversion transitions of NH_3 with different excitation energies will allow us to trace the material down to disk scales and to derive the properties of the collapse and of the accretion disks that will help us to better constrain theories of high-mass star formation. In particular, by studying the infall velocity field, i.e., whether infall spins down or spins up, we will infer what controls the gravitational collapse in high-mass star-forming regions.

Acknowledgments. V.M.R. is funded by the European Union's Horizon 2020 research and innovation programme under the Marie Skłodowska-Curie grant agreement No 664931.

References

Basu, S., & Mouschovias, T. Ch. 1994, ApJ, 432, 720
Beltrán, M. T., & de Wit, W. J. 2016, A&ARv, 24, 6
Beltrán, M. T., Cesaroni, R., Codella, C., Testi., L. et al. 2006a, Nature, 443, 427
Beltrán, M. T., Brand, J., Cesaroni, R. et al. 2006b, A&A, 447, 221
Beltrán, M. T., Cesaroni, R., Rivilla, V. M. et al. 2018, A&A, arXiv:1803.05300
Bonnell, I. A., & Bate, M. R. 2006, MNRAS, 370, 488
Caratti o Garatti, A., Stecklum, B., Garcia López, R. et al. 2017, Nature Physics, 13, 276
Cesaroni, R., Galli, D., Lodato, G. et al. 200, Nature, 444, 703
Girart, J. M., Beltrán, M. T., Zhang, Q. et al. 2009, Science, 324, 1408
Goddi, C., Zhang, Q., & Moscadelli, L. 2015, A&A, 573, A108
Goddi, C., Ginsburg, A., Maud, L. et al. 2018, arXiv:1805.05364

Kahn, F. 1974, A&A, 37, 149
Keto, E. R., Ho, P. T. P., & Haschick, A. D. 1988, ApJ, 324, 920
Klassen, M., Pudritz, R. E., Kuiper, R., Peters, Th., Banerjee, R. 2016, ApJ, 823, 28
Krumholz, M. R., Klein, R. I., McKee, C. F., Offner, S. S. R., & Cunningham, A. J. 2009, Science, 323, 754
Kuiper, R., Klahr, H., Beuther, H., & Henning, T. 2010, ApJ, 722, 1556826, 161
Ho, P. T. P., & Haschick, A. D. 1986, ApJ, 304, 501
Jijina, J., & Adams, F. C. 1996, ApJ, 462, 874
McKee, C. F., & Tan, J. C. 2002, Nature, 416, 59
Nakano, T. 1989, ApJ, 345, 464
Osorio, M., Anglada, G., Lizano, S., D'Alessio, P. 2009, ApJ, 694, 29
Rivilla, V. M., Fontani, F., Beltrán, M. T. et al. 2016, ApJ,
Shu, F., Allen, A., Shang, H. et al. 1999, NATO Adv. Sci. Institutes Ser. C., Lada, C. & Kylafis, N. (ed) NATO Advanced Science Institutes (ASI) Series C, 540, 193
Tomisaka, K. 1998, ApJL, 502, 163
Wolfire, M, & Cassinelli, J. 1987, ApJ, 319, 850
Yorke, H. W., & Krügel, E. 1977, A&A, 54, 183
Zapata, L., Palau, A., Ho, P. T. P. et al. 2008, A&A, 479, L25
Zhang, Q., & Ho, P. T. P. 1997, ApJ, 488, 241

Science with a Next-Generation Very Large Array
ASP Conference Series, Monograph 7
Eric J. Murphy, ed.

Star-forming Filaments and Cores on a Galactic Scale

James Di Francesco[1], Jared Keown[2], Tyler Bourke[3], and Paola Caselli[4]
[1]*National Research Council of Canada, Victoria, BC, Canada;* `james.difrancesco@nrc-cnrc.gc.ca`

[2]*University of Victoria, Victoria, BC, Canada;* `jkeown@uvic.ca`

[3]*Square Kilometre Array Organization, Macclesfield, UK;* `t.bourke@skatelescope.org`

[4]*Max Planck Institute for Extraterrestrial Physics, Garching, Germany;* `caselli@mpe.mpg.de`

Abstract. Continuum observations of molecular clouds have revealed a surprising amount of substructure in the form of filaments of a few pc length and cores of ~0.1 pc diameter. Understanding the evolution of these substructures towards star formation requires the kinematic and dynamical insights provided uniquely by sensitive line observations at high angular and spectral resolution. In this Chapter, we describe how an ngVLA can probe effectively the dynamics of filaments and cores in nearby star-forming molecular clouds using the NH_3 rotation-inversion transitions at 24 GHz. Such emission has been proven to trace well the high column density environments of star-forming cores and filaments but higher-resolution observations are needed to reveal important details of how dense gas is flowing within and onto these substructures. In particular, we describe how 150 × 18-m antennas with a maximum baseline of 1 km can be used to map sensitively NH_3 emission across high column density locations in clouds in roughly an order of magnitude less time than with the current Jansky VLA.

1. Introduction

Stars form out of molecular cloud gas, when dense pockets (i.e., "cores") become gravitationally unstable and collapse (see Di Francesco et al. 2007 for a review). Recent far-infrared/submillimeter continuum observations (e.g., from *Herschel* or the JCMT) of Galactic clouds at distances < 3 kpc have revealed close connections between the detailed substructures of clouds and star formation. First, molecular clouds are suffused with filaments, regardless of their star-forming activity (André et al. 2010; Ward-Thompson et al. 2010). Second, clouds can have hundreds of cores, many of which appear bound and hence likely to form stars in the future (Könyves et al. 2010). Third, core formation, and hence star formation, appears to be most efficient within supercritical filaments above a given column density threshold equivalent to $A_V \sim 7$ magnitudes (André et al. 2010, 2014). Indeed, the resulting core mass function strikingly resembles the initial stellar mass function, suggesting the process that forms cores also ultimately determines stellar masses (Könyves et al. 2015). Finally, high-mass star and clus-

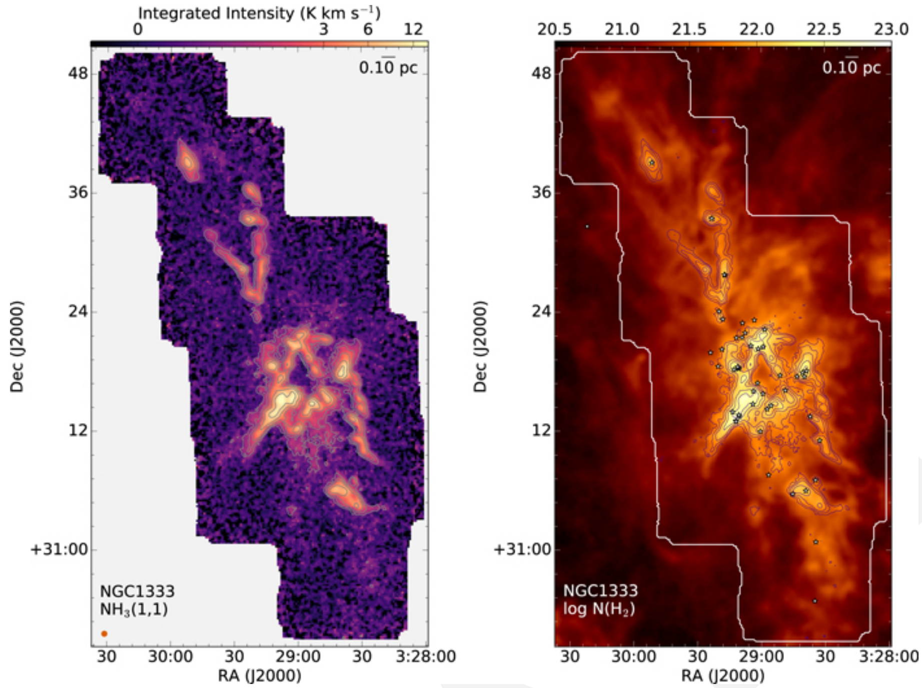

Figure 1. Left: integrated intensity map of the NH_3 (1, 1) line for the NGC 1333 region obtained by the Green Bank Ammonia Survey (Friesen et al. 2017). Contours are drawn at [3, 6, 12, 24, ...]-σ, where 1 $\sigma \approx 1.0$ K km s^{-1} was estimated from emission-free pixels. Beam size and scale bar are shown in the bottom left and top right corners, respectively. Right: the H_2 column density, log10 [N(H_2) cm^{-2}], derived from SED fitting of Herschel submillimeter dust continuum data (A. Singh et al. 2018, in preparation). Contours show the NH_3 (1,1) integrated intensity, as in the left panel. White contours show the GAS map extent. Stars show the locations of Class 0/I and flat-spectrum protostars (Dunham et al. 2015).

ter formation occur most efficiently where supercritical filaments appear to intersect (Schneider et al. 2012).

Understanding the relationships between filamentary substructures and star formation requires kinematic and dynamical insights. For example, how does gas in clouds assemble into filaments and cores? Also, how will the gas in these sub-structures evolve? Are there substructures within filaments (e.g., "fibers"; Hacar et al. 2013, 2017). The continuum observations that identified these substructures do not have the ability to trace their kinematics and dynamics. Instead, observations of line emission are essential to determine how mass flows within filaments and cores and whether or not such substructures are stable. More specifically, to understand the structure and dynamical evolution of molecular clouds in general, large-scale surveys of lines must be performed at sensitivities and resolutions not possible with currently available observatories.

The NH_3 rotation-inversion transitions at 24 GHz (e.g., (1,1), (2,2), (3,3), etc.) can probe effectively the kinematics and dynamics of star-forming substructures in nearby molecular clouds. NH_3 emission has been shown repeatedly to trace best the locations of significant column density revealed by continuum emission from dust (e.g., Benson & Myers 1989). This behavior follows partly because the NH_3 transitions are

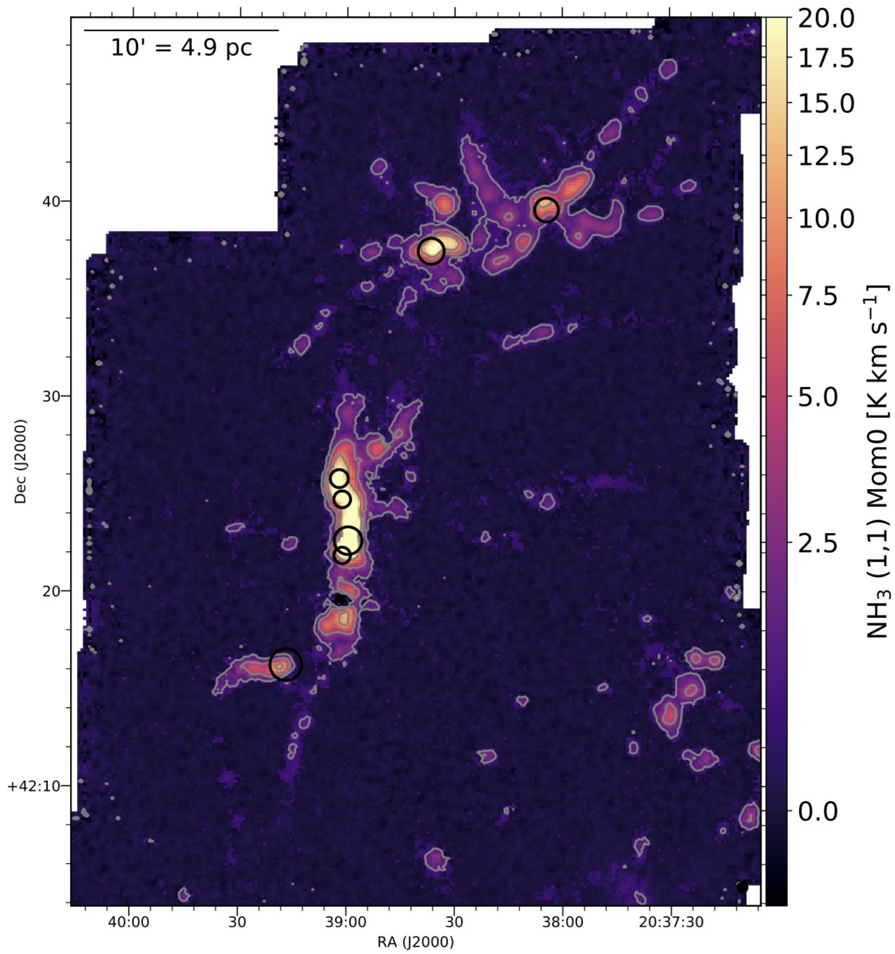

Figure 2. Integrated intensity map of the NH_3 (1, 1) line for the Cygnus X North region, including DR21, obtained by the KEYSTONE survey (Keown et al. 2018). Colors range from -1 K km s^{-1} (black) to 10 K km s^{-1} (yellow). Contours are at 1.0, 3.5, and 10 K km s^{-1}. Circles show the locations of H_2O maser emission simultaneously detected during the NH_3 observations. The size of the circle indicates the relative brightness of the maser emission.

excited in moderately dense gas; e.g., the critical densities of (1,1) and (2,2) at 10 K are 10^{3-4} cm^{-3} (Ho & Townes 1983). In addition, these NH_3 transitions have hyperfine structure that spreads out their overall optical depths over numerous components, enabling better probes of all dense gas along the line of sight (Crapsi et al. 2007). In contrast, other molecules have emission that is too optically thick to sample such environments (e.g., ^{12}CO) or have been themselves too drastically depleted in cold dense gas to be effective probes (e.g., C^{18}O; see Di Francesco et al. 2007). Even other less-abundant "dense gas tracers" like HCN or CN emission may yet suffer from optical depth and depletion issues on the scales of cores and filaments. Furthermore, the hyperfine structure of the NH_3 transitions further allows, through simultaneous fitting, direct determinations of excitation temperature and opacity, and hence column density. Finally, these NH_3 transitions can directly provide the gas kinetic temperature along the line of sight via their ratios (Walmsley & Ungerechts 1983), unlike those of other nitrogen-based molecules (e.g., N_2H^+).

Given the utility of NH_3 emission, it is being widely observed to trace the kinematics and dynamics of moderately dense gas in molecular clouds, especially in filaments and cores. These programs are being largely run from the Green Bank Telescope (GBT) using its unique K-band Focal Plane Array (KFPA) instrument to map many square degrees of sky in nearby molecular clouds, Giant Molecular Clouds, and large swaths of the Galactic Plane. Figures 1 and 2 show examples of recent wide-field GBT KFPA observations of NH_3 (1,1) emission toward star-forming molecular clouds. Figure 1 (left) shows the integrated intensities of NH_3 (1,1) emission toward the NGC 1333 star-forming region of the Perseus molecular cloud from the Green Bank Ammonia Survey with the KFPA (Friesen et al. 2017), while Figure 1 (right) shows the H_2 column densities of the same region derived from continuum data obtained by *Herschel* (Singh et al. 2018). Figure 2 shows the integrated intensity of NH_3 (1,1) emission toward the Cygnus X North region, including DR21, from the K-band Examinations of Young STellar Object Natal Environments (KEYSTONE) survey (Keown et al. 2018). In both cases, widespread NH_3 emission indicative of dense, star-forming gas is seen, much of it in filaments.

Though observations such as those in Figures 1 and 2 are ideal for determining where NH_3 emission occurs, it remains challenging to recover details of the kinematics and dynamics of the dense gas from such data. For context, the GBT's relatively low angular resolution, i.e., $33''$ at 24 GHz, is equivalent to 0.07 pc at the 420 pc distance of the Orion molecular cloud complex, but cores and filaments each have characteristic widths of 0.1 pc (Di Francesco et al. 2007; Arzoumanian et al. 2011). Hence, the GBT observations do not resolve the gas kinematics and dynamics of such structures in clouds much more distant that Orion. Indeed, higher-resolution observations are critical for such targets, to probe for further substructure and allow details of mass flow and dynamical stability to be recovered. Though the Jansky VLA can be currently used to observe NH_3 emission at 24 GHz, its limited point-source sensitivity to line emission, its relatively small field-of-view, and its insensitivity to moderate spatial scales, qualities effectively hardwired since the beginning of the VLA's operations in 1980, make it challenging to map the internal details of multi-pc long filaments and numerous cores. Instead, a next generation Very Large Array (ngVLA) with improved sensitivities and wider fields-of-view will enable acquisition of the data needed to probe best the kinematics and dynamics of dense star-forming gas. With an flexible ngVLA, targets could include large samples of targeted individual pre-/protostellar cores and their host filaments or wide-field mapping across star-forming molecular clouds.

2. NH_3 observing with ngVLA

This science is uniquely addressed by an ngVLA design with sensitive access to K-band. As stated above, the Jansky VLA does not have the sensitivity or field-of-view in K-band for wide-field imaging of NH_3 emission (see also below). The GBT is useful for locating NH_3 emission but it does not have the intrinsic angular resolution to resolve cores and filaments beyond Orion, e.g., in several key Giant Molecular Clouds like Cygnus X (see Figure 2). No other single-dish radio telescope on the planet is as optimally equipped for wide-field K-band observing than the GBT. The SKA's current specifications on sensitivity only go up to 15 GHz. While there is a specification for aperture efficiency at 20 GHz, the SKA antennas are not being optimized for performance above 15 GHz. (We note that design work indicates that performance of the SKA antennas will be good at 25 GHz but their actual performance remains to be determined.) ALMA can observe emission from N_2H^+, a nitrogen-based molecule chemically similar to NH_3 that can also trace dense gas, but the critical density of its lowest rotational transition is 1-2 orders of magnitude higher than those of the lower NH_3 transitions, suggesting it is less able to map typically lower density filaments or the transition regions between dense cores and the filaments within which they are embedded. Moreover, N_2H^+ cannot be used to determine kinetic gas temperatures directly as NH_3 can. The high spectral resolution and sensitivity of an ngVLA will allow better disentangling of velocity components along the line of sight.

No other facilities are planned to sample K-band frequencies with the sensitivity and resolution of the ngVLA. Synergies may exist with future far-infrared/submillimeter space missions like SPICA and OST, if such far-infrared/submillimeter facilities have wide-field continuum imaging capabilities. In particular, the potential addition of polarizers on these telescopes would provide high-resolution information on magnetic field morphologies, from which ngVLA line data could allow magnetic field strengths to be determined using the Davis-Chandrasekhar-Fermi method. Though cores and filaments emit largely at far-infrared and submillimeter wavelengths, maps of their internal structures at resolutions higher than *Herschel* or the JCMT, i.e., 1-3$''$, could arise from extinction mapping of molecular cloud material using deep wide-field near-infrared observations from next-generation facilities such as TMT/E-ELT or LSST. Complementarity with kinematic information on such scales is therefore vital.

There are hundreds of known molecular clouds, from those situated relatively near the Sun (0.1-0.5 kpc distance) to those largely confined to the Galactic Plane (~10 kpc distance), so there are several targets available from any potential ngVLA site. The targets, however, are generally within 30 degrees of the Galactic Plane. Dense gas is found within molecular clouds in relatively isolated locations, a small percentage of total cloud surface areas. Nominally, such locations exhibit extended NH_3 emission over $\sim 10' \times 10'$ scales in single-dish maps. The typical peak brightnesses of NH_3 (1,1) emission are 1-3 K (T_{mb}) in a 33$''$ beam. Assuming no beam dilution, those brightnesses translate to 7.5-25 mJy beam^{-1} for a "standard resolution" $\sim 4''$ beam (see below). Detection of such emission at an SNR of ~5, the minimum needed for high-quality line fitting, requires per channel sensitivities of ~5 mJy beam^{-1}.

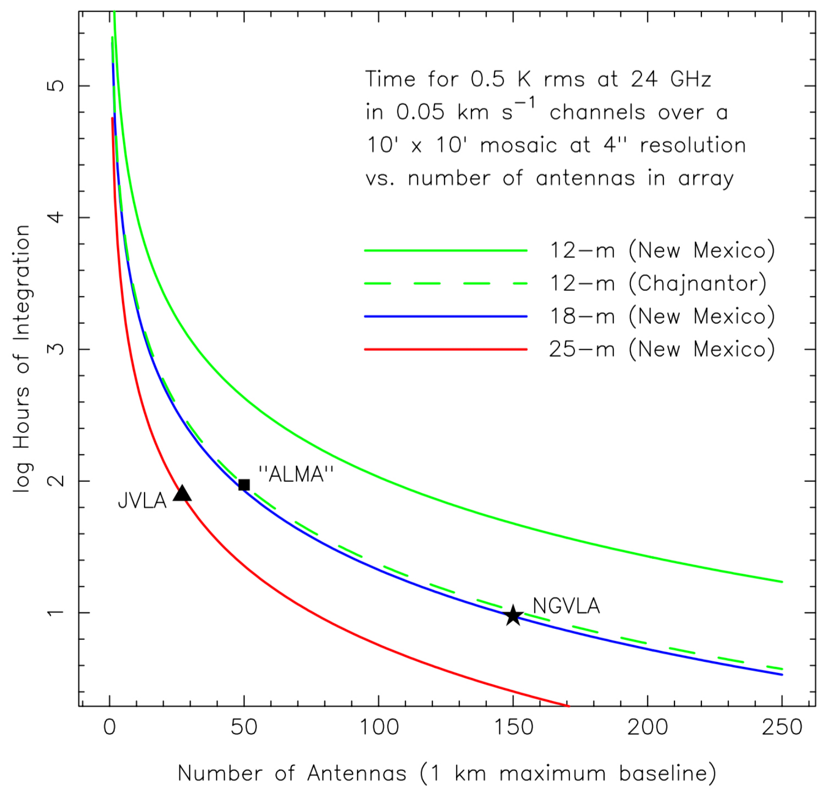

Figure 3. Hours of integration required to reach a 1 σ rms = 0.5 K at 24 GHz in a 0.05 km s^{-1} channel over a $10' \times 10'$ mosaic at $4''$ FWHM resolution given the number of antennas in an array. Note that this resolution requirement means the number of antennas within about ~1 km maximum baseline. The number of hours is obtained using the current Jansky VLA Exposure Calculator and scaling the integration time by the D^2N^4 scaling relation for mapping speed. (D is the antenna diameter and N is the number of antennas.) The solid red line shows the number of 25-m antennas within 1 km needed to reach this target sensitivity in New Mexico (i.e., assuming Jansky VLA site conditions). The black triangle indicates the current Jansky VLA of 27 antennas. The solid green line shows the number of 12-m diameter antennas within 1 km needed in New Mexico, while the dashed green line shows the number of 12-m ALMA-like antennas required at the Llano de Chajnantor in Chile which has superior site conditions. For reference, the black square indicates the 50 × 12-m antennas of ALMA, though ALMA has no plans for K-band receivers for the foreseeable future. The solid blue line shows the number of 18-m antennas within 1 km needed to reach the target sensitivity in New Mexico, with a star indicating the reasonable number (150) needed in a compact distribution of ngVLA antennas.

3. Example ngVLA Mosaic Observations

To determine some reasonable observations for an ngVLA, we first assume a standard resolution of 4″ FWHM, similar to that provided by the D configuration of the Jansky VLA. Going to higher resolution has a profound impact on surface brightness sensitivity, so there are tradeoffs expected between sensitivity and field-of-view. Of course, more distant clouds for which higher resolution may be most beneficial will be intrinsically more compact and require fewer pointings per mosaic. Single-dish data show NH_3 emission in dense gas regions of nearby molecular clouds to be extended over $\sim 10' \times 10'$ fields, leading to a mapped image size of ∼100 sq. arcmin. In addition, the target maximum angular scale is ∼30″, i.e., the minimum scale seen in single-dish maps. Given that cores and filaments are intrinsically low surface brightness features, inclusion of arrays of smaller diameter antennas in very compact configurations and total power antennas are important to recover all scales between 1-4″ and 30″.

We expect that a target sensitivity of ∼0.5 K in channels 0.05 km s^{-1} wide over a mosaic of $10' \times 10'$ provides a reasonable minimum goal for ngVLA observations of dense gas in star-forming regions. Such high spectral resolution is necessary to resolve NH_3 lines at low temperatures, e.g., the thermal line width of NH_3 at 10 K is 0.07 km s^{-1}. According to the VLA Exposure Calculator[1], 24 GHz can be observed in a single pointing to 0.5 K sensitivity in 0.05 km s^{-1} channels with 25 antennas in D configuration (i.e., ∼3-4″ FWHM resolution) in ∼1.2 hours of winter time on source or ∼2.3 hours with overheads. (Baselines of up to 4 km are needed to reach 1″ resolution.) A $\sim 10' \times 10'$ field of dense gas, however, requires ∼126 pointings for Nyquist sampling in a mosaic. Indeed, a mosaic may benefit from a $\sqrt{2}$ increase in sensitivity from overlapping pointings, equivalent to a savings of time by a factor of 2. Accordingly, the Jansky VLA can reach the target sensitivity over a $10' \times 10'$ mosaic in approximately 78 hours. Though tractable for a small cloud of 100 sq. arcmin. size or less, mapping the NH_3 emission of larger clouds with the Jansky VLA would take numerous such mosaics to cover their entirety, and hence would require a prohibitively large amount of observing time. For example, the mapped region of Cygnus X shown in Figure 2 consists of eleven such $10' \times 10'$ fields.

Figure 3 shows the number of hours needed to reach the target sensitivity of 0.5 K in 0.05 km s^{-1} channels over a $10' \times 10'$ mosaic for various numbers of antennas of different size. The trends follow the well-known D^2N^4 scaling relation for mapping speed, where D and N are the diameter and number of the antennas, respectively. The hours needed for the Jansky VLA of 27 antennas of 25-m diameter is indicated, as is the impact on observing time given a lesser or greater number of such antennas. Also shown in Figure 3 are curves indicating the observing times needed to reach the target sensitivity for 18-m and 12-m diameter antennas in New Mexico, again following the D^2N^4 scaling relation. For further comparison, a curve is also shown in Figure 3 for ALMA-like 12-m antennas on the Llano de Chajnantor in Chile, which has site conditions superior to those in New Mexico (e.g., a 50% better atmospheric opacity at 24 GHz is assumed). ALMA has 50×12-m antennas and the specific hours of integration needed for it to reach the target sensitivity is indicated in Figure 3. Note, however, that there are no plans to install K-band receivers on ALMA for the foreseeable future. Also, the sensitivity performance of ALMA equipped with K-band receivers would be

[1] https://obs.vla.nrao.edu/ect/

merely comparable to that of the Jansky VLA. Figure 3 shows that 150×18-m antennas within 1 km distance would be sufficient to improve the observing speed of observing such a mosaic to the target sensitivity by roughly an order of magnitude, i.e., 9.4 hours. In contrast, hundreds of 12-m antennas in New Mexico would be needed to reach a similar performance improvement. Note that for the ngVLA curves in Figure 3 we assumed current Jansky VLA receiver and antenna performances and did not include further sensitivity improvements from receiver upgrades or better dish surfaces.

We conclude that ~150 antennas with a maximum baseline of ~1 km are required to fulfill this science case. Such antenna numbers are needed as an absolute minimum to enable roughly an order of magnitude improvement over the current Jansky VLA. Furthermore, compact placement of the ngVLA antennas is critical for the ability to image low surface brightness emission from dense gas. For context, a circular area of 1-km diameter has the same surface area as 1600 antennas of 25-m diameter, so the required configuration will be tight but doable. At present, however, the ngVLA concept includes $\sim 220 \times 18$-m antennas of which only ~40% (i.e., 88) would be located within 2 km and another ~40% located within 50 km. Hence, it may be worthwhile for the inner ngVLA antennas to have some limited reconfigurability for low surface brightness imaging. Alternatively, a suite of antennas with smaller antennas and/or antennas dedicated to total power observations would be needed. Indeed, continued access to a large aperture single-dish facility would be particularly welcome, e.g., the 100-m diameter GBT with its current KFPA or an expanded K-band focal-plane array with significantly more receivers.

Acknowledgments. JDF and JK acknowledge the support of a Discovery Grant by the Natural Science and Engineering Council of Canada.

References

André, Ph., Di Francesco, J., Ward-Thompson, D., et al. 2014, in Protostars and Planets VI, ed. H. Beuther, R. S. Klessen, C. P. Dullemond, & T. Henning, (University of Arizona Press, Tucson), p. 27-51
André, Ph., Men'shchikov, A., Bontemps, S., et al. 2010, A&A, 518, L102
Arzoumanian, D., André, Ph., Didelon, P., et al. 2011, A&A, 529, L6
Benson, P., & Myers, P. C. 1989, ApJS, 71, 89
Crapsi, A., Caselli, P., Walmsley, M., et al. 2007, A&A, 470, 221
Di Francesco, J., Evans, N. J., II., Caselli, P., et al. in Protostars and Planets V, ed. B. Reipurth, D. Jewitt & K. Keil, (University of Arizona Press, Tucson), p. 17
Dunham, M. M., Allen, L. E., Evans, N. J., II, et al. 2015, ApJS, 220, 11
Friesen, R. K., Pineda, J. E., Rosolowsky, E., et al. 2017, ApJ, 843, 63
Hacar, A., Tafalla, M., & Alves, J. 2017, A&A, 606, 24
Hacar, A., Tafalla, M., Kauffmann, J., & Kovács, A. 2013, A&A, 554, 55
Ho, P. T. P., & Townes, C. H. 1983, ARA&A, 21, 239
Keown, J., Di Francesco, J., Rosolowsky, E., et al. 2018, in preparation
Könyves, V., André, Ph., Men'shchikov, A. et al. 2015, A&A, 584, A91
Könyves, V., André, Ph., Men'shchikov, A., et al. 2010, A&A, 518, L106
Schneider, N., Csengeri, T., Hennemann, M., et al. 2012, A&A, 540, L11
Singh, A., et al. 2018, in preparation
Walmsley, M., & Ungerechts, H. 1983, A&A, 122, 164
Ward-Thompson, D., Kirk, J., André, Ph., et al. 2010, A&A, 518, L92

Science with a Next-Generation Very Large Array
ASP Conference Series, Monograph 7
Eric J. Murphy, ed.

DRAFT EDITION

Resolving the Structure and Kinematics of the Youngest HII Regions and Radio Jets from Young Stellar Objects

Roberto Galván-Madrid[1], Maite Beltrán[2], Adam Ginsburg[3], Carlos Carrasco-González[1], Hauyu Baobab Liu[4], Luis F. Rodríguez[1], Stanley Kurtz[1]
[1]*Instituto de Radioastronomía y Astrofísica, Universidad Nacional Autónoma de México, Apdo. Postal 72-3 (Xangari), Morelia, Michoacán 58089, Mexico.;* `r.galvan@irya.unam.mx`

[2]*INAF-Osservatorio Astrofisico di Arcetri, Largo E. Fermi 5, I-50125 Firenze, Italy.*

[3]*National Radio Astronomy Observatory, 1003 Lopezville Rd., Socorro, NM 87801, USA.*

[4]*European Southern Observatory, Karl-Schwarzschild-Straße 2, D-85748 Garching bei München, Germany.*

Abstract. In this contribution we explore the new science that a Next Generation Very Large Array (ngVLA) would be able to perform on the topics of the youngest HII regions and (proto)stellar jets. Free-free continuum and radio recombination line (RRL) emission are often the only way of peering into the dense envelopes surrounding (proto)stars of all masses, and trace their initial feedback in the form of 'radio jets', 'hypercompact HII regions', or photoevaporating, partially-ionized flows. Properly disentangling free-free from dust emission is also mandatory in studies of protoplanetary and accretion disks. Current VLA research has reached an impasse in which a population of faint ionized radio sources, probably corresponding to the above mentioned objects, is detected, but their nature is mostly unknown. The ngVLA would allow us to resolve the density structure and kinematics of such sources, revolutionizing our knowledge of star formation across the entire stellar-mass spectrum.

1. Introduction

1.1. Free-free and Recombination Line Emission from High-Mass Young Stellar Objects

Thermal free-free emission from ionized gas is a ubiquitous signpost of the physical processes associated with star formation. Such emission is complementary to and as important as that from dust and cold gas. Massive (proto)stars can produce enough Lyman continuum photons to significantly ionize their own envelopes. The VLA was key to the discovery and understanding of ultracompact (UC) and hypercompact (HC) HII regions: the small (< 0.1 pc ≈ 20000 au) pockets of ionized gas associated with newborn massive ($M_\star > 15\ M_\odot$) stars (Dreher & Welch 1981; Ho & Haschick 1981; Kurtz et al. 1994; De Pree et al. 2014; Kalcheva et al. 2018). The nature of the fainter ionized sources detected by the VLA in massive star formation regions (Rosero et al.

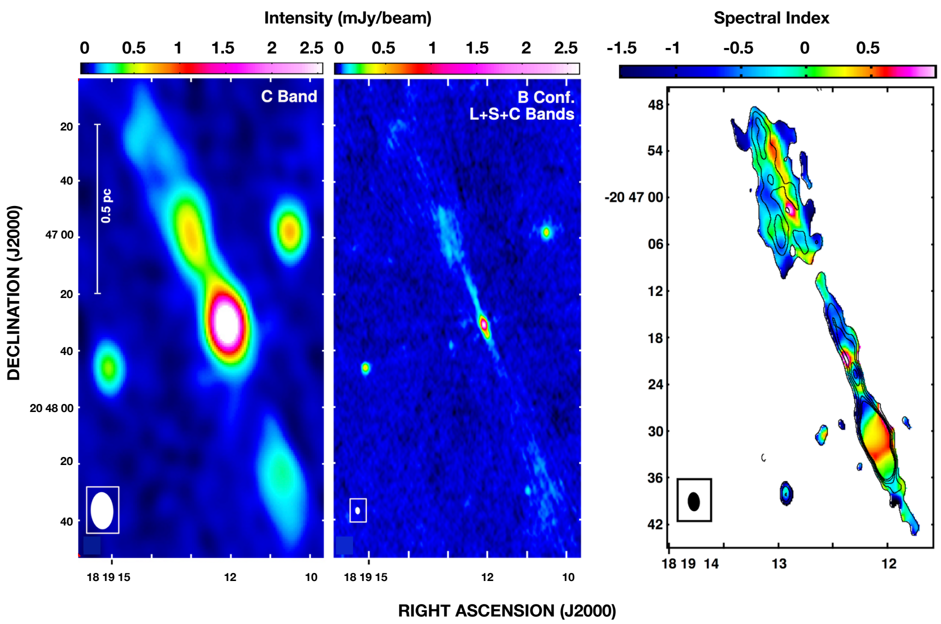

Figure 1. The radio jet from IRAS 18162–2048, which powers Herbig-Haro objects 80 and 81. This object is the prototypical example of a radio jet from a high-mass YSO, well studied thanks to its proximity (1.7 kpc), brightness, and anomalously large (pc) extension. The *left* and *central* panels show low and high (arcsecond) angular resolution views of the thermal jet core and inner jet knots. The *right* panel shows the spectral index derived from multifrequency synthesis imaging over the *L*, *S* and *C* bands. Positive values at the core and jet axis mark the thermal free-free component, while negative spectral indices pinpoint to non-thermal emission. Taken from Rodríguez-Kamenetzky et al. (2017). The ngVLA will allow us to perform this type of studies in statistically significant samples of radio jets from both nearby low-mass YSOs and high-mass YSOs at kpc distances.

2016; Moscadelli et al. 2016) is not clear, however, since they are barely detected (fluxes $\lesssim$ 100 μJy at $\nu >$ 30 GHz) and mostly unresolved (sizes < 100 mas, or < 500 au at 5 kpc).

Competing theoretical models suggest that these faint free-free sources could either be: i) gravitationally trapped HII regions (Keto 2003), expected to exist in the late stages of accretion in the formation of stars more massive than 20 to 30 $M_{\odot}$; ii) outflow-confined HII regions (Tanaka et al. 2016), expected to form if there is a photoionized disk-wind outflow; or iii) radio jets similar to those found in their lower-mass counterparts (Beltrán et al. 2016; Purser et al. 2016). Figure 1 shows the iconic HH 80–81 radio jet, one of the brightest known, that is powered by the $\sim$ 10 $M_{\odot}$ protostar IRAS 18162–2048 (Girart et al. 2017). A significant fraction of the faint radio sources in massive star formation regions could be stellar winds from very young (Carrasco-González et al. 2015) or unembedded massive stars (Dzib et al. 2013), or even colliding-wind binaries with synchrotron excesses at $\nu <$ 4 GHz (Williams et al. 1990; Pittard & Dougherty 2006; Ginsburg et al. 2016). Figure 2 illustrates the differences between the relatively bright HC HIIs in W51A, whose nature as photoionized regions around young massive

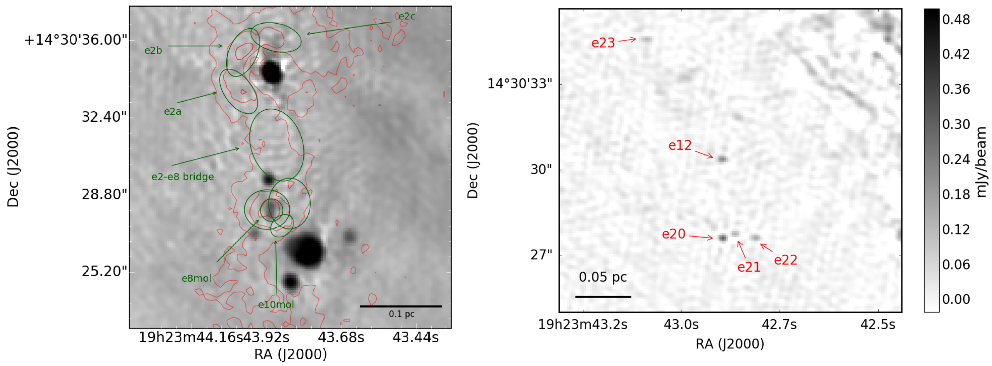

Figure 2. *Left:* Examples of bright hypercompact (HC) HII regions: the well-known e2/e8 system in the massive cluster forming region W51A. Gray-scale shows the free-free 2-cm continuum observed at 0.3 arcsec resolution. Contours show their surrounding molecular (formaldehyde) emission. Current facilities such as the VLA can map the continuum of all HII regions and the recombination line emission of some of these with $S_{\rm cm} \sim 10 - 100$ mJy. *Right:* Examples of faint ionized sources that are candidate HC HIIs, radio jets, or stellar-wind systems. Their fluxes $S_{\rm cm} \lesssim 0.1 - 1$ mJy and sizes $l < 100$ mas require the ngVLA to be characterized. Taken from Ginsburg et al. (2016).

stars is well established, and the compact, fainter sources that are candidates to be HC HIIs, thermal radio jets, or stellar-wind systems.

The high angular resolution and sensitivity of the ngVLA in both cm continuum and Radio Recombination Lines (RRLs) would open a new window to perform systematically detailed studies of the density and velocity distribution of the ionized gas present in the formation of massive stars. In Sections 2 and 3, we give more detailed sensitivity estimates for this scientific case. Regardless of whether or not current theoretical models are correct in detail, free-free emission is the only way of tracing the stellar content in the deeply embedded regions where the formation of massive stars occurs.

The Next Generation VLA will allow us to finally resolve the structure and kinematics of ionized material, the closest gaseous component to the (proto)star, in both low- and high-mass star formation regions.

1.2. Free-free and Recombination Line Emission from Low-Mass Young Stellar Objects

The VLA was the most important tool for the discovery of and understanding that low-mass Young Stellar Objects (YSOs) have at their centers collimated jets of free-free emission, known as thermal radio jets, powering the observed molecular outflows and Herbig-Haro systems at larger scales (Rodríguez et al. 1994; Anglada 1995; Rodríguez 1997; Beltrán et al. 2001; Liu et al. 2014; Tychoniec et al. 2018). This finding was an important confirmation of a key prediction of star formation theories (Shu et al. 1994). Low-mass YSOs do not emit significant EUV photons from their photospheres. Thus, ionization produced by photons arising from the shock of the – mostly – neutral stellar wind against the surrounding high-density gas was established as a viable mechanism (Torrelles et al. 1985; Curiel et al. 1987; Anglada et al. 1998). Figure 3 shows a compilation of measurements of bolometric and radio luminosities of sources interpreted as being radio jets, compared to the theoretical expectations for their 'jet vs HII region' nature.

In the most embedded and youngest low-mass YSOs (Class 0 and I, or low-mass protostars), the radio jets are the only way of peering into the dense envelopes and tracing the ejection processes close (< 10 au) to the central objects. Even with the $\sim 10\,\mu$Jy sensitivity and $\sim$ 10 au resolution currently achievable with the VLA for the nearest low-mass star forming regions, however, our understanding of ejection phenomena in low-mas YSOs is far from complete. Specifically, the relatively bright radio jets from Class 0 and I YSOs are barely resolved in the continuum, and their kinematics are unknown due to the practical impossibility of detecting their RRL emission. Furthermore, jet emission in the more evolved Class II YSOs – the protoplanetary disks, now one of the most active fields in astronomy – is far weaker and hardly detectable by the VLA in the most optimistic cases (Galván-Madrid et al. 2014; Macías et al. 2016). For Class II (primordial disks) and Class III (remnant disks) YSOs, other physical processes become observable. Disk photoevaporation, one of the main candidates to cause protoplanetary disk dispersal, may be detected through faint free-free and RRL emission (Pascucci et al. 2012; Owen et al. 2013). Also, unresolved non-thermal (gyro)synchrotron emission from active magnetospheres is often detected with the VLA in some of these more-evolved YSOs (Forbrich & Wolk 2013; Liu et al. 2014; Rivilla et al. 2015). The ngVLA will enable us to resolve, for the first time, the structure and kinematics of the free-free emission from YSOs at all proto-stellar and young-stellar evolutionary stages from Class 0 to Class III, as well as disentangle it from other 'contaminating' processes such as (gyro)synchrotron emission. A full characterization of the free-free emission from YSOs at frequencies $\nu > 30$ GHz is also necessary to separate it from dust emission. This disentangling is a mandatory issue to address in studies of planet formation, which need to get accurate measurements of the mass distribution of disks around low-mass YSOs.

2. Scientific Capabilities with Continuum Observations

We estimate here the scientific outcome of deep (rms noise 0.5 μJy/beam) continuum total intensity observations from 1 to 50 GHz with an angular resolution of 30 mas or better. These values are about the ngVLA 1-hr sensitivity and resolution quoted in the project overview by Carilli et al. (2015). All the science cases described below require such wide frequency coverage to image the respective free-free emission and disentangle it from other 'contaminating' emission mechanisms. At $\nu < 4$ GHz, there could be a contribution from (gyro)synchrotron emission that would need to be properly subtracted (see chapter by Hull et al.). At $\nu > 50$ GHz dust emission starts to dominate in some objects. This transition region also needs to be covered to disentangle properly the competing emission mechanisms (Isella et al. 2015).

A wide field-of-view and the ability to mosaic are needed to make studies over statistically significant samples, except for highly clustered regions (e.g., Forbrich et al. 2016). A recent VLA survey of YSOs in a nearby star formation region needed 134 pointings to create a Nyquist-sampled mosaic of an area equivalent to 0.5 deg^2 (Hauyu Baobab Liu, personal communication). Under the assumption of 18-m dishes, the ngVLA would need about half the number of pointings than the current VLA. At the sensitivities considered in the following Sections, a full survey of the entire YSO

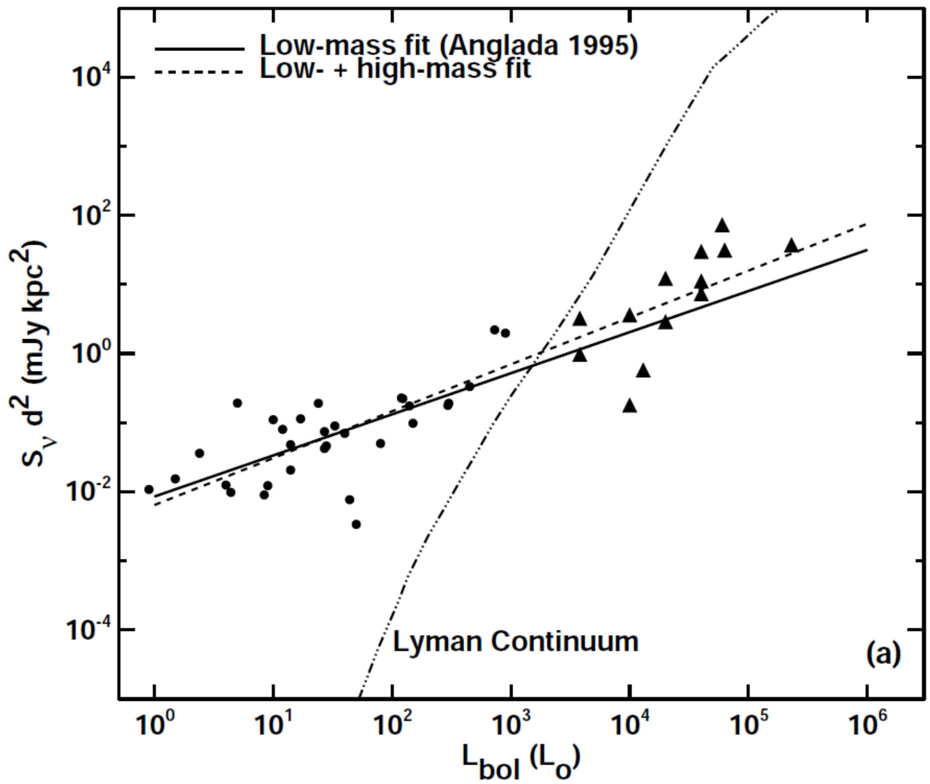

Figure 3. Empirical correlations between the YSO bolometric luminosity $L_{\rm bol}$ and the cm radio luminosity $S\,d^2$. The plotted points and fits correspond to objects best interpreted as radio jets, from the low- to high-luminosity regime. The steeper dash-dotted line shows the expected radio luminosity for HII regions produced by a ZAMS star of the corresponding $L_{\rm bol}$. HC and UC HIIs are observed to populate this locus for $L_{\rm bol} > 10^3\ L_\odot$ (not plotted). The nature of radio objects close to the intersection – of which exact value is somewhat model dependent – is particularly difficult to determine (jet vs HII region). These objects at $\sim 10^3 - 10^4\ L_\odot$ are highly relevant for understanding the formation of intermediate- and high-mass stars. The ngVLA will allow us to perform systematically resolved studies of radio jets in nearby star formation regions down to the brown-dwarf regime, and of HC HIIs at kpc distances down to $\lesssim 10^3\ L_\odot$. Taken from Carrasco-González (2010). See also the recent review by Anglada et al. (2018).

population ($\sim 10^3$ sources) in a nearby star-forming cloud could be completed with a time investment of tens of hours.

2.1. Radio Jets from Low-Mass YSOs

We use the empirical correlations between the radio luminosity of YSOs and their bolometric luminosity (Anglada 1995; Shirley et al. 2007; Anglada et al. 2015), which appear to hold even in the brown dwarf regime (Morata et al. 2015). We also assume a distance of 140 pc throughout this section, characteristic of nearby low-mass star formation regions such as Taurus and Ophiuchus (Ortiz-León et al. 2017). For the lowest-luminosity case, $L_{\rm bol} = 0.01\,L_\odot$, this relation gives a 3.6 cm flux $F_{3.6\rm cm} = 10\,\mu$Jy, which is only detectable with deep VLA integrations. The jet is comprised of a jet core and extended emission typically in the form of jet knots (see Fig. 1 for one of the few well studied cases). The jet core is usually the brightest and we consider it to have ~ 50% of the total jet emission, ($F_{3.6\rm cm,core} = 5\,\mu$Jy). Such emission would be detectable easily with the ngVLA at S/N ~ 10 in ~ 1 hr integrations (Carilli et al. 2015).

Depending on its driving mechanism, evolutionary stage, and mass, the jet core emission can be spread through very different scales (Frank et al. 2014), from magnetospheric (diameter ~ 0.1 au = 0.7 mas at 140 pc) in the X-wind model to disk-wind scales (~ 10 au = 70 mas). The ngVLA with an angular resolution of 5-20 mas would be able to distinguish between jet launching models, detecting unresolved or barely resolved cores for the former scenario and resolved ones for the latter. It is also possible that some jets are collimated externally through ambient pressure or magnetic fields, in which case the emission would extend to tens of au (Albertazzi et al. 2014) and be more easily resolved. For an unresolved X-wind jet core, most of the flux would be inside the beam, so it would be easily detected. For an resolved disk-wind jet core, sensitivity to different parts of the emission is model dependent, but assuming a conservative electron temperature $T_e = 5000$ K, then $T_B = 50 - 5000$ K for $\tau = 0.01 - 1$, so the fainter optically-thin emission could be detected at S/N ~ $50/7$ =~ 7 for 1 hr integration at 10 GHz (Carilli et al. 2015).

2.2. Photoevaporating Flows from Class II YSOs

During the Class II stage, free-free emission from the radio jet becomes weaker due to the much lower accretion rates compared to the Class 0 and I stages. Free-free emission from disk photoevaporation by EUV photons could then take over as the principal continuum emission (Pascucci et al. 2014; Galván-Madrid et al. 2014; Macías et al. 2016). The possibility of detecting and imaging this emission is highly relevant for understanding the mechanisms of protoplanetary disk dispersal (Alexander et al. 2014). Pascucci et al. (2012) applied the photoevaporation-flow model of Hollenbach et al. (1994) to estimate the free-free continuum and hydrogen recombination line emission due to EUV photoevaporation. Using their prescription, disks with an ionizing photon luminosity as low as $\Phi = 10^{40}$ s^{-1} at 140 pc would have centimetric fluxes (almost constant with frequency) $S_{\rm cm} \sim 4\,\mu$Jy. Therefore, EUV photoevaporation happening in low-mass protoplanetary disks could be easily detectable with the ngVLA at S/N ~ 10 in 1-hour integrations (Carilli et al. 2015).

2.3. Faint Ionized Sources in High-Mass Star Formation

The VLA has been the main tool for discovering and characterizing the small pockets of ionized gas around newly formed O-stars: the so-called ultracompact (UC) and hypercompact (HC) HII regions. In the following, we assume ionization equilibrium – something debatable in the faintest sources that the ngVLA will help to understand – and use the observational calibration for main-sequence OB stars of Vacca et al. (1996). We also assume a typical distance of 5 kpc for massive star formation regions throughout this section. A B0 main sequence star of 20 $M_\odot$ has $L_{\rm bol} = 10^{4.8}\ L_\odot$ and Lyman continuum photon rate $N_{\rm Ly} = 10^{48.1}$ s^{-1}, which translates into a 8-GHz optically-thin flux ≈ 480 mJy (quite constant across frequencies since the dependency for optically thin emission is $\nu^{-0.1}$). This emission level indeed defined the target sensitivities for the past few decades (Wood & Churchwell 1989; Kurtz et al. 1994; Urquhart et al. 2009).

Extrapolating the empirical calibration used above to lower masses, the HC HII of an intermediate-mass star with $L_{\rm bol} = 10^3\ L_\odot$ has an 8-GHz flux of 120 μJy (e.g., Cesaroni et al. 2015). The VLA is currently allowing observers to detect, but not to resolve, a population of radio sources in massive star formation regions with centimeter fluxes $\lesssim 100\ \mu$Jy (e.g., Rosero et al. 2016; Moscadelli et al. 2016). Their interpretation as faint HC HIIs, however, is not unique, and many of them can be as well interpreted as radio jets from high-mass YSOs. Extrapolating the radio-jet flux to bolometric luminosity correlation to high masses gives jet centimeter fluxes that are below HC HII fluxes for all bolometric luminosities above $L_{\rm bol} \sim 10^3\ L_\odot$ (see Fig. 3, we note that the exact intersection is model dependent). Radio jets, however, are often assumed to have ionization fractions ~ 0.1 for low-mass YSOs, whereas UC and HC HIIs are considered to be fully ionized. The theoretically expected quenching of HC HIIs due to their surrounding neutral accretion flows (Walmsley 1995; Peters et al. 2010) and a higher ionization fraction in jets from intermediate- and high-mass YSOs could easily invert the relative radio brightnesses of the two different physical scenarios. Observationally, there is evidence that a jet nature may be the correct interpretation for the faint ionized sources of some YSOs with luminosities up to $L_{\rm bol} \sim 10^4\ L_\odot$ (Rosero et al. 2016; Moscadelli et al. 2016; Purser et al. 2016). At these luminosities there could be a transition to HII-region-dominated emission (Guzmán et al. 2016).

The ngVLA is needed to understand the nature of this population of objects with cm fluxes $S_{\rm cm} \lesssim 100\ \mu$Jy and sizes $l \lesssim 100$ mas (see Fig. 2). Assuming a conservative electron temperature $T_e = 5000$ K, then $T_B = 50 - 5000$ K for $\tau = 0.01 - 1$, so a 1 hour integration with an rms noise $\sim 0.5\ \mu$Jy/beam ~ 10 K would suffice to map very optically thin emission at $5 - 30$ mas resolution, which would correspond to $25 - 150$ au at 5 kpc.

3. Scientific Capabilities with Recombination Line Observations

We estimate here the scientific outcome of deep (rms noise of 100 μJy/beam in channels 5 km/s wide) total intensity observations of RRLs from H78α (5.0 GHz) to H40α (99.0 GHz). The desired maximum angular resolution is 100 mas for unresolved detections, 30 mas for resolved detections, or slightly better for the few brightest cases. A hundred milliarcseconds correspond to 14 au for objects in nearby (140 pc) low-mass star forming regions, or to 500 au at 5 kpc.

Continuum imaging is not enough to model and fully interpret ionized sources in star formation. The kinematic information inferred from hydrogen recombination lines is also needed. Recombination lines in the cm radio and (sub)mm are weak compared to the often used optical and infrared lines such as Hα, Lyα, and Brγ. They are unobscured, however, which makes RRLs a unique tool for revealing the kinematics in the embedded regions where star formation occurs (Martín-Pintado et al. 1989; Peters et al. 2012; Jiménez-Serra et al. 2013; Plambeck et al. 2013; Zhang et al. 2017).

The VLA, ALMA, and other interferometers have been able to detect systematically RRLs from the UCs and HC HIIs produced by O and early-B type stars (Keto et al. 2008), but not for lower masses. The resolved kinematics of ionized gas in star formation is almost unexplored except for the brighter UC HIIs and some HC HIIs (e.g., Garay et al. 1986; Liu et al. 2012). Also, only a couple of detections of RRL emission from the brightest, massive radio jets have been reported (Guzmán et al. 2016). Attempts to detect RRLs in iconic objects such as the jet of IRAS 18162–

2048 (Fig. 1 shows its continuum emission) have produced negative results (Roberto Galván-Madrid, unpublished). Indeed, RRLs are more easily detected in HC HIIs than in radio jets because the former tend to be brighter and their line widths are one order of magnitude smaller. Even 'broad linewidth' HC HIIs have $\Delta V \sim 30 - 50$ km s^{-1}, whereas jet motions appear to have ΔV of several hundreds of km s^{-1}, as inferred from their proper motions (Curiel et al. 2006; Rodríguez-Kamenetzky et al. 2016) and a few tentative RRL detections (Jiménez-Serra et al. 2011). Therefore, ngVLA measurements of RRL line widths alone, even if angularly unresolved, would serve as a discriminator for competing models of the interpretation of faint ionized sources in massive star formation.

Lines such as H51α are detectable for $L_{\rm bol} = 10^5\ L_\odot$ objects even with the sensitivities of the VLA before its upgrade (e.g., Galván-Madrid et al. 2009). In the following, we consider the detectability of RRL emission from fainter sources at kpc distances with the ngVLA. The LTE line-to-continuum ratio $S_{\rm line}\Delta V/S_{\rm cont}$ goes as $\nu^{1.1}$ (Gordon & Sorochenko 2002). Observationally, it has been measured to be $S_{\rm line}\Delta V/S_{\rm cont}$ = $30 - 100$ km s^{-1} for the H30α line (231.9 GHz) for HC HIIs with $L_{\rm bol} \sim 10^5 L_\odot$ (Keto et al. 2008). We consider $S_{\rm line}\Delta V/S_{\rm cont} = 50$ km s^{-1} for the H30α line and $\Delta V = 25$ km s^{-1} for all lines. This estimate translates into $S_{\rm line}\Delta V/S_{\rm cont} \sim 17.6$ km s^{-1} for H41α (90.0 GHz), 8.9 km s^{-1} for H51α (48.1 GHz), and 0.8 km s^{-1} for H106α (5.4 GHz). We further consider a HC HII region with a 48 GHz continuum flux $S_{\rm 48GHz} = 1$ mJy, such as the ones detected in $L_{\rm bol} \sim 10^4\ L_\odot$ YSOs by van der Tak & Menten (2005). This HC HII would have a velocity-integrated H51α flux $S_{\rm line}\Delta V = 8.9$ mJy km s^{-1}. At this frequency, the expected ngVLA noise in a 5 km s^{-1} channel for a 10-hour integration is $\sim 32\ \mu$Jy/beam (Carilli et al. 2015). For the assumed FWHM linewidth of 25 km s^{-1}, the line peak would be $S_{\rm peak} \sim 334\ \mu$Jy, detectable at S/N ~ 10.

The above discussion applies to beam-matched or angularly unresolved observations with a HPBW ~ 100 mas. Observations at higher angular resolution would need to aim at brighter objects or integrate longer. The S/N of individual line detections for these faint HII regions would go up by factors ~ 2 for the H41α line at 90 GHz, so resolved RRL mapping would be less expensive using high-frequency RRLs. Lines in the frequency range $50 < \nu < 100$ GHz could be the right compromise between high brightness and the absence of contamination from molecular lines compared to RRLs at ALMA frequencies. Therefore, RRL observations are an important motivation for the ngVLA to operate at frequencies $\nu > 50$ GHz.

Non-detections at frequencies $\nu < 20$ GHz or in fainter objects could be solved by taking advantange of stacking of lines from neighbouring quantum numbers. The VLA Ka and Q bands ($36 - 50$ GHz) harbor 12 α hydrogen RRLs (H62α to H51α) that could be stacked together in a given object to decrease the noise by factors of $\sim 3 - 4$. This opportunity highlights the importance of having a large simultaneous frequency coverage.

Although the previous discussion considered a HC HII from a massive (proto)star at kpc distances, it also applies to radio jets from low-mass YSOs at the canonical distance of 140 pc. These radio jets have cm fluxes $S_{\rm cm} \sim 1$ mJy for luminosities $L_{\rm bol} > 10\ L_\odot$ (see Fig. 3). Their RRL emission could be spread through several hundred km s^{-1}. Assuming that the radio-jet line width is $\times 10$ larger than for HC HIIs, the S/N would decrease by factors of $\sim 10^{0.5} \sim 3$ if the velocity binning increases from $5 - 50$ km s^{-1}.

In conclusion, although more expensive than continuum observations, kinematical imaging of hydrogen recombination line emission is feasible with the ngVLA. Such observations would open for the first time a window into understanding the kinematics of ionized gas in the formation of both low- and high-mass stars.

4. Peering into the Innermost Regions in the Formation of Stars of all Masses

From the previous sections, it can be concluded that the ngVLA will allow us to perform, for the first time, studies of statistically significant samples of the resolved structure and kinematics of the ionized gas associated with stars in formation and young stars of all masses. This ionized gas is often the closest gaseous component to the (proto)star itself. Table 1 summarizes the basic continuum properties of the objects that we have considered in detail among the anticipated 'radio zoo'.

Object	Typical distance [kpc]	8 GHz Flux [μJy]	Size [mas (au)]
Faint HC HII or massive radio jet	5	< 100	< 100 (< 500)
Very low luminosity radio jet	0.14	5	0.7 – 70 (0.1 – 10)
Photoevaporation flow from low-mass disk	0.14	4	7 – 350 (1 – 50)

Table 1. Free-free continuum properties of the considered objects.

5. Uniqueness of ngVLA Capabilities

Only the VLA and a future ngVLA can observe the free-free continuum emission associated with star formation in the range of frequencies where it dominates ($4 - 50$ GHz). At frequencies < 4 GHz and > 50 GHz, (gyro)synchrotron and dust emission, respectively, can be a significant 'contaminant', or even dominate the observed flux. Having a telescope with frequency coverage beyond the overlapping ranges is needed to model properly and subtract the contribution to the emission from those other mechanisms. Conversely, properly subtracting the free-free contribution will be mandatory in the much anticipated studies of dust emission in protoplanetary disks.

Similarly, hydrogen radio recombination lines from about 20 to 100 GHz have the right compromise between brightness (they are too faint at lower frequencies) and the absence of confusion with the rich molecular forest seen at higher (ALMA) frequencies.

A field-of-view of at least a few arcminutes size, as given by the proposed 18-m dishes, is needed to perform surveys of large numbers of sources in areas of the order of a square degree in reasonably long integrations of tens of hours.

Although not discussed at length in this paper (see chapter by Hull et al.), the capability to image in full polarization mode is highly desirable, since a few radio jets are known to have synchrotron emission beyond the thermal core (Carrasco-González et al. 2010), and that might be the rule rather than the exception.

Finally, a large instantaneous bandwidth (of the order of the central frequency where possible) would uniquely open the time-domain window in a systematic way. Radio jets (Liu et al. 2014) and some HC HIIs (De Pree et al. 2014) are known to be variable in timescales from days to years, a phenomenon with important implications to the properties of accretion in YSOs (Galván-Madrid et al. 2011; Hunter et al. 2017).

6. Synergies at other Wavelengths

The ngVLA would naturally complement and enhance the star formation research done with ALMA and the SKA. The studies of free-free and recombination line emission proposed in this chapter will consistently be put in the context of ALMA observations of the corresponding dust and molecular line emission. All tracers are needed to have a comprehensive physical picture. SKA observations at lower-frequencies would greatly help to disentangle non-thermal emission mechanisms. The proposed ngVLA research would also benefit observations with the next generation of ground- and space-based near- and mid-IR telescopes, such as the TMT, GMT, E-ELT, JWST, and WFIRST, since those observations are the most efficient to discover and classify YSOs. Finally, high-angular resolution mid-IR and far-IR observations, such as the ones provided by SOFIA and other future facilities, are in high demand to pinpoint the sources of luminosity at resolutions that are not too coarse compared with instruments like ngVLA, ALMA, and JWST.

Acknowledgments. The National Radio Astronomy Observatory is a facility of the National Science Foundation operated under cooperative agreement by Associated Universities, Inc. RGM acknowledges support from UNAM-PAPIIT program IA102817.

References

Albertazzi, B. 2014, Science, 346, 325
Alexander, R., Pascucci, I., Andrews, S., Armitage, P., & Cieza, L. 2014 Protostars and Planets VI ed H. Beuther et al (Tucson, AZ: Univ. Arizona Press) 475
Anglada, Guillem 1995, RMxAC, 1, 67
Anglada, G., Rodríguez, L. F., Carrasco-González, C. Advancing Astrophysics with the Square Kilometre Array (AASKA14) 121
Anglada, G., Rodríguez, L. F., Carrasco-González, C. 2018, Astronomy and Astrophysics Review (A&AReV), in press
Anglada, Guillem, Villuendas, Eva, Estalella, Robert, Beltrán, Maria T., Rodríguez, Luis F., Torrelles, José M., Curiel, Salvador 1998, AJ, 116, 2953
Beltrán, M. T., Cesaroni, R., Moscadelli, L., Sánchez-Monge, A., Hirota, T., Kumar, M. S. N. 2016, A&A, 593A, 49
Beltrán, Maria T., Estalella, Robert, Anglada, Guillem, Rodríguez, Luis F., Torrelles, José M. 2001, AJ, 121, 1556
Carrasco-González, Carlos. 2010, PhD Thesis, Universidad de Granada.
Carrasco-González, Carlos, Rodríguez, Luis F., Anglada, Guillem, Martí, Josep, Torrelles, José M., Osorio, Mayra 2010, Science, 330, 1209
Carrasco-González, C., et al. 2015, Science, 348, 114
Carilli, C. L., et al. 2015, arXiv:1510.06438
Cesaroni, R., Pestalozzi, M., Beltrán, M. T., Hoare, M. G., Molinari, S., Olmi, L., Smith, M. D., Stringfellow, G. S., Testi, L., Thompson, M. A. 2015, A&A, 579A, 71
Curiel, Salvador, Cantó, Jorge, Rodríguez, Luis F. 1987, RMxAA, 14, 595
Curiel, Salvador, et al. 2006, ApJ, 638, 878

De Pree, C. G., Peters, T., Mac Low, M.-M., Wilner, D. J., Goss, W. M., Galván-Madrid, R., Keto, E. R., Klessen, R. S., Monsrud, A. 2014, ApJ, 781, L36
Dreher, J. W., Welch, W. J. 1981, ApJ, 245, 857
Dzib, S. A., Rodríguez-Garza, C. B., Rodríguez, L. F., Kurtz, S. E., Loinard, L., Zapata, L. A., Lizano, S. 2013, ApJ, 772, 151
Forbrich, J., Wolk, S. J. 2013, A&A, 551A, 56
Forbrich, J., Rivilla, V. M., Menten, K. M., Reid, M. J., Chandler, C. J., Rau, U., Bhatnagar, S., Wolk, S. J., Meingast, S. 2016, ApJ, 822, 93
Frank, A., et al. 2014 Protostars and Planets VI ed H. Beuther et al (Tucson, AZ: Univ. Arizona Press) 451
Galván-Madrid, Roberto, Keto, Eric, Zhang, Qizhou, Kurtz, Stan, Rodríguez, Luis F., Ho, Paul T. P. 2009, ApJ, 706, 1036
Galván-Madrid, R., Liu, H. B., Manara, C. F., Forbrich, J., Pascucci, I., Carrasco-González, C., Goddi, C., Hasegawa, Y., Takami, M., Testi, L. 2014, A&A, 570, L9
Galván-Madrid, R., Peters, T., Keto, E. R., Mac Low, M.-M., Banerjee, R., Klessen, R. S. 2011, MNRAS, 416, 1033
Garay, Guido, Rodríguez, Luis F., van Gorkom, J. H. 1986, ApJ, 309, 553
Ginsburg, Adam, et al. 2016, A&A, 595A, 27
Girart, J. M., et al. 2017, ApJ, 847, 58
Gordon, M. A. & Sorochenko, P. N. 2002, Radio Recombination Lines: Their Physics and Astronomical Applications (Dordrecht: Kluwer)
Guzmán, Andrés E., Garay, Guido, Rodríguez, Luis F., Contreras, Yanett, Dougados, Catherine, Cabrit, Sylvie 2016, ApJ, 826, 208
Hollenbach, David, Johnstone, Doug, Lizano, Susana, Shu, Frank 1994, ApJ, 428, 654
Ho, P. T. P., Haschick, A. D. 1981, ApJ, 248, 622
Hunter, T. R., Brogan, C. L., MacLeod, G., Cyganowski, C. J., Chandler, C. J., Chibueze, J. O., Friesen, R., Indebetouw, R., Thesner, C., Young, K. H. 2017, ApJ, 837, L29
Isella, Andrea, et al. 2015, arXiv:1510.06444
Jiménez-Serra, I., Martín-Pintado, J., Báez-Rubio, A., Patel, N., Thum, C. 2011, ApJ, 732, L27
Jiménez-Serra, I., Báez-Rubio, A., Rivilla, V. M., Martín-Pintado, J., Zhang, Q., Dierickx, M., Patel, N. 2013, ApJ, 764, L4
Kalcheva, I. E., Hoare, M. G., Urquhart, J. S., Kurtz, S., Lumsden, S. L., Purcell, C. R., Zijlstra, A. A. 2018, arXiv:1803.09334
Keto, Eric. 2003, ApJ, 599, 1196
Keto, Eric, Zhang, Qizhou, Kurtz, Stanley 2008, ApJ, 672, 423
Kurtz, S., Churchwell, E., Wood, D. O. S. 1994, ApJS, 91, 659
Liu, Hauyu Baobab, et al. 2014, ApJ, 780, 155
Liu, Hauyu Baobab, Jiménez-Serra, Izaskun, Ho, Paul T. P., Chen, Huei-Ru, Zhang, Qizhou, Li, Zhi-Yun 2012, ApJ, 756, 10
Macías, Enrique, et al. 2016, ApJ, 829, 1
Martín-Pintado, J., Bachiller, R., Thum, C., Walmsley, M. 1989, A&A, 215, L13
Morata, Oscar, et al. 2015, ApJ, 807, 55
Moscadelli, L., Sánchez-Monge, A., Goddi, C., Li, J. J., Sanna, A., Cesaroni, R., Pestalozzi, M., Molinari, S., Reid, M. J.
2016, A&A, 585A, 71
Ortiz-León, Gisela, et al. 2017, ApJ, 834, 141O
Owen, James E., Scaife, Anna M. M., Ercolano, Barbara 2013, MNRAS, 434, 3378
Pascucci, I., Gorti, U., Hollenbach, D. 2012, ApJ, 751, L42
Pascucci, I., Ricci, L., Gorti, U., Hollenbach, D., Hendler, N. P., Brooks, K. J., Contreras, Y. 2014, ApJ, 795, 1
Plambeck, R. L., et al. 2013, ApJ, 765, 40
Peters, Thomas, Banerjee, Robi, Klessen, Ralf S., Mac Low, Mordecai-Mark, Galván-Madrid, Roberto, Keto, Eric R. 2010, ApJ, 711, 1017
Peters, Thomas, Longmore, Steven N., Dullemond, Cornelis P. 2012, MNRAS, 425, 2352
Pittard, J. M., Dougherty, S. M. 2006, MNRAS, 372, 801

Purser, S. J. D., Lumsden, S. L., Hoare, M. G., Urquhart, J. S., Cunningham, N., Purcell, C. R., Brooks, K. J., Garay, G., Guzmán, A. E., Voronkov, M. A. 2016, MNRAS, 460, 1039
Rivilla, V. M., Chandler, C. J., Sanz-Forcada, J., Jiménez-Serra, I., Forbrich, J., Martín-Pintado, J. 2015, ApJ, 808, 146
Rodríguez, L. F. 1997, in IAU Symp. 182, Herbig-Haro Flows and the Birth of Stars, ed B. Reipurth and C. Bertout (Cambridge: Cambridge Univ. Press) 83
Rodríguez, Luis F., Garay, Guido, Curiel, Salvador, Ramirez, Solange, Torrelles, José M., Gómez, Yolanda, Velazquez, Arturo 1994, ApJ, 430, L65
Rodríguez-Kamenetzky, Adriana, Carrasco-González, Carlos, Araudo, Anabella, Torrelles, José M., Anglada, Guillem, Martí, Josep, Rodríguez, Luis F., Valotto, Carlos 2016, ApJ, 818, 27
Rodríguez-Kamenetzky, Adriana, Carrasco-González, Carlos, Araudo, Anabella, Romero, Gustavo E., Torrelles, José M., Rodríguez, Luis F., Anglada, Guillem, Martí, Josep, Perucho, Manel, Valotto, Carlos 2017, ApJ, 851, 16
Rosero, Viviana, et al. 2016, ApJS, 227, 25
Shirley, Yancy L., Claussen, Mark J., Bourke, Tyler L., Young, Chadwick H., Blake, Geoffrey A. 2007, ApJ, 667, 329
Shu, Frank, Najita, Joan, Ostriker, Eve, Wilkin, Frank, Ruden, Steven, Lizano, Susana. 1994, ApJ, 429, 781
Tanaka, Kei E. I., Tan, Jonathan C., Zhang, Yichen 2016, ApJ, 818, 52
Torrelles, J. M., Ho, P. T. P., Rodríguez, L. F., Cantó, J. 1985, ApJ, 288, 595
Tychoniec, Ł, et al. 2018, arXiv:1806.02434
Urquhart, J. S., Hoare, M. G., Purcell, C. R., Lumsden, S. L., Oudmaijer, R. D., Moore, T. J. T., Busfield, A. L., Mottram, J. C., Davies, B. 2009, A&A, 501, 539
van der Tak, F. F. S., Menten, K. M. 2005, A&A, 437, 947
Vacca, William D., Garmany, Catharine D., Shull, J. Michael 1996, ApJ, 460, 914
Walmsley, M. 1995, RMxAC, 1, 137
Williams, P. M., van der Hucht, K. A., Pollock, A. M. T., Florkowski, D. R., van der Woerd, H., Wamsteker, W. M. 1990, MNRAS, 243, 662
Wood, Douglas O. S., Churchwell, Ed 1989, ApJS, 69, 831
Zhang, Qizhou, Claus, Brian, Watson, Linda, Moran, James 2017, ApJ, 837, 53

Science with a Next-Generation Very Large Array
ASP Conference Series, Monograph 7
Eric J. Murphy, ed.

Understanding Massive Star Formation through Maser Imaging

Todd R. Hunter,[1] Crystal L. Brogan,[1] Anna Bartkiewicz,[2] James O. Chibueze,[3,4,5] Claudia J. Cyganowski,[6] Tomoya Hirota,[7] Gordon C. MacLeod,[8] Alberto Sanna,[9] and José-Maria Torrelles[10]

[1]*NRAO, Charlottesville, VA, USA;* thunter@nrao.edu, cbrogan@nrao.edu

[2]*Nicolaus Copernicus University, Torun, Poland;* annan@astro.umk.pl

[3]*Department of Physics and Astronomy, University of Nigeria, Nsukka, Nigeria*

[4]*SKA South Africa, Cape Town, South Africa;* james.chibueze@gmail.com

[5]*Centre for Space Research, Physics Department, North-West University, Potchefstroom, South Africa*

[6]*SUPA, School of Physics and Astronomy, University of St. Andrews, St. Andrews, UK;* cc243@st-andrews.ac.uk

[7]*National Astronomical Observatory of Japan, Mitaka, Tokyo, Japan;* tomoya.hirota@nao.ac.jp

[8]*Hartebeesthoek Radio Astronomy Observatory, Krugersdorp, South Africa;* gord@hartrao.ac.za

[9]*Max-Planck-Institut für Radioastronomie, Bonn, Germany;* asanna@mpifr-bonn.mpg.de

[10]*Institut de Ciéncies de l'Espai, Barcelona, Spain;* chema.torrelles@ice.cat

Abstract. Imaging the bright maser emission produced by several molecular species at centimeter wavelengths is an essential tool for understanding the process of massive star formation because it provides a way to probe the kinematics of dense molecular gas at high angular resolution. Unimpeded by the high dust optical depths that affect shorter wavelength observations, the high brightness temperature of these emission lines offers a way to resolve accretion and outflow motions down to scales as fine as ~1-10 au in deeply embedded Galactic star-forming regions, and at sub-pc scales in nearby galaxies. The Next Generation Very Large Array will provide the capabilities needed to fully exploit these powerful tracers.

1. Introduction: The Scientific Importance of Masers

The process of star formation leads to the concentration of molecular gas to high densities in molecular cloud cores. The potential energy released by gravitational collapse and accretion onto the central protostars heats and excites the surrounding material through infrared radiation and high velocity bipolar outflows. Both of these feedback mechanisms (radiative and mechanical) naturally produce population inversions between specific pairs of energy levels in several abundant molecules, including H_2O, CH_3OH, OH, NH_3, SiO, and H_2CO. The resulting non-thermal maser emission in the corresponding spectral transitions provides a beacon whose brightness temperature far exceeds the more commonly-excited thermal emission lines. Consequently, maser lines at centimeter wavelengths have traditionally provided a powerful probe of star formation through single-dish surveys and interferometric imaging. In general, they trace hot, dense molecular gas, revealing the kinematics of star-forming material within a few 1000 au from very young stars, including accretion disks and their associated jets, as well as shocks in the outflow lobes where the jets impact ambient gas. Masers are generally more prevalent in regions surrounding massive protostars, due to their higher luminosities and more energetic outflows. Furthermore, masers are sensitive indicators of sudden changes in the pumping conditions near the protostars, and, recently, it has been recognized that maser flares, in those lines which are pumped by infrared photons, can be directly associated with bursts of accretion onto the stars. In this context, maser emission provides a unique tool for probing how massive stars form, allowing us to reconstruct the gas dynamics in the vicinity of young stars with tens of Solar masses, as well as to study the accretion process in the time domain.

2. Description of the problem and limits of current facilities

With the advent of the Atacama Large Millimeter/submillimeter Array (ALMA), imaging thermal lines at high resolution has become easier, and recent results have begun to place previous and ongoing maser studies into better physical context (see, e.g., Orion Source I, Plambeck & Wright 2016; Hirota et al. 2017). At the distances of more typical massive star-forming regions, however, the brightness temperature sensitivity of ALMA is still not sufficient to trace the accretion flow and accompanying jet structures that surround massive protostars, because of the high angular and spectral resolution required. Moreover, at the shorter wavelengths of ALMA, the combination of molecular line confusion and high dust opacity toward the hot cores in protoclusters will often block the most interesting details from ALMA's view. In contrast, the centimeter maser transitions propagate unobscured from the innermost regions, providing a strong signal for self-calibration, and thus enabling high dynamic range imaging on long baselines.

Unfortunately, the angular resolution of the VLA is insufficient to resolve the details of accreting gas, particularly in the 6 GHz band where the beamsize is limited to ~0.3 arcsec. In the handful of nearest examples of massive star formation (d~1 kpc), this resolution corresponds to 300 au (e.g., Brogan et al. 2016). However, in the majority of star-forming sites across the Milky Way at several kpc from the Sun, it exceeds 1000 au, which is often more than the separation of protostars in the centers of massive protoclusters (e.g., Palau et al. 2013). Thus, an order of magnitude improvement in angular resolution (requiring at least ~300 km baselines) is needed to resolve the spatial morphology and kinematics of disks, or other accretion structures, at scales of 10-100 au in a large sample of massive protostars. Such a resolution would also enable three dimensional measurements of gas velocity via multi-epoch proper motions. For instance, with an angular resolution of 10 mas in the bright H_2O maser line, it is possible to determine the maser positions with an accuracy better than 0.1 mas (assuming S/N > 100), and then to measure proper motions of order 10 km s^{-1} in a few months only, for sources located up to several kpc distance. Furthermore, proper motion measurements of different maser species toward the same region have the potential to trace simultaneously the complementary kinematic structures around a young star, providing a unique picture of the gas dynamics locally (Sanna et al. 2010; Goddi et al. 2011). These measurements are currently conducted by means of Very Long Baseline Interferometry (VLBI) observations, but with the small number of available antennas their sensitivity is limited to non-thermal processes exceeding brightness temperatures of $\sim 10^7$ K (e.g. Matsumoto et al. 2014; Bartkiewicz et al. 2009). An example of proper motion observations at these scales, using three different VLBI facilities, is shown in Fig. 1 (Burns et al. 2017).

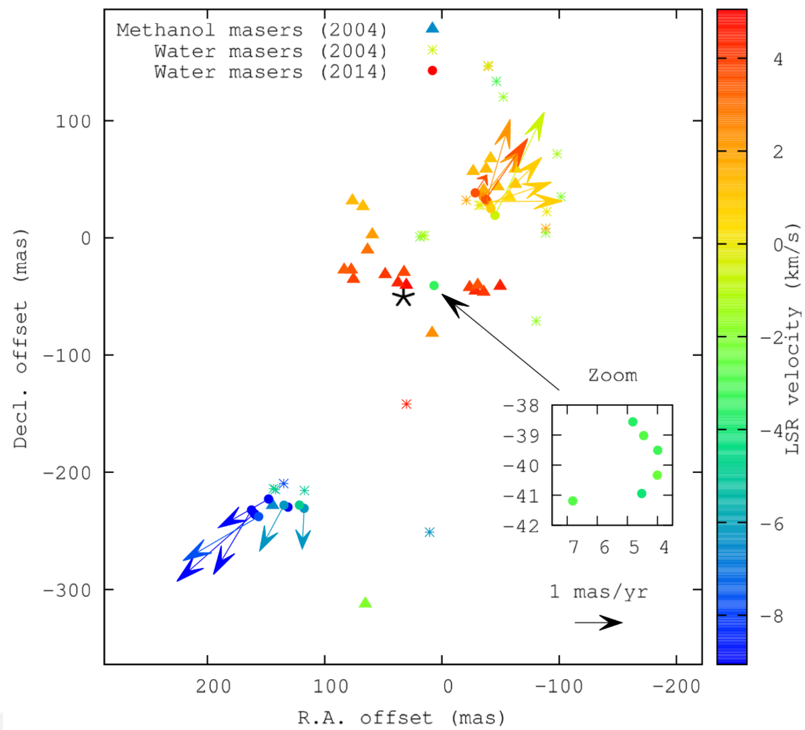

Figure 1. Central region of the dominant member (MM1) of the massive proto-cluster AFGL 5142 (figure extracted from Burns et al. (2017)). Combined view of 22-GHz water masers (filled circles) observed with VERA in 2010, 22-GHz water masers (asterisk) observed with the VLBA in 2004 (Goddi & Moscadelli 2006) and 6.7-GHz methanol masers (triangles) observed with the EVN in 2004 (Goddi et al. 2007). The inset shows the trajectory of maser feature A, moving in a clockwise fashion. The trajectory of feature A and proper motions of other masers are all converted to the YSO frame. The black asterisk symbol indicates the approximate origin of the episodic ejections, estimated from least-squares fitting of ellipses to the VERA maser data.

While current VLBI facilities (VLBA, EVN, eMERLIN, KVN, VERA, and LBA) have the requisite angular resolution to trace maser proper motions accurately, studies at these scales currently suffer from poor surface brightness sensitivity, which affects the science in two key ways. First, only the brightest maser spots can be detected, reducing the fidelity with which kinematic structures can be delineated in a single epoch, and reducing the number of potential spots that will persist over multiple epochs (used for proper motion studies). Second, the thermal radio continuum emission which arises in the immediate vicinity of massive protostars, with flux densities of < 1 mJy typically (Cyganowski et al. 2011), cannot be observed with the masers simultaneously, leading to (relative) positional uncertainties between the protostellar and maser components. The resulting ambiguity of the dynamical center severely hinders the interpretation of multi-epoch proper motion measurements, which are essential to understand the mass, momentum, and kinetic energy of the inner jet where it transitions into a bipolar molecular outflow.

Studying additional objects at scales of 10-100 au in a comprehensive list of maser lines, and with sufficient brightness sensitivity to image simultaneously the associated thermal free-free continuum emission, will be an important task for the next generation Very Large Array (ngVLA); see the accompanying chapter on Jets from YSOs (Galvan-Madrid et al. 2018). These studies will test and expand our current picture of massive star formation into the broader context of the Milky Way. Moreover, with 300 km baselines, it will also be possible to trace molecular gas structures down to 0.2-pc scales in the star-forming clouds in nearby extragalactic nuclei (e.g., Maffei 2 / IC 342 / M82) in the bright water maser and Class I methanol maser lines, enabling the study of individual massive protoclusters in these objects for the first time.

3. Astronomical Impact

While each maser transition offers a unique view into particular phenomena of massive star formation, masers can be broadly classified into major categories. The Class II CH_3OH maser lines, primarily at 6.7 GHz, 12.2 GHz, and 19.9 GHz, trace hot molecular gas that is (at least) moderately close to the youngest massive protostars ($\lesssim$ 1000 au), such that they can provide sufficiently intense mid-infrared emission to pump the maser transitions (e.g., Moscadelli et al. 2011; Bartkiewicz et al. 2014). The light curves of this maser species also show intriguing properties. Quasi-periodic flares in one or more Class II CH_3OH maser lines (120-500 days) have been observed in about a dozen objects (e.g., Goedhart et al. 2014); in one case, the 4.83 GHz H_2CO maser also shows correlated flaring (Araya et al. 2010). Recently, two spectacular accretion outbursts in massive protostars have been accompanied by strong flaring of these lines, S 255 NIRS3 (Caratti o Garatti et al. 2017; Moscadelli et al. 2017) and NGC 6334I-MM1 (Hunter et al. 2017, 2018; MacLeod et al. 2018), supporting the idea that maser flares might be caused by a variable accretion rate onto the central protostar. These extraordinary events led to the formation of the international Maser Monitoring Organization (M2O), with the goal of detecting and reporting future maser flares so that interferometers can be alerted to study the accretion event while it is still underway. Such an accretion event is also expected to yield variation in the continuum emission from the thermal jet (Cesaroni et al. 2018) and/or the hypercompact HII region (Brogan et al. 2018). Since both of these phenomena are powered by the protostar, the ability of ngVLA to perform simultaneous observations of the continuum and the masers will enable direct measurements of the correlations between them, yielding important constraints on the physics of the accretion mechanism.

The Class II CH_3OH maser lines (Sobolev et al. 1997; Cragg et al. 2005), along with the 1.6 GHz ground state OH lines and several excited state OH lines which are radiatively pumped (at 4.66 GHz, 4.75 GHz, 4.765 GHz, 6.030 GHz, and 6.035 GHz), are also seen to trace the ionization front of ultracompact HII regions (e.g., Fish & Reid

2007), which are powered by the more evolved massive protostars and Zero-Age Main Sequence (ZAMS) OB stars. Although excited OH lines are generally considered rare, a recent unbiased survey found that the 6.035 GHz line is detected toward nearly 30% of Class II CH_3OH masers and with a similar distribution in Galactic latitude (Avison et al. 2016). A similar detection rate is seen in survey of the 4.765 GHz line (Dodson & Ellingsen 2002). A simple explanation is these excited OH masers always occur in the same objects that power Class II masers, but simply have a correspondingly shorter mean lifetime or duty cycle, perhaps reflecting how long they remain above current sensitivity levels following each successive accretion outburst. In rare cases, the main line OH masers can also trace outflow motion (e.g., W75N and W3OH-TW Fish et al. 2011; Argon et al. 2003).

The strong water maser line at 22 GHz also traces gas close to massive and intermediate mass protostars. Often these lines span a broad (LSR) velocity range, of several tens of km s^{-1}, about the systemic velocity of the young stars, particularly compared to both classes of methanol masers ($\lesssim 10\,\mathrm{km\,s^{-1}}$). In some cases, water masers clearly arise from gas in the first few hundred au of the jet, such as in Cepheus A (e.g., Torrelles et al. 2011; Chibueze et al. 2012), or in bow shocks somewhat further out (e.g., Sanna et al. 2012; Burns et al. 2016). With continent-scale baselines, proper motion studies of these masers reveal the 3D velocities and orientations of collimated jets and/or wide-angle winds in the inner few 1000 au from the central protostars (e.g., Torrelles et al. 2001, 2003, 2014; Moscadelli et al. 2007; Sanna et al. 2010; Burns et al. 2017). When these studies are combined with high-resolution radio continuum observations of radio thermal jets, they can allow us to quantify the outflow energetics directly produced by the star formation process (e.g., Moscadelli et al. 2016; Sanna et al. 2016), as opposed to estimates of the molecular outflow energetics that are attainable on scales greater than 0.1 pc (typically through CO isotopologues). Long-term monitoring studies demonstrate that water masers are also highly variable (e.g., Felli et al. 2007), and their primary pumping mechanism is not believed to be radiative but collisional. Thus, since water masers are fundamentally produced in specific ranges of gas density and temperature within shocked gas layers, they are likely to trace different types of coherent motions at different stages of protostellar evolution. This is the case, for instance, of the star-forming region W75 N, where the 22 GHz masers (and the radio continuum) show different spatial distributions around two distinct young stars at different evolutionary stages (Torrelles et al. 2003; Carrasco-González et al. 2015). The 22 GHz line is also unique in exhibiting the 'superburst' phenomenon, in which brief flares reach 10^5 Jy or more. It has happened in only a few objects including Orion KL (Hirota et al. 2014, and references therein) and G25.65+1.05 (Lekht et al. 2018), but it has repeated in both, and appears to be due to interaction of the jet with high density clumps in the ambient gas, but within a few thousand au of the central protostar. In addition to Galactic studies, the detection and imaging of water masers in nearby star-forming galaxies provides a powerful probe of optically-obscured areas of star formation like the overlap region of the Antennae (Brogan et al. 2010). Additional uses of extragalactic masers are described in the accompanying chapter on Megamaser Cosmology (Braatz et al. 2018).

In contrast to H_2O masers and Class II CH_3OH masers, the Class I CH_3OH maser lines (primarily at 25 GHz, 36 GHz, 37 GHz, 44 GHz, and 95 GHz, but see Müller et al. (2004) for a more complete list) typically arise from collisionally-excited gas located much further from the protostar (~0.1-0.5 pc) where the bipolar molecular outflow lobes impact ambient gas. VLA surveys of these masers show that they often coincide with 4.5 micron emission that traces shocked gas in active outflows (Towner et al. 2017; Cyganowski et al. 2012, 2009). A similar maser phenomenon occurs in the ortho-NH_3 (3,3) and (6,6) lines at 23.87 GHz and 25.06 GHz (Brogan et al. 2011; Kraemer & Jackson 1995). Unfortunately, the VLA beam size is insufficient to resolve the structure of individual Class I maser features but VLBI observations resolve out most of the emission. Furthermore, the sensitivity of VLBI arrays is insufficient to map weak maser features detected by the VLA and single dishes (e.g. Matsumoto et al. 2014). We note that a portion of Class II maser emission also tends to be resolved out on VLBI scales (Pandian et al. 2011; Bartkiewicz et al. 2009; Minier et al. 2002). Thus, the ngVLA will provide a unique tool to study the spatial and velocity structures of both types of methanol masers.

The Class I CH_3OH masers are particularly abundant in the Galactic Center star-forming clouds (McEwen et al. 2016), and have recently been detected in starburst galaxies (Ellingsen et al. 2017; McCarthy et al. 2017). With ngVLA sensitivity and resolution, these masers could be used to probe such star-forming clouds in nearby galaxies (including Maffei 2 / IC 342 / M82).

Many maser lines are significantly polarized, thus it is important to observe them with full Stokes products in order to obtain the highest fidelity imaging. Furthermore, recent full polarization images of various Class I and Class II methanol maser lines (e.g., Surcis et al. 2013; Dall'Olio et al. 2017; Momjian & Sarma 2017) and the 22 GHz water line (e.g., Surcis et al. 2011; Goddi et al. 2017) have been used successfully to measure the magnetic field toward massive protostars via Zeeman splitting. These maser lines thus offer the potential to help us understand the degree to which magnetic fields influence or control accretion and outflows in massive protostars by providing very valuable information of magnetic field and velocity vectors in the same maser features (Sanna et al. 2015; Goddi et al. 2017).

Finally, maser emission from the vibrationally-excited levels of SiO offers a powerful (though rare) probe of the innermost hot gas surrounding massive protostars. For example, in one spectacular nearby case (Orion KL), movies of the vibrationally-excited SiO J=1-0, v=0 and v=1 transitions at 43 GHz have revealed a complicated structure of disk rotation and outflow (Matthews et al. 2010). Additional massive protostars (at greater distances) have recently been detected in these lines (Cordiner et al. 2016; Ginsburg et al. 2015; Zapata et al. 2009). The increased sensitivity of the ngVLA will no doubt yield further detections and enable new detailed images of the inner accretion structures in these objects. Additional uses of all maser species is described in the accompanying chapter on Evolved Stars (Matthews et al. 2018).

4. Connection to Unique ngVLA Capabilities

With its proposed frequency span, the ngVLA will uniquely provide access to all of the most important maser transitions from OH at 1.6 GHz to CH_3OH at 109 GHz. While the Long Baseline Observatory's Very Long Baseline Array (VLBA) also covers most of this frequency span, it lacks the sensitivity at the critical baseline lengths of up to 300 km to image simultaneously the continuum emission. The ngVLA will provide the required balance between angular resolution and brightness sensitivity, filling an important gap in existing capabilities. With the ability to image the non-thermal and thermal processes simultaneously, it will finally be possible to link the studies of the 3D gas dynamics (using the masers) with studies of the physical conditions of the ionized and molecular gas (using the continuum and strong, compact thermal lines like ammonia, respectively) at the same spatial resolution. Also, the ability to acquire high-fidelity images of all of these maser lines in just a few tunings will promote more uniform surveys of massive protostars as well as enable rapid monitoring of protostars currently undergoing an accretion outburst. Furthermore, the broader bandwidth receivers will provide more robust measurements of the spectral index of the continuum emission by promoting the ability to obtain all the necessary observations at a common epoch. Finally, the high spectral resolution and full polarization capability of the ngVLA will allow measurements of the magnetic field in the masing molecular gas via the Zeeman effect in methanol and water, which is a fundamental quantity for understanding the physics of star formation.

5. Experimental layout

In addition to studies of individual high mass protostellar objects (HMPOs), such as those currently undergoing an outburst, one can foresee a large ngVLA project to perform multi-epoch imaging of a significant sample of (several dozen) high-mass star-forming regions (HMSFRs). These HMSFRs typically contain clusters of massive protostars in diverse evolutionary states, a phenomenon that is often termed a "proto-Trapezium" (Megeath et al. 2005) or a "protocluster" (Minier et al. 2005). The following project would allow us: (1) to take a census of the young stellar objects across a broad mass range in these protoclusters, directly measuring the initial-mass-function; (2) to measure the kinematics of the gas undergoing maser emission, which will trace the flow of gas near the most massive stars; and (3) to study the way massive stars feed energy back into the protocluster environment and influence the formation of Solar-mass stars (and vice versa), by combining points (1) and (2).

Most protoclusters will be easily encompassed by a single pointing of the ngVLA in the lower bands, in which the primary beam full width half power (FWHP) is envisioned to be $\sim 10'$ (15 pc at 5 kpc) at 6.7 GHz. The largest ones may require a few pointings at the highest band where the beam is only $\sim 40''$ (1 pc at 5 kpc) at 100 GHz. Given that protostars at different stages of evolution may excite different masers, imaging these fields in all the ngVLA bands, and using all available antennas with full polarization products will efficiently identify all the massive protostars via their continuum emission (ionized gas and/or dust) and various maser lines. To illustrate the level of sensitivity required, we consider the continuum emission from jets which are closely linked to maser activity (see §3). Furthermore, we consider specifically jets from intermediate-mass protostars in order to define a sensitivity that will probe a broad range of massive protostars. The emission from individual clumps in jets observed by the VLA toward intermediate-mass protostars is approximately 1 mJy at 2-20 GHz in nearby (400 pc) regions like Serpens (Rodríguez-Kamenetzky et al. 2016), which translates to only 6 μJy for similar examples that are expected to populate more massive protoclusters at 5 kpc. In order to measure the SED of such an object, we require a $\approx 6\sigma$ detection in each 1 GHz subband. With the current VLA, we would need 44 hr of VLA observing time to reach 1 μJy rms in X-band alone. With the increased effective collecting area of the ngVLA, this time requirement would drop to $\lesssim 1$ hr per band, meaning that a multi-band survey of many fields would become feasible. Also, with this sensitivity, young lower-mass T Tauri stars, which are chromospherically active stars associated with highly-variable faint (synchrotron) radio continuum emission, will be also detected in the lower frequency bands (e.g., C-band), providing information about the low-mass population (Forbrich et al. 2017).

The available correlator channels will be distributed accordingly among low resolution continuum windows and up to 20 high-resolution spectral line windows in each of the 6 bands. Due to the 300 km baselines, we note that the maximum channel width for a 24 GHz (K-band) continuum observation is 0.5 MHz in order to limit bandwidth smearing to less than 2% across the FWHP of the primary beam, which means that ~28000 dual-polarization channels will be needed for the 14 GHz instantaneous bandwidth available in that band. In addition, the high-resolution line windows will require between 256 channels and 1024 channels each in order to provide Hanning-smoothed spectra with 0.1 km s^{-1} resolution across a velocity width of 12 km s^{-1} to 50 km s^{-1}. The broadest lines (primarily water) will require 4096 channels to cover ~200 km s^{-1}, so an additional ~20000 full-polarization channels are also needed for the maser lines. Thus, the number of correlator resources needed for the line observations is comparable to that needed for the continuum. A list of maser lines detectable in each band is summarized in Table 1.

Table 1. Detected maser lines in each ngVLA band; see Table 1 of Menten (2007) for further details

Band	Range (GHz)	Species and line frequencies (GHz)	# lines
1	1.2 - 3.5	ground-state OH (1.612, 1.665, 1.667, 1.720)	4
2	3.5 - 12.3	excited OH (4.66, 4.75, 4.765, 6.031, 6.035, 6.049)	6
		CH_3OH Class I (9.936)	1
		CH_3OH Class II (6.668, 12.18)	2
		ortho-H_2CO (4.83)	1
3	12.3 - 20.5	CH_3OH Class II (19.97)	1
		excited OH (13.441, Baudry et al. 1981; Caswell 2004)	1
4	20.5 - 34	H_2O (22.235)	1
		CH_3OH J_2-J_1-series Class I (24.9-30.3)	15
		CH_3OH Class I (23.445, Voronkov et al. 2011)	1
		CH_3OH Class II (23.12, Cragg et al. 2004))	1
		ortho-NH_3 (3,3) (6,6) (9,9) (12,12)	4
		other NH_3 inversion lines (thermal and/or maser)	~dozen
		excited OH (23.8, Baudry et al. 1981)	1
5	30.5 - 50.5	Class I CH_3OH (36.169, 44.069)	2
		Class II CH_3OH (37.7, 38.29, 38.45)	3
		SiO 1-0 v=1,2 (43.12, 42.82)	2
6	70 - 116	CH_3OH Class I (84.521, 95.169, 104.3)	3
		CH_3OH Class II (76.2, 76.5, 85.5, 86.6, 104.1, 107, 108.8)	7
		SiO 2-1 v=1,2 (86.24, 85.64)	2

With the calibrated uv-data, we will first construct multi-band continuum images with a matched resolution of 0.05″ in the range 5-100 GHz, using all the baselines (~360 km) at 5 GHz, and tapering the data to 60 km at 30 GHz and 18 km at 100 GHz. The photometry from these images will provide the spectral energy distributions of all the individual protostars (or compact binaries) on scales of 250 au $\times(d/5$ kpc), giving an immediate census of the protocluster. At these scales, images of thermal line emission from tracers of warm dense gas can also be attempted. Finer details of the individual objects can then be pursued by imaging the continuum using the longer baselines in the higher frequency bands, for instance, as fine as $0.01''$ at 22 GHz (50 au $\times$(d/5kpc)). This step will allow us to distinguish between jets (linearly-shaped emission), ultracompact and hypercompact HII regions (more symmetric emission), and T Tauri stars (non-thermal point-like emission). At this scale, in the higher frequency bands, disk-like accretion structures may be visible in the (still) optically-thin dust emission. Next, we can image the full field in the individual maser lines at moderate spectral resolution ($\sim$1 km s^{-1}) and in both polarizations, tabulating which transitions are associated with each object. In some cases, this process will include identifying the angular scale at which the emission becomes resolved in order to maintain sensitivity to the weakest features. We can then make spatially smaller cubes of each maser line, imaging several smaller sub-fields (i.e., those containing all the strong sources) taking advantage of the highest angular and spectral resolution ($\sim$0.1 km s^{-1}) in order to analyze the maser gas kinematics associated with each protostar. In many cases, we would make these cubes with full polarization in order to measure the magnetic fields. Finally, the strongest compact features can then be used to measure proper motions over several months or years.

On the one hand, such an ambitious project would require the efforts of many students and researchers at many international institutions, but on the other hand, it will foster new synergies between astronomers with diverse expertise, and provide a global picture of the youngest star-forming sites across the Milky Way.

6. Complementarity with respect to existing and planned (>2025) facilities

The science described here will share many synergies with other future facilities. Of course, ALMA will likely be the closest complementary facility as it can observe the dust emission and strong thermal lines at comparable angular resolutions. The Square Kilometer Array (SKA) will provide access to high resolution imaging of the lowest frequency masers, such as OH at 1612 MHz, 1665 MHz, 1667 MHz and 1720 MHz, as well as covering the southern Galactic plane in the additional maser lines that will be accessible in its highest frequency bands including Class II methanol masers. Toward many target regions, imaging at mid-infrared wavelengths by the Thirty Meter Telescope (TMT) and the European Extremely Large Telescope (ELT) will be quite informative as these facilities can potentially deliver 0.05-0.2 arcsec resolution at 7-28 μm which can probe through a portion of the typically high column of extinction. The James Webb Space Telescope (JWST) can also provide sensitive integral field images for regions where saturation is not prohibitive. In both cases, the short wavelengths will delineate outflow cavities on larger scales, while the longer wavelengths (when combined with ALMA observations) will enable measurements of the luminosities of the individual massive protostars. Finally, future X-ray space telescopes such as Lynx (Vikhlinin 2018) can potentially provide crucial measurements of transient hot gas following accretion outbursts in massive protostars, as well as study the variable emission from the lower mass members of the protocluster (see, e.g., Montes et al. 2015; Townsley et al. 2014).

Acknowledgments. The National Radio Astronomy Observatory is a facility of the National Science Foundation operated under agreement by Associated Universities, Inc.

References

Araya, E. et al. 2010, ApJ, 717, 133
Argon, A. L., Reid, M. J., & Menten, K. M. 2003, ApJ, 593, 925
Avison, A., Quinn, L. J., Fuller, G. A., et al. 2016, MNRAS, 461, 136
Bartkiewicz, A., Szymczak, M., & van Langevelde, H. J. 2014, A&A, 564, A110
Bartkiewicz, A., Szymczak, M., van Langevelde, H. J., Richards, A. M. S., & Pihlström, Y. M. 2009, A&A, 502, 155
Baudry, A., Walmsley, C. M., Winnberg, A., & Wilson, T. L. 1981, A&A, 102, 287
Braatz, J., et al. 2018, this volume
Brogan, C.L., et al. 2018, in Proc. of IAU Symp. 336, ed. A. Tarchi, M.J. Reid & P. Castangia, Cambridge University Press
Brogan, C.L., et al. 2016, ApJ, 832, 187
Brogan, C. L., Hunter, T. R., Cyganowski, C. J., et al. 2011, ApJ, 739, L16
Brogan, C., Johnson, K., & Darling, J. 2010, ApJ, 716, L51
Burns, R. A., Handa, T., Imai, H., et al. 2017, MNRAS, 467, 2367
Burns, R. A., Handa, T., Nagayama, T., Sunada, K., & Omodaka, T. 2016, MNRAS, 460, 283
Caratti o Garatti, A., Stecklum, B., Garcia Lopez, R., et al. 2017, Nature Physics, 13, 276
Carrasco-González, C., Torrelles, J. M., Cantó, J., et al. 2015, Science, 348, 114
Caswell, J. L. 2004, MNRAS, 352, 101
Cesaroni, R., Moscadelli, L., Neri, R., et al. 2018, A&A, 612, 103, arXiv:1802.04228
Chibueze, J. O., Imai, H., Tafoya, D., et al. 2012, ApJ, 748, 146
Cordiner, M. A., Boogert, A. C. A., Charnley, S. B., et al. 2016, ApJ, 828, 51
Cragg, D. M., Sobolev, A. M., & Godfrey, P. D. 2005, MNRAS, 360, 533
Cragg, D. M., Sobolev, A. M., Caswell, J. L., Ellingsen, S. P., & Godfrey, P. D. 2004, MNRAS, 351, 1327
Cyganowski, C. J., Brogan, C. L., Hunter, T. R., et al. 2012, ApJ, 760, L20
Cyganowski, C. J., Brogan, C. L., Hunter, T. R., & Churchwell, E. 2011, ApJ, 743, 56
Cyganowski, C.J., et al. 2009, ApJ, 702, 1615
Dall'Olio, D., Vlemmings, W. H. T., Surcis, G., et al. 2017, A&A, 607, A111
Dodson, R. G., & Ellingsen, S. P. 2002, MNRAS, 333, 307
Ellingsen, S. P., Chen, X., Breen, S. L., & Qiao, H.-H. 2017, MNRAS, 472, 604
Felli, M., Brand, J., Cesaroni, R., et al. 2007, A&A, 476, 373
Fish, V. L., Gray, M., Goss, W. M., & Richards, A. M. S. 2011, MNRAS, 417, 555
Fish, V. L., & Reid, M. J. 2007, ApJ, 670, 1159
Forbrich, J., Reid, M. J., Menten, K. M., et al. 2017, ApJ, 844, 109
Galvan-Madrid, R., et al. 2018, this volume
Ginsburg, A., Walsh, A., Henkel, C., et al. 2015, A&A, 584, L7
Goddi, C., et al. 2017, A&A, 597, 43
Goddi, C., Moscadelli, L., & Sanna, A. 2011, A&A, 535, L8
Goddi, C., Moscadelli, L., Sanna, A., Cesaroni, R., & Minier, V. 2007, A&A, 461, 1027
Goddi, C., & Moscadelli, L. 2006, A&A, 447, 577
Goedhart, S., et al. 2014, MNRAS, 437, 1808
Hirota, T., Machida, M. N., Matsushita, Y., et al. 2017, Nature Astronomy, 1, 0146
Hirota, T., Tsuboi, M., Kurono, Y., et al. 2014, PASJ, 66, 106
Hunter, T. R., Brogan, C. L., et al. 2018, ApJ, 854, 170
Hunter, T. R., Brogan, C. L., MacLeod, G. C., et al. 2017, ApJ, 837, L29
Kraemer, K. E., & Jackson, J. M. 1995, ApJ, 439, L9
Lekht, E. E., et al. 2018, Astronomy Reports, 62, 213
MacLeod, G. C., et al. 2018, MNRAS, 478, 1077, arXiv: 1804.05308

Matsumoto, N., Hirota, T., Sugiyama, K., et al. 2014, ApJ, 789, L1
Matthews, L., et al. 2018, this volume
Matthews, L., et al. 2010, ApJ, 708, 80
McCarthy, T. P., Ellingsen, S. P., Chen, X., et al. 2017, ApJ, 846, 156
McEwen, B. C., Sjouwerman, L. O., & Pihlström, Y. M. 2016, ApJ, 832, 129
Megeath, S. T., Wilson, T. L., & Corbin, M. R. 2005, ApJ, 622, L141
Menten, K. M. 2007, Astrophysical Masers and their Environments, IAU Symposium 242, 496
Minier, V., Burton, M. G., Hill, T., et al. 2005, A&A, 429, 945
Minier, V., Booth, R. S., & Conway, J. E. 2002, A&A, 383, 614
Momjian, E. & Sarma, A. 2017, ApJ, 834, 168
Montes, V. A., Hofner, P., Anderson, C., & Rosero, V. 2015, ApJS, 219, 41
Moscadelli, L., Sanna, A., Goddi, C., et al. 2017, A&A, 600, L8
Moscadelli, L., Sánchez-Monge, Á., Goddi, C., et al. 2016, A&A, 585, A71
Moscadelli, L., Sanna, A., & Goddi, C. 2011, A&A, 536, A38
Moscadelli, L., Goddi, C., Cesaroni, R., Beltrán, M. T., & Furuya, R. S. 2007, A&A, 472, 867
Müller, H. S. P., Menten, K. M., & Mäder, H. 2004, A&A, 428, 1019
Palau, A., Fuente, A., Girart, J. M., et al. 2013, ApJ, 762, 120
Pandian, J. D., Momjian, E., Xu, Y., Menten, K. M., & Goldsmith, P. F. 2011, ApJ, 730, 55
Plambeck, R. L., & Wright, M. C. H. 2016, ApJ, 833, 219
Rodríguez-Kamenetzky, A., Carrasco-González, C., Araudo, A., et al. 2016, ApJ, 818, 27
Sanna, A., Moscadelli, L., Cesaroni, R., et al. 2016, A&A, 596, L2
Sanna, A., Surcis, G., Moscadelli, L., et al. 2015, A&A, 583, L3
Sanna, A., Reid, M. J., Carrasco-González, C., et al. 2012, ApJ, 745, 191
Sanna, A., Moscadelli, L., Cesaroni, R., et al. 2010, A&A, 517, A78
Sobolev, A. M., Cragg, D. M., & Godfrey, P. D. 1997, A&A, 324, 211
Surcis, G., Vlemmings, W. H. T., van Langevelde, H. J., et al. 2013, A&A, 556, A73
Surcis, G., Vlemmings, W. H. T., Curiel, S., et al. 2011, A&A, 527, A48
Torrelles, J. M., Trinidad, M. A., Curiel, S., et al. 2014, MNRAS, 437, 3803
Torrelles, J. M., Patel, N. A., Curiel, S., et al. 2011, MNRAS, 410, 627
Torrelles, J. M., Patel, N. A., Anglada, G., et al. 2003, ApJ, 598, L115
Torrelles, J. M., Patel, N. A., Gómez, J. F., et al. 2001, Nat, 411, 277
Towner, A. P. M., Brogan, C. L., Hunter, T. R., et al. 2017, ApJS, 230, 22
Townsley, L. K., Broos, P. S., Garmire, G. P., et al. 2014, ApJS, 213, 1
Vikhlinin, A. 2018, American Astronomical Society Meeting Abstracts #231, #103.04
Voronkov, M. A., Walsh, A. J., Caswell, J. L., et al. 2011, MNRAS, 413, 2339
Zapata, L. A., Menten, K., Reid, M., & Beuther, H. 2009, ApJ, 691, 332

Science with a Next-Generation Very Large Array
ASP Conference Series, Monograph 7
Eric J. Murphy, ed.

DRAFT EDITION

New Frontiers in Protostellar Multiplicity with the ngVLA

John J. Tobin

University of Oklahoma, `jjtobin@ou.edu`

Patrick Sheehan

University of Oklahoma

Doug Johnstone

NRC-Herzberg

Abstract. The ngVLA will enable significant advances in our understanding of the formation and evolution of multiple star systems in the protostellar phase, building upon the breakthroughs enabled by the VLA. The high-sensitivity and resolution at 3 mm wavelengths and longer will enable closer multiple systems to be discovered in the nearby star forming regions. The ngVLA is incredibly important for multiplicity studies because dust opacity at short wavelengths (<3 mm) can hide multiplicity and the long wavelengths are needed to reveal forming multiples in the youngest systems. The samples sizes can be expanded to encompass star forming regions at distances of at least 1.5 kpc, enabling statistical studies that are on par with studies of field star multiplicity. We verify the capability of the ngVLA to detect and resolve multiple star systems at distances out to 1.5 kpc using empirical examples of systems detected by the VLA and scaling them to greater distances. We also use radiative transfer models and simulations to verify that the ngVLA can resolve close binary systems from their dust emission at these distances. The ngVLA will also have excellent imaging capability and the circum-multiple environments can also be examined in great detail.

1. Introduction

Star formation occurs as a consequence of dense gas clouds collapsing under their own gravity, once the gravitational force is able to overcome sources of support (e.g., thermal pressure, magnetic fields, turbulence; McKee & Ostriker 2007). The star formation process frequently results in the formation of two or more stars that comprise a gravitationally bound system, given that nearly half of Sun-like stars (in terms of stellar mass) are found in binary or higher-order multiple systems (Duquennoy & Mayor 1991; Raghavan et al. 2010). The degree of stellar multiplicity strongly depends on stellar mass. Stars more massive than the Sun have a higher fraction of multiplicity and stars less massive than the Sun have a lower degree of multiplicity, but still with a multiplicity fraction upwards of 25%; see Duchêne & Kraus (2013) for a recent review. Thus, multiple star formation is a common outcome of the star formation process for all stellar masses and a comprehensive understanding of star formation must account for multiplicity.

Recent surveys in the infrared, millimeter, and centimeter have also shown a high degree of multiplicity in the protostar phase (Connelley et al. 2008; Looney et al. 2000). Both the youngest protostars (Class 0 sources, André et al. 1993) and more evolved protostars (Class I), show a higher degree of multiplicity than field stars (e.g., Reipurth et al. 2004; Chen et al. 2013; Tobin et al. 2016b). The largest mass reservoir is available during the protostellar phase, making it the most promising epoch for companion star formation to occur (Tohline 2002). Thus, the distribution of field star multiplicity is likely derived from the primordial distribution of companions that form during the protostar phase. While the mechanisms of multiple star formation are still uncertain, the distribution of separations in the protostellar phase may reveal the signature of their formation process. The peak of the companion separation distribution for field solar-type stars is ~50 AU (Raghavan et al. 2010), but the formation route for these systems cannot be determined from evolved stellar populations alone because they have undergone Myr to Gyr of dynamical evolution. Moreover, not all systems that form as multiples may remain multiple throughout their lives, but they may still have formed in the presence of one or more companion stars (Sadavoy & Stahler 2017). Some companions can be ejected through dynamical interactions (e.g., Reipurth & Mikkola 2012) or become unbound after the dispersal of the star forming core. This means that the formation of nascent planetary systems may have been influenced by companion stars, even if they are no longer bound to the system. Thus, to reveal the origins of stellar multiplicity and its effects on proto-planetary systems, multiplicity must be characterized during the earliest stage of the star formation process.

There are two favored routes to explain the formation of multiple star systems: disk fragmentation due to gravitational instability (e.g., Stamatellos & Whitworth 2009; Kratter et al. 2010) and turbulent fragmentation within the molecular cloud (e.g., Padoan & Nordlund 2002; Offner et al. 2010). Disk fragmentation will preferentially result in the formation of close (<500AU) multiple star systems and requires a large (R_{disk} ~50 AU) and massive rotationally-supported disk to have formed around the primary star. Turbulent fragmentation can result in the formation of both wide and close multiple systems. In this scenario, the initial protostars form with separations ~1000 AU, and depending on their relative motions and masses they can migrate inward to radii ~100 AU (Offner et al. 2010), remain at wide radii, or drift further apart. However, the expected trends can only be revealed statistically, requiring large samples of protostars to be observed with spatial resolution better than 50 AU (the average field star separation). It is also important to point out that rotation of the protostellar cloud itself has also been suggested as a mechanism to form multiple star systems (Burkert & Bodenheimer 1993), but current observational evidence points more toward turbulence for the formation of wide companions (Lee et al. 2016).

A key difference in examining the formation of multiple stars at radio/millimeter wavelengths versus optical/infrared is that direct emission from the protostellar photosphere is not being detected. Instead, the dust emission from the individual circumstellar disks and/or free-free emission from the base of the protostellar jet are being probed. Thus, the observations are tracing fragmentation, but cannot directly confirm the protostellar nature of the multiple observed sources. Tobin et al. (2016b) examined the nature of the emission detected and concluded that multiple sources of emission very likely correspond to true multiplicity, but we note, however, that the possibility of a small percentage of false positives cannot be excluded. Nevertheless, observations at millimeter/centimeter wavelengths are generally the only available tool to study multiplicity toward such deeply embedded objects.

The multiplicity statistics of field stars have the benefit of large samples and are not subject to the same limitations of protostellar multiplicity studies. Nonetheless, it is useful to use the field multiplicity studies as a baseline for the survey requirements of future protostellar multiplicity studies. The most recent compendium of field solar-type star multiplicity had a sample of 454 stars in a volume limited sample, finding a total of 259 companions with an average companion separation of 50 AU in an approximate Gaussian distribution (Raghavan et al. 2010). Assuming that the field multiplicity distribution represents the distribution of protostellar multiplicity (it probably does not), we can use this distribution in order to estimate how many protostellar multiples would need to be detected in order to obtain the same level of statistical accuracy. Restricting the relevant parameter space to a separation range between 1 AU and 1000 AU, the Raghavan et al. (2010) sample contains ∼126 companion stars within this range. It is necessary to limit the parameter space in this regard because scales less than 1 AU will likely be difficult to examine for protostars and scales greater than 1000 AU will be dominated by clustering and not physical association. In order to observe 126 protostellar companions to match the sample size, at least 630 protostars must be observed if the average companion frequency of protostars is in this range is 20% (Tobin et al. 2016b). This would require that all protostars within the Gould Belt be observed, sampling over different star formation conditions. If the youngest (Class 0) protostars are required for such characterization, then there are much less than 630 in the entire Gould Belt (Dunham et al. 2014). Surveys of more distant, massive star forming regions are therefore required to observe this number of protostars in a single region.

2. Setting the Stage: The VANDAM Survey

A first large, systematic survey to examine protostellar multiplicity in an entire star forming region was carried out by the VLA Nascent Disk and Multiplicity (VANDAM) Survey (Tobin et al. 2015). This survey was carried out toward the Perseus star forming region, observing 45 Class 0 protostars (including possible objects in transition; Class 0/I), 37 Class I protostars, and 12 Class II young stars. All protostars were observed at a wavelength of 9 mm (33 GHz), at a uniform sensitivity of ∼9 μJy, and at a uniform resolution of 15 AU (0.065′′). From these data, we identified 18 systems that were multiple with companion separations <500 AU; 16 of these companions were new detections by the VANDAM survey. We also detected a number of systems with separations >500 AU as well as many hierarchical multiple systems. Some multiple systems had separations as small as ∼19 AU, near the limit of our spatial resolution. Figure 1 shows an example of a very close multiple system. Figure 2 then shows an example of a hierarchical system toward L1448 IRS3 where there is a triple, a binary, and a single system all within 5000 AU. The triple was revealed by ALMA to have a circum-multiple disk, strongly indicating that the system formed via disk fragmentation (Tobin et al. 2016a), and the system as a whole in Figure 2 illustrates how fragmentation is a multi-scale process.

The separations of all companion stars detected in the VANDAM survey, are shown as a histogram in Figure 3. Two features are obvious: 1) there appears to be two peaks, one at ∼75 AU and another >1000 AU, and 2) the separation distribution is in excess of the field, except for separations between ∼300 AU and ∼1000 AU. It is argued in Tobin et al. (2016b) that this bimodality results from both disk fragmentation (∼75 AU part) and turbulent fragmentation (>1000 AU part) happening to produce the observed distribution. There are a lower number of detected companions between

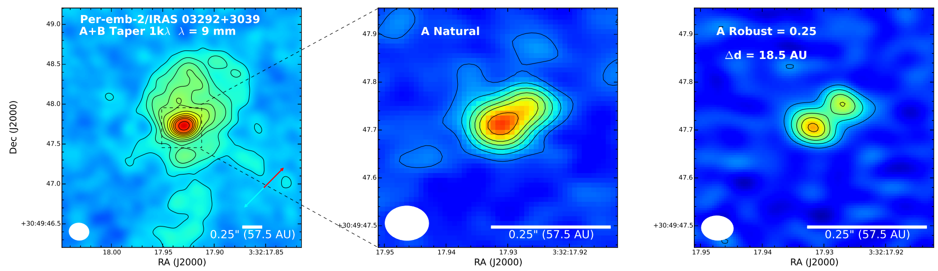

Figure 1. Images of Per-emb-2 (IRAS 03292+3039) at 9 mm from the VLA at increasing resolution from left to right. The left panel, with the lowest resolution and most sensitivity to extended structure, shows significant/structured emission surrounding a bright source that we interpret as the position of the main protostar; the middle and right panels zoom-in on the region outlined with a dashed box. The middle panels with higher resolution have resolved-out the extended structure and only detect the bright peak at the position of the protostar; however, the source appears extended at this resolution. The highest resolution image in the right panel shows that the source is resolved into two sources separated by 18.5 AU. The contours in each panel are [-6, -3, 3, 6, 9, 12, 15, 20, 25, 30, 35, 40, 50, 60, 70, 80, 90, 100, 150] $\times\ \sigma$, where σ = 7.3 μJy, 9.6 μJy, 11.9 μJy from left to right at 9 mm.

~300 AU and ~1000 AU, indicating that neither formation mechanism is efficient at these scales.

While this survey of Perseus represents a major advance, it was limited in terms of the number of sources. Considering uncertainties, the distribution could be consistent with a flat separation distribution (when considering the logarithm of the separation). Thus, it is clear that greater numbers are required and more than one star forming region needs to be examined in order to understand if this is a common distribution or an outlier. However, Perseus still offers an excellent template for studies of multiplicity to larger samples and more distant star forming regions. It remains to be seen if the separation distribution observed toward Perseus is 'universal,' and its implications for the formation mechanisms of multiple stars are just beginning to be understood (Tobin et al. 2016a; Lee et al. 2016; Offner et al. 2016).

Expanding on the discussion at the end of the Section 1, it will be important to determine if the observed bimodality is statistically significant. One way to do this is to obtain enough statistics such that the uncertainties in the individual bins of Figure 3 are statistically distinct. Assuming the same distribution of companion separations in Perseus, the bin at 1.875 log(AU) will be inconsistent with the bin at 2.375 log(AU) at the 4σ level when the sample size reaches ~500. Thus, samples in excess of 500 protostars are needed to statistically distinguish between bimodal and log-flat distributions.

A challenge to observing larger numbers of protostars is that the most populous star forming regions are more distant. Orion is ~400 pc away and the VLA offers a best spatial resolution of ~30 AU at 8 mm, this is just a bit better that the typical separation of field solar-type stars and there are likely to be more multiple systems lurking at separations below 30 AU. Perseus has at least three systems with separations ~20 AU (Figures 1 and 3). Another limiting issue in Orion is that sources are 3× fainter due to the increased distance, so observing with the same sensitivity requires 9× more observing time as compared to Perseus. It quickly becomes impractical to

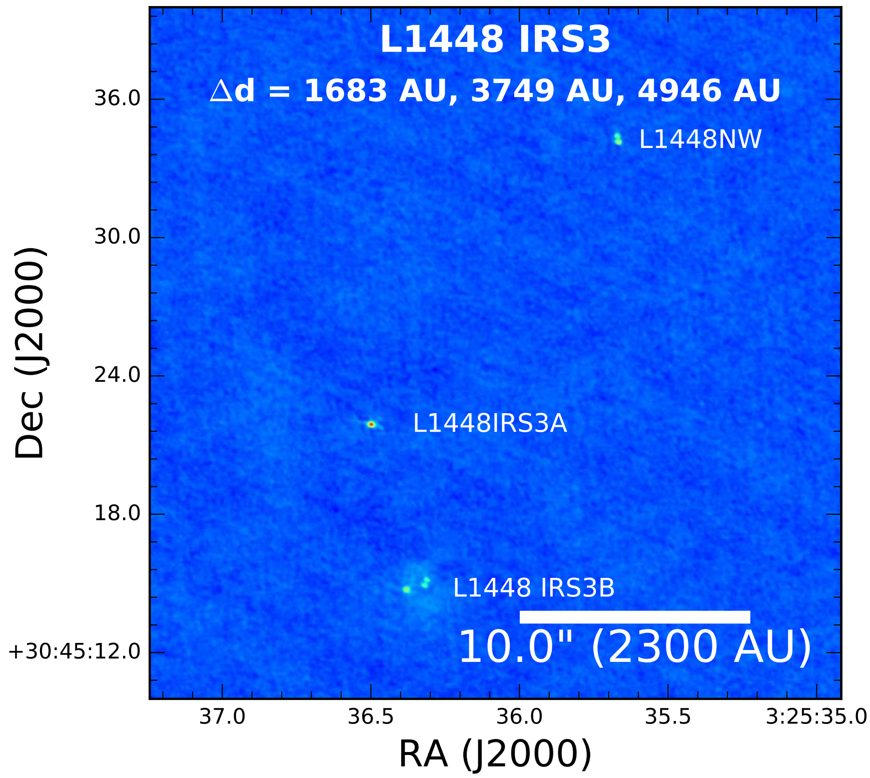

Figure 2. Image of the L1448-N or IRS3 region at 9 mm from the VLA. L1448 IRS3B is a close triple, L1448NW (L1448 IRS3C) is a binary, and L1448 IRS3A is single at the limit of our resolution. Both L1448 IRS3B and L1448NW are Class 0 sources while L1448 IRS3A is a Class I system. Separations written inside the figure are relative to L1448 IRS3B.

observe even more distant star forming regions with sensitivity to protostars having typical luminosities (i.e., 1-3 $L_{\odot}$; Fischer et al. 2017).

Finally, it is important to highlight that in the VANDAM survey, the spatial association of young stars was observed and not boundedness, which could not be evaluated from the data at hand. Many (or most) of the companions shown in Figure 2 at separations > 1000 AU do not likely reflect bound systems. Some could be line of sight associations (more frequent with increasing separation), or when they finish accreting material, outflows may have removed enough mass such that they are unbound. The closer companions (< 500 AU) have a higher likelihood of being bound, but even so, interactions may alter or destroy some of these multiple systems. Thus, the observed companion separation distribution in the protostellar phase may reflect the initial companion separation distribution and it will dynamically evolve over Myr to Gyr toward toward the field star separation distribution.

The ngVLA has excellent potential to evaluate the boundedness of systems with <50 AU separations. The angular resolution in the nearby regions will uncover closer

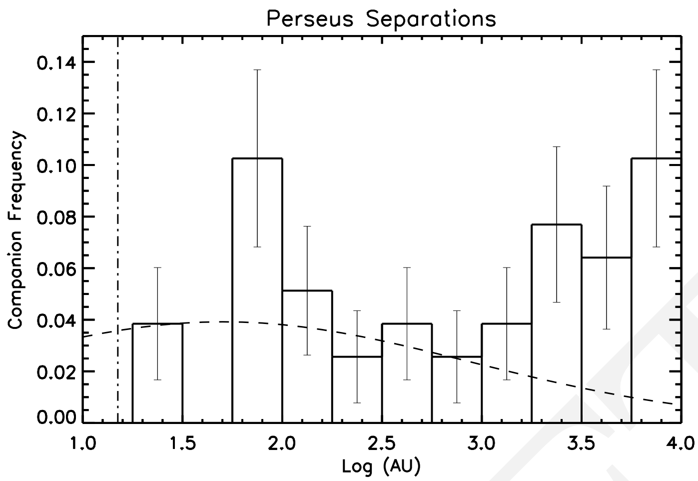

Figure 3. Histogram of companion star frequency versus separation for the entire sample of multiple sources in Perseus. The dashed curve is the Gaussian fit to the field star separation distribution from Raghavan et al. (2010). The vertical dot-dashed line corresponds to the approximate resolution limit of the VLA in A-configuration (~15 AU) toward Perseus at a distance of 230 pc.

multiple systems, and the positional accuracy granted by the increased angular resolution will enable the orbital motion of <50 AU companions to be measured on time scales of ~5 years. Such analysis can incorporate previous VLA data as needed to establish likely orbital solutions with an extended time baseline. Such measurements of binary/multiple orbits will also offer constraints on the protostar masses.

3. Examining Close Multiplicity Studies out to ≥1.5 kpc

The ngVLA offers a number of features that overcome the limitations of the current VLA. The full array will provide an angular resolution of 0.01″ at 7.3 mm and 0.014″ at 1.1 cm (ngVLA Memo #17). These two wavelength bands are ideal for examining protostellar multiplicity because they probe both dust and free-free emission. The addition of free-free emission to the dust emission makes the protostars themselves stand out, enhancing their detectability. The dramatically increased resolution of the ngVLA will enable the range of separations to be expanded, with better sensitivity to close companions. For Perseus (d=230 pc), we will be able to look for companions down to 2.3 AU separations. Toward Orion (d=400 pc), the separation limit will be pushed down to 4 AU, and in more distant, more populous star forming regions (e.g., Cygnus-X at 1500 pc) the separation limit will be 15 AU. The ngVLA will enable us to examine separations in these distant Galactic star forming regions down to the same scale that we are currently able to do in Perseus!

Angular resolution improvements alone, however, are not sufficient to address questions of protostellar multiplicity, because these studies require statistics and not a few case studies. With the drastic increase in the number of antennas, and hence the collecting area, projected for the ngVLA, it is important to consider the detectability of protostellar multiple systems in progressively more distant star forming regions. Using IRAS 03292+3039 from Perseus (Figure 1) as a case study, current VLA observations detect sources A and B with peak flux densities of 170 μJy and 130 μJy, respectively. If a similar system were located at the distance of Cygnus-X, their respective flux densities would be 4 μJy and 3 μJy. These flux densities are completely impractical to observe at 30 GHz for the current VLA; reaching a S/N of 10 with the VLA would take 10 days! However, the ngVLA can reach a sensitivity of 0.26 μJy beam^{-1} (S/N$\sim$10) in 1 hour on-source. Thus, detecting such faint and close companions in massive, distant star forming regions will be routine with the ngVLA because the increased sensitivity.

We have concentrated on the capabilities of the ngVLA at $\sim$7.3 mm because of the ability to directly compare with data from the VANDAM surveys. However, the 3 mm band of the ngVLA also holds significant potential to enable studies of multiplicity out to star forming regions even more distant than Cygnus-X. At 3 mm, most emission will be from pure dust emission, and the brightness of this emission increases steeply with decreasing wavelength $\lambda^{-(2+\beta)}$ (increasing with frequency $\nu^{2+\beta}$), where β is the dust opacity spectral index which is typically observed to be between 0 and 2 in disks (e.g., Ricci et al. 2010). IRAS 03292+3039 was also observed with ALMA at 3 mm using 14 km baselines, obtaining nearly the highest resolution offered by the facility at 3 mm. The 3 mm flux densities of the two companions were 1200 μJy and 1050 μJy, respectively. Scaling these to the distance of Cygnus-X they could be detected with S/N > 20 with the ngVLA in 1 hr on-source with a sensitivity of 0.86 μJy beam^{-1}. At an even greater distance of $\sim$3 kpc, they could be detected with a S/N=8 in 1 hr as well! Thus, the increased sensitivity of the ngVLA, coupled with the higher angular resolution will radically enhance the study of multiple star formation. Furthermore, the addition of a 3 mm band to the ngVLA would be particularly advantageous for the detection of multiple protostars in even more distant regions than possible with the 7.3 mm band due to the better resolution and the fact that dust emission increases steeply with decreasing wavelength.

Obtaining sensitive images will still take a few hours of time with overheads toward the more distant star forming regions, but star forming regions at greater distances occupy less area of the sky in terms of their solid angle. The wide field of view offered by the ngVLA (a factor of 2 increase in solid angle over the VLA), coupled with the increased sensitivity, means that many more protostars can be captured in a single pointing than in the nearby star forming regions, this will somewhat offset the need for longer integrations times because more sources will be observed in a single observation.

While ALMA of course has unmatched sensitivity to dust emission at shorter wavelengths, the shorter wavelength becomes a disadvantage when attempting to study the youngest protostars. On scales less than $\sim$100 AU, the dense inner envelope or disks of protostars can be opaque at wavelengths as long as 1.3 mm and 3 mm, hiding small-scale multiplicity (see Chapter 'Exploring Protostellar Disk Formation with the ngVLA'). Moreover, at higher frequencies the field of view of ALMA becomes small, making it unable to simultaneously observe as many protostars at high resolution. Thus the ngVLA capability of 0.01″ or better resolution at wavelengths between 2 cm and 3 mm is an absolutely unique and critical capability to examine the formation of multiple stars during the early stages of protostellar evolution.

Because detection of dust emission from the small circumstellar disks in multiple systems is the most well-defined route to detection, it is important to further demonstrate their detectability. We ran a few radiative transfer models of protostars with small disks in binary star systems and simulated their observation with the full ngVLA using the CASA *simobserve* task. The modeling is described in more detail in the Chapter ‘Exploring Protostellar Disk Formation with the ngVLA.’ We show the results of our simulations in Figure 4, where we have simulated the observation of two protostars, separated by 5 AU, each with a 1 AU radius and 0.001 $M_\odot$ disk. These protostars are simulated at a distance of 400 pc, and they can be well-detected by the ngVLA with S/N = 20 in 1 hr. We also computed a model for a 15 AU separation binary system at a distance of 1.5 kpc and each disk having a radius of 3 AU and a mass of 0.01 $M_\odot$. The 1.5 kpc binary can be detected by the ngVLA with S/N = 10 in 1 hr. Thus, the ngVLA will enable the detection of extremely close binary protostars with separations as small as 3 AU (at 230 pc) from their dust emission alone, under the assumption that circumstellar disks have radii of order their separation/3 (Artymowicz & Lubow 1994). However, if each component has some free-free emission, in addition to the dust, they can likely be resolved at closer separations and their disks would not need to be as massive.

In addition to the ngVLA’s ability to examine extremely close companions, the imaging capabilities of the ngVLA are superb enough to enable circum-multiple environments to be characterized. Using an ALMA image at 0.87 mm of L1448 IRS3B system, a triple system with a surrounding circum-multiple disk with spiral structure (Tobin et al. 2016a), we scaled the surface brightness assuming optically thin dust emission and β=1, implying a flux density scaling as λ^{-3} (see discussion in preceding paragraphs). Then we simulated a 1 hour observation at 3 mm, and a 2 hour observation at 7.3 mm using the 168 antenna ‘Plains array,’ keeping the distance at 230 pc. We show the results of modeling in Figure 5; the structure observed at 0.87 mm is fully recovered with high fidelity at 3 mm and the image is also well-recovered at 7.3 mm but with lower S/N due to the fainter dust emission. Thus, the ngVLA will also enable the imaging of circum-multiple environments simultaneously while probing for multiplicity. At 3 mm and 7.3 mm, the sensitivity of the ngVLA will superior to that of ALMA at these wavelengths and have higher angular resolution even with only the ‘Plains’ array. The circum-multiple emission is more likely to be optically thin at these wavelengths as compared to shorter wavelengths with ALMA.

The ngVLA will open up three exciting regions of parameter space in protostellar multiplicity studies. It will conduct high-S/N imaging toward nearby star forming regions (i.e., Perseus, Taurus) with enough angular resolution to search for companion protostars that have ~5× smaller separation than can be examined with the VLA. The ngVLA will also enable studies of protostellar multiplicity to obtain far greater statistics through the simultaneous observation of larger numbers of protostars in more distant regions (e.g., Cygnus-X) with the same or better sensitivity than is currently possible toward the nearby regions. Finally, the ngVLA can examine the environments around multiple star systems with high-S/N, with best results at the shortest wavelengths.

4. Synergies with Other Facilities

While the ngVLA will be able to identify very close multiple systems perhaps out to 3 kpc, ALMA will be very useful in characterizing the immediate surroundings of multiple star systems. The brighter dust emission at shorter wavelengths may make ALMA an ideal complement to very high resolution studies with the ngVLA, both in the dust continuum and molecular lines, provided that the dust emission is not too optically

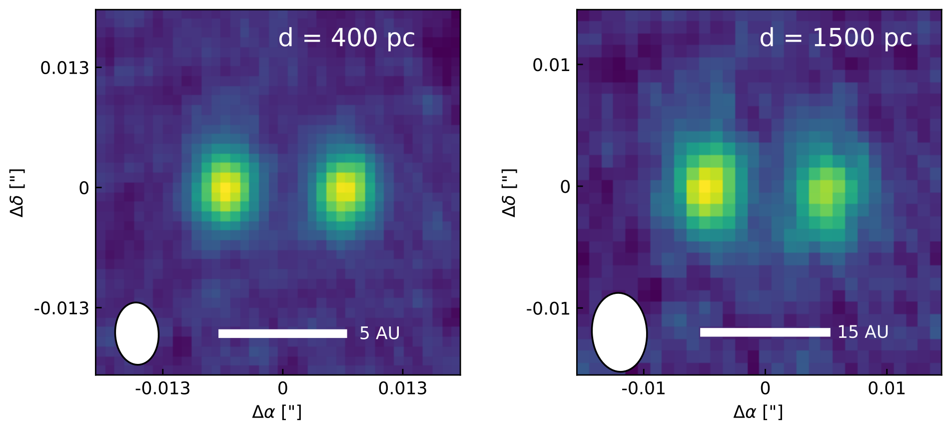

Figure 4. Synthetic ngVLA observations of binary systems comprised of emission from compact circumstellar disks. The left panel is at a distance of 400 pc having R_{disk} = 1 AU and M_{disk} = 0.001 $M_\odot$, and the right pane is at a distance of 1.5 kpc R_{disk} = 3 AU and M_{disk} = 0.01 $M_\odot$. Thus, these models demonstrate the feasibility of detecting small disks in multiple star systems at close separations.

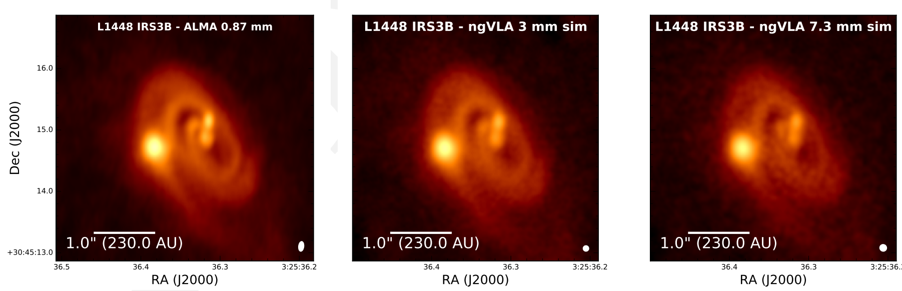

Figure 5. Synthetic ngVLA observations of the triple system L1448 IRS3B using only the 168 antenna 'Plains' array. These simulations used a scaled ALMA 0.87 mm image as the model (left) and utilize the maximum bandwidth available for the respective ngVLA bands, 40 GHz (3 mm; middle) and 20 GHz (7.3 mm; right). The 3 mm simulation is one hour on-source and is imaged using Briggs weighting, robust=0.5, and a taper at 2000 kλ; the 7.3 mm simulation is two hours on-source and the rest of the imaging parameters are the same as the 3 mm.

thick. ALMA will be able to provide access to the necessary molecular lines to characterize the immediate environs around proto-multiple systems. This is because many of the most abundant, disk-tracing molecules have their strongest rotation transitions at wavelengths shorter than 3 mm; the ngVLA will only be able to access the ($J = 1 \rightarrow 0$) transitions for most molecules, and these transitions do not generally have the brightest emission in the warm (>20 K) regions in the immediate vicinity of protostars. Furthermore, ALMA dust continuum observations can detect circum-multiple disks around the protostar that might have column densities too low to detect with the ngVLA, but as shown in Figure 5 the ngVLA will have this capability as well.

The more distant star forming regions have a disadvantage relative to the nearby ones in that their protostellar content is not as well-characterized due to the low resolution (>1″) of previous mid-to-far-infrared surveys. The James Webb Space Telescope will undoubtedly survey numerous massive star forming regions and infrared dark clouds (IRDCs) that harbor significantly more young stars than the nearby regions at wavelengths between 10 and 28 μm. Thus, by the time the ngVLA is conducting early science, the protostellar content of more distant star forming regions is likely to be much more well-characterized, enabling the multiplicity results obtained by the ngVLA to be put into a similar context as the results toward nearby star forming regions.

5. Summary

The ngVLA will open a new window into the study of multiplicity during the protostellar phase, providing a much clearer picture of where most companion stars are forming. Thus, the ngVLA will improve our understanding of just how many stars and proto-planetary disks begin their lives initially as part of a multiple system and how multiplicity affects the evolution of planetary systems, whether or not the system remains a multiple in its main sequence life. The increased resolution of the ngVLA will enable both closer multiples to be detected than previously possible for protostellar systems, and coupled with the increased sensitivity, larger numbers of multiple star systems can be observed in order to obtain statistics that equal or surpass that of the field solar-type stars.

References

André, P., Ward-Thompson, D., & Barsony, M. 1993, ApJ, 406, 122
Artymowicz, P., & Lubow, S. H. 1994, ApJ, 421, 651
Burkert, A., & Bodenheimer, P. 1993, MNRAS, 264, 798
Chen, X., Arce, H. G., Zhang, Q., et al. 2013, ApJ, 768, 110
Connelley, M. S., Reipurth, B., & Tokunaga, A. T. 2008, AJ, 135, 2526
Duchêne, G., & Kraus, A. 2013, ARA&A, 51, 269
Dunham, M. M., Stutz, A. M., Allen, L. E., et al. 2014, Protostars and Planets VI, 195
Duquennoy, A., & Mayor, M. 1991, A&A, 248, 485
Fischer, W. J., Megeath, S. T., Furlan, E., et al. 2017, ApJ, 840, 69
Kratter, K. M., Matzner, C. D., Krumholz, M. R., & Klein, R. I. 2010, ApJ, 708, 1585
Lee, K. I., Dunham, M. M., Myers, P. C., et al. 2016, ApJ, 820, L2
Looney, L. W., Mundy, L. G., & Welch, W. J. 2000, ApJ, 529, 477
McKee, C. F., & Ostriker, E. C. 2007, ARA&A, 45, 565
Offner, S. S. R., Dunham, M. M., Lee, K. I., Arce, H. G., & Fielding, D. B. 2016, ApJ, 827, L11

Offner, S. S. R., Kratter, K. M., Matzner, C. D., Krumholz, M. R., & Klein, R. I. 2010, ApJ, 725, 1485
Padoan, P., & Nordlund, Å. 2002, ApJ, 576, 870
Raghavan, D., McAlister, H. A., Henry, T. J., et al. 2010, ApJS, 190, 1
Reipurth, B., & Mikkola, S. 2012, Nat, 492, 221
Reipurth, B., Rodríguez, L. F., Anglada, G., & Bally, J. 2004, AJ, 127, 1736
Ricci, L., Testi, L., Natta, A., et al. 2010, A&A, 512, A15
Sadavoy, S. I., & Stahler, S. W. 2017, MNRAS, 469, 3881
Stamatellos, D., & Whitworth, A. P. 2009, MNRAS, 392, 413
Tobin, J. J., Dunham, M. M., Looney, L. W., et al. 2015, ApJ, 798, 61
Tobin, J. J., Kratter, K. M., Persson, M. V., et al. 2016a, Nat, 538, 483
Tobin, J. J., Looney, L. W., Li, Z.-Y., et al. 2016b, ApJ, 818, 73
Tohline, J. E. 2002, ARA&A, 40, 349

Science with a Next-Generation Very Large Array
ASP Conference Series, Monograph 7
Eric J. Murphy, ed.

DRAFT EDITION

Exploring Protostellar Disk Formation with the ngVLA

John J. Tobin

University of Oklahoma, `jjtobin@ou.edu`

Patrick Sheehan

University of Oklahoma

Doug Johnstone

NRC-Herzberg

Rajeeb Sharma

University of Oklahoma

Abstract. The formation and evolution of disks early in the protostellar phase is an area of study in which the ngVLA is poised to make significant breakthroughs. The high-sensitivity and resolution at wavelengths of 3 mm and longer will enable forming disks to be examined with unprecedented detail. The need to observe dust emission at wavelengths of 3 mm and longer is motivated by the fact that dust emission at these wavelengths is more likely to be optically thin, which is essential to understanding the structure of these disks. We explore the feasibility of detecting and resolving protostellar disks with a variety of radii, masses, and distances, out to distances as large as 1.5 kpc using radiative transfer models and simulations with the proposed ngVLA configuration. We also examine the potential for the ngVLA to enable studies of grain growth and radial migration of dust particles early in the protostellar phase with the broad multi-wavelength coverage. Studies of grain growth will require wavelength coverage extending at least to ~4 cm to characterize and quantify the location and intensity of free-free emission, which is expected to be generated at <10 AU scales.

1. Introduction

The formation of disks occurs as a natural consequence of angular momentum conservation during the star formation process. As such, proto-planetary disks are found nearly ubiquitously toward pre-main sequence stars, with higher fractions of disks found toward members of clusters/associations having younger collective ages (Hernández et al. 2008). The origins of proto-planetary disks can be traced to the disks that form during the early phase of the star formation process, around Class 0 protostars. Class 0 protostars are characterized by a dense envelope of infalling material that feeds the protostellar disk. As the envelope dissipates due to continued accretion and erosion of the envelope by protostellar outflows (e.g., Frank et al. 2014), it becomes a Class I protostar. The Class 0 phase is expected to last ~150 kyr, while the combined Class 0 and

Class I phases are expected to last ~0.5 Myr (Dunham et al. 2014); these ages estimates are based on the assumption that pre-main sequence stars hosting proto-planetary disks (objects in the Class II phase) have an average age of ~2 Myr. These young, embedded disks are often collectively referred to as protostellar disks.

Protostellar disks are important for the formation and mass assembly of the star, as well as the planet formation process. Most of the mass that is accreted onto a star must pass through the disk, and these protostellar disks are the initial conditions for disk evolution into a proto-planetary disk. The radius and mass of the forming disk can be regulated by the angular momentum of the infalling material, and magnetic fields can remove angular momentum efficiently in the absence of dissipative processes (e.g., Li et al. 2014). As such, the structure of these protostellar disks is expected to be connected to their formation conditions, and clear detections of rotationally supported disks have been found toward Class 0 and I protostars (Tobin et al. 2012; Harsono et al. 2014). The disks may also increase in radius later via viscous evolution and the outward transport of angular momentum (e.g., Manara et al. 2016). Furthermore, if gravitational instability in disks is a viable mechanism for angular momentum transport, the formation of multiple star systems, and possibly giant planet formation, the disks in the protostellar phase are those most likely to have the requisite conditions (Kratter et al. 2010; Tobin et al. 2016). Finally, the growth of solid material can begin during the protostellar phase and this may catalyze the later formation of planets via the core accretion process if the protostellar disk is able to efficiently grow dust grains to pebble/rock sizes in order to promote planetesimal growth.

Typical proto-planetary disks have masses of ~0.005 $M_\odot$, radii of ~50 AU, and surface density profiles $\propto R^{-1}$, meaning that most of the disk mass is at large radii (Andrews et al. 2013; Ansdell et al. 2016). Proto-planetary disks tend to be significantly lower in mass than the protostellar disks, which can have masses >0.1 $M_\odot$ (Tobin et al. 2015; Jørgensen et al. 2009; Tychoniec et al. 2018). The typical masses, radii, and/or surface density profiles for protostellar disks are still poorly constrained, and the ngVLA has significant potential to unlock some of these characteristics.

2. Resolving and Characterizing Youngest Disks

Observational studies of young disks have only just begun to reach samples larger than 10-20 systems (Tobin et al. 2015; Segura-Cox et al. 2016), and young protostar systems (Class 0 and Class I phases) are inherently more rare than pre-main sequence stars hosting proto-planetary disks. This is because the lifetime of the protostar phase is expected to be at least ~4× shorter than the lifetime of a PMS star with a disk (Dunham et al. 2014). Specifically, the *Spitzer cores2disks* survey along with the entire *Spitzer* Gould Belt survey contain only ~200[1] Class 0 and I protostars. Thus, to observe large numbers of protostellar disks, more populous star forming regions need to be observed and these are only present at distances ≥ 400 pc. For example, Orion alone contains ~315 Class 0 and I protostars. The need to examine protostellar disks at 100s of pc distances makes their characterization difficult to achieve with the same mass sensitivity and spatial resolution as the more nearby proto-planetary disk systems. Moreover, high mass sensitivity is particularly difficult at long wavelengths where the dust emis-

[1]This number corresponds to sources with the most firm characterization based on bolometric temperature.

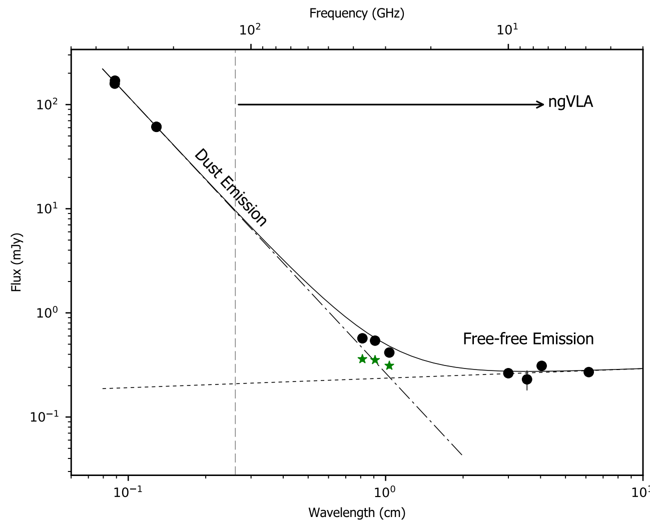

Figure 1. Spectrum from millimeter to centimeter wavelengths of a typical protostar in Orion. The emission from dust dominates at short wavelengths and free-free dominates at long wavelengths. The ngVLA will fully probe the transition from dust emission to free-free. The 8 mm to 1 cm bands have some free-free emission that is typically removed in current studies using power-law fits to the long wavelength emission. the ngVLA will enable improvements by spatially resolving the free-free emitting region(s). The points at 0.87 mm and 1.3 mm are from ALMA, the points at all longer wavelengths are from the VLA; the green star points are the flux densities between 8 mm and 1 cm with the extrapolated free-free contribution subtracted. Error bars are plotted with each point, but in most cases the statistical uncertainties are smaller than the points plotted.

sion is intrinsically fainter ($F_\lambda \propto \lambda^{-(2+\beta)}$, where β is the dust opacity spectral index). Figure 1 shows an example radio spectrum of a protostar from the submillimeter to centimeter wavelengths which illustrates the expected spectral properties of protostar systems as a function of wavelength. Protostars often exhibit free-free emission that dominates at wavelengths >1 cm, but can can contribute to the overall flux density at 7.5 mm. Thus, multi-wavelength observations are important to measure and remove the contribution of free-free emission to the flux density at wavelengths where we aim to trace dust emission. We will discuss this aspect further in section 4. For the sake of discussion, throughout this chapter we will use the dust opacity normalization of 0.899 cm^2 g^{-1} (dust only) at 1.3 mm from (Ossenkopf & Henning 1994), assuming β=1 for extrapolation to longer wavelengths (0.155 cm^2 g^{-1} at 7.5 mm).

The advent of the Karl G. Jansky Very Large Array (VLA) with its enhanced continuum sensitivity has enabled surveys of protostellar disks at wavelengths between 6.7 mm and 1 cm. Dust emission is more optically thin than at shorter wavelengths and thus the emission better traces column density due to the power-law decrease of dust opacity with increasing wavelength (Hildebrand 1983). Two VLA Nascent Disk and Multiplicity (VANDAM) surveys have been carried out with the VLA toward the Perseus and Orion star forming regions, observing a total of over 200 protostar systems

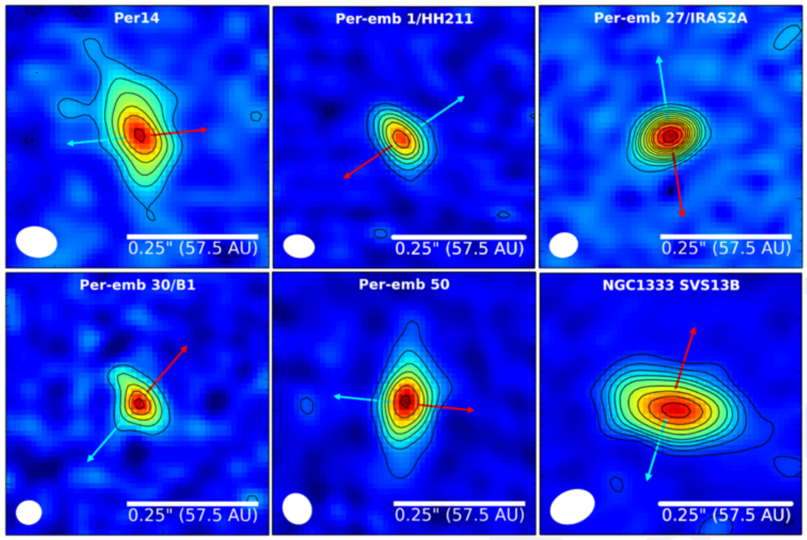

Figure 2. Images of some well-resolved disks from the VANDAM: Perseus survey at 8 mm, from Segura-Cox et al. (2016). The contours in each panel are [-6, -3, 3, 6, 9, 12, 15, 20, 25, 30, 35, 40, 50, 60, 70, 80, 90, 100, 150] $\times\,\sigma$, where σ = 11 μJy at 8 mm.

in each region. The VANDAM surveys took ~600 hours of time on the VLA. These surveys were conducted in Ka-band at a central wavelength of 9 mm, while observing at the highest possible angular resolutions, translating to spatial resolutions of ~15 AU and ~30 AU in Perseus and Orion, respectively. Example images of disks observed with the VLA are shown in Figure 2. Also note that the VANDAM: Perseus survey observed the entire sample at 4.1 cm and 6.4 cm, but we focus on the dust emission at 5.9 mm to 10 mm in this chapter. This corresponds to the proposed ngVLA band that is most similar to the wavelengths used in VANDAM and is centered at ~7.5 mm.

The VANDAM: Perseus survey detected candidate disks, meaning that extended dust continuum emission was resolved, toward only 12/42 Class 0 protostars and even fewer toward Class I protostars 5/37 (Segura-Cox et al. 2018 submitted). We show examples of some of the well-resolved disks detected in the VANDAM: Perseus survey in Figure 2 (Segura-Cox et al. 2016). The disks in Perseus were further characterized by Tychoniec et al. (2018), focusing on the integrated dust emission at 9 mm toward all sources whether or not they were resolved. Tychoniec et al. (2018) found that Class 0 protostars tend to have more mass within radii <100 AU relative to the Class I protostars. Furthermore, both Class 0 and Class I protostars had higher masses than the more-evolved proto-planetary disks (Class II sources). The low percentage of well-resolved disks toward Class 0 and I protostars may be due to both the limited spatial resolution and sensitivity of the VLA. The sensitivity may be especially limiting for Class I protostars as, due to their disk evolution, they have less overall mass (thus lower flux densities). The ability to observe at wavelengths of ~9 mm is extremely important for examining protostellar disks, especially around Class 0 targets. If they are compact (R< 50 AU) and massive (>0.01 $M_\odot$), they are likely optically thick at shorter wavelengths, but remain optically thin at most radii at 9 mm. We show radial surface

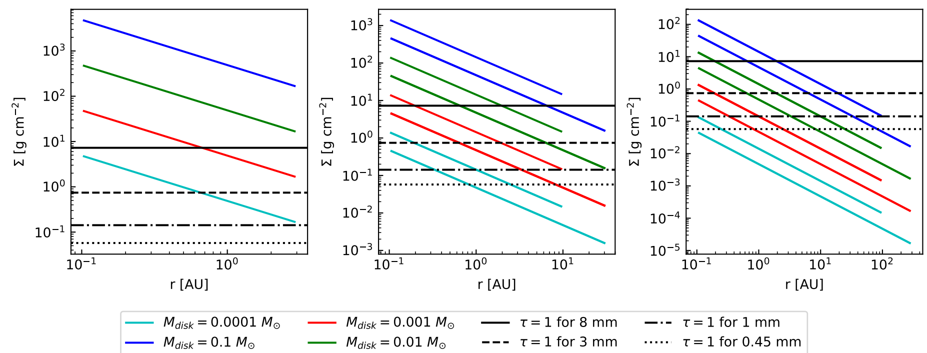

Figure 3. Surface density profiles of modeled disks versus radius. Note that range of radius plotted increases from left to right; the 3 AU disks are plotted in the left panel, the 10 AU and 30 AU disks are plotted in the middle panel, and the 100 AU and 300 AU disks are plotted in the right panel. Horizontal lines are plotted that denote the surface density corresponding to $\tau = 1$ at 7.5 mm (solid), 3 mm (dashed), 1 mm (dash-dot), and 0.45 mm (dotted). Observations at 7.5 mm will not be immune to dust opacity effects, but they can probe surface densities 10× larger without becoming optically thick. The dust mass opacities calculated are 0.15, 1.35, 7.03, 17.43 cm^2 g^{-1} at wavelengths of 7.5, 3, 1, and 0.45 mm, respectively.

density profiles for model protostellar disks and their corresponding radii where $\tau = 1$ in Figure 3, thereby underscoring that long wavelength observations of dust emission are essential to resolve and quantify the majority of the mass within protostellar disks. The opacity of disks at different wavelengths depending on mass and radius will be discussed in more detail in the following section.

Despite the advances enabled by the VLA surveys, they are not without limitations. Due to the increased distance to Orion, the VANDAM: Orion survey had 2.2× less mass sensitivity than the Perseus survey, despite spending 2× more time on source. The VANDAM: Orion survey used 240 hours in the VLA A-configuration to observe 100 Class 0 protostars, accounting for ~50% of the available array time at high-frequencies. Thus, high-sensitivity at ~8 mm wavelengths toward large protostar samples at a distance of ≥400 pc requires a significant utilization of available observing time for the current VLA; the time required quickly becomes unrealistic for protostars at much greater distances.

The ngVLA is needed to further advance studies of disks because ALMA will also not be as sensitive to long wavelength dust emission as the ngVLA. Using ALMA at 3 mm, 1 hour of integration will achieve a sensitivity of 15 μJy. Assuming a distance of 230 pc, this translates to a 1σ mass sensitivity of 1.6×10^{-4} M$_\odot$. Therefore, ALMA Band 1 (~7.5 mm) will only be about as sensitive as the current VLA. The ngVLA will reach 1σ mass sensitivities of 5.0×10^{-5} M$_\odot$ and 8.2×10^{-6} M$_\odot$ at wavelengths of 7.5 mm and 3 mm, respectively. Thus, the ngVLA will be vastly superior to ALMA at these long wavelengths for the characterization of dust emission from protostellar disks. However, these mass estimates assume that all emission is within one beam. We will conduct a more realistic assessment of the ngVLA's ability to detect resolved disks in the following section.

3. Detectability of Protostellar Disks with the ngVLA

The VANDAM: Perseus survey was able to detect disks with total masses > 0.025 $M_\odot$ (gas+dust, assuming a gas-to-dust ratio of 100:1 and a 5σ detection limit) and resolve disks with observed radii >10 AU at a wavelength of 8 mm (Segura-Cox et al. 2018). However, most of the resolved disks have masses > 0.1 $M_\odot$. The sensitivity of the ngVLA will enable a ~10× leap in both resolution and sensitivity. In order to quantitatively characterize the ability of the ngVLA to detect and resolve disks toward both nearby and distant star forming regions, we have computed a small suite of radiative transfer models at wavelengths of 7.5 mm and 3 mm, varying luminosity (1.0, 10.0, 100.0 $L_\odot$), disk radius (3.0, 10.0, 30.0, 100.0, 300.0 AU), and disk mass (10^{-4}, 10^{-3}, 10^{-2}, 10^{-1} $M_\odot$). The disks are assumed to have a radial surface density profile proportional to R^{-1}, scale height (H/R) of 0.1 at 1 AU, and flaring $H \propto R^{1.15}$; the disk density profiles are truncated at the specified radii and do not exponentially drop-off. All models have a surrounding envelope with a mass of 0.1 $M_\odot$ and a radius of 1500 AU. The dust opacities we use are derived from Woitke et al. (2016) and have a maximum particle size of 1 mm, yielding dust mass opacities of 0.15 cm^2 g^{-1} and 1.35 cm^2 g^{-1} at 7.5 mm and 3 mm, respectively. Radiative transfer was computed with the RADMC3D code (Dullemond et al. 2012), and model images were generated at three distances (230, 400, and 1500 pc) and three viewing geometries (i = 25, 45, and 75°). We simulated ngVLA observations of these models with the CASA *simobserve* task using the full ngVLA configuration, assuming 1 hour on source and the estimated noise of 0.26 μJy from this same integration time (ngVLA Memo #17).

A subset of these models are shown in Figure 4 at a wavelength of 7.5 mm, distances of 230 pc, 400 pc, and 1.5 kpc, and at an inclination of 75°. At distances of 230 pc and 400 pc, disks with masses of >0.001 $M_\odot$ toward protostars with luminosities of 10 $L_\odot$ can be detected and resolved. We note, however, that at a mass of 0.001 $M_\odot$, the 300 AU radius disk is not as well detected due to the mass being spread over a larger disk size. We also find that disks with radii of 3 and 10 AU can also be detected for a disk mass as small as 0.0001 $M_\odot$.

At a distance of 1.5 kpc and the same luminosity, disks with masses of 0.1 $M_\odot$ can be detected and resolved at all radii, and at a mass of 0.01 $M_\odot$ the disks with $R_{disk} \leq 100$ AU can still be detected. Disks with masses much below 0.01 $M_\odot$ are not well-detected in a 1 hour observation. While optimal imaging parameters will depend on the radii and mass of each disk, the visibility data themselves can be utilized to fit the disk radii with greater accuracy from the images alone, given the possible limitations of maximum recoverable scale and surface brightness. The ngVLA will enable the physical structure of protostellar disks with radii as small as ~3 AU to be characterized in the nearby star forming regions. The ngVLA is the only facility that will be able to do this given the necessity of very high angular resolution and long-wavelengths; this will be a major advance in the capability of examining small-scale structures in protostellar systems.

Furthermore, observations at 3 mm (not shown for brevity) enable the detection of all the disks detected at 7.5 mm (Figure 4), but lower mass disks will be able to be detected as well given the factor of ~6 - 16× increase in flux density going from 7.5 mm to 3 mm (depending on dust opacity spectral index). The 3 mm band will be especially effective for the detection of disks in star forming regions out to 1.5 kpc, as disk masses of 0.001 $M_\odot$ can be detected more robustly. Thus, both the 7.5 mm and 3 mm ngVLA bands will be essential to further characterizing disks in the protostellar phase, and the

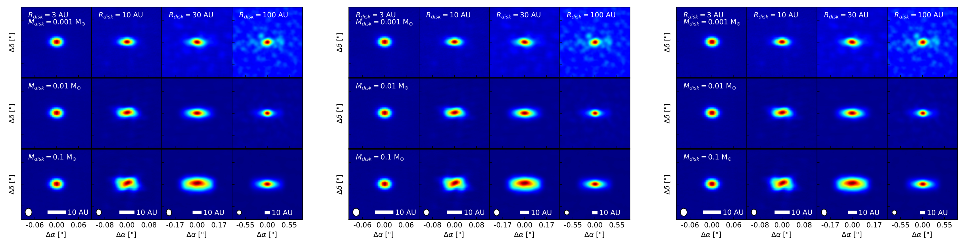

Figure 4. Model images of protostellar disks at 7.5 mm computed for a three distances 230 pc (top), 300 pc (middle), and 1500 pc (bottom). For each distance we have generated synthetic observations for a variety of radii and disk masses and run through a simulated observation of 1 hr with the full ngVLA configuration. UV-tapering has been applied to the disks with $R_{disk} \geq 30$ AU at the level of $R_{disk}/5.0$ translated to angular units.

full ngVLA will enable disks to be detected and resolved out to star forming regions at distances of at least 1.5 kpc. This capability will greatly expand the number of disks that can be observed compared with the current VLA by enabling significantly smaller radii and masses to be detected and resolved. By including all star forming regions out to ~1.5 kpc (e.g., Cygnus-X; Kryukova et al. 2014), more than 1000 additional protostars and their disks will be accessible to the ngVLA. Moreover, the 100s of protostars star-forming regions at distances of 400 pc or less (Dunham et al. 2014) will be able to have their disks resolved, where only unresolved observations were possible with the current VLA.

Optical depth is another significant advantage of the ngVLA over other millimeter interferometers like ALMA that primarily operate at wavelengths shorter than 3 mm. The surface density profiles for the modeled disks are shown in Figure 3 with horizontal lines marking the surface density corresponding to $\tau = 1$ for wavelengths between 7.5 mm and 0.45 mm. Due to the fixed grid of masses and varying radii, the surface density profiles are larger for smaller disk radii. However, it can be seen that 7.5 mm wavelengths can trace about 10× higher surface densities than at 1 mm before becoming optically thick. The opacity can be significant even at 7.5 mm, particularly for disks with $M_{disk} = 0.1\ M_\odot$. For the 100 and 300 AU radius and $M_{disk} = 0.1\ M_\odot$ disks, only the inner few AU are optically thick at 7.5 mm, while the entire 100 AU disk is optically thick at 1 mm. The disks with radii between 10 and 30 AU and $M_{disk} = 0.1\ M_\odot$ are optically thick out to ~10 AU in both cases, but lower mass disks in this range of radii are only optically thick in their inner few AU. However, these disks are completely optically thick at 1 mm and 0.45 mm until the disk masses are ~0.0001 $M_\odot$. Note that τ in Figure 3 is calculated for an inclination of 0° (face-on), and intermediate to edge-on inclinations will have substantially more opacity for a given surface density profile. Therefore, we can conclude that 7.5 mm wavelengths are not necessarily immune to issues of opacity, but they are significantly less affected than 1 mm and 0.45 mm. This will enable ngVLA to significantly improve on the characterization of protostellar disks, while the ability of ALMA to probe their structure is more limited.

The ability to detect these low-mass, small radius disks is also extremely important for the characterization of multiple star systems from the emission of their circumstellar disks. This capability is described in more detail in the Chapter 'New Frontiers in Protostellar Multiplicity with the ngVLA.' Furthermore, while we do not specifically address the likelihood of substructure in protostellar disks, growing numbers of proto-planetary disks exhibit a variety of substructure when observed with sufficiently high resolution in the dust continuum (ALMA Partnership et al. 2015; Andrews et al. 2016; Sheehan & Eisner 2018, Andrews et al. 2018 in prep.). Therefore, it is entirely possible that protostellar disks themselves will also not have smooth structures. The higher-resolution at longer wavelengths of the ngVLA will be crucial for characterizing whether or not protostellar disks exhibit significant substructure. This is because, as discussed previously, the more massive protostellar disks are largely opaque at shorter wavelengths and the longer wavelengths with lower opacity are more ideal to reveal substructure if present.

4. Characterizing Early Grain Growth

The ability to detect and resolve disks with a variety of radii in the nearby star forming regions makes it possible to characterize the spectral index of dust emission both in the limit of integrated flux densities and spatially-resolved emission throughout the disks. With a shortest wavelength of 3 mm, the ngVLA can characterize the spectral index of dust emission at least between 3 mm and 1 cm. The sensitivity of the >1 cm wavelength ngVLA bands will also have the capability of detecting and resolving dust emission. This capability is incredibly important because the rate of growth for solids in disks can be examined as a function of evolution through the protostellar phase. However, at wavelengths >1 cm dust emission becomes more difficult to detect due to the power-law decrease in flux density of dust emission at longer wavelengths, thus the ngVLA is crucial to enable the detection of dust emission at wavelengths >1 cm because the current VLA does not have the needed angular resolution or sensitivity.

The ability to measure the spectral index of dust emission over a wide range of wavelengths is important because it is connected to both the maximum dust grain sizes and the slope of the assumed power-law dust size distribution; dust grains are most efficiently detected when observed at a wavelength comparable to their size. Through radiative transfer modeling, using the same techniques that generated the images in Figure 4, the dust emission over a wide range of wavelengths can be used to determine the maximum particle sizes. Such studies are currently possible toward a few select systems, but the limited sensitivity of the VLA makes detection of dust emission out to large disk radii and low disk masses challenging. Furthermore, the low angular resolution of the current VLA at long wavelengths means that characterizing dust emission a wavelengths of several cm must use integrated flux densities. Resolved studies of disk spectral indices have been done for a few of the most nearby disk-hosting PMS stars (Pérez et al. 2012, 2015). Doing such modeling for protostars spanning the full range of evolution will enable the rate of grain growth to be understood, and we will learn whether or not this is a linear/universal process, or if it varies strongly between protostars. However, in order to accomplish this, greater sensitivity and resolution than are possible with the VLA are needed to sufficiently resolve the inner regions of protostellar disks and accurately separate free-free emission from dust emission.

Separating the free-free jet emission from dust emission is incredibly important, especially for examining dust emission at >1 cm (Figure 1). The resolution of the ngVLA will enable the dust emission to be resolved from the free-free emission out to wavelengths of several cm. However, the disk needs to be well-resolved for this to be possible. Compact free-free emission is expected to originate from the inner ~10 AU

(Anglada et al. 1998) and the ngVLA will have a spatial resolution of ~11.5 AU in the 3.75 cm (8 GHz) band for protostars at a distance of 230 pc. Thus, the emission from the two distinct processes can be separated spatially with multi-wavelength observations, and the region containing free-free emission can be isolated and removed from the analysis. This is not possible with the angular resolution of the current VLA and will be an unique capability of the ngVLA. We also note that free-free emission can also originate from a disk wind, but without the ngVLA we cannot fully characterize the nature of free-free emission to properly account for it. Finally, free-free emission is can still contribute at wavelengths <1 cm (Figure 1), and the higher angular resolution at shorter wavelengths will help further characterize its nature.

ALMA can add to the characterization of dust growth with its equivalent angular resolution at shorter wavelengths. While small disks and the inner radii of large disks will be optically thick (Figure 3), ALMA observations should be more sensitive to the outer regions of protostellar disks where the concentration of large grains is expected to be lower. This is because grain growth is slower at larger radii, having lower densities, and the radial drift process is expected to move large particles to smaller radii (Weidenschilling 1977). Therefore, in the regions where the dust emission is not optically thick, short wavelength observations from ALMA will be helpful to characterize dust growth at all disk radii, especially if the dust emission is more compact at longer wavelengths (Pérez et al. 2012, 2015; Segura-Cox et al. 2016).

Furthermore, the ngVLA may not be able to probe the transition from the envelope to disk as well as ALMA, because the envelope will have significantly lower column density and thereby low surface brightness. On top of that, if the envelopes have mostly small dust grains < 10 μm, the dust emission drops much faster in wavelength than it does in the disk due to the smaller grains. Thus, ALMA will enable the connection of the disk to the infalling/rotating envelope to be better understood through both the observations of shorter wavelength dust and molecular lines tracing envelope and disk kinematics. The ngVLA then will be the ideal instrument for examining the presence and structure of the disks around protostars to smaller radii. This will complement ALMA's ability to examine the structure of proto-planetary disks around more evolved young stars.

5. Uniqueness of ngVLA Capabilities

The ngVLA will have extraordinary capabilities to examine disks toward protostars throughout the Class 0 and I phases. It is crucial to examine the disks at long wavelengths where the dust emission is optically thin over a large range of radii to probe nearly the entire disk mass reservoir. Moreover, the ngVLA will be able to fully resolve young disks with radii as small as ~3 AU in the nearby star forming regions. While ALMA can reach such spatial scales at short wavelengths, the disks around protostars are likely to be optically thick at such small radii (Figure 3), making it impossible for ALMA to examine the internal structure of their protostellar disks in many cases.

Due to the optical depth of disks (Figure 3), the radial distribution of dust particle sizes cannot be explored with short wavelength data from ALMA. Longer wavelength observations and ~10 mas resolution are crucial to map the radial distribution of dust emission. While ALMA has 3 mm receivers and is expected to have ~1 cm receivers (Band 1) in the future, the best angular resolution at 3 mm is ~0.05″, and ~0.14″ at 1 cm. Thus, ALMA at 3 mm will only have the spatial resolution that VANDAM had with the VLA toward Perseus at 8 mm, and ALMA will have lower angular resolution at 1 cm; ALMA will not be able to improve upon the resolution of the VANDAM survey at wavelengths where dust emission is less affected by opacity. Furthermore, ALMA will be significantly less sensitive than the ngVLA at these same wavelengths; see section 2. In summary, the ngVLA will be superior to ALMA in examining protostellar disks at wavelengths of 3 mm and longer.

Lastly, the ngVLA will be able to examine the vertical settling of large dust grains for edge-on disks. In nearby star forming regions, (e.g., Taurus, Oph at 140 pc), edge-on disks can be observed to determine how settled the disk midplanes are. The disk midplanes can be examined from 3 mm to 1 cm to see if there is variation with wavelength in the vertical extent of the dust emission. If the vertical structure of the dust emission is approximately H/R $\sim$0.1, then at a radius of 14 AU the vertical height of the dust at 7.5 mm can be resolved (assuming 0.01$''$ resolution at 140 pc). This study also cannot be done with ALMA at shorter wavelengths because the disk midplanes are opaque (Lee et al. 2016). Through modeling, it can be determined if the dust emission is more concentrated in the disk midplanes going to longer wavelengths, consistent with expectations of dust settling (D'Alessio et al. 2006) and low levels of turbulence in the disks (e.g., Flaherty et al. 2017).

6. Summary

The ngVLA will enable a new revolution in the study of protostellar disks with the ability to probe the spatial structure of protostellar disks, where many of these disks cannot be resolved with current instrumentation. The ngVLA will enable us to resolve dust emission from disks that are as small as 3 AU in the nearby star forming regions and examine the full spatial extents of protostellar disks using emission from optically thin dust. Together, this information will enable us to determine the spectral index and thereby the sizes of the emitting dust grains to be characterized as a function of radius, and perhaps height for edge-on disks. The ngVLA will enable the structure and early grain growth of protostellar disks to be better understood, in addition to how quickly the conditions for planet formation are established in disks.

References

ALMA Partnership, Brogan, C. L., Pérez, L. M., et al. 2015, ApJ, 808, L3
Andrews, S. M., Rosenfeld, K. A., Kraus, A. L., & Wilner, D. J. 2013, ApJ, 771, 129
Andrews, S. M., Wilner, D. J., Zhu, Z., et al. 2016, ApJ, 820, L40
Anglada, G., Villuendas, E., Estalella, R., et al. 1998, AJ, 116, 2953
Ansdell, M., Williams, J. P., van der Marel, N., et al. 2016, ApJ, 828, 46
D'Alessio, P., Calvet, N., Hartmann, L., Franco-Hernández, R., & Servín, H. 2006, ApJ, 638, 314
Dullemond, C. P., Juhasz, A., Pohl, A., et al. 2012, RADMC-3D: A multi-purpose radiative transfer tool, Astrophysics Source Code Library, ascl:1202.015
Dunham, M. M., Stutz, A. M., Allen, L. E., et al. 2014, Protostars and Planets VI, 195
Frank, A., Ray, T. P., Cabrit, S., et al. 2014, ArXiv e-prints, arXiv:1402.3553
Harsono, D., Jørgensen, J. K., van Dishoeck, E. F., et al. 2014, A&A, 562, A77
Hernández, J., Hartmann, L., Calvet, N., et al. 2008, ApJ, 686, 1195
Hildebrand, R. H. 1983, QJRAS, 24, 267
Jørgensen, J. K., van Dishoeck, E. F., Visser, R., et al. 2009, A&A, 507, 861
Kratter, K. M., Matzner, C. D., Krumholz, M. R., & Klein, R. I. 2010, ApJ, 708, 1585

Kryukova, E., Megeath, S. T., Hora, J. L., et al. 2014, AJ, 148, 11
Lee, K. I., Dunham, M. M., Myers, P. C., et al. 2016, ApJ, 820, L2
Li, Z.-Y., Banerjee, R., Pudritz, R. E., et al. 2014, Protostars and Planets VI, 173
Manara, C. F., Rosotti, G., Testi, L., et al. 2016, A&A, 591, L3
Ossenkopf, V., & Henning, T. 1994, A&A, 291, 943
Pérez, L. M., Carpenter, J. M., Chandler, C. J., et al. 2012, ApJ, 760, L17
Pérez, L. M., Chandler, C. J., Isella, A., et al. 2015, ApJ, 813, 41
Segura-Cox, D. M., Harris, R. J., Tobin, J. J., et al. 2016, ApJ, 817, L14
Sheehan, P. D., & Eisner, J. A. 2018, ApJ, 857, 18
Tobin, J. J., Hartmann, L., Chiang, H.-F., et al. 2012, Nat, 492, 83
Tobin, J. J., Dunham, M. M., Looney, L. W., et al. 2015, ApJ, 798, 61
Tobin, J. J., Kratter, K. M., Persson, M. V., et al. 2016, Nat, 538, 483
Tychoniec, Ł., Tobin, J. J., Karska, A., et al. 2018, ArXiv e-prints, arXiv:1806.02434
Weidenschilling, S. J. 1977, MNRAS, 180, 57
Woitke, P., Min, M., Pinte, C., et al. 2016, A&A, 586, A103

Science with a Next-Generation Very Large Array
ASP Conference Series, Monograph 7
Eric J. Murphy, ed.

DRAFT EDITION

Magnetic fields in forming stars with the ngVLA

Charles L. H. Hull,[1,2,3] Carlos Carrasco-González,[4] Peter K. G. Williams,[5] Josep M. Girart,[6] Timothy Robishaw,[7] Roberto Galván-Madrid,[4] and Tyler Bourke[8]

[1]*National Astronomical Observatory of Japan, NAOJ Chile Observatory, Alonso de Córdova 3788, Office 61B, Vitacura 763 0422, Santiago, Chile;* `chat.hull@nao.ac.jp`

[2]*Joint ALMA Observatory, Alonso de Córdova 3107, Vitacura 763 0355, Santiago, Chile*

[3]*NAOJ Fellow*

[4]*Instituto de Radioastronomía y Astrofísica (IRyA-UNAM), Universidad Nacional Autónoma de México, Campus Morelia, Apartado Postal 3-72, 58090 Morelia, Michoacán, Mexico*

[5] *Harvard-Smithsonian Center for Astrophysics, 60 Garden St, MS 20, Cambridge, MA 02138, USA*

[6]*Institut de Ciències de l'Espai (CSIC-IEEC), Campus UAB, Carrer de Can Magrans S/N, E-08193 Cerdanyola del Vallès, Catalonia, Spain*

[7]*Dominion Radio Astrophysical Observatory, National Research Council Canada, PO Box 248, Penticton, BC, V2A 6J9, Canada;*

[8]*Square Kilometre Array Organization, Jodrell Bank Observatory, Lower Withington, Macclesfield, Cheshire SK11 9DL, UK;*

1. Introduction

The magnetic field plays an important role in every stage of the star-formation process from the collapse of the initial protostellar core to the star's arrival on the main sequence. Consequently, the goal of this science case is to explore a wide range of magnetic phenomena that can be investigated using the polarization capabilities of the Next Generation Very Large Array (ngVLA). These include (1) magnetic fields in protostellar cores via polarized emission from aligned dust grains, including in regions optically thick at wavelengths observable by the Atacama Large Millimeter/submillimeter Array (ALMA); (2) magnetic fields in both protostellar cores and molecular outflows via spectral-line polarization from the Zeeman and Goldreich-Kylafis effects; (3) magnetic fields in protostellar jets via polarized synchrotron emission; and (4) gyrosynchrotron emission from magnetospheres around low-mass stars.

2. Scientific Importance & Anticipated Results

2.1. Dust polarization in low-mass protostellar objects

Mapping the morphology of magnetic fields in the cores and envelopes surrounding young, low-mass protostars is critical to further our understanding of how magnetic fields affect the star-formation process at early times. Under most circumstances, and for the typical grain sizes found in the ISM ($\ll$100 μm), elongated dust grains are thought to align themselves with their long axes perpendicular to magnetic field lines (e.g., Hildebrand 1988; Lazarian 2007; Hoang & Lazarian 2009; Andersson et al. 2015), resulting in thermal radiation from the grains that is polarized perpendicular to the magnetic field (see Heiles et al. 1993 for a description of not only linear dust polarization, but also the other polarization mechanisms that are mentioned in the following sections). Thus, this type of observation can be used to infer the magnetic field morphology in the plane of the sky.

Polarized thermal dust emission from both low- and high-mass protostellar objects has been studied extensively at millimeter wavelengths at 1–2″ resolution by the Berkeley Illinois Maryland Association millimeter array (BIMA; e.g., Rao et al. 1998; Girart et al. 1999; Lai et al. 2001; Matthews et al. 2005; Cortes & Crutcher 2006; Kwon et al. 2006), the Submillimeter Array (SMA; e.g., Girart et al. 2006, 2009; Tang et al. 2009; Alves et al. 2011; Zhang et al. 2014), the Combined Array for Research in Millimeter-wave Astronomy (CARMA; e.g., Hull et al. 2013; Hughes et al. 2013; Hull et al. 2014; Stephens et al. 2014; Segura-Cox et al. 2015), and ALMA (e.g., Cortes et al. 2016; Hull et al. 2017b,a; Cox et al. 2018; Maury et al. 2018). With the upgraded Karl G. Jansky Very Large Array (JVLA), it has recently become possible to begin performing dust polarization studies at centimeter wavelengths, using the highest-frequency bands available: K, Ka, and Q bands (18–50 GHz). Both Cox et al. (2015, see Figure 1) and Liu et al. (2016) studied the polarized dust emission at 37 and 43 GHz from NGC 1333-IRAS 4A, one of the first sources to be imaged in full polarization and high resolution at submillimeter wavelengths using the SMA (Girart et al. 2006). More recently, Liu et al. (2018) have studied the 40–48 GHz polarization toward the Class 0 protostar IRAS 16293, another bright source that was an early target for millimeter-wave polarization observations (Rao et al. 2009, 2014).

For the JVLA, NGC 1333-IRAS 4A and IRAS 16293 are two of the very few sources with polarized dust emission bright enough that they can be imaged within a few hours. A typical protostellar core may be $\sim 10\times$ fainter than IRAS 4A or IRAS 16293. In order to probe the magnetic field in the innermost $\sim$ 1000–100 au regions (which can be resolved with the 1000–10 mas scales recoverable with the ngVLA) of these more "normal" objects, we need the sensitivity and the resolution of the ngVLA at the $\sim$ 30–90 GHz wavelengths where there is still appreciable dust emission, but where material is still optically thin even in the densest inner regions. For example, the peak flux of IRAS 4A at 30 GHz as detected by Cox et al. (2015) is $\sim 3000\,\mu$Jy in an 0.25″ synthesized beam. In < 1 hr of integration time, the ngVLA will be able to detect 1% polarized dust emission at a frequency of 30 GHz at a level $> 3\sigma$ in objects $10\times$ fainter than IRAS 4A.

2.1.1. Polarization in protoplanetary disks

Regarding protoplanetary disk polarization at long wavelengths: a notable non-detection is HL Tau—one of the brightest known protoplanetary disks—where exceptionally

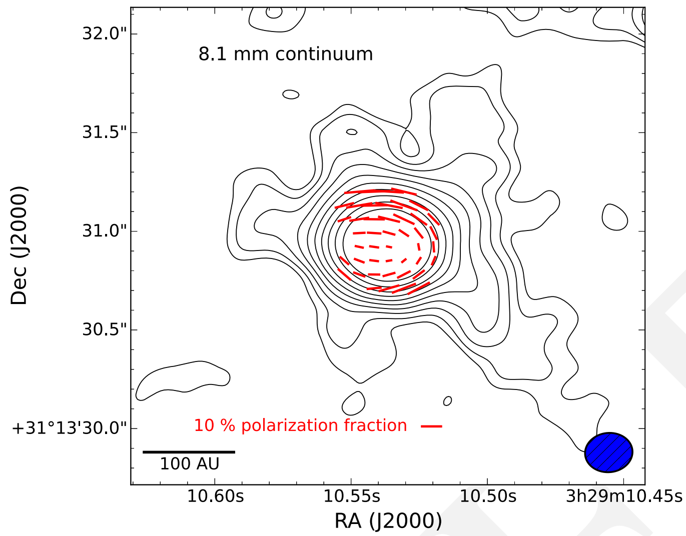

Figure 1. VLA 8 mm polarization observations of the embedded Class 0 protostellar source NGC 1333-IRAS 4A (Cox et al. 2018). Contours show total intensity (Stokes *I*) emission; red line segments show the inferred magnetic field, rotated by 90° relative to the dust polarization. IRAS 4A is one of the brightest low-mass protostellar sources known; typical sources are not bright or polarized enough for dust polarization to be detected toward them with the JVLA.

deep 7 mm VLA observations by Carrasco-González et al. (2016) were unable to detect dust polarization, despite having an rms noise of $\sim 3\,\mu$Jy beam^{-1} (after integrating for nearly 15 hrs on source), simply because the dust emission is too faint at those long wavelengths. Polarization fractions of $\sim 1\%$ are expected in protostellar disks; thus, an order-of-magnitude improvement in sensitivity is needed in order to detect polarization in these sources.

HL Tau is $\sim 10\times$ brighter than a "typical" extended protoplanetary disk: for example, the subsample of transition disks in the ALMA survey of ρ Oph by Cox et al. (2017) has a median integrated flux of ~ 260 mJy at 850 μm, whereas HL Tau has an integrated flux of brightness of ~ 2.4 Jy at the same wavelength (Stephens et al. 2017). Assuming this approximate factor of 10 ratio holds at longer wavelengths, a typical large disk would have a peak 3 mm flux of ~ 3 mJy in a ~0.5″ beam, $10\times$ lower than the value reported in Stephens et al. (2017). In < 1 hr of integration time, the ngVLA will be able to detect 1% polarized dust emission at a wavelength of 3 mm at a level $> 3\sigma$ in such an object, enabling studies of long-wavelength polarization in a statistically significant sample of many of the famous, extended disks present in a wide range of star-forming regions. These studies will also allow us to characterize the polarization in regions optically thick at ALMA wavelengths (e.g., in HL Tau; ALMA Partnership et al. 2015; Carrasco-González et al. 2016; Jin et al. 2016); will enable us to characterize the polarization properties of grains by observing the polarization spectrum—i.e., the source polarization as a function of wavelength—from infrared to (sub)millimeter to centimeter wavelengths; and will allow us to better understand the physics behind the transition from magnetic alignment of dust grains to other polarization mechanisms (see below), which are thought to be dependent on dust-grain growth.

Recent ALMA polarization observations toward several protoplanetary disks have revealed different mechanisms causing the polarization: self-scattering at 870 μm (observational: Kataoka et al. 2016; Stephens et al. 2017; Lee et al. 2018; Girart et al. 2018; Hull et al. 2018; theoretical: Kataoka et al. 2015; Yang et al. 2017), alignment with the dust-emission gradient at 3 mm (observational: Kataoka et al. 2017; theoretical: Tazaki et al. 2017), and a seemingly linear combination of the two at 1.3 mm (Stephens et al. 2017). Recent (sub)millimeter ALMA polarization observations of younger, more embedded Class 0/I protostars have even shown hints of scattering in the innermost, ~ 100 au regions of a few sources (Cox et al. 2018; Harris et al. 2018; Sadavoy et al. 2018). However, self-scattering is a highly wavelength-dependent phenomenon, and it is maximum around a wavelength of $2\pi a_{\max}$, where $a_{\max}$ is the maximum grain size. Thus, at long wavelengths far from this value (i.e., those accessible to the ngVLA), it may be possible that grains aligned with the magnetic field dominate the dust polarization.

Considering that ALMA will eventually have Band 1 (~ 40 GHz), and that it already has a functioning polarization system at Band 3 (~ 100 GHz), lower-frequency K and Ka band (18–40 GHz) observations with the ngVLA would be complementary, and possibly unique to the instrument. Also, without considering the unknown polarization efficiency as a function of wavelength, 18–40 GHz observations are easier than higher Q band (40–50 GHz) observations at the JVLA site due to the weather constraints.

2.2. Spectral-line polarization: Zeeman and Goldreich-Kylafis effects

Molecular and atomic lines are sensitive to magnetic fields, which cause their spectral levels to split into magnetic sub-levels. When threaded by a magnetic field, atomic hydrogen and molecules with a strong magnetic dipole moment will have the degeneracy in magnetic sub-levels lifted for states with non-zero angular momentum. Examples lying within the nominal 1.2–116 GHz frequency range of the ngVLA include lines from H at 1.42 GHz; OH at 1.61–1.72 GHz & 6.01–6.05 GHz; CH_3OH at 6.7, 36, & 44 GHz; C_4H at 9.5 & 19.0 GHz; CCS at 11, 22, 33, & 45 GHz; C_2H at 87 GHz; SO at 13, 30, 63, 86, & 99 GHz; and CN at 113.1–113.6 GHz. This lifting of the degeneracy will split the radio frequency transitions into a number of linearly and elliptically polarized components slightly separated in frequency. This is known as the Zeeman effect (Troland & Heiles 1986; Heiles et al. 1993; Crutcher 1999). Measuring this effect is the only way to directly measure the magnetic field strength (yielding either the line-of-sight field strength for Zeeman-broadened transitions, or the entire field strength for transitions that are completely split, e.g., Galactic OH masers[1]). Directly measuring the magnetic field strength is essential to achieve a more robust understanding of the dynamical relevance of the magnetic fields before and during the collapse of the star-forming core. Galactic OH masers can also be used to map out the large-scale magnetic field in the Milky Way since the star-forming regions in which they're found seem to retain information about the large-scale field in their vicinity (Davies 1974; Reid & Silverstein 1990). The ngVLA will play a critical role in extending Zeeman measurements beyond our Galaxy by detecting magnetic fields from extragalactic OH masers in nearby

[1] Linear and circular polarization from maser emission of centimeter and millimeter lines of SiO, CH_3OH, H_2O, and OH would allow us to probe the dense environment around young stellar objects and the circumstellar material around evolved stars.

galaxies like M33 and M31 and from OH megamasers in distant starbursting galaxies (Robishaw et al. 2008).

For other types of molecules, linear polarization can arise whenever an anisotropy in the radiation field yields a non-LTE population of magnetic sub-levels. This is the so-called Goldreich-Kylafis (G-K) effect, which traces the plane-of-sky magnetic field orientation (Goldreich & Kylafis 1981, 1982; Kylafis 1983; Deguchi & Watson 1984). This effect is expected to be easiest to observe where the lines have an optical depth of ~ 1; when the ratio of the collision rate to the radiative transition rate (i.e., the spontaneous emission rate) is also ~ 1; and for the lowest rotational transitions of simple molecules such as CO, CS, HCN, SiO, or HCO^+. So far, the G-K effect has been measured mostly around molecular outflows (e.g., Girart et al. 1999; Lai et al. 2003; Cortes et al. 2005; Vlemmings et al. 2012; Girart et al. 2012; Ching et al. 2016). This suggests that G-K observations with the ngVLA at 7 mm (SiO, CS) or 3 mm (CO, SiO, HCO^+) will provide new insight into the properties of the putative helical magnetic field near the launching point of bipolar outflows around young stellar objects, where a significant fraction of the outflow appears to be molecular. Molecular outflows from protostellar objects tend to have a parabolic, multi-layered, "onion-skin" type structure, with the lowest/highest-velocity material located in the outermost/innermost shells. Therefore, measuring the polarization at different velocities enables us to reconstruct the 3-dimensional magnetic field morphology in the source.

Polarization from thermal lines requires detection of emission with a high signal-to-noise ratio at high spectral resolution. The layout of the ngVLA (including the high-density central core of antennas) will yield excellent brightness sensitivity over a range of spatial scales relevant to star formation (approximately 10–1000 mas). The types of sources where the ngVLA would have a clear science impact detecting the Zeeman splitting and the G-K effect include the inner regions of various types of star-forming cores (e.g., warm cores, hot corinos, hot cores), proto/circumstellar envelopes, the launching regions of molecular outflows and jets, and disks.

2.3. Synchrotron emission from protostellar jets

Jets play an important role in the star-formation process. They are believed to regulate accretion from the disk onto the protostar at the earliest (Class 0/I) stages of star formation. However, jets are not only important in the field of the star formation—protostellar jets are usually considered a less energetic manifestation of the powerful relativistic jets driven by supermassive black holes at the center of active galaxies or stellar-mass black holes in our own Galaxy (e.g., de Gouveia Dal Pino 2005). Despite their importance, we still do not know how protostellar jets are launched and collimated. In the case of relativistic jets, observations of polarized synchrotron emission suggest that a helical configuration of the magnetic field is responsible for the collimation of the jet (e.g., Lyutikov et al. 2005; Gómez et al. 2008). In the case of protostellar jets, theoretical models also point to a fundamental role of the magnetic field, which is thought to have a helical configuration (e.g., Shu et al. 1994); helical magnetic fields are a consequence of the rotation of the protostar-disk system. As for the collimation of jets, they may be collimated internally. However, other collimation mechanisms by external agents, such as ordered magnetic fields present in the protostar's neighborhood, have also been proposed (e.g., Albertazzi et al. 2014); some observations are consistent with external collimation mechanisms (e.g., Carrasco-González et al. 2015).

The magnetic field is extremely difficult to study in the case of protostellar jets. Jets have been observed in great detail at radio wavelengths, although they emit mainly continuum thermal radiation (e.g., Anglada 1996), which contains no information about the magnetic field. However, in the last decades, very sensitive observations have shown that synchrotron emission can also be present in some protostellar jets (see Carrasco-González et al. 2010 and references therein). While the material in the jet moves at velocities of a few $\times$ 100 km s^{-1}, it has been shown that under some conditions, a population of particles can be accelerated up to relativistic velocities in strong shocks against the ambient medium (e.g., Rodríguez-Kamenetzky et al. 2016). Under these conditions, these accelerated particles can emit synchrotron emission, thus allowing the study of the magnetic field in the jet via synchrotron polarization. However, synchrotron emission in these objects is extremely weak, with intensities on the order of only a few $\times$ 10 μJy in Stokes *I*. At the beginning of the 2000s, we only knew of a handful of bright objects that show hints of synchrotron emission (i.e., negative spectral indices at centimeter wavelengths). In the last few years, more candidates have been detected as a result of the recently improved sensitivity in the ATCA and JVLA (e.g., Purser et al. 2016; Osorio et al. 2017). Yet, it has only been possible to detect linearly polarized emission in a single object, HH 80-81 (Carrasco-González et al. 2010, see Figure 2). Even though HH 80-81 is the brightest known protostellar jet, this unique detection at a single wavelength (6 cm) was only possible with significant observational effort (15 hrs of observations with the pre-upgrade VLA). Therefore, given the sensitivity of current instruments, it is still prohibitive to extend this study to multiple wavelengths in a sample of several protostellar jets.

In order to infer the 3-dimensional configuration of the magnetic field in the jet it is necessary to study the properties of the polarization of the synchrotron emission at several wavelengths. For example, for a helical magnetic field, we expect to observe gradients of the polarization fraction and the rotation measure (RM) across the jet width (Lyutikov et al. 2005). This implies the necessity to observe with high sensitivity to detect very low polarization fractions in intrinsically weak emission, and with high angular resolution to resolve the jet width (a few $\times$ 10 milliarcseconds). In principle, these requirements could be reached by the JVLA. However, protostellar jets are very dense (electron densities of the order of a few $\times$ 1000 cm^{-3}), and thus large RMs are expected. High sensitivity is currently achieved by averaging large frequency ranges. However, this introduces depolarization across the bandwidth when large RMs are present, rendering the polarized signal impossible to detect. It is therefore necessary to obtain high sensitivities even in narrow frequency ranges, which can only be achieved by increasing the observation time and/or the number of antennas in the interferometer.

Finally, it is not only desirable to detect polarization at several frequencies, but also at very different physical scales. The jet is expected to show complex morphology: extended diffuse emission, bow shocks, extended lobes, highly collimated parts, and compact internal shocks (e.g., Rodríguez-Kamenetzky et al. 2017). We also expect to see changes in the density across and along the jet. All of these characteristics imply dramatic changes of the properties of the emission (e.g., RM, brightness, and polarization fraction) at different scales. These changes can actually be used to obtain information about the jet's physical structure by, for example, using new wide-band spectropolarimetry modeling techniques that have been successfully applied to very bright, but unresolved, radio galaxies (e.g., O'Sullivan et al. 2017; Pasetto et al. 2018). While this type of study would be very difficult to perform in distant extragalactic jets, in nearby protostellar jets it could be performed simply by being sensitive simultane-

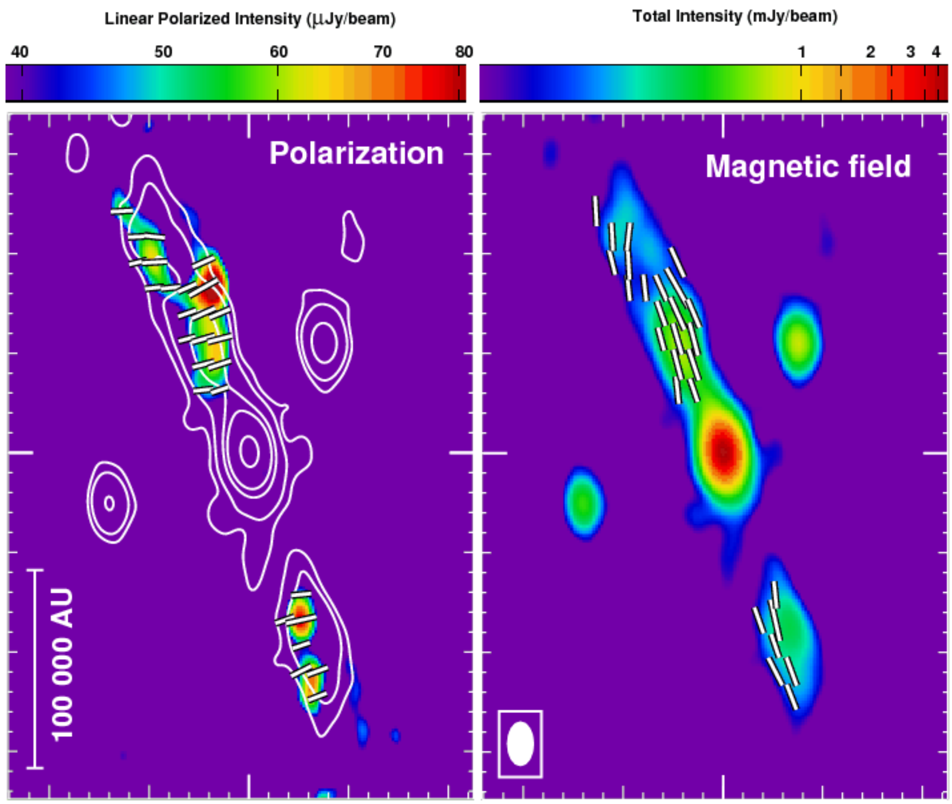

Figure 2. Observations of linearly polarized emission at 6 cm in the protostellar jet HH 80-81 (Carrasco-González et al. 2010). This is the first and only time that polarized emission has been detected in a protostellar jet. This result demonstrated that detecting polarized synchrotron emission is possible in protostellar jets, and allowed the study of the magnetic field in this object using techniques similar to those used in relativistic jets. However, the weakness of the emission and the likelihood of large rotation measures make it extremely difficult to extend this kind of study to other wavelengths and/or protostellar jets using current instruments. *Left:* Color scale is the linearly polarized emission at 6 cm. Line segments indicate the polarization orientation of the electric field. Contours are the total 6 cm emission from the protostellar jet. *Right:* White line segments indicate the orientation of the inferred (projected on the plane of the sky) magnetic field obtained from the polarization measurements. Color scale is the total 6 cm emission of the jet. The apparent magnetic field is parallel to the direction of the jet. This is consistent with a helical magnetic field configuration. However, in order to to infer the 3-dimensional configuration of the magnetic field it is necessary to study the polarization properties at several wavelengths.

ously to scales from a few milliarcseconds to several arcseconds. This will be easily achieved by an interferometer such as the ngVLA, with a large number of antennas spread over a few thousand kilometers.

2.4. Gyrosynchrotron from active magnetospheres around young stellar objects

Gyrosynchrotron radio emission from active magnetospheres is present in low-mass young stellar objects (YSOs) (e.g., Andre 1996) as well as their more evolved counterparts (Güdel & Benz 1993), including our Sun (Nita et al. 2004). Studying this emission in pre-main-sequence stars sheds light on their magnetic activity and the overall "space weather" that they drive, which has important effects on the chemistry and evolution of the surrounding protoplanetary and debris disks (e.g., Wilner et al. 2000).

The characterization of magnetospheric radio emission is also necessary for the proper analysis of YSO dust emission, because the two processes lead to emission at overlapping radio frequencies—in particular, the range of frequencies where the ngVLA will be most powerful. Non-thermal gyrosynchrotron emission can be distinguished from thermal emission mainly through its variability on timescales from minutes to months (Forbrich et al. 2015), its generally (but not always) negative spectral index (Garay et al. 1996), circular polarization fraction of a few to ~20% (Andre 1996), and its brightness temperatures $\gg 10^4$ K (Ortiz-León et al. 2017). Even the upgraded JVLA, however, has difficulty achieving the performance needed to fully understand YSO radio emission at centimeter wavelengths. In a study using the JVLA, Liu et al. (2014) characterized the radio flux, variability, and circular polarization of YSOs from Class 0 to Class III, achieving a noise of $\sim 20\,\mu$Jy using observing blocks of a few hours and averaging over a few GHz of bandwidth. The results were consistent with earlier findings (e.g., Gibb 1999) showing that centimeter radio emission from YSOs (1) is dominated by free-free emission from collimated winds or radio jets in the early Class 0 and I stages (Anglada et al. 2015); (2) is difficult to detect in Class IIs (Galván-Madrid et al. 2014); and (3) is detectable in some but not all Class III YSOs (Forbrich et al. 2007; Dzib et al. 2013). The emission from Class IIIs appears to be dominated by gyrosynchrotron radiation, but in Class IIs there are individual case studies pointing toward either free-free or gyrosynchrotron (Macías et al. 2016; Galván-Madrid et al. 2014).

The high sensitivity, wide frequency coverage, and angular resolution of the ngVLA would transform studies of both thermal and non-thermal YSO radio emission, allowing robust disentanglement of the two processes in snapshot observations as short as a few seconds. Scaling the nominal sensitivities reported by Carilli et al. (2015), the ngVLA could obtain full-polarization measurements with noise levels of $\sim 10\ \mu$Jy in 5-second integrations. Moreover, the large simultaneous bandwidth would allow full characterization of the non-thermal radio SEDs and their overlap with free-free or dust thermal emission truly simultaneously, something that has not been possible with the VLA. It is quite likely that the non-thermal SEDs of YSOs have complexities due to multiple magnetospheric components, binary interactions (Salter et al. 2010), and other phenomena yet to be discovered.

The same attributes of the ngVLA that will make it a transformative tool for studies of YSO magnetospheres will produce similar gains in studies focusing on other objects with comparable magnetic properties. In particular, the magnetospheres of fully-convective YSOs can be dipolar and rotation-dominated, with strong commonalities to those found in very-low-mass stars and brown dwarfs, magnetic chemically peculiar (MCP) stars, and even the Solar System giant planets (Donati & Landstreet 2009; Schrijver 2009). The magnetism of these objects is quite different from that of the Sun, being driven by a fully-convective dynamo and resulting in large-scale current systems, coherent maser emission, and potentially trapped particle radiation belts (Hallinan et al.

2006; Williams 2017). The resulting radio emission is generally quite broadband and highly polarized (e.g., Williams et al. 2015), and current studies are often sensitivity-limited; for example, the JVLA is unable to detect even the 2 pc-distant ultracool dwarf binary Luhman 16AB (Osten et al. 2015). The ngVLA will therefore enable an entirely new class of time-resolved, full-polarization studies of magnetospheric activity in YSOs and beyond.

3. Measurements Required

Continuum polarization observations are relatively straightforward, generally requiring a single-pointing per source, integrating down to the point where a ~ 1–3% polarization signal can be detected at the 3+ sigma confidence level across the desired region of the source. Spectral line polarization requires high spectral resolution, where the rule of thumb is ~ 6 channels across the full-width-at-half-max (FWHM) of the line. This is especially important for Zeeman observations of masers, where a velocity resolution of < 0.1 km/s is required. Polarization levels can be low, on the order of a few $\times$ 0.1%, so an accurate characterization of the instrumental polarization is required, down to a level of $\sim 0.1\%$, similar to what is achievable with the ALMA polarization system. The more compact sources (disks, protostellar envelopes, etc.) will generally fill only a fraction of the primary beam; however, for more extended sources, and in the event that there is more than one source (e.g., a few disks or protostars) in one field of view, either separate pointings and/or mosaics will have to be performed, or the wide-field polarization characteristics will have to be well characterized in order to correct for off-axis effects (see, e.g., work done by Jagannathan et al. 2017, 2018). Other standard polarization-specific calibration requirements involve solving for leakages (D-terms) and the XY (or RL) phase of the reference antenna.

The design of the ngVLA antennas and feeds should be informed by careful consideration of polarimetric goals—unfortunately, there is always a polarimetric sacrifice to be made for any given design. Linearly polarized radiation (Stokes Q and U)—especially weak polarization—is best measured via the cross-correlation of the orthogonal outputs from native circular feeds (with a penalty in measuring Stokes V); likewise, circularly polarized radiation is best measured by cross-correlating the outputs from orthogonal native linear feeds (with a penalty in measuring Stokes Q). New interferometers, except for the JVLA, are employing native dual-linear feeds. While these feeds can be converted to dual-circular by means of hybrids or dielectric quarter-wave phase shifters, such devices provide frequency-dependent polarization, operate over narrow bandwidths, and can increase not only the system temperature, but also the complexity and the cost of the receiver design.

An altitude-azimuth (alt-az) mount is ideal for polarization measurements because it causes a linearly polarized astronomical source to rotate relative to the feed as a source is tracked. This rotation greatly reduces systematic effects and makes calibration much easier. The Australian Square Kilometre Array Pathfinder (ASKAP) interferometer has been designed with dishes on alt-az mounts, but the designers have opted to rotate their entire dish structure with the sky—mimicking the behavior of an equatorial mount—in order to simplify wide-field polarimetric imaging. This is even better than a standard alt-az mount because the polarization rotation can be done instantaneously, without having to wait for the angle to change while tracking.

A final polarization consideration involves the choice to use an off-axis Gregorian secondary-focus design for the dishes. When it comes to measuring polarization, symmetry is better: sidelobes and spillover radiation tend to be polarized by an amount that increases with asymmetry. Moreover, ground radiation is highly polarized.

4. Uniqueness to ngVLA Capabilities

The centimeter-wave/$\sim$ 30 GHz capabilities of the ngVLA are unique in that the other extant telescope that can currently perform such observations—namely, the JVLA—doesn't have the sensitivity to perform the type of observations we require. In the case of future ALMA Band 1 observations at $\sim$ 1 cm wavelengths, the ngVLA's resolution and sensitivity will be much higher, enabling the studies we discuss above. Lower frequency telescopes probe physical phenomena that are completely different from the various polarization mechanisms we discuss above.

5. Synergies at Other Wavelengths

For continuum science, as an interferometer the ngVLA will fill a gap between the Square Kilometre Array (SKA)—which will address many different topics related to magnetic fields and polarization—and ALMA, which will look at many of the same objects, but at high frequencies where the material in the regions of interest (i.e., the inner parts of protoplanetary disks) is sometimes optically thick. The ngVLA will perform extremely high-resolution, high-sensitivity, targeted polarization science at the same time that the Origins Space Telescope (OST), if funded and constructed, is performing surveys of continuum and spectral-line polarization toward entire star-forming clouds across the Galaxy. The ngVLA will perform long-wavelength follow-up of observations from the myriad telescopes that are currently available (or are soon coming online) and have polarization capabilities at far-infrared and (sub)millimeter wavelengths, including ALMA, SOFIA (HAWC+ polarimeter), the James Clark Maxwell Telescope (JCMT; POL2 polarimeter), the Large Millimeter Telescope (LMT; TolTEC polarimeter), and the BLAST-TNG balloon-borne experiment.

Acknowledgments. The authors thank Carl Heiles for his help in clarifying the implications of the ngVLA receiver design on the telescope's polarimetric capabilities. C.L.H.H acknowledges the support of the JSPS KAKENHI grant 18K13586. J.M.G. is supported by the MINECO (Spain) AYA2017-84390-C2 grant. R.G.-M. acknowledges support from UNAM-PAPIIT program IA102817. P.K.G.W. acknowledges support for this work from the National Science Foundation through Grant AST-161477. The National Radio Astronomy Observatory is a facility of the National Science Foundation operated under cooperative agreement by Associated Universities, Inc.

References

Albertazzi, B., Ciardi, A., Nakatsutsumi, M., Vinci, T., Béard, J., Bonito, R., Billette, J., Borghesi, M., Burkley, Z., Chen, S. N., Cowan, T. E., Herrmannsdörfer, T., Higginson, D. P., Kroll, F., Pikuz, S. A., Naughton, K., Romagnani, L., Riconda, C., Revet, G., Riquier, R., Schlenvoigt, H.-P., Skobelev, I. Y., Faenov, A. Y., Soloviev, A., Huarte-Espinosa, M., Frank, A., Portugall, O., Pépin, H., & Fuchs, J. 2014, Science, 346, 325

ALMA Partnership, Brogan, C. L., Pérez, L. M., Hunter, T. R., Dent, W. R. F., Hales, A. S., Hills, R. E., Corder, S., Fomalont, E. B., Vlahakis, C., Asaki, Y., Barkats, D., Hirota, A., Hodge, J. A., Impellizzeri, C. M. V., Kneissl, R., Liuzzo, E., Lucas, R., Marcelino, N., Matsushita, S., Nakanishi, K., Phillips, N., Richards, A. M. S., Toledo, I., Aladro, R., Broguiere, D., Cortes, J. R., Cortes, P. C., Espada, D., Galarza, F., Garcia-Appadoo, D., Guzman-Ramirez, L., Humphreys, E. M., Jung, T., Kameno, S., Laing, R. A., Leon, S., Marconi, G., Mignano, A., Nikolic, B., Nyman, L.-A., Radiszcz, M., Remijan, A., Rodón, J. A., Sawada, T., Takahashi, S., Tilanus, R. P. J., Vila Vilaro, B., Watson, L. C., Wiklind, T., Akiyama, E., Chapillon, E., de Gregorio-Monsalvo, I., Di Francesco, J., Gueth, F., Kawamura, A., Lee, C.-F., Nguyen Luong, Q., Mangum, J., Pietu, V., Sanhueza, P., Saigo, K., Takakuwa, S., Ubach, C., van Kempen, T., Wootten, A., Castro-Carrizo, A., Francke, H., Gallardo, J., Garcia, J., Gonzalez, S., Hill, T., Kaminski, T., Kurono, Y., Liu, H.-Y., Lopez, C., Morales, F., Plarre, K., Schieven, G., Testi, L., Videla, L., Villard, E., Andreani, P., Hibbard, J. E., & Tatematsu, K. 2015, ApJ, 808, L3. 1503.02649

Alves, F. O., Girart, J. M., Lai, S.-P., Rao, R., & Zhang, Q. 2011, ApJ, 726, 63. 1011.0475

Andersson, B.-G., Lazarian, A., & Vaillancourt, J. E. 2015, ARA&A, 53, 501

Andre, P. 1996, in Radio Emission from the Stars and the Sun, edited by A. R. Taylor, & J. M. Paredes, vol. 93 of Astronomical Society of the Pacific Conference Series, 273

Anglada, G. 1996, in Radio Emission from the Stars and the Sun, edited by A. R. Taylor, & J. M. Paredes, vol. 93 of Astronomical Society of the Pacific Conference Series, 3

Anglada, G., Rodríguez, L. F., & Carrasco-Gonzalez, C. 2015, Advancing Astrophysics with the Square Kilometre Array (AASKA14), 121. 1412.6409

Carilli, C. L., McKinnon, M., Ott, J., Beasley, A., Isella, A., Murphy, E., Leroy, A., Casey, C., Moullet, A., Lacy, M., Hodge, J., Bower, G., Demorest, P., Hull, C., Hughes, M., di Francesco, J., Narayanan, D., Kent, B., Clark, B., & Butler, B. 2015, ArXiv e-prints. 1510.06438

Carrasco-González, C., Henning, T., Chandler, C. J., Linz, H., Pérez, L., Rodríguez, L. F., Galván-Madrid, R., Anglada, G., Birnstiel, T., van Boekel, R., Flock, M., Klahr, H., Macias, E., Menten, K., Osorio, M., Testi, L., Torrelles, J. M., & Zhu, Z. 2016, ApJ, 821, L16. 1603.03731

Carrasco-González, C., Rodríguez, L. F., Anglada, G., Martí, J., Torrelles, J. M., & Osorio, M. 2010, Science, 330, 1209. 1011.6254

Carrasco-González, C., Torrelles, J. M., Cantó, J., Curiel, S., Surcis, G., Vlemmings, W. H. T., van Langevelde, H. J., Goddi, C., Anglada, G., Kim, S.-W., Kim, J.-S., & Gómez, J. F. 2015, Science, 348, 114. 1507.05285

Ching, T.-C., Lai, S.-P., Zhang, Q., Yang, L., Girart, J. M., & Rao, R. 2016, ApJ, 819, 159. 1601.05229

Cortes, P., & Crutcher, R. M. 2006, ApJ, 639, 965. astro-ph/0607357

Cortes, P. C., Crutcher, R. M., & Watson, W. D. 2005, ApJ, 628, 780. astro-ph/0504258

Cortes, P. C., Girart, J. M., Hull, C. L. H., Sridharan, T. K., Louvet, F., Plambeck, R., Li, Z.-Y., Crutcher, R. M., & Lai, S.-P. 2016, ApJ, 825, L15. 1605.08037

Cox, E. G., Harris, R. J., Looney, L. W., Chiang, H.-F., Chandler, C., Kratter, K., Li, Z.-Y., Perez, L., & Tobin, J. J. 2017, ApJ, 851, 83. 1711.03974

Cox, E. G., Harris, R. J., Looney, L. W., Li, Z.-Y., Yang, H., Tobin, J. J., & Stephens, I. 2018, ArXiv e-prints. 1802.00449

Cox, E. G., Harris, R. J., Looney, L. W., Segura-Cox, D. M., Tobin, J., Li, Z.-Y., Tychoniec, Ł., Chandler, C. J., Dunham, M. M., Kratter, K., Melis, C., Perez, L. M., & Sadavoy, S. I. 2015, ApJ, 814, L28. 1511.00685

Crutcher, R. M. 1999, ApJ, 520, 706

Davies, R. D. 1974, in Galactic Radio Astronomy, edited by F. J. Kerr, & S. C. Simonson (Dordrecht: Reidel), vol. 60 of IAU Symp., 275

de Gouveia Dal Pino, E. M. 2005, Advances in Space Research, 35, 908. astro-ph/0406319

Deguchi, S., & Watson, W. D. 1984, ApJ, 285, 126

Donati, J. F., & Landstreet, J. D. 2009, ARA&A, 47, 333. URL http://dx.doi.org/10.1146/annurev-astro-082708-101833

Dzib, S. A., Loinard, L., Mioduszewski, A. J., Rodríguez, L. F., Ortiz-León, G. N., Pech, G.,

Rivera, J. L., Torres, R. M., Boden, A. F., Hartmann, L., Evans, N. J., II, Briceño, C., & Tobin, J. 2013, ApJ, 775, 63. 1307.5105
Forbrich, J., Preibisch, T., Menten, K. M., Neuhäuser, R., Walter, F. M., Tamura, M., Matsunaga, N., Kusakabe, N., Nakajima, Y., Brandeker, A., Fornasier, S., Posselt, B., Tachihara, K., & Broeg, C. 2007, A&A, 464, 1003. astro-ph/0703316
Forbrich, J., Rodríguez, L. F., Palau, A., Zapata, L. A., Muzerolle, J., & Gutermuth, R. A. 2015, ApJ, 814, 15. 1510.01233
Galván-Madrid, R., Liu, H. B., Manara, C. F., Forbrich, J., Pascucci, I., Carrasco-González, C., Goddi, C., Hasegawa, Y., Takami, M., & Testi, L. 2014, A&A, 570, L9. 1409.7110
Garay, G., Ramirez, S., Rodriguez, L. F., Curiel, S., & Torrelles, J. M. 1996, ApJ, 459, 193
Gibb, A. G. 1999, MNRAS, 304, 1
Girart, J. M., Beltrán, M. T., Zhang, Q., Rao, R., & Estalella, R. 2009, Science, 324, 1408
Girart, J. M., Crutcher, R. M., & Rao, R. 1999, ApJ, 525, L109
Girart, J. M., Fernandez-Lopez, M., Li, Z.-Y., Yang, H., Estalella, R., Anglada, G., Añez-Lopez, N., Busquet, G., Carrasco-Gonzalez, C., Curiel, S., Galvan-Madrid, R., Gomez, J. F., de Gregorio-Monsalvo, I., Jimenez-Serra, I., Krasnopolsky, R., Marti, J., Osorio, M., Padovani, M., Rao, R., Rodriguez, L. F., & Torrelles, J. M. 2018, ArXiv e-prints. 1803.06165
Girart, J. M., Patel, N., Vlemmings, W. H. T., & Rao, R. 2012, ApJ, 751, L20. 1204.4381
Girart, J. M., Rao, R., & Marrone, D. P. 2006, Science, 313, 812. arXiv:astro-ph/0609177
Goldreich, P., & Kylafis, N. D. 1981, ApJ, 243, L75
— 1982, ApJ, 253, 606
Gómez, J. L., Marscher, A. P., Jorstad, S. G., Agudo, I., & Roca-Sogorb, M. 2008, ApJ, 681, L69. 0805.4797
Güdel, M., & Benz, A. O. 1993, ApJ, 405, L63. URL http://dx.doi.org/10.1086/186766
Hallinan, G., Antonova, A., Doyle, J. G., Bourke, S., Brisken, W. F., & Golden, A. 2006, ApJ, 653, 690. URL http://dx.doi.org/10.1086/508678
Harris, R. J., Cox, E. G., Looney, L. W., Li, Z.-Y., Yang, H., Fernández-López, M., Kwon, W., Sadavoy, S., Segura-Cox, D., Stephens, I., & Tobin, J. 2018, ArXiv e-prints. 1805.08792
Heiles, C., Goodman, A. A., McKee, C. F., & Zweibel, E. G. 1993, in Protostars and Planets III, edited by E. H. Levy, & J. I. Lunine, 279
Hildebrand, R. H. 1988, QJRAS, 29, 327
Hoang, T., & Lazarian, A. 2009, ApJ, 697, 1316. 0812.4576
Hughes, A. M., Hull, C. L. H., Wilner, D. J., & Plambeck, R. L. 2013, AJ, 145, 115. 1302.4745
Hull, C. L. H., Girart, J. M., Tychoniec, Ł., Rao, R., Cortés, P. C., Pokhrel, R., Zhang, Q., Houde, M., Dunham, M. M., Kristensen, L. E., Lai, S.-P., Li, Z.-Y., & Plambeck, R. L. 2017a, ApJ, 847, 92. 1707.03827
Hull, C. L. H., Mocz, P., Burkhart, B., Goodman, A. A., Girart, J. M., Cortés, P. C., Hernquist, L., Springel, V., Li, Z.-Y., & Lai, S.-P. 2017b, ApJ, 842, L9. 1706.03806
Hull, C. L. H., Plambeck, R. L., Bolatto, A. D., Bower, G. C., Carpenter, J. M., Crutcher, R. M., Fiege, J. D., Franzmann, E., Hakobian, N. S., Heiles, C., Houde, M., Hughes, A. M., Jameson, K., Kwon, W., Lamb, J. W., Looney, L. W., Matthews, B. C., Mundy, L., Pillai, T., Pound, M. W., Stephens, I. W., Tobin, J. J., Vaillancourt, J. E., Volgenau, N. H., & Wright, M. C. H. 2013, ApJ, 768, 159. 1212.0540
Hull, C. L. H., Plambeck, R. L., Kwon, W., Bower, G. C., Carpenter, J. M., Crutcher, R. M., Fiege, J. D., Franzmann, E., Hakobian, N. S., Heiles, C., Houde, M., Hughes, A. M., Lamb, J. W., Looney, L. W., Marrone, D. P., Matthews, B. C., Pillai, T., Pound, M. W., Rahman, N., Sandell, G., Stephens, I. W., Tobin, J. J., Vaillancourt, J. E., Volgenau, N. H., & Wright, M. C. H. 2014, ApJS, 213, 13. 1310.6653
Hull, C. L. H., Yang, H., Li, Z.-Y., Kataoka, A., Stephens, I. W., Andrews, S., Bai, X., Cleeves, L. I., Hughes, A. M., Looney, L., Pérez, L. M., & Wilner, D. 2018, ArXiv e-prints. 1804.06269
Jagannathan, P., Bhatnagar, S., Brisken, W., & Taylor, A. R. 2018, AJ, 155, 3. 1711.00875
Jagannathan, P., Bhatnagar, S., Rau, U., & Taylor, A. R. 2017, AJ, 154, 56. 1706.01501

Jin, S., Li, S., Isella, A., Li, H., & Ji, J. 2016, ApJ, 818, 76. 1601.00358
Kataoka, A., Muto, T., Momose, M., Tsukagoshi, T., Fukagawa, M., Shibai, H., Hanawa, T., Murakawa, K., & Dullemond, C. P. 2015, ApJ, 809, 78. 1504.04812
Kataoka, A., Tsukagoshi, T., Momose, M., Nagai, H., Muto, T., Dullemond, C. P., Pohl, A., Fukagawa, M., Shibai, H., Hanawa, T., & Murakawa, K. 2016, ApJ, 831, L12. 1610.06318
Kataoka, A., Tsukagoshi, T., Pohl, A., Muto, T., Nagai, H., Stephens, I. W., Tomisaka, K., & Momose, M. 2017, ApJ, 844, L5. 1707.01612
Kwon, W., Looney, L. W., Crutcher, R. M., & Kirk, J. M. 2006, ApJ, 653, 1358. arXiv:astro-ph/0609176
Kylafis, N. D. 1983, ApJ, 267, 137
Lai, S.-P., Crutcher, R. M., Girart, J. M., & Rao, R. 2001, ApJ, 561, 864. astro-ph/0107322
Lai, S.-P., Girart, J. M., & Crutcher, R. M. 2003, ApJ, 598, 392. arXiv:astro-ph/0308051
Lazarian, A. 2007, J. Quant. Spec. Radiat. Transf., 106, 225. 0707.0858
Lee, C.-F., Li, Z.-Y., Ching, T.-C., Lai, S.-P., & Yang, H. 2018, ApJ, 854, 56. 1801.03802
Liu, H. B., Galván-Madrid, R., Forbrich, J., Rodríguez, L. F., Takami, M., Costigan, G., Manara, C. F., Yan, C.-H., Karr, J., Chou, M.-Y., Ho, P. T.-P., & Zhang, Q. 2014, ApJ, 780, 155. URL http://dx.doi.org/10.1088/0004-637X/780/2/155
Liu, H. B., Hasegawa, Y., Ching, T.-C., Lai, S.-P., Hirano, N., & Rao, R. 2018, ArXiv e-prints. 1805.02012
Liu, H. B., Lai, S.-P., Hasegawa, Y., Hirano, N., Rao, R., Li, I.-H., Fukagawa, M., Girart, J. M., Carrasco-González, C., & Rodríguez, L. F. 2016, ApJ, 821, 41. 1602.04077
Lyutikov, M., Pariev, V. I., & Gabuzda, D. C. 2005, MNRAS, 360, 869. astro-ph/0406144
Macías, E., Anglada, G., Osorio, M., Calvet, N., Torrelles, J. M., Gómez, J. F., Espaillat, C., Lizano, S., Rodríguez, L. F., Carrasco-González, C., & Zapata, L. 2016, ApJ, 829, 1. 1607.04225
Matthews, B. C., Lai, S.-P., Crutcher, R. M., & Wilson, C. D. 2005, ApJ, 626, 959
Maury, A. J., Girart, J. M., Zhang, Q., Hennebelle, P., Keto, E., Rao, R., Lai, S.-P., Ohashi, N., & Galametz, M. 2018, MNRAS. 1803.00028
Nita, G. M., Gary, D. E., & Lee, J. 2004, ApJ, 605, 528
Ortiz-León, G. N., Loinard, L., Kounkel, M. A., Dzib, S. A., Mioduszewski, A. J., Rodríguez, L. F., Torres, R. M., González-Lópezlira, R. A., Pech, G., Rivera, J. L., Hartmann, L., Boden, A. F., Evans, N. J., II, Briceño, C., Tobin, J. J., Galli, P. A. B., & Gudehus, D. 2017, ApJ, 834, 141. 1611.06466
Osorio, M., Díaz-Rodríguez, A. K., Anglada, G., Megeath, S. T., Rodríguez, L. F., Tobin, J. J., Stutz, A. M., Furlan, E., Fischer, W. J., Manoj, P., Gómez, J. F., González-García, B., Stanke, T., Watson, D. M., Loinard, L., Vavrek, R., & Carrasco-González, C. 2017, ApJ, 840, 36. 1703.07877
Osten, R. A., Melis, C., Stelzer, B., Bannister, K. W., Radigan, J., Burgasser, A. J., Wolszczan, A., & Luhman, K. L. 2015, ApJ, 805, L3+. URL http://dx.doi.org/10.1088/2041-8205/805/1/L3
O'Sullivan, S. P., Purcell, C. R., Anderson, C. S., Farnes, J. S., Sun, X. H., & Gaensler, B. M. 2017, MNRAS, 469, 4034. 1705.00102
Pasetto, A., Carrasco-González, C., O'Sullivan, S., Basu, A., Bruni, G., Kraus, A., Curiel, S., & Mack, K.-H. 2018, ArXiv e-prints. 1801.09731
Purser, S. J. D., Lumsden, S. L., Hoare, M. G., Urquhart, J. S., Cunningham, N., Purcell, C. R., Brooks, K. J., Garay, G., Gúzman, A. E., & Voronkov, M. A. 2016, MNRAS, 460, 1039. 1605.01200
Rao, R., Crutcher, R. M., Plambeck, R. L., & Wright, M. C. H. 1998, ApJ, 502, L75+. arXiv:astro-ph/9805288
Rao, R., Girart, J. M., Lai, S.-P., & Marrone, D. P. 2014, ApJ, 780, L6. 1311.6225
Rao, R., Girart, J. M., Marrone, D. P., Lai, S.-P., & Schnee, S. 2009, ApJ, 707, 921. 0910.5269
Reid, M. J., & Silverstein, E. M. 1990, ApJ, 361, 483
Robishaw, T., Quataert, E., & Heiles, C. 2008, ApJ, 680, 981. 0803.1832

Rodríguez-Kamenetzky, A., Carrasco-González, C., Araudo, A., Romero, G. E., Torrelles, J. M., Rodríguez, L. F., Anglada, G., Martí, J., Perucho, M., & Valotto, C. 2017, ApJ, 851, 16. 1711.02554

Rodríguez-Kamenetzky, A., Carrasco-González, C., Araudo, A., Torrelles, J. M., Anglada, G., Martí, J., Rodríguez, L. F., & Valotto, C. 2016, ApJ, 818, 27. 1512.02980

Sadavoy, S. I., Myers, P. C., Stephens, I. W., Tobin, J., Commercon, B., Henning, T., Looney, L., Kwon, W., Segura-Cox, D., & Harris, R. 2018, ArXiv e-prints. 1804.05968

Salter, D. M., Kóspál, Á., Getman, K. V., Hogerheijde, M. R., van Kempen, T. A., Carpenter, J. M., Blake, G. A., & Wilner, D. 2010, A&A, 521, A32. 1008.0981

Schrijver, C. J. 2009, ApJ, 699, L148. URL http://dx.doi.org/10.1088/0004-637X/699/2/L148

Segura-Cox, D. M., Looney, L. W., Stephens, I. W., Fernández-López, M., Kwon, W., Tobin, J. J., Li, Z.-Y., & Crutcher, R. 2015, ApJ, 798, L2. 1412.1085

Shu, F., Najita, J., Ostriker, E., Wilkin, F., Ruden, S., & Lizano, S. 1994, ApJ, 429, 781

Stephens, I. W., Looney, L. W., Kwon, W., Fernández-López, M., Hughes, A. M., Mundy, L. G., Crutcher, R. M., Li, Z.-Y., & Rao, R. 2014, Nat, 514, 597. 1409.2878

Stephens, I. W., Yang, H., Li, Z.-Y., Looney, L. W., Kataoka, A., Kwon, W., Fernández-López, M., Hull, C. L. H., Hughes, M., Segura-Cox, D., Mundy, L., Crutcher, R., & Rao, R. 2017, ApJ, 851, 55. 1710.04670

Tang, Y.-W., Ho, P. T. P., Girart, J. M., Rao, R., Koch, P., & Lai, S.-P. 2009, ApJ, 695, 1399. 0812.3444

Tazaki, R., Lazarian, A., & Nomura, H. 2017, ApJ, 839, 56. 1701.02063

Troland, T. H., & Heiles, C. 1986, ApJ, 301, 339

Vlemmings, W. H. T., Ramstedt, S., Rao, R., & Maercker, M. 2012, A&A, 540, L3. 1203.2922

Williams, P. K. G. 2017, in Handbook of Exoplanets, edited by H. J. Deeg, & J. A. Belmonte (Springer Verlag). URL http://adsabs.harvard.edu/abs/2017arxiv170704264

Williams, P. K. G., Berger, E., Irwin, J., Berta-Thompson, Z. K., & Charbonneau, D. 2015, ApJ, 799, 192+. URL http://dx.doi.org/10.1088/0004-637X/799/2/192

Wilner, D. J., Ho, P. T. P., Kastner, J. H., & Rodríguez, L. F. 2000, ApJ, 534, L101. astro-ph/0005019

Yang, H., Li, Z.-Y., Looney, L. W., Girart, J. M., & Stephens, I. W. 2017, MNRAS, 472, 373. 1705.05432

Zhang, Q., Qiu, K., Girart, J. M., Liu, H. B., Tang, Y.-W., Koch, P. M., Li, Z.-Y., Keto, E., Ho, P. T. P., Rao, R., Lai, S.-P., Ching, T.-C., Frau, P., Chen, H.-H., Li, H.-B., Padovani, M., Bontemps, S., Csengeri, T., & Juárez, C. 2014, The Astrophysical Journal, 792, 116. URL http://stacks.iop.org/0004-637X/792/i=2/a=116

Part VI

Galaxy Ecosystems:

Science with a Next-Generation Very Large Array
ASP Conference Series, Monograph 7
Eric J. Murphy, ed.

DRAFT EDITION

Radio Continuum Emission from Galaxies: An Accounting of Energetic Processes

Eric J. Murphy,[1] James J. Condon,[1] Antxon Alberdi,[2] Loreto Barcos-Muñozarcos,[3,1] Robert J. Beswick,[4] Elias Brinks,[5] Dillon Dong,[6] Aaron S. Evans,[7,1] Kelsey E. Johnson,[7,1] Rober C. Kennicutt Jr.,[8] Sean T. Linden,[7,1] Tom W. B. Muxlow,[4] Miguel Pérez-Torres,[2] Eva Schinnerer,[9] Mark T. Sargent,[10] Fatemeh S. Tabatabaei,[2,11] and Jean L. Turner[12]

[1]*National Radio Astronomy Observatory, Charlottesville, VA, 22903;* `emurphy@nrao.edu`

[2]*Instituto de Astrofisica de Andalucía (IAA, CSIC); Glorieta de la Astronomía s/n, 18008-Granada, Spain*

[3]*Joint ALMA Observatory, Alonso de Córdova 3107, Vitacura, Santiago, Chile*

[4]*Jodrell Bank Centre for Astrophysics/e-MERLIN, The University of Manchester, Manchester, M13 9PL, UK*

[5]*School of Physics, Astronomy and Mathematics, University of Hertfordshire, Hatfield AL10 9AB, UK*

[6]*California Institute of Technology, MC 100-22, Pasadena, CA 91125, USA*

[7]*Department of Astronomy, University of Virginia, 3530 McCormick Road,Charlottesville, VA 22904, USA*

[8]*Institute of Astronomy, University of Cambridge, Madingley Road, Cambridge CB3 0HA, UK*

[9]*Max Planck Institut für Astronomie, Königstuhl 17, Heidelberg D-69117, Germany*

[10]*Astronomy Centre, Department of Physics and Astronomy, University of Sussex, Brighton BN1 9QH, UK*

[11]*Departamento de Astrofísica, Universidad de La Laguna, E-38206 La Laguna, Spain*

[12]*Department of Physics and Astronomy, UCLA, Los Angeles, CA 90095, USA*

Abstract. Radio continuum observations have proven to be a workhorse in our understanding of the star formation process (i.e., stellar birth and death) from galaxies both in the nearby universe and out to the highest redshifts. In this chapter we focus on how the ngVLA will transform our understanding of star formation by enabling one to map and decompose the radio continuum emission from large, heterogeneous samples of nearby galaxies on $\gtrsim$ 10 pc scales to conduct a proper accounting of the energetic processes powering it. At the discussed sensitivity and angular resolution, the ngVLA will simultaneously be able to create maps of current star formation activity at ~100 pc scales, as well as detect and characterize (e.g., size, spectral shape, density, etc.) discrete HII regions and supernova remnants (SNRs) on 10 pc scales in galaxies out to the distance of the Virgo cluster. Their properties can then be used to see how they relate to the local and global ISM and star formation conditions. Such investigations are essential for understanding the astrophysics of high-z measurements of galaxies, allowing for proper modeling of galaxy formation and evolution.

1. Introduction

Radio continuum observations have proven to be a workhorse in our understanding of the star formation process (i.e., stellar birth and death) from galaxies both in the nearby universe and out to the highest redshifts. A next-generation Very Large Array (ngVLA), as currently proposed, would revolutionize our understanding of the emission mechanisms that power the radio continuum emission in and around galaxies by enabling the routine construction of $\sim 1.2 - 116$ GHz radio spectral maps. Coupled with its nearly order of magnitude increased sensitivity compared to the current Jansky VLA, the ngVLA makes it possible to use this frequency window to investigate the distinct physical processes linked to stellar birth and death for large, heterogeneous samples of galaxies for the first time. Furthermore, by delivering such a finely sampled spectrum over this entire frequency range with a single instrument will allow robust separation of the various emission components, which is currently the main challenge for multi-frequency radio studies. Each observation will provide enough sensitivity and spectral coverage to robustly decompose and accurately quantify the individual energetic components powering the radio continuum, thus providing unique information on the non-thermal plasma, ionized gas, and cold dust content in the disks and halos of galaxies.

In this chapter we focus on how the ngVLA can be used to map and decompose the radio continuum emission from large heterogeneous samples of nearby galaxies on $\gtrsim 10$ pc scales to conduct a proper accounting of their energetics. In doing so, we will be able to determine how star formation, AGN, and physical conditions in the ISM give rise to varying contributions of:

- non-thermal synchrotron emission powered by accelerated CR electrons/positrons
- free-free emission from young massive star-forming (HII) regions
- anomalous microwave emission (AME), which is a dominant, but completely unconstrained, foreground in CMB experiments.
- cold, thermal dust emission that accounts for most of the dust and total mass content of the ISM in galaxies.

2. The Energetic Processes Powering Radio Continuum Emission

Radio continuum emission from galaxies covering $\sim 1.2 - 116$ GHz is powered by an eclectic mix of physical emission processes, each providing completely independent information on the star formation and ISM properties of galaxies (see Figure 1). As such,

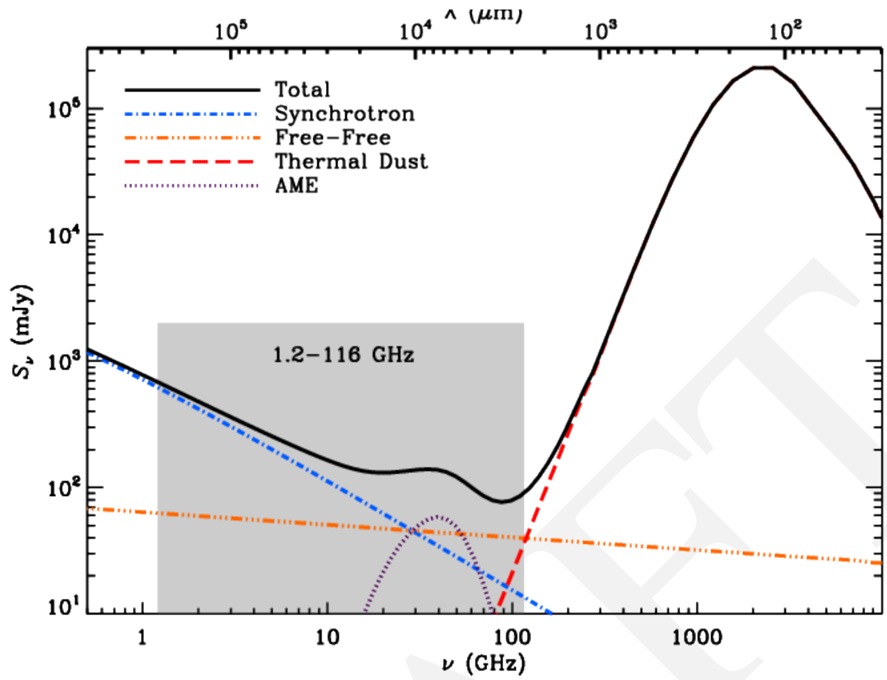

Figure 1. A model spectrum illustrating the various emission processes (non-thermal synchrotron, free-free, AME, thermal dust) that contribute to the observed radio frequency range to be covered by the ngVLA. Only in the proposed ngVLA frequency range (1.2−116 GHz, highlighted) do all major continuum emission mechanisms contribute at similar levels, making this range uniquely well-suited to next-generation continuum studies.

it provides a unique window into the ISM and the process of star formation in galaxies. These processes include non-thermal synchrotron, free-free (thermal bremsstrahlung), anomalous microwave, and thermal dust emission that are directly related to the various phases of the ISM and provide a comprehensive picture of how galaxies convert their gas into stars. Each of these emission components, described in detail below, are of low surface brightness in the $\sim 30 - 116$ GHz frequency range, and therefore difficult to map in a spatially resolved manner at $\sim 10 - 100$ pc scales in the general ISM of nearby galaxies using existing facilities. Consequently, our current knowledge about the emissions processes over this frequency range is limited to the brightest star-forming regions/nuclei in the most nearby sources (e.g., Leroy et al. 2011; Clemens et al. 2008, 2010; Murphy 2013; Murphy et al. 2015; Barcos-Muñoz et al. 2015), providing no information on how the situation may change in drastically different ISM conditions (e.g., Tabatabaei et al. 2018) that may be more representative of those in high-redshift galaxies, where we have to rely on globally integrated measurements.

- **Non-Thermal Synchrotron Emission:** At ~GHz frequencies, radio emission from galaxies is dominated by non-thermal synchrotron emission resulting, indirectly, from star formation. Stars more massive than $\sim 8\,M_{\odot}$ end their lives as core-collapse supernovae, whose remnants are thought to be the primary accelerators of cosmic-ray (CR) electrons, giving rise to the diffuse synchrotron emission observed from star-forming galaxies. Thus, the synchrotron emission observed from galaxies provides a direct probe of the still barely understood relativistic (magnetic field + CRs) component of the ISM. As illustrated in Figure 1, the synchrotron component has a steep spectral index, typically scaling as $S_\nu \propto \nu^{-0.83}$ with a measured rms scatter of 0.13 (Niklas et al. 1997). By covering a frequency range spanning $1.2 - 116$ GHz, the ngVLA will be sensitive to CR electrons spanning an order of magnitude in energy (i.e., $\sim 1 - 30$ GeV), including the population that may drive a dynamically-important CR-pressure term in galaxies (e.g., Socrates et al. 2008). Further, the ngVLA will allow for investigations of the radio spectra of galaxies that are not self-similar across a range of physical scales as the injection of fresh CRs are able to modify the spectra locally.

- **Free-Free Emission:** The same massive stars whose supernovae are directly tied to the production of synchrotron emission in star-forming galaxy disks are also responsible during their lifetime for the creation of HII regions. The ionized gas produces free-free emission, which is directly proportional to the production rate of ionizing (Lyman continuum) photons and optically-thin at radio frequencies. In contrast to optical recombination line emission, no hard-to-estimate attenuation term is required to link the free-free emission to ionizing photon rates, making it an ideal, and perhaps the most reliable, measure of the current star formation in galaxies. Unlike non-thermal synchrotron emission, free-free emission has a relatively flat spectral index, scaling as $S_\nu \propto \nu^{-0.1}$. Globally, free-free emission begins to dominate the total radio emission in normal star-forming galaxies at $\gtrsim$30 GHz (e.g., Condon 1992; Murphy et al. 2012), exactly the frequency range for which the ngVLA will be delivering an order of magnitude improvement compared to any current or planned facility.

- **Thermal Dust Emission:** At frequencies $\gtrsim$100 GHz, (cold) thermal dust emission on the Rayleigh-Jeans portion of the galaxy far-infrared/sub-millimeter spectral energy distribution can begin to take over as the dominant emission component for regions within normal star-forming galaxies. This in turn provides a secure handle on the cold dust content in galaxies, which dominates the total dust mass. For a fixed gas-to-dust ratio, the total dust mass can be used to infer a total ISM mass (e.g., Heiles et al. 1988; Dame et al. 2001; Scoville et al. 2016). Given the large instantaneous bandwidth offered by the ngVLA, approximately an order of magnitude increase in mapping speed at 100 GHz compared to ALMA (Carilli 2017), such observations will simultaneously provide access to the $J = 1 \rightarrow 0$ line of CO revealing the molecular gas fraction for entire disks of nearby galaxies. Alternatively, combining HI observations (also obtained with the ngVLA) with $J = 1 \rightarrow 0$ CO maps, one can instead use the thermal dust emission to measure the spatially varying gas-to-dust ratio directly.

- **Anomalous Microwave Emission (AME):** In addition to the standard Galactic foreground components described above, an unknown component has been found to dominate over these at microwave frequencies between $\sim 10 - 90$ GHz, and is seemingly correlated with 100 μm thermal dust emission. Cosmic microwave background (CMB) experiments were the first to discover the presence of AME (Kogut et al. 1996; Leitch et al. 1997), whose origin still remains unknown (see Dickinson et al. 2018, for a review). Its presence as a foreground is problematic as the precise characterization and separation of foregrounds remains a major challenge for current and future CMB experiments (e.g., BICEP2/Keck Collaboration et al. 2015; Planck Collaboration et al. 2016). At present, the most widely accepted explanation for AME is the spinning dust model (Erickson 1957; Draine & Lazarian 1998; Planck Collaboration et al. 2011; Hensley & Draine 2017) in which rapidly rotating very small grains, having a nonzero electric dipole moment, produce the observed microwave emission. The increased sensitivity and mapping speed of the ngVLA will allow for an unprecedented investigation into the origin and prominence of this emission component both within our own galaxy and others, ultimately helping to improve upon the precision of future CMB experiments.

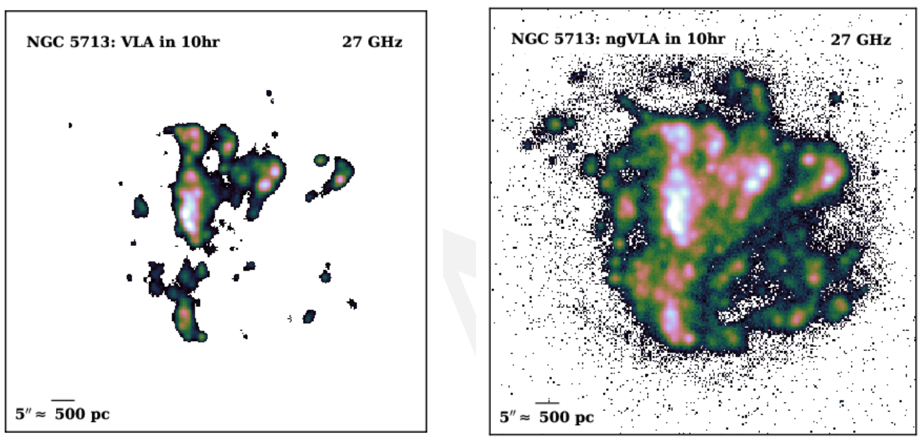

Figure 2. Both panels show a model 27 GHz free-free emission image of NGC 5713 ($d_L \approx 21.4$ Mpc, SFR $\approx 4\,M_\odot\,\mathrm{yr}^{-1}$) based on an existing H$\alpha$ narrow band image at its native ($\approx 1''$) angular resolution taken from SINGS (Kennicutt et al. 2003). The left and right panels indicate the emission that would be detected at the 3σ level after a 10 hr on-source integration time using the current VLA in C-configuration ($1\sigma \approx 1.5\,\mu\mathrm{Jy\,bm^{-1}}$) and the ngVLA with a $1''$ sculpted beam ($1\sigma \approx 0.17\,\mu\mathrm{Jy\,bm^{-1}}$). In a relatively modest integration, the ngVLA is able to recover a significant fraction of star formation activity that is completely missed by the VLA.

3. Robust Mapping of Star Formation within Nearby Galaxies on a Range of Physical Scales

For a proper decomposition of the radio continuum emission into its component parts, one needs to have spectral coverage at frequencies low enough (i.e., < 10 GHz) to be dominated by the non-thermal, steep spectrum component, having a spectral index of -0.83 (Condon 1992; Niklas et al. 1997; Murphy et al. 2011) and at frequencies high enough (i.e., > 50 GHz) where the emission becomes completely dominated by thermal emission, having a spectral index of -0.1. Given the potential for a significant contribution from AME (e.g., Murphy et al. 2010, 2018; Scaife et al. 2010; Hensley et al. 2015), peaking at frequencies $\sim 20-40$ GHz, coarse coverage spanning that spectral region is critical to account for such a feature. To date, the shape of the AME feature is largely unconstrained, and has not been carefully measured in the ISM of extragalactic sources. This is largely due to the insensitivity of current facilities to conduct a proper search for AME in nearby galaxies and map the feature with enough frequency resolution to provide useful constraints on its shape.

Broadband imaging spanning the full ngVLA frequency range of 1.2 − 116 GHz will therefore be extremely powerful to properly decompose radio continuum emission from galaxies into its constituent parts. Additionally having frequency coverage below 8 GHz provides sensitivity to free-free absorption, which is common in nearby luminous infrared galaxies (e.g., Condon et al. 1991; Clemens et al. 2010; Barcos-Muñoz et al. 2015). For individual (ultra compact) HII regions, the turnover frequency can be as high as ≈20 GHz (Murphy et al. 2010). A fundamental goal of the ngVLA will be to produce star formation maps for a large, heterogenous samples of nearby galaxies at ≈1″ resolution. This will deliver Hα-like images that optical astronomers have relied on heavily for decades without having the additional complications of extinction and contamination by nearby [NII] emission, which make such images challenging to interpret.

By achieving arcsecond-like resolution that is commensurate with ground-based optical facilities, the ngVLA will be able to probe ≈100 pc scales out to the distance of Virgo (the nearest massive cluster at $d \approx 16.6$ Mpc), which are the typical sizes of giant molecular clouds (GMCs) and giant HII regions. At an rms sensitivity of 0.15 μJy bm^{-1} at 27 GHz, such radio maps will reach a sensitivity espressed in terms of star formation rate (SFR) density of $\approx 0.005\,M_\odot\,\mathrm{yr}^{-1}\mathrm{kpc}^{-2}$, matching the sensitivity of extremely deep Hα images such as those included in the Local Volume Legacy survey (Kennicutt et al. 2008). An example of this is illustrated in Figure 2 where an existing Hα narrow band image taken from SINGS (Kennicutt et al. 2003) was used to create a model 27 GHz free-free emission map at 1″ resolution for the nearby star-forming galaxy NGC 5713. With a 10 hr integration the ngVLA will be able to map the entire disk of NGC 5713 down to an rms of ≈0.15 μJy bm^{-1} (≈35 mK). A comparison of what can currently be delivered with the VLA for the same integration time is also shown, indicating that only the brightest star-forming peaks are able to be detected. To make a map to the same depth using the current VLA would take $\gtrsim$800 hr! This is the same amount of time it would take to roughly survey $\gtrsim$80 galaxies with the ngVLA.

Using the same data, but applying a different imaging weighing scheme to create finer resolution maps (i.e., 0.″1, or even higher for brighter systems), similar multi-frequency radio continuum analyses can be performed for discrete HII regions and SNRs to complement high-resolution, space-based optical/NIR observations (e.g., *HST*, *JWST*, *WFIRST*, etc.). At an angular resolution of 0.″1, the data would sample ≈10 pc scales in galaxies out to the distance of Virgo to resolve and characterize (e.g., size, spectral shape, density, etc.) discrete HII regions and SNRs with a sensitivity to diffuse free-free emission corresponding to a SFR density of $\approx 0.5\,M_\odot\,\mathrm{yr}^{-1}\mathrm{kpc}^{-2}$.

This is a transformational step for studies of star formation in the local universe covering a large, heterogeneous set of astrophysical conditions. This statement is independent of the fact that with such observations using the ngVLA, having its wide-bandwidth, a number of RRL's will come for free (see Balser et al. 2018, in this Volume) The detection of such lines (individually or through stacking), coupled with the observed continuum emission, can be used to quantify physical conditions for the HII regions such as electron temperature. It is without question that the ngVLA will make radio observations a critical component for investigations carried out by the entire astronomical community studying star formation and the ISM of nearby galaxies.

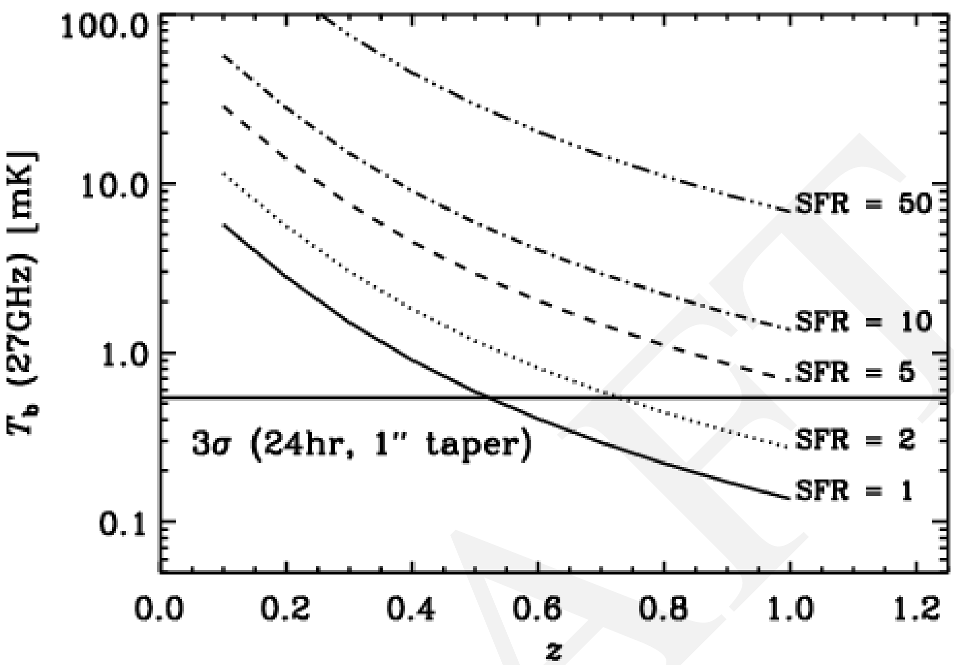

Figure 3. Observed 27 GHz brightness temperature plotted against redshift indicating the expected brightness temperature of an 4 kpc disk galaxy forming stars at a rate of 1, 2, 5, 10, and 50 $M_\odot\,\mathrm{yr}^{-1}$. Given the current sensitivity specifications, by tapering to a 1″ synthesized beam, the ngVLA will have enough brightness temperature sensitivity to resolve a Milky Way like galaxy forming stars at a rate of a $\sim 3\,M_\odot\,\mathrm{yr}^{-1}$ out to $z \sim 1$ after a 24 hr integration. Using the existing VLA, the detection of such a galaxy would take $\gtrsim$2000 hr!

4. A Robust Star Formation Indicator at All Redshifts

While deep field surveys aimed at studying the cosmic star formation activity at high redshifts is the focus of another chapter in this volume (i.e., Barger et al. 2018), we briefly describe what the ngVLA can do for studies of star formation out to moderate redshifts (i.e., $z \lesssim 1$). With the increased collecting area and bandwidth of the ngVLA, one would be able to measure and resolve rest-frame 60 GHz emission from a Milky Way like galaxy out to $z \sim 1$ forming stars at rates of $\sim 3\,M_\odot\,\mathrm{yr}^{-1}$ after a 24 hr integration. This is illustrated in Figure 3 which shows the observed 27 GHz brightness temperature of 4 kpc diameter disk galaxies with a range of SFRs. We note that a choice of 4 kpc for a typical disk diameter may be slightly conservative, given that the 10 GHz sizes found for μJy sources at $z \sim 1$ in deep VLA observations of GOODS-N are reported to be ~ 1.2 kpc (Murphy et al. 2017). The $3\,\sigma$ 27 GHz brightness temperature rms of the ngVLA tapered to a 1″ synthesized beam is based on the updated sensitivities given in (Selina & Murphy 2017)[1]. Accordingly, such observations provide highly robust extinction-free measurements of SFRs for comparison with other optical/UV diagnostics to better understand how extinction on both galactic scales and within individual star-forming regions, evolves with redshift. By coupling these higher frequency observations with those at lower radio frequencies one can accurately measure radio spectral indices as a function of redshift to better characterize thermal and non-thermal energetics independently. This therefore enables one to determine if these physically distinct components remain in rough equilibrium with one another or if there are changes which in turn affects the global star formation activity as a function of look-back time.

5. Uniqueness of ngVLA Capabilities

While the VLA has frequency coverage up to 50 GHz, it lacks the higher frequencies ($\gtrsim$ 50 GHz) necessary to measure the location where the radio spectrum is completely dominated by free-free emission and/or properly constrain the spectral shape of AME. This is required to robustly account for the energetic contributions of each emission component to the total radio continuum emission of star-forming galaxies. Furthermore, at the top end of the ngVLA frequency range, cold thermal dust emission associated with the molecular ISM may also be detectable at low surface brightness levels, which can be characterized by a rising spectrum. Perhaps most importantly, the lack of sensitivity by the VLA and other telescopes (e.g., ALMA, NOEMA, etc.) makes such continuum mapping for entire galaxies, rather than just the brightest HII regions within them, impossible, requiring the factor of $\gtrsim 10\times$ improvement in sensitivity afforded by the ngVLA. It is only with the ngVLA that the full potential of the radio continuum spectrum can be used as a tool to properly constrain the various energetic processes that power its emission for a broad range of heterogeneous conditions in galaxies.

6. Synergies at Other Wavelengths

Nearby galaxies provide our only laboratory for understanding the detailed physics of star formation and AGN activity across much larger ranges of physical conditions than offered by our own Milky Way. They are the workhorses for testing and applying physical models of star formation and their associated feedback processes that are used in galaxy evolution models to explain statistical observations for large populations of galaxies at high redshifts, for which it is impossible to conduct the detailed astrophysical experiments described here. Consequently, the transformational set of observations enabled by the ngVLA, and discussed in this chapter, will illuminate the relation between thermal and non-thermal energetic processes in the ISM and be highly synergistic with observations from shorter wavelength ground- and space-based telescopes that have access to large numbers of other diagnostic (line and continuum imaging) that may be difficult to interpret due to extinction at both low and high redshift. The same can be said for synergy with longer wavelength, far-infrared telescopes that will provide access to dust continuum and fine structure line emission that can be used to

[1] http://ngvla.nrao.edu/page/refdesign

characterize the cold/warm neutral phase of the ISM, but lack the angular resolution necessary to study discrete ($\gtrsim$ 10 pc) star-forming regions in large samples of galaxies.

References

Barcos-Muñoz, L., Leroy, A. K., Evans, A. S., et al. 2015, ApJ, 799, 10

Barger, A., Kohno, K., Murphy, E. J., et al., 2018, 2018, ASP Monograph 7, Title of the Book, ed. E. Murphy (San Francisco, CA: ASP)

Balser, D. S., Anderson, L. D., Bania, T. M., et al. 2018, 2018, ASP Monograph 7, Title of the Book, ed. E. Murphy (San Francisco, CA: ASP)

BICEP2/Keck Collaboration, Planck Collaboration, Ade, P. A. R., et al. 2015, Physical Review Letters, 114, 101301

Carilli, C., 2017, ngVLA Memo #12

Clemens, M. S., Vega, O., Bressan, A., et al. 2008, A&A, 477, 95

Clemens, M. S., Scaife, A., Vega, O., & Bressan, A. 2010, MNRAS, 405, 887

Condon, J. J., Huang, Z.-P., Yin, Q. F., & Thuan, T. X. 1991, ApJ, 378, 65

Condon, J. J. 1992, ARA&A, 30, 575

Dame, T. M., Hartmann, D., & Thaddeus, P. 2001, ApJ, 547, 792

Dickinson, C., Ali-Haïmoud, Y., Barr, A., et al. 2018, NewAR, 80, 1

Draine, B. T., & Lazarian, A. 1998, ApJ, 494, L19

Erickson, W. C. 1957, ApJ, 126, 480

Heiles, C., Reach, W. T., & Koo, B.-C. 1988, ApJ, 332, 313

Hensley, B., Murphy, E., & Staguhn, J. 2015, MNRAS, 449, 809

Hensley, B. S., & Draine, B. T. 2017, ApJ, 836, 179

Kennicutt, Jr., R. C., Armus, L., Bendo, G., et al. 2003, PASP, 115, 928

Kennicutt, R. C., Jr., Lee, J. C., Funes, J. G., et al. 2008, ApJS, 178, 247-279

Kogut, A., Banday, A. J., Bennett, C. L., et al. 1996, ApJ, 460, 1

Leroy, A. K., Evans, A. S., Momjian, E., et al. 2011, ApJ, 739, L25

Leitch, E. M., Readhead, A. C. S., Pearson, T. J., & Myers, S. T. 1997, ApJ, 486, L23

Murphy, E. J., Helou, G., Condon, J. J., et al. 2010a, ApJ, 709, L108

Murphy, E. J., Condon, J. J., Schinnerer, E., et al. 2011, ApJ, 737, 67

Murphy, E. J., Bremseth, J., Mason, B. S., et al. 2012, ApJ, 761, 97

Murphy, E. J. 2013, ApJ, 777, 58

Murphy, E. J., Dong, D., Leroy, A. K., et al. 2015, ApJ, 813, 118

Murphy, E. J., Momjian, E., Condon, J. J., et al. 2017, ApJ, 839, 35

Murphy, E. J., Linden, S. T., Dong, D., et al. 2018, ApJ, in press (arXiv:1805.05965)

Murphy, T., Cohen, M., Ekers, R. D., et al. 2010b, MNRAS, 405, 1560

Niklas, S., Klein, U., & Wielebinski, R. 1997, A&A, 322, 19

Planck Collaboration, Ade, P. A. R., Aghanim, N., et al. 2011, A&A, 536, A20

Planck Collaboration, Adam, R., Ade, P. A. R., et al. 2016, A&A, 586, A133

Scaife, A. M. M., Nikolic, B., Green, D. A., et al. 2010, MNRAS, 406, L45

Scoville, N., Sheth, K., Aussel, H., et al. 2016, ApJ, 820, 83

Selina, R. and Murphy, E. J., 2017, ngVLA Memo #17

Socrates, A., Davis, S. W., & Ramirez-Ruiz, E. 2008, ApJ, 687, 202-215

Tabatabaei, F. S., Minguez, P., Prieto, M. A., & Fernández-Ontiveros, J. A. 2018, Nature Astronomy, 2, 83

Science with a Next-Generation Very Large Array
ASP Conference Series, Monograph 7
Eric J. Murphy, ed.

DRAFT EDITION

Radio Recombination Lines from H II Regions

Dana S. Balser,[1] L. D. Anderson,[2], T. M. Bania,[3] John M. Dickey,[4] D. Anish Roshi,[1] Trey V. Wenger,[5] and T. L. Wilson[6]
[1]*National Radio Astronomy Observatory, Charlottesville, VA, USA;* dbalser@nrao.edu, aroshi@nrao.edu

[2]*West Virginia University, Morgantown, WV, USA;* loren.anderson@mail.wvu.edu

[3]*Boston University, Boston, MA, USA ;* bania@bu.edu

[4]*University of Tasmania, Hobart, TAS, Australia;* John.Dickey@utas.edu.au

[5]*University of Virginia, Charlottesville, VA, USA ;* tvw2pu@virginia.edu

[6]*Max-Planck-Institut für Radioastronomie, Bonn, Germany;* twilson@mpifr-bonn.mpg.de

Abstract.
The ngVLA will create a Galaxy-wide, volume-limited sample of H II regions; solve some long standing problems in the physics of H II regions; and provide an extinction-free star formation tracer in nearby galaxies.

1. Introduction

Here we discuss three scientific areas that could be revolutionized by ngVLA observations of radio recombination line (RRL) and continuum emission from H II regions: Galactic structure, H II region physics, and star formation in nearby galaxies.

H II regions are zones of ionized gas surrounding recently-formed high-mass OB-type stars. They are the archtypical tracer of spiral structure. Since they are young (< 10 Myr), their chemical abundances represent Galactic abundances today, and reveal the effects of billions of years of Galactic chemical evolution. H II regions are often part of a high-mass star formation complex that consists of a thin neutral photodissociation region (PDR) between a hot ($\sim 10^4$ K) H II region and dense, cool ($\sim 10 - 100$ K) molecular material from which the stars were formed.

H II regions are the brightest objects in the Milky Way at infrared and mm wavelengths and can be detected across the Galaxy. They are characterized in the infrared by $\sim 20\,\mu$m emission from stochastically heated small dust grains mixed with the ionized gas surrounded by $\sim 10\,\mu$m emission from polycyclic aromatic hydrocarbon (PAH) molecules located in the PDR (Anderson et al. 2014). The ionized gas produces bright, free-free (thermal) radio continuum emission that is coincident with the $\sim 20\,\mu$m infrared emission. When free electrons recombine and cascade to the ground state they produce recombination line emission which is found at radio wavelengths for the higher principal quantum number levels (n > 50). Currently, only emission from hydrogen and helium is detected in H II regions at radio wavelengths, but heavier elements (e.g., carbon) are detected in the denser, cooler PDRs (Wenger et al. 2013).

RRLs are an excellent, extinction-free diagnostic of H II regions. Unlike radio continuum emission, they uniquely probe the thermal emission and therefore unambiguously identify an H II region. The RRL parameters alone provide information about H II region kinematics (Anderson et al. 2012), turbulent motions (Roshi 2007), and He/H abundance ratios (Balser 2006). Measuring the RRL and continuum emission together allows the calculation of many physical H II region properties: electron (thermal) temperature, rms electron density, the H-ionizing stellar luminosity (number of OB-type stars), etc. (Gordon & Sorochenko 2009).

The main limitation of using RRLs to probe Galactic structure and star formation compared to similar tracers at optical or infrared wavelengths is that they have much lower intensities. This is particularly an issue in external galaxies. For example, RRL emission has been primarily detected from nearby starburst galaxies powered by massive young star clusters. Recently, however, RRL emission was detected in the normal galaxies M51 and NGC 628 at centimeter wavelengths (Luisi et al. 2018). Moreover, for some radio facilities the spatial resolution is not sufficient to resolve individual H II regions, which limits the analysis. The ngVLA will provide both the sensitivity and spatial resolution to remedy these problems and place RRLs as an H II region diagnostic on par with, for example, Hα.

2. Galactic Structure

The ngVLA is necessary to create a Galaxy-wide, volume-limited sample of H II regions. Since radio waves penetrate the dust located within the Galactic disk, an H II region map of the entire Milky Way is possible at these wavelengths. This is needed to understand the global properties of the Milky Way, and to compare its star formation to that of external galaxies. There is strong evidence that we have only discovered about 25% of the H II regions in the Milky Way, which impedes our understanding of Galactic structure and Galactic chemical evolution (Anderson et al. 2014).

The implications for Galactic structure studies using RRLs were recognized shortly after their discovery in 1965 and prompted large-scale H II region surveys (Wilson et al. 1970; Reifenstein et al. 1970). RRLs measure the systemic velocity of an H II region and therefore their motion around the center of the Galaxy. Using a rotation curve model together with the velocity yields the Heliocentric distance of the H II region. Distances computed in this way are known as "kinematic distances." Improvements in receiver performance resulted in follow-up surveys in the 1980s that increased the number of sources (Wink et al. 1983; Caswell & Haynes 1987; Lockman 1989). These RRL surveys, however, were limited in sensitivity and had inaccurate distance determinations. A third generation of Galactic H II region discovery surveys (HRDS) is almost complete using primarily the Green Bank Telescope (GBT) in the Northern sky (Bania et al. 2010) and the Australia Telescope Compact Array (ATCA) in the Southern sky (Brown et al. 2017). The HRDS has doubled the number of known H II regions. It has the sensitivity to detect all nebulae ionized by an O-type star out to a distance of 20 kpc from the Sun. This has primarily been achieved by the flexibility of spectrometers that can simultaneously observe multiple RRLs which can be averaged together to increase the signal-to-noise ratio (SNR). Maser parallax distances together with better models of Galactic rotation have improved our understanding of kinematic distance determinations (Reid et al. 2014; Wenger et al. 2018).

These new surveys have made several discoveries about the morphological and chemical structure of the Milky Way. *Cold H I gas and molecular clouds are often used to define spiral structure but such tracers are not always associated with high-mass star formation* (Anderson et al. 2009). Therefore, Koo et al. (2017) used H I surveys together with the HRDS to characterize the spiral structure in the outer Galaxy and found that a four-arm spiral model with pitch angle of 12° was a good fit to the data. Yet the number of H II regions sampling the outer-most spiral arms is limited. For example, deep RRL observations with the GBT were only able to detect a handful of H II regions in the outer Scutum-Centaurus arm (Armentrout et al. 2017). (N.B., the RRL spectral sensitivity of the Jansky Very Large Array (JVLA) is comparable to the GBT.)

For H II regions in thermal equilibrium the nebular electron temperature is determined by the abundance of the coolants (O, N, and other heavy elements). Balser et al. (2015) used this to derive electron temperatures for a sub-set of the HRDS H II regions and used them to derive the nebular [O/H] abundances. Figure 1 shows the resulting metallicity map and reveals the chemical structure of the Milky Way disk. The radial metallicity gradient is obvious from this map and has been detected before, but there is also azimuthal structure that was revealed for the first time. This may be due to radial mixing from the Galactic Bar whose major axis is aligned toward an azimuth of about 30°. The sample is limited, however, since only the most accurate RRL and continuum data is selected. More sources are required to better characterize this chemical structure and therefore constrain the physical mechanisms that might be in play. The ngVLA will add thousands of sources to Figure 1 (see below) and reveal any detailed metallicity structure across the Galactic disk.

The *WISE* catalog of Galactic H II regions contains about 8000 objects identified by their mid-infrared and radio properties as H II region (Anderson et al. 2014). Currently only $\sim$ 2000 sources in this catalog are known H II regions with RRL or Hα emission. Of the remaining sources $\sim$ 2000 have spatially coincident radio continuum emission and are very likely H II regions, and $\sim$ 4000 are radio quiet at the sensitivity limits of existing radio continuum surveys. There is some evidence that the radio quiet sources in the *WISE* H II region catalog are bona fide H II regions (Armentrout et al. 2018, in prep.). Because of their extreme luminosities, H II regions are essential for computing extragalactic star formation rates in combination with infrared and other radio data. The HRDS, when complete, will be the first survey to detect all H II regions created by at least one O-type star, but there will remain thousands of likely H II regions whose RRL emission cannot be detected with extant facilities.

The ngVLA will have the sensitivity to create a Galaxy-wide, volume-limited sample of H II regions. The optimal frequency range is 4-12 GHz (ngVLA band 2), where classical H II regions are optically thin, in LTE, and many adjacent transitions can be averaged to increase the SNR. The HRDS spectral sensitivity at these frequencies is $\sim$ 1 mJy. To detect all sources in the *WISE* Galactic H II region catalog requires a spectral sensitivity of $\sim$ 3 μJy (Anderson et al. 2014). This assumes a radio continuum flux density of 0.2 mJy at 21 cm, a SNR of 5, an optically thin nebula, and a line-to-continuum ratio of 0.1 at 8 GHz (e.g., Brown et al. 2017). Using the ngVLA spectral

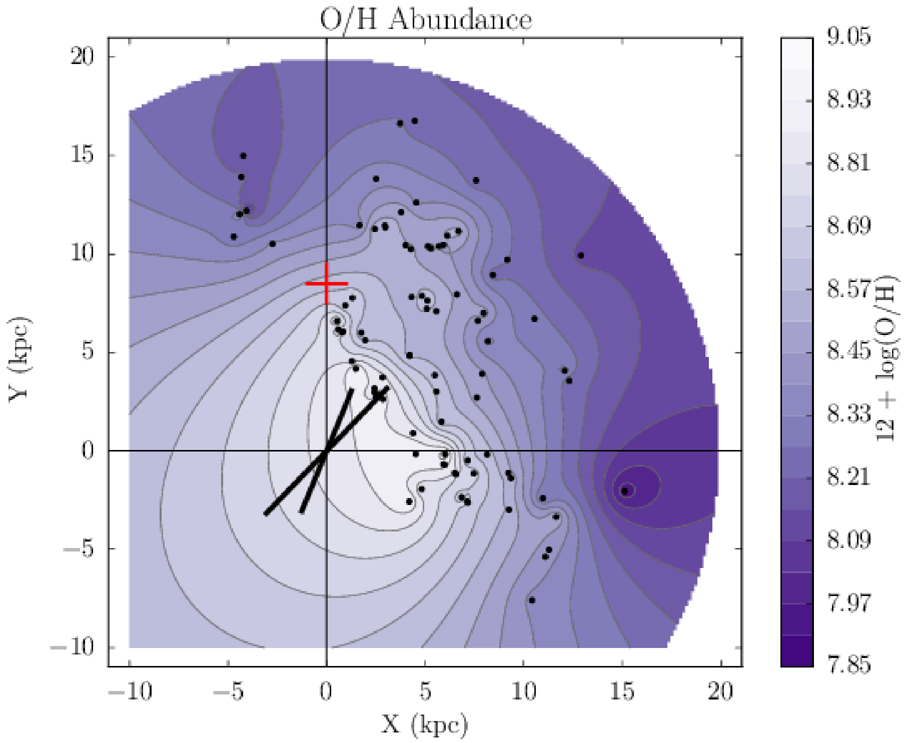

Figure 1. Face-on Galactic [O/H] abundance ratio image using Kriging to interpolate between the discrete H II region values taken from Balser et al. (2015). The points indicate the location of the discrete H II regions. The solid lines intersect at the Galactic Center. The red lines mark the location of the Sun. The thick lines correspond to the central locii of the putative "short" and "long" bars.

sensitivity from Selina & Murphy (2017) for a 50 mas beam[1], the weakest sources in the *WISE* catalog would require 15 hr of integration time. The ngVLA sensitivity will be less for sources that are resolved by the longest baselines. At a distance of 20 kpc an H II region with a physical size of 1 pc has an angular size of 10″. Since the ngVLA core of antennas will contain a large fraction of the collecting area the sensitivity should not be significantly reduced. In principle, the GBT could fill in the missing flux density. Phased array feeds in the central ngVLA core would increase the efficiency. Such a survey would complement MeerGAL, a high frequency (~ 10 GHz) survey of the Galactic plane with MeerKat in the Southern sky.

A Galactic H II region pointed survey toward *WISE* H II region candidates may be possible with the *James Webb Space Telescope* (JWST), which will be sensitive to wavelengths from 0.6 – 28μm, using collisonally excited lines (CELs) in the mid-infrared. RRLs provide a more direct measure of the ionizing flux, but CELs probe the hardness of the radiation field. Most optical and near-infrared studies, however, trace

[1]The ngVLA spectral rms is 37.3 μJy beam^{-1} for a beam size of 50 mas at 8 GHz with an integration time of 1 hr and a FHWM line width of 10 km s^{-1}.

the kinematic and chemical structure of stars. Recent surveys such as APOGEE, GAIA-ESO, LAMOS, and RAVE are sampling hundreds of thousands of stars and will soon have accurate distances from GAIA. But these surveys do not probe the gas component of the Milky Way or very far into the disk due to extinction by dust. Understanding the morphological and chemical structure of both the stars **and** the gas is critical to constrain Galactic formation and evolution models (e.g., Kubryk et al. 2013).

3. H II Region Physics

The ngVLA could solve some long standing problems in the physics of H II regions including, for example, constraining the collision rates from free electrons, characterizing temperature fluctuations, and understanding the role of magnetic fields within H II regions.

Recombination lines from hydrogen and helium at radio wavelengths are strongly affected by collisions from free electrons and therefore accurate collision rates are important for predicting the line opacity. Under some physical conditions the opacities can vary by as much as a factor of five depending on the rates used (F. Guzmán, private comm.; also see Guzmán et al. 2016). Accurate measurements of the RRL intensity ratio over a frequency range wide enough for the opacity to vary significantly would provide vital observational constraints for the collision rates. For example, the flexible spectrometer on the ATCA allows RRLs to be observed simultaneously from 6-12 GHz so that we can begin to constrain the atomic physics (see Figure 2). We are working on a detailed strategy to detect each RRL transition with a high SNR over a variety of physical conditions. This will require the sensitivity of the ngVLA.

One of the key problems in the physics of ionized nebulae is that abundances derived from recombination lines (RLs) are significantly larger, by as much as a factor of two, than those derived from CELs (Garcá-Rojas & Esteban 2007). These differences can be explained by temperature fluctuations in the ionized gas. The concept of temperature fluctuations was developed by Peimbert (1967) to explain how electron temperatures derived from RLs were different than those derived from CELs. Temperatures are also expected to increase at the H II region boundary because of photon hardening. That is, photons with energies of 20 eV have a smaller absorption cross section so they can reach the nebular boundary where they are absorbed and thus raise the electron temperature. Wilson et al. (2015) suggested that optical observations produced different electron temperature profiles in the Orion nebula compared with RRLs due to the effects of dust. The radio observations were performed with the GBT instead of the JVLA because Orion is extended, but to probe small-scale structure requires better spatial resolution. The smallest scales over which the temperatures vary is not known. Therefore to measure both the small and large-scale temperature variations in H II regions requires calculating the radio line-to-continuum ratio over a wide range of spatial scales with high sensitivity. This may be possible by combing data from the JVLA and GBT, but the systematic errors using this method may be too large. The internal calibration with the ngVLA would provide a more accurate measure of the electron temperature over a wider range of spatial scales with significantly better sensitivity.

Magnetic fields may play an important role in the formation of stars and the Zeeman effect is the only method that directly measures the *in-situ* magnetic field strength, but it is a challenging experiment. Most of the work thus far has probed molecular (e.g., CN) or neutral (e.g, H I) components of high-mass star formation regions (Crutcher et

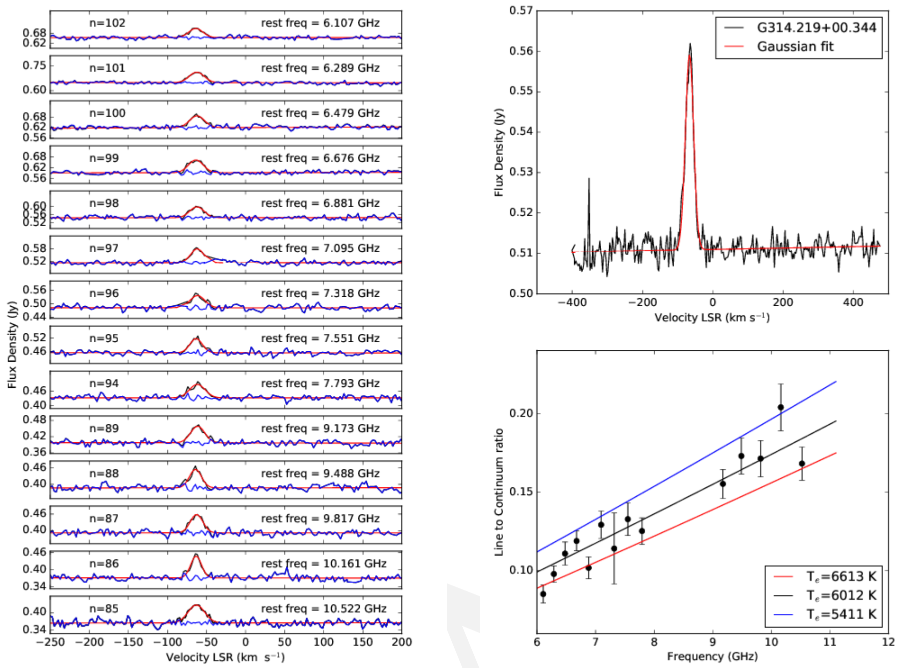

Figure 2. RRL spectra for G314.219+00.344 using the ATCA taken from Brown et al. (2017). Individual spectra (left) and an averaged spectrum (upper-right) are shown where the red curves are Gaussian fits to the data. The lower-right panel plots the line-to-continuum ratio as a function of frequency.

al. 2010). To our knowledge there has never been a Zeeman detection from RRLs (e.g., Troland & Heiles 1977), so an ngVLA detection would be the first. Such a measurement is difficult since the hydrogen RRL width ($\sim$ 25 km s^{-1}) is broader than the Zeeman splitting and therefore a very high SNR is required. High spatial resolution is necessary since magnetic field variations have been detected and will be averaged over a large beam. Since many bright H II regions are extended, however, the larger spatial scales, or shorter baselines for an interferometer, must be sampled.

We estimate the sensitivity of the ngVLA for Zeeman measurements in H II regions by assuming a hydrogen RRL intensity of 50 mJy beam^{-1} and a line width of 30 km s^{-1} observed with a resolution of 1 arcsec at 8 GHz. Using the ngVLA spectral sensitivity from Selina & Murphy (2017) for a 1 arcsec beam and Equation 2 from Troland & Heiles (1982), we estimate a 3 σ limiting line-of-sight magnetic field strength of 295 μG in 1 hr of integration time. This assumes we are able to average 20 RRLs with six spectral channels across the FWHM line width.

4. Star Formation in Nearby Galaxies

Using RRLs the ngVLA will provide an extinction-free star formation tracer in nearby galaxies that is comparable to Hα for the sensitivity and spatial resolution afforded by existing optical instruments. That is particularly important in extreme environments with clusters of massive stars since star formation may proceed differently in these objects. These environments are, moreover, often opaque at ultraviolet, optical, or near infrared wavelengths due to dust.

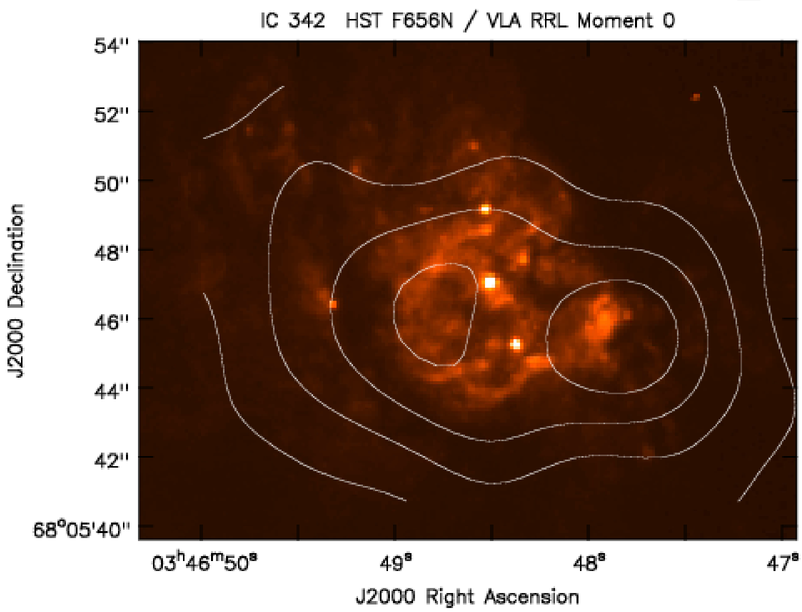

Figure 3. Star formation diagnostics in the IC 342 nuclear region taken from Balser et al. (2017). Shown in color is the HST Hα (F656N) image together with the JVLA Ka-band RRL-integrated intensity map in contours. The contour levels are 0.2, 0.4, 0.6, and 0.8 times the peak intensity (0.1324 Jy beam^{-1} km s^{-1}). The JVLA synthesized beam size is $4\farcs5 \times 4\farcs5$.

Radio continuum measurements are excellent probes of these regions since they can penetrate the gas and dust that surrounds the young star clusters. Observations at multiple frequencies measure the thermal emission associated with H II regions and non-thermal emission related to supernova remnants (e.g., Turner & Ho 1983; Johnson et al. 2004). Radio recombination lines are fainter than radio continuum emission, but they directly measure the thermal emission and yield important information about the dynamics of these star clusters. Anantharamaiah et al. (2000) combined both RRL and continuum data at several different frequencies to constrain models of these young massive star clusters. Technical improvements provided by the JVLA increased the sensitivity of such work by almost an order of magnitude (Kepley et al. 2011), and enabled RRL studies of less massive star clusters. For example, Balser et al. (2017) detected RRL emission in IC 342 for the first time and revealed thermal emission to the east and west of the nuclear star cluster that was associated with giant molecular clouds (see Figure 3). The best fit model is a collection of many hundreds of compact ($\sim$ 0.1 pc) H II regions ionized by an equivalent of $\sim$ 2000 O6 stars. Even with the increased sensitivity of the JVLA these observations are challenging and we do not detect RRL emission in gas located beyond the most central regions. Better sensitivity over many spatial scales is required. Also, Anantharamaiah et al. (2000) showed that because of free-free opacity effects the RRL are brighter at higher frequencies and therefore it is important to observe RRLs over a large range of frequencies (e.g., 1-100 GHz).

The ngVLA has the required sensitivity spanning a wide range of spatial and frequency scales. Ideally, we want to resolve individual H II regions but also have the sensitivity to detect extended emission (e.g., the diffuse ionized gas). So we need to probe scales from $\sim 1 - 1000$ pc in galaxies with distances between 1-20 Mpc, or angular scales $0\farcs01 - 200''$. To estimate the required spectral sensitivity we use a model H II region. We assume a homogeneous sphere ionized by an O5 star at a distance of 2 Mpc with an electron density and temperature of 1,000 cm^{-3} and 8,000 K, respectively. Using the stellar models of Martins et al. (2005) the continuum flux density at a frequency of 5 GHz is 0.1 mJy (see appendix G.1 in Balser 1995). This continuum flux density estimate is similar to the values found in compact sources in nearby galaxies (e.g., Tsai et al. 2006). Assuming a line-to-continuum ratio of 0.1 yields a RRL intensity of 10 μJy. Using the ngVLA sensitivity from Selina & Murphy (2017) for a 50 mas beam, we estimate an integration time of 35 hr assuming a SNR of 5, a spectral resolution of 5 km s^{-1}, and averaging 20 RRLs. This is over two orders of magnitude more sensitive than our JVLA RRL observations. For an optically thin, unresolved H II region the results are not very sensitive to the electron density, electron temperature, or frequency. Moreover, the flux density only increases by approximately a factor of two for an O3 star relative to an O6 star. The integration time can therefore be approximated as $t_{\rm intg} \approx 35 * (D/2\,{\rm Mpc})^4$ hr for detecting RRL emission from H II regions ionized by a single star, where D is the distance.

The RRL data probe the ionized gas and will complement observations that sample the neutral (H I; ngVLA) and molecular (CO; ALMA, ngVLA) components to characterize these star formation complexes. Detection of submillimeter H and He RRLs with ALMA trace the hardness of the radiation field, or indirectly the high-mass end of the initial mass function, in nearby massive young star clusters (e.g., see Scoville & Murchikova 2013). Similar observations with the ngVLA are possible at 3 mm assuming the ngVLA is about five times more sensitive than ALMA (A. Bolatto, private comm.). In principle the JWST Paα and ngVLA RRL intensity ratio could directly measure the dust extinction as a function of velocity.

5. Summary

The ngVLA will allow for sensitive observations of RRLs and impact the following areas:

- *Galactic Structure:* The ngVLA will have the sensitivity to create a Galaxy-wide, volume-limited sample of H II regions for the first time. This is needed to determine the global star formation properties of the Milky Way, and to better characterize both the morphological and chemical structure of the Galactic disk.

- *H II Region Physics:* The ngVLA could solve several long standing problems in H II region physics. These include discriminating between different models of the collision rates from free electrons that determine the opacity, characterizing temperature fluctuations which effect abundance determinations, and directly measuring the magnetic field strength within H II regions.

- *Star Formation in Nearby Galaxies:* The ngVLA will have both the necessary sensitivity and spatial resolution to probe star formation in a statistically significant sample of nearby galaxies. RRLs provide an extinction-free tracer of the physical conditions and dynamics of the ionized gas.

References

Anantharamaiah, K. R., Viallefond, F., Mohan, N. R. et al. 2000, ApJ, 537, 613
Anderson, L. D., Bania, T. M., Balser, D. S., & Rood, R. T. 2012, ApJ, 754, 62
Anderson, L. D., Bania, T. M., Balser, D. S., et al. 2014, ApJS, 212, 1
Anderson, L. D., Bania, T. M., Jackson et al. 2009, ApJS, 181, 255
Armentrout, W. P., Anderson, L. D., Balser, D. S. et al. 2017, ApJ, 841, 121
Balser, D. S. 1995, PhD thesis
Balser, D. S. 2006, AJ, 132, 2326
Balser, D. S., Roshi, D. A., Jeyakumar, S. et al. 2016, ApJ, 816, 22
Balser, D. S., Wenger, T. V., Anderson, L. D., & Bania, T. M. 2015, ApJ, 806, 199
Balser, D. S., Wenger, T. V., Goss, W. M., Johnson, K. E., & Kepley, A. A., 2017, ApJ, 844, 73
Bania, T. M., Anderson, L. D., Balser, D. S., & Rood, R. T. 2010, ApJ, 718, L106
Brown, C., Jordan, C., Dickey, J. M. 2017, AJ, 154, 23
Caswell, J. L., & Haynes, R. F. 1987, A&A, 171, 261
Crutcher, R. M., Wandelt, B., Heiles, C. et al. 2010, ApJ, 725, 466
Garcá-Rojas, J., & Esteban, C. 2007, ApJ, 670, 457.
Gordon, M. A., & Sorochenko, R. L. 2009, ASSL, Vol. 282, Radio Recombination Lines
Guzmán, F., Badnell, N. R., Williamns, R. J. R. et al. 2016, MNRAS, 459, 3498
Johnson, K. E., Indebetouw, R., Watson, C., & Kobulnicky, H. A. 2004, AJ, 128, 610
Kepley, A. A., Chomiuk, L., Johnson, K. E. et al. 2011, ApJ, 739, L24
Koo, B.-C., Park, G., Kim, W.-T. et al. 2017, PASP, 129, 94102
Kubryk, M., Prantzos, N., & Athanassoula, E. 2013, MNRAS, 436, 1479
Lockman, F. J. 1989, ApJS, 71, 469
Luisi, M., Anderson, L. D., Bania, T. M. et al. 2018, PASP, in press (ArXiv:1805.11460)
Martins, F., Schaerer, D., & Hillier, D. J. 2005, A&A, 436, 1049
Peimbert, M. 1967, ApJ, 150, 825
Reid, M. J., Menten, K. M., Brunthaler, A., et al. 2014, ApJ, 783, 130
Reifenstein, E. C., III, Wilson, T. L., Burke, B. F. et al. 1970, A&A, 4, 357
Roshi, D. A. 2007, ApJ, 658, L41
Scoville, N., & Murchikova, L. 2013, ApJ, 779, 75
Selina, R., & Murphy, E. 2017, ngVLA Memo 17.
Troland, T. H. & Heiles, C. 1977, ApJ, 214, 703
Troland, T. H. & Heiles, C. 1982, ApJ, 252, 179
Tsai, C.-W., Turner, J. L., Beck, S. C. et al. 2006, AJ, 132, 2383
Turner, J.L. & Ho, P.T.P. 1983, ApJ, 268, L79
Wenger, T. V., Balser, D. S., Anderson, L. D. & Bania, T. M. 2018, ApJ, 856, 52
Wenger, T. V., Bania, T. M., Balser, D. S., & Anderson, L. D. 2013, ApJ, 764, 34
Wilson, T. L., Bania, T. M., & Balser, D. S. 2015, ApJ, 812, 45
Wilson, T. L., Mezger, P. G., Gardner, F. F., & Milne, D. K. 1970, A&A, 6, 364
Wink, J. E., Wilson, T. L., & Bieging, J. H. 1983, A&A, 127, 211

Science with a Next-Generation Very Large Array
ASP Conference Series, Monograph 7
Eric J. Murphy, ed.

DRAFT EDITION

How Do Cold Gas Outflows Shape Galaxies?

Alberto D. Bolatto,[1] Lee Armus,[2] Adam K. Leroy,[3] Sylvain Veilleux,[4] Fabian Walter,[5] and Richard Mushotzky[6]

[1] *University of Maryland, Department of Astronomy, College Park, MD 20742, USA;* bolatto@astro.umd.edu

[2] *Infrared Processing and Analysis Center, California Institute of Technology, 1200 E. California Boulevard, Pasadena, CA 91125, USA;* lee@ipac.caltech.edu

[3] *Ohio State University, Department of Astronomy, Columbus, OH 43210, USA;* leroy.42@osu.edu

[4] *University of Maryland, Department of Astronomy, College Park, MD 20742, USA;* veilleux@astro.umd.edu

[5] *Max Planck Institute for Astronomy, Heidelberg, Germany;* walter@mpia.de

[6] *University of Maryland, Department of Astronomy, College Park, MD 20742, USA;* richard@astro.umd.edu

Abstract. The ngVLA will obtain breakthrough observations of the cold phases (molecular and atomic) of galactic outflows. These observations will be key to study the driving mechanisms of cold winds, the fate of the gas, the mass-loss rates, the conditions that trigger cold outflows, the fraction of gas that escapes galaxies, the effects of winds on suppressing star formation and slowing black hole growth, the statistical properties of outflows, and the relation between large scale outflows and UFOs and BAL outflows. Finally, we highlight the ngVLA complementarity with existing and planned facilities, such as ALMA/SKA, OST/SPICA, and Lynx/ATHENA.

1. The Importance of Galaxy-scale Winds

It has become increasingly clear over the last two decades that it is impossible to understand how galaxies form and evolve through cosmic time without a deeper understanding of how star formation and black hole accretion affect the growth of galaxies and the state of their gas reservoirs. The failure of both large-scale cosmological simulations and detailed physical simulations of individual galaxies to reproduce the observed characteristics of the galaxy population has driven home the point - understanding how feedback works is probably the key open question in galaxy evolution. This is intimately linked to one of the fundamental questions identified in the *"New Worlds, New Horizons"* decadal report: how do baryons cycle in and out of galaxies?

Galactic winds are thought to shape the galaxy mass function, heat the circumgalactic medium, play a critical role in quenching star formation, and pollute the intergalactic medium with heavy elements (e.g., Veilleux et al. 2005). Galaxies are not closed systems, and winds are necessary to explain chemical evolution, as well as playing a key role in shaping the disk-halo interface. The fastest and most energetic winds arise due to feedback from active galactic nuclei (AGN) or strong starbursts, while less powerful, and more localized, galactic fountains due to clustered star formation recycle material between the disk and the halo even in less active galaxies. On smaller scales, super star clusters can also drive outflows that shape their final stellar mass and affect their environment (e.g., Herrera & Boulanger 2017).

Detailed studies of nearby systems have frequently focused on the warm or hot phases of galactic winds, which are often visible in X-rays or optical emission lines. The manifestation of these hot winds can often be quite spectacular, consisting of huge, bipolar nebulae (e.g., Strickland et al. 2004), but they typically carry very little mass $M_{Xray} \sim 10^6\,\mathrm{M}_\odot$ (e.g., Lehnert et al. 1999). One of the important effects of winds is to shut down star formation by removal of gas, but this hot gas is very low density compared to the cold gas out of which young stars will ultimately form. But galactic winds are multi-phase phenomena (Figure 1). When present, colder phases, containing neutral atomic and dense molecular gas, can dominate the mass budget of the outflow (Walter et al. 2002; Rupke et al. 2005; Feruglio et al. 2010; Alatalo et al. 2011; Rupke & Veilleux 2013).

Until recently, observations of the cooler phases of galactic outflows have been hindered by a lack of sensitivity and/or spatial resolution to properly image the low surface brightness wind and unambiguously connect it to the processes in the disk that power the outflow. With Herschel, it has been possible to detect fast, dense outflows in a number of local Ultraluminous Infrared and starburst galaxies (e.g., Sturm et al. 2011; Veilleux et al. 2013). In some cases the mass outflow rates are comparable to, or larger than, the star formation rates of the galaxies themselves, suggesting a significant impact on the lifetime of the active phase. However, with Herschel it was only possible to detect the nearest, brightest sources, and the winds were nearly always unresolved. ALMA and the IRAM Plateau de Bure Interferometer are currently making important advances in finding and imaging molecular outflows (Bolatto et al. 2013a; Combes et al. 2013; Cicone et al. 2014; Sakamoto et al. 2014; García-Burillo et al. 2014; Zschaechner et al. 2016; Veilleux et al. 2017), but the resolution and surface brightness sensitivity requirements make identifying and characterizing molecular winds challenging with present-day facilities.

2. The Need for the ngVLA

The ngVLA will have the sensitivity and frequency coverage to enable a giant leap in our understanding of the cold phases of galactic winds. The ngVLA will be able to: 1) identify molecular and neutral atomic winds using sensitive, high resolution imaging, 2) characterize their mass, outflow rate, and physical state using molecular multi-line spectroscopy and 21 cm emission, 3) diagnose their fate by imaging their extent with high surface brightness sensitivity across multiple phases and providing detailed kinematics, and 4) study their physical launching mechanisms.

Imaging galactic outflows requires the combination of high spectral sensitivity, resolution, and the ability to recover a wide range of spatial scales – all things for which the ngVLA excels. Close to the source, typical column densities may correspond to optical extinction (A_V) of a few magnitudes, rapidly decaying with distance from the source as the outflow expands and gets diluted. The hydrogen column density

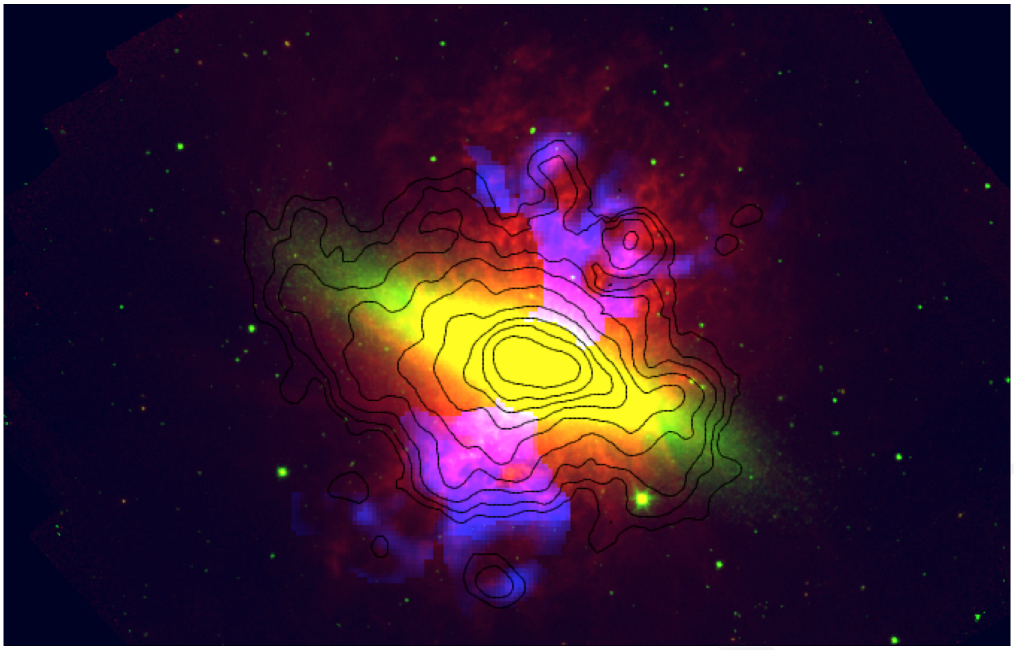

Figure 1. The cooler phases of the starburst-driven wind in the prototypical starburst M 82. The red, green, and blue colors correspond respectively to PAH emission (from IRAC 8.0 μm), the stellar component (from IRAC 3.6 μm), both from (Kennicutt et al. 2003), and HI emission kinematically identified to be part of the outflow (from Leroy et al. 2015) imaged at 24″ resolution. The black contours show the CO emission (in this case CO 2 − 1) at 20″ resolution obtained by the IRAM 30m telescope. The contours correspond to both the disk and the outflow emission (also from Leroy et al. 2015).

corresponding to $A_V \sim 1$ is N(H) $= 1.9 \times 10^{21}\,\mathrm{cm}^{-1}$ (Bohlin et al. 1978; Rachford et al. 2009). At $\lambda = 21$ cm the ngVLA is capable of attaining an atomic hydrogen column density RMS of N(H) $\sim 5.2 \times 10^{20}\,\mathrm{cm}^{-1}$ in $10\,\mathrm{km\,s}^{-1}$ in one hour, at a resolution of 1″. Therefore assuming a linewidth of 30 km/s and an integration time of 24 hours, it can detect and image atomic outflows down to N(H) $\sim 3 \times 10^{20}\,\mathrm{cm}^{-1}$ at 5σ, which corresponds to $A_V \sim 0.1$ mag in $30\,\mathrm{km\,s}^{-1}$ (equivalent to a surface density of $\Sigma_{\mathrm{HI}} \sim 1.5\,\mathrm{M}_\odot\,\mathrm{pc}^{-2}$, or a mass M(HI) $\sim 2.5 \times 10^4\,\mathrm{M}_\odot$ at D=30 Mpc).

The molecular content of outflows may decrease faster than their atomic content, as molecular cloudlets get shattered and dissociated (see, for example, Leroy et al. 2015). At $\lambda = 3$ mm the ngVLA has a line sensitivity of 10 mK in 10 km/s at a resolution of 1″. Assuming a CO $1-0$ emission with linewidth of 30 km/s, and a CO-to-H_2 factor of $X_{\mathrm{CO}} \sim 0.5 \times 10^{20}\,\mathrm{cm}^{-2}\,(\mathrm{K\,km\,s}^{-1})^{-1}$ (intermediate between Milky Way GMCs and optically thin emission, Bolatto et al. 2013a,b), the ngVLA will be capable of detecting molecular outflows down to $A_V \sim 0.01$ mag at 5σ (equivalent to $\Sigma_{\mathrm{H2}} \sim 0.15\,\mathrm{M}_\odot\,\mathrm{pc}^{-2}$, or M($\mathrm{H}_2$) $\sim 2.5 \times 10^3\,\mathrm{M}_\odot$ at D=30 Mpc) in 24 hours at 1″ resolution. ALMA is capable of comparable Rayleigh-Jeans brightness temperature sensitivities in CO $J = 3-2$. However, the factor of ~ 27 higher critical density required to excite the $J = 3-2$ transition compared to $J = 1-0$ means that only very dense molecular gas will be bright in the CO $J = 3-2$ line. As we emphasize below, the combination of the ngVLA and ALMA provides a powerful set of tools for studying a wide range of density and excitation conditions in molecular outflows.

Some of the key open questions that ngVLA observations will help answer are:

1. What are the driving mechanisms of cold winds? Mechanical feedback from supernovae (e.g., Fujita et al. 2009), radiation pressure (e.g., Murray et al. 2011), cosmic ray pressure gradients (e.g., Uhlig et al. 2012), entrainment facilitated by Kelvin-Helmholtz instabilities (e.g., Heckman et al. 2000), and direct driving by interaction with AGN jets (e.g., Wagner & Bicknell 2011) have all been proposed as ways to inject momentum in the gas. It remains unclear, however, how they combine, and which one if any dominates (Hopkins et al. 2012; Muratov et al. 2015). A combination of high-resolution and sensitivity observations of the cold phases as they are ejected are key to solve this problem. For example, it appears that radiation pressure is insufficient to explain the high-resolution properties of the NGC 253 molecular outflow (Walter et al. 2017).

2. What is the fate of the launched gas? Is molecular gas reformed in the wind? Does expelled gas change phases? Imparting momentum to molecular cloudlets without destroying them has proven difficult in numerical simulations, while at the same time it is expected that part of the hot phase outflow may cool and reform a cold phase (e.g., Thompson et al. 2016). Observations of the outflow in M 82 strongly suggest that there is conversion of molecular into neutral atomic gas as the outflowing gas progresses away from the galaxy (Leroy et al. 2015). High sensitivity, resolved imaging in neutral atomic gas and molecular tracers is needed to answer these questions.

3. What are the wind mass loss rates? What is the mass-loss to star-formation-rate ratio (the mass loading parameter)? Are mass-loading parameters and mass-loss rates as high as predicted for low-mass galaxies? These parameters are key inputs to cosmological simulations, necessary to understand the precise effects of feedback on galaxy growth. Current estimates of the efficiency with which momentum is imparted to the different gas phases, implemented as sub-grid recipes in physical galaxy simulations, suggest mass loading parameters of order $\eta \sim 10$ for massive galaxies, and as high as $\eta \sim 100$ for dwarf galaxies (Muratov et al. 2015). While higher mass galaxies are expected to retain most of their metals in their circum-galactic environment, dwarf galaxies should heavily pollute the IGM (Muratov et al. 2017). Such values of η appear to be necessary to reproduce galaxy properties in cosmological simulations. It remains unclear, however, how to precisely attain such high mass loading efficiencies in detailed simulations Kim & Ostriker (2018). Most of the mass loss is due to the denser, cold phases, likely dominated by the neutral atomic and molecular gas that is directly observable with the ngVLA. The key to measuring accurate molecular mass loss rates is an understanding of the density structure in the wind, critically dependent on observations of several molecular species in the outflowing gas. These observations require extremely high sensitivity, wide bandwidth, and the ability to spatially and kinematically map the emission from the outflow.

4. What are the conditions triggering cool outflows? Observations suggest the existence of a star formation surface density threshold for launching large outflows (e.g., Newman et al. 2012), and a similar threshold in luminosity appears to exist

for AGN-launched outflows (e.g., Veilleux et al. 2013; Wylezalek et al. 2017). Lower velocity galactic fountains and even radiation pressure-driven outflows, can also occur over extended areas of disks. Systematic demographics of the different properties of the multiphase outflows and their hosts, collected through a combination of radio and other multi-wavelength observations (see below), will provide valuable information about the conditions and triggers of outflows.

5. What fraction of the outflowing gas reaches escape velocity versus falling back and being reaccreted/recycled? Detailed simulations suggest that winds and fountains go through phases, dominated alternatively by outflow and inflow (Kim & Ostriker 2018). Observations show velocity gradients in the expelled gas, that can be interpreted in some cases as acceleration (Walter et al. 2017), or deceleration (Martini et al. 2018). Generally, recycled material may play an important role in lengthening the gas depletion timescale of galaxies (Davé et al. 2011), feeding galaxies at late cosmic times, and allowing for the exchange of processed gas between galaxies (Anglés-Alcázar et al. 2017b). Understanding the fraction of escaping gas and the relative amounts of expelled and recycled material, requires high sensitivity and high angular resolution observations of molecular and atomic gas tracers in galaxies and their circum-galactic environments.

6. Are winds only effective at suppressing the formation of stars (negative feedback), or can they also trigger star formation in galaxies? Although outflows driven by star formation or AGN are frequently invoked as mechanisms to expel gas and/or quench star formation (e.g., Alatalo et al. 2015), star formation can also be enhanced by compressive turbulence driven by the mechanical energy input of the wind (e.g., van Breugel et al. 1985; Croft et al. 2006). These positive feedback processes can also have an important effect on galaxy evolution (Silk 2013). Multi-wavelength radio techniques are particularly well suited to studying this problem, since they can be used to simultaneously image the outflowing gas and measure the gas kinematics, as well as derive the star formation rate (via the thermal free-free radio continuum emission) on sub-kpc scales.

7. How do winds affect the growth of black holes? Simulations suggest that black hole growth, particularly at early times, is limited by stellar feedback, which expels gas from galactic nuclei, limiting accretion. As a consequence, black holes can be undermassive in low-mass galaxies with respect to their high-mass counterparts, causing them to fall below the $M_{BH} - \sigma_{halo}$ relation (e.g., Anglés-Alcázar et al. 2017a). The ability of the ngVLA to resolve and measure gas content and kinematics in the innermost regions of galaxies, is key to quantifying the effects of winds on the growth of supermassive black-holes.

8. What are the statistical properties of cold winds in the universe? Are these a rare phenomenon confined to AGN and starbursts, or are they a general feature of galaxies? What is the redshift evolution of starburst- and quasar-driven winds? Observations suggest that galactic winds are ubiquitous at high redshift (e.g., Newman et al. 2012). We know very little about their cold components, except in a handful of spectacular examples (e.g., Maiolino et al. 2012). Fast outflows are seen in powerful IR galaxies in the local Universe (Veilleux et al. 2013), but studies have been limited to a handful of the brightest, most energetic sources. Large, sensitive, systematic surveys of molecular outflows reaching out to epochs where

most galaxies are rapidly evolving are necessary to establish the importance of outflows in a cosmological context.

9. What is the relation between the large scale cold outflows and the AGN that seem to trigger them? Are the ultra-fast outflows (UFOs) seen in the X-rays on sub-parsec scale the ultimate drivers of the most powerful cold outflows, or are the more common but slower soft X-ray and ultraviolet (UV) warm absorbers and UV broad absorption line (BAL) outflows seen on larger scale than the UFOs a better predictor of these cold outflows? How is the energy in these nuclear winds transferred to drive the galaxy-scale cold outflows? The kinetic power that is available from an AGN wind scales with v_{out}^3, rising quite rapidly with outflow velocity. Thus the fastest outflows are the ones that can potentially produce the largest feedback effects, provided they couple with the ISM effectively. X-ray observations identify a type of outflow that can reach modestly relativistic speeds $v_{out} \sim 0.03\,c - 0.3\,c$, consisting of a highly ionized flow originating from the accretion disk itself with column densities as high as 10^{24} cm^{-2} (Reeves et al. 2003; Tombesi et al. 2010). In theory, these very fast accretion-disk winds can drive shocks into the host galaxy ISM and create shock-driven over-pressurized bubbles that give rise to the large-scale outflows observed in ionized, neutral, and molecular gas (Faucher-Giguère & Quataert 2012; Tombesi et al. 2015). Testing these models, and directly linking fast accretion disk outflows with galactic winds requires high-quality, velocity-resolved imaging of the molecular and neutral atomic gas at high spatial resolution in the central regions of AGN with identified X-ray UFOs. A more complete survey of AGN will help relate the cold outflows to the more prevalent warm absorbers (Crenshaw & Kraemer 2012) and Broad Absorption Line (BAL) outflows (Gibson et al. 2009). The prospects are good that ngVLA and future UV-optical facilities will be able to spatially resolve the regions where the BAL outflows interact with the ISM of the AGN host galaxies (Moe et al. 2009; Bautista et al. 2010; Dunn et al. 2010).

3. The Unique Discovery Space of the ngVLA

The ngVLA has a unique part of the discovery space to fill, of surface brightness sensitivity at high enough resolution to spatially resolve outflows close in and trace them far out from galaxy centers while at the same time studying the launching mechanisms and compositions.

Obtaining these measurements requires imaging and kinematics of the cool molecular and atomic component. This requires high surface brightness sensitivity on physical scales of $20 - 100$ pc out to 100 Mpc, with good imaging dynamic range (frequently the faint wind emission in next to bright line or continuum emission from the galaxy/AGN). A distance of 100 Mpc encloses a volume big enough to find several examples of LIRGs/ULIRGs and powerful AGN. Physical resolution of $20-100$ pc (~ 20 pc is the width of the streamers in NGC253) is necessary to study the base of the outflows and their launching mechanisms, while high surface brightness sensitivity allows us to follow the outflow further out and search for accelerations/velocity gradients that constrain the final velocity. Even higher resolution is useful to study the disk/nucleus next to the outflow (usually much brighter), and investigate the connections to energy sources such as super star clusters, collections of supernova remnants, or SMBH accretion disks. To find and trace the extent and composition of winds it is necessary to image the CO, HI, and OH lines along with the continuum, as well as a host of tracers of local physical conditions. To characterize the physical state of winds and their mass loss, CO isotopologues, shock tracers, probes of the diverse excitation mechanisms (IR/UV/CR/X-ray) and tracers of the density distribution are key (e.g., Lindberg et al. 2016; Walter et al. 2017).

4. Complementarity with Existing and Planned Facilities

Three of the NASA flagship mission concepts under study have significant complementarity for the study of galaxy outflows, which are naturally multi-phase, multi-wavelength phenomena. In the following we focus on the complementary capabilities brought by the Infrared *Origins Space Telescope* (OST), the X-ray Lynx Telescope, and the Large UV/Optical/Infrared Surveyor (LUVOIR), while also discussing the *Square Kilometer Array* (SKA) and the Atacama Large Millimeter/submillimeter Array (ALMA).

With a huge leap in line and surface brightness sensitivity over all previous and planned IR missions, high spatial resolution, and the ability to quickly map large areas of the sky to generate unbiased spectroscopic samples, the OST will be able to find cool outflows spanning from the present day to over 90% of the age of the Universe. These targets will be prime targets for detailed follow-up study with the ngVLA at high angular and spectral resolution. For example, the Medium Resolution Survey Spectrometer (MRSS) on OST can detect columns of extra-planar neutral gas with $N_{HI} \sim 10^{20}\,\mathrm{cm}^{-2}$ and $n_H \sim 1\,\mathrm{cm}^{-3}$ via [CII] at sub-kpc resolution out to 30 Mpc in 10 minutes, and fine-structure lines in fast moving galactic winds down to $\sim 2x10^{-21}\,\mathrm{W\,m}^{-2}$ in one hour, mapping nearby galaxies and detecting sources well into the epoch of re-ionization. For example, outflow signatures such as P-Cygni profiles (blueshifted absorption and redshifted emission) are easily detectable in the far-infrared molecular OH feature at $\lambda_{rest} = 79\,\mu$m from a source like Mrk 231 out to $z \sim 5$ in an hour, making surveys of large numbers of galaxies feasible in the far-infrared for the first time. Through blind, low-resolution spectroscopic surveys and detailed studies of nearby starbursts and AGN, OST working together with the ngVLA, will deliver a complete picture of feedback on the cold and warm atomic and molecular ISM in rapidly evolving galaxies. The proposed JAXA/ESA mission SPICA, recently selected as one of three candidate missions to be further studied for ESA's M5 mission call, will also be an extremely capable observatory for studying galactic outflows in the infrared (González-Alfonso et al. 2017), although it will have significantly less collecting area than OST and a narrower wavelength coverage.

While OST searches for cool outflows, Lynx will characterize the highly ionized $10^6 - 10^7$ K plasma phase (although measurements in absorption can also measure cold phases). The crucial capabilities of the Lynx telescope for galactic winds are high angular resolution ($\sim 0.5''$), high spectral resolution of ~ 2 eV FWHM independent of energy (corresponding to $R \sim 700$ at the very strong OVII line, and high signal-to-noise imaging over a field of view of $\sim 5'$. Lynx also has a grating with energy-resolution of 0.3 eV, capable of resolving the kinematics of the hot wind phases, and producing density diagnostics for the soft X-ray emitting winds. This combination of parameters allows measurement of dynamics (velocities of $\sim 200\,\mathrm{km\,s}^{-1}$), chemical composition (through lines from C, N, O, Ne, Mg, Si, S, Fe, and Ni), and diagnostics of ionization state. This allows Lynx to study the narrow emission-line regions of hot plasma bubbles inflated by AGN, as well as measuring metallicities outside the cores of massive clusters out to a redshift $z \sim 3$, and determining the mechanisms of gas ionization. In dusty winds Lynx can also distinguish dust features in absorption as the binding energy of atoms in grains is ~ 1 eV, allowing it to detect whether oxygen is bound in grains or in the gas phase. Lynx's planned sensitivity will allow the study of M 82-like starbursts at moderate redshifts, the most luminous starbursts at $z \sim 2-3$, and lensed objects at $z \sim 4$. In addition Lynx's high sensitivity and resolution in the Fe K band will allow a detailed analysis of the ultrafast outflows, determining their energetics and geometry over a wide range of redshifts, luminosities and black hole masses. Similarly, ESA's Advanced Telescope for High Energy Astrophysics (ATHENA) to be launched in the early 2030s, will also be able to detect and measure the hot gas associated with galactic outflows. However, ATHENA's significantly lower spatial and spectral resolution compared to Lynx ($5''$ and 2.5 eV compared to $1''$ and 0.3 eV, respectively) will make it better suited to studying outflows from powerful AGN, and likely limit its usefulness for low-velocity, starburst-driven winds.

LUVOIR will bring a leap in sensitive high-resolution imaging and spectroscopy across the full UVOIR ($0.1-3\ \mu$m) bandpass, with the capability to resolve structures on scales of 100 parsecs or smaller in all galaxies at $z \leq 4$. The excellent match in resolution between LUVOIR and ngVLA will allow for direct comparisons between the warm and cool phases of the outflows and their impact on these galaxies. In particular, LUVOIR will provide spatially resolved maps of the UV BAL outflows in quasars to directly probe the mechanisms involved in driving the most extreme cold outflows. The 50–100 times larger UV spectroscopic sensitivity of LUVOIR compared with *HST* will bring a hundredfold more UV-bright quasars within its reach. It will also be able to use the much more numerous UV-bright galaxies as background sources. With this dramatic gain in sensitivity, LUVOIR will be able to efficiently probe gas and metals outside of galaxies, and the complex interplay between accretion flows onto galaxies and gas outflowing from the galaxies. These results will nicely complement the low surface brightness maps of galaxies and their halos produced by ngVLA.

The mid-frequency SKA has significant overlap with the low-frequency capabilities of the ngVLA, and so it will be able to perform HI and low-frequency OH studies of outflowing gas. The SKA phase 1 is comparable to the ngVLA, with a somewhat smaller collecting area but without the high-frequency capabilities. The precise sensitivity comparison will depend on decisions about array configurations, and the upper frequency cutoff of the SKA. However, it is clear that much of the molecular and high-resolution science associated with the outflows will be out of reach of even a phase 2 mid-frequency SKA. With a full mid-frequency SKA built, the complementarity with the ngVLA will be excellent, with the former focusing on the low frequency science while the ngVLA observes at higher frequencies ($\nu > 10-20$ GHz).

Compared to the the ngVLA, ALMA, which currently drives much of the research on high-resolution studies of molecular outflows in galaxies, will have significantly lower line sensitivity in the region of frequency overlap (ALMA bands 1 to 3). But because of its extensive high frequency coverage the combination of ALMA and ngVLA will be extremely complementary, particularly for studies of and launching mechanisms and chemistry and excitation in outflows.

Acknowledgments. ADB acknowledges support from NSF-AST 1412419.

References

Alatalo, K., Blitz, L., Young, L. M., et al. 2011, ApJ, 735, 88
Alatalo, K., Lacy, M., Lanz, L., et al. 2015, ApJ, 798, 31
Anglés-Alcázar, D., Faucher-Giguère, C.-A., Quataert, E., et al. 2017, MNRAS, 472, L109
Anglés-Alcázar, D., Faucher-Giguère, C.-A., Kereš, D., et al. 2017, MNRAS, 470, 4698
Bautista, M. A., Dunn, J. P., Arav, N., Korista, K. T., Moe, M., & Benn, C. 2010, ApJ,713, 553
Bohlin, R. C., Savage, B. D., & Drake, J. F. 1978, ApJ, 224, 132
Bolatto, A. D., Wolfire, M., & Leroy, A. K. 2013, ARA&A, 51, 207
Bolatto, A. D., Warren, S. R., Leroy, A. K., et al. 2013, Nat, 499, 450
van Breugel, W., Filippenko, A. V., Heckman, T., & Miley, G. 1985, ApJ, 293, 83
Cicone, C., Maiolino, R., Sturm, E., et al. 2014, A&A, 562, A21
Combes, F., García-Burillo, S., Casasola, V., et al. 2013, A&A, 558, A124
Crenshaw, D. M., & Kraemer, S. B. 2012, ApJ, 753, 75
Croft, S., van Breugel, W., de Vries, W., et al. 2006, ApJ, 647, 1040
Davé, R., Oppenheimer, B. D., & Finlator, K. 2011, MNRAS, 415, 11
Dunn, J. P., Bautista, M., Arav, N., et al. 2010, ApJ, 709, 611
Faucher-Giguère, C.-A., & Quataert, E. 2012, MNRAS, 425, 605
Feruglio, C., Maiolino, R., Piconcelli, E., et al. 2010, A&A, 518, L155
Fujita, A., Martin, C. L., Mac Low, M.-M., New, K. C. B., & Weaver, R. 2009, ApJ, 698, 693
García-Burillo, S., Combes, F., Usero, A., et al. 2014, A&A, 567, A125
Gibson, R. R., Jiang, L., Brandt, W. N., et al. 2009, ApJ, 692, 758
González-Alfonso, E., Armus, L., Carrera, F. J., et al. 2017, PASA, 34, e054
Heckman, T. M., Lehnert, M. D., Strickland, D. K., & Armus, L. 2000, ApJS, 129, 493
Herrera, C. N., & Boulanger, F. 2017, A&A, 600, A139
Hopkins, P. F., Quataert, E., & Murray, N. 2012, MNRAS, 421, 3522
Kennicutt, R. C., Jr., Armus, L., Bendo, G., et al. 2003, PASP, 115, 928
Kim, C.-G., & Ostriker, E. C. 2018, ApJ, 853, 173
Lehnert, M. D., Heckman, T. M., & Weaver, K. A. 1999, ApJ, 523, 575
Leroy, A. K., Walter, F., Martini, P., et al. 2015, ApJ, 814, 83
Lindberg, J. E., Aalto, S., Muller, S., et al. 2016, A&A, 587, A15
Maiolino, R., Gallerani, S., Neri, R., et al. 2012, MNRAS, 425, L66
Martini, P., Leroy, A. K., Mangum, J. G., et al. 2018, arXiv:1802.04359
Moe, M., Arav, N., Bautista, M. A., & Korista, K. T. 2009, ApJ, 706, 525
Muratov, A. L., Kereš, D., Faucher-Giguère, C.-A., et al. 2015, MNRAS, 454, 2691
Muratov, A. L., Kereš, D., Faucher-Giguère, C.-A., et al. 2017, MNRAS, 468, 4170
Murray, N., Ménard, B., & Thompson, T. A. 2011, ApJ, 735, 66
Newman, S. F., Genzel, R., Förster-Schreiber, N. M., et al. 2012, ApJ, 761, 43
Rachford, B. L., Snow, T. P., Destree, J. D., et al. 2009, ApJS, 180, 125
Reeves, J. N., O'Brien, P. T., & Ward, M. J. 2003, ApJ, 593, L65
Rupke, D. S. N., & Veilleux, S. 2013, ApJ, 768, 75
Rupke, D. S., Veilleux, S., & Sanders, D. B. 2005, ApJS, 160, 115
Sakamoto, K., Aalto, S., Combes, F., Evans, A., & Peck, A. 2014, ApJ, 797, 90
Silk, J. 2013, ApJ, 772, 112
Sturm, E., González-Alfonso, E., Veilleux, S., et al. 2011, ApJ, 733, L16
Strickland, D. K., Heckman, T. M., Colbert, E. J. M., Hoopes, C. G., & Weaver, K. A. 2004, ApJS, 151, 193
Thompson, T. A., Quataert, E., Zhang, D., & Weinberg, D. H. 2016, MNRAS, 455, 1830
Tombesi, F., Cappi, M., Reeves, J. N., et al. 2010, A&A, 521, A57
Tombesi, F., Meléndez, M., Veilleux, S., et al. 2015, Nat, 519, 436
Uhlig, M., Pfrommer, C., Sharma, M., et al. 2012, MNRAS, 423, 2374
Veilleux, S., Cecil, G., & Bland-Hawthorn, J. 2005, ARA&A, 43, 769
Veilleux, S., Meléndez, M., Sturm, E., et al. 2013, ApJ, 776, 27
Veilleux, S., Bolatto, A., Tombesi, F., et al. 2017, ApJ, 843, 18
Wagner, A. Y., & Bicknell, G. V. 2011, ApJ, 728, 29

Walter, F., Weiss, A., & Scoville, N. 2002, ApJ, 580, L21
Walter, F., Bolatto, A. D., Leroy, A. K., et al. 2017, ApJ, 835, 265
Wylezalek, D., Schnorr Müller, A., Zakamska, N. L., et al. 2017, MNRAS, 467, 2612
Zschaechner, L. K., Walter, F., Bolatto, A., et al. 2016, ApJ, 832, 142

Science with a Next-Generation Very Large Array
ASP Conference Series, Monograph 7
Eric J. Murphy, ed.

DRAFT EDITION

SMBH Formation and Feedback in Nearby Low-mass Galaxies

Kristina Nyland[1] and Katherine Alatalo[2]

[1]*National Radio Astronomy Observatory, Charlottesville, VA, 22903;* `knyland@nrao.edu`

[2]*Space Telescope Science Institute, 3700 San Martin Dr., Baltimore, MD 21218, USA;* `kalatalo@stsci.edu`

Abstract. The ngVLA will facilitate deep surveys capable of detecting the faint and compact signatures of accreting supermassive black holes (SMBHs) with masses below one million solar-masses hosted by low-mass ($< 10^9$ solar-masses) galaxies. This will provide important new insights on both the origins of supermassive black holes and the possible impact of active galactic nucleus-driven feedback in a currently unexplored mass regime.

1. Introduction and Motivation

It is now well-established that supermassive black holes (SMBHs) with masses ranging from $10^6 - 10^{10}\ M_\odot$ commonly reside in the nuclei of galaxies. A number of lines of evidence, including the observed scaling relations between SMBHs and their hosts, further suggest that the formation and growth of SMBHs and their hosts are inextricably linked (Kormendy & Ho 2013; Heckman & Best 2014). Despite their prevalence and importance to our understanding of galaxy evolution, the origin of supermassive SMBHs at high redshift (e.g., hierarchical merging vs. direct gas collapse) and their formation efficiency remains an open area of research (Volonteri 2010; Bellovary et al. 2011; Shirakata et al. 2016). Thus, a key observational parameter for constraining the formation of SMBHs is the mass distribution of so-called SMBH "seeds" (Greene et al. 2012; Reines & Volonteri 2015; Mezcua et al. 2016).

1.1. Insights on SMBH Formation from Nearby Low-mass Galaxies

Knowledge of the shape of the SMBH seed mass distribution at high redshift ($z > 6$) would provide strong constraints on the dominant SMBH formation channel, thus elucidating a key missing element in our understanding of SMBH-galaxy co-evolution. While direct mass measurements of SMBH seeds in the early universe are not yet feasible (Volonteri et al. 2017), the detection of their radiative signatures provides information on the SMBH occupation fraction as well as indirect SMBH mass constraints. Thus far, such studies of high-z SMBHs have been limited to luminous quasars, which may have formed via atypical processes to build the massive SMBHs needed to power their central engines at such early cosmic epochs (e.g., Mortlock et al. 2011). The population of accreting SMBHs with $M_{\rm BH} < 10^6\ {\rm M}_\odot$ in the local universe residing in lower-mass and dwarf galaxies offers an alternative means for studying SMBH seed formation since these systems have not experienced substantial merger or accretion driven growth (e.g., Mezcua 2017).

1.2. SMBH-driven Feedback in Low-mass Galaxies?

In addition to their importance for constraining SMBH seed formation and growth scenarios, accreting SMBHs hosted by low-mass galaxies may also impact their hosts though energetic feedback. While supernova-driven feedback is believed to be the dominant regulatory mechanism associated with low-mass galaxies (e.g., Martin-Navarro & Mezcua 2018), recent observational and theoretical evidence suggests that active galactic nuclei (AGNs) powered by the sub-million-solar-mass SMBHs residing in their nuclei may also be capable of producing significant energetic feedback. From a theoretical standpoint, analytical models suggest that AGN feedback in low-mass galaxies may provide an efficient mechanism for the displacement of gas from the host galaxy (Silk 2017; Dashyan et al. 2018), though this possibility remains controversial (e.g., Trebitsch et al. 2018). This scenario may be most plausible in galaxies with stellar masses in the range of $10^7 \lesssim M_* \lesssim 10^9$ $\mathrm{M}_\odot$ when preceded by substantial supernova feedback capable of rarefying the ISM, thus making it more susceptible to disruption via AGN feedback (Prieto et al. 2017; Hartwig et al. 2018).

Observational evidence for AGNs hosted by low-mass galaxies has become increasingly common over the past decade (Barth et al. 2008; Greene & Ho 2007; Reines et al. 2013; Moran et al. 2014; Lemons et al. 2015; Sartori et al. 2015; Nucita et al. 2017; Mezcua et al. 2018), though the identification of AGN-driven feedback in low-mass and dwarf galaxies has remained challenging due to the resolution and sensitivity limitations of existing telescopes. However, recent spatially-resolved optical emission line studies have provided tentative support for AGN feedback in the low-mass-galaxy regime (e.g., Penny et al. 2018).

At radio frequencies, the identification of dwarf galaxies harboring jetted AGNs with the potential to impart feedback on their hosts is also challenging with current instruments such as the Karl G. Jansky Very Large Array (JVLA; Nyland et al. 2016; Padovani 2016), which lack adequate collecting area and angular resolution to detect their faint, compact signatures. Despite their importance for probing the impact of jet-driven feedback physics in the low-mass regime, only a handful of candidate jetted AGNs hosted by low-mass galaxies with $M_{\mathrm{BH}} < 10^6\, M_\odot$ are known, including NGC 4395 (Wrobel & Ho 2006), Henize 2-10 (Reines et al. 2011, 2013), and NGC 404 (Nyland et al. 2017).

1.3. NGC 404: A Case Study

In Figure 1, we illustrate the multiwavelength nuclear properties of the nearby dwarf galaxy NGC 404, which harbors a nuclear radio jet with an extent of ~10 pc characterized by a steep radio spectral index from 1 to 18 GHz ($\alpha \sim -1$; Nyland et al. 2017). The spatial coincidence of the radio source, hard X-ray source, dynamical center of NGC 404, and the rotating circumnuclear CO(2–1) disk are most consistent with a confined radio jet launched by the central low-mass ($M_{\mathrm{BH}} < 10^5\, M_\odot$ from stellar dynamical modeling; Nguyen et al. 2017), low-Eddington-ratio ($L_{\mathrm{bol}}/L_{\mathrm{Edd}} \sim 10^{-6}$; Nyland et al. 2012) SMBH that has been disrupted by the ambient interstellar medium (ISM). Multiwavelength evidence for shock excitation supports the possibility of an interaction between the confined jet and the ISM. This includes the detection of extended Hα and soft X-ray emission from *HST* and *Chandra*, respectively, as well as strong [Fe II] at

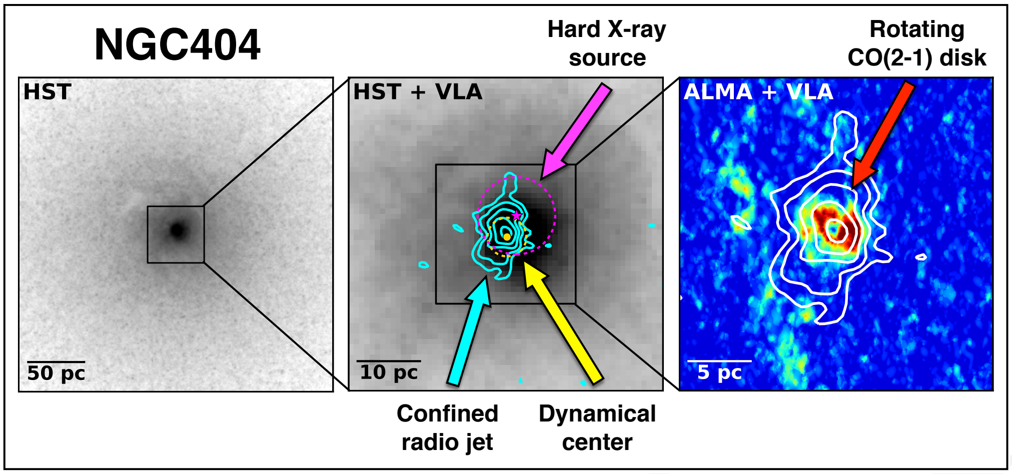

Figure 1. *HST*, VLA, *Chandra* and ALMA data identify a confined radio jet possibly interacting with the ambient ISM in the nucleus of the dwarf galaxy NGC 404. Adapted from Nyland et al. (2017).

26 μm and rotational H_2 emission in archival *Spitzer* spectroscopic data (Nyland et al. 2017).

The nucleus of NGC 404 therefore offers a unique local laboratory for directly constraining the energetic impact on the ambient ISM by a jetted AGN hosted by a dwarf galaxy. However, the identification of additional jetted AGNs in low-mass galaxies will ultimately be needed to place NGC 404 in the broader context of galaxy evolution. Given the limited sensitivity and resolution of current radio telescopes, building a larger sample of jetted low-mass AGNs must await the availability of next generation instruments such as the Next-generation Very Large Array (ngVLA).

2. Prospects for the ngVLA

2.1. Demographics and Energetics of a Hidden SMBH Population

The ngVLA, with its roughly order of magnitude increase in sensitivity and angular resolution compared to the JVLA, will greatly improve our ability to study compact radio sources in the nuclei of low-mass galaxies associated with SMBH accretion. The local volume of nearby galaxies within ~10 Mpc encompasses 869 galaxies, about 75% of which are dwarf galaxies (Karachentsev et al. 2013). Recent studies (e.g., Mezcua et al. 2016) have suggested that accreting SMBHs with masses in the range of $10^3 \lesssim M_{\rm BH} \lesssim 10^6$ $M_\odot$ may commonly reside in the nuclei of nearby low-mass galaxies, thus motivating deep searches for the radio continuum signatures of this population. However, identifying SMBHs in this population of galaxies is inherently difficult due to their expected low masses ($M_{\rm BH} < 10^6\ M_\odot$) and faint accretion signatures.

The identification of NGC 404 analogs in other dwarf or low-mass galaxies would offer new insights into the occupation fraction of SMBHs analogous to the SMBH seeds that formed at high redshift, thus profoundly impacting our understanding of the origin of SMBHs. Deep, high-angular-resolution observations with the ngVLA will both help constrain the SMBH seed mass distribution and also provide new constraints on the

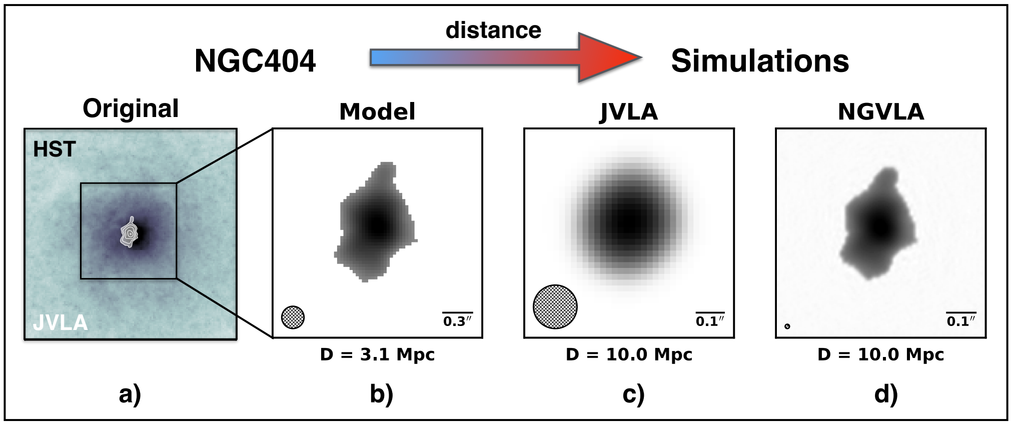

Figure 2. Simulated VLA and ngVLA images of an analog to the jetted AGN hosted by the nearby dwarf galaxy NGC 404 as it would appear if it were ~3X more distant. **a)** An *HST* optical image is shown in the background colorscale and the VLA *Ku*-band (15 GHz) radio contours are overlaid in white. The angular resolution of the radio data is $\theta_{\rm FWHM} = 0.20''$ and the extent of the radio jets from end to end is 1.13″ (17 pc). The NGC 404 VLA data were originally published in Nyland et al. (2017). **b)** Model radio image of NGC 404 based on the original data shown in panel a) and shown at the true source distance of $D = 3.1$ Mpc. **c)** Simulated VLA A-configuration map of an NGC 404 analog shifted to a distance of $D = 10.0$ Mpc at 15 GHz with $\theta_{\rm FWHM} = 0.15''$. **d)** Simulated map of an NGC 404 analog at $D = 10.0$ Mpc as it would appear if imaged with the ngVLA at 15 GHz. The angular resolution is $\theta_{\rm FWHM} = 0.014''$. Adapted from Nyland et al. (2018).

energetic impact of AGN feedback associated with SMBHs with masses below one million solar-masses. These new insights will provide crucial tests of our understanding of SMBH-galaxy co-evolution.

2.2. Imaging Simulations

We present ngVLA and JVLA simulations of a more distant analog to the confined jet with an extent of ~10 pc in the center of NGC 404 in Figure 2. To produce the input model, we scaled the image pixel size such that it corresponds to an NGC 404 analog located at 10 Mpc, or ~3X further than the true distance to NGC 404. For the ngVLA simulations, we used the ngVLA configuration with 300 antennas and maximum baselines of $B_{\rm max} \sim 513$ km as shown in (Nyland et al. 2018). The JVLA simulations were performed in the A-configuration, which has $B_{\rm max} = 36.4$ km.

Figure 2 illustrates the inability of the VLA to spatially resolve the morphology of a 10 pc jet at a distance of 10 Mpc in the most extended A configuration. This is in contrast to the simulated ngVLA observations, which successfully resolve the extended structure of a ~10-pc-scale jet at a distance of 10 Mpc at 15 GHz. As discussed in detail in Nyland et al. (2018), both the JVLA in the A configuration and the ngVLA would be able to detect emission from an NGC 404 analog at a distance of 10 Mpc in a reasonable amount of on-source integration time ($\lesssim$ 15 hr). However, only the ngVLA would be able to spatially resolve the emission. Given the low-luminosity of NGC 404

($L_{15\,\mathrm{GHz}} \sim 3.4 \times 10^{17}$ W Hz^{-1}), spatially resolving the morphology of the source is crucial to distinguish its origin from nuclear star formation (Nyland et al. 2017).

3. Summary

In addition to placing constraints on the basic physical properties (e.g., extent, luminosity, and energy) of jetted AGNs in nearby low-mass galaxies, observations of the molecular ISM as traced by the CO(1–0) line at 115 GHz will probe the amount of energy transferred to the ISM and, in conjunction with supporting multiwavelength ancillary data from telescopes such as ALMA and the *James Webb Space Telescope*, its impact on the ambient star formation efficiency. Thus, the unprecedented capabilities of the ngVLA will enable new advancements in our understanding of SMBH formation and the impact of jet-driven feedback driven by SMBH seed analogs in the local universe.

References

Barth, A. J., Greene, J. E., & Ho, L. C. 2008, AJ, 136, 1179. 0807.3316

Bellovary, J., Volonteri, M., Governato, F., Shen, S., Quinn, T., & Wadsley, J. 2011, ApJ, 742, 13. 1104.3858

Dashyan, G., Silk, J., Mamon, G. A., Dubois, Y., & Hartwig, T. 2018, MNRAS, 473, 5698. 1710.05900

Greene, J. E., & Ho, L. C. 2007, ApJ, 670, 92. 0707.2617

Greene, J. E., Zakamska, N. L., & Smith, P. S. 2012, ApJ, 746, 86. 1112.3358

Hartwig, T., Volonteri, M., & Dashyan, G. 2018, MNRAS, 476, 2288. 1707.03826

Heckman, T. M., & Best, P. N. 2014, ARA&A, 52, 589. 1403.4620

Karachentsev, I. D., Makarov, D. I., & Kaisina, E. I. 2013, AJ, 145, 101. 1303.5328

Kormendy, J., & Ho, L. C. 2013, ARA&A, 51, 511. 1304.7762

Latif, M. A., & Ferrara, A. 2016, PASA, 33, e051. 1605.07391

Lemons, S. M., Reines, A. E., Plotkin, R. M., Gallo, E., & Greene, J. E. 2015, ApJ, 805, 12. 1502.06958

Martin-Navarro, I., & Mezcua, M. 2018, ArXiv e-prints. 1802.07277

Mezcua, M. 2017, International Journal of Modern Physics D, 26, 1730021. 1705.09667

Mezcua, M., Civano, F., Fabbiano, G., Miyaji, T., & Marchesi, S. 2016, ApJ, 817, 20. 1511.05844

Mezcua, M., Civano, F., Marchesi, S., Suh, H., Fabbiano, G., & Volonteri, M. 2018, MNRAS. 1802.01567

Moran, E. C., Shahinyan, K., Sugarman, H. R., Vélez, D. O., & Eracleous, M. 2014, AJ, 148, 136. 1408.4451

Mortlock, D. J., Warren, S. J., Venemans, B. P., Patel, M., Hewett, P. C., McMahon, R. G., Simpson, C., Theuns, T., Gonzáles-Solares, E. A., Adamson, A., Dye, S., Hambly, N. C., Hirst, P., Irwin, M. J., Kuiper, E., Lawrence, A., & Röttgering, H. J. A. 2011, Nat, 474, 616. 1106.6088

Nguyen, D. D., Seth, A. C., den Brok, M., Neumayer, N., Cappellari, M., Barth, A. J., Caldwell, N., Williams, B. F., & Binder, B. 2017, ApJ, 836, 237. 1610.09385

Nucita, A. A., Manni, L., De Paolis, F., Giordano, M., & Ingrosso, G. 2017, ApJ, 837, 66. 1704.03182

Nyland, K., Davis, T. A., Nguyen, D. D., Seth, A., Wrobel, J. M., Kamble, A., Lacy, M., Alatalo, K., Karovska, M., Maksym, W. P., Mukherjee, D., & Young, L. M. 2017, ApJ, 845, 50. 1707.02303

Nyland, K., Harwood, J. J., Mukherjee, D., Jagannathan, P., Rujopakarn, W., Emonts, B., Alatalo, K., Bicknell, G. V., Davis, T. A., Greene, J. E., Kimball, A., Lacy, M., Lonsdale, C., Lonsdale, C., Maksym, W. P., Molnár, D. C., Morabito, L., Murphy, E. J., Patil, P., Prandoni, I., Sargent, M., & Vlahakis, C. 2018, ApJ, 859, 23. 1803.02357

Nyland, K., Marvil, J., Wrobel, J. M., Young, L. M., & Zauderer, B. A. 2012, ApJ, 753, 103. 1204.3089

Nyland, K., Young, L. M., Wrobel, J. M., Sarzi, M., Morganti, R., Alatalo, K., Blitz, L., Bournaud, F., Bureau, M., Cappellari, M., Crocker, A. F., Davies, R. L., Davis, T. A., de Zeeuw, P. T., Duc, P.-A., Emsellem, E., Khochfar, S., Krajnović, D., Kuntschner, H., McDermid, R. M., Naab, T., Oosterloo, T., Scott, N., Serra, P., & Weijmans, A.-M. 2016, MNRAS, 458, 2221. 1602.05579

Padovani, P. 2016, A&A Rev., 24, 13. 1609.00499

Penny, S. J., Masters, K. L., Smethurst, R., Nichol, R. C., Krawczyk, C. M., Bizyaev, D., Greene, O., Liu, C., Marinelli, M., Rembold, S. B., Riffel, R. A., Ilha, G. d. S., Wylezalek, D., Andrews, B. H., Bundy, K., Drory, N., Oravetz, D., & Pan, K. 2018, MNRAS, 476, 979. 1710.07568

Prieto, J., Escala, A., Volonteri, M., & Dubois, Y. 2017, ApJ, 836, 216. 1701.06172

Reines, A. E., & Comastri, A. 2016, PASA, 33, e054. 1609.03562

Reines, A. E., Greene, J. E., & Geha, M. 2013, ApJ, 775, 116. 1308.0328

Reines, A. E., Sivakoff, G. R., Johnson, K. E., & Brogan, C. L. 2011, Nat, 470, 66. 1101.1309

Reines, A. E., & Volonteri, M. 2015, ApJ, 813, 82. 1508.06274

Sartori, L. F., Schawinski, K., Treister, E., Trakhtenbrot, B., Koss, M., Shirazi, M., & Oh, K. 2015, MNRAS, 454, 3722. 1509.08483

Shirakata, H., Kawaguchi, T., Okamoto, T., Makiya, R., Ishiyama, T., Matsuoka, Y., Nagashima, M., Enoki, M., Oogi, T., & Kobayashi, M. A. R. 2016, MNRAS, 461, 4389. 1604.05317

Silk, J. 2017, ApJ, 839, L13. 1703.08553

Trebitsch, M., Volonteri, M., Dubois, Y., & Madau, P. 2018, MNRAS. 1712.05804

Volonteri, M. 2010, A&A Rev., 18, 279. 1003.4404

Volonteri, M., Reines, A. E., Atek, H., Stark, D. P., & Trebitsch, M. 2017, ApJ, 849, 155. 1704.00753

Wrobel, J. M., & Ho, L. C. 2006, ApJ, 646, L95. astro-ph/0606600

Science with a Next-Generation Very Large Array
ASP Conference Series, Monograph 7
Eric J. Murphy, ed.

DRAFT EDITION

Radio Jet-ISM Feedback

Kristina Nyland,[1] Jeremy J. Harwood,[2] Dipanjan Mukherjee,[3] Isabella Prandoni,[4] Katherine Alatalo,[5] and Anna D. Kapińska[6]

[1]*National Radio Astronomy Observatory, Charlottesville, VA, 22903;* `knyland@nrao.edu`

[2]*ASTRON, The Netherlands Institute for Radio Astronomy, Postbus 2, 7990 AA, Dwingeloo, The Netherlands;* `jeremy.harwood@physics.org`

[3]*Dipartimento di Fisica Generale, Universita degli Studi di Torino, Via Pietro Giuria 1, 10125 Torino, Italy;* `dipanjan.mukherjee@unito.it`

[4]*INAF-Istituto di Radioastronomia, via P. Gobetti 101, 40129, Bologna, Italy;* `prandoni@ira.inaf.it`

[5]*Space Telescope Science Institute, 3700 San Martin Dr., Baltimore, MD 21218, USA;* `kalatalo@stsci.edu`

[6]*National Radio Astronomy Observatory, Socorro, NM, 87801;* `akapinska@nrao.edu`

Abstract. Energetic feedback by active galactic nuclei (AGNs) plays an important evolutionary role in the regulation of star formation (SF) on galactic scales. However, the effects of this feedback as a function of redshift and galaxy properties such as mass, environment and cold gas content remain poorly understood. Given its unique combination of frequency range, angular resolution, and sensitivity, the ngVLA will serve as a transformational new tool in our understanding of how radio jets affect their surroundings. By combining broadband continuum data with measurements of the cold gas content and kinematics, the ngVLA will quantify the energetic impact of radio jets hosted by gas-rich galaxies as the jets interact with the star-forming gas reservoirs of their hosts.

1. Introduction

Energetic feedback produced by Active Galactic Nuclei (AGNs) is believed to play an important role in galaxy evolution through the regulatory effect it may have on the star formation rate and efficiency of the host galaxy. AGN feedback may be driven by radiative winds launched by the accretion disks of powerful quasars or spurred by radio jets/lobes as they heat, expel, or shock their surroundings. Observational evidence for both modes of feedback have been reported (e.g., Fabian 2012, and references therein). Villar Martín et al. (2014) show that, on average, radio jets appear to be capable of producing more extreme gas outflows than accretion disk winds. However, the relative importance of each mode, and the dependence on redshift and other factors, such as galaxy mass and environment, remain open areas of research.

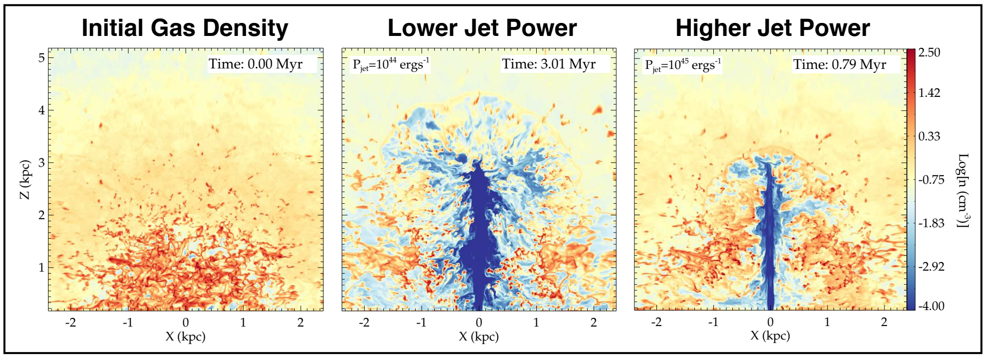

Figure 1. Snapshots from the relativistic hydrodynamic radio jet simulations (Mukherjee et al. 2016, 2017) showing the effect on an identical initial ISM (left) made by a radio jet with $P_{\rm jet} = 10^{44}$ erg s^{-1} (center) and $P_{\rm jet} = 10^{45}$ erg s^{-1} (right). The more powerful radio jet is able to more quickly "drill" through the ISM of its host galaxy, while the "wimpier" radio jet is trapped by the ISM and able to disrupt the surrounding gas for a longer time period and over a larger volume.

We also lack a fundamental understanding of exactly how radio jets transfer energy to their surroundings, how much energy is transferred to the different gas phases, and under what conditions significant positive/negative feedback is produced. We know that radio jets may deposit energy into their surroundings through a variety of mechanisms including heating, shocks, and/or turbulence (Fabian 2012; Alatalo et al. 2015; Soker 2016), and may also directly couple to gas in their surroundings and physically expel it (e.g., Morganti et al. 2013). However, the details of these processes – and under which conditions and environments different mechanisms dominate – are poorly understood. This is primarily due to the observational challenges of identifying systems with jet-driven feedback (e.g., sensitivity, angular resolution, and the need for extensive multi-wavelength data) that have prevented statistical studies of radio jets interacting with their surroundings.

2. Observing Jet-ISM Feedback with the ngVLA

The ngVLA will complement source morphologies and energetics constraints from deep, high-resolution continuum observations with spectral line data that encode information on the ISM content and conditions. The combination of broadband continuum and spectral line imaging will allow the ngVLA to uniquely probe the energetic impact of radio jets on the ambient cold gas. Spectral line measurements of molecular and atomic gas on comparable angular scales can be used to identify AGN-driven outflows (as well as gas inflow associated with fueling), perform detailed kinematic studies to gauge the amount of energy injected into the gas via feedback, and address the future evolutionary impact on local/global scales caused by the AGN feedback. Molecular gas and continuum estimates of the energetics of the outflow and jet can be directly compared with state-of-the art simulations, such as those shown in Figure 1, to deeply probe the underlying feedback physics.

Continuum + cold gas ngVLA studies would – for the first time – provide constraints on the prevalence and energetic importance of jet-ISM feedback in the dominant population of low-luminosity ($L_{1.4\,\mathrm{GHz}} < 10^{24}$ W Hz^{-1}) AGNs residing in "normal" galaxies. This is a particularly exciting prospect given recent observational evidence that lower-power radio AGNs may be able to significantly affect the interstellar medium (ISM) conditions of their hosts through feedback from sub-galactic-scale radio jets (e.g., Alatalo et al. 2011, 2015; Davis et al. 2012; Nyland et al. 2013; Godfrey & Shabala 2016; Querejeta et al. 2016; Zschaechner et al. 2016). From a theoretical standpoint, recent relativistic hydrodynamic simulations of radio jets propagating through a dense ISM (Mukherjee et al. 2016, 2017; Figure 1) provide further support for this possibility, demonstrating that while powerful radio jets rapidly "drill" through the ISM, lower-power jets become entrained in the ISM and are ultimately able to transfer energy over a much larger volume and for a longer period of time.

2.1. Probing a Unique Range of Jet Angular Scales

In Figure 2, we illustrate the redshift dependence of the observed angular jet extent for a wide range of radio jet size scales ranging from sub-parsec jets to giant radio galaxies with Mpc-scale lobes. The maximum angular resolution (defined as $\theta_{\mathrm{max}} = \lambda/B_{\mathrm{max}}$) for each of the proposed ngVLA observing bands (assuming $B_{\mathrm{max}} \approx 500$ km) is also shown in this figure. Future ngVLA studies of radio jets with intrinsic extents of a few pc to a few kpc will be able to fully utilize the unique combination of angular resolution, collecting area, and frequency coverage of the ngVLA over a wide range of redshifts. This range of angular scales, combined with the frequency range of the ngVLA, highlights the suitability of the ngVLA for studies of jet-ISM feedback associated with lower-power radio AGNs with sub-galactic jets. Observations of more extended radio jets that may be engaged in feedback on intergalactic or intracluster medium scales will be possible with suitable combinations of weighting and *uv*-tapering. However, the poor surface brightness sensitivity on the longest ngVLA baselines will prevent radio AGN studies of extended sources at the maximum resolution of the array.

2.2. ISM Content and Conditions

2.2.1. Atomic Gas

The absorption of atomic hydrogen at 21 cm against background continuum emission associated with a radio AGN provides a powerful means of directly identifying jet-driven outflows and quantifying their effect on the cold ISM (e.g., Morganti et al. 2013). HI absorption offers a key advantage over studies of the HI line in emission in terms of detectability, since the detection of HI absorption is independent of redshift and depends solely on the underlying strength of the background continuum source. In addition, the relatively low spin temperature of HI of $\sim$100$-$150 K (Condon & Ransom 2016) makes the detection of emission at high angular resolution difficult or impossible due to brightness temperature sensitivity limitations (see Section 2.2.3). HI absorption observations, on the other hand, depend only on the brightness temperature of the background continuum source, and may therefore be performed on much smaller (e.g., milliarcsecond) scales. In the context of jet-driven feedback, the detection of a blue-shifted spectral component in HI absorption is a signature of an outflow, which can be unambiguously distinguished from other possibilities, such as inflow or rotation. Additionally, kinematic constraints from HI absorption observations probe the gas conditions by providing direct measurements of the kinetic energy of any outflow components (Nyland et al. 2013) as well as characterizing the degree of turbulence (Lacy et al. 2017).

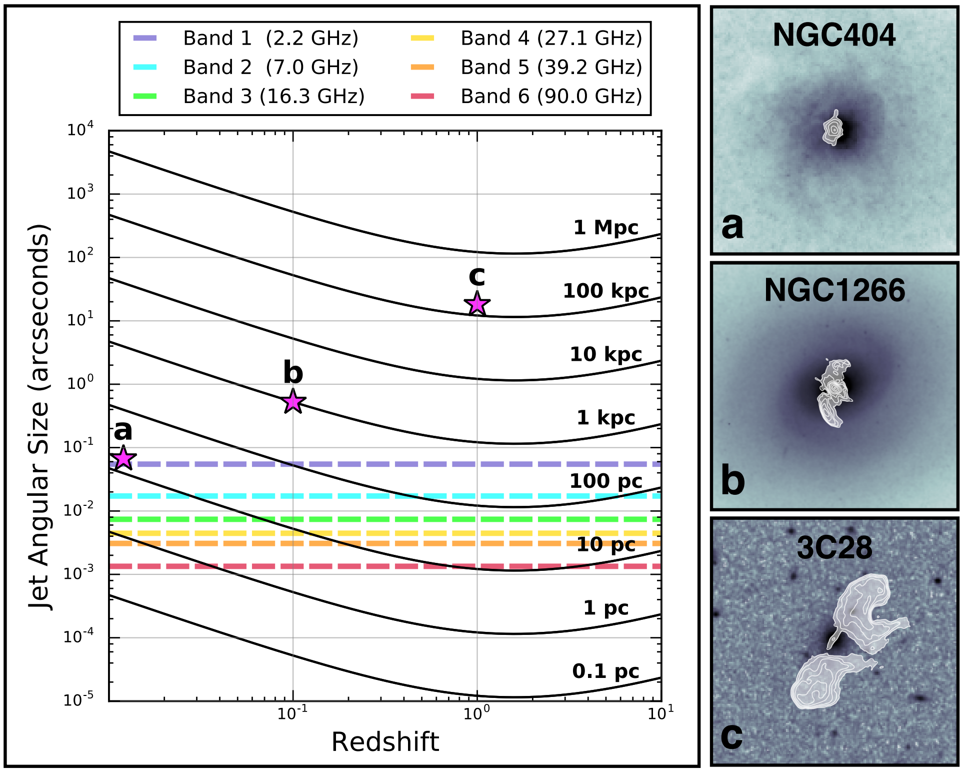

Figure 2. Jet angular size as a function of redshift. The black solid lines trace the redshift dependence of the angular extent of a jetted AGN for intrinsic jet sizes (measured from end to end along the major axis of the jet) from 0.1 pc to 1 Mpc. The maximum angular resolution of the ngVLA at the center of each of the ngVLA bands as defined in Selina & Murphy (2017) is denoted by the dashed colored lines. The magenta stars and thumbnails to the right of the main figure indicate three jetted radio AGNs representing a wide range of jet size scales: **a)** the dwarf galaxy NGC 404 with a jet extent of 10 pc, **b)** the jet-driven feedback host NGC 1266 with a jet extent of 1 kpc, and **c)** the radio galaxy 3C28 with a jet extent of 150 kpc. The redshifts of the representative sources correspond to simulated ngVLA maps from Nyland et al. (2018) at $z \approx 0$ (D = 10 Mpc), z = 0.1, and z = 1.0, respectively. Figure adapted from Nyland et al. (2018).

The ability of the ngVLA to observe the HI line will ultimately depend on the lower frequency cutoff of its observing range. Assuming the ngVLA will observe down to 1.2 GHz, HI studies would be limited to nearby galaxies ($0 < z < 0.1$). HI absorption surveys of bright (1.4 GHz fluxes $\gtrsim$ a few tens of mJy), nearby radio AGNs with existing radio telescopes have reported detection rates of ~30% (Geréb et al. 2014; Maccagni et al. 2017), suggesting that blind surveys of HI absorption in even lower-luminosity systems may be possible. The possibility of extending the ngVLA's frequency range below 1 GHz (e.g., Taylor et al. 2017) would greatly expand the redshift range over which HI would be observable with the ngVLA. We refer readers to Morganti et al. (2015b) for a more detailed discussion of the prospects for HI absorption studies with future radio telescopes being designed to operate over more favorable frequency ranges for HI science, such as the SKA and its pathfinders.

2.2.2. Molecular Gas

Identifying jet-driven molecular outflows is crucial for understanding the multiphase nature of AGN feedback (e.g., Rupke & Veilleux 2013; Emonts et al. 2014; Sakamoto et al. 2014; Alatalo et al. 2015; Morganti et al. 2015a). Molecular outflows may be identified on the basis of their spectral line shapes, such as the presence of broad wings or a shifted component (e.g., NGC 1266; Alatalo et al. 2011) or a P Cygni profile (Sakamoto et al. 2009). A survey of the cold gas properties of a large statistical sample of AGNs spanning a wide range of environments, host galaxy morphologies, SMBH masses, and nuclear activity classifications (e.g., high/low Eddington ratios, jetted/radio quiet, Compton thick/unobscured, etc.) would ultimately help establish an observationally-motivated model for the cosmic importance of outflows launched by active nuclei. We emphasize that improving our understanding of AGN feedback through ngVLA molecular gas observations will not be limited to objects with detectable outflows. A significant increase in the turbulence of the gas, or a substantial change in star formation efficiency/depletion time in the vicinity of the AGN (e.g., at the location the jet), may also provide an indirect means of studying more subtle feedback effects (e.g., Alatalo et al. 2015; Oosterloo et al. 2017).

The lowest energy transitions of the CO molecule, CO(1–0), CO(2–1), and CO(3–2) at rest frequencies of 115, 230, and 345 GHz, respectively, trace the total molecular gas reservoir at relatively low densities ($n_{\mathrm{H}_2} \sim 10^3$ cm^{-3}). The CO(1–0) line will be accessible to the ngVLA over the redshift ranges $0 < z \lesssim 0.5$ and $z \gtrsim 1.5$. The gap from $z \approx 0.5$ to 1.5 is due to the high telluric opacity of molecular oxygen that precludes ground-based observations from 52 to 68 GHz. Observations of the CO(2–1) line will be possible from $1 \lesssim z \lesssim 2$ and $z \gtrsim 3.5$, and the CO(3–2) line will be accessible over the range $2 \lesssim z \lesssim 4$ and also at $z \gtrsim 6$ (though see Section 2.2.3 regarding important caveats). We note that none of the low-J CO lines will be observable from $z = 0.5 - 1.0$, though transitions of other species probing denser gas, such as SiO and CS, will be accessible. For a graphical description of the redshift dependence of a wide variety of molecular gas species and transitions observable with the ngVLA, we refer readers to Figures 2 and 9 in Casey et al. (2015).

2.2.3. Important Caveats

The long ngVLA baselines of a few hundred km – although advantageous for pinpointing AGNs and resolving their continuum morphologies – will naturally lead to poor brightness temperature sensitivity, making it virtually impossible to study CO at the maximum angular resolution afforded by the array. With maximum ngVLA baselines of ~500 km in the north-south direction, the maximum angular resolution at 93 GHz would be ~10 mas, corresponding to a brightness temperature sensitivity[1] of $\sigma_{T_\mathrm{B}} \sim 350$ K for an integration time of 1 hr, a channel width of 10 km s^{-1}, and

[1]The brightness temperature sensitivity of a point source is defined as $\sigma_{T_\mathrm{B}} = \left(\frac{S}{\Omega_\mathrm{A}}\right)\frac{\lambda^2}{2k}$, where S is the flux density in units of W m^{-2} Hz^{-1}, k is the Boltzmann constant (1.38×10^{-23} Jy K^{-1}), and λ is the observing wavelength in meters. The quantity Ω_A is the beam solid angle and defined as $\Omega_\mathrm{A} = \frac{\pi\theta^2_\mathrm{FWHM}}{4\ln(2)}$, where θ_FWHM is the angular resolution in units of radians.

robust weighting (Selina & Murphy 2017). This is substantially higher than the minimum excitation temperature of the CO(1–0) line of 5.53 K. Thus, significant tapering of the data, as well as the application of new weighting schemes, will be necessary for studying jet-ISM feedback through ngVLA observations of the low-J CO transitions.

At high redshifts, the increasing influence of the cosmic microwave background (CMB) may also hinder the detectability of CO, particularly in the lower-J transitions. The increasing CMB temperature at high redshifts[2] both reduces the contrast of the CO emission against the background (particularly in cold molecular clouds with $T_{\rm kinetic} \sim$ 20 K) and changes the shape of the CO spectral line energy distribution by exciting a greater proportion of higher-J rotational levels (e.g., da Cunha et al. 2013; Zhang et al. 2016). As da Cunha et al. (2013) concluded, this will become particularly problematic for ngVLA observations of cold molecular clouds in non-starbursting galaxies at $z \sim 4$, where $T_{\rm CMB} = 13.65$ K. However, CMB heating is expected to be less problematic in molecular clouds in the vicinity of AGNs and jets, since AGN heating may increase the gas kinetic temperature to hundreds of degrees (Matsushita et al. 1998; Krips et al. 2008; Viti et al. 2014; Glenn et al. 2015; Richings & Faucher-Giguere 2017).

3. Multiwavelength Synergy

The unique combination of high sensitivity, resolution, and broad frequency range of the ngVLA will facilitate exciting advancements in our understanding of AGN feedback and its broader connection to galaxy evolution, particularly when combined with multiwavelength data from other state-of-the-art instruments. For example, observations with the Atacama Large Millimeter and Sub-millimeter Array (ALMA) at frequencies above the ngVLA's limit of 116 GHz will provide key insights on the energetic and chemical impact of jet-driven feedback on the dense gas phase of the ISM. At lower radio frequencies, the ngVLA and the Square Kilometre Array (SKA) will both probe the 21 cm line and trace jet-ISM feedback in the atomic phase through HI absorption at low redshifts. While only the SKA can observe the neutral HI content of the universe out to $z \sim 1$ to 2, which approaches the peak epoch of cosmic galaxy assembly, it cannot target the higher frequency tracers of molecular gas. The ngVLA will be uniquely suited for studying the molecular gas content of galaxies over a wide range of redshifts by targeting the lower$-J$ transitions of CO. In the optical and infrared, new 30m-class optical telescopes as well as the *James Webb Space Telescope* will further probe jet-ISM feedback via thir abilities to detect warm ionized outflows

JWST will also play an exciting role in direct studies of AGN feedback through the detection of outflows. In the NIR and MIR, *JWST* will observe the ro-vibrational lines of warm/hot molecular H_2 gas, using integral-field spectroscopy. By comparing the distribution and kinematics of warm/hot H_2 with that of the cold molecular gas, as traced by the low-J CO lines with ngVLA, the physics of AGN-driven outflows of molecular gas can be studied in detail (see, e.g., Rupke & Veilleux 2013; Emonts et al. 2014; **?**). MIR spectral-line diagnostics of features such as [NeV], the coronal line [SiVI], and polycyclic aromatic hydrocarbons (PAHs) will help distinguish between nuclear engines powered by AGN/star formation out to $z \sim 1.5$ (**?**).

[2]The redshift dependence of the CMB temperature follows the relation $T_{\rm CMB} = T^{z=0}_{\rm CMB} \times (1 + z)$, where $T^{z=0}_{\rm CMB} = 2.73$ K is the CMB temperature at $z = 0$.

References

Alatalo, K., Blitz, L., Young, L. M., Davis, T. A., Bureau, M., Lopez, L. A., Cappellari, M., Scott, N., Shapiro, K. L., Crocker, A. F., Martín, S., Bois, M., Bournaud, F., Davies, R. L., de Zeeuw, P. T., Duc, P.-A., Emsellem, E., Falcón-Barroso, J., Khochfar, S., Krajnović, D., Kuntschner, H., Lablanche, P.-Y., McDermid, R. M., Morganti, R., Naab, T., Oosterloo, T., Sarzi, M., Serra, P., & Weijmans, A. 2011, ApJ, 735, 88. 1104.2326

Alatalo, K., Lacy, M., Lanz, L., Bitsakis, T., Appleton, P. N., Nyland, K., Cales, S. L., Chang, P., Davis, T. A., de Zeeuw, P. T., Lonsdale, C. J., Martín, S., Meier, D. S., & Ogle, P. M. 2015, ApJ, 798, 31. 1410.4556

Casey, C. M., Hodge, J. A., Lacy, M., Hales, C. A., Barger, A., Narayanan, D., Carilli, C., Alatalo, K., da Cunha, E., Emonts, B., Ivison, R., Kimball, A., Kohno, K., Murphy, E., Riechers, D., Sargent, M., & Walter, F. 2015, ArXiv e-prints. 1510.06411

Condon, J. J., & Ransom, S. M. 2016, Essential Radio Astronomy

da Cunha, E., Groves, B., Walter, F., Decarli, R., Weiss, A., Bertoldi, F., Carilli, C., Daddi, E., Elbaz, D., Ivison, R., Maiolino, R., Riechers, D., Rix, H.-W., Sargent, M., & Smail, I. 2013, ApJ, 766, 13. 1302.0844

Davis, T. A., Krajnović, D., McDermid, R. M., Bureau, M., Sarzi, M., Nyland, K., Alatalo, K., Bayet, E., Blitz, L., Bois, M., Bournaud, F., Cappellari, M., Crocker, A., Davies, R. L., de Zeeuw, P. T., Duc, P.-A., Emsellem, E., Khochfar, S., Kuntschner, H., Lablanche, P.-Y., Morganti, R., Naab, T., Oosterloo, T., Scott, N., Serra, P., Weijmans, A.-M., & Young, L. M. 2012, MNRAS, 426, 1574. 1207.5799

Emonts, B. H. C., Piqueras-López, J., Colina, L., Arribas, S., Villar-Martín, M., Pereira-Santaella, M., Garcia-Burillo, S., & Alonso-Herrero, A. 2014, A&A, 572, A40. 1409.4468

Fabian, A. C. 2012, ARA&A, 50, 455. 1204.4114

Geréb, K., Morganti, R., & Oosterloo, T. A. 2014, A&A, 569, A35. 1407.1799

Glenn, J., Rangwala, N., Maloney, P. R., & Kamenetzky, J. R. 2015, ApJ, 800, 105. 1502.02041

Godfrey, L. E. H., & Shabala, S. S. 2016, MNRAS, 456, 1172. 1511.06007

Krips, M., Neri, R., García-Burillo, S., Martín, S., Combes, F., Graciá-Carpio, J., & Eckart, A. 2008, ApJ, 677, 262-275. 0712.0319

Lacy, M., Croft, S., Fragile, C., Wood, S., & Nyland, K. 2017, ApJ, 838, 146. 1703.03006

Maccagni, F. M., Morganti, R., Oosterloo, T. A., Geréb, K., & Maddox, N. 2017, A&A, 604, A43. 1705.00492

Matsushita, S., Kohno, K., Vila-Vilaro, B., Tosaki, T., & Kawabe, R. 1998, ApJ, 495, 267

Morganti, R., Frieswijk, W., Oonk, R. J. B., Oosterloo, T., & Tadhunter, C. 2013, A&A, 552, L4. 1302.2236

Morganti, R., Oosterloo, T., Oonk, J. B. R., Frieswijk, W., & Tadhunter, C. 2015a, A&A, 580, A1. 1505.07190

Morganti, R., Sadler, E. M., & Curran, S. 2015b, Advancing Astrophysics with the Square Kilometre Array (AASKA14), 134. 1501.01091

Mukherjee, D., Bicknell, G. V., Sutherland, R., & Wagner, A. 2016, MNRAS, 461, 967. 1606.01143

— 2017, MNRAS, 471, 2790

Nyland, K., Alatalo, K., Wrobel, J. M., Young, L. M., Morganti, R., Davis, T. A., de Zeeuw, P. T., Deustua, S., & Bureau, M. 2013, ApJ, 779, 173. 1310.7588

Nyland, K., Harwood, J. J., Mukherjee, D., Jagannathan, P., Rujopakarn, W., Emonts, B., Alatalo, K., Bicknell, G. V., Davis, T. A., Greene, J. E., Kimball, A., Lacy, M., Lonsdale, C., Lonsdale, C., Maksym, W. P., Molnár, D. C., Morabito, L., Murphy, E. J., Patil, P., Prandoni, I., Sargent, M., & Vlahakis, C. 2018, ApJ, 859, 23. 1803.02357

Oosterloo, T., Raymond Oonk, J. B., Morganti, R., Combes, F., Dasyra, K., Salomé, P., Vlahakis, N., & Tadhunter, C. 2017, A&A, 608, A38. 1710.01570

Querejeta, M., Schinnerer, E., García-Burillo, S., Bigiel, F., Blanc, G. A., Colombo, D., Hughes, A., Kreckel, K., Leroy, A. K., Meidt, S. E., Meier, D. S., Pety, J., & Sliwa, K. 2016,

A&A, 593, A118. 1607.00010
Richings, A. J., & Faucher-Giguere, C.-A. 2017, ArXiv e-prints. 1706.03784
Rupke, D. S. N., & Veilleux, S. 2013, ApJ, 775, L15. 1308.4988
Sakamoto, K., Aalto, S., Combes, F., Evans, A., & Peck, A. 2014, ApJ, 797, 90. 1403.7117
Sakamoto, K., Aalto, S., Wilner, D. J., Black, J. H., Conway, J. E., Costagliola, F., Peck, A. B., Spaans, M., Wang, J., & Wiedner, M. C. 2009, ApJ, 700, L104. 0906.5197
Selina, R., & Murphy, E. 2017, Next Generation Very Large Array Memo Series, 17. http://library.nrao.edu/ngvla.shtml
Soker, N. 2016, ArXiv e-prints. 1605.02672
Taylor, G., Dowell, J., Malins, J., Clarke, T., Kassim, N., Giacintucci, S., Hicks, B., Kooi, J., Peters, W., Polisensky, E., Schinzel, F., & Stovall, K. 2017, ArXiv e-prints. 1708.00090
Villar Martín, M., Emonts, B., Humphrey, A., Cabrera Lavers, A., & Binette, L. 2014, MNRAS, 440, 3202. 1403.1175
Viti, S., García-Burillo, S., Fuente, A., Hunt, L. K., Usero, A., Henkel, C., Eckart, A., Martin, S., Spaans, M., Muller, S., Combes, F., Krips, M., Schinnerer, E., Casasola, V., Costagliola, F., Marquez, I., Planesas, P., van der Werf, P. P., Aalto, S., Baker, A. J., Boone, F., & Tacconi, L. J. 2014, A&A, 570, A28. 1407.4940
Zhang, Z.-Y., Papadopoulos, P. P., Ivison, R. J., Galametz, M., Smith, M. W. L., & Xilouris, E. M. 2016, Royal Society Open Science, 3, 160025. 1605.03885
Zschaechner, L. K., Walter, F., Bolatto, A., Farina, E. P., Kruijssen, J. M. D., Leroy, A., Meier, D. S., Ott, J., & Veilleux, S. 2016, ApJ, 832, 142. 1609.06316

Science with a Next-Generation Very Large Array
ASP Conference Series, Monograph 7
Eric J. Murphy, ed.

DRAFT EDITION

Astrometry and Long Baseline Science

Mark Reid[1], Laurent Loinard[2] and Thomas Maccarone[3]

[1]*Harvard-Smithsonian CfA, Cambridge, MA, USA;* reid@cfa.harvard.edu

[2]*Centro de Radioastronomía – UNAM, Morelia, Michoacán, Mexico;* l.loinard@crya.unam.mx

[3]*Texas Tech University, Lubbock, TX, USA;* Thomas.Maccarone@ttu.edu

1. Introduction

Astrometry at centimeter to millimeter wavelengths has advanced dramatically over the last decade. VLBI techniques have been perfected and relative positional accuracy of $\approx 10\,\mu$as is routinely achieved for compact sources relative to background quasars (Reid & Honma 2014). Indeed, this demonstrated astrometric accuracy exceeds that of the *Gaia* mission goal and, since radio waves can penetrate even hundreds of magnitudes of visual extinction, provides unique opportunities to fully explore the Galactic plane and deeply embedded sources in star forming regions. Long baseline radio interferometry has produced some remarkable results, including 1) detailed mapping of accretion sub-parsec scale disks around supermassive black holes in galaxies well into the Hubble flow, yielding "gold standard" masses for the black holes and direct estimates of the Hubble constant independent of all other methods (Gao et al. 2016), and 2) measurements of trigonometric parallax to masers in star forming regions across large portions of the Milky Way, revealing its true spiral structure, size, and rotation curve (Reid et al. 2014).

Many potential applications of radio astrometry are currently limited by the sensitivity of long baseline interferometry with, for example, ten antennas of 25-m diameter. The ngVLA with long baselines comparable to size of North America could provide a sensitivity increase of more than an order of magnitude, which translates to the ability to detect > 30-times more sources (for $N \propto S^{-3/2}$), both for astrometric targets and background quasars. The greatly increased background source counts project to a decrease in target-quasar separation by a factor of $\sqrt{30}$, which directly translates to improved astrometric accuracy by the same factor. Thus, the ngVLA could potentially achieve astrometric accuracies of $\approx 1\,\mu$as! In this chapter we explore some of the applications of the astounding capabilities of the ngVLA with long baselines based on our current knowledge of the Universe. Of course, by 2030 and later, new and unknown applications are almost certain to be important for the advancement of astrophysics.

2. Gravitational Wave Sources

The ngVLA has the potential to directly observe the last stages of the inspiral of compact binaries, as well as post merger activity, across the Universe. The merger of two neutron stars, such as recently observed by *LIGO*, or a neutron star and a black hole, can produce emission across the electromagnetic spectrum. Even at distances of hundreds of Mpc, the ngVLA could make movies of expanding ejecta or jets, since at cosmological source distances, scales of $\sim$ 1 pc correspond to $\sim$ 1 mas (Alexander et al. 2017). One can also expect to witness the inspiral of supermassive black holes (SMBHs), complementing a future space-based gravitational wave detector like *LISA*, by providing the only way to achieve *resolved* images of electromagnetic counterparts.

The International Pulsar Timing Array goal is to detect gravitational waves by timing an array of about 30 pulsars. While distances to these pulsars can be solved for from the timing data, having to solve for these terms introduces a noise term and some parameter correlations. Obtaining independent pulsar distances via trigonometric parallaxes will be possible with long baselines on the ngVLA, and this could substantially increase the sensitivity of gravitational wave detections.

3. Black Holes

Fermi has detected an amazing variety of energetic phenomena, including beams of particles of unexpectedly high energy. Some of the most energetic sources in the universe are found in AGN. One of the most important and long-standing problems in astrophysics is to answer how do cosmic accelerators work and what are they accelerating? VLBA imaging of AGNs has revealed that gamma-ray emission comes from jet components (Hodgson et al. 2017), and not always from the immediate vicinity of SMBHs. Still, important questions remain: Are jets proton-electron or positron-electron plasma? What powers and collimates AGN jets and how do these jets evolve and interact with their host galaxy? Long baseline radio interferometry provides the highest angular resolution possible to make movies of these amazing phenomena on scales down to the ergospheres of nearby SMBHs. Note that recent advances in theory and computation have opened the possibility of fully relativistic, magneto-hydrodynamic simulations in 3-dimensions. High sensitivity and resolution observations with long baselines on the ngVLA will be critical to guide simulations and finally arrive at a deep understanding of these fundamental astrophysical phenomena.

H_2O masers in AGN accretion disks have been used to measure accurate SMBH masses and the Hubble constant. But they also have the potential to determine physical properties of these sub-parsec scale disks. Of particular interest is mapping the magnetic fields in these disks via spatially resolved polarization measurements (Zeeman effect). Currently, observations have provided upper limits to magnetic field strength (Modjaz et al. 2005), but, with the greatly increased sensitivity of the ngVLA, detection should be possible. Indeed, it will be the only telescope that can make such resolved measurements in the foreseeable future.

Stellar mass black holes pose equally fascinating questions. Do these black holes form from supernova (SN) or by direct collapse without explosions? What is the origin of black hole spin? The ngVLA will be able to provide unique clues that address these questions by measuring parallax and proper motions. For example, the long-standing controversy over the distance to Cyg X-1 (the source of the famous wager between Thorne and Hawking) was recently resolved by long baseline radio astrometry; its accurate parallax distance of 1.86 ± 0.12 kpc (Reid et al. 2011) allowed a precise determination of the mass of the compact object of $15{\pm}1\ M_\odot$ (Orosz et al. 2011), clearly indicating a black hole, and was key to determining that the black hole is spinning maximally with a*>0.92 (Gao et al. 2011). This binary is too young for accretion to have appreciably spun up the black hole, indicating it was born with great spin. Regarding its birth, its measured distance and proper motion (peculiar motion of only 20 km/s) matches that of the Cyg OB3 star-forming cluster, establishing that it was born in this young cluster. Since a SN explosion would have disrupted the region, the black hole probably formed with a quiet, prompt stellar collapse (Mirabel & Rodrigues 2003). But this is only one source and similar measurements of many more, weaker sources with the ngVLA are needed to understand their complete demographics and determine how they formed. It is important to note that most known black hole X-ray binaries are both too far and too extincted for precise Gaia parallaxes.

At the present time, measurements of astrometric wobble of the black hole (induced by the secondary star in the binary) are marginally possible in one X-ray binary, Cygnus X-1 (Reid et al. 2011). With the ngVLA, if it has enough collecting area on long baselines, proper tracing of orbits should become possible for a few X-ray binaries, both due to the increased sensitivity and the ability to work at higher frequencies, which will allow both better angular resolution and more easily manageable systematics due to less extended emission from jets. This is vital, because the biggest uncertainty in black hole mass measurements usually comes from the precision of the estimation of the inclination angle of the orbit, since the inferred mass scales as $\sin^3 i$. Additional uncertainties come into play from having incorrect inclination angles using either the disk continuum method for spin estimation (e.g. Steiner et al. 2017) or the reflection method (e.g. Garcia et al., 2013).

Understanding the distribution of masses of black holes and neutron stars is one of the few means we have to probe the actual process of supernova explosions. At the present time, there appears to be a gap between the lowest mass black holes and the highest mass neutron stars, which would imply that whatever instability causes supernovae to actually blow up must be relatively rapid (Belczynski et al. 2012), but it remains quite possible that the gap is an artifact of the biases in inclination angle measurements from ellipsoidal modulations (Kreidberg et al. 2012). Having even a few systems where direct inclination angle measurements from astrometric wobble can be used to calibrate the ellipsoidal modulation of the secondary's light would be vital for building samples of well-understood black hole masses and spins.

4. Fundamental Physics

Pulsar parallaxes and proper motions precisely locate these stellar remnants in the Galaxy and provide full phase-space information. Coupled with rotation and dispersion measurements, this can be used to model the magnetic field and electron density of the Milky Way (Cordes et al. 1991). Peculiar motions (after removing Galactic rotation) give direct information on "kicks" received at birth by asymmetrical SN explosions. Additionally, knowing distances to pulsars allows accurate mass measurements. Pulsar mass is the key parameter to discriminating among competing models for the equation-of-state of material at the extreme density of neutron stars.

One interesting problem critically dependent on the Galaxy's fundamental parameters (eg, R_0 & Θ_0; see the Milky Way section below) involves the interpretation of the orbital decay of the Hulse-Taylor binary pulsar system, owing to gravitational radiation as predicted by General Relativity. In 1993, the Nobel Prize in Physics was awarded for this measurement. In order to properly interpret the observed decay rate, one needs to account for the accelerations of the Sun (Θ_0^2/R_0) and the pulsar ($\Theta(R)^2/R$) from their Galactic orbits. In 1993, uncertainties in the values of R_0 and Θ_0 limited the Relativity test to ±0.23%. With improved values based on maser parallaxes, this uncertainty was reduced by a factor of 3. Interestingly, with these values, there is a 3σ discrepancy from General Relativity, using the pulsar distance of 9.9 kpc assumed in 1993. This discrepancy would vanish if the pulsar distance is 7.2 kpc (Reid et al. 2014). An accurate pulsar parallax is critical to test this prediction, but may require the sensitivity of the ngVLA as the pulsar is weak. Of course there are other binaries that can be used to test General Relativity, and distances to these coupled with accurate models of the Galaxy are needed and could be supplied by the ngVLA with long baselines.

Are physical "constants," such as the fine-structure constant and the proton-to-electron mass ratio, different in the early Universe? Does the cosmic microwave background temperature evolve as predicted with redshift? These and other questions (see section on Galaxy Evolution) can be addressed by imaging molecular clouds at high redshift in absorption against bright AGNs. However, high sensitivity and angular resolution (~ 1 mas) are crucial to detecting and isolating (resolving) individual pc-scale clouds, since observations at lower resolutions blend together clouds that have a wide range of physical conditions (Sato et al. 2013).

5. Galaxy Evolution

The Local Group offers a critical opportunity to study the formation and evolution of galaxies with extremely high resolution (ie, local cosmology). Long baseline observations have been able to measure the proper motions of two of Andromeda's satellite galaxies, M 33 (Brunthaler et al. 2005) and IC10 (Brunthaler et al. 2007). Fig. 1 schematically shows the locations of the Milky Way, M 31 (Andromeda) and M 33, along with the motion of M 33. These constrain values of the distance and mass of Andromeda. The key parameter for determining the the distribution of dark matter and the history and fate of the Local Group is the proper motion of Andromeda itself, which would give its 3-D velocity relative to the Milky Way.

Current estimates of Andromeda's proper motion vary considerably, from values near zero to over 100 km/s. This range allows scenarios in which Andromeda directly hits the Milky Way in a few billion years or instead they could orbit each other for a very long time. The most direct and accurate measurement to solve this problem would be astrometric measurements of the AGN in Andromeda, M 31*, with μas accuracy over several years. This may only be possible with the ngVLA sensitivity coupled with long baselines, since M 31* is extremely weak, ~ 10 μJy.

How early do SMBHs form and how do they relate to their protogalaxies? When studying protogalaxies, it is crucial to understand what portion of the emission is attributable to a SMBH and what comes from a more extended star-burst. At $z \approx 6$, a 100 pc sized star-burst nucleus subtends 18 mas (and smaller at intermediate redshifts). For a radio-bright SMBH, the best telescope to resolve and separate AGN from star-bursts would be the ngVLA with long baselines.

Are molecular clouds seen toward high redshift galaxies different than those seen locally? Molecular absorption line observations at the high angular resolution afforded by long baselines on the ngVLA may be the only foreseeable way to probe the density, temperature, and structure (filamentary?) of molecular clouds in the early Universe.

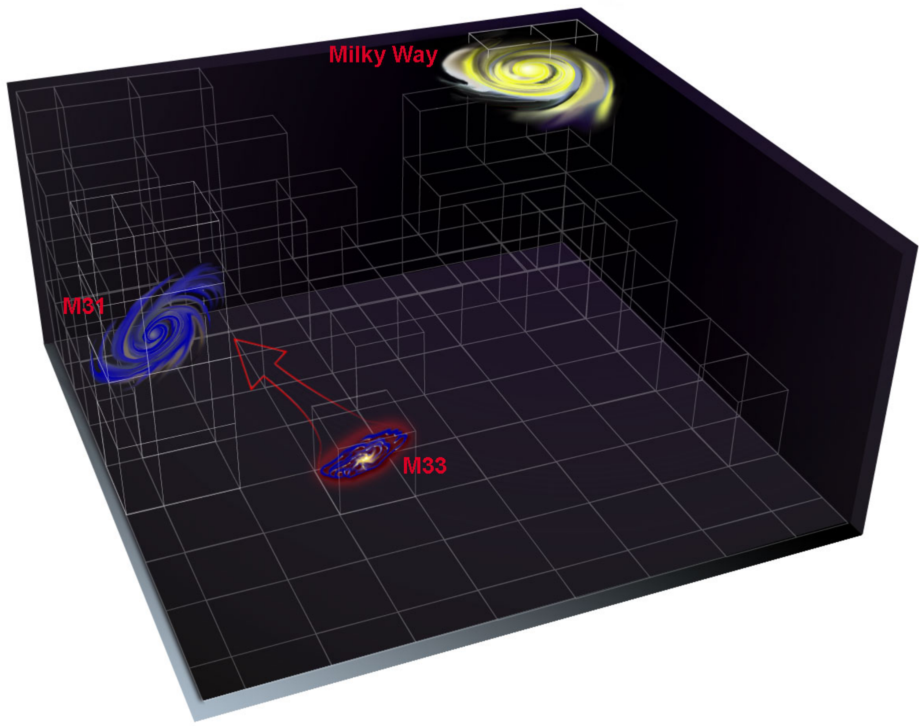

Figure 1. Local Group proper motions. Schematic view of the Local Group of Galaxies with the Milky Way in the upper right and the Andromeda galaxy (M 31) in the left. The measured 3-D motion of M 33 is indicated with the red arrow. Only the radial component, approaching the Milky Way at $\approx$ 110 km s^{-1}, of the motion of Andromeda is known. If Andromeda's proper motion is small it will collide with the Milky Way in a few billion years. However, if it has a substantial proper motion ($\sim$ 100 km s^{-1}), Andromeda and the Milky Way will orbit each other for a very long time.

6. Milky Way Structure

VLBI parallax and proper motions of masers have been measured for $\approx$ 200 high mass star formation regions (HMSFRs), as shown in Fig. 2. These clearly trace spiral structure across large portions of the Milky Way (Reid et al. 2014), and provide the most accurate estimates of the distance to the Galactic center, R_0 (currently with about 2% accuracy), the rotation speed of the Galaxy at the Sun, Θ_0, and the Galaxy's rotation curve. However, with current sensitives, very few sources are detected that are beyond the Galactic center. So, roughly half of the Milky Way remains "terra incognito." The ngVLA with baselines of thousands of km would have the sensitivity and angular resolution to complete a map of the Milky Way. The greater sensitivity of the ngVLA, compared to the current VLBA, allows the use of weaker QSOs that are then closer in angle to the target sources. This yields improved parallax accuracy which coupled with an increased sample size should allow estimation of R_0 to 1% accuracy.

Pulsar parallaxes can provide an accurate map of their locations in the Galaxy. Coupled with rotation and dispersion measurements, they can be used to model the

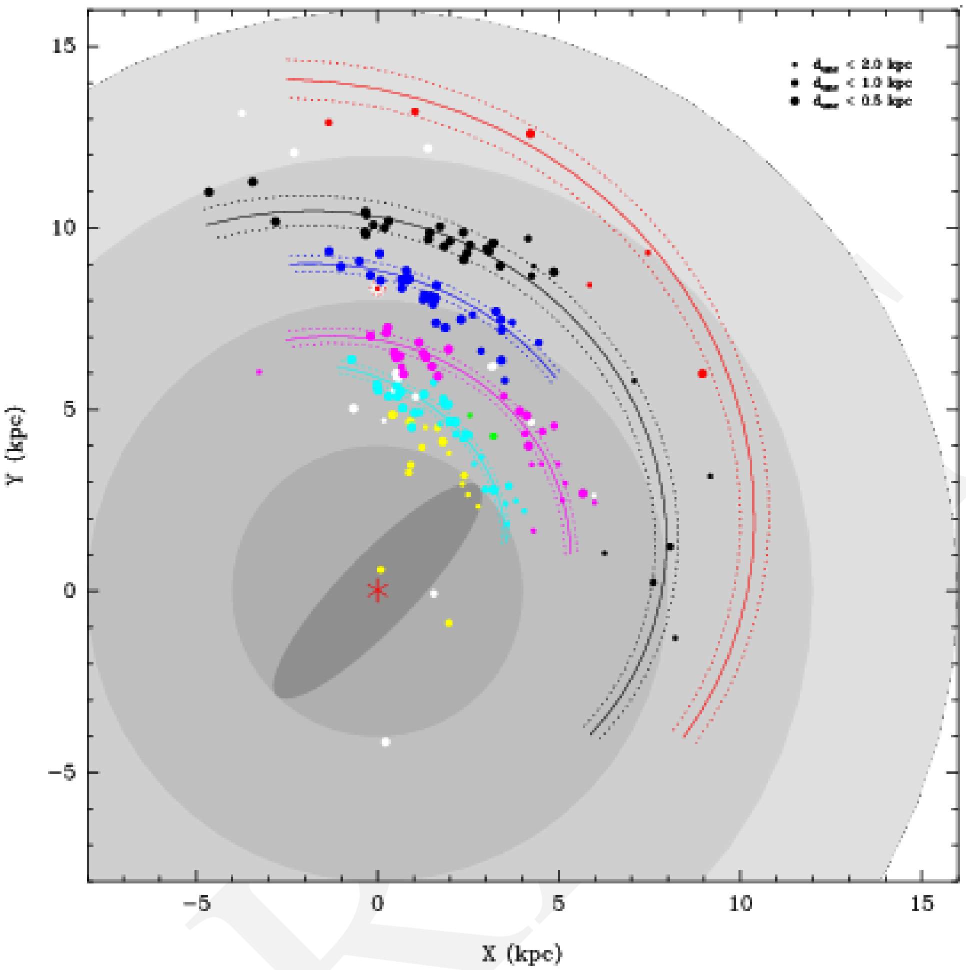

Figure 2. Plan view of the Milky Way showing the locations of high-mass star forming regions (HMSFRs) with trigonometric parallaxes measured with VLBI (Reid et al, in preparation). The Galactic center (*red asterisk*) is at (0,0) and the Sun (*red Sun symbol*) is at (0,8.34). HMSFRs were assigned to spiral arms based primarily on association with structure seen in $\ell - V$ plots of CO and hydrogen emission (and not based on the measured parallaxes): Inner Galaxy sources, *yellow dots*; Scutum arm, *cyan octagons*; Sagittarius arm, *magenta hexagons*; Local arm, *blue pentagons*; Perseus arm, *black squares*; Outer arm, *red triangles*. Distance errors are indicated in the legend. The background grey disks provide scale, with radii corresponding in round numbers to the Galactic bar region ($\approx$ 4 kpc), the solar circle ($\approx$ 8 kpc), co-rotation of the spiral pattern and Galactic orbits ($\approx$ 12 kpc), and the end of major star formation ($\approx$ 16 kpc). The "long" bar is indicated with a shaded ellipse. The *solid* curved lines trace the centers (and *dotted* lines the 1σ widths) of the spiral arms. Note that there are few measurements for sources beyond the Galactic center (negative Y values); long baselines with the ngVLA will provide the sensitivity and angular resolution to help finish this map.

magnetic field and electron density of the Milky Way. Since radio astrometry improves dramatically at frequencies above a few GHz (to minimize the turbulent and difficult to model ionosphere), the greatly improved sensitivity of the ngVLA, compared to current long baseline interferometers, is needed to do astrometry on these very steep-spectrum sources.

7. Young Stars and Stellar Systems

The evolution of a star is almost entirely determined by its mass (and, to a much smaller extent, its chemical composition). Thus, direct stellar mass measurements are of great importance to constrain theoretical stellar evolution models. Such measurements can be obtained in multiple stellar systems if the orbital motions are monitored with sufficient accuracy and over a period covering a significant fraction of an orbital period. For main and pre-main sequence stars, this is best achieved using optical and near-infrared imaging techniques (adaptive optics, aperture masking interferometry, etc.). However, for protostellar objects one must turn to longer wavelengths on account of the high extinction that affects such deeply embedded objects. Millimeter and centimeter interferometric observations are critical, since they can reach both very high angular resolution and high astrometric accuracy.

At the moment, monitoring of orbital motions has only been possible for a small number of very young (class 0) stellar systems: eg, IRAS 16293–2422 (Loinard et al. 2002), L1551 IRS5 (Rodriguez et al. 2003), and YLW15 (Curiel et al. 2002), via multi-epoch VLA observations. However, none of these observations cover a sufficient fraction of an orbit to enable a reliable mass estimate. The ngVLA with baselines longer than 300 km and a sensitivity 10-times higher than the VLA would permit significant progress in two ways. First, relative positions between the members of binary systems could be measured to at least 10-times higher accuracy, and this would result in a much higher precision in orbit (and, therefore, mass) determination. Second, the higher resolution of the ngVLA would enable the identification of much tighter systems (with separations as small as $\sim$ 10 mas, compared with $\sim$ 100 mas for the VLA) with commensurably shorter orbital periods. Reliable mass measurements would be attained for such systems. It is worth emphasizing that the very early evolution of stars is still a very open research topic and that accurate mass measurements at the earliest protostellar stages would have a great impact.

Protostellar jets are ubiquitous in young stellar objects, and two mechanisms have been proposed to explain their launching. In magnetospheric models, they are associated with the accretion mechanisms that occur on scales of $\sim$ 0.1 AU ($\sim$ 1 mas at the distance of nearby star-forming regions). For disk-wind models, in contrast, the launching occurs on scales comparable with those of the inner accretion disk region ($\sim$ 10 AU; or 100 mas). Baselines of at least 300 km would provide an angular resolution in the centimeter regime of about 10 mas, which would be sufficient to discriminate between the two mechanisms, and to resolve the jets in the transversal direction if the disk-wind hypothesis holds. However, baselines of at least a few thousand kilometers would be required to resolve jets launched through magneto-centripetal acceleration.

8. Commercial Applications

While the benefits of the ngVLA to classical astrophysics have been discussed above, there may be significant other benefits to society. VLBI observations supply accurate telescope locations on a global scale. This is used to calibrate GPS positioning, which is an integral part of our economic activity. Also VLBI has demonstrated that it can track spacecraft with exceptional accuracy. Had VLBI been used to track the Martian lander that crashed into its surface, the metric-vs-English units error that lead to the multi-billion dollar disaster could have been caught and rectified. As the USA aims to send robotic crafts and humans to Mars and beyond, it seems foolish (and dangerous) not to use the best independent method of spacecraft tracking, which the ngVLA with long baselines could provide.

References

Alexander, K. D. et al. 2017, ApJ, 848, 21
Belczynski, K., Wiktorowicz, G., Fryer, C. L. et al. 2012, ApJ, 757, 91
Brunthaler, A. et al. 2005, Sci, 307, 1440
Brunthaler, A. et al. 2007, A&A, 462, 101
Cordes, J. M. et al. 1991, Nat, 354, 121
Curiel, S., Girart, J. M., Rodriguez, L. F. & Canto, J. 2002, ApJ, 638, 878
Gao, L. et al. 2011, ApJ, 742, 85
Gao, F. et al. 2016, ApJ, 817, 128
Garcia, J., Dauser, T. Reynolds, C. S. et al. 2013, ApJ, 768, 146
Hodgson, J. A. et al. 2017, A&A, 597, 80
Kreidberg, L., Bailyn, C. D., Farr, W. M. & Kalogera, V. 2012, ApJ, 757, 36
Loinard, L. 2002, RMxAA, 38, 61
Mirabel, I. F. & Rodrigues, I. 2003, Sci, 300, 1119
Modjaz, M., Moran, J. M., Kondratko, P. T. & Greenhill, L. J. 2005, ApJ, 626, 104
Orosz, J. A. et al. 2011, ApJ, 742, 84
Reid, M. J. et al. 2011, ApJ, 742, 83
Reid, M. J. & Honma, M. 2014, ARA&A, 52, 339
Reid, M. J. et al. 2014, ApJ, 700, 137
Rodriguez, L. F. et al. 2003, ApJ, 583, 330
Sato, M., Reid, M. J., Menten, K. M. & Carilli, C. L. 2013, ApJ, 764, 132
Steiner, J. F., Garcia, J. A., Eikmann, W. et al. 2017, ApJ, 836, 119

Science with a Next-Generation Very Large Array
ASP Conference Series, Monograph 7
Eric J. Murphy, ed.

DRAFT EDITION

Unwinding Star Formation with Next-Generation Galactic Plane Survey

Erik Rosolowsky,[1] Adam Ginsburg,[2] and Adam Leroy[3]
[1]*University of Albera, Edmonton, AB, Canada;* rosolowsky@ualberta.ca

[2]*National Radio Astronomy Observatory, Socorro, NM, USA;* adam.g.ginsburg@gmail.com

[3]*The Ohio State University, Columbus, OH, USA;* leroy.42@osu.edu

Abstract. The ngVLA will enable for efficient surveys of a large fraction of the Galactic plane in a suite of molecular gas tracers from the 3mm band, including both low (CO) and high (HCN, HCO^+, N_2H^+) critical density transitions. The key motivation for a next generation Galactic Plane survey is spanning a wide dynamic range of scales at high sensitivity. Such a survey will determine the connections between the kiloparsec scale galactic processes like feedback and instabilities down through the turbulent cascade to the thermal scales where individual stellar cores form (0.1 pc). While current facilities must stitch together these effects over different regions, only the ngVLA will have the mapping efficiency required to map square-degree areas with the 1" resolution to deduce how galactic physics regulates all aspects of star formation.

1. Introduction

Star formation is the dominant process in the secular evolution of galaxies, and understanding how galaxies form stars through cosmic time remains a vital open question in understanding the evolution of the Universe. The ngVLA is uniquely able to provide the definitive census of the dominant physical and chemical processes that shape the molecular ISM and govern how stars form. Historically, studies of star formation in the context of galaxy evolution have focused on the rate of star formation as a function of gas properties and local galactic environment. However, the properties of the molecular gas must set the other outputs of star formation: the initial mass function, cluster masses and properties, and distribution of binary masses and orbital properties. All of these outputs establish the resulting stellar populations, the patterns of enrichment, and the nature of feedback into a galaxy.

One of the major data products from the ngVLA should be to survey a large fraction of the Milky Way disk at spatial scales resolving the thermal dissipation length in molecular clouds (0.1 pc). This survey will (1) conclusively identify the critical scales governing star formation and (2) definitively link variations in local Galactic properties to changes in star formation for all the outputs of the process (IMF, binary properties, clusters). While we routinely observe on scales from < 0.1 pc in nearby clouds to 10s of pc scales across the disk, we are lacking a unified survey that covers the full range of these scales over a substantial fraction of the Galactic volume. Using the full suite of molecular line diagnostics available throughout the ngVLA observational bands, we will directly measure the flow of energy, mass and momentum through the interstellar medium into newly forming stars and their feedback on the surrounding gas.

2. Scientific Motivation

The molecular ISM is shaped by gravitation, turbulence, magnetism, radiation, and chemistry. These effects play out on a wide range of scales from the scale length of the disk (kpc) down to the thermal dissipation scale (< 0.1 pc). Since the molecular medium hosts all star formation in the modern universe, understanding how the conditions in the ISM establish star formation has been a subject of study for decades. While vast progress has been made, the subject remains unsolved and the primary difficulty in making progress arises because the process is both *multi-physics* and *multi-scale*. With the ngVLA, it is possible to establish the definitive observational data set that will lay the groundwork for overcoming these barriers. This possibility comes because only the ngVLA has the capability of making a multi-tracer study of the Galactic plane (to address multi-physics) over a vast spatial dynamic range (to address multi-scale). Unlike other proposed instruments, the ngVLA can efficiently observe the smallest scales over a large part of the disk. By observing a suite of molecular gas tracers, we will be able to establish the definitive inventory of physics at play in disk galaxies.

Wide Spatial Dynamic Range:The ngVLA makes it possible to measure *all* the relevant scales in the molecular medium and calculate the interplay between the governing physical effects. This will reveal whether the outer scales of the molecular medium (the clouds) represent a significant feature in the hierarchy of the ISM. The proposed observations will trace this hierarchy down to the turbulent dissipation scales across the disk, identifying how the balance of physical forces evolves with scale throughout the galaxy, making a direct connection to the regulation of the star formation process. This wide range of scales is required since the best probes of turbulence require characterization over a wide range. Critically, these data will test conjectures that the properties of the turbulent flows account for variations in modes of star formation through the disk. Given the sensitivity and range of scales proposed by the ngVLA, this survey would enable the definitive and ultimate tests of the physics of galaxy-scale star formation given our current understanding.

To date, the molecular ISM has already be surveyed at these different scales in different objects (Figure 1). Studies of nearby molecular clouds probe down to the thermal scales of the emission (e.g., Ridge et al. 2006; Kong et al. 2018). Surveys of the Milky Way disk span larger scales that can reach the scale height and length of the disk (e.g., Dame et al. 2001; Jackson et al. 2006; Dempsey et al. 2013) but are limited in their dynamic range at the small scales. While these disjoint data have been at the foundation of our understanding of star formation, we are hampered by having to synthesize across different galactic environments. Specifically, changes in the efficiency of the star formation process arise in different galactic environments but our understanding of how star formation plays out at small scales is extrapolated from our observations of local clouds.

Efficient Observation of Multiple Tracers: The centimeter to millimeter bands provide tracers of all the relevant physical processes in star formation. With wide instantaneous bandwidth, it becomes possible for the ngVLA to sample these all simultaneously. While molecular hydrogen is difficult to observe directly, our understanding of ISM properties comes through different chemical species. We can trace the location of the material through relatively uniform bulk gas tracers like the isotopologues of CO, which trace $n \sim 10^2$ cm^{-3} gas (Shirley 2015). With excellent spectral resolution, we use the velocity information to understand ISM dynamics and therefore turbulence and gravitation. High-dipole-moment species such as HCN, CS, N_2H^+, and CN provide similar observations but only in the highest density gas associated with star formation ($n \sim 10^{4.5}$-10^5 cm^{-3}; Shirley 2015). Molecular line excitation also directly traces the influence of the radiation field (e.g., ^{12}CO excitation in Figure 1). Recombination lines and centimetre-wave continuum data directly identify regions of high mass star formation. Polarized continuum data can unwind the structure of the magnetic field. While all these are accessible to the ngVLA, here we focus on the utility of the millimetre-wave molecular line toolkit.

3. ngVLA Observations and Complementary Facilities

This science case proposes the Next Generation Galactic Plane Survey (ngGPS) in several tracers across the 3 mm band. This science case is built around the idea that the ngVLA will be able to survey several spectral lines separated by up to ~ 10 GHz. With this assumption, the proposed survey focuses on two spectral windows: the CO isotopologues near 110 GHz (^{12}CO, ^{13}CO, C^{18}O as well as CN) and a suite of dense gas tracers (HCN, HCO^+, CS, N_2H^+) near 90 GHz. The molecular disk observable by the ngVLA spans ~ 300 deg^2 which should be imaged from the largest possible angular scales down to 1″. The maximum resolution corresponds to two resolution elements across the 0.1 pc thermal scale at a distance of 10 kpc. We target 500 mK sensitivity in an 0.2 km/s channel, representative of detecting faint tracers of dense gas at the thermal line width for H_2. Using the ngVLA reference design, reaching this depth and resolution requires 70 seconds of integration time. With a primary beam size of 0.4 arcmin^2, covering 1 deg^2 would take 175 hours per tuning. For reference, using ALMA to map 1 deg^2 would require 2300 hours of 12-m array time. Thus, individual regions can be mapped in the scope of PI on the ngVLA projects and an extra-large program can provide the ultimate Galactic plane survey.

The high surface brightness sensitivity of the ngVLA over a wide range of spatial scales is what enables the ngGPS. While ALMA can observe many of the same properties, it will be restricted to small scale studies in the Milky Way. A broad census of the entire Galaxy remains prohibitive to other facilities, especially spanning the wide range of scales. However, it is precisely the wide area survey that will provide the progress toward understanding star formation. In overlapping portions of the sky,

ALMA can readily probe the higher rotational transitions of the target species over small regions. However, the ngVLA is uniquely able to probe regions in first and second Galactic quadrants, including the nearest signs of interaction with the spiral structure found in the Cygnus X region. The complementary access to higher-energy transitions probes the thermodynamics of GMCs using CO spectral-line energy distributions. ALMA and potentially the Origins Space Telescope will necessarily focus on small regions whereas OST will have relatively poor resolution. The ngVLA data set provides the best available channel to stitch together these complementary views of the molecular ISM. No other facility would be able to provide the wide-dynamic-range imaging of the Galaxy in these spectral lines.

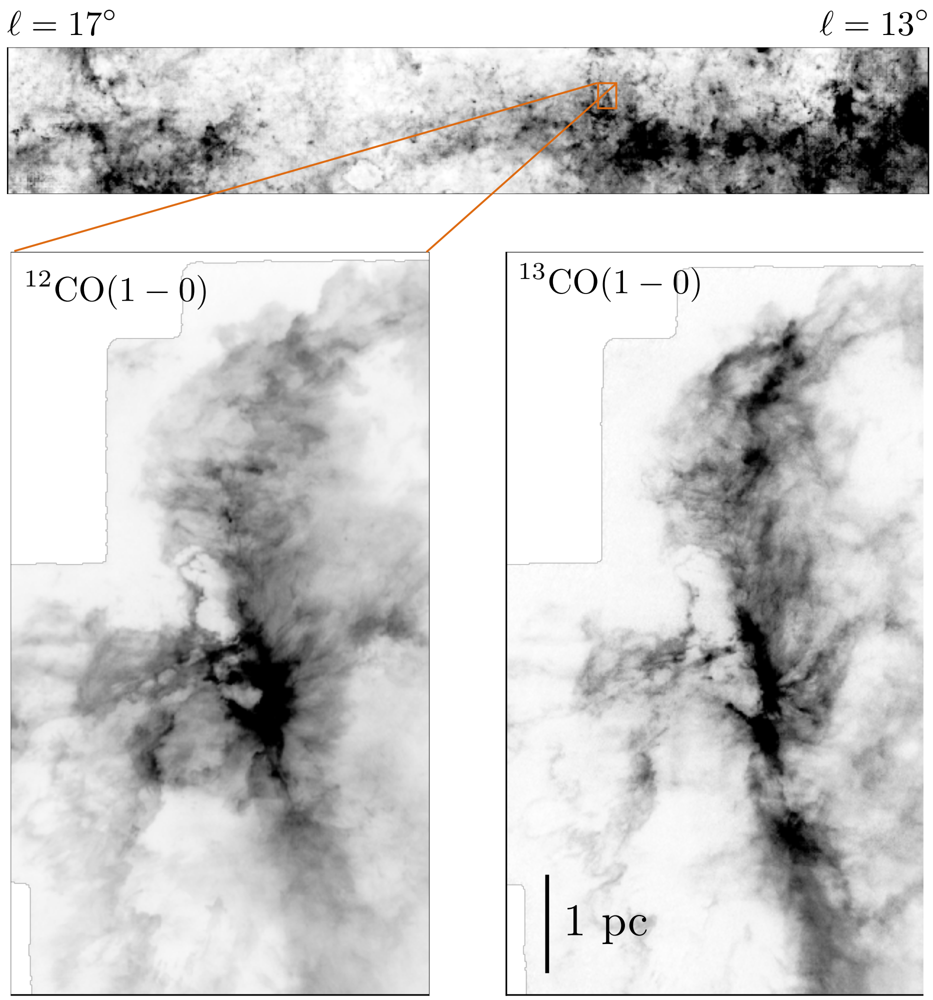

Figure 1. Example data quality that would be provided through ngGPS observations of the Galactic plane based on example data sets. The top panel shows observations taken from the JCMT CO High Resolution survey in ^{12}CO(3-2) which is the highest resolution molecular line image of the Galactic Plane available (14″ Dempsey et al. 2013). The bottom panels show integrated intensity maps for ^{12}CO(1-0) and ^{13}CO(1-0) of the Integral Shaped Filament in Orion obtained through the CARMA-NRO Orion Survey (Kong et al. 2018). The ngGPS would provide a high-resolution, multi-tracer survey of the Galactic plane with linear resolution comparable to the Orion data.

4. Scientific Strategy

The ngGPS aims to characterize the star forming interstellar medium. The broadest impact of such a survey would be from the release of survey data products for general use, immediately becoming the definitive ground truth survey of the molecular medium in the Milky Way.

Used as a survey, the data can be used to infer the physical properties of the molecular medium throughout the Milky Way. The CO isotopologues reveal the opacity and excitation conditions within molecular clouds, which is challenging to do from single line studies alone. With a wide dynamic range in spatial resolutions, observing low opacity lines is essential for a complete census of high column density regions (e.g., $C^{18}O$). Tracers that are only excited in high density regions (e.g., HCN, HCO^+, N_2H^+) are key for tracing mass and momentum flow into the regions that immediately host star formation. By tracing down to 0.1 pc scales, the ngGPS will identify the *core* populations throughout the visible Galactic plane, which will provide a link to IMF variations and show how clusters form and evolve.

While the 3-mm band provides a robust physical toolkit, the key advantage of a Galactic plane survey is to use this full toolkit to trace how star forming gas evolves in different Milky Way environments. With a progressively refined understanding of the longitude-velocity space founded on trigonometric parallax (Reid et al. 2014), it will possible to map molecular emission to three dimensional position in the Galaxy. The three key contrasts dynamical environment (arm vs. interarm vs. center), radial (tracing different stellar potentials, metallicities) and vertical (tracing different pressure levels). The survey will trace the mass distribution, and the flow of momentum (through Doppler shift analyses) and energy flux (through Doppler shift and molecular line cooling studies). While it is difficult to predict the exact questions that will directly drive a Galactic plane survey after ngVLA construction, such a data set would immediately answer a myriad of questions about Galactic evolution that currently face the community. By directly tracing gas motion in the molecular medium throughout the galaxy, we could directly measure how turbulence regulates star formation (McKee & Ostriker 2007) by relating its power spectrum, anisotropy, and solenoidal fraction to local star formation rates. With a broad census of molecular clouds, we could trace the life cycle of molecular clouds including their thermodynamics, and chemistry. We would have the data required to measure variations of the core mass function in time and evolution, establishing the understanding the stellar initial mass function. Furthermore, we would also know the angular momentum distribution within molecular clouds and determining how this regulates binary star formation.

Depending on the flexibility of the ngVLA instrument, commensal science goals could easily be achieved through a flexible deployment of correlator and receiver resources. For example, continuum observations will reveal compact HII regions, bright dust emission features, and non-thermal events. Stacking radio recombination line emission will provide opacity-free measurements of the dynamics of ionized regions as well as tracers of the ionizing radiation field. Finally, a multi-epoch survey strategy may be ideal for revealing transient sources for further study.

Acknowledgments. ER acknowledges the support of the Natural Sciences and Engineering Research Council of Canada (NSERC), funding reference number RGPIN-2017-03987.

References

Dame, T. M., Hartmann, D., & Thaddeus, P. 2001, ApJ, 547, 792
Dempsey, J. T., Thomas, H. S., & Currie, M. J. 2013, ApJS, 209, 8
Jackson, J. M., Rathborne, J. M., Shah, R. Y., et al. 2006, ApJS, 163, 145
Kong, S., Arce, H. G., Feddersen, J. R., et al. 2018, arXiv:1803.11522
McKee, C. F., & Ostriker, E. C. 2007, ARA&A, 45, 565

Reid, M. J., Menten, K. M., Brunthaler, A., et al. 2014, ApJ, 783, 130
Ridge, N. A., Di Francesco, J., Kirk, H., et al. 2006, AJ, 131, 2921
Shirley, Y. L. 2015, PASP, 127, 299

Science with a Next-Generation Very Large Array
ASP Conference Series, Monograph 7
Eric J. Murphy, ed.

DRAFT EDITION

Neutral Atomic Hydrogen in the Local Universe

D.J. Pisano,[1,2] Fabian Walter,[3] and Snežana Stanimirović[4]

[1]*Dept. of Physics & Astronomy and Center for Gravitational Waves & Cosmology, West Virginia University, Morgantown, WV, USA*
[2]*Adjunct Astronomer at Green Bank Observatory, Green Bank, WV, USA;* `djpisano@mail.wvu.edu`

[3]*Max Planck Institute für Astronomie, Heidelberg, Germany;* `walter@mpia.de`

[4]*Dept. of Astronomy, U. Wisconsin-Madison, Madison, WI, USA;* `sstanimi@astro.wisc.edu`

Abstract. One of the outstanding questions in astronomy today is how gas flows from the circumgalactic medium (CGM) onto the disks of galaxies and then transitions from the diffuse atomic medium into molecular star-forming cores. For studies of the CGM, the Next Generation Very Large Array (ngVLA) will have the sensitivity and resolution to measure the sizes of the neutral atomic hydrogen (HI) disks of galaxies and complete a census of the HI content around galaxies. Within galaxies, the ngVLA will be able to resolve HI clouds in large numbers of galaxies beyond the Local Group providing measurements of the physical conditions of gas across a wide range of galaxy types. Finally, within our own Milky Way, the ngVLA will provide a dense grid of HI absorption spectra in the cold and warm neutral medium constraining the temperature and density of atomic gas as it transitions into molecular gas. Combined with radio continuum and molecular line data from the ngVLA plus multi-wavelength data from other planned facilities, ngVLA will have a key role in understanding star-formation in the local universe while complementing future studies with the Square Kilometer Array.

1. Introduction

The Next Generation Very Large Array (ngVLA) will play a crucial role in the studies of 21-cm atomic neutral hydrogen (HI) emission in and around galaxies in the local Universe. The unprecedented sensitivity and resolution of the ngVLA will provide key information on the atomic gas reservoir in the circumgalactic medium (CGM) and its flow onto the gas disks of galaxies. The ngVLA will connect this large scale view of HI to individual star-forming cores to study the relatively unexplored transition from atomic to molecular gas in nearby galaxies and ultimately how gas is converted into stars.

In order to understand how gas flows onto galaxies and is then converted into molecular gas and, eventually, stars, there are three regimes to study: HI around galaxies in the circumgalactic medium; HI within nearby galaxies; and HI in the Milky Way. We will take these up in turn.

2. HI in the Circumgalactic Medium

The extent, morphology and dynamics of the gas in the very far outskirts of galaxies are still essentially unexplored observationally. These outer parts of galaxies are the interface between the inner star-forming disk and the cosmic web, and likely these are also the regions where galaxies accrete gas, possibly through the “cold accretion" process (e.g. Kereš et al. 2005). Measuring the very extended gas distributions in galaxies, and its connection to the cosmic web, will be a main science driver for the ngVLA.

To date, most of the exploration of the CGM has come through UV absorption line studies. The COS-HALOS project (Tumlinson et al. 2013; Werk et al. 2014) has used background quasars to study the Lymanα absorption in the halos of low redshift galaxies. The project has found that HI absorption at $N_{HI} \gtrsim 10^{14}$cm^{-2} is ubiquitous out to 150 kpc for star-forming galaxies and present in 75% of passive galaxies as well (Tumlinson et al. 2013). This cool CGM gas represents 25%-45% of the total baryon mass within the virial radius of the galaxy (Werk et al. 2014)[1]. Unfortunately, above $N_{HI} \sim 10^{16}$cm^{-2} saturation of absorption lines makes it difficult to get an accurate measure of N_{HI}; these are the Lyman Limit Systems. While below $N_{HI} \sim 10^{16-17}$cm^{-2}, HI absorption is common, particularly in the intergalactic medium, it is impossible to image in 21-cm HI emission. Obtaining deep HI emission observations with the ngVLA is the only way forward: while Lyman-α absorption observations can reach very low column densities, their pencil-beam nature make it extremely difficult to reconstruct the full gas distribution and its kinematics.

In galaxy disks the HI surface density is declining as a function of radius, but observations with current L-band facilities are typically not sensitive enough (reaching column density sensitivities just below 10^{20}cm^{-2}) to map the HI distribution at larger radii and correspondingly lower column densities. Does the azimuthally averaged HI surface density profile continue to decline at the same rate as in the inner disk, or do other effects start to play a role in determining the shape of the very outer radial HI profile? For example, when HI column densities decrease, one expectation is that the density of the neutral gas is no longer sufficient for self shielding and this could cause the majority of the gas to become ionized by the intergalactic radiation field. Models that include this ionization from the intergalactic radiation field predict that the steep radial decline of neutral gas surface density will transition, below column densities of $\sim 10^{18}$cm^{-2}, to a more extended, low column density outer disk with a flatter radial profile (e.g. Maloney 1993; Popping et al. 2009; Braun 2012), but many of the details are model-dependent. Gas accretion is not included in these models, and it is currently not known to what degree this process will affect the outskirts of the gaseous disks of galaxies. Simulations and some tentative observations indicate the presence of low-column density, kpc-sized gas features near galaxy disks (e.g. Braun & Thilker 2004; Popping et al. 2009; Wolfe et al. 2013, 2016). It is certainly conceivable that these could also have a big impact on the HI distribution at very low column densities. In order to detect such features, it is important to have both sensitive observations and resolution that is well matched to the size of the emitter. This can be seen in Figure 1. The ngVLA will have both the sensitivity and resolution to map this diffuse HI at low N_{HI} for a large number of galaxies.

[1] Our current understanding of the state of the CGM is well-summarized in the review by Tumlinson et al. (2017)

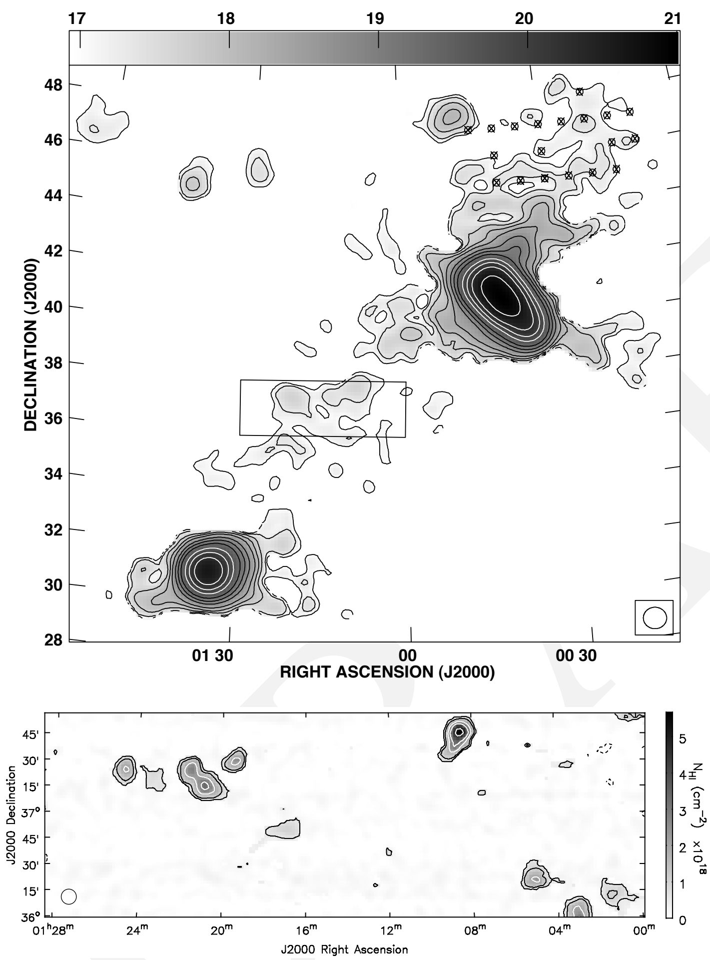

Figure 1. Top: A map of the total HI emission associated with M 33 (lower left) and M 31 (upper right) from Braun & Thilker (2004). The contours are at log N_{HI}=17.0, 17.3, 17.7, 18.0, 18.3, 18.7, 19.0, 19.3, 19.7, 20.0, 20.3, and 20.7 [cm^{-2}]. The beamsize is shown in the lower right of the panel. The box shows the region mapped by Wolfe et al. (2016) with the GBT. Bottom: The GBT HI map from Wolfe et al. (2016). The contours are at -1, 1, 2, 4, 6, and 10 times $5{\times}10^{17}$cm^{-2}. The beam size is the circle in the lower left of the image. Note that the HI structures detected by Braun & Thilker (2004) are revealed to be much smaller, higher-N_{HI} features by Wolfe et al. (2016), illustrating the critical importance of resolution and sensitivity.

Besides characterizing the sizes of the gas disks in nearby galaxies, observing the extended HI distribution will at the same time constrain the numbers of individual HI clouds around the target galaxies. Based on the relative kinematics and morphologies/locations, one can distinguish between tidal dwarfs, compact high velocity clouds (HVCs), and tidal material that could be present around the galaxies under consideration. This will provide a link to the missing galaxy problem, i.e. satellites with clumps of cool HI, but no star-formation. Cloud sizes and masses will then provide key insights into the physical state of gas in the CGM, which can be compared to cosmological simulations of the structure of the CGM of galaxies (e.g. Shen et al. 2013). Such simulations indicate that the most compelling signature of the cold accretion phenomenon onto galaxies is a high covering factor ∼20-30% of Lyman limit system absorption in the CGM on scales out to ∼100 kpc (scales that can be easily covered with the ngVLA with small mosaics).

In addition to this deep ngVLA HI imaging, newly developed techniques are now available to obtain azimuthally averaged measurements at previously inaccessible radii based on the shifting and stacking technique described in Ianjamasimanana et al. (2012). This method uses an extrapolation of the (typically flat) rotation curve to create a model velocity field at large radii well beyond that of the directly detected HI disk. This is then used to shift all spectra in the data cube in velocity by the amount indicated by the extrapolated velocity field at that position. This ensures that all (potential) HI signals are lined up at the same reference velocity. Using the same tilted-ring model that was used for the shifting step, the spectra are then selected in annuli of increasing galaxy radius and are stacked. The stacked spectrum will have a lower noise value, and if any underlying HI signal has been lined up through the shift process, the signal-to-noise ratio will have increased and signatures of otherwise undetected very low column density HI can be detected. Testing this methodology using THINGS and HALOGAS data has demonstrated that the HI column density limit can be pushed down by an order of magnitude (Ianjamasimanana et al. 2018). The combination of ngVLA's sensitivity, together with the above stacking technique thus will enable measurements at unprecedented HI columns ($\ll 10^{17}\mathrm{cm}^{-2}$), that have only been accessible via Lyman α absorption measurements. In summary, through the combination of ngVLA observations and new techniques to enhance HI column density sensitivities through stacking will reach depths in HI column densities that were previously inconceivable. This measurement will provide the currently completely unexplored connection to the cosmic HI web.

3. HI in Nearby Galaxies

Understanding the processes that drive star formation in galaxies is one of the most challenging astrophysical topics, both observationally and theoretically. Of particular interest are studies of how stars form out of the interstellar medium (ISM) on scales comparable to the Jeans mass and Jeans length of neutral atomic clouds, and how, in turn, these stars shape the structure and physical properties of their ambient ISM. Of key importance n any such study are high resolution observations of the different tracers of the ISM (in particular HI and CO observations) and the stellar population (e.g. broad band and Hα imaging). For such studies, resolutions of 5-150 pc are needed to resolve the giant molecular cloud (GMC) complexes and the related individual sites of star formation. It is also on these scales where the feedback of individual supernovae and/or massive stars is expected to be most profound.

Although arcsecond resolutions are routinely achieved using ground–based optical telescopes, it is observations of similar resolutions at radio wavelengths, in particular the HI, that are lacking. In fact, to date, this is the limiting factor of all coherent ISM studies on these small, critical scales. In the era of ALMA, observations of the molecular gas phase (using CO as a tracer) are now routinely pushed to arcsecond resolutions. These CO observations are typically limited to the central few arcminutes of the target galaxies (given by the primary beam size of millimeter interferometers) and do not recover the atomic gas phase – they thus cannot be used to understand global star formation processes in galaxies. Recently observations of OH emission in the Milky Way have been shown to trace molecular gas that is unseen in CO emission (Allen et al. 2012, 2015). The ngVLA may be able to detect such molecular gas clouds in other galaxies.

On the contrary, most nearby galaxies are small enough to fit within the primary beam of existing radio interferometers (FWHM_{VLA} ~$30'$) for HI observations and the angular resolution is the limiting factor. Typically resolutions of order $15''$ are achieved; only the VLA has been pushing these resolutions down to ~$6''$ for large samples of galaxies. The HI Nearby Galaxy Survey (THINGS; Walter et al. 2008) demonstrated that $6''$ resolution can be achieved for a sample of 35 galaxies of any size (i.e. dwarfs to spirals) with the VLA. Only a couple of galaxies have been imaged in HI emission at higher resolution, ~$1.6''$, with the VLA (van Zee et al. 2006), but this requires an extremely large time commitment with the VLA. The ngVLA will fundamentally change this situation. The possibility of mapping nearby galaxies at linear resolutions of 5-150 pc opens the prospects of exploring processes in the ISM on scales which have hitherto been inaccessible. Although some notable exceptions exist, such as: the LMC: (Kim et al. 2003); the SMC: (Staveley-Smith et al. 1997); IC 10: (Wilcots & Miller 1998); and other Local Group dwarfs: (Begum et al. 2006), but these galaxies are not representative of the galaxy main sequence at low redshift. Figure 2 shows a THINGS image of a typical spiral galaxy at ~90 pc resolution; ngVLA will achieve better resolution and sensitivity for larger samples of galaxies in the same amount of time that the VLA took for THINGS.

(Sub-)arcsec resolution is commonly reached through massive optical/NIR imaging efforts (ground and space based, currently with HST, and in the near future, JWST [dust/PAH emission, embedded SFR tracers]). Resolution-matched HI imaging will enable measurements on the ISM conditions required for H_2 formation (Krumholz et al. 2009; Krumholz 2013), and the distribution of, e.g., the HI/H_2 ratio will constrain the evolution of molecular clouds. For example, recent sub-pc scale studies of GMCs in the Milky Way have shown that the HI surface density and the H_2 fraction agree well with the equilibrium model predictions (e.g. Lee et al. 2012). ngVLA HI observations of Local Group galaxies will provide crucial tests for the HI surface density and the H_2 fraction on pc-scales in galaxies of varying metallicity and interstellar radiation field required to test both equilibrium and non-equilibrium models for H_2 formation and molecular cloud evolution. Observations at GMC-scale resolution are also crucial to study turbulence in the ISM. It is at these scales that energy gets injected into the ISM which then cascades down to smaller scales. We can test if the HI power spectra indeed follow the predicted power-law scales for turbulence like that found in the

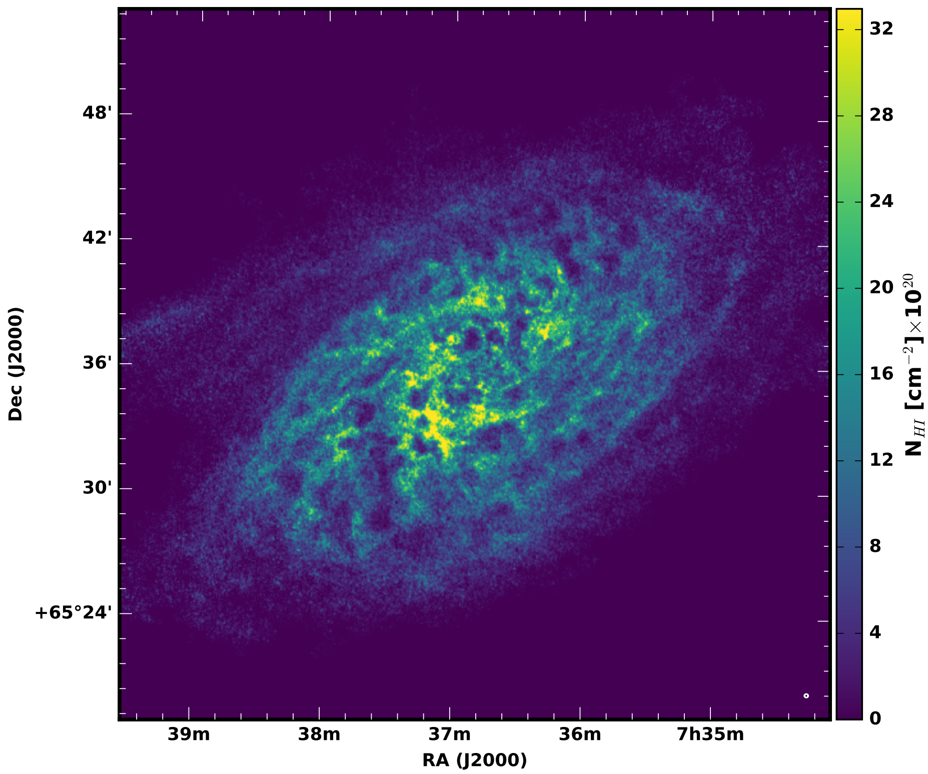

Figure 2. A total HI intensity (moment 0) image of NGC 2403 from THINGS (Walter et al. 2008). These data were imaged with robust weighting resulting in a resolution of ~6″. At the distance of NGC 2403, 3.2 Mpc, this corresponds to a physical resolution of 93 pc. The ngVLA will be able to achieve better resolution and sensitivity for larger samples of galaxies in the same amount of time as the VLA.

SMC (Stanimirovic et al. 1999; Elmegreen et al. 2001) in a large range of extragalactic environments.

ngVLA GMC-resolution imaging of the HI emission will allow us to study the fine scale structure of the ISM in galaxies of different types. To date, the only galaxies for which similar linear resolutions have been achieved have been Local Group dwarfs, notably the LMC/SMC (e.g. Kim et al. 2003). These studies have shown how the emission breaks up in filaments and shells, even at the smallest currently accessible scales. The presence of fractal-like structure in the HI emission is also evident from recent HI imaging of our Galaxy (Beuther et al. 2016, in particular the large VLA THOR project). The ngVLA will reach sensitivities and column densities that this work can be replicated in galaxies across the Hubble sequence, including main sequence galaxies in the local universe. GMC-scale resolution represents a critical and fundamental scale as it samples the typical sizes of individual giant molecular and atomic clouds that are the precursors of star formation. Observations at this resolution will also enable us to directly study the feedback/energy input from individual supernovae due to massive stars.

A unique feature of the high-resolution HI imaging is that they will, for the first time, enable us to study non-circular motions in the HI disks of galaxies at scales that are directly relevant for the ΛCDM cusp/core controversy. HI observations have the immediate advantage that the kinematics in the very centers of galaxies can be immediately linked to their outskirts. The large range of Hubble types that can be studied (including the important dwarf galaxies whose kinematics/DM content cannot be studied through ALMA imaging using CO) will also enable precise quantification of the effects of the non-circular motions on the dark matter profile as a function of e.g. disk mass, depth of the potential, etc. Measuring the strength of shocks and other non-rotation velocity components at these scales (e.g. across spiral arms/bars) will allow us to derive independent estimates of the mass in the disk (see e.g. descriptions in Weiner et al. 2001b,a), another crucial input in the derivation of dark matter profiles in galaxies. This information will also provide important insights in assessing the local stability of gas clouds against gravitational collapse.

GMC-scale resolution data will resolve the giant atomic cloud complexes for the first time in galaxies beyond the local group and will allow investigations of if and how the peak HI temperature of the warm HI changes of a function of galaxy type. Of particular interest is the question if peak HI temperature is different in low-metallicity dwarfs as compared to more metal-rich spirals. Such studies will directly constrain the physical conditions of the interstellar medium on sub-100 pc scales. In addition, background continuum sources will be bright enough to perform HI absorption studies. In this context, ngVLA's 1″ resolution is essential to isolate the absorption from the surrounding emission. This then opens the possibility to determine directly the HI spin temperature, something which has largely only been possible in Local Group galaxies (e.g. Dickey & Brinks 1993; Braun 1997).

4. Cloud Scale Imaging of HI in the Milky Way

The increased sensitivity of the ngVLA will be crucial for addressing major outstanding questions in ISM physics. The diffuse neutral ISM exists in two flavors: the cold neutral medium (CNM) and the warm neutral medium (WNM). The CNM is easily studied with the 21-cm line absorption and its properties have been measured extensively, while only several measurements of the WNM temperature exist so far. The main reason for this observational paucity is the low optical depth of the WNM, $\tau \sim 10^{-3}$. This makes the WNM one of the least understood phases of the ISM. To constrain theoretical and numerical models of the ISM, temperature distributions over the full temperature range from $\sim$20 to $\sim 10^4$ K are essential. Using the upgraded Very Large Array (project 21-SPONGE), Murray et al. (2014, 2015, 2017) demonstrated that already the VLA can detect HI absorption lines with a peak optical depth $\sim 10^{-3}$. However, the existing sample size of the current measurements is of order 50 directions - way too low to start building proper statistical samples for a comparison with numerical simulations and understanding of how the CNM-WNM phase mix vary with interstellar environments.

In addition, the HI excitation processes are still not fully understood. Using a stacking analysis, Murray et al. (2014) detected statistically the presence of a widespread WNM population with T_s=7200 K. This demonstrated that the non-collisional excitation of HI is significant even at high Galactic latitudes. As Lyα scattering is the most likely candidate for additional excitation of HI, the Murray et al. results show that the fraction of Lyα photons, and/or the photon propagation throughout the ISM, are likely more complicated than what is commonly assumed. For example, both a theoretical study by Liszt (2001) and state-of-the-art numerical simulations (Kim et al. 2014) assume a uniform flux of Lyα photons throughout the ISM and result is the expected $T_s < 4000$ K. In that regard, the high sensitivity enabled by the ngVLA will allow direct measurements of WNM spin temperature and its spatial variations in the Milky Way by observing hundreds to thousands of directions with σ_T <0.05. By stacking selectively different interstellar environments will be probed for the first time. Finer scale variations may also be possible to measure by imaging resolved continuum sources to map out variations on sub-parsec scales (e.g. Faison et al. 1998; Lazio et al. 2009; Roy et al. 2012).

Simultaneously, the ngVLA will be able to map out the raw fuel for H_2 formation across major GMCs in the Milky Way. While it is commonly assumed that the CNM is the key ingredient for making H_2 because of its high density, the observational evidence whether GMC precursors are in the form of dense HI clouds, diffuse HI, or smaller molecular clouds, is still lacking (Dobbs & Pringle 2013). In addition, numerical simulations suggest that GMCs grow via accretion of the CNM from the envelopes. Recent Green Bank Telescope results, (Allen et al. 2012, 2015), have shown that OH is tracing diffuse molecular gas that is not seen via CO measurements. This may represent an intermediate stage in forming GMCs. Constraining where the fuel for H_2 formation is in and around GMCs, what are its physical properties, and what is the accretion rate of this material onto the GMCs, are essential next steps. Due to sensitivity limitations, almost all HI absorption measurements (e.g. 21- SPONGE) have focused on random directions, utilizing strong background radio sources. The ngVLA can provide, for the first time, dense grids of HI absorption spectra in the direction of selected GMCs. The ngVLA has thus potential to revolutionize our understanding of the ISM physics, in particular the critical phase transition from the WNM to the CNM to H_2 formation.

5. Limitations of Current Astronomical Instrumentation

Current radio interferometers lack the combination of resolution and surface brightness sensitivity. In addition, the larger dishes of the VLA and WSRT restrict the field of view limiting the region of study. These all combine to make it near impossible to map the low-N_{HI} gas within the virial radius of nearby galaxies, while being able to resolve any features. While single-dish telescopes, like the GBT, have the surface brightness sensitivity, they lack the resolution to map filamentary structures beyond the Local Group. For high resolution studies of HI in nearby galaxies or in the Milky Way, the sparse nature of the VLA or WSRT mean that a lot of flux is missing in these data.

In terms of planned interferometers, MeerKAT is nearing completion and will be well-suited to mapping the diffuse, low-N_{HI} gas around nearby galaxies; the MHONGOOSE survey (de Blok et al. 2017) will do exactly this for a sample of 30 galaxies. The IMAGINE survey, currently being undertaken with the Australia Telescope Compact Array (ATCA) and the Parkes radio telescope is also studying the diffuse HI around galaxies, but both of these surveys will only reach the needed sensitivity over a beam size of ~30″. Neither survey will have the high resolution, ~1″ that will be needed to study the internal structure of galaxies at sufficient detail.

6. Unique Capabilities of the ngVLA for HI Science

The planned technical capabilities of the ngVLA at 1.4 GHz should be matched by the SKA. The SKA, however, will be located in the southern hemisphere leaving many nearby galaxies (e.g. M 31) and the outer portions of the Milky Way inaccessible. Furthermore, current plans are for the SKA to operate in a survey mode. The ngVLA has the opportunity to be PI-driven allowing for a wider variety of science to be done. In addition, for sources that extend over a large area, total power HI measurements will be required. While the ngVLA has a dense core and will be able to recover flux on much larger angular scales than the VLA, short spacing data will still be needed for some observations. This can be provided with existing instrumentation using the Green Bank Telescope (Frayer 2017). Finally, since ngVLA will be able to operate at higher frequencies than the SKA, much of the science that requires complementary multi-wavelength data (see below) will require the ngVLA, even if the HI data comes from SKA observations.

7. Experimental Layout

The reference configuration of the ngVLA, Spiral214, can be divided into three parts: the “core" array, the “plains" array, and the full array. For the science described here, only the core array (with B_{max} ~1 km) and the plains array (with B_{max} ~30 km), will be useful (ngVLA memo 17). Some HI absorption studies, such as using background radio galaxies to map small-scale, high-N_{HI} gas, may use the full array. Using the reference design sensitivity, the core array will be able to reach σ_{NHI} ~10^{18}cm^{-2} in 1 hour over a 10 km s^{-1} channel with a beamsize of ~40″, while the plains array will reach σ_{NHI} ~6×10^{20}cm^{-2} for the same time and channel width over a beam of ~1″.

For studies of the CGM of nearby galaxies, astronomers will want to use the ngVLA to study HI at N_{HI}~10^{17-18}cm^{-2} for a ~20 km s^{-1} linewidth. To get a 3σ detection of HI at N_{HI}=10^{18}cm^{-2} will require ~30 hours. To reach N_{HI}=10^{17}cm^{-2} would require ~3000 hours at a resolution of 43″. If we degrade the resolution to ~1′, then we could do this in about 600 hours for a single target. These time requirements roughly match those of the SKA1-MID telescope (see de Blok et al. 2017, for examples). Given the planned, semi-random distribution of antennas in the core array, we can anticipate that the sensitivity will improve with additional tapering. As diffuse HI emission could be extended over large angular scales, single-dish, total power HI data may be needed. This can easily be provided by the GBT using an array receiver, such as FLAG (Roshi et al. 2018). Since the HI filaments expected from models of cold flow accretion are on the scale of 1–10 kpc across (Popping et al. 2009, e.g.), we can probe to $N_{HI}\lesssim10^{17}$cm^{-2} for a small sample of nearby galaxies (D<10 Mpc) with relatively modest time requirements (<1000 hours) and we can study a much larger sample of galaxies out to larger distances at N_{HI}=10^{18}cm^{-2} in a similar amount of time.

For studies of HI within nearby galaxies, we will want the high angular resolution of the plains array (θ ~1″). Samples of galaxies at distances of 1 Mpc<D<30 Mpc are ideal targets–and a wide range of different types of galaxies can be studied in this volume. At these distances, 1″ resolution corresponds to spatial resolutions of 5-150 pc. In 1 hour, for a 10 km s^{-1} channel width, the ngVLA will yield σ_{NHI} ~6×10^{20}cm^{-2}. Even this sensitivity will allow astronomers to study the high-N_{HI} associated with the gas transitioning between the atomic and molecular phases. In a couple of days of observing we could then redo a survey like THINGS at much higher physical resolution and sensitivity.

In addition to direct observations of HI in nearby galaxies and the Milky Way, we would want to get commensal observations of OH, radio recombination lines, and radio continuum with full polarization. These data will help map out the full transition of gas from the atomic to the molecular to the ionized phase.

8. Complementarity

First and foremost, the ngVLA study of HI within nearby galaxies, including the Milky Way, will be complemented by the ngVLA's studies at other wavelengths of other molecules in these systems, such as CO, HCN, NH_3, etc., as well as the radio continuum associated with star formation and heated dust. This will yield one of the most detailed pictures of how gas is accreted onto galaxies, transitions into molecular clouds, and then turns into stars. Complementing the data from ngVLA will be a broad range of facilities. In the infrared, from the near IR through the far IR, will be JWST, Euclid, SPICA, WFIRST, and ALMA. These telescopes will be able to study warm dust, important cooling lines in the ISM (such as [CII]), protostars and obscured star formation in general.

In the study of the CGM around galaxies, new X-ray facilities such as eROSITA and Athena should allow for the study of the hot halos of galaxies, either directly or via stacking. Unfortunately, at present there are no planned UV telescopes that could probe the CGM and IGM in absorption, tracing the WHIM with better sensitivity and towards a denser grid of background sources around many galaxies. Such a mission would allow astronomers to both map the hot gas in the X-rays, the warm-hot ionized gas in the CGM using UV absorption lines, and then diffuse, warm neutral hydrogen with the ngVLA. This would give us a complete census of the gas available to accrete onto galaxies and fuel future star formation in the local universe.

Acknowledgments. The authors thank Nickolas Pingel for his assistance in making figures.

References

Allen, R. J., Hogg, D. E., & Engelke, P. D. 2015, AJ, 149, 123. 1502.00657

Allen, R. J., Ivette Rodríguez, M., Black, J. H., & Booth, R. S. 2012, AJ, 143, 97. 1202.4434

Begum, A., Chengalur, J. N., Karachentsev, I. D., Kaisin, S. S., & Sharina, M. E. 2006, MNRAS, 365, 1220. astro-ph/0511253

Beuther, H., Bihr, S., Rugel, M., Johnston, K., Wang, Y., Walter, F., Brunthaler, A., Walsh, A. J., Ott, J., Stil, J., Henning, T., Schierhuber, T., Kainulainen, J., Heyer, M., Goldsmith, P. F., Anderson, L. D., Longmore, S. N., Klessen, R. S., Glover, S. C. O., Urquhart, J. S., Plume, R., Ragan, S. E., Schneider, N., McClure-Griffiths, N. M., Menten, K. M., Smith, R., Roy, N., Shanahan, R., Nguyen-Luong, Q., & Bigiel, F. 2016, A&A, 595, A32. 1609.03329

Braun, R. 1997, ApJ, 484, 637. astro-ph/9702111

— 2012, ApJ, 749, 87. 1202.1840

Braun, R., & Thilker, D. A. 2004, A&A, 417, 421. astro-ph/0312323

de Blok, W. J. G., Adams, E. A. K., Amram, P., Athanassoula, E., Bagetakos, I., Balkowski, C., Bershady, M. A., Beswick, R., Bigiel, F., Blyth, S.-L., Bosma, A., Booth, R. S., Bouchard, A., Brinks, E., Carignan, C., Chemin, L., Combes, F., Conway, J., Elson, E. C., English, J., Epinat, B., Frank, B. S., Fiege, J., Fraternali, F., Gallagher, J. S., Gibson, B. K., Heald, G., Henning, P. A., Holwerda, B. W., Jarrett, T. H., Jerjen, H., Józsa, G. I., Kapala, M., Klöckner, H.-R., Koribalski, B. S., Kraan-Korteweg, R. C., Leon, S., Leroy, A., Loubser, S. I., Lucero, D. M., McGaugh, S. S., Meurer, G. R., Meyer, M., Mogotsi, M., Namumba, B., Oh, S., Oosterloo, T. A., Pisano, D. J., Popping, A., Ratcliffe, S., Sellwood, J. A., Schinnerer, E., Schröder, A. C., Sheth, K., Smith, M. W. L., Sorgho, A., Spekkens, K., Stanimirovic, S., van der Heyden, K., van Driel, W., Verdes-Montenegro, L., Walter, F., Westmeier, T., Wilcots, E., Williams, T., Wong, O. I., Woudt, P. A., & Zijlstra, A. 2017, ArXiv e-prints. 1709.08458

Dickey, J. M., & Brinks, E. 1993, ApJ, 405, 153

Dobbs, C. L., & Pringle, J. E. 2013, MNRAS, 432, 653. 1303.4995

Elmegreen, B. G., Kim, S., & Staveley-Smith, L. 2001, ApJ, 548, 749. astro-ph/0010578

Faison, M. D., Goss, W. M., Diamond, P. J., & Taylor, G. B. 1998, AJ, 116, 2916

Frayer, D. T. 2017, ArXiv e-prints. 1706.02726

Ianjamasimanana, R., de Blok, W. J. G., Walter, F., & Heald, G. H. 2012, AJ, 144, 96. 1207.5041

Ianjamasimanana, R., Walter, F., de Blok, W. J. G., Heald, G. H., & Brinks, E. 2018, ArXiv e-prints. 1803.10291

Kereš, D., Katz, N., Weinberg, D. H., & Davé, R. 2005, MNRAS, 363, 2. astro-ph/0407095

Kim, C.-G., Ostriker, E. C., & Kim, W.-T. 2014, ApJ, 786, 64. 1403.5566

Kim, S., Staveley-Smith, L., Dopita, M. A., Sault, R. J., Freeman, K. C., Lee, Y., & Chu, Y.-H. 2003, ApJS, 148, 473

Krumholz, M. R. 2013, MNRAS, 436, 2747. 1309.5100

Krumholz, M. R., McKee, C. F., & Tumlinson, J. 2009, ApJ, 693, 216. 0811.0004

Lazio, T. J. W., Brogan, C. L., Goss, W. M., & Stanimirović, S. 2009, AJ, 137, 4526. 0903.0672

Lee, M.-Y., Stanimirović, S., Douglas, K. A., Knee, L. B. G., Di Francesco, J., Gibson, S. J., Begum, A., Grcevich, J., Heiles, C., Korpela, E. J., Leroy, A. K., Peek, J. E. G., Pingel, N. M., Putman, M. E., & Saul, D. 2012, ApJ, 748, 75. 1110.2745

Liszt, H. 2001, A&A, 371, 698. astro-ph/0103246

Maloney, P. 1993, ApJ, 414, 41

Murray, C. E., Lindner, R. R., Stanimirović, S., Goss, W. M., Heiles, C., Dickey, J., Pingel, N. M., Lawrence, A., Jencson, J., Babler, B. L., & Hennebelle, P. 2014, ApJ, 781, L41. 1401.1215

Murray, C. E., Stanimirović, S., Goss, W. M., Dickey, J. M., Heiles, C., Lindner, R. R., Babler, B., Pingel, N. M., Lawrence, A., Jencson, J., & Hennebelle, P. 2015, ApJ, 804, 89. 1503.01108

Murray, C. E., Stanimirović, S., Kim, C.-G., Ostriker, E. C., Lindner, R. R., Heiles, C., Dickey, J. M., & Babler, B. 2017, ApJ, 837, 55. 1612.02017

Popping, A., Davé, R., Braun, R., & Oppenheimer, B. D. 2009, A&A, 504, 15. 0906.3067

Roshi, D. A., Shillue, W., Simon, B., Warnick, K. F., Jeffs, B., Pisano, D. J., Prestage, R., White, S., Fisher, J. R., Morgan, M., Black, R., Burnett, M., Diao, J., Ruzindana, M., van Tonder, V., Hawkins, L., Marganian, P., Chamberlin, T., Ray, J., Pingel, N. M., Rajwade, K., Lorimer, D. R., Rane, A., Castro, J., Groves, W., Jensen, L., Nelson, J. D., Boyd, T., & Beasley, A. J. 2018, AJ, 155, 202. 1803.04473

Roy, N., Minter, A. H., Goss, W. M., Brogan, C. L., & Lazio, T. J. W. 2012, ApJ, 749, 144. 1203.2925

Shen, S., Madau, P., Guedes, J., Mayer, L., Prochaska, J. X., & Wadsley, J. 2013, ApJ, 765, 89. 1205.0270

Stanimirovic, S., Staveley-Smith, L., Dickey, J. M., Sault, R. J., & Snowden, S. L. 1999, MNRAS, 302, 417

Staveley-Smith, L., Sault, R. J., Hatzidimitriou, D., Kesteven, M. J., & McConnell, D. 1997, MNRAS, 289, 225

Tumlinson, J., Peeples, M. S., & Werk, J. K. 2017, ARA&A, 55, 389. 1709.09180

Tumlinson, J., Thom, C., Werk, J. K., Prochaska, J. X., Tripp, T. M., Katz, N., Davé, R., Oppenheimer, B. D., Meiring, J. D., Ford, A. B., O'Meara, J. M., Peeples, M. S., Sembach, K. R., & Weinberg, D. H. 2013, ApJ, 777, 59. 1309.6317

van Zee, L., Cannon, J. M., & Skillman, E. D. 2006, in American Astronomical Society Meeting Abstracts, vol. 38 of Bulletin of the American Astronomical Society, 1136

Walter, F., Brinks, E., de Blok, W. J. G., Bigiel, F., Kennicutt, R. C., Jr., Thornley, M. D., & Leroy, A. 2008, AJ, 136, 2563-2647. 0810.2125

Weiner, B. J., Sellwood, J. A., & Williams, T. B. 2001a, ApJ, 546, 931. astro-ph/0008205

Weiner, B. J., Williams, T. B., van Gorkom, J. H., & Sellwood, J. A. 2001b, ApJ, 546, 916. astro-ph/0008204

Werk, J. K., Prochaska, J. X., Tumlinson, J., Peeples, M. S., Tripp, T. M., Fox, A. J., Lehner, N., Thom, C., O'Meara, J. M., Ford, A. B., Bordoloi, R., Katz, N., Tejos, N., Oppenheimer, B. D., Davé, R., & Weinberg, D. H. 2014, ApJ, 792, 8. 1403.0947

Wilcots, E. M., & Miller, B. W. 1998, AJ, 116, 2363

Wolfe, S. A., Lockman, F. J., & Pisano, D. J. 2016, ApJ, 816, 81. 1507.05237

Wolfe, S. A., Pisano, D. J., Lockman, F. J., McGaugh, S. S., & Shaya, E. J. 2013, Nat, 497, 224. 1305.1631

Part VII

Galaxy Formation and Evolution:

Science with a Next-Generation Very Large Array
ASP Conference Series, Monograph 7
Eric J. Murphy, ed.

DRAFT EDITION

Imaging Molecular Gas at High Redshift

C.L. Carilli & Y. Shao
National Radio Astronomy Observatory, Socorro, NM, 87801;
`ccarilli@nrao.edu`, `yshao@nrao.edu`

Abstract.
We perform simulations of the capabilities of the Next Generation Very Large Array in the context of imaging low order CO emission from typical high redshift star forming galaxies at ∼ 1kpc resolution. We adopt as a spatial and dynamical template the CO 1-0 emission from M51, scaled accordingly for redshift, transition, and total gas mass. The molecular gas masses investigated are factors of 1.4, 3.5, and 12.5 larger that of M51, at $z = 0.5$, 2, and 4.2, respectively. The $z = 2$ galaxy gas mass is comparable to the lowest mass galaxies currently being discovered in the deepest ALMA and Noema cosmological CO line surveys, corresponding to galazies with star formation rates ∼ 10 to 100 $M_\odot$ year^{-1}. The ngVLA will perform quality imaging at 1kpc resolution of the gas distribution and dynamics over this disk. We recover the overall rotation curve, galaxy orientation properties, and molecular ISM internal velocity dispersion. The model at $z = 4.2$ corresponds to a massive star forming main sequence disk (SFR ∼ 130 $M_\odot$ year^{-1}). The ngVLA can obtain 1kpc resolution images of such a system in a reasonable integration time, and recover the basic galaxy orientation parameters, and, asymptotically, the maximum rotation velocity. We compare the ngVLA results with capabilities of ALMA and the JVLA. ALMA and the JVLA can detect the integrated low order CO emission from these galaxies, but lack the sensitivity to perform the high resolution imaging to recover the dynamics at 1kpc scales. To do so would require of order 1000 hours per galaxy with these current facilities. We investigate a 'minimal' ngVLA configuration, removing the longest baselines and much of the very compact core, and find good imaging can still be performed at 1kpc resolution.

1. Introduction

The 'Next Generation Very Large Array' (ngVLA), is being considered as a future large radio facility operating in the 1GHz to 115GHz range. The current design involves ten times the effective collecting area of the JVLA and ALMA, with ten times longer baselines, providing mas-resolution, plus a dense core on km-scales for high surface brightness imaging. The ngVLA opens unique new parameter space in the imaging of thermal emission from cosmic objects ranging from protoplanetary disks to distant galaxies, as well as unprecedented broad band continuum polarimetric imaging of non-thermal processes (McKinnon et al. 2016; Carilli et al. 2015; Selina & Murphy 2017; Bolatto et al. 2017).

One of the primary science drivers for the ngVLA involves study of the molecular gas content of galaxies throughout cosmic time (Carilli et al. 2015). Cool molecular gas provides the fuel for star formation in galaxies, and hence represents a key constituent in the study of the Baryon cycle during galaxy evolution (Carilli & Walter 2013). A

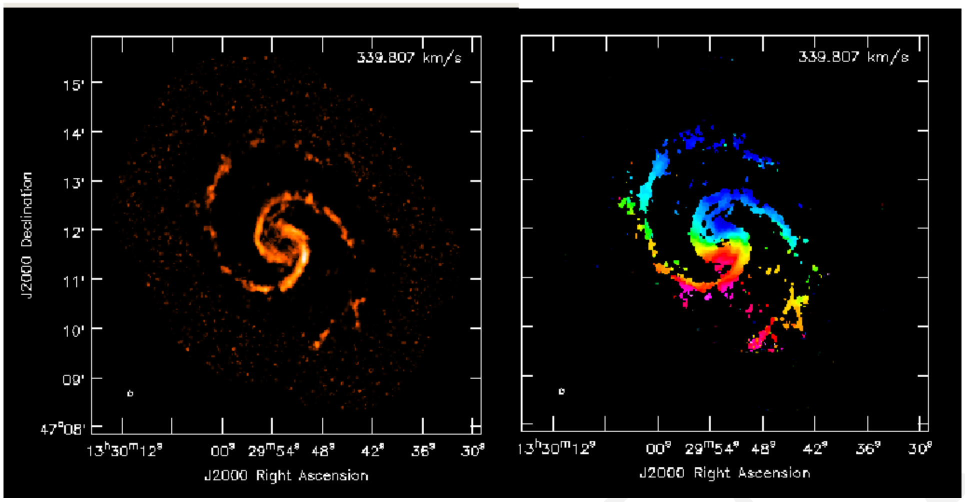

Figure 1. BIMA SONG CO 1-0 observations of M51 at 200pc resolution (5.5”; (Helfer et al. 2003)

standard method for deriving the molecular gas mass in galaxies involves an empirical calibration of the relationship between the CO 1-0 tracer and total gas mass (Bolatto et al. 2013). The high sensitivity and wide fractional bandwidth of the ngVLA provides a powerful tool to study the evolution of the molecular content of galaxies, through observations of the low order CO transitions.

An area that is currently poorly explored is the detailed distribution and kinematics of the molecular gas in early galaxies. Progress has been made using ALMA, the VLA, and Noema, but these studies are time comsuming (tens of hours per galaxy), and remain limited in spatial resolution (few kpc). The ngVLA will revolutionize this field, through sub-kpc resolution observations of the molecular gas down to very low brightnesses in galaxies out to the highest redshifts (Carilli & Walter 2013). In particular, the full frequency range from 30GHz to 100GHz, covers both low and high order CO transitions at high redshift, with 10x the sensitivity of ALMA and the VLA.

We investigate the ability of the ngVLA to image the molecular ISM in high redshift galaxies at $\leq$ 1kpc resolution. This scale corresponds to the giant molecular star forming clumps being discovered in active star forming galaxies during the peak epoch of cosmic star formation, around $z \sim 2$ (Genzel et al. 2011). We compare the capabilities of the ngVLA to observe typical ’main sequence’ star forming galaxies, with those of ALMA and the JVLA. We also consider a minimal array design with which such measurements could be made with reasonable accuracy.

2. Template: CO 1-0 emission from M51

We adopt as a spatial template the CO 1-0 emission from the nearby star forming disk galaxy, M51. M51 is one of the best studied galaxies in molecular gas (Schinnerer et al. 2013). M51 is at a distance of 7.6 Mpc (recessional velocity = 463 km/s), with an integrated CO 1-0 luminosity of $L'_{C0} = 1.6 \times 10^9$ K km/s pc^2, implying a molecular gas mass of 5.5×10^9 $(\alpha/3.4)$ M$_\odot$, where $\alpha = 3.4$, corresponding to the Galactic conversion factor for CO 1-0 luminosity to total molecular gas mass. We give the galaxy properties for M51 and the higher redshift models in Table 1. The rotation curve of M51 is well studied, and the numbers are given in our comparitive dynamical analysis below. We employ the public BIMA SONG CO 1-0 data cubes (Helfer et al. 2003), as the starting point of the models. The moment 0 and 1 images (velocity-integrated CO emission and intensity weighted mean velocity) for these data are shown in Figure 1.

We then redshift the source to $z = 0.5$ and $z = 2$, and generate mock observations of the CO emission with the ngVLA and ALMA. For the $z = 0.5$ calculation, we adopt the 1-0 line, redshifted to 77GHz. For the $z = 2$ calculation, we adopt the CO 2-1 line, redshifted to 77GHz. We assume thermalized line excitation at least to the 2-1 line, and hence increase the line flux densities (in Jy), by a factor four over the 1-0 flux densities. The CO 1-0 luminosity has been one of the primary diagnostics for deriving total molecular gas mass in galaxies (Bolatto et al. 2013). One of the issues in the study of high redshift galaxies historically is that many observations of CO emission have employed higher order transitions, thereby requiring an assumption about the excitation ladder of CO to derive a total molecular gas mass. Observing CO 1-0 directly avoids this extrapolation. Moreover, it has been found that the 2-1 line is almost always thermally excited (ie. a luminosity four times that of 1-0, in Jy km s^{-1}), in high z galaxies, hence a factor 4 extrapolation is justified. However, as shown by Casey et al. (2015), going to higher order leads to substantial uncertainty in extrapolation to the 1-0 luminosity due to varying sub-thermal excitation in different galaxies. Hence, the importance of observing the low order transitions (Daddi et al. 2015; Carilli & Walter 2013).

An important recent discovery with regards to the molecular gas in galaxies is the observation of a rapid increase in the gas mass to stellar mass ratio with redshift. Studies of main sequence star forming disks galaxies show an order of magnitude increase in this ratio from $z = 0$ to 2. The peak epoch of cosmic star formation corresponds to an epoch when the baryon content of typical star forming disk galaxies is dominated by gas, not stars (Tacconi et al. 2010, 2018; Genzel et al. 2015; Schinnerer et al. 2016; Daddi et al. 2010; Geach et al. 2011; Scoville et al. 2017; Decarli et al. 2016). To make some allowance for this increase in gas mass fraction with redshift, we increase the CO luminosity by a factor 1.4 for the $z = 0.5$ model, and 3.5 for the $z = 2$ model, relative to M51.

The CO 2-1 luminosity for the $z = 2$ model is then: $L'_{C0} = 5.8 \times 10^9$ K km/s pc^2, implying a molecular gas mass of '2.0×10^{10} $(\alpha/3.4)$ $\mathrm{M}_\odot$. This is at the extreme low end of the galaxies currently being discovered in the deepest ALMA, JVLA, and Noema cosmological surveys for molecular line emission from $z \sim 2$ galaxies (Walter et al. 2016, 2014; Decarli et al. 2016). Using the standard relationship between IR luminosity and CO luminosity for main sequence galaxies leads to: $L_{IR} \sim 2.5 \times 10^{11}$ $\mathrm{L}_\odot$, and a star formation rate ~ 25 $\mathrm{M}_\odot$ year^{-1} (Daddi et al. 2010).

We also adopt the CO 2-1 line at $z = 2$ because it will be less affected by brightness contrast relative to the CMB (Zhang et al. 2016). Since all observations are made relative to the mean background of the CMB, the increasing temperature of the CMB with redshift can depress the observed surface brightness of the CO and dust emission of high redshift galaxies, with the effect becoming more noticeable for low order transitions. Their calculation shows that at $z \sim 2$, the effect on the CO 2-1 brightness should be minimal.

As a final comparison, we consider a galaxy at $z = 4.2$ with 3.5× higher CO luminosity than the $z = 2$ model (12.5× M51), and a total velocity width a factor three larger. We adopt the CO 2-1 line, redshifted to 44GHz. This system would correspond to the more massive star forming disk galaxies seen at high redshift (SFR $\sim$ 130 $M_\odot$ year^{-1}; (Casey et al. 2014)).

3. Configuration

We employ the Southwest configuration, distributed across New Mexico and Chihuahua[1]. The array includes 45% of the antennas in a core of diameter ~ 1km, centered on the VLA site. Then some 35% of the antennas out to VLA A array baselines of 30km, and the rest to baselines as long as 500km, into Northern Mexico.

For the ngVLA noise calculation at 77GHz, we assume the radiometer equation, using an 18m diameter antenna, with 70% efficiency, 70K system temperature at 77GHz, and a 30 hour observation. For the ngVLA noise calculation at 44GHz, we use an 18m diameter antenna, with 75% efficiency, 55K system temperature, and a 30 hour observation.

For the ALMA simulations, we use the ALMA-out18 and ALMA-out22 configurations. These have 50 antennas extending to baselines that give a naturally weighted beam at 77GHz of 0.45" and 0.19", respectively. For the ALMA noise calculation, we assume antennas of 12m diameter, with an efficiency of 75%, and 70K system temperature, and a 30hour integration. Note that these observations require ALMA band 2, currently under design.

For the JVLA simulation, we employ the B configuration, with 27 antennas of 25m diameter, with an efficiency of 35%, and 65K system temperature, and a 30 hour observing time.

The noise in the final images is also dictated by the channel width and visibility weighting, with natural weighting (robust = 2) giving the optimal noise performance. The different ALMA configurations are designed to give a reasonable synthesized beam for natural weighting.

The ngVLA has a very non-uniform antenna distribution. The naturally weighted beam for this centrally condensed distribution leads to a PSF with a high resolution core of a few mas width at 77 GHz, plus a broad, prominent pedestal or plateau in the synthesized beam with a response of ~ 50% over ~ 1" scale. This prominent pedestal leads to severe problems when trying to image complex structure. The imaging process entails a balance between sensitivity and synthesized beam shape, using visibility tapering and Briggs robust weighting (Carilli et al. 2018; Cotton & Condon 2017; Carilli 2017, 2016,?; **?**).

---

[1]These simulations were performed with a slightly older, 300 antenna configuration, vs. the latest 214 antenna configuration. However, the uv-weighting employed downweights both the longer spacings (beyond 30km), and the core (within 1km), while the intermediate spacing array is much the same as the latest configuration. Hence, the results will not change appreciably using SW214.

4. Mechanics of the simulation

The starting model is the BIMA SONG observations of CO 1-0 at about 5.5" resolution (Helfer et al. 2003). This corresponds to 0.20 kpc at the distance of M51. The channel width is 10 km s^{-1} = 3.8MHz at 115GHz. Details of the process can be found in (**?**). In brief, we adjust the frequency, pixel size, and flux density of the model to match the line luminosity and galaxy size as a function of redshift.

We employed the SIMOBSERVE task within CASA to generate uv data sets. Instructions on how this is done are found on the ngVLA web page. We simulated a 30 hour observation, made up of a series of 3 hour scheduling blocks around transit.

In all cases we employed the CLEAN algorithm with Briggs weighting, and adjusted the robust parameter and uvtaper to give a reasonable synthesized beam and noise performance. Our target resolution was ~ 0.2", which corresponds to ~ 1kpc physical for $z \geq 0.5$. Synthesized beams for different weighting schemes are given in Table 2. We use a cell size of 0.01" throughout.

5. Results

5.1. $z = 0.5$

We focus our more detailed analysis on the $z = 2$ model. However, for reference, we have performed a mock observation of M51 at $z = 0.5$.

Figure 2, row 1 shows the CO 1-0 moment images for a 30hr observation for the $z = 0.5$ model with the ngVLA. The observing frequency is 77 GHz. Our targer resolution is ~ 0.2" ~ 1 kpc at $z = 0.5$. To achieve a well behaved synthesized beam (ie. no pedestal), but retain reasonable sensitivity, we employ the imaging parameters listed in Table 1. The rms per 20 km s^{-1} channel, is about 16μJy beam^{-1}.

We generate moment images of the CO 1-0 emission blanking at surface brightnesses below about 1.5σ. The results in Figure 2 show that the ngVLA will make quality images of the velocity integrated intensity, as well as the overall velocity field. The emission is dominated by the central regions, but emission from the spiral arms remains clear, as well the large-scale galaxy velocity structure in the extended regions. The minimum measured velocity dispersions are 20km/s, which is at the limit of the measurements.

5.2. $z = 2.0$

We next generate a mock observation of the CO 2-1 emission from the model galaxy at $z = 2$. Again, 30hrs integration is assumed, and the observing frequency is 77 GHz. The imaging parameters are given in Table 2. Figure 3 shows the resulting CO 2-1 channel images for the $z = 2$ model. The rms per 20 km s^{-1} channel (5.1MHz), is 16μJy beam^{-1}. The corresponding 3σ gas mass limit per channel is $\sim 2 \times 10^8$ $(\alpha/3.4)$ $M_\odot$.

Emission is clearly detected over the full velocity range of the galaxy, starting with the northern arm at low velocity, through the main gas distribution at the galaxy center, to the southern arm at high velocity.

Figure 2, row 2 shows the moment images for this system derived from the ngVLA observations. While the spiral arms are less prominent, the emission is still seen over most of the disk, and the velocity field is reasonable clear.

Figure 4 shows the integrated spectrum of the CO emission from the galaxy. The red curve is derive from the mock ngVLA observation. The blue curve shows the intrinsic emission derived from a model with no noise added. The integrated emission profile is very well recovered, with a mean flux density of 0.65 mJy beam^{-1}, and a total velocity width of 150 km s^{-1}.

The CO 2-1 luminosity is $L'_{C0} = 5.8 \times 10^9$ K km/s pc^2, implying a molecular gas mass of 2.0×10^{10} $(\alpha/3.4) M_\odot$. This corresponds to a CO luminosity a factor 3.5× larger than M51 itself.

We next consider a similar 30hr observation using ALMA. To achieve a similar spatial resolution of ∼ 1kpc, we employ the 'out22' configuration and natural weighting of the visibilities. This leads to an rms noise of 75 μJy beam^{-1} per 20 km s^{-1} channel. Figure 5 shows the velocity integrated emission from the ALMA observation, compared to that from the ngVLA observation. ALMA barely detects the velocity integrated emission at this resolution. To recover the dynamics at the level of detail seen in Figure 2, row 2 would required about 700 hours of integration time on ALMA.

We then use a smaller ALMA array (out18 to achieve 0.45" resolution), to avoid over-resolving the emission, and again integrating for 30hrs. The spatially integrated spectrum is shown as the yellow curve in Figure 4. The spatially integrated emission is detected in the spectrum, although still at relatively low signal-to-noise.

5.3. Rotation curve analysis

We have analyzed our mock CO 2-1 ngVLA observations of the $z = 2$ disk using the standard tools for galaxy dynamical analysis available in AIPS and GIPSY. The details of the process can be found in (Jones et al. 2017a).

In brief, we generate an optimal moment 1 image (intensity weighted mean velocity), using the XGAUS routine in AIPS. This routine fits a Gaussian function in frequency (velocity) at each pixel in the cube to obtain the mean velocity.

We then run the resulting moment 1 image through the ROTCUR program in GIPSY. This program assumes the gas has a pure circular rotation in a gas disk, and fits the velocity field with a series of tilted rings as a function of radius with a given thickness (Rogstad et al. 1974). Each ring has a number of parameters that are used in the fitting, including rotation velocity, inclination angle of the normal to the line of sight, and position angle of the projected major axis of the ring on the sky.

Figure 6 shows the results, including the moment 1 image from XGAUS, the resulting fit dynamical disk, and the residuals (fit - observed). The data are reasonably well fit by the tilted ring model. The fit position angle of the major axis is 172^o, as compared to the 'true' value for M51 of 162^o (Oikawa & Sofue 2014). The fit inclination angle is 21^o, as compared to 24^o for the nominal 'true' value of M51 (Shetty et al. 2007). Note that M51 has a warped disk, but the warp starts at radius ∼ 7kpc, which is outside our sensitivity area (Oikawa & Sofue 2014).

The fit rotation velocities (corrected for inclination) for the rings versus radius are shown in Figure 7a. The blue curve is the rotation curve of M51 from (Oikawa & Sofue 2014). While the error bars are substantial, the magnitude in the outer rings matches well the 'true' rotation velocity of ∼ 200 km s^{-1}. This plot also shows the limitations of such a process: recovering the inner steep rise in the rotation curve within ∼ 1 to 2kpc radius remains problematic with data that has only 1kpc resolution.

5.4. $z = 4.2$

As a final example, we present CO 2-1 emission from a massive disk galaxy at z = 4.2. Note that at this redshift, the combination of CMB excitation, and the fact that observations always measure the surface brightness relative to the CMB, may become issues. At $z \sim 4$, for cold molecular clouds (20K), the 'CMB effect' could lower the observed 2-1 surface brightnesses by up to 60%, while for warmer gas (50K), the CMB effect is $\leq$ 20% (Zhang et al. 2016). Given the galaxy in question is a massive star forming galaxy, we assume the latter.

We again assume 30hr integration. The observing frequency is 44GHz. The imaging parameters are given in Table 1, resulting in a PSF with a FWHM = 0.19" and no pedestal. The resulting rms noise per 30 km s^{-1} channel, is 10μJy beam^{-1}.

Figure 2, row 4 shows the moment images for this system derived from the ngVLA observations. While the spiral arms are less prominent, the emission is still seen over most of the disk, including the north and south arms, and the overall velocity field is clear.

Figure 8 shows the integrated spectrum of the CO emission from this galaxy. The red curve is derived from the mock ngVLA observation. The blue curve shows the intrinsic emission derived from a model with no noise added. The integrated emission profile is very well recovered, with a mean flux density of 0.22 mJy beam^{-1}, and a total velocity width of 450 km s^{-1}.

The implied CO 2-1 luminosity is: $L'_{C0} = 2.0 \times 10^{10}$ K km/s pc^2, implying a molecular gas mass of 6.9×10^{10} $(\alpha/3.4)$ $M_\odot$. The implied star formation rate for this galaxy based on the standard star formation law for disk galaxies would be $\sim$ 130 $M_\odot$ year^{-1} (Daddi et al. 2010). Such a galaxy corresponds to a more massive star forming disk galaxy ('main sequence'), observed at high redshift (Carilli & Walter 2013; Casey et al. 2014).

We next consider a 30hr observation using the current JVLA. To achieve a similar spatial resolution of $\sim$ 1kpc, we employ the B-configuration and natural weighting of the visibilities, but include a taper parameter of 0.15". This leads to an rms noise of 80 μJy beam^{-1} per 30 km s^{-1} channel, and a spatial resolution of 0.22"). The signal is not detectable above the noise in the channel images. We created a spatially integrated spectrum, as shown as the yellow curve in Figure 8, smoothed to 60 km s^{-1} channel^{-1}. The emission can be seen in this integrated spectrum, but at marginal signal-to-noise. To reach the required signal-to-noise to perform the imaging in Figure 2, row 4 would require 2000hrs with the current JVLA.

We again perform a rotation curve analysis using XGAUS and ROTCUR on the ngVLA most observations. Figure 9 shows the results, including the moment images and the resulting fit dynamical disk, and the residuals (observed - fit). The fit position angle of the major axis is 173^o, as compared to the 'true' value for M51 of 162^o (Oikawa & Sofue 2014). The fit inclination angle is 26^o, as compared to 24^o for the nominal 'true' value of M51 (Shetty et al. 2007).

The fit rotation velocities (corrected for inclination) for the rings versus radius are shown in Figure 7b. The blue curve is the rotation curve of M51 from (Oikawa & Sofue 2014), scaled up by a factor three. In this case, the measured rotation curve appears to asymptote to the maximum rotation velocity at 6kpc radius. This under-estimation over much of the radius may result from the marginal measurement of the velocity field on the southern (fainter) spirals arms of the galaxy. These results indicate the limitations of this kind of analysis, for a given signal to noise and spatial resolution.

5.5. Minimal Array

We investigate a 'miminal array configuration' that would be adequate to perform the CO imaging at $z = 2$ considered in section 5.2.

We revised the Southwest configuration as follows. First, we remove all antennas outside the area covered by the current VLA Y configuration (all antennas beyond 15km radius of the array core). These antennas are heavily down-weighted due to the desire to obtain ~ 0.2" resolution, which correponds to baselines of about 4km at 77GHz and 8km at 44GHz. This removes about 1/3 of the antennas. Then we remove 2/3 of the core antennas, or 82 antennas. The core antennas were also down-weighted by the use of the robust parameter in the imaging analysis above. This leaves us with 114 antennas (out of the original 300), in an array that has good baseline coverage on scales out to 30km.

We then perform the same mock observation as above for the $z = 2$ model (30hrs). In this case, we could employ robust R=1, along with the same cell and taper as before, to achieve similar resolution (0.21"). The rms noise per 20km s^{-1} channel is now 24uJy $beam^{-1}$.

The resulting moment images are shown in Figure 2, Row 3. The resolution is slightly lower, but the signal to noise is still adequate to recover all the main structures of the galaxy as seen with the original SW array.

The green curve on Figure 4 shows the resulting integrated spectrum. This matches well the true spectrum shown in the blue.

6. Conclusions

We have performed a detailed analysis of the capabilities of the ngVLA to image at 1kpc resolution the low order CO emission from high redshift main sequence star forming galaxies. The template for the galaxy size and dynamics is M51. The model galaxies include: (i) a galaxy with CO luminosity 40% higher than M51 at $z = 0.5$ (star formation rate ~ 7 $M_\odot$ $year^{-1}$), (ii) a modest star forming main sequence disk galaxy at $z = 2$ (SFR ~ 25 $M_\odot$ $year^{-1}$), and (iii) a massive star forming disk at $z = 4.2$ (SFR ~ 130 $M_\odot$ $year^{-1}$). The main results are as follows:

- The overall gas distribution and dynamics are recovered in all cases by the ngVLA.
- Detailed analysis of the mock rotation curves recover the main galaxy orientation parameters, such as inclination angle and position angle of the major axis, to within 10% in all cases.
- The rotation velocity versus radius is determined reasonably out to the maximum radius of the CO disk (6kpc) for the $z = 0.5$ and $z = 2$, with the exception of the rapid rise in the rotation curve in the inner 2kpc, which cannot be recovered at 1kpc resolution.
- The rotation curve analysis for the $z = 4.2$ galaxy asymptotes to the maximum rotation velocity of the system. This is likely due to the more limited signal-to-noise on the southern spiral arm emission.

- ALMA and the JVLA can detect the integrated emission from these galaxies, but neither can recover the dynamics at high spatial resolution. To do so would require of order 1000 hours per galaxy with these current facilities.
- We explore a 'minimal array' to perform this measurement involving 1/3 of the dense 1km core, and no antennas beyond the current VLA foot-print, giving an array of 114 antennas to radii of about 15km. We can still recover the source dynamics at 0.22" resolution, with a noise figure higher by about 50% relative to the full array when suitably tapered and weighted.

Observing detailed galaxy dynamics is one of the critical, and yet under explored, elements in studies of high redshift galaxies. Multiple techniques are now being employed, with the Hα and IFU specroscopy in the near-IR employed on large telescopes for galaxies at $z \sim 2$ (Forster-Schreiber et al. 2018), and [CII] 158μm spectroscopy with ALMA at $z \geq 3$ (Jones et al. 2017b). The CO observations play a complementary role, tracing the molecular gas, as opposed to the ionized or neutral atomic gas.

The National Radio Astronomy Observatory is a facility of the National Science Foundation operated under cooperative agreement by Associated Universities, Inc.

Table 1. Galaxy Model parameters

Model	CO flux	CO line	z	D_L	L'_{CO}	M_{H2}	L_{IR}	SFR
	Jy km s^{-1}			Mpc	10^9 K km/s pc^2	$(\alpha/3.4)10^{10}$ $M_\odot$	$\times10^{10}$ $L_\odot$	$M_\odot$ year^{-1}
M51	10150	1-0	0.0015	7.6	1.6	0.55	4.7	4.7
z=0.5	0.15	1-0	0.5	2860	2.3	0.8	7.4	7.4
z=2	0.1	2-1	2.0	15800	5.8	2.0	25	25
z=4.2	0.1	2-1	4.2	38800	20	6.9	130	130

Table 2. Imaging parameters

Array	Frequency	Channel Width	Robust	UV Taper	Resolution	rms noise
	GHz	MHz		arcsec	arcsec	μJy beam^{-1} channel^{-1}
ngVLA CO 1-0	77	5.1	0.5	0.15	0.22	16
ngVLA CO 2-1	77	5.1	0.25	0.15	0.19	16
ALMA-out22	77	5.1	2		0.19	75
ALMA-out18	77	5.1	2		0.45	75
ngVLA-min	77	5.1	1	0.15	0.21	24
ngVLA	44	4.5	0.5	0.1	0.19	10
JVLA	44	4.5	2		0.22	80

References

Bolatto, A. et al. 2013, ARAA, 51, 207
Bolatto, A. et al. 2017, ngVLA Memo No. 19
Carilli, C. et al. 2018, ngVLA Memo No. 35
Carilli, C. 2018, ngVLA Memo No. 47
Carilli, C. 2017, ngVLA Memo No. 16
Carilli, C. 2016, ngVLA Memo No. 12
Carilli, C. et al. 2015, ngVLA Memo No. 5 (arXiv:1510.06438)

Carilli, C.L. & Walter, F. 2013, ARAA 51, 105
Casey, C. et al. 2014, PhR, 541, 45
Cotton, W. & Condon, J. 2017, ngVLA Memo No. 30
Daddi, E. et al. 2015, A& A, 577, 46
Daddi, E et al. 2010, ApJ, 713, 686
Decarli, R. et al. 2016, ApJ, 833, 70
Forster-Schreiber et al. 2018, arXiv:1802.07276
Geach, J. et al. 2011, ApJ, 730, L19
Genzel, R. et al. 2015, ApJ, 800, 20
Genzel, R. et al. 2011, ApJ, 733, 101
Helfer, T. et al. 2003, ApJS, 145, S259
Jones, G.C. et al. 2017, ApJ, 850, 180
Jones, G.C. et al. 2017, ApJ, 845, 175
McKinnon, M. et al. 2016, SPIE, 9906, 27
Oikawa & Sofue 2014, PASJ, 66, 77
Rogstad et al. 1974, ApJ, 193, 309
Schinnerer, E. et al. 2016, ApJ, 833, 112
Schinnerer, E. et al. 2013, ApJ, 779, 42
Shetty et al. 2007, ApJ, 665, 1138
Selina, R. & Murphy, E. 2017, ngVLA Memo. No. 17
Tacconi, L. et al. 2010, Nature, 463, 781
Tacconi, L. et al. 2018, ApJ, 853, 179
Scoville, N. et al. 2017, ApJ, 837, 150
Walter, F. et al. 2016, ApJ, 833, 67
Walter, F. et al. 2014, ApJ, 782, 79
Zhang et al. 2016, Royal Society Open Science, Volume 3, Issue 6, id.160025

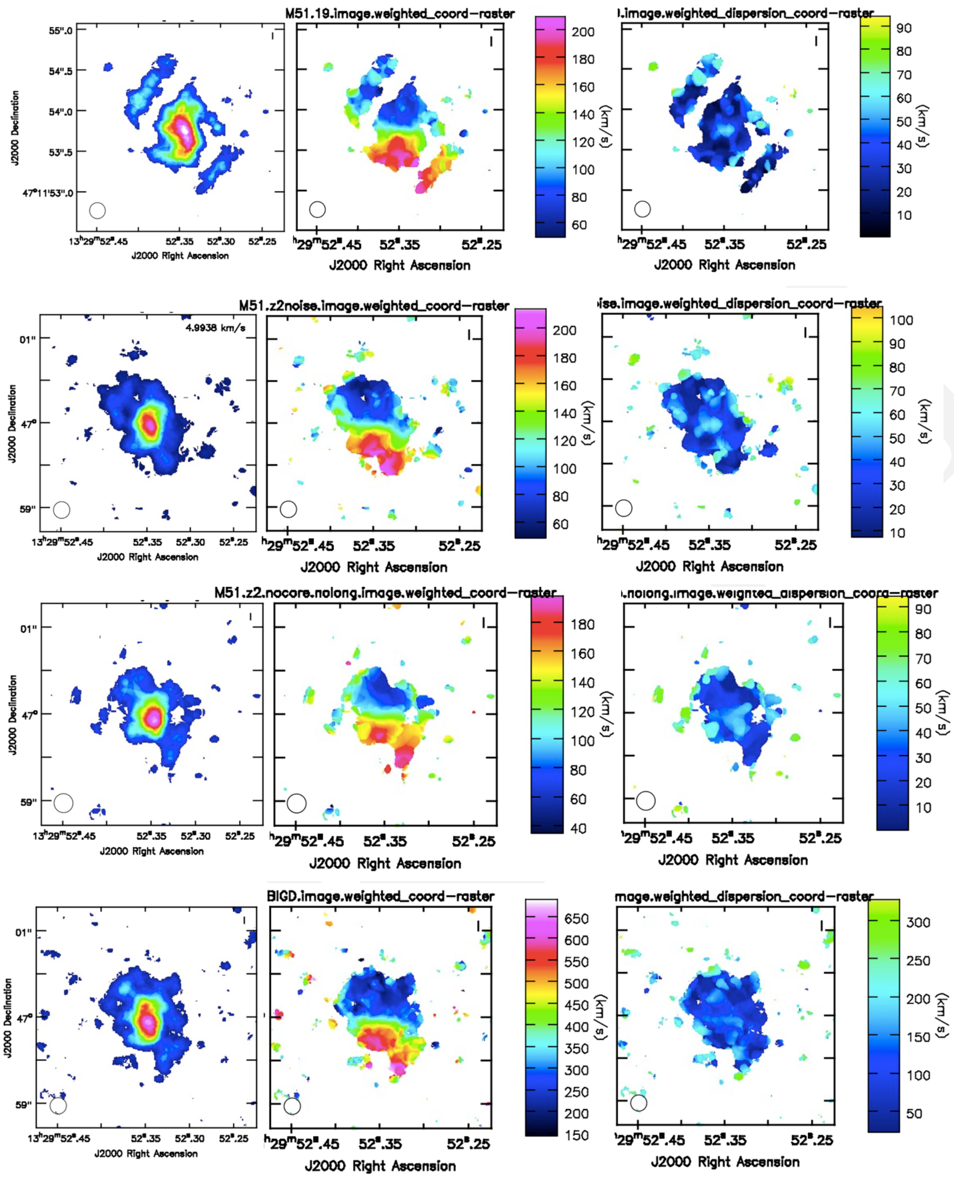

Figure 2. **Top row***: Simulated ngVLA observations using at 77 GHz of the CO 1-0 emission from an M51 analog at z = 0.5 for a 30 hour observation ($SFR \sim 7\ M_{\odot}\ year^{-1}$). The left frame shows the velocity integrated emission. The middle shows the intensity weighted mean velocity, and the right shows the velocity dispersion. (Frames are the same in all four examples). The spatial resolution is* 0.19”. **Second row***: Simulated ngVLA observation at 77 GHz of the CO 2-1 emission from the $z = 2$ model galaxy ($SFR \sim 25\ M_{\odot}\ year^{-1}$). The spatial resolution is* 0.19”. **Third row***: Simulated observation using a ’minimal configuration’ of the ngVLA (only 1/3 of the core, and no antennas at radii outside the original VLA Y), at 77 GHz of the CO 2-1 emission from the z = 2 model. The spatial resolution is* 0.19”. **Bottom row***: Simulated ngVLA observation at 44GHz of the CO 2-1 emission from a massive star forming disk galaxy at $z = 4.2$ ($SFR \sim 130\ M_{\odot}\ year^{-1}$). The spatial resolution is* 0.22”.

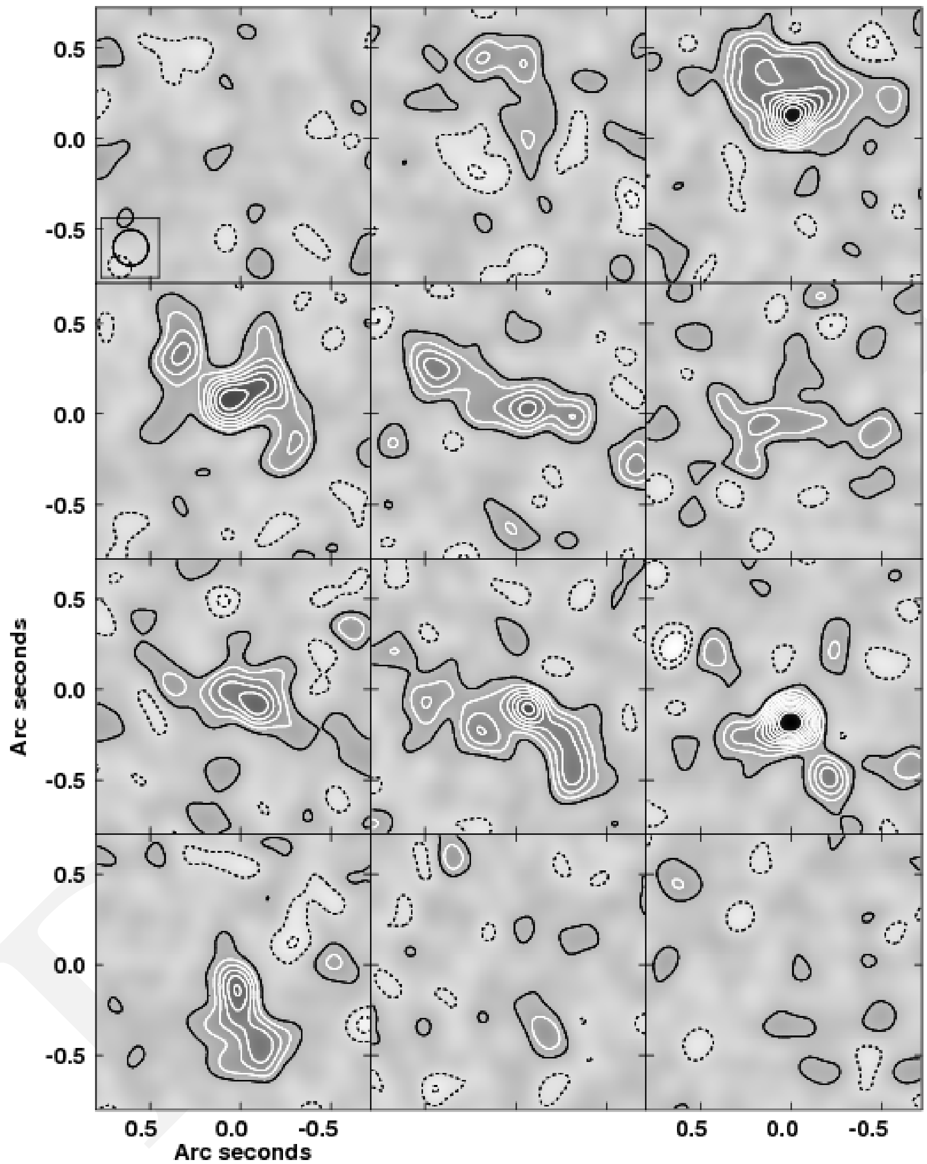

Figure 3. Spectral channel images of the CO 2-1 emission from star forming disk galaxy at $z = 2$ ($SFR \sim 25$ $M_\odot$ year^{-1}), from the 30hr ngVLA observations tapered to 0.19” resolution. The first contour level is 26μJy beam^{-1}, and the contours are linear. Negative contours are dashed.

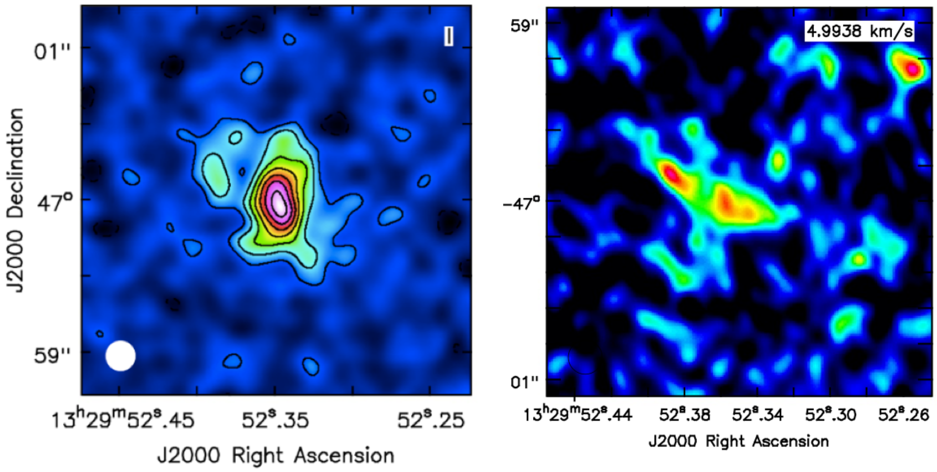

Figure 4. Right: Simulated observations using ALMA at 77 GHz of the velocity-integrated total CO 2-1 emission from the $z = 2$ model. Left: The ngVLA velocity integrated CO emission as per Figure 2, row 2, for comparison.

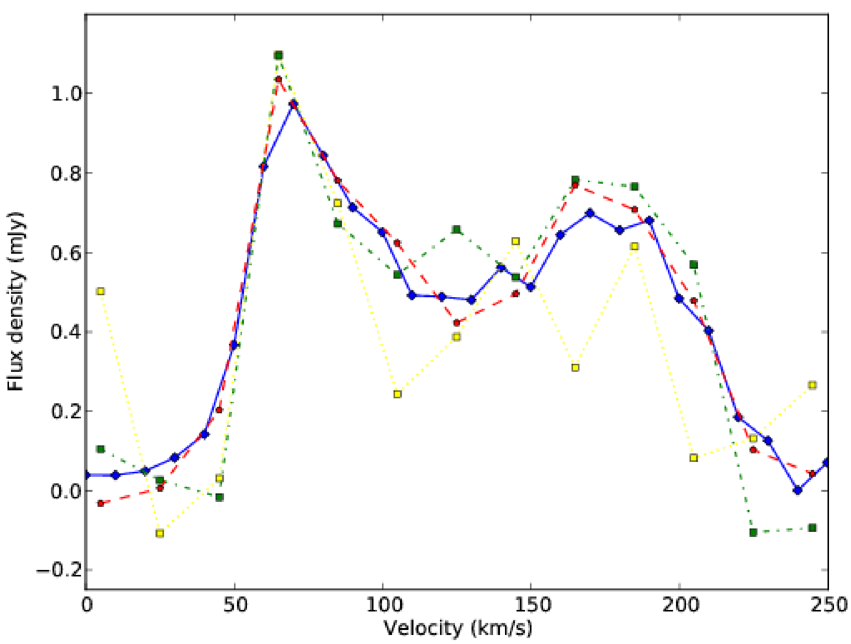

Figure 5. The spatially integrated CO 2-1 spectrum of the $z = 2$ model galaxy. Blue is the input model with no noise added, and 10 km s^{-1} channel^{-1}. The red is for the tapered ngVLA 30hr observation shown in Figure 2, row 2, at 20 km s^{-1} channel^{-1}. The yellow is for the ALMA observation shown in Figure 5, at 20 km s^{-1} channel^{-1}. The green is for the minimal ngVLA array (30% core, Y-only), 30hr observation shown in Figure 2, row 3, at 20 km s^{-1} channel^{-1}.

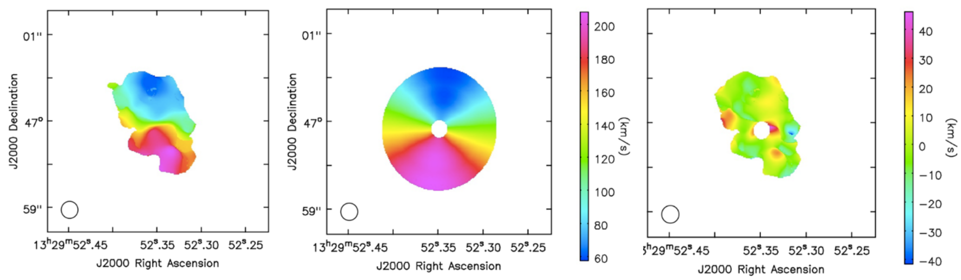

Figure 6. Left: the mean velocity of the CO emission from the z=2 model derived from the ngVLA using the XGAUS technique descibed in section 5.3. Center: the model for the rotation curve derived using ROTCUR. Right: the residuals from differencing the model and observation.

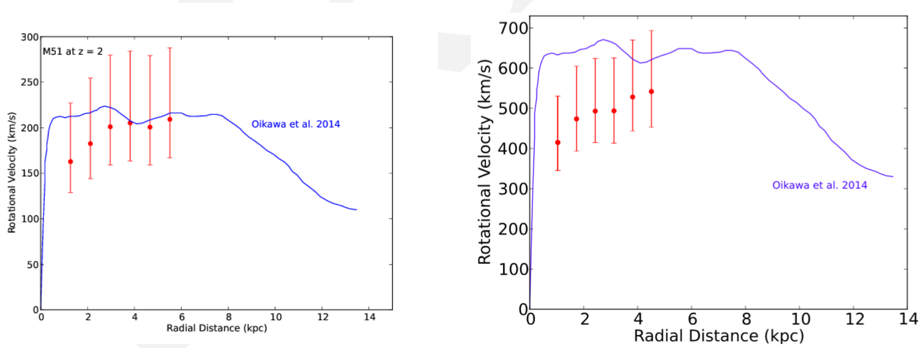

Figure 7. **Left**: The rotation curve derived for the z=2 model from the ngVLA data using ROTCUR (red points plus errors). The blue line shows the true rotation curve (Oikawa & Sofue 2014). **Right:** The rotation curve derived for the z=4.2 massive star forming disk galaxy, derived from the ngVLA data using ROTCUR (red points plus errors). The blue curve shows the input model scaled by a factor 3 (Oikawa & Sofue 2014).

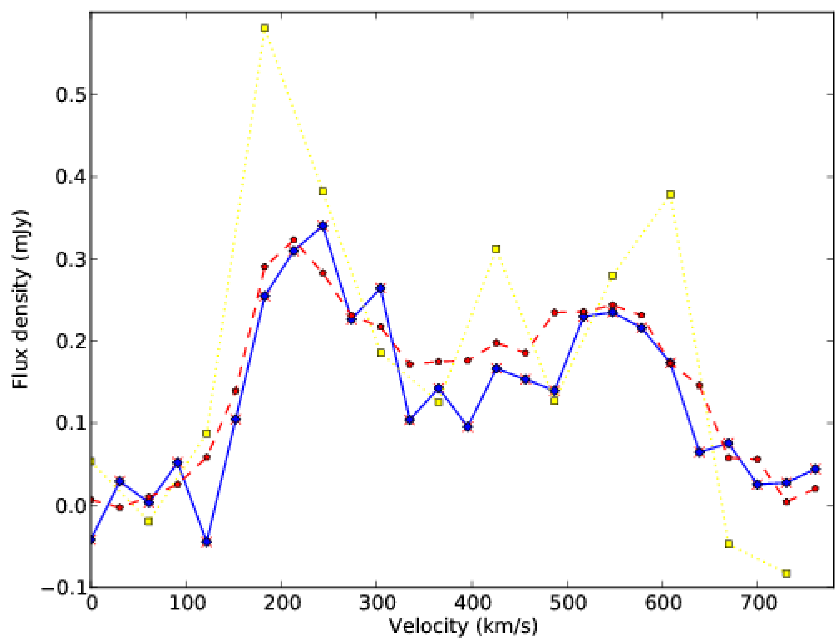

Figure 8. The integrated spectrum of the CO 2-1 emission from the z = 4.2 massive star forming disk galaxy. Blue is the input model with no noise and 30 km s^{-1} channel^{-1}. The red is for the tapered ngVLA 30hr observation shown in Figure 2, row 4, at 30 km s^{-1} channel^{-1}. The yellow is for a 30hr JVLA observation, at 60 km s^{-1} channel^{-1}.

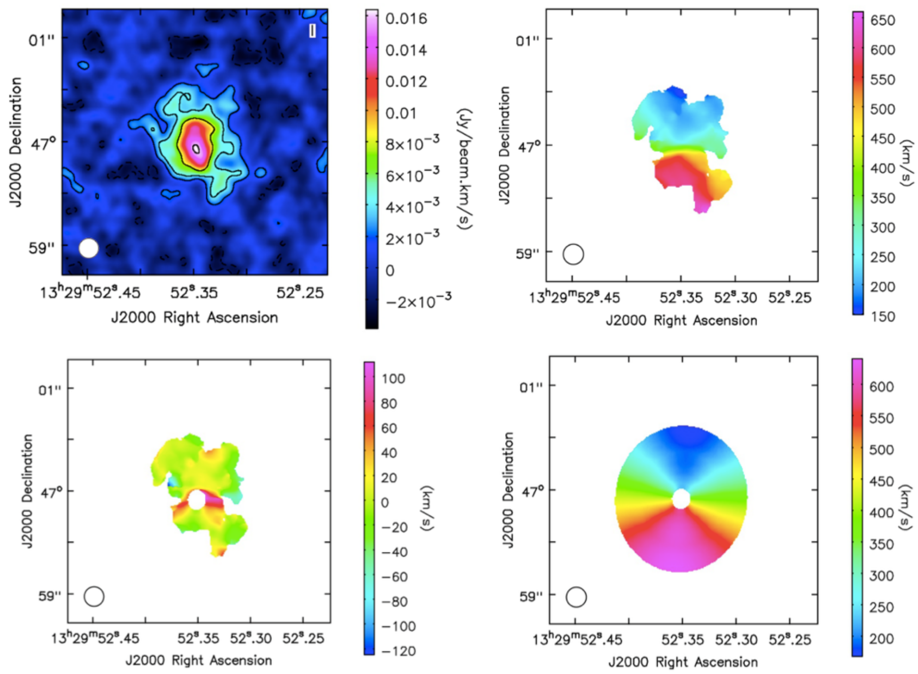

Figure 9. Upper Left: the velocity integrated CO 2-1 emission from the z=4.2 galaxy, Upper right: the mean velocity, derived from the ngVLA using the XGAUS technique descibed in section 5.3. Lower right: the model for the rotation curve derived using ROTCUR. Lower left: the residuals from the model and observation difference.

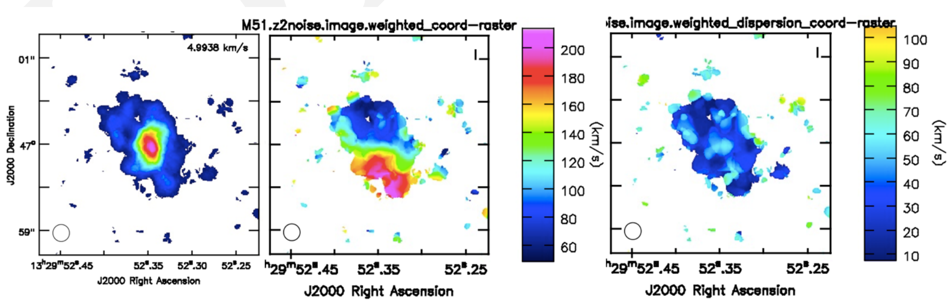

Figure 10. Simulated observation using the ngVLA at 80GHz of the CO 2-1 emission from the $z = 2$ model galaxy. The left frame shows the velocity integrated emission. The middle shows the intensity weighted mean velocity, and the right shows the velocity dispersion. The spatial resolution is 0.19”.

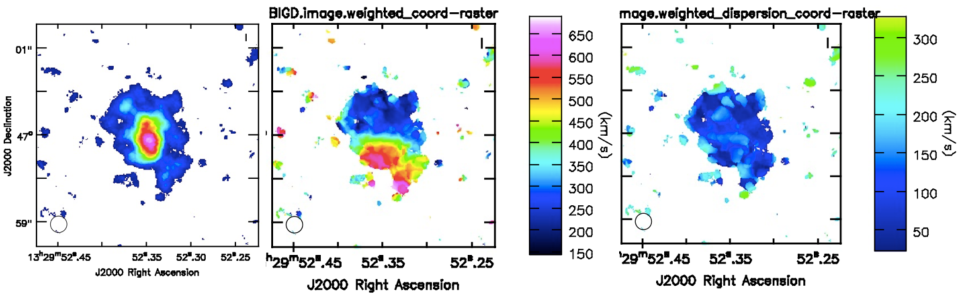

Figure 11. Simulated observation using the ngVLA at 44GHz of the CO 2-1 emission from a massive star forming disk galaxy at $z = 4.2$ ($SFR \sim 130$ $M_\odot$ year^{-1}). The left frame shows the velocity integrated emission. The middle shows the intensity weighted mean velocity, and the right shows the velocity dispersion. The spatial resolution is 0.22".

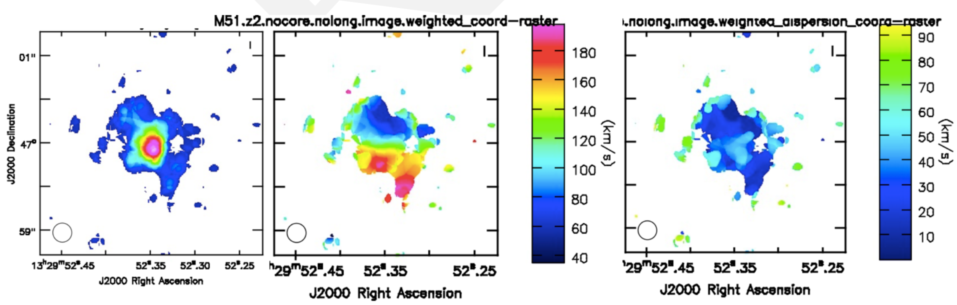

Figure 12. Simulated observation using a 'minimal configuration' of the ngVLA (only 1/3 of the core, and no antennas at radii outside the original VLA Y), at 77 GHz of the CO 2-1 emission from the $z = 2$ model. The left frame shows the velocity integrated emission. The middle shows the intensity weighted mean velocity, and the right shows the velocity dispersion. The spatial resolution is 0.19".

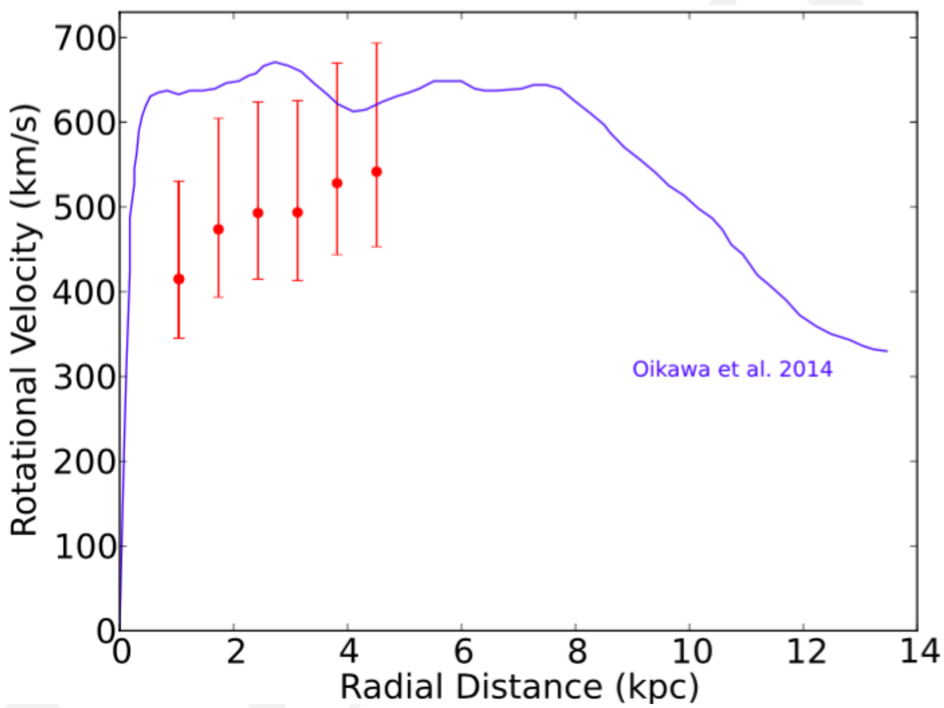

Figure 13. The 1D rotation curve derived for the z=4.2 massive star forming disk galaxy, derived from the ngVLA data using ROTCUR (red points plus errors). The blue curve shows the input model scaled by a factor 3 (Oikawa & Sofue 2014).

Science with a Next-Generation Very Large Array
ASP Conference Series, Monograph 7
Eric J. Murphy, ed.

DRAFT EDITION

Continuum Surveys

Amy J. Barger,[1] Kotaro Kohno,[2] Mark T. Sargent[3], Eric J. Murphy[4], James J. Condon[4]

[1]*University of Wisconsin-Madison, Madison, WI, USA;* barger@astro.wisc.edu

[2]*University of Tokyo, Tokyo, Japan;* kkohno@ioa.s.u-tokyo.ac.jp

[3]*University of Sussex, Brighton, UK;* Mark.Sargent@sussex.ac.uk

[4]*National Radio Astronomy Observatory, Charlottesville, VA, USA;* emurphy@nrao.edu, jcondon@nrao.edu

1. Introduction

The rest-frame UV light density has been successfully mapped to beyond $z \sim 10$ using the *Hubble Space Telescope*. However, very luminous galaxies emit much of their light at far-infrared (FIR) to millimeter (mm) wavelengths and may be extremely faint in the UV/optical. Thus, long-wavelength observations are needed to determine how much star formation we are missing from UV/optical surveys. Indeed, the universe produces comparable amounts of energy in the FIR and optical (Puget et al. 1996; Fixsen et al. 1998), requiring a detailed understanding of the FIR population at all redshifts.

Uniformly selected samples are key for determining the dusty star formation history, and there are various ways we can try and construct such samples. One route is to observe at submm wavelengths, which are unique in that they are equally sensitive to high and low redshifts due to the negative K-correction (i.e., with increasing redshift, the fixed submm bandpass samples higher on the Rayleigh-Jeans tail of the blackbody emission produced by the galaxy's dust, which compensates for the inverse square law dimming). Imaging surveys with single-dish submm and mm telescopes and cameras have the advantage of being able to cover large fields and produce uniformly selected samples in a single bandpass to a well-established flux limit. Their main disadvantage is low resolution. This is particularly problematic for blank field observations, since the confusion limit can be reached at fairly high fluxes. (Confusion refers to the blending of sources and/or the noise being dominated by unresolved contributions from fainter sources.) In contrast, interferometric submm and mm imaging surveys enjoy high spatial resolution and sensitivity, but their fields-of-view are small.

An alternative route is to conduct surveys at radio wavelengths. The advantages of such surveys are large areas, high spatial resolution, and no extinction. However, at current sensitivities, the positive K-correction at these wavelengths results in redshift limitations ($z \lesssim 3$) for even the most luminous galaxies. Differentiating star-forming galaxies from active galactic nuclei (AGNs) at radio wavelengths is also challenging.

Fortunately, the ngVLA is poised to revolutionize radio continuum surveys and make it possible to construct a complete star formation history. In this chapter, we describe an ngVLA survey that will complement the *James Webb Space Telescope (JWST)* deep fields by providing high-resolution imaging of star formation, unbiased by dust, for a large, homogeneous sample of galaxies with a wide range of luminosities and star formation rates (SFRs) out to redshifts of $z \sim 6$.

2. Scientific Importance and Survey Considerations

Single-dish submm imaging surveys have revealed a significant population of extremely luminous, dusty star-forming galaxies to the highest redshifts (see Casey et al. 2014 for a review). These galaxies have dramatically changed our understanding of the star formation history of the universe and have challenged cosmological simulations in producing them. At some point, the submm selected population will begin to overlap in SFR with the optically selected population. To obtain large samples of submm galaxies to the depths necessary to observe the overlap with the optical population, we can use next generation radio continuum surveys that cover large areas, have high spatial resolution, and are insensitive to extinction. In order to determine the optimal frequency continuum survey to be made with the ngVLA, we need to consider the dominant physical mechanisms that contribute to the radio emission at high redshifts.

From the well-established FIR-radio correlation (e.g., Condon 1992), we know that non-thermal synchrotron emission is a valuable tracer of the total amount of star formation in galaxies, unbiased by dust. Synchrotron emission is dominant in lower frequency radio observations ($\sim$ 1 GHz). The large fields-of-view at these frequencies are an advantage for measuring substantial numbers of very high-redshift galaxies; however, AGNs are a contaminant in the star-forming galaxy samples. Moreover, there are uncertainties in the conversion from radio flux to SFR. The sensitivity of current facilities at these frequencies is very limiting. For example, the deepest existing 1.4 GHz VLA image (5σ of 11.5 μJy of the *Chandra* Deep Field-North; Owen 2018) is only able to probe luminosities of ultraluminous infrared galaxies or ULIRGs ($L_{IR} = 10^{12}\,L_\odot$) to $z \sim 3$ and luminous infrared galaxies or LIRGs ($L_{IR} = 10^{11}\,L_\odot$) to $z \sim 1$ (see Figure 14 in Barger et al. 2014).

Inverse Compton (IC) scattering of relativistic electrons off of cosmic microwave background radiation (CMBR) photons may also have an impact on synchrotron emission. When the CMBR radiation energy density exceeds the galaxy magnetic energy density, the IC scattering dominates (e.g., Condon 1992; Murphy 2009). There is a redshift dependence in the amount of IC scattering that occurs, since the energy density of the CMBR goes as $(1 + z)^4$. There is also a luminosity dependence, since the synchrotron emission will be highly quenched in moderate SFR galaxies at high redshifts but possibly never in ULIRGs where the magnetic energy density is higher. This means that high-redshift galaxies with moderate SFRs will be totally free-free, modulo the possible contribution from anomalous dust emission (Planck Collaboration et al. 2015), which may arise from spinning dust grains (e.g., Draine & Lazarian 1998).

Free-free emission is directly proportional to the production rate of ionizing photons by young, massive stars, making it useful for measuring SFRs (see, e.g., Murphy et al. 2015). Free-free emission is dominant at rest-frame tens of GHz and is straightforwardly understood. There are also no issues with the conversion of radio flux to SFR. However, there can still be substantial synchrotron contributions that have to be taken into account.

3. Anticipated Results and Astronomical Impact

The sweet spot for field-of-view versus resolution with the ngVLA is around 10 GHz. By covering the maximum size of the *JWST* deep fields (1 deg^2), which are the most heavily studied regions on the sky, to a sensitivity of 0.1 μJy per beam at 10 GHz ($0\farcs1$ resolution), critical dust-free information about the star formation rates and morphologies of the galaxies in these fields can be obtained. In particular, such a survey will allow the detection of many thousands of galaxies at $z \sim 2$ to 4 L^*, as well as galaxies with $L_{IR} > 5 \times 10^{12}\ L_\odot$ out to $z \sim 8$, where we have no current knowledge of the numbers of such luminous galaxies.

By combining the data for a large sample of 10 GHz selected galaxies with observations at other frequencies from 1 to 50 GHz, ideally also made with the ngVLA as part of the survey, we could map the radio spectral energy distributions (SEDs) of the galaxies, which would make it possible to separate the free-free contributions from the synchrotron contributions, and to separate the AGNs from the star-forming galaxies. This is critical for the construction of the total star formation history from radio data. In addition, with such a large frequency range, we could make measurements of low CO lines to obtain redshifts for many of the galaxies—particularly the more dusty galaxies where it is very difficult to measure redshifts from optical and near-infrared spectroscopy—and to provide information on the gas masses of the galaxies.

Another interesting outcome of mapping the radio SEDs for a number of galaxies of a given luminosity is that by seeing at what redshift the shape changes from synchrotron plus free-free to free-free only, we will get a rough galactic magnetic field measurement for that luminosity by equating it to the CMBR energy density. We show this in Figure 1, where we plot energy density versus redshift for a local spiral and a ULIRG (from McBride et al. 2014 following Carilli 2001) and for the redshift-dependent CMBR. We show the magnetic field strength on the right-hand vertical axis.

4. Uniqueness to ngVLA Capabilities

Single-dish submm images have low resolution, and blank field observations hit the confusion limit at relatively bright fluxes ($\sim$ 2 mJy). Interferometric submm/mm images have high spatial resolution and sensitivity but suffer from small fields-of-view. The deepest existing continuum surveys with the VLA are limited to finding complete samples of ULIRGs to $z \sim 3$ and LIRGs to $z \sim 1$ (e.g., see Figure 14 of Barger et al. 2014), while Milky Way luminosities can only be detected in the local region ($z \ll 0.5$). The unprecedented sensitivity of continuum imaging surveys with the ngVLA will push the boundaries of galaxy evolution studies considerably (see Figure 2). Moreover, with the ngVLA's broad high-frequency coverage, we will be able to estimate the fraction of light being produced by free-free versus synchrotron as a function of frequency.

Although the SKA1 will do similar science at lower frequencies, where there is the advantage of larger fields-of-view for getting large numbers of very high-redshift galaxies, the SKA1's upper frequency limit of 24 GHz will prohibit it from mapping the region where free-free emission is highly dominant. If the ngVLA goes down to 3 GHz, then the imaging will be superior to the SKA1, which will likely be dynamic range limited due to their dish design.

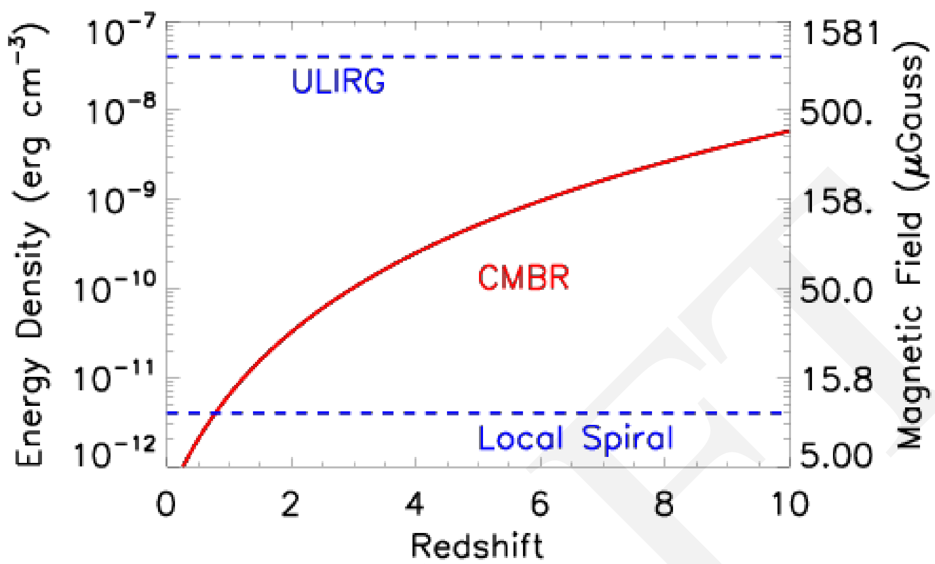

Figure 1. Energy density vs. redshift for a ULIRG and a local spiral (Carilli 2001; McBride et al. 2014), and for the redshift-dependent CMBR. The corresponding magnetic field strength is shown on the right-hand axis.

5. Experimental Layout and Complementarity

We require the mapping of a 1 deg^2 area at 10 GHz to an rms value of 0.1 μJy. As we show in Figure 2, we should be able to detect a galaxy at the 5σ level with a SFR of 20 $M_\odot$ yr^{-1} to beyond $z \sim 3$, and a galaxy with a SFR of 100 $M_\odot$ yr^{-1} to beyond $z \sim 6$. Specifically, given the current sensitivity specifications, by tapering to a 1″ synthesized beam the ngVLA will have enough brightness temperature sensitivity to detect galaxies forming stars at a rate of $> 50\, M_\odot$ yr^{-1} into the Epoch of Reionization after a 300 hr integration (i.e., rms $\approx$ 30 nJy/bm). Using the existing VLA, the detection of such a galaxy would take ~10,000 hr.

The ngVLA observations will add enormous value to the JWST deep fields by providing high-resolution, dust-free images of the galaxies to study the morphologies of the star formation. They will also provide complementary observations to SKA1, allowing a better understanding of the radio production mechanisms.

References

Barger, A. J., Cowie, L. L., Chen, C.-C., et al. 2014, ApJ, 784, 9
Carilli, C. L. 2001, in Starburst Galaxies: Near and Far, ed. L. Tacconi and D. Lutz, 309
Casey, C. M., Narayanan, D., Cooray, A. 2014, Physics Reports, 541, 45
Condon, J. J. 1992, ARA&A, 30, 575
Draine, B. T., & Lazarian, A, 1998, ApJ, 494, L19
Fixsen, D. J., Dwek, E., Mather, J. C., Bennett, C. L., & Shafer, R. A. 1998, ApJ, 508, 123

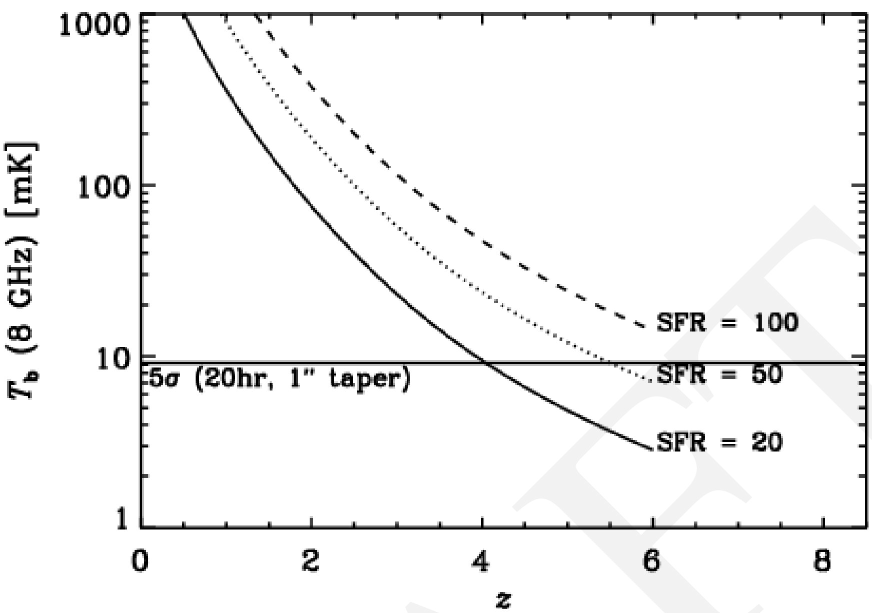

Figure 2. Observed 8 GHz brightness temperature vs. redshift indicating the expected brightness temperature of a 4 kpc disk galaxy forming stars at a rate of 20, 50, and 100 $M_\odot$ yr^{-1}. These values include estimates for synchrotron dimming due to IC scattering of cosmic ray electrons in galaxies due to the increasing CMBR temperature with redshift.

McBride, J., Quataert, E., Heiles, C., Bauermeister, A. 2014, ApJ, 780, 182
Murphy, E. J. 2009, ApJ, 706, 482
Murphy, E. J., Sargent, M. T., Beswick, R. J., et al. 2015, Advancing Astrophysics with the Square Kilometre Array (AASKA14), 85
Owen, F. N. 2018, ApJS, 235, 34
Planck Collaboration, Adam, R., Ade, P. A. R., Aghanim, N., et al. 2015, A&A, 594, A10
Puget, J.-L., Abergel, A., Bernard, J.-P., et al. 1996, A&A, 308, L5

Science with a Next-Generation Very Large Array
ASP Conference Series, Monograph 7
Eric J. Murphy, ed.

DRAFT EDITION

[CII] 158μm emission from $z \geq 10$ galaxies

C. L. Carilli[1,2], E.J. Murphy[3], A. Ferrara[4], P. Dayal[5]
[1]*National Radio Astronomy Observatory, Socorro, NM, 87801;*
`ccarilli@nrao.edu`

[2]*Cavendish Astrophysics, Cambridge, UK;*

[3]*National Radio Astronomy Observatory, Charlottesville, VA, 22903;*
`emurphy@nrao.edu`

[4]*Scuola Normale Superiore, Piazza dei Cavalieri 7, I-56126 Pisa, Italy;*

[5]*Kapteyn Astronomical Institute, University of Groningen, P.O. Box 800, 9700 AV Groningen, The Netherlands;*

Abstract.
We consider the capabilities of ALMA and the ngVLA to detect and image the [CII] 158 μm line from galaxies into the cosmic 'dark ages' ($z \sim 10$ to 20). The [CII] line may prove to be a powerful tool in determining spectroscopic redshifts, and galaxy dynamics, for the first galaxies. In 40 hr, ALMA has the sensitivity to detect the integrated [CII] line emission from a moderate metallicity, active star-forming galaxy [$Z_A = 0.2\,Z_\odot$; star formation rate (SFR) = 5 $M_\odot$ yr^{-1}], at $z = 10$ at a significance of 6σ. The ngVLA will detect the integrated [CII] line emission from a Milky-Way like star formation rate galaxy ($Z_A = 0.2\,Z_\odot$, SFR = 1 $M_\odot$ yr^{-1}), at $z = 15$ at a significance of 6σ. Imaging simulations show that the ngVLA can determine rotation dynamics for active star-forming galaxies at $z \sim 15$, if they exist. The [CII] detection rate in blind surveys will be slow (of order unity per 40 hr pointing).[1]

1. Introduction

The $z \sim 15$ Universe is at the edge of our current understanding. A handful of theoretical studies have speculated on the cosmic star formation rate (SFR) density at these redshifts (Mashian et al. 2016; Duffy et al. 2017; Chary & Pope 2010; Dayal et al. 2014; Yue et al. 2015; Topping & Shull 2015). Observational constraints on extreme redshift galaxies are poor, based on extrapolation of the few galaxies and AGN known at $z \sim 7$ to 8, and the even fewer galaxy candidates at $z \sim 8$ to 11.

Encouraging results come from observations of a relatively mature interstellar medium, and active star formation, in some of the very high redshift sources discovered to date. The last few years have seen an explosion in the number of [CII] 158μm detections at high redshift, including high resolution imaging of the gas dynamics on

[1]This paper is a brief synopsis of a paper presented in the Astrophysical Journal (Carilli et al. 2017). We refer the interested reader to the Journal article for more detail.

kpc-scales in both AGN host galaxies and in more normal star-forming galaxies at $z \sim 5.5$ to 7.5 (see Carilli et al. (2017) for a summary). The most recent results include the detection of the [OIII] 88μm fine structure line and/or the [CII] line, from galaxies at $z = 7.2$, 8.4, and 9.1 (Laporte et al. 2017; Hashimoto et al. 2018a,b) and the detection of strong [CII] and dust continuum emission from a quasar host galaxy at $z = 7.5$ (Venemans et al. 2017). While encouraging, observations remain sparse, and the most basic questions remain on the nature, and even existence, of galaxies at $z \sim 15$.

Given the uncertainty in our knowledge of galaxies at extreme redshifts, in this study we focus on a few simple of questions: if such extreme redshift galaxies exist, what kind of facility is required to detect, and possibly image, the [CII] 158 μm line emission? How do the prospects depend on basic galaxy properties, such as metallicity and star formation rate? And based on what little we know of galaxy demographics at very early epochs, what kind of numbers can we expect in blind cosmological spectral deep fields?

2. The [CII] 158μm line

The [CII] 158 μm line is one of the brightest spectral line from star-forming galaxies at far-infrared wavelengths and longer, carrying between 0.1% to 1% of the total far infrared luminosity of star forming galaxies (Stacey et al. 1991; Carilli & Walter 2013). The [CII] fine structure line traces both neutral and ionized gas in galaxies, and is the dominant coolant of star-forming gas in galaxies (Velusamy et al. 2015). While the line is only visible from space in the nearby Universe, it becomes easier to observe with increasing redshift, moving into the most sensitive bands of large ground based millimeter telescopes, such as NOEMA[2], and the ALMA[3].

As a predictor for the [CII] 158 μm luminosity from early galaxies we use the Vallini et al. (2015) relationship (their Equation 8). This theoretical and observational analysis considers in detail the relationships between star formation rate, galaxy metallicity, and [CII] luminosity. We adopt a few representative galaxy characteristics, including the main parameters of star formation rate, metallicity, redshift, and [CII] luminosity, and compare these to the capabilities of the given facilities.

3. Telescopes

The relevant ALMA bands are 3, 4, and 5, corresponding to frequencies of 84 − 116 GHz, 125 − 163 GHz, and 163 − 211 GHz, respectively. These bands then cover the [CII] line (1900.54 GHz rest frequency), between $z = 10$ and 20, almost continuously, with gaps of a few MHz due to atmospheric O_2 absorption at 118 GHz and 183 GHz. The current bandwidth for ALMA is 8 GHz, with a upgrade to 16GHz or 32GHz being considered sometime in the future. We employ the ALMA sensitivity calculator, under good weather conditions (3rd octile), with 50 antennas. For the sake of illustration, we adopt a fiducial line width of 100 km s^{-1} (see below) and an on-source integration time of 40 hr. The rms sensitivity per channel is 21 μJy beam^{-1} channel^{-1}, roughly

[2] `http://iram-institute.org/EN/noema-project.php`

[3] `http://www.almaobservatory.org`

independent of frequency due to the increasing channel width in Hz for a fixed velocity resolution, offsetting decreasing system sensitivity with increasing frequency.

Table 1. Facilities

Facilities	Redshifts	Frequencies GHz	rms μJy beam^{-1}	Bandwidth GHz
ngVLA	15 – 20	116 – 90	2.0	26
ALMA	10 – 15	173 – 116	21	8 (32^b)

For the ngVLA we employ the “Southwest" configuration, and we adopt sensitivity parameters consistent with ngVLA memo 17 (Selina & Murphy 2017). The maximum redshift we consider is $z = 20$, so we only consider frequencies between 90 GHz and 116GHz. The current reference design has a nominal maximum bandwidth of 20GHz, although broader bandwidths are under investigation. For the sake of number counts, the $z = 18.8$ to 20 range (90 GHz to 96 GHz), contributes very little to the total number of sources detected in blind searches. For the purpose of estimating the sensitivity of the ngVLA for realistic observations, and to explore the imaging capabilities in the event of the discovery of any relatively luminous sources, we have employed the CASA simulation tools (Carilli & Shao 2017), developed for the ngVLA project.

We simulate a 40 hr observation, and we employ the CLEAN algorithm with Briggs weighting. We adjust the ROBUST parameter, the (u, v)-taper, and the cell size, to give a reasonable synthesized beam and noise performance. Our target resolution is $\sim 0\farcs4$ for detection, and $\sim 0\farcs2$ for imaging.

We adopt as a spatial and dynamical template, the observed CO 1-0 emission from the nearby star-forming disk galaxy, M 51 (Helfer et al. 2003). We arbitrarily reduce the physical size of the disk by a factor three, with the idea that very early galaxies are likely smaller than nearby galaxies. Again, this exercise is for illustrative purposes, and the input model is just a representative spatial/dynamical template for a disk galaxy, with the relevant parameters being size, velocity, and luminosty. We then adjust the line luminosity per channel per beam, to achieve a given integrated [CII] 158 μm luminosity at a given redshift.

4. Results

4.1. Spectroscopic Confirmation of $z \gtrsim 10$ Candidates

An obvious application of the [CII] 158 μm line search will be to determine spectroscopic redshifts for near-IR dropout candidate galaxies at $z \sim 10$ to 20.

We start with the relationship between the [CII] velocity integrated line flux, in the standard flux units of Jy km s^{-1}, versus redshift. We adopt a metallically of $Z_A = 0.2\,Z_\odot$, and star formation rates of 1 $M_\odot$ yr^{-1} and 5 $M_\odot$ yr^{-1}. Figure 1 shows the predicted [CII] line flux versus redshift for the two models, along with the 1σ sensitivity of ALMA and the ngVLA.

This image simulation shows that, in 40 hr, the ngVLA will be able to detect the integrated [CII] line emission from moderate metallicity and star formation rate galaxies ($Z_A = 0.2$, SFR = 1 $M_\odot$ yr^{-1}), at $z = 15$ at a significance of 6σ. This significance reduces to 4σ at $z = 20$.

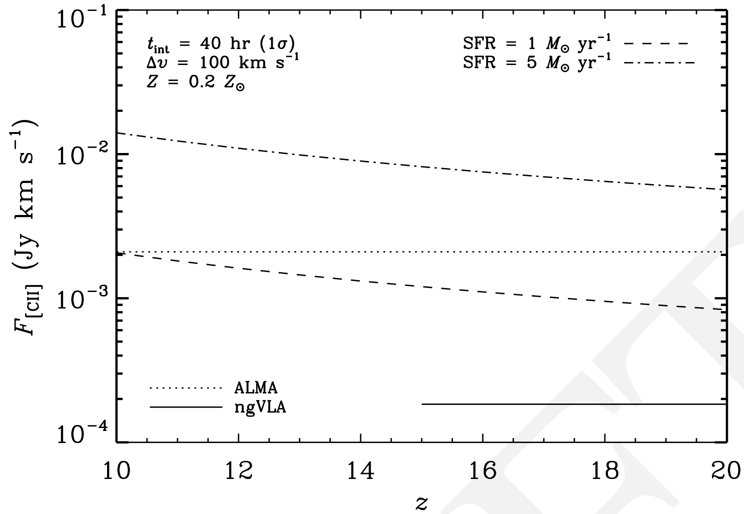

Figure 1. *[CII] 158 µm velocity integrated line flux versus redshift for galaxies with star formation rates of 1 $M_\odot$ yr^{-1} and 5 $M_\odot$ yr^{-1}, and metallicity of 0.2 $Z_\odot$, based on the relationship given in Equation 12 of Vallini et al. (2015). The rms sensitivity in a 100 km s^{-1} channel and 40 hr integration is shown for both ALMA and the ngVLA.*

In 40 hr, ALMA will be able to detect the integrated [CII] line emission from a higher star formation rate galaxy ($Z_A = 0.2\,Z_\odot$, SFR = 5 $M_\odot$ yr^{-1}), at $z = 10$ at a significance of 6σ. This significance reduces to 4σ at $z = 15$. ALMA will be hard-pressed to detect a moderate metallicity ($Z_A = 0.2\,Z_\odot$), lower star formation rate (1 $M_\odot$ yr^{-1}) galaxy, requiring 1000 hr for a 5σ detection of the velocity integrated line flux, even at $z = 10$.

We next consider dependence on metallicity. Figure 2 shows the relationship between [CII] luminosity (in Solar units), to star formation rate, for three different metallicities: $Z_A = 0.04$, 0.2, and 1.0 $Z_\odot$, for a galaxy at $z = 15$. Again shown are the ALMA and ngVLA sensitivities in 40 hr, 100 km s^{-1} channels. The Vallini et al. (2015) model has the [CII] luminosity as a strong function of metallicity. If the gas has Solar metallicity, the ALMA detection threshold (4σ) reduces to a galaxy with a star formation rate of 2.5 $M_\odot$ yr^{-1} (compared to 5 $M_\odot$ yr^{-1} for $Z_A = 0.2$), while that for the ngVLA reduces to 0.4 $M_\odot$ yr^{-1} (compared to 1 $M_\odot$ yr^{-1} for $Z_A = 0.2$). Conversely, for a low metallicity galaxy of $Z_A = 0.04\,Z_\odot$, these values increase to 100 $M_\odot$ yr^{-1} and 10 $M_\odot$ yr^{-1}, respectively.

4.2. Kinematics of $z \gtrsim 10$ Galaxies

We investigate the potential for obtaining kinematic information from such galaxies using the ngVLA. We find that the best even the ngVLA can do for a $z = 15$, $Z_A = 0.2\,Z_\odot$, and SFR = 1 $M_\odot$ yr^{-1} galaxy, in 40 hr is a 5.5σ detection of the integrated emission, with little or no dynamical information.

For a higher SFR galaxy ($z = 15$, $Z_A = 0.2\,Z_\odot$, 5 $M_\odot$ yr^{-1} galaxy), in a 40 hr observation, the ngVLA can recover the overall rotational dynamics of the system. The

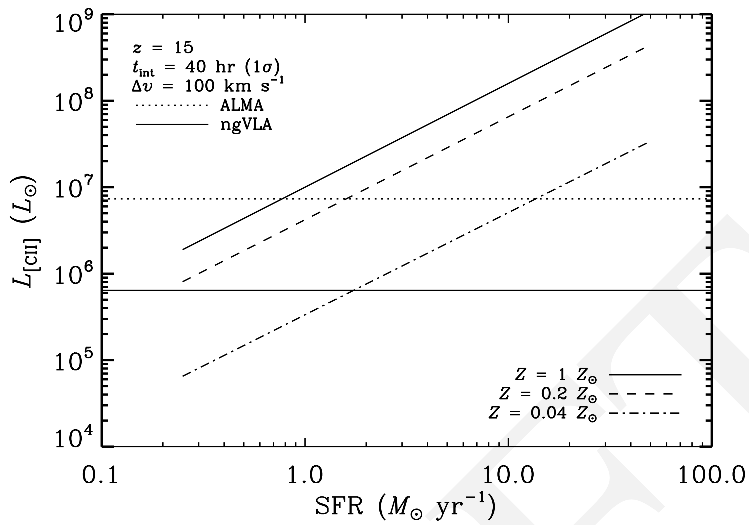

Figure 2. *[CII] 158 μm line luminosity versus star formation rate and metallicity, based on the relationship given in Equation 12 of Vallini et al. (2015). Three different metallicities are shown. Also shown is the rms sensitivity of ALMA and the ngVLA for a galaxy at z = 15, assuming a 100 km s^{-1} channel and 40 hr integration.*

imaging results for the velocity integrated emission (mom 0), and the intensity weighted mean velocity (mom 1), are shown in Figure 3. The beam size in this case is FWHM $\sim$ 0.″2, and the channel images at 20 km s^{-1} channel^{-1} have an rms noise of 4.5 μJy beam^{-1}.

4.3. The Potential for Blind Searches of $z \gtrsim 10$ Galaxies

Another application for the [CII] line will be blind cosmological deep fields. The advent of very wide bandwidth spectrometers has led to a new type of cosmological deep field, namely, spectral volumetric deep fields, in which a three dimensional search for spectral lines can be made, with redshift as the third dimension (Walter et al. 2016).

Table 2. Number of Detections per 40 hr Pointing

Model z	ngVLA 15 to 16	ngVLA 15 to 20	ALMA 10 to 10.5 (8GHz)	ALMA 11 to 14 (32GHz)
CP10, 1 $M_\odot$ yr^{-1}	0.29	1.3	–	–
CP10, 5 $M_\odot$ yr^{-1}	0.11	0.48	0.29	0.68
Dayal14, 1 $M_\odot$ yr^{-1}	0.36	0.64	–	–
Dayal14, 5 $M_\odot$ yr^{-1}	6.9×10^{-4}	7.3×10^{-4}	2.8	1.4

Given the large uncertainty in the predicted galaxy luminosity function beyond $z \sim 10$, we investigated two theoretical predictions for the [CII] luminosity function with very different methodologies. The first method used star forming galaxy number counts of Chary & Pope (2010, CP10). These galaxy counts are based on backward-evolving

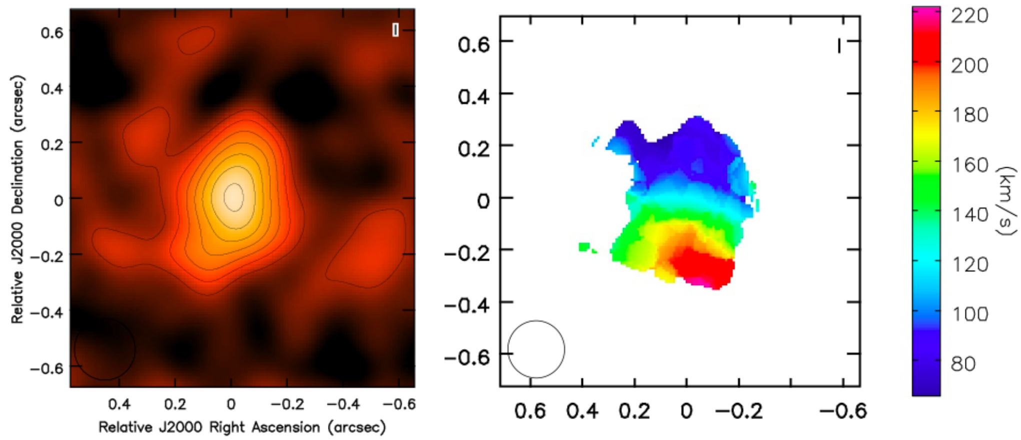

Figure 3. *Left: A simulated image of the velocity integrated [CII] 158 μm emission from a $z = 15$ galaxy with a star formation rate of 5 $M_\odot$ yr^{-1}, and a metallicity of 0.2 $Z_\odot$, assuming for a 40 hr observation with the ngVLA. Left is the velocity integrated line emission. The contour levels are -6, -3, 3, 6, 9, 12, 15, 18, 21 μJy beam^{-1}. The rms noise on the image is about 1.8 μJy beam^{-1}, and the synthesized beam FWHM is 0.″22. Right: The intensity weighted mean [CII] velocity (moment 1).*

models for the infrared luminosity function of Chary & Elbaz (2001), anchored by a variety of observational data from *Spitzer* and *Herschel*.

The second method employed the calculations of high redshift galaxy formation of Dayal et al. (2014). This model aims at isolating the essential physics driving early galaxy formation via a merger-tree based semi-analytical model including the key physics of star formation, supernova feedback, and the growth of progressively more massive systems (via halo mergers and gas accretion). This model reproduces well both the slope and amplitude of the UV LF from $z = 5$ to $z = 10$.

The two models predict the cummulative co-moving number density of star-forming galaxies above a given star formation rate as a function of redshift. These values can be converted to cummulative number densities of [CII] emitting galaxies as a function of line flux, using the models of Vallini et al. (2015). The [CII] number densities vs. flux can then be turned into the number of observed galaxies in a given integration time, bandwidth, and field of view, using the sensitivities, field sizes, and bandwidths of the ngVLA and ALMA, as discussed in §3.

The ngVLA covers the 90 GHz to 116 GHz range, corresponding to $z = 20$ to 15. We also consider just the number of galaxies between $z = 15$ and 16. ALMA has receivers that will cover from $z = 10$ to 15, or frequencies from 173 GHz to 116 GHz. Currently, the bandwidth is limited to 8 GHz. We consider an 8 GHz blind search in the Band 5 from 165 GHz to 173 GHz ($z = 10.5$ to 10), and one covering most of Band 4 with a hypothetical 32 GHz bandwidth system, from 126 GHz to 158 GHz ($z = 11$ to 14).

In Table 2, we tabulate the number of galaxies detected in [CII] emission per 40 hr integration per frequency tuning, for the ngVLA and ALMA, and for the different models. For the ngVLA, and for SFR $\geq 1\ M_\odot$ yr^{-1}, the models predict that one to two independent pointings will be required to detect one galaxy over the full redshift range, on average. For the CP10 model, these sources have a broader redshift distribution, with 22% of the sources at $z = 15$ to 16. For the Dayal14 model, the majority (64%), of the sources are in this lowest redshift bin.

For ALMA and SFR $\geq 5\,M_\odot\,\mathrm{yr}^{-1}$, the predicted number of detections differs significantly between models. For the 8 GHz bandwidth search in Band 5 ($z = 10$ to 10.5), the CP10 model requires about three pointings for a single detection, on average, while the Dayal14 model has more low redshift, brighter galaxies, with three sources per pointing expected. For the hypothetical 32 GHz bandwidth search in Band 4 ($z = 11$ to 14), the values are roughly two pointings needed for a single detection for the CP10 model, and one pointing needed for the Dayal14 model.

Overall, the detection rates in blind surveys will be slow (of order unity per 40 hr pointing). However, the observations are well suited to commensal searches on all programs employing the very wide bands that may be available in future.

A key issue in blind searches is spurious detections and verifying sources, especially given the large number of voxels searched for emission in the proposed surveys (see Carilli et al. (2017)). Recent blind line searches have developed some techniques for making statistical corrections to number counts based on e.g., comparing the number of negative and positive detections at a give level (Decarli et al. 2016; Walter et al. 2016; Aravena et al. 2016). However, the problem still remains as to how to verify that a given detection is associated with a $z > 10$ galaxy. One possible method will be broad band near-IR colors from e,g., *JWST*, or large ground based telescopes. Likewise, follow-up spectroscopy with large ground and space-based telescopes may reveal atomic lines (Barrow et al. 2017). Lastly, ALMA could be used to search for [OIII] 88μm emission, in cases of low metallicity galaxies (Cormier et al. 2015; Hashimoto et al. 2018a,b).

5. Conclusions

We have considered observing [CII] 158μm emission from $z = 10$ to 20 galaxies. The [CII] line may prove to be a powerful tool to determine spectroscopic redshifts, and galaxy dynamics, for the first galaxies at the end of the dark ages, such as identified as near-IR dropout candidates by *JWST*.

In 40 hr, the ngVLA has the sensitivity to detect the integrated [CII] line emission from moderate metallicity and (Milky-Way like) star formation rate galaxies ($Z_A = 0.2$, SFR = $1\,M_\odot\,\mathrm{yr}^{-1}$), at $z = 15$ at a significance of 6σ. This significance reduces to 4σ at $z = 20$. In 40 hr, ALMA has the sensitivity to detect the integrated [CII] line emission from a higher star formation rate galaxy ($Z_A = 0.2\,Z_\odot$, SFR = $5\,M_\odot\,\mathrm{yr}^{-1}$), at $z = 10$ at a significance of 6σ. This significance reduces to 4σ at $z = 15$. We also consider dependencies on metallically and star formation rate.

We perform imaging simulations using a plausible model for the gas dynamics of disk galaxies, scaled to the sizes and luminosities expected for these early galaxies. The ngVLA will recover rotation dynamics for active star-forming galaxies ($\gtrsim 5\,M_\odot\,\mathrm{yr}^{-1}$ at $z \sim 15$), in reasonable integration times.

We adopt two models for very high redshift galaxy formation, and calculate the expected detection rate for [CII] emission at $z \sim 10$ to 20, in blind, wide bandwidth, spectroscopic deep fields. The detection rates in blind surveys will be slow (of order unity per 40 hr pointing). However, the observations are well suited to commensal searches on all programs employing the very wide bands that may be available in future.

Acknowledgments. PD acknowledges support from the European Research Council's starting grant ERC StG-717001 and from the European Commission's and University of Groningen's CO-FUND Rosalind Franklin program. The National Radio Astronomy Observatory is a facilites of the National Science Foundation operated under cooperative agreement by Associated Universities, Inc.. We thank Ranga-Ram Chary for discussions on the models and the paper, and N. Scoville for bringing up the possibility of very high z [CII] in the ngVLA context.

References

Aravena, M.; Decarli, R.; Walter, F.; Bouwens, R.; Oesch, P. A. et al. 2016, ApJ, 833, 71
Barrow, Kirk S. S.; Wise, John H.; Norman, Michael L.; O'Shea, Brian W.; Xu, Hao 2017, MNRAS, 469, 4863
Carilli, C. L. & Shao, Y. 2017, Next Generation Very Large Array Memo No. 13 (http://library.nrao.edu/ngvla.shtml)
Carilli, C. L., & Walter, F. 2013, ARA&A, 51, 105
Carilli, C. L., Murphy, E., Ferrara, A., Dayal, P. 2017, ApJ, 848, 49
Chary, R.-R., & Pope, A. 2010, arXiv:1003.1731
Chary, R. & Elbaz, D. 2010, ApJ, 556, 562
Cormier, D., Madden, S. C., Lebouteiller, V., et al. 2015, A&A, 578, A53
Dayal, P., Ferrara, A., Dunlop, J. S., & Pacucci, F. 2014, MNRAS, 445, 2545
Decarli, Roberto; Walter, Fabian; Aravena, Manuel; Carilli, Chris; Bouwens, Rychard et al. 2016, ApJ, 833, 69
Duffy, A. R., Mutch, S. J., Poole, G. B., et al. 2017, arXiv:1705.07255
Helfer, T. T., Thornley, M. D., Regan, M. W., et al. 2003, ApJS, 145, 259
Hashimoto, T., Laporte, N., Mawatari, K. et al. et al. 2018, Nature, 557, 392
Hashimoto, T., Inoue, A., Mawatari, K. et al. et al. 2018, PASJ, submitted
Laporte, N., Ellis, R. S., Boone, F., et al. 2017, arXiv:1703.02039
Mashian, N., Oesch, P. A., & Loeb, A. 2016, MNRAS, 455, 2101
Selina, R. & Murphy, E. 2017, Next Generation Very Large Array Memo No. 17 (http://library.nrao.edu/ngvla.shtml)
Stacey, G. J., Geis, N., Genzel, R., et al. 1991, ApJ, 373, 423
Topping, M.W. & Shull, J.M. 2015, ApJ, 800, 97
Vallini, L., Gallerani, S., Ferrara, A., Pallottini, A., & Yue, B. 2015, ApJ, 813, 36
Velusamy, T., Langer, W. D., Goldsmith, P. F., & Pineda, J. L. 2015, A&A, 578, A135
Venemans, B. P., Walter, F., Decarli, R., Banados, E., Carilli, C. et al. 2017, ApJ, 851, 8
Walter, Fabian; Decarli, Roberto; Aravena, Manuel; Carilli, Chris; Bouwens, Rychard et al. 2016, ApJ, 833, 67
Yue, B., Ferrara, A., Pallottini, A., Gallerani, S., & Vallini, L. 2015, MNRAS, 450, 3829

Science with a Next-Generation Very Large Array
ASP Conference Series, Monograph 7
Eric J. Murphy, ed.

DRAFT EDITION

Cold gas in High-z Galaxies: The molecular gas budget

R. Decarli,[1,2] C. Carilli[3,4], C. Casey[5], B. Emonts[6], J.A. Hodge[7], K. Kohno[8], D. Narayanan[9], D. Riechers[10], M.T. Sargent[11], F. Walter[2,3]

[1]*INAF – Osservatorio di Astrofisica e Scienza dello Spazio, via Gobetti 93/3, 40129 Bologna, Italy;* `roberto.decarli@inaf.it`

[2]*Max Planck Institut für Astronomie, Königstuhl 17, 69117 Heidelberg, Germany*

[3]*National Radio Astronomy Observatory, Pete V. Domenici Array Science Center, P.O. Box O, Socorro, NM 87801, USA*

[4]*Cavendish Laboratory, University of Cambridge, 19 J.J. Thomson Avenue, Cambridge CB3 0HE, UK*

[5]*Department of Astronomy, The University of Texas at Austin, 2515 Speedway Blvd Stop C1400, Austin, TX 78712*

[6]*National Radio Astronomy Observatory, 520 Edgemont Road, Charlottesville, VA 22903, USA*

[7]*Leiden Observatory, Niels Bohrweg 2, 2333 CA Leiden, The Netherlands*

[8]*Institute of Astronomy, School of Science, The University of Tokyo, 2-21-1 Osawa, Mitaka, Tokyo 181-0015, Japan*

[9]*Department of Astronomy, University of Florida, 211 Bryant Space Science Center, Gainesville, FL 32611, USA*

[10]*Cornell University, 220 Space Sciences Building, Ithaca, NY 14853, USA*

[11]*Astronomy Centre, Department of Physics and Astronomy, University of Sussex, Brighton, BN1 9QH, UK*

1. Science Goals

The goal of this science case is to accurately pin down the molecular gas content of high redshift galaxies. By targeting the CO ground transition, we circumvent uncertainties related to CO excitation. The ngVLA can observe the CO(1-0) line at virtually any $z > 1.5$, thus exposing the evolution of gaseous reservoirs from the earliest epochs down to the peak of the cosmic history of star formation. The order-of-magnitude improvement in the number of CO detections with respect to state-of-the-art observational campaigns will provide a unique insight on the evolution of galaxies through cosmic time.

2. Scientific rationale

Our understanding of the evolution of galaxies, and in particular of the cosmic history of star formation, is limited by our ignorance of the amount of cold gas that galaxies could use to fuel star formation in various cosmic epochs. The bulk of the Universe's cold gas reservoir is comprised of hydrogen gas in the form of atomic hydrogen, HI, and molecular hydrogen, H_2, the latter of which is responsible for star formation in cold, condensed molecular clouds. A key goal of the ngVLA will be to assess the molecular gas content in high-redshift galaxies.

Although abundant, H_2 is not directly observable under normal circumstances in the star-forming medium. The bright transitions of carbon monoxide (CO), the second most abundant molecule in the universe, are thus the workhorse for investigating the molecular content of galaxies through cosmic time. Indeed, the vast majority of the few hundred molecular line detections reported so far at $z > 1$ have been of CO (see more in reviews of Solomon & vanden Bout 2005, Carilli & Walter 2013). Due to frequency shifting at sufficiently high-redshift, millimeter-operating facilities like IRAM's PdBI/NOEMA, CARMA, and ALMA can only observe the higher-J transitions of CO. The intrinsic brightness of these lines depends not only on the amount of molecular gas, but primarily on the excitation of the CO molecules, which is affected by the temperature and density of the gas. The so-called CO Spectral Line Energy Distribution (SLED) might vary substantially in different regions of a galaxy by up to factors of five, and even between the relatively low-J transitions from CO(3-2) to CO(1-0) — this implies that high-J transitions cannot be used to gauge the molecular gas mass. On the other hand, the lower-J transitions, including the ground state CO(1-0) transition, are only accessible to longer wavelength radio observatories like the VLA (see Figure 1).

From the CO luminosity one can infer molecular gas masses M_{H2} via the CO–to–H_2 conversion factor, X_{CO} or α_{CO}. This conversion varies by up to a factor of five depending on the conditions of the gas in the ISM, including metallicity. Recent work has focused on using dust continuum measurements to scale to gas masses (Magdis et al. 2011, 2012; Santini et al. 2014; Scoville et al. 2014, 2016). However, this technique typically assumes that the dust-to-gas ratio is fixed across a wide range of galaxies and redshifts, which has been shown to be a poor assumption in some cases (Rémy-Ruyer et al. 2014; Capak et al. 2015). In particular, the dust-to-gas ratio is known to depend strongly on metallicity (e.g., Issa et al. 1990; Lisenfeld & Ferrara 1998; Draine et al. 2007; Bolatto et al. 2013; Berta et al. 2016). Furthermore, the important kinematic signatures that come along with molecular line measurements are missed in dust continuum measurements.

The ideal probe of the cold molecular gas reservoir is therefore the ground state transition of CO, CO(1-0), where the scaling to molecular hydrogen mass has only the uncertainty in X_{CO} with which to contend. Constraining X_{CO} in high-z galaxies is possible via empirical relations linking the conversion factor with the dynamical mass and stellar mass, which further reduce the uncertainty on gas mass. The JVLA, GBT, and ATCA have detected CO(1-0) in a number of high-redshift starburst galaxies, albeit a few at a time with long integrations (Ivison et al. 2011; Hodge et al. 2012; Papadopoulos et al. 2012; Greve et al. 2014; Emonts et al. 2014). These initial detections of CO(1-0) at high-redshift have not only constrained the total molecular gas mass of hydrogen in these high-z systems, but also highlighted the importance of understanding the spatial distribution of gas in distant galaxies. While the submillimeter-luminous galaxy population, i.e., dusty star forming galaxies (DSFGs) have been found to be relatively

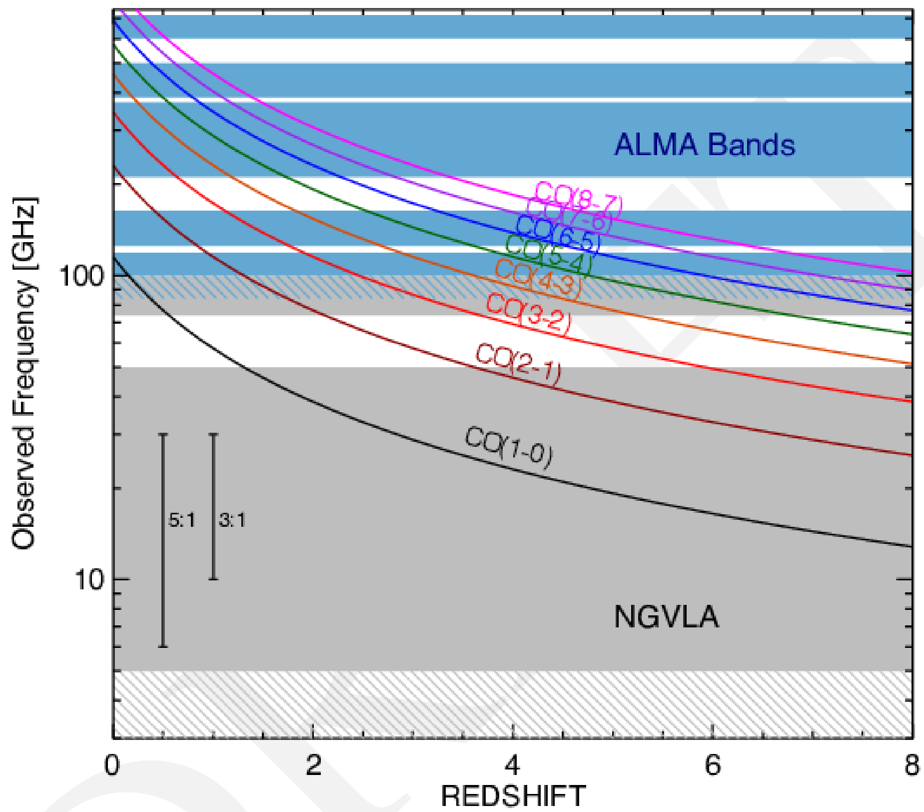

Figure 1. The observed frequencies of various transitions of CO from z=0 to z=8. While the ALMA bands (blue shading) are sensitive to many transitions of CO at low redshift, the low-J CO lines redshift out of the bands beyond $z \sim 0.5 - 2$. These low-J CO lines are critical for characterization of the total molecular gas reservoir in high-z galaxies and are only currently accessible for high-redshift galaxies using the VLA. The gray region indicates the ngVLA coverage of 5–100 GHz, with a gap around the 59–75 GHz water band. The gray hashed region represents the reach capabilities for ngVLA at low frequencies. With the advent of very wide-bandwidth setups for the ngVLA, we will be able to obtain multiple CO transitions for galaxies beyond $z \sim 3.5$ in one correlator setup, which will be revolutionary for studying dust and gas in very high-redshift galaxies. Figure adapted from Casey et al. (2015).

compact in high-J transitions (Tacconi et al. 2008; Bothwell et al. 2010), consistent with the idea that they are scaled-up analogs to local ULIRGs (Sanders & Mirabel 1996), their CO(1-0) maps are dramatically different, showing gas extending as far as 16 kpc from the galaxy centers (Ivison et al. 2011; Spilker et al. 2015; see also Decarli et al. 2016b). Studies of high-redshift proto-cluster radio galaxies even revealed bright CO(1-0) reservoirs out to distances of ~60 kpc from the central galaxy (Emonts et al. 2014). While these larger sizes are more suggestive of disk-like rotation dynamics and widespread molecular gas reservoirs in the halo environment of massive galaxies, the number of galaxies surveyed at the current VLA sensitivity makes it difficult to infer large-scale population dynamics or draw comparisons between low-z and high-z galaxy populations — a situation that will not significantly change even after ALMA starts to offer band 1&2 observations. The ngVLA is desperately needed to dramatically increase the number of galaxies surveyed in CO(1-0) at high-redshift — by factors in the thousands, in line with what is currently observed from high-redshift galaxies via direct starlight. Figure 2 illustrates the anticipated improvement in ngVLA sensitivity over the current VLA and ALMA depths across 10–120 GHz.

To demonstrate the dramatic impact of ngVLA on detection rates of CO(1-0) in high-z samples, we generated a mock observation with a 3:1 bandwidth ratio tuned to 11–33 GHz. This frequency range will pick up the CO(1-0) transition from $2.5 < z < 9.5$ *in a single frequency setting*. The RMS reached after a one hour integration with five times the collecting area of the current VLA is $\sim 10\ \mu\text{Jy beam}^{-1}$ RMS in 2 MHz bins, sufficient to resolve individual CO lines into 3–5 spectral bins across the entire bandwidth.

To estimate the number of galaxies accessible to CO(1-0) detection within one ngVLA pointing in a 11–33 GHz frequency scan, we computed the flux distribution of CO emitters expected based on state-of-the-art semi-analytical models of galaxy formation and evolution (Popping et al. 2012, 2014, 2016). These models couple a semi-analytic model of galaxy formation with a radiative transfer code to make predictions for the luminosity function of CO. They treat the interstellar medium as a density distribution for each galaxy, and assume a log-normal density distribution for the gas within clouds. They then consider only the UV contribution to the heating (no X-rays), and model the CO chemistry based on a fit to results from the photodissociation region code of Wolfire et al. (2010). The value of $\alpha_{\rm CO}$ is left free to vary from galaxy to galaxy based on the various galaxy properties (mass, compactness, SFR, etc). We transform the luminosity function of CO(1-0) computed at various redshifts into flux distributions, focusing on the redshift interval $z > 2.5$. We consider the volume corresponding to the ngVLA primary beam (assuming 25m antennas) integrated along the line of sight in various contiguous redshift slices. The total volume of the universe sampled with such a scan is ~88,500 comoving Mpc^3. By scaling the CO luminosity / flux distributions to this volume, we obtain the expected number of CO-emitting galaxies at various redshifts in our spectral scan. If we restrict our search to the limit of $\sim 10\ \mu\text{Jy beam}^{-1}$ RMS in 2 MHz bins, we consider a typical line width of 200 km s^{-1}, and we require secure > 5-σ detections, we expect 33 CO(1-0) detections at $z \sim 2$; 43 at $z \sim 4$; and even 2 at $z \sim 6$ (see Figure 3). To first order, these estimates are in general agreement with the relatively coarse observational constraints on the CO luminosity functions at high redshift available so far (Walter et al. 2014; Decarli et al. 2016a) and with predictions based on recent estimates of the integrated infrared luminosity function (Casey et al. 2014; Vallini et al. 2016) which is roughly complete out to $z \sim 2$, translated into a best-guess CO(1-0) luminosity function using a conservative estimate of a ULIRG-

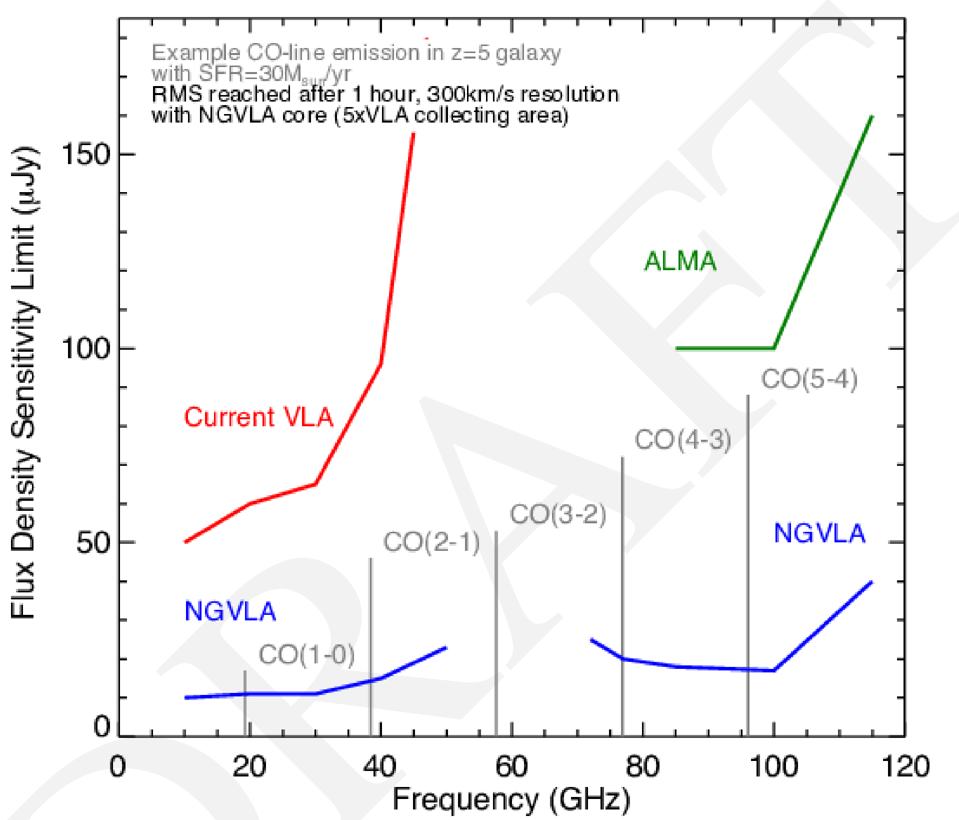

Figure 2. The projected sensitivity limits of the proposed ngVLA core, which will have five times the effective collecting area of the current VLA. This plot also shows the sensitivity limits of ALMA alongside the current VLA and projected ngVLA as a function of frequency (the gap from 50–75 GHz is due to atmosphere). Overplotted are the anticipated CO line strengths, from CO(1-0) to CO(5-4) of a typical z=5 galaxy (with SFR=30 $M_\odot$ yr^{-1}). This type of galaxy is currently well below the detection limit of existing facilities, including ALMA, yet is crucial for understanding the star forming budget of the Universe's first galaxies. Figure adapted from Casey et al. (2015).

type $L'_{\rm CO(1-0)}$-to-$L_{\rm IR}$ scaling (Bothwell et al. 2013) and assuming a line width of 200 km s^{-1}. Further support to these estimates is derived from the empirical predictions for the number of line emitters in a CO deep field by da Cunha et al. (2013a), based on a physically motivated spectral energy distribution model along with empirical relations between the observed CO line and infrared luminosities of star-forming galaxies. These estimates capitalized on the deepest available optical/near-infrared data for the Hubble Ultra Deep Field (UDF). Given all of the assumptions that went into the models, and particularly since the estimates were derived in very different ways, this relative agreement is encouraging. Intriguingly, preliminary results from larger campaigns blindly searching for molecular gas emission in deep fields suggest that the predictions based on semi-analytical models might underestimate the number of CO–bright sources at the high–luminosity end of the luminosity functions (see results from ASPECS LP in Decarli et al. 2018, in prep; and from COLDz in Riechers et al. 2018, in prep). If these preliminary results are confirmed, the expected number of CO detections per ngVLA pointings might exceed 100.

The mock observation described in this paper will not only be sensitive to CO(1-0), but also CO(2-1) emission at early epochs. However, the sensitivity and field of view for CO(2-1) will be significantly different for the same redshift regime given the differences in frequency, and will more closely mirror the coverage for the low-redshift CO(1-0) emitters. The survey sensitivity with respect to CO(2-1) depends on source excitation as the ratio of $S_{\rm CO(2-1)}$=$S_{\rm CO(1-0)}$ can vary from 2–4. Perhaps counter-intuitively, the depth of CO(2-1) observations at high-z will be greater than for CO(1-0), although the number of expected sources per single pointing will not differ substantially from the expected CO(1-0) emitters given the limited field of view. Line degeneracy may then be of concern, since it will be difficult to disentangle low-redshift CO(1-0) emitters and high-redshift CO(2-1) emitters. Other multiwavelength information (and perhaps parallel ALMA observations) would be necessary to break this degeneracy.

The estimates discussed so far refer to an individual pointing with 25m antennas. Clearly, smaller antenna dishes would correspond to an increased surveyed area, and therefore larger number of detections at a given survey depth. In case of a mosaic, we note that weaving a series of single pointings together will have unique advantages with such a wide bandwidth. For a single pointing example above, the low frequency space probes the largest volumes, but at shallower luminosity limits at high-redshifts. Tiling a mosaic together by maximizing overlap for the low-frequency observations will dramatically reduce the RMS at higher-redshifts, while mapping a large area. Figure 4 shows the effect of mosaicing on the CO(1-0) luminosity limit out to high-redshifts, sensitive to objects in the gray parameter space.

While direct molecular gas detections are certainly the main focus of future ngVLA extragalactic deep fields, it is worth noting that these surveys will be done in well-surveyed legacy fields, where there is already substantial ancillary data including spectroscopic redshifts. With large numbers of spectroscopic redshifts, stacking to measure the median molecular gas reservoir in LBGs would become possible as a function of redshift, environment, or other physical factors.

An important caveat is that, at sufficiently high redshift, the temperature of the CMB is non-negligible and can contribute to dust continuum and gas heating within galaxies. While this extra heating of the gas (and dust) will boost the intrinsic fluxes, the CMB also becomes a stronger background against which these fluxes must be measured. The net effect of these two competing effects on CO emission is less straightfor-

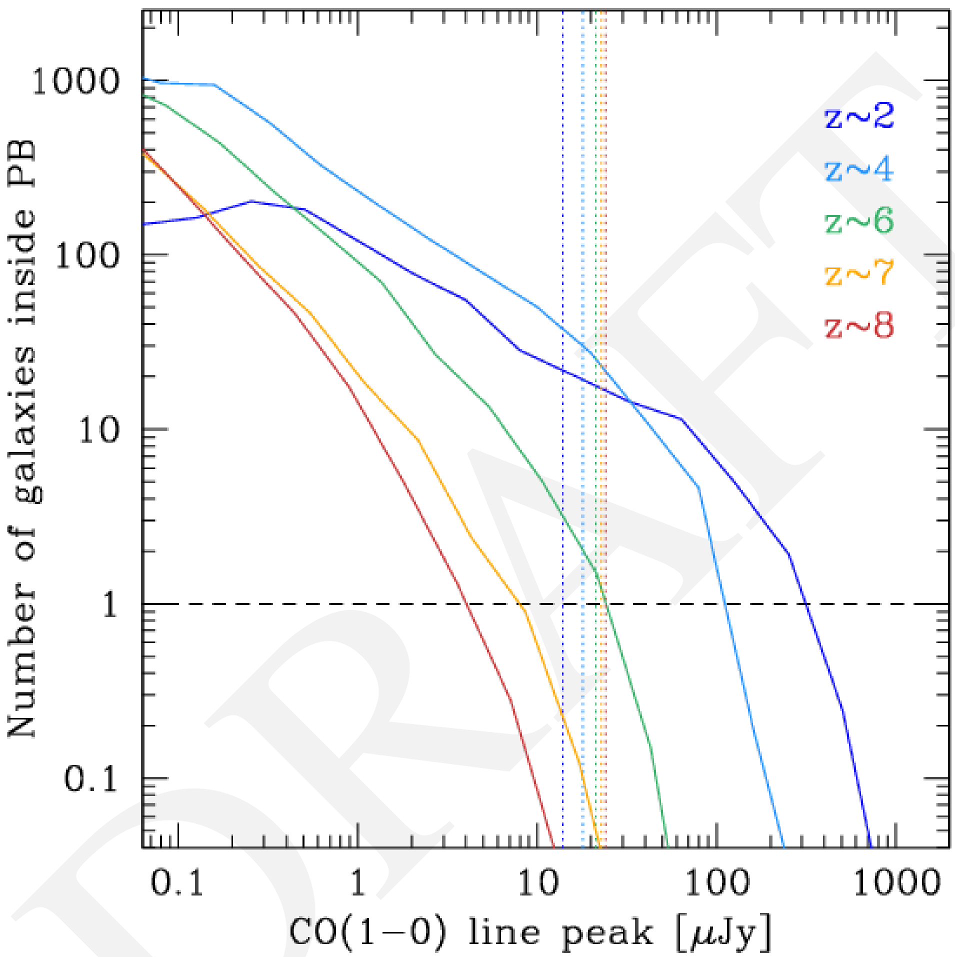

Figure 3. Predicted CO(1-0) flux distributions in various redshift bins, according to the semi-analytical models by Popping et al. (2012, 2014, 2016). The vertical lines mark the sensitivity that we will reach with ngVLA in the example of molecular deep field outlined in the text. Tens of galaxies at $z = 2-4$ will be detected within a single pointing. Recent molecular deep field investigations (ASPECS: Decarli et al. 2016a, 2018 in prep.; COLDz: Riechers et al. 2018 in prep.) suggest that semi-analytical models tend to underpredict the bright end of the CO luminosity function, i.e., the expected detection counts per ngVLA pointing might exceed 100. For a comparison, at the present sensitivity only a handful of detections per pointings are expected.

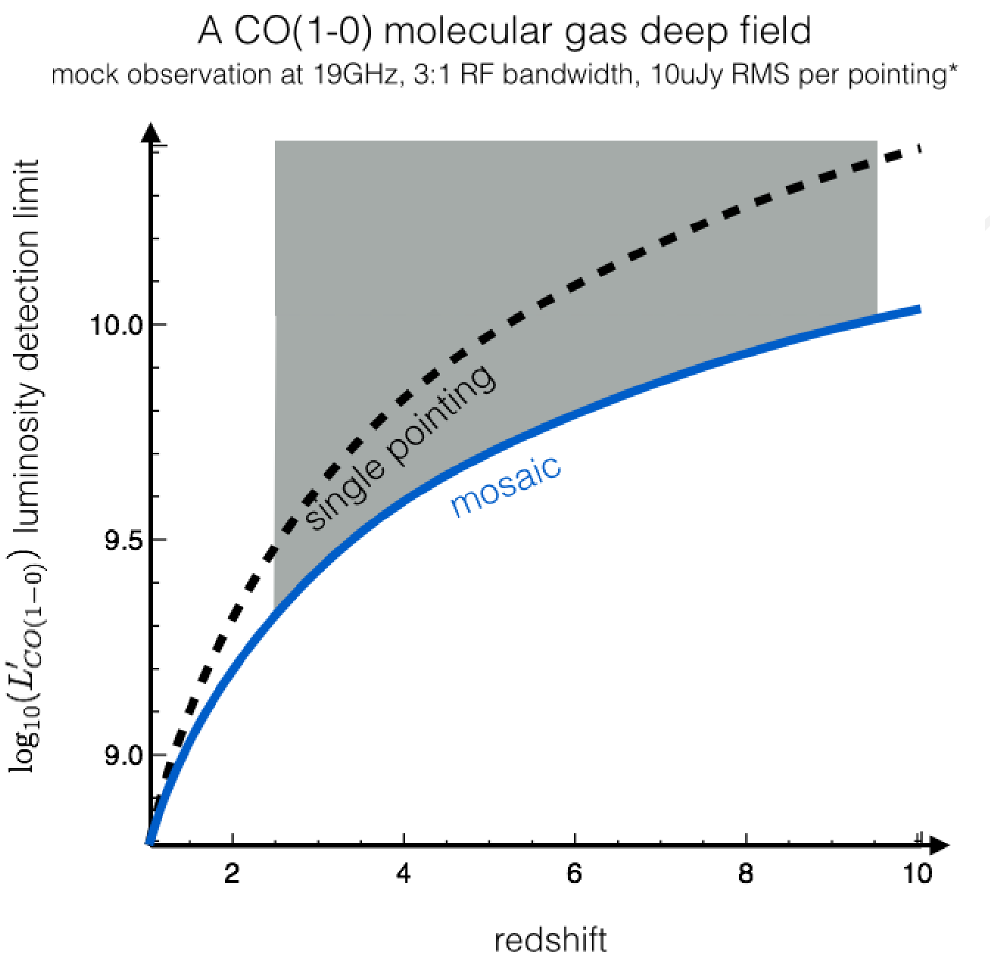

Figure 4. Luminosity limit per pointing reached in a molecular deep field initiative, with a single pointing and with a mosaic. By tiling different pointings with appropriate overlap, we significantly improve on the final depth of the data in any given region. Figure adapted from Casey et al. (2015).

ward than for the dust continuum emission (da Cunha et al. 2013b), as the regions of cold molecular gas may not be in local thermal equilibrium, or the kinetic temperature of the gas may not be thermally coupled to the dust in an obvious way, particularly in early-Universe galaxies. However, the overall effect of CMB heating will be to cut down the number of direct detections in the $z \gtrsim 6$ Universe at low gas temperatures ($T \lesssim 20$ K).

On a technical note, using phased array feeds (PAFs) with multiple pixels instead of single pixel feeds would allow the ngVLA to survey areas of sky corresponding to volumes of ~0.1 Gpc^3, covering the full range of cosmic environments. For example, if we were to use a 3×3 pixel PAF we could survey the entire 2 deg^2 COSMOS field to this depth in a few hundred hours, detecting $\sim 10^5$ CO emitting galaxies. This would allow us, for example, to compute 2-point correlation functions within the CO emitting population, and cross-correlations between CO emitting galaxies and other populations such as galaxies with large stellar masses, galaxy clusters and AGN, all of which can be compared directly with the output of simulations. This is critical for assessing the collapse of large scale structure and environmental impact on star formation in galaxies.

2.1. Measurements Required

The science goals presented here require the detection of faint lines distributed over large volumes. The key features will be the sensitivity to faint lines, and the wide simultaneous coverage in terms of both field of view and redshift (i.e., frequency) space.

2.2. Uniqueness to ngVLA Capabilities (e.g., frequency coverage, resolution, etc.)

The key features needed in order to successfully address the proposed science goals are:
1) sensitivity to faint line observations in the 12–50 GHz range, in order to sample CO(1-0) at the highest redshifts;
2) imaging capabilities to 1–3″ scales, in order to unambiguously identify counterparts without out-resolving the faint line emission;
3) large bandwidth: $\Delta\nu/\nu > 1$, in order to maximize the simultaneous CO redshift coverage and therefore the survey speed;
4) large field of view: > 1 arcmin^2 per pointing at any frequency, again to insure rapid coverage of large volumes. The combination of requirements 1 and 2 forces us to restrict to radio interferometers. The VLA in principle has the power to achieve these goals, but lacks the required sensitivity (see Figure 2). ALMA performs better in terms of sensitivity at ~3 millimeter wavelengths, but it lacks the frequency coverage below 80 GHz, which is crucial to observe CO(1-0) at high redshift.

2.3. Longevity/Durability: with respect to existing and planned (>2025) facilities

The molecular scan efforts will inevitably focus on well studied fields where exquisitely deep observations at various wavelengths are already in place, and more will come in the coming years. E.g., all the key extragalactic fields (HDF-N, HUDF, GOODS, COSMOS, EGS, etc) have been heavily hammered with HST, Spitzer, Herschel, ALMA, Chandra, XMM, VLT, Keck, and will be natural targets for extensive investigations with upcoming facilities and observatories, such as JWST, WFIRST, TMT/E-ELT. Optical/NIR images will be used to characterize the stellar populations in the galaxies detected in CO(1-0) in the ngVLA molecular scans. Optical/NIR spectroscopy will provide precise redshifts that can be used to further push the sensitivity of the ngVLA observations via stacks. For the brightest sources, optical/NIR spectra will also provide information on, e.g., the gas metallicity and other properties of the ISM thanks to rest-frame optical diagnostics. X-ray observations will allow to separate AGN from quiescent galaxies, thus allowing us to put the ngVLA measurements into the broader context of galaxy and black hole joint evolution. The multi-wavelength photometric coverage will provide precise stellar masses and star formation rates, which will be crucial to complement the molecular gas information provided by ngVLA. JWST data will enormously improve on the existing data, both in terms of wavelength coverage, sensitivity, and angular resolution (especially in the MIR), and in terms of spectroscopic capabilities at NIR and MIR wavelengths. Similarly, the advent of 30 m class telescopes will open up the possibility of spectroscopically characterizing sources that are barely detected in broad-band photometry with the state-of-the-art instrumentation — again fostering an obvious synergy with the ngVLA effort.

References

Berta S., Lutz D., Genzel R., Förster-Schreiber N.M., Tacconi L.J., 2016, A&A, 587, 73
Bolatto A.D., Wolfire M., Leroy A.K. 2013, ARA&A, 51, 207
Bothwell M.S., Chapman S.C., Tacconi L., Smail I., Ivison R.J., Casey C.M., Bertoldi F., Beswick R., et al. 2010, MNRAS, 405, 219
Bothwell M.S., Smail I., Chapman S.C., Genzel R., Ivison R.J., Tacconi L.J., Alaghband-Zadeh S., Bertoldi, F., et al. 2013, MNRAS, 429, 3047
Capak P.L., Carilli C., Jones G., Casey C.M., Riechers D., Sheth K., Carollo C.M., Ilbert O., et al. 2015, Nature, 522, 455
Carilli C.L. & Walter F., 2013, ARA&A, 51, 105
Casey C.M., Narayanan D., Cooray A. 2014, PhR., 541, 45
Casey C.M., Hodge J.A., Lacy M,. et al. 2015, arXiv:1510.06411
da Cunha E., Walter F., Decarli R., Bertoldi F., Carilli C., Daddi E., Elbaz D., Ivison R., et al., 2013a, ApJ, 765, 9
da Cunha E., Groves B., Walter F., Decarli R., Weiß A., Bertoldi F., Carilli C., Daddi E., Elbaz D., Ivison R., et al., 2013b, ApJ, 766, 13
Decarli R., Walter F., Aravena M., Carilli C., Bouwens R., da Cunha E., Daddi E., Ivison R.J., et al. 2016a, ApJ, 833, 69
Decarli R., Walter F., Aravena M., Carilli C., Bouwens R., da Cunha E., Daddi E., Elbaz D., et al. 2016b, ApJ, 833, 70
Draine B.T., Dale D.A., Bendo G., Gordon K.D., Smith J.D.T., Armus L., Engelbracht C.W., et al. 2007, ApJ, 663, 866
Emonts B.H.C., Norris R.P., Feain I., Mao M.Y., Ekers R.D., Miley G., Seymour N., Röttgering H.J.A., Villar-Martín M., Sadler E.M. 2014, MNRAS, 438, 2898
Greve T.R., Leonidaki I., Xilouris E.M., Weiß A., Zhang Z.-Y., van der Werf P., Aalto S., Armus L., et al. 2014, ApJ, 794, 142
Hodge J.A., Carilli C.L., Walter F., de Blok W.J.G., Riechers D., Daddi E., Lentati L. 2012, ApJ, 760, 11
Issa M.R., MacLaren I., Wolfendale A.W. 1990, A&A, 236, 237
Ivison R.J., Papadopoulos P.P., Smail I., Greve T.R., Thomson A.P., Xilouris E.M., Chapman S.C. 2011, MNRAS, 412, 1913
Lisenfeld U. & Ferrara A. 1998, ApJ, 496< 145
Magdis G.E., Daddi E., Elbaz D., Sargent M., Dickinson M., Dannerbauer H., Aussel H., Walter F., et al. 2011, ApJ, 740, L15
Magdis G.E., Daddi E., Sargent M., Elbaz D., Gobat R., Dannerbauer H., Feruglio C., Tan Q., et al. 2012, ApJ, 758, L9

Papadopoulos P.P., van der Werf P.P., Xilouris E.M., Isaak K.G., Gao Y., Mühle S. 2012, MNRAS, 426, 2601
Popping G., Caputi K.I., Somerville R.S., Trager S.C. 2012, MNRAS, 425, 2386
Popping G., Somerville R.S., Trager S.C., 2014a, MNRAS, 442, 2398
Popping G., van Kampen E., Decarli R., Spaans M., Somerville R.S., Trager S.C. 2016, arXiv:1602.02761
Rémy-Ruyer A., Madden S.C., Galliano F., Galametz M., Takeuchi T.T., Asano R.S., Zhukovska S., Lebouteiller V., et al. 2014, A&A, 563, A31
Sanders D.B. & Mirabel I.F. 1996, ARA&A, 34, 749
Santini P., Maiolino R., Magnelli B., Lutz D., Lamastra A., Li Causi G., Eales S., Andreani P., et al. 2014, A&A, 562, A30
Scoville N., Aussel H., Sheth K., Scott K.S., Sanders D., Ivison R., Pope A., Capak P., et al. 2014, ApJ, 783, 84
Scoville N., Sheth K., Aussel H., Vanden Bout P., Capak P., Bongiorno A., Casey C.M., Murchikova L., et al. 2016, ApJ, 820, 83
Solomon P.M. & vanden Bout P.A., 2005, ARA&A, 43, 677
Spilker J.S., Aravena M., Marrone D.P., Béthermin M., Bothwell M.S., Carlstrom J.E., Chapman S.C., Collier J.D., et al. 2015, ApJ, 811, 124
Tacconi L.J., Genzel R., Smail I., Neri R., Chapman S.C., Ivison R.J., Blain A., Cox P., et al. 2008, ApJ, 680, 246
Vallini L., Gruppioni C., Pozzi F., Vignali C., Zamorani G. 2016, MNRAS, 456, L40
Walter F., Decarli R., Sargent M., Carilli C., Dickinson M., Riechers D., Ellis R., Stark D., et al. 2014, ApJ, 782, 79
Wolfire M.G., Hollenbach D., McKee C.F. 2010, ApJ, 716, 1191

Science with a Next-Generation Very Large Array
ASP Conference Series, Monograph 7
Eric J. Murphy, ed.

DRAFT EDITION

Cold gas in High-z Galaxies: The dense ISM

R. Decarli,[1,2] C. Carilli[3,4], C. Casey[5], B. Emonts[6], J.A. Hodge[7], K. Kohno[8], D. Narayanan[9], D. Riechers[10], M.T. Sargent[11], F. Walter[2,3]
[1]*INAF – Osservatorio di Astrofisica e Scienza dello Spazio, via Gobetti 93/3, 40129 Bologna, Italy;* `roberto.decarli@inaf.it`

[2]*Max Planck Institut für Astronomie, Königstuhl 17, 69117 Heidelberg, Germany*

[3]*National Radio Astronomy Observatory, Pete V. Domenici Array Science Center, P.O. Box O, Socorro, NM 87801, USA*

[4]*Cavendish Laboratory, University of Cambridge, 19 J.J. Thomson Avenue, Cambridge CB3 0HE, UK*

[5]*Department of Astronomy, The University of Texas at Austin, 2515 Speedway Blvd Stop C1400, Austin, TX 78712*

[6]*National Radio Astronomy Observatory, 520 Edgemont Road, Charlottesville, VA 22903, USA*

[7]*Leiden Observatory, Niels Bohrweg 2, 2333 CA Leiden, The Netherlands*

[8]*Institute of Astronomy, School of Science, The University of Tokyo, 2-21-1 Osawa, Mitaka, Tokyo 181-0015, Japan*

[9]*Department of Astronomy, University of Florida, 211 Bryant Space Science Center, Gainesville, FL 32611, USA*

[10]*Cornell University, 220 Space Sciences Building, Ithaca, NY 14853, USA*

[11]*Astronomy Centre, Department of Physics and Astronomy, University of Sussex, Brighton, BN1 9QH, UK*

1. Science Goals

The goal of this science case is to study physical conditions of the interstellar medium (ISM) in distant galaxies. In particular, its densest component is associated with the inner cores of clouds – this is where star formation takes place. Carbon monoxide is usually used to trace molecular gas emission; however, its transitions are practically opaque, thus preventing astronomers from piercing through the clouds, into the deepest layers that are most intimately connected with the formation of stars. Other dense gas tracers are required, although they are typically too faint and/or at too low frequencies to be effectively observed in high redshift galaxies. The ngVLA will offer for the first time the sensitivity at radio frequencies that is needed to target $[\mathrm{C\,I}]_{1-0}$ (at $z > 5$), as well as the ground transitions of dense gas tracers of the ISM such as HCN, HNC, HCO+ (at various redshifts $z > 1$), beyond the tip of the iceberg of the hyper-luminous sources that could be studied up to now. These new tools will critically contribute to our understanding of the intimate interplay between gas clouds and star formation in different environments and cosmic epochs.

2. Scientific rationale

While undoubtedly the carbon monoxide (CO) rotational emission lines are extremely useful to gauge the molecular gas mass in distant galaxies, they have a limited power in exposing the diversity of properties and the complexity of the multi-phased ISM. For instance, both observational and theoretical studies revealed substantial amount of diffuse molecular gas that is not associated with CO emission (e.g., Langer et al. 2014; Glover & Smith 2016). On the other hand, CO transitions reach optical depth values close to unity even at very modest column densities, i.e., CO-emitting regions appear opaque. Furthermore, the critical density required to collisionally de-excite CO is relatively low ($n_{\rm H2} \sim 10^2 - 10^3$ cm^{-3} for the lower-J transitions), meaning that CO is a fairly poor tracer of the dense molecular cores, where star-formation within distant galaxies is ultimately taking place.

The neutral carbon fine structure lines [CI] at 609 and 370 μm arise in the external parts of molecular clouds, where the radiation field is too intense for CO molecules to survive, but at not enough to ionize the carbon atoms (optical extinction $A_V = 1 -$ 5 mag). The 370 μm transition has been detected even at $z \approx 7$ (Venemans et al. 2017). The two neutral carbon fine structure lines are ideal tracers of the more diffuse molecular ISM (see, e.g., Glover et al. 2015). In particular, because of the different critical densities, their ratio is an excellent tracer of the gas density. Furthermore, in combination with other lines (such as CO or [CII]) they can be used to infer physical properties of the ISM such as the gas density and the intensity of the incident radiation field (see, e.g., Meijerink et al. 2008; Popping et al. 2018). [CI] is also considered a complementary tracer of the cold gas mass, which can be used to infer either an independent measurement of the CO–to–H$_2$ conversion factor, $\alpha_{\rm CO}$, or to measure the neutral carbon abundance, $X_{\rm CI}$ (see, e.g., Bothwell et al. 2017; Popping et al. 2017).

To date, only about 40 galaxies at $z > 1$ have been detected in [CI]. This list mostly consists of sub-mm galaxies and quasar host galaxies. E.g., Bothwell et al. (2017) use [CI] 609 μm observations, in combination with other ISM lines, to infer molecular gas mass, density and intensity of the radiation field in 13 dusty, star–forming galaxies at $2<z<5$ using ALMA. They find a higher density and stronger UV field for the star–forming medium in these galaxies than estimated by previous studies of similar sources. At higher redshifts, however, the [CI]$_{1-0}$ transition is shifted outside the ALMA bands at $z > 4.8$. This ground transition is a better mass tracer than the [CI]$_{2-1}$ transition (observable with ALMA at these high redshifts), which is also sensitive to the excitation temperature. Furthermore, only the detection of both these lines provides a direct measure of the neutral gas density. The detection of the [CI]$_{1-0}$ line at higher redshift thus requires sensitive observations in the frequency ranges that will be covered by the ngVLA.

In addition to neutral carbon, other molecular gas tracers can provide us with precious complementary information than CO. E.g., high dipole moment molecules like hydrogen cyanide (HCN) are only collisionally de-excited at very high densities, making them much more reliable tracers of the very dense gas directly associated with the formation of individual stars. Some studies of HCN in the nearby universe have even found evidence that the ratio of HCN luminosity to FIR luminosity remains constant over >8 orders of magnitude in HCN luminosity, suggesting that HCN may be a fundamental direct probe of star forming 'units', and that the only difference between star formation on different scales and in different environments is the number of these fundamental star-forming units (e.g., Gao & Solomon 2004; Wu et al. 2005, 2010; Zhang et al. 2014).

However, not much is known about dense gas tracers in the more distant universe. Owing to the fact that they only trace the densest regions of the ISM and are therefore less abundant, emission from the rotational transitions of molecules like HCN is usually an order of magnitude fainter than CO, complicating efforts to detect and study these tracers at high-z. As a result, only a few high-z galaxies have been detected in dense gas tracers to-date — most of which are either intrinsically extremely luminous, or strongly lensed (e.g., Solomon et al. 2003; Vanden Bout et al. 2004; Carilli et al. 2005; Gao et al. 2007; Riechers et al. 2007, 2011; Danielson et al. 2011). With ALMA now online, the situation will clearly improve dramatically in the near future. However, as with CO, ALMA will only be able to detect the mid- and high-J transitions of dense gas tracers like HCN, HNC, and HCO+. These higher-level transitions are less directly tied to the total dense gas mass, requiring assumptions about the (highly uncertain) excitation ratios. In addition, these higher-J transitions are more likely to be affected by IR pumping, which local studies find may be common in ultraluminous galaxies (e.g., Aalto et al. 2007). Thus, while necessary to understand the overall excitation properties of high-z sources, the ALMA-detectable transitions may be unsuitable as tracers of the total dense gas mass.

The current JVLA probes the right frequency range to detect the crucial low-J transitions of these high critical density molecules (Figure 1). However, its limited sensitivity means that the current state-of-the-art for high-z detections consists of a smattering of strongly lensed hyper-starbursting quasar hosts (e.g., Vanden Bout et al. 2004; Riechers et al. 2007, 2011). With significantly increased sensitivity, the ngVLA would extend studies of the dense gas mass at high-z beyond this handful of extreme objects for the first time. In addition to tracing the dense gas mass at high-z, such studies are critical for constraining models of star formation based on the gas density PDF, as these models make testable predictions about the FIR-HCN relation in FIR-luminous objects (e.g., Krumholz & Thompson 2007; Narayanan et al. 2008). Finally, while angular resolution is not a priority for these photon-starved studies, the brightest objects could even be spatially resolved by a ngVLA on ~kpc scales (requiring baselines on the order of the current VLA). The ngVLA would thus enable detailed studies of the dense gas at high-redshift such as are currently only possible in the local universe.

2.1. Measurements Required

This science goal requires integrated flux measurements of faint lines in high redshift galaxies. The sensitivity and the coverage in the radio bands are prime technical requirements for these observations. The targeted lines will be >10× fainter than CO (in temperature units). A galaxy with stellar mass $M_* \approx 10^{11}\,\mathrm{M}_\odot$ on the massive main sequence of star–forming galaxies at $z \sim 2$ has SFR$\approx$100 $\mathrm{M}_\odot\,\mathrm{yr}^{-1}$ (Santini et al. 2017). This corresponds to an IR luminosity $L_{\mathrm{IR}} \approx 5\times10^{11}\,\mathrm{L}_\odot$. Assuming the CO–to–IR luminosity empirical relation from Carilli & Walter (2013), we infer an expected CO(1-0) luminosity of 7.0×10^9 K km s^{-1} pc^2, or 345,000 $\mathrm{L}_\odot$. For a CO(1-0)/HCN(1-0)$\approx$10 (see Fig. 2), we infer an expected flux density for the HCN(1-0) transition of 7 μJy (assum-

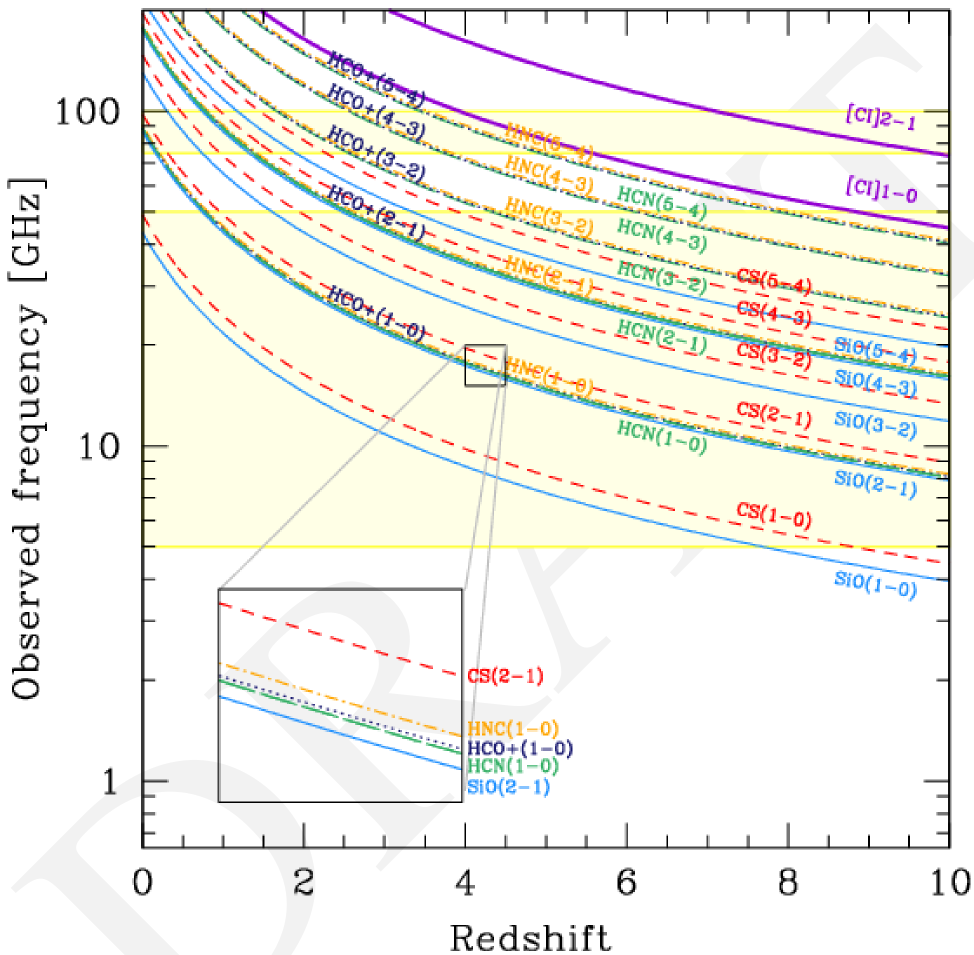

Figure 1. Redshifted frequencies of dense gas tracers, many of which will be accessible in single-tuning setups with the ngVLA at high-redshift. In particular, the 1-0 and 2-1 transitions of HNC, HCO+, HCN and SiO lines are spaced very closely in frequency (see inset zoom-in). While ALMA can detect the mid- and high-J transitions of these molecules at high-redshift, significant uncertainties regarding excitation mean that the low-J transitions accessible with the ngVLA are more suitable as tracers of the total dense gas mass.

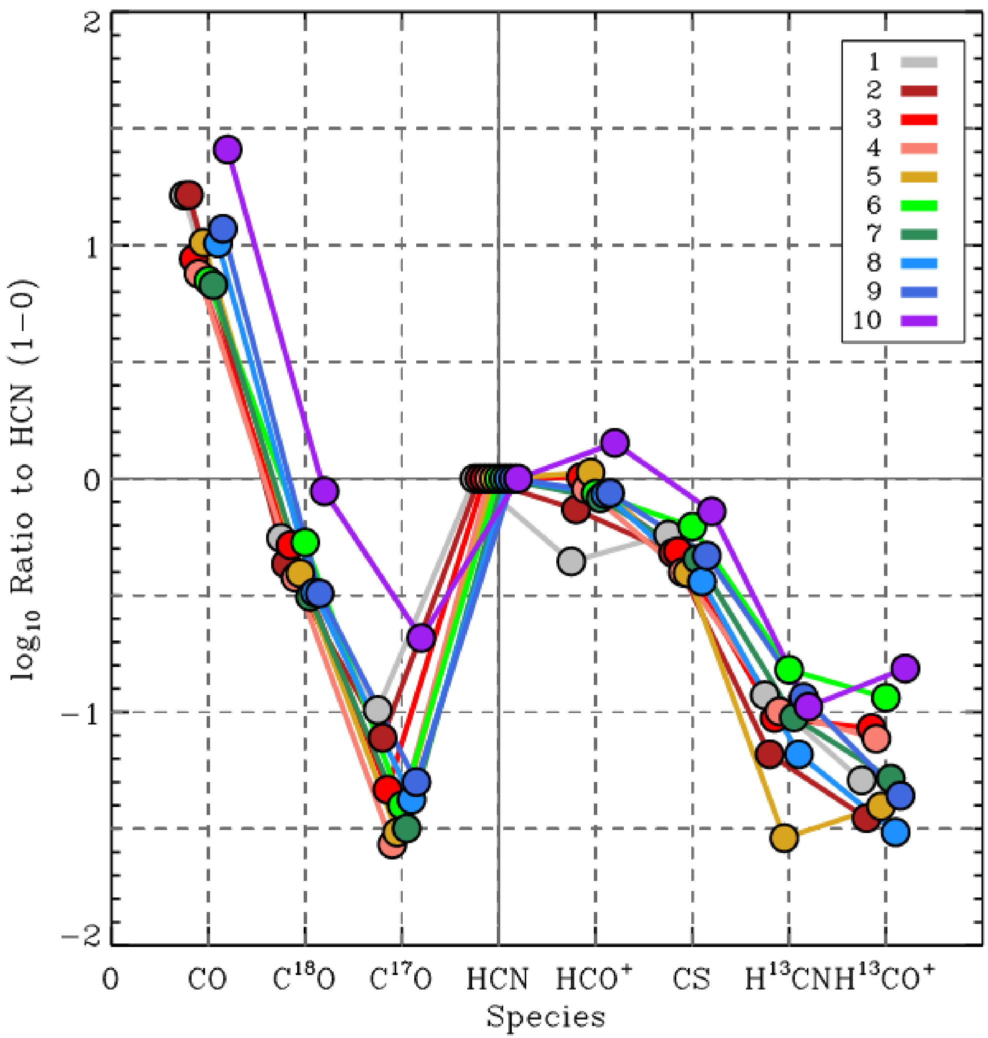

Figure 2. The intensity (in units of temperature) of the ground transitions of CO, $C^{18}O$, $C^{17}O$, HCN, HCO^{+}, CS, and $H^{13}CNH^{13}CO^{+}$ in various clouds (labeled 1–10) in the local starburst galaxy NGC253, normalized to the observed HCN(1-0) flux. CO is at least 10× brighter than other dense gas tracers – in order to detect these other lines at high redshift, the unprecedented sensitivity of ngVLA at radio frequencies will be instrumental. Figure adapted from Leroy et al. (2015).

ing a line width of 300 km s^{-1}). Such a line can be detected at 3-σ significance with 26 hr of integration, assuming that ngVLA will have 5× the collecting area of the current JVLA. No existing instrument has the sensitivity at radio frequencies to perform the proposed observations.

Imagining requirements are limited at $\sim 1-3''$ resolution, in order to avoid confusion with other sources in the field, and at the same time limit the risk of out-resolving the faint emission. A large bandwidth would allow to simultaneously cover multiple ISM tracers (see Figure 1) in one shot, i.e., it would be ideal although it is not a strict requirement.

2.2. Longevity/Durability: with respect to existing and planned (>2025) facilities

There are obvious synergies with other key observatories to envision in the context of the characterization of the ISM in high-z galaxies. In particular, ALMA can provide coverage of the intermediate and high-J transitions of the dense gas tracers, as well as of the [CI]$_{2-1}$ line, whereas ngVLA will focus on the lower-J lines and on the [CI]$_{1-0}$ transition (see Fig. 1). The combinations of CO transitions ranging from low to high J, together with the denser gas tracers targeted with ngVLA + ALMA, will enable an unprecedentedly detailed study of the properties of the densest parts of the ISM, which are not currently accessible. This will enable a direct link between the gas properties and the on-going star formation, given that the dense gas tracers are intimately connected with birthplace of stars. JWST and the 30m class telescope will provide sensitive spectroscopy of rest-frame UV/optical/NIR ISM tracers, mostly associated with the ionized phase of the gas, thus paving the way for a coherent description of the gas cycle in galaxies throughout cosmic history.

Acknowledgments. ...

References

Aalto S., Spaans M., Wiedner M.C., Hüttemeister S. 2007, A&A, 464, 193
Bothwell M.S., Aguirre J.E., Aravena M., et al. 2017, MNRAS, 466, 2825
Carilli C.L., Solomon P., Vanden Bout P., Walter F., Beelen A., Cox P., Bertoldi F., Menten K.M., Isaak K.G., Chandler C.J., Omont A. 2005, ApJ, 618, 586
Carilli C.L. & Walter F., 2013, ARA&A, 51, 105
Danielson A.L.R., Swinbank A.M., Smail I., Cox P., Edge A.C., Weiß A., Harris A.I., Baker A.J., De Breuck C., Geach J.E., et al. 2011, MNRAS, 410, 1687
Gao Y., Solomon P.M. 2004, ApJ, 606, 271
Gao Y., Carilli C.L., Solomon P.M., Vanden Bout P.A. 2007, ApJ, 660, L93
Glover S.C.O., Clark P.C., Micic M., Molina F. 2015, MNRAS, 448, 1607
Glover S.C.O., Smith R.J. 2016, MNRAS, 462, 3011
Krumholz M.R., Thompson T.A. 2007, ApJ, 669, 289
Langer W.D., Velusamy T., Pineda J.L., Willacy K., Goldsmith P.F. 2014, A&A, 561, A122
Leroy A., Bolatto A.D., Ostriker E.C., et al. 2015, ApJ, 801, L25
Meijerink R., Glassgold A.E., Najita J.R. 2008, ApJ, 676, 518
Narayanan D., Cox T.J., Hernquist L. 2008, ApJ, 681, L77
Popping G., Decarli R., Man A.W.S., et al. 2017, A&A, 602, A11
Popping G., Narayanan D., Somerville R.S., et al. 2018, arXiv:1805.11093
Riechers D.A., Walter F., Carilli C.L., Bertoldi F. 2007, ApJ, 671, L13
Riechers D.A., Walter F., Carilli C.L., Cox P., Weiß A., Bertoldi F., Menten K.M. 2011, ApJ, 726, 50
Santini P., Fontana A., Castellano M., et al. 2017, ApJ, 847, 76

Solomon P.M., Vanden Bout P., Carilli C., Guelin M. 2003, Nature, 426, 636
Vanden Bout P.A., Solomon P.M., Maddalena R.J. 2004, ApJ, 614, L97
Venemans B.P., Walter F., Decarli R., Ferkinhoff C., Weiß A., Findlay J.R., McMahon R.G., Sutherland W.J., Meijerink R. 2017, ApJ, 845, 154
Wu J., Evans N.J. II, Gao Y., Solomon P.M., Shirley Y.L., Vanden Bout P.A. 2005, ApJ, 635, L173
Wu J., Evans N.J. II, Shirley Y.L., Knez C. 2010, ApJS, 188, 313
Zhang Z.-Y., Gao Y., Henkel C., Zhao Y., Wang J., Menten K.M., Güsten R. 2014, ApJ, 784, L31

Science with a Next-Generation Very Large Array
ASP Conference Series, Monograph 7
Eric J. Murphy, ed.

DRAFT EDITION

Cold gas in High-z Galaxies: CO as redshift beacon

R. Decarli,[1,2] C. Carilli[3,4], C. Casey[5], B. Emonts[6], J.A. Hodge[7], K. Kohno[8], D. Narayanan[9], D. Riechers[10], M.T. Sargent[11], F. Walter[2,3]
[1]*INAF – Osservatorio di Astrofisica e Scienza dello Spazio, via Gobetti 93/3, 40129 Bologna, Italy;* `roberto.decarli@inaf.it`

[2]*Max Planck Institut für Astronomie, Königstuhl 17, 69117 Heidelberg, Germany*

[3]*National Radio Astronomy Observatory, Pete V. Domenici Array Science Center, P.O. Box O, Socorro, NM 87801, USA*

[4]*Cavendish Laboratory, University of Cambridge, 19 J.J. Thomson Avenue, Cambridge CB3 0HE, UK*

[5]*Department of Astronomy, The University of Texas at Austin, 2515 Speedway Blvd Stop C1400, Austin, TX 78712*

[6]*National Radio Astronomy Observatory, 520 Edgemont Road, Charlottesville, VA 22903, USA*

[7]*Leiden Observatory, Niels Bohrweg 2, 2333 CA Leiden, The Netherlands*

[8]*Institute of Astronomy, School of Science, The University of Tokyo, 2-21-1 Osawa, Mitaka, Tokyo 181-0015, Japan*

[9]*Department of Astronomy, University of Florida, 211 Bryant Space Science Center, Gainesville, FL 32611, USA*

[10]*Cornell University, 220 Space Sciences Building, Ithaca, NY 14853, USA*

[11]*Astronomy Centre, Department of Physics and Astronomy, University of Sussex, Brighton, BN1 9QH, UK*

1. Science Goals

The goal of this science case is to address the use of a ngVLA as a CO redshift machine for dust-obscured high-redshift galaxies which lack of clear counterparts at other wavelengths. Thanks to its unprecedentedly large simultaneous bandwidth and sensitivity, the ngVLA will be able to detect low–J CO transitions at virtually any $z > 1$. In particular, at $z > 4.76$ two CO transitions will be covered in a single frequency setting, thus ensuring unambiguous line identification. The ngVLA capabilities fill in a redshift range where other approaches (e.g., photometric redshifts, search for optical/radio counterparts, etc) typically fail due to the combination of intrinsically faint emission and increasing luminosity distance. This will allow us to explore the formation of massive galaxies in the early cosmic times.

2. Scientific rationale

Since the identification of the first sub-mm galaxies and dusty star-forming galaxies (DSFGs; e.g., Hughes et al. 1998; Ivison et al. 1998, 2002; Smail et al. 2002; Chapman et al. 2005), it has been clear that obtaining precise redshift measurements for these sources would represent a major challenge, especially at the highest redshifts (e.g., Riechers et al. 2013; Marrone et al. 2018). A combination of intrinsic faintness, high redshift, and dust reddening limits the detectability of rest-frame optical/UV spectral features that could be used to pin down the redshift to ~50% of the DSFGs studied so far (e.g., Danielson et al. 2017). This is particularly severe for those galaxies for which the estimated unobscured star formation is only a tiny fraction of the total star–formation rate. The peak wavelength of the dust spectral energy distribution can be used as a tentative redshift proxy (see, e.g., Riechers et al. 2013; da Cunha et al. 2015), although it is highly degenerate with the dust temperature. The search for radio continuum counterparts biases the selection against high redshifts (as the radio continuum does not benefit of the negative *k*-correction that is in place at sub-mm wavelengths). As a result, the intrinsic redshift distribution of these sources is still under debate (see Casey et al. 2014, for a review). The question of whether the unconfirmed DSFGs sit at similar redshifts or higher redshifts than the others is yet to be clarified, with the incompleteness being a strong function of redshift. The discovery of bright dusty galaxies like HFLS3 (Riechers et al. 2013) and SPT0311–58 (Marrone et al. 2018), and the four [CII]–bright galaxies in the field of four $z > 6$ quasars (Decarli et al. 2017) hint at the existence of such a population at very high redshifts, but so far, confirming such sources (especially at lower luminosities or in the absence of gravitational lensing) in a systematic way has not been efficient.

A promising way forward consists in searching for multiple CO transitions. Since DSFGs are very luminous at IR wavelengths, and the CO luminosity correlates with $L_{\rm IR}$ (see, e.g., Carilli & Walter 2013), CO transitions are expected to be bright in DSFGs. CO transitions have rest frequencies of ~115.2 $J_{\rm up}$ GHz. The detection of two transitions might leave some degeneracy in the redshift interpretation [e.g., if one line is observed at 2× the frequency of the other, they could be CO(1-0) and CO(2-1), or CO(2-1) and CO(4-3), or CO(3-2) and CO(6-5), etc]. However, by combining the line detection with ancillary information (e.g., broad-band optical/NIR photometry) one could significantly restrict the number of possible identifications. Furthermore, the CO spectral energy distribution is typically fairly regular, so that if one observe, e.g., CO(2-1) and CO(4-3), the flux of the CO(3-2) can be predicted pretty accurately. The presence or lack of intermediate transitions can then further trim the parameter space of allowed interpretations.

The main drawback of CO-based redshifts is that large frequency ranges need to be sampled in order to find one or more lines. At any redshift, CO transitions are spaced by several tens of GHz in the observed frame — thus representing an observational challenge, as multiple frequency setting need to be combined in order to effectively sample a large bandwidth (see Fig. 1). Weiß et al. (2013) used existing capability of ALMA to scan a large fraction of the 3mm band, and searched for high-J CO emission in 26 DSFGs. Each source was observed in 5 different frequency settings, for a total of ~10 min on source. However, the high detection rate (~90% of sources have been detected in at least 1 CO transition) of such short observations was only possible thanks to the extreme brightness of the strongly-magnified sources in their sample. A similar effort with PdBI targeting the non-lensed galaxy HDF850.1 resulted in the first redshift

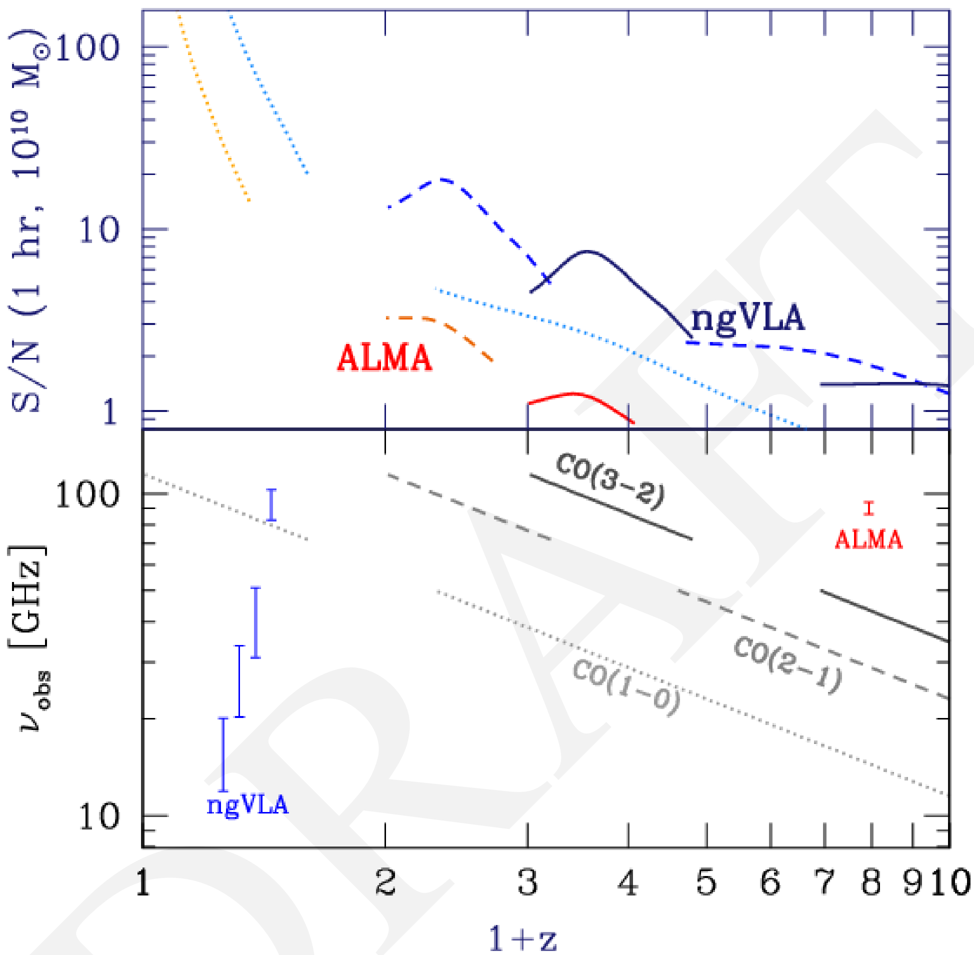

Figure 1. The power of ngVLA as a redshift beacon, compared to ALMA. *Top* — The expected S/N of CO(1-0) (dotted), CO(2-1) (dashed), and CO(3-2) (solid lines) emission for a galaxy with molecular mass $M_{\rm H2} = 10^{10}\,{\rm M}_\odot$, as a function of redshift. We assume 1 hr of integration, a line width of 300 km s^{-1}, a CO–to–H_2 conversion of $\alpha_{\rm CO}$=3.6 M$_\odot$ (K km s^{-1} pc^2)$^{-1}$ (Daddi et al. 2010), and a CO excitation typical of main sequence galaxies (Daddi et al. 2015). The ngVLA (blue lines) will provide 5–10× higher S/N for the same integration time than ALMA (red lines) in the overlapping frequency ranges, and will expand the redshift coverage of low–J CO transitions to much higher redshifts, virtually covering every redshift $z > 1$. *Bottom* — The observed frequency of the same CO transitions as a function of redshift, compared with the simultaneous bandwidth of ngVLA and ALMA (shown as vertical bars). The large bandwidth of ngVLA will enable to sample wide CO redshift ranges in a single frequency setting.

determination of this archetypal source (z=5.183); this however required ∼100 hr of integration (e.g., Walter et al. 2012). Even with full ALMA, redshift scans are going to be expensive in "normal" DSFGs that are not lensed. Additionally, by focusing on wavelengths equal to or larger than 3mm, we can only sample intermediate to high J CO transitions, thus the method would be applicable only to highly excited sources.

The ngVLA is going to revolutionize this line of search, as 1) the large simultaneous bandwidth coverage will maximize the probability of detecting the CO(1-0) line at $z > 2$ from any source with only a few frequency settings, even if only very coarse constraints on the redshift are available; 2) by focusing on the lowest-J transitions, it will be insensitive to excitation bias, i.e., the method will be applicable to any CO-emitting gaseous reservoir, not only to the most excited; 3) at $z > 4.76$, it will provide coverage of both the CO(1-0) and CO(2-1) lines. This will provide unambiguous redshift identification for all the DSFGs at the highest redshift, where the optical/NIR spectroscopy and the radio continuum follow-up are extremely incomplete.

This is quantitatively demonstrated in Fig. 1, where we show the expected S/N of CO(1-0), CO(2-1), and CO(3-2) in a galaxy with molecular gas mass $M_{\rm H2}$=10^{10} $M_\odot$, line width Δv=300 km s^{-1}, a CO–to–H_2 conversion factor $\alpha_{\rm CO}$=3.6 $M_\odot$ (K km s^{-1} pc^2)$^{-1}$ (Daddi et al. 2010), and a CO excitation typical for main sequence galaxies (Daddi et al. 2015). In only a few hours of integration, the ngVLA will be able to securely detect CO(1-0) in two wide redshift windows ($z < 0.5$ and $2.2 < z < 10$), as well as CO(2-1) and/or CO(3-2) at virtually any redshift $z > 1$. For a comparison, ALMA will only target intermediate to high J transitions at $z > 3$, and their detection will require several hours per frequency settings, and multiple frequency settings to compensate for the smaller bandwidth. The ngVLA will therefore represent the main facility for CO redshift searches in DSFGs over most of the cosmic history in the future decades. For a comparison, the Square Kilometer Array will only be competitive with ngVLA in this line of search if it will have a dedicated high–frequency (5–50 GHz) band, which is still under debate: The intermediate frequency band (0.3–10 GHz) becomes sensitive to CO only at $z > 10.5$, where we do not expect a significant population of dusty galaxies to be already in place, and other redshift tracers than CO (e.g., fine structure lines at rest–frame far–infrared wavelengths, which are shifted in the ALMA 1–3 mm bands at these redshifts) become more effective redshift tracers.

2.1. Measurements Required

We need to pin down the redshift of dusty galaxies with unknown or poorly constrained redshift via the observation of the CO(1-0) [and possibly CO(2-1)] line.

2.2. Uniqueness to ngVLA Capabilities (e.g., frequency coverage, resolution, etc.)

Thanks to the large simultaneous band coverage, the ngVLA will be a unparalleled facility to blindly search for lines associated with dusty, high-redshift galaxies. For any galaxy at $z > 2$, the coverage of one/two lines is ensured irrespective of the redshift. By targeting the lowest J transitions, this line search circumvents any potential excitation bias (that would inevitably affect a similar endeavor with, e.g., ALMA). Finally, thanks to the improved sensitivity with respect to the VLA, this approach will become applicable even to relatively CO-faint sources, whereas to date it has only been used for the very brightest sources.

2.3. Longevity/Durability: with respect to existing and planned (>2025) facilities

The advent of JWST and the 30m class telescopes will significantly push the sensitivity of optical/NIR/MIR spectroscopic investigations, thus mitigating the spectroscopic incompleteness that currently prevents us from characterizing DFSGs, especially at high redshift. However, even these facilities will have a hard time in measuring redshifts of the reddest sources at the dawn of galaxy formation. For these galaxies, the ngVLA will play a unique role as a redshift machine.

References

Carilli C.L. & Walter F., 2013, ARA&A, 51, 105

Casey C.M., Narayanan D., Cooray A. 2014, PhR., 541, 45

Chapman S.C., Blain A.W., Smail I., Ivison R.J. 2005, ApJ, 622, 772

da Cunha E., Walter F., Smail I.R., Swinbank A.M., Simpson J.M., Decarli R., Hodge J.A., Weiß A., et al. 2015, ApJ, 806, 110

Daddi E., Bournaud F., Walter F., Dannerbauer H., Carilli C.L., Dickinson M., Elbaz D., Morrison G.E., et al., 2010, ApJ, 713, 686

Daddi E., Dannerbauer H., Liu D., Aravena M., Bournaud F., Walter F., Riechers D., Magdis G., et al. 2015, A&A, 577, 46

Danielson A.L.R., Swinbank A.M., Smail I., Simpson J.M., Casey C.M., Chapman S.C., da Cunha E., Hodge J.A., et al. 2017, ApJ, 840, 78

Decarli R., Walter F., Venemans B.P., Bañados E., Bertoldi F., Carilli C., Fan X., Farina E.P., et al. 2017, Nature, 545, 457

Hughes D.H., Serjeant S., Dunlop J., Rowan-Robinson M., Blain A., Mann R.G., Ivison R., Peacock J., et al. 1998, Nature, 394, 241

Ivison R.J., Smail I., Le Borgne J.-F., Blain A.W., Kneib J.-P., Bezecourt J., Kerr T.H., Davies J.K. 1998, MNRAS, 298, 583

Ivison R.J., Greve T.R., Smail I., Dunlop J.S., Roche N.D., Scott S.E., Page M.J., Stevens J.A., et al. 2002, MNRAS, 337, 1

Marrone D.P., Spilker J.S., Hayward C.C., Vieira J.D., Aravena M., Ashby M.L.N., Bayliss M.B., Béthermin M., et al. 2018, Nature, 553, 51

Riechers D.A., Bradford C.M., Clements D.L., Dowell C.D., Pérez-Fournon I., Ivison R.J., Bridge C., Conley A., et al. 2013 Nature, 496, 329

Smail I., Ivison R.J., Blain A.W., Kneib J.-P. 2002, MNRAS, 331, 495

Walter F., Decarli R., Carilli C., Bertoldi F., Cox P., da Cunha E., Daddi E., Dickinson M., et al., 2012, Nature, 486, 233

Weiß A., De Breuck C., Marrone D.P., Vieira J.D., Aguirre J.E., Aird K.A., Aravena M., Ashby M.L.N., Bayliss M., Benson B.A., et al. 2013, ApJ, 767, 88

Science with a Next-Generation Very Large Array
ASP Conference Series, Monograph 7
Eric J. Murphy, ed.

DRAFT EDITION

The Molecular High-z Universe on Large Scales: Low-surface-brightness CO and the strength of the ngVLA Core

Bjorn Emonts[1], Chris Carilli[2], Desika Narayanan[3,4,5], Matthew Lehnert[6], Kristina Nyland[1]

[1]*National Radio Astronomy Observatory, 520 Edgemont Road, Charlottesville, VA 22903* (bemonts@nrao.edu)

[2]*National Radio Astronomy Observatory, P.O. Box 0, Socorro, NM 87 801*

[3]*Department of Astronomy, University of Florida, 211 Bryant Space Science Center, Gainesville, FL 32611*

[4]*University of Florida Informatics Institute, 432 Newell Drive, CISE Bldg E251, Gainesville, FL 32611*

[5]*Cosmic Dawn Centre (DAWN), University of Copenhagen, Julian Maries vej 30, DK-2100, Copenhagen, Denmark*

[6]*Sorbonne Université, CNRS, UMR 7095, Institut d'Astrophysique de Paris, 98bis bvd Arago, 75014, Paris, France*

Abstract. The Next-Generation Very Large Array (ngVLA) will revolutionize our understanding of the Early Universe by tracing the coldest phase of molecular gas -the raw ingredient for star formation- in the most distant galaxies and galaxy-clusters. The km-scale core of the ngVLA will be densely packed with antennas, making it a prime instrument for imaging low-surface-brightness emission from large-scale molecular gas in the high-z circum- and inter-galactic medium (CGM/IGM). Recent studies indicate that large amounts of cold molecular gas are hiding in the 10s−100 kpc environments of distant galaxies, but that technical limitations on existing telescope arrays have prevented us from efficiently detecting these large molecular reservoirs. This may have led to a severly biased view of the molecular Universe. We present the science case for low-surface-brightness CO observations of the Early Universe, and how the core of the ngVLA will reveal the cold molecular Universe to limits and at scales not currently detectable by radio telescopes. As such, the ngVLA core will be a powerful instrument for studying the cold baryon cycle that drives the early evolution of galaxies and clusters.

1. Introduction

The evolution of galaxies is tightly linked to processes in the circum- and inter-galactic medium (CGM/IGM). Unfortunately, most of the baryons in the CGM/IGM are too faint to be easily detected. At high-z, we view glimpses of dark baryonic halos through quasar absorption lines, or cooling-radiation emitted as Lyα. Absorption-line work inferred the presence of large, ∼100 kpc halos of warm/cool (T∼10^4 K), metal-enriched gas around high-z quasars (e.g., Prochaska et al. 2014; Lau et al. 2016). However, a direct connection to the stellar growth of massive galaxies remains missing, because we have yet to identify the ultimate reservoir of halo gas that has sufficient mass to fuel widespread star-formation, namely the cold molecular gas (T~10−100 K).

The massive Spiderweb Galaxy at z=2.2 (Miley et al. 2006) revealed the first evidence for the existence of a cold molecular CGM in the distant Universe (Emonts et al. 2016, Fig. 1). CO(1-0) observations with very compact array configuration of the Australia Telescope Compact Array (ATCA) traced a 70 kpc reservoir of molecular halo gas across the CGM of this massive forming proto-cluster galaxy (Emonts et al. 2016). The extended CO follows diffuse blue light from star formation that occurs in-situ within the CGM (Hatch et al. 2008, see Fig. 1). This is evidence that there is a massive ($M_{H2} \sim 10^{11}\ M_{\odot}$) reservoir of gas in the CGM that cooled well beyond the temperature of Lyα-emitting gas (T ~ few $10^3 - 10^4$ K), and is actively feeding star formation across the halo. More recent observations of [C I] $^3P_1$-$^3P_0$ and CO(4-3) with the Atacama Large Millimeter Array (ALMA) revealed that the cold CGM has densities of several 100 cm^{-3}, with average carbon abundance and excitation conditions resembling those of starforming galaxies (Emonts et al. 2018). This does not corroborate models of efficient and direct stream-fed accretion of relatively pristine gas (Dekel et al. 2009). Instead, the [CI] and CO properties agree with more complex recycling models, where the gas in the IGM is a melange from various sources − metal-enriched outflows, mass transfer among galaxies, gas accretion, and mergers (see Emonts et al. 2018).

Other studies using very compact interferometers also found CO-emitting gas on scales of tens of kpc around high-z massive galaxies (e.g., Emonts et al. 2014; Cicone et al. 2015; Emonts et al. 2015; Ginolfi et al. 2017; Dannerbauer et al. 2017). These results are starting to reveal a picture that the CGM is truly multi-phase, and that the Early Universe may contain much more molecular gas hiding outside galaxies than has thus far been observed. However, many questions remain about the nature of the cold molecular CGM/IGM, and its role in early galaxy evolution. How common is the presence of a cold CGM, in particular among the more general population of high-z galaxies? Is the cold gas diffuse or associated with star-formation? What is its origin (tidal debris, outflows, mixing, or accretion)? And how can we observe this cold CGM/IGM?

In this paper, we will explain that technical limitations on array designs have mostly prevented us from reaching the sensitive low-surface-brightness levels needed to efficiently image widespread molecular gas across the CGM/IGM. This likely produced a severely biased view of the molecular Universe. The core of the Next-Generation VLA (ngVLA) will be a powerful instrument for tracing the molecular CGM, allowing us to study the cold baryon cycle that governs the early growth of massive galaxies.

2. Low-surface-brightness CO

Some of the strongest tracers for molecular gas are the various rotational transitions of carbon-monoxide, ^{12}CO(J,J-1). With the Atacama Large Millimeter Array (ALMA), it has become routine to observe CO, and other molecular species, in high-z galaxies. However, imaging the cold molecular medium outside galaxies on tens to hundred kpc scales has been limited by two observational challenges:

• **Excitation conditions of the molecular medium.** The critical density of CO(J,J-1) scales roughly with $n_{crit} \propto J^3$. The ground-transition CO(1-0) (ν_{rest} = 115.27 GHz) has an effective critical density of only several 100 cm^{-3}, and the $J = 1$ level of CO is

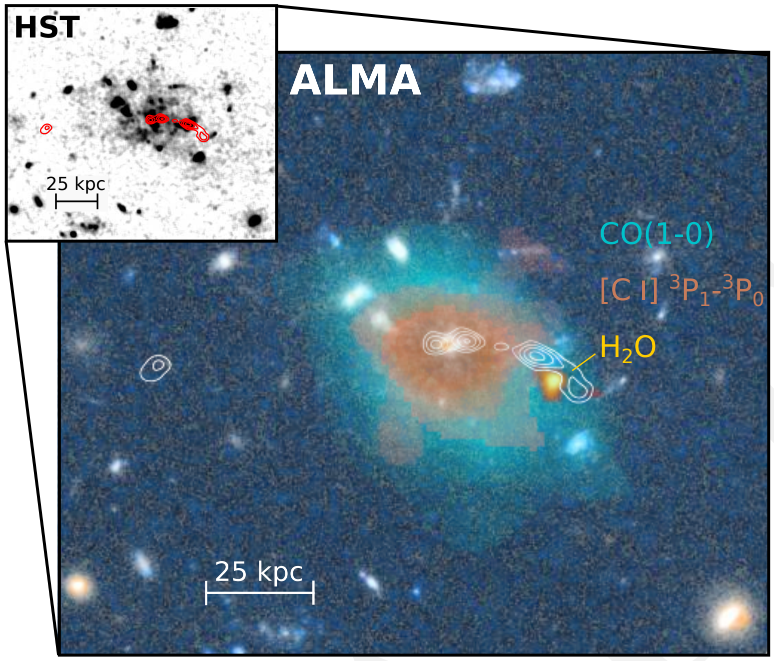

Figure 1. The cold circum-galactic medium of the Spiderweb Galaxy ($z = 2.2$). A total intensity image of the CO(1-0) emission is shown in light-blue in the main panel, as detected with the ATCA (Emonts et al. 2016). Superposed in brown are various channel maps of atomic carbon, [C I] $^3P_1 - ^3P_0$, as detected with ALMA (Emonts et al. 2018). A bright spot of H_2O emission is shown in yellow (Gullberg et al. 2016). The background image is taken with the *Hubble Space Telescope* Advanced Camera for Surveys (*HST*/ACS) in the F475W and F814W filters (Miley et al. 2006). The radio source is shown in white contours, as observed with the VLA in the C-configuration at 35 GHz (Emonts et al. 2016). The in-set in the top-left corner shows the combined *HST*/ACS F475W+F814W image of the same region as the main panel (Miley et al. 2006), but optimized to visualize the diffuse optical light from in-situ star formation (Hatch et al. 2008).

substantially populated down to $T \sim 10$ K (Papadopoulos et al. 2004). However, these values increase by an order of magnitude or more for the high-J transitions, like CO(3-2) and higher. This means that these high-J transitions trace the warmer and denser molecular gas in starburst and AGN regions, and may severely underestimate masses from colder, lower density, and sub-thermally excited gas components (Papadopoulos et al. 2000). To get robust estimates of the *total* molecular gas mass in galaxies at $z > 1.5$, it is vital that CO(1-0) or CO(2-1) are observed in the 20-50 GHz regime. *This is particularly important for widespread CO-emitting reservoirs of molecular gas in the circum- and inter-galactic medium, as the excitation conditions and temperature of the molecular gas in these environments may be low compared to the ISM of galaxies.*

• **Short-spacing problem of radio interferometers.** Radio interferometers sample the sky at discrete intervals, set by the length of antennas pairs ('baselines'), frequency coverage and scan-time. Because large-scale features are filtered out by widely separated antennas, *low-surface-brightness emission can only be imaged with compact*

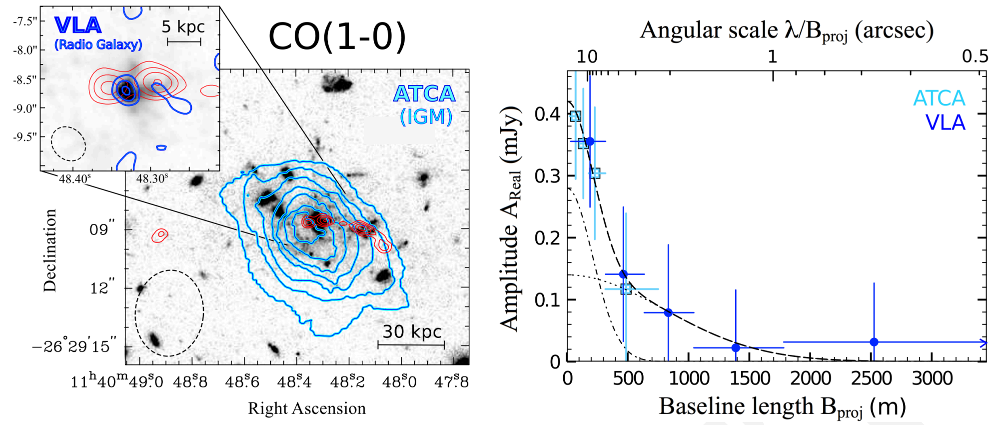

Figure 2. Low-surface-brightness CO(1-0) from Fig. 1 across the halo of the Spiderweb Galaxy (z=2.2), reproduced from Emonts et al. (2016) Left: ATCA CO(1-0) contours (blue) are overlaid onto the *HST*/ACS F475W+F814W image from Miley et al. (2006). Contour levels: 0.020, 0.038, 0.056, 0.074, 0.092, 0.110, 0.128 Jy beam^{-1} $\times$ km s^{-1}. The inset shows the CO(1-0) total-intensity contours from the VLA in DnC+CnB-configuration at 3.5, 4.5σ. The full-resolution VLA data reveal only a third of the total CO imaged on large scales with ATCA. Right: Visibility-amplitudes of the CO(1-0) emission are plotted as function of the projected baseline length in data from the ATCA (light-blue squares) and VLA DnC+CnB (dark-blue dots). As described in Emonts et al. (2016): "The amplitude plotted on the Y-axis is the real part of the complex interferometer visibility for the CO-signal, when vector-averaged across the velocity range -100 to +200 km/s and over all baselines covered by the horizontal error bars. The $\pm 1\sigma$ uncertainty in the amplitude of the averaged signal is indicated with the vertical error bars. The dashed line shows a model where we superimposed a Gaussian distribution with FWHM = 3" (dash-dotted line) and a Gaussian distribution with FWHM = 0.8" (dotted line)." This plot illustrates that it is essential to use short-baseline configurations to recover extended CO emission.

array-configurations at relatively low spatial resolution. This problem is particularly severe when studying extended gas reservoirs in the mm regime. For example, to recover CO at $z \sim 2$ on scales $\geq$15 kpc requires antennas to be placed <1 km apart at 35 GHz, and less than a few 100m for the lower ALMA bands! This problem is visualized in Fig. 2.

Unfortunately, millimeter observatories, like ALMA, generally operate at frequencies >85 GHz. This means that the ground-transition CO(1-0) rapidly redshifts out of the receiver bands. Several of the traditional cm-observatories, like the Very Large Array (VLA) and ATCA, can target redshifted CO(1-0) and CO(2-1) in the 20-50 GHz regime, but they crucially lack sensitivity on very short (<<1 km) baselines for efficiently imaging the cold molecular CGM/IGM (Fig. 2).

3. The strength of the ngVLA core

The core of the next-generation VLA (ngVLA) (Carilli 2016) will be densely packed with antennas that will vastly supersede the current VLA D-configuration in number of short baselines. The current reference design for the core includes 94 antennas with

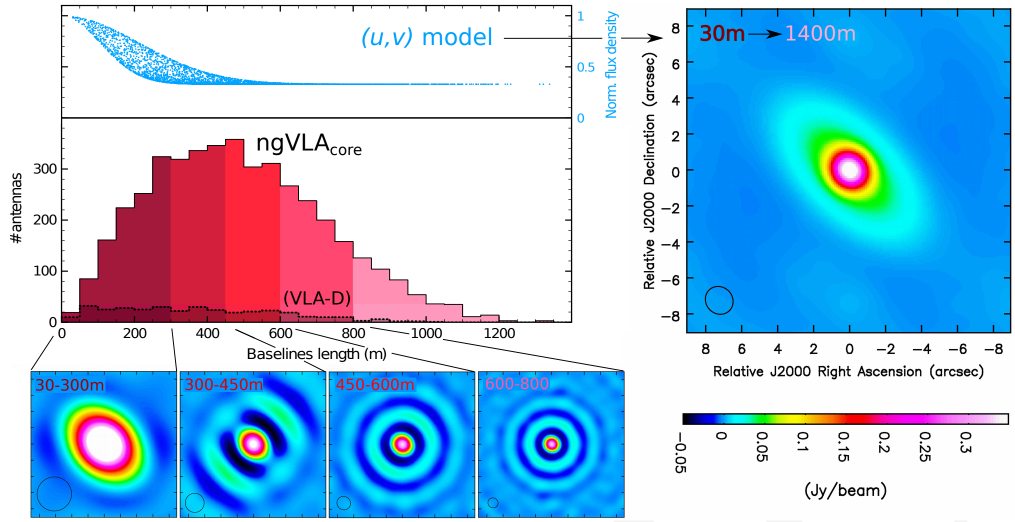

Figure 3. Simulated observations with the ngVLA core. *Top left:* Red-colored histogram of the baseline distribution of the 18m antennas in the ngVLA core, using the reference design of Carilli (2018). The colors from dark to light red contain 24% (30−300m), 23% (300−450m), 22% (450−600m), 20% (600−800m) and 11% (800−1400m) of the total number of baselines in the core. The overlaying black histogram at the bottom shows the baseline distribution of the VLA in D-configuration. The blue dots at the top of the figure are drawn on the same x-axis and represent a simulated snap-shot observation of a target model at the zenith, using the simulation tools in the Common Astronomy Software Applications (CASA) software (McMullin et al. 2007). This model consists of a Gaussian function that represents extended emission with a superposed delta-function of an unresolved point-source component, both placed at the phase center. The Gaussian has FWHM $b_{\rm maj} = 6''$ and $b_{\rm min} = 3''$ with PA = 45°, which corresponds to about 50×25 kpc at $z = 2$. The signal is normalized and placed in a single channel of width 30 MHz, with 2/3rd (1/3rd) of the total flux in the Gaussian (point-source) component. No noise has been added to the simulation and a basic clean of 1000 iterations down to 0.1 × the peak flux was applied. *Top right:* Total intensity image of the simulated emission of the target model using the ngVLA core with an exposure time of 8h. The image includes all the baselines in the range 30−1400m. *Bottom:* The small panels show the total intensity image when restricting the uv-coverage to the baselines indicated in the colored parts of the histogram (i.e., 30−300m, 300−450m, 450−600m and 600−800m). The dimensions and color-scaling for all four panels are the same as for the main image of the target model in the top right panel. This figure illustrates that the shortest (≤ several 100m) baselines in the core of the ngVLA are crucial for recovering and imaging extended low-surface-brightness emission.

a diameter of 18m that cover baselines out to about 1 km (Carilli 2018). While the longer ngVLA baselines will not be able to detect extended CO because they resolved out the emission, the ngVLA core will be a revolutionary new instrument for unlocking the cold molecular Universe. This is further visualized in Fig. 3, where we show the baseline coverage of the ngVLA core (Carilli 2018), as well as simulated imaging of extended emission. The simulation shown in Fig. 3 is simplistic, and does not take into account noise or gas kinematics and clumpiness. Nevertheless, it shows the need for sufficient sensitivity on baselines less than several × 100m in the core of the ngVLA, in order to optimize low surface brightness observations.

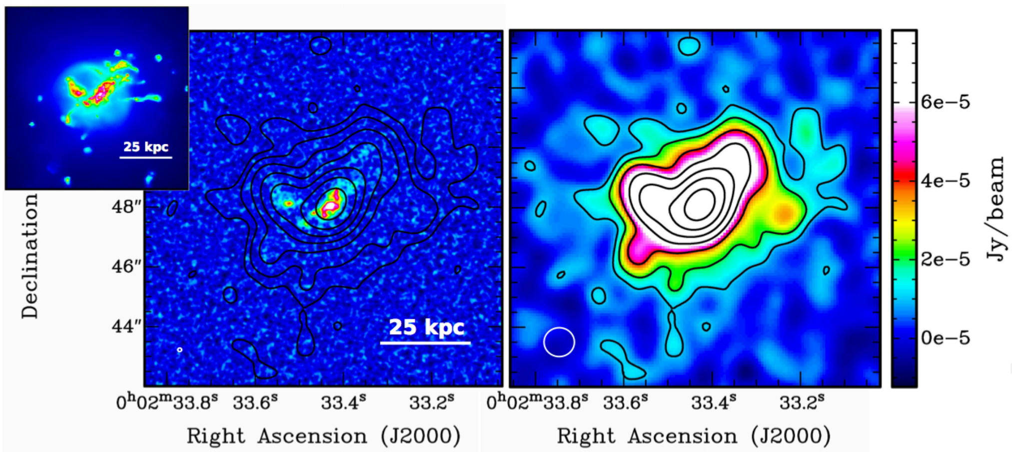

Figure 4. Simulated CO(1-0) observation of a merging system with extended halo from the cosmological simulations of Narayanan et al. (2015) (top-left inset), using the ngVLA reference design of Carilli (2018). The simulations were performed in CASA, and assume $z = 2$, exposure time $t_{exp} = 48$h, channel width of 9 MHz (~ 70 km s^{-1}), and total CO(1-0) luminosity $I_{CO(1-0)} = 0.21$ Jy beam^{-1} km s^{-1} (i.e., similar to that of the Spiderweb Galaxy in Fig. 2; Emonts et al. 2016). Noise has been added to the visibilities, based on a theoretical root-mean-square (rms) noise of 2.3 μJy beam^{-1} when taking the inner 168 antennas of the array and using natural weighting. *Left:* Simulated CO(1-0) image at a resolution of 0.126″ (~1 kpc), using a robust weighting of 0 and uv-tapering of 0.09″. This taper provides a resolution relevant only to the antennas that are distributed across the Plains of San Augustin with baselines ≤30 km, while down-weighting the core. The synthesized beam is shown in white in the bottom-left corner. The rms noise level is 3.0 μJy beam^{-1}, with a 3σ surface brightness limit of 0.5 K, and 3σ limit for H_2 mass clumps of $5.6\,(\alpha_{CO}/0.8) \times 10^8$ M$_\odot$. *Right:* Simulated CO(1-0) image at resolution of 1″, using a robust weighting of 0.5 and uv-tapering of 0.85″. This taper provides a resolution relevant to the km-scale core of the array, and down-weights the longer spacings. The synthesized beam is shown in white in the bottom-left corner. The rms noise level is 3.4 μJy beam^{-1}, with a 3σ surface brightness limit of 9 mK. The halo gas is detected at 3σ across ~80 kpc, and includes ~60% more CO(1-0) flux than the 0.13″ plot on the left. The black contours start at 3σ (10 μJy) and increase by factors of 2. For visualization purposes, the same contours are also overlaid in the left plot. More details are given in Carilli (2018).

A more realistic simulation is shown in Fig. 4. Here we simulate the expected CO(1-0) emission observed with the ngVLA in a massive ($M_* \sim 10^{12}\,M_\odot$) high-$z$ merger system. The CO luminosities are calculated using the Narayanan et al. (2012) scaling relations between X_{CO} and Σ_{H2}, and the Narayanan & Krumholz (2014) model relationship between CO excitation ladders and Σ_{SFR}. For the purposes of modeling the CO flux, the system is placed at $z = 2$ and has its overall flux scaled to the CO(1-0) intensity observed in the Spiderweb Galaxy (Fig. 2). The system contains bright merging components across ~30 kpc and a halo stretching twice as far out. We simulate a 48h observation with the ngVLA (Carilli 2018), and apply different tapers to increase the surface brightness sensitivity. When going from a moderately tapered 0.13″ resolution to a heavily tapered 1″ resolution, the surface brightness sensitivity increases by almost two orders of magnitude, reaching an rms noise level of 3 mK at 1″ resolution. At this brightness sensitivity, we detect the CO(1-0) across the halo environment on a scale of ~80 kpc. In the simulated 1″ image we detect ~60 % more CO(1-0) flux at a level above 3σ than in the 0.13″ image.

Low-surface-brightness observations of molecular gas with the ngVLA core will be complemented by ALMA, provided that ALMA is used in its most compact configurations, because the baseline length *in* $k\lambda$ increases rapidly at the higher frequencies. ALMA can target not only the high-J transition of CO, but also atomic carbon [C I], which is expected to be concomitant with CO(1-0) and can serve as an important alternative mass tracer (Papadopoulos et al. 2004, see also Fig. 1). With the advent of Band 1 (Huang et al. 2016), ALMA will be able to observe down to 35 GHz, where it can target CO(1-0) out to $z \leq 2.3$. This is also roughly the redshift out to which the Square Kilometre Array (SKA) in its phase-1 will be sensitive for imaging the 21 cm line of neutral hydrogen in the most massive galaxies. For targeting the low-J CO lines at higher redshifts (15-50 GHz regime), where we can unravel the cold gas content of the very Early Universe, the ngVLA is needed.

As a note of caution, CO lines become dimmer when observed at higher redshifts as a result of reduced contrast against the increasing temperature of the Cosmic Microwave Background (da Cunha et al. 2013; Zhang et al. 2016). For extended CO(1-0), this dimming can reach anywhere from the typical 30-40% expected for the coldest (T~20 K) component of the ISM at $z \sim 2$ to up to factors of a few for gas in the CGM at higher redshifts. A detailed investigation into the dimming of the low-J CO lines is beyond the scope of this paper. However, to account for this dimming by the CMB, the vastly increased sensitivity of the ngVLA core over existing instruments, like the VLA, is critical.

Therefore, the ngVLA will be the only instrument in the foreseeable future than can target the crucial CO(1-0) transition at $z \geq 2.3$ with a core-configuration that has the brightness sensitivity to reveal the full extent of the cold molecular Universe.

4. Concluding remarks

While the Next-Generation VLA will be a powerful instrument to study the radio Universe with unprecedented resolution, it is crucial to consider its surface brightness performance during the design phase. The core of the ngVLA, i.e., the baselines in the inner km, will act as a world-leading instrument for unlocking the large-scale cold gas content of the Early Universe. To make optimal use of this capability, it is important to consider the following specifications:

• To maximize the surface-brightness sensitivity of the ngVLA, it is essential to optimize the sensitivity on the shortest (≤ several 100m) baselines.

• To utilize the ngVLA core as a unique stand-alone instrument, it is worth considering sub-array functionality between the inner and outer antennas.

Currently, the inclusion of a Short Baseline Array as part of the ngVLA is under consideration. Such a Short Baseline Array aims at recovering emission on the largest spatial scales, and would be analogous to the Atacama Compact Array (a.k.a. Morita Array) of the ALMA observatory. The current reference design envisions that this Short Baseline Array consists of 19 antennas of 6m and 4 total-power dishes of 18m diameter, with interferometric baselines ranging from 11−56m (Mason et al 2018). It will be essential to investigate to what extent the limited sensitivity of this Short Baseline Array will contribute to efficiently mapping faint, low-surface-brightness CO emission at high redshifts, but this is beyond the scope of this paper.

Concluding, the core of the ngVLA will reveal the cold molecular medium in the Early Universe to limits and at scales not currently detectable with existing millimeter observatories. As such, it will be the most powerful instrument for investigating the cold baryon cycle that drives the early evolution of galaxies and clusters.

Acknowledgments. We thank Brian Mason for his feedback on the Short Baseline Array. The National Radio Astronomy Observatory is a facility of the National Science Foundation operated under cooperative agreement by Associated Universities, Inc.

References

Carilli, C. L. 2016, Next Generation VLA Memo Series, 12
Carilli, C. L. 2018, Next Generation VLA Memo Series, 41
Cicone, C., Maiolino, R., Gallerani, S., et al. 2015, A&A, 574, A14
da Cunha, E., Groves, B., Walter, F., et al. 2013, ApJ, 766, 13
Dannerbauer, H., Lehnert, M. D., Emonts, B., et al. 2017, A&A, 608, A48
Dekel, A., Birnboim, Y., Engel, G., et al. 2009, Nature, 457, 451
Emonts B. H. C., et al., 2014, MNRAS, 438, 2898
Emonts, B. H. C., Mao, M. Y., Stroe, A., et al. 2015, MNRAS, 451, 1025
Emonts B. H. C., et al., 2016, Science, 354, 1128
Emonts, B. H. C., et al. 2018, MNRAS, 477, L60
Ginolfi, M., et al. 2017, MNRAS, 468, 3468
Gullberg, B., et al. 2016, A&A, 591, 73
Hatch N. A., et al., 2008, MNRAS, 383, 931
Huang, Y. D. (., Morata, O., Koch, P. M., et al. 2016, Proceeding of the SPIE, 9911, 99111V
Lau, M. W., Prochaska, J. X., & Hennawi, J. F. 2016, ApJS, 226, 25
Mason, B. 2018, Next Generation VLA Memo Series, 43.
McMullin, J. P., et al. 2007, ASP Conference Series, 376, 127
Miley G. K., et al., 2006, ApJL, 650, L29
Narayanan, D., Krumholz, M. R., Ostriker, E. C., & Hernquist, L. 2012, MNRAS, 421, 3127
Narayanan, D., & Krumholz, M. R. 2014, MNRAS, 442, 1411
Narayanan D., et al., 2015, Nature, 525, 496
Papadopoulos, et al. 2000, ApJ, 528, 626
Papadopoulos P., Thi W., Viti S., 2004, MNRAS, 351, 147
Prochaska J. X., Lau M., Hennawi J., 2014, ApJ, 796, 140
Zhang, Z.-Y., Papadopoulos, P. P., Ivison, R. J., et al. 2016, Royal Society Open Science, 3, 160025

Science with a Next-Generation Very Large Array
ASP Conference Series, Monograph 7
Eric J. Murphy, ed.

DRAFT EDITION

Young Radio AGNs in the ngVLA Era

Pallavi Patil[1,4], Kristina Nyland[1], Jeremy J. Harwood[2], Dipanjan Mukherjee[3], and Anna D. Kapińska[5]

[1]*National Radio Astronomy Observatory, Charlottesville, VA, 22903;* knyland@nrao.edu ; ppatil@nrao.edu

[2]*ASTRON, The Netherlands Institute for Radio Astronomy, Postbus 2, 7990 AA, Dwingeloo, The Netherlands;* jeremy.harwood@physics.org

[3]*Dipartimento di Fisica Generale, Universita degli Studi di Torino, Via Pietro Giuria 1, 10125 Torino, Italy;* dipanjan.mukherjee@unito.it

[4]*University of Virginia, Department of Astronomy, Charlottesville, VA 22903, USA;* pp3uq@virginia.edu

[5]*National Radio Astronomy Observatory, Socorro, NM, 87801;* akapinska@nrao.edu

Abstract. Young, compact radio sources associated with accreting supermassive black holes (SMBHs) represent an important phase in the life cycles of jetted active galactic nuclei (AGNs) for understanding AGN triggering and duty cycles. Yet, this the population of young radio AGNs remains poorly studied. The superb sensitivity and resolution of the ngVLA, coupled with its broad frequency coverage, will enable exciting new insights in our understanding of the life cycles of radio AGNs and their impact on galaxy properties. With broadband continuum coverage from 1 to 116 GHz, the ngVLA will excel at studies of low-redshift ($z < 1$) sources as old as 30 to 40 years.

1. Introduction

Young radio active galactic nuclei (AGNs) are radio galaxies that have recently (re)ignited their central engines within the past 10^2 to 10^4 years, resulting in sub-galactic jet extents of ~10 pc to a few kpc. Young, compact radio sources associated with accreting massive black holes (MBHs) represent a key phase in the life cycles of jetted AGNs. One of the unique characteristics of these galaxies is the concave radio spectral energy distributions (SEDs) with steep spectral slopes. Well studied classes of radio sources, called Compact Steep-Spectrum (CSS) sources, Gigahertz-peaked Spectrum (GPS) sources and High-frequency Peakers (HFP), also show a characteristic spectral turnover that peak from hundreds of MHz to a few GHz and jet extents ranging from tens of kpc to a few pc, respectively (O'Dea 1998; Orienti 2016). These sources are now thought be young radio AGNs, and some of which may evolve to become large and powerful FR I/FR II galaxies (Fanaroff & Riley 1974; Snellen et al. 2000; Kunert-Bajraszewska et al. 2010). The wide frequency range and high angular resolution of the ngVLA are well tuned for the studies of young radio AGNs.

An open question regarding young radio AGNs is their energetic impact on the interstellar medium (ISM) of the host galaxy. As radio jets are still contained within the host, spatially and spectrally resolved analysis of the radio emission will enable us to probe the jet-ISM interactions directly. A growing number of studies have reported detections of multiphase outflow signatures associated with young radio AGNs engaged in jet-ISM feedback (e.g., Chandola et al. 2011; Holt et al. 2011; Morganti et al. 2013), but the importance of this feedback in the context of galaxy evolution remains unclear. The ngVLA will address this issue through both continuum and spectral line observations. Broad-band continuum measurements of the turnover frequency of the radio SEDs of young radio sources can give a direct handle on the density distribution of the ISM for sources at low redshift (Bicknell et al. 1997, 2017; Jeyakumar 2016). Follow-up spectral line observations probing the conditions of the ISM in the vicinity of the jets of the young radio AGNs will provide further constraints on the kinematics of the gas, thus probing the energetic impact of the jet-driven feedback.

Young radio AGNs also hold vital clues about radio triggering and duty cycles, which are still poorly understood (Tadhunter 2016). The host galaxies of AGN exhibit different physical properties which can result in different types of triggering and fueling mechanisms (Maccagni et al. 2014; Tadhunter 2016). An exact understanding of duty cycles and the nature of black hole accretion mechanisms can provide insights into the impact of black hole growth on the host galaxy assembly and their star formation histories (Shulevski et al. 2015). Molecular gas line or HI absorption diagnostics can establish a link between fueling and different triggering mechanisms (Maccagni et al. 2014). A large amount of dense gas is observed in young radio AGNs (O'Dea 1998), and several studies have found that neutral Hydrogen gas is more often detected in GPS, CSS sources as compared to other radio galaxies (Geréb et al. 2014; O'Dea 1998 and references therein). Therefore, the investigation of these newly born AGNs can give us a direct view of many transient processes and help better constrain the simulations of the galaxy formation and evolution.

2. Anticipated Results

2.1. Resolving Young Radio AGNs with the ngVLA

In Figure 1, we show examples of candidate young radio AGNs with jet extents of 60 to 85 pc based on high-resolution continuum observations with the Very Long Baseline Array (Patil et al., in preparation). These radio AGNs were drawn from the sample of extremely infrared luminous sources identified in Lonsdale et al. (2015) that are believed to be in a unique evolutionary stage just after the (re)ignition of the radio AGN but while the host galaxy is still experiencing substantial starburst activity. The ngVLA offers an ideal combination of angular resolution, frequency range, and sensitivity to efficiently resolve the structures of young radio AGNs, such as the sources highlighted in Figure 1, and constrain their ages through broadband continuum observations. The planned longest baselines of a few hundred km are required to provide the milliarcsecond resolution. The ngVLA can easily detect radio galaxies found between redshifts, $z \sim 1 - 6$, and having sub-parsec scale structures over its entire frequency range. The significant increase in brightness sensitivity will enable the detection of radio emission in reasonable integration time.

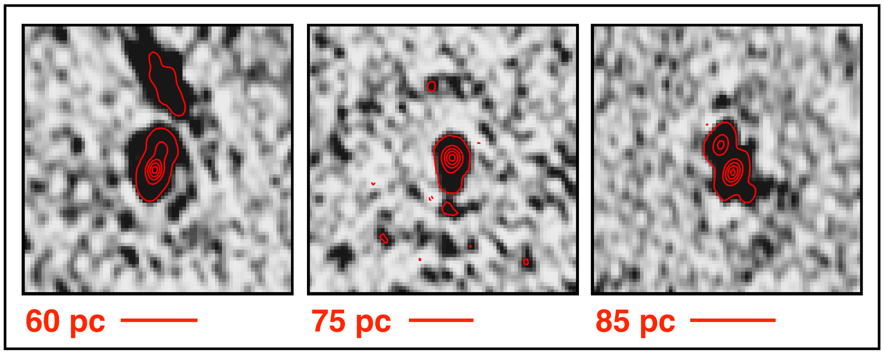

Figure 1. Example VLBA continuum images from (Nyland et al. 2018; Patil et al. in preparation) of young, compact radio AGNs with extents of tens of pc. These sources are drawn from the sample presented in Lonsdale et al. (2015), which selects heavily obscured, powerful AGNs embedded in luminous starbursting galaxies at intermediate redshifts with compact radio emission based on their properties from the Wide-Field Infrared Survey Explorer (Wright et al. 2010) and the NRAO–VLA Sky Survey (Condon et al. 1998). The high collecting area and angular resolution of the ngVLA will facilitate deep, spatially-resolved surveys of compact radio jets with comparable extents in a wide range of systems, providing new insights into the energetic impact of young radio jets under a wide range of host galaxy conditions and properties.

Simulations of relativistic jets interacting with ISM (Mukherjee et al. 2016; Bicknell et al. 2017; Mukherjee et al. 2018) have shown that jets drive shocks in the ISM via an energy bubble. Mukherjee et al. (2018) have found that jet powers, inclinations, and densities affect the AGN-driven outflows. Therefore, high-resolution radio imaging is warranted to obtain structural, spectral and polarimetric information of radio jets. Direct measurements of flux densities and size-scales can give us estimates of energy densities and pressure in synchrotron plasma which can then be used to constrain ISM densities, and the rate of advance of shock front into the medium. By obtaining limits on Faraday rotation measures, polarized emission can constrain models of the nuclear environment. One example of the resolved radio imaging is the eMerlin legacy survey of the local universe, low luminosity AGNs (LeMMINGs) by Baldi et al. (2018). Observations with continental baselines such as in LeMMINGs survey are helpful in the robust detections of the radio emission in the local as well as high redshift galaxies.

2.2. Radio Spectral Ages

In theory, for an electron population in a fixed magnetic field with an initial energy distribution described by a power law such that $N(E) = N_0 E^{-\delta}$, the energy losses scale as $\tau = \frac{E}{dE/dt} \propto 1/E \propto 1/\nu^2$, ultimately leading to a preferential cooling of higher energy electrons. In the absence of any further particle acceleration, this produces a spectrum that becomes increasingly curved over time allowing us to determine the characteristic age of a source (e.g., Myers & Spangler 1985; Harwood et al. 2013).

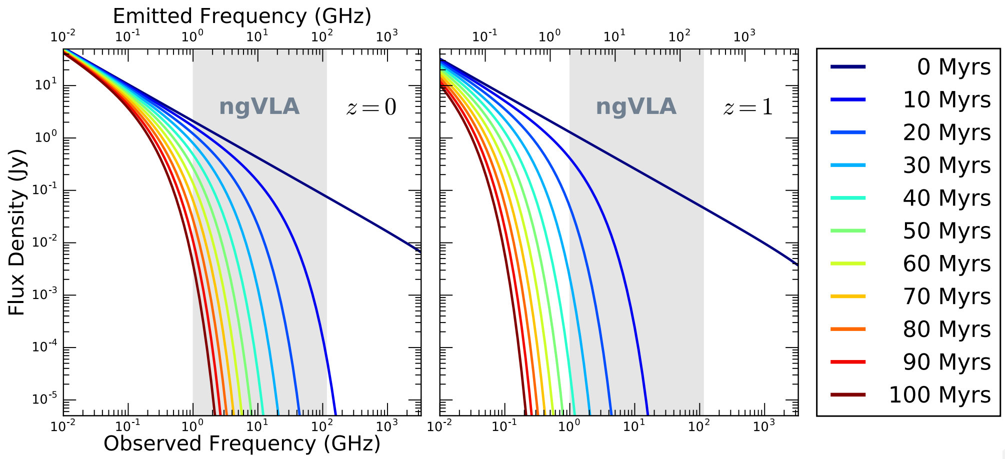

Figure 2. Example of JP model (Jaffe & Perola 1973) spectral ages calculated using the BRATS software (Harwood et al. 2013) demonstrating the need for ngVLA observations spanning a wide range of frequencies. The left and center panels correspond to redshifts of 0 and 1, respectively. The flux density values shown on the *y*-axis have been arbitrarily scaled. Because of its advantages of the wide frequency range and angular resolution compared to the SKA, the ngVLA will uniquely excel in studies of low-redshift radio AGNs that are young, or higher-redshift AGNs that are embedded in dense environments.

In Figure 2, we show an example of Jaffe-Perola (JP) model (Jaffe & Perola 1973) spectral ages calculated using the BRATS software[1] (Harwood et al. 2013) for an arbitrary jetted radio AGN at $z = 0$ and $z = 1$. As indicated by the spectral age curves shown in this figure, the ngVLA will excel in studies of radio AGNs spanning a wide range of ages at low redshift, as well as radio AGNs that are young or embedded in dense environments at higher redshifts. As shown by results from the Australia Telescope 20 GHz (AT20G) survey (Murphy et al. 2010), continuum measurements in the tens of GHz range are needed to model the radio spectral energy distributions (Sadler et al. 2006, 2008) adequately. This is particularly important for modeling the ages of young, low-redshift sources less than 10 Myrs old. Lower frequency radio continuum data in the MHz range are important for constraining the ages of high-z sources; however, the inclusion of the lowest-frequency ngVLA bands down to ∼1 GHz would provide sufficient frequency coverage for measuring ages of sources as old as 30–40 Myrs at $z \sim 1$.

2.3. Characterizing Spectral Turnover

CSS, GPS and HFP sources show an inverse correlation between the spectral peak frequency and their linear sizes (O'Dea 1998; Orienti & Dallacasa 2014). The relation could suggest an evolutionary link between all three classes. However, details of the absorption model which causes the turnover are still unknown (Callingham et al. 2015). Therefore, a high-resolution broadband spectral modeling on both sides of the peak is

[1] http://www.askanastronomer.co.uk/brats/

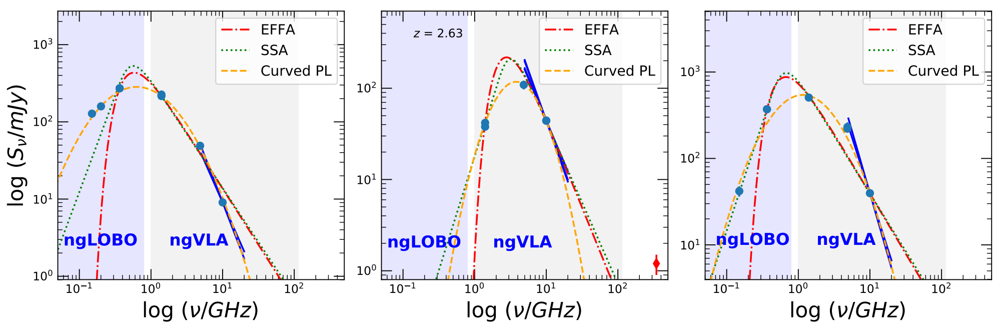

Figure 3. An example of radio SED fitting in GPS/HFP sources. These sources are taken from a parent sample of heavily obscured and hyper-luminous quasars having compact radio emission (Lonsdale et al. 2015). The observation at 10 GHz is a part of the high-resolution JVLA imaging of these young radio AGNs at 10 GHz (Patil et al. in preparation). The blue bow-tie is the in-band spectral index of the JVLA data point. Remaining data points are taken from archival radio sky surveys. The source in the second panel has a known redshift, and the red diamond is the ALMA Band-7 observation taken in cycle-0. The curves are the best-fit solutions of different radio SED models: red dashed dot line is for the external free-free absorption model (EFFA), dotted green line corresponds to the synchrotron self-absorption model (SSA), and the yellow dashed line is for the generic curved power law model. The ngVLA and ngLOBO can spatially map the radio SED in these sources and will be able to distinguish between different theoretical models.

essential for the identification of the absorption process. As shown in Figure 3, the inclusion of low-frequency observations around 1 GHz or lower would enhance studies of the turnover in the optically thick radio SEDs of young radio AGNs. This would provide new insights into the dominant physical mechanism responsible for the turnover (e.g., synchrotron self-absorption vs. free-free absorption; Kellermann 1966) in young radio AGNs over larger parameter space. The Next Generation LOw Band Observatory (ngLOBO; Taylor et al. 2017), which is a proposed enhancement to the basic ngVLA reference design that would extend the ngVLA's frequency range below 1 GHz, would thus enable more robust radio SED and spectral aging model studies with the ngVLA, particular for slightly older (> 10 Myr) and more distant ($z > 1$) sources.

3. Uniqueness to ngVLA Capabilities

The broad frequency range (1–116 GHz) of the ngVLA will facilitate surveys of the radio spectral ages of *young* AGNs residing in gas-rich galaxies at low and intermediate redshifts. We emphasize that unlike other next-generation radio facilities that will operate primarily at lower frequencies (e.g., the SKA), the planned observing frequency range of the ngVLA from 1–116 GHz makes it uniquely equipped for measuring the ages of *young* radio AGNs potentially engaged in jet-ISM feedback.

4. Multiwavelength Synergy

We now know that most galaxies will go through an AGN phase either once or multiple times in their life. Furthermore, this transient phase affects an overall evolution of the host galaxy, and the AGN itself. Young radio AGNs are ideal candidates to study such interactions between the host and central engines as they provide a direct view of short-lived processes. Upcoming or current facilities at radio, as well as other wavelengths, will be essential to probe different components of young radio AGNs as the evolution of all those components is interdependent.

- SKA: The ngVLA and SKA will both allow broadband studies of radio SEDs over their respective wide frequency ranges, thus providing the temporal information from spectral aging models necessary for interpreting the evolutionary stage of the source. The SKA will be able to detect emission associated with the fading radio lobes, tracing the regime of radio AGN with older spectral ages ("AGN archaeology"; Morganti 2017). In Figure 2, we showed that the 1–116 GHz observing range of the ngVLA is advantageous for studies of low-redshift radio AGNs, or intermediate redshift sources that are very young. Such young sources are often embedded in dense environments, and are known to drive multi-phase gas outflows (e.g., Holt et al. 2008; Geréb et al. 2015). Broadband radio continuum surveys with both the ngVLA and SKA will, therefore, be needed to construct a complete picture of the life cycles of radio AGNs and their connection to galaxy evolution.

- ALMA: The high-frequency range of ngVLA is in a spot where both synchrotron emission and star formation can significantly contribute to the continuum, whereas ALMA can map the dust-continuum, and trace the higher transitions in molecular gas. Combining ngVLA and ALMA will allow determination of both of these components. The powerful radio galaxies tend to reside in high-density environments (Wylezalek et al. 2013). Therefore, some young radio AGN could be found in proto-cluster regions, and ALMA CO-line diagnostics can probe the companion star-forming galaxies.

- Optical/Infrared (IR) Telescopes: Next-generation optical/IR telescopes such as *James Webb* Space Telescope *(JWST)*, Thirty Meter Telescope (TMT), Giant Magellan Telescope (GMT) and Wide-Field Infrared Survey Telescope *(WFIRST)* can provide wealth of complimentary information about the host galaxies and the physical conditions of young radio AGNs. Some of the science goals that can be achieved by these planned facilities are: resolving host morphologies, studying the kinematics of the warm ionized gas via spectroscopy, delineating star-formation and AGN via MIR imaging, and tracing AGN-driven outflows and their excitation mechanisms.

References

Baldi, R. D., Williams, D. R. A., McHardy, I. M., Beswick, R. J., Argo, M. K., Dullo, B. T., Knapen, J. H., Brinks, E., Muxlow, T. W. B., Aalto, S., Alberdi, A., Bendo, G. J., Corbel, S., Evans, R., Fenech, D. M., Green, D. A., Klöckner, H.-R., Körding, E., Kharb, P., Maccarone, T. J., Martí-Vidal, I., Mundell, C. G., Panessa, F., Peck, A. B., Pérez-Torres,

M. A., Saikia, D. J., Saikia, P., Shankar, F., Spencer, R. E., Stevens, I. R., Uttley, P., & Westcott, J. 2018, MNRAS, 476, 3478. 1802.02162

Bicknell, G. V., Dopita, M. A., & O'Dea, C. P. O. 1997, ApJ, 485, 112

Bicknell, G. V., Mukherjee, D. D., Wagner, A. Y., & Sutherland, R. S. 2017, MNRAS, submitted

Callingham, J. R., Gaensler, B. M., Ekers, R. D., Tingay, S. J., Wayth, R. B., Morgan, J., Bernardi, G., Bell, M. E., Bhat, R., Bowman, J. D., Briggs, F., Cappallo, R. J., Deshpande, A. A., Ewall-Wice, A., Feng, L., Greenhill, L. J., Hazelton, B. J., Hindson, L., Hurley-Walker, N., Jacobs, D. C., Johnston-Hollitt, M., Kaplan, D. L., Kudrayvtseva, N., Lenc, E., Lonsdale, C. J., McKinley, B., McWhirter, S. R., Mitchell, D. A., Morales, M. F., Morgan, E., Oberoi, D., Offringa, A. R., Ord, S. M., Pindor, B., Prabu, T., Procopio, P., Riding, J., Srivani, K. S., Subrahmanyan, R., Udaya Shankar, N., Webster, R. L., Williams, A., & Williams, C. L. 2015, ApJ, 809, 168. 1507.04819

Chandola, Y., Sirothia, S. K., & Saikia, D. J. 2011, MNRAS, 418, 1787. 1108.2242

Condon, J. J., Cotton, W. D., Greisen, E. W., Yin, Q. F., Perley, R. A., Taylor, G. B., & Broderick, J. J. 1998, AJ, 115, 1693

Fanaroff, B. L., & Riley, J. M. 1974, MNRAS, 167, 31P

Geréb, K., Maccagni, F. M., Morganti, R., & Oosterloo, T. A. 2015, A&A, 575, A44. 1411.0361

Geréb, K., Morganti, R., & Oosterloo, T. A. 2014, A&A, 569, A35. 1407.1799

Harwood, J. J., Hardcastle, M. J., Croston, J. H., & Goodger, J. L. 2013, MNRAS, 435, 3353. 1308.4137

Holt, J., Tadhunter, C. N., & Morganti, R. 2008, MNRAS, 387, 639. 0802.1444

Holt, J., Tadhunter, C. N., Morganti, R., & Emonts, B. H. C. 2011, MNRAS, 410, 1527. 1008.2846

Jaffe, W. J., & Perola, G. C. 1973, A&A, 26, 423

Jeyakumar, S. 2016, MNRAS, 458, 3786. 1601.05406

Kellermann, K. I. 1966, Australian Journal of Physics, 19, 195

Kunert-Bajraszewska, M., Gawroński, M. P., Labiano, A., & Siemiginowska, A. 2010, MNRAS, 408, 2261. 1009.5235

Lonsdale, C. J., Lacy, M., Kimball, A. E., Blain, A., Whittle, M., Wilkes, B., Stern, D., Condon, J., Kim, M., Assef, R. J., Tsai, C.-W., Efstathiou, A., Jones, S., Eisenhardt, P., Bridge, C., Wu, J., Lonsdale, C. J., Jones, K., Jarrett, T., & Smith, R. 2015, ApJ, 813, 45. 1509.00342

Maccagni, F. M., Morganti, R., Oosterloo, T. A., & Mahony, E. K. 2014, A&A, 571, A67

Morganti, R. 2017, Nature Astronomy, 1, 9

Morganti, R., Frieswijk, W., Oonk, R. J. B., Oosterloo, T., & Tadhunter, C. 2013, A&A, 552, L4. 1302.2236

Mukherjee, D., Bicknell, G. V., Sutherland, R., & Wagner, A. 2016, MNRAS, 461, 967. 1606.01143

Mukherjee, D., Bicknell, G. V., Wagner, A. Y., Sutherland, R. S., & Silk, J. 2018, ArXiv e-prints. 1803.08305

Murphy, T., Sadler, E. M., Ekers, R. D., Massardi, M., Hancock, P. J., Mahony, E., Ricci, R., Burke-Spolaor, S., Calabretta, M., Chhetri, R., de Zotti, G., Edwards, P. G., Ekers, J. A., Jackson, C. A., Kesteven, M. J., Lindley, E., Newton-McGee, K., Phillips, C., Roberts, P., Sault, R. J., Staveley-Smith, L., Subrahmanyan, R., Walker, M. A., & Wilson, W. E. 2010, MNRAS, 402, 2403. 0911.0002

Myers, S. T., & Spangler, S. R. 1985, ApJ, 291, 52

Nyland, K., Harwood, J. J., Mukherjee, D., Jagannathan, P., Rujopakarn, W., Emonts, B., Alatalo, K., Bicknell, G. V., Davis, T. A., Greene, J. E., Kimball, A., Lacy, M., Lonsdale, C., Lonsdale, C., Maksym, W. P., Molnár, D. C., Morabito, L., Murphy, E. J., Patil, P., Prandoni, I., Sargent, M., & Vlahakis, C. 2018, ApJ, 859, 23. 1803.02357

O'Dea, C. P. 1998, PASP, 110, 493

Orienti, M. 2016, Astronomische Nachrichten, 337, 9. 1511.00436

Orienti, M., & Dallacasa, D. 2014, MNRAS, 438, 463. 1311.2999

Sadler, E. M., Ricci, R., Ekers, R. D., Ekers, J. A., Hancock, P. J., Jackson, C. A., Kesteven,

M. J., Murphy, T., Phillips, C., Reinfrank, R. F., Staveley-Smith, L., Subrahmanyan, R., Walker, M. A., Wilson, W. E., & de Zotti, G. 2006, MNRAS, 371, 898. astro-ph/0603437

Sadler, E. M., Ricci, R., Ekers, R. D., Sault, R. J., Jackson, C. A., & de Zotti, G. 2008, MNRAS, 385, 1656. 0709.3563

Shulevski, A., Morganti, R., Barthel, P. D., Harwood, J. J., Brunetti, G., van Weeren, R. J., Röttgering, H. J. A., White, G. J., Horellou, C., Kunert-Bajraszewska, M., Jamrozy, M., Chyzy, K. T., Mahony, E., Miley, G., Brienza, M., Bîrzan, L., Rafferty, D. A., Brüggen, M., Wise, M. W., Conway, J., de Gasperin, F., & Vilchez, N. 2015, A&A, 583, A89. 1510.01479

Snellen, I. A. G., Schilizzi, R. T., Miley, G. K., de Bruyn, A. G., Bremer, M. N., & Röttgering, H. J. A. 2000, MNRAS, 319, 445. astro-ph/0002130

Tadhunter, C. 2016, A&A Rev., 24, 10. 1605.08773

Taylor, G., Dowell, J., Malins, J., Clarke, T., Kassim, N., Giacintucci, S., Hicks, B., Kooi, J., Peters, W., Polisensky, E., Schinzel, F., & Stovall, K. 2017, ArXiv e-prints. 1708.00090

Wright, E. L., Eisenhardt, P. R. M., Mainzer, A. K., Ressler, M. E., Cutri, R. M., Jarrett, T., Kirkpatrick, J. D., Padgett, D., & et al. 2010, AJ, 140, 1868. 1008.0031

Wylezalek, D., Galametz, A., Stern, D., Vernet, J., De Breuck, C., Seymour, N., Brodwin, M., Eisenhardt, P. R. M., Gonzalez, A. H., Hatch, N., Jarvis, M., Rettura, A., Stanford, S. A., & Stevens, J. A. 2013, ApJ, 769, 79. 1304.0770

Science with a Next-Generation Very Large Array
ASP Conference Series, Monograph 7
Eric J. Murphy, ed.

DRAFT EDITION

Probing Obscured MBH Accretion and Growth since Cosmic Dawn

Wiphu Rujopakarn[1,2,3], Kristina Nyland[4], Amy E Kimball[5], and Isabella Prandoni[6]

[1]*Department of Physics, Faculty of Science, Chulalongkorn University, 254 Phayathai Road, Pathumwan, Bangkok 10330, Thailand;* wiphu.r@chula.ac.th

[2]*National Astronomical Research Institute of Thailand (Public Organization), Don Kaeo, Mae Rim, Chiang Mai 50180, Thailand*

[3]*Kavli Institute for the Physics and Mathematics of the universe (WPI), The University of Tokyo Institutes for Advanced Study, The University of Tokyo, Kashiwa, Chiba 277-8583, Japan*

[4]*National Radio Astronomy Observatory, Charlottesville, VA, 22903, USA;* knyland@nrao.edu

[5]*National Radio Astronomy Observatory, Socorro, NM, 87801, USA;* akimball@nrao.edu

[6]*INAF-Istituto di Radioastronomia, via P. Gobetti 101, 40129, Bologna, Italy;* prandoni@ira.inaf.it

1. Introduction

The convergence of theory and observation in galaxy evolution is a major milestone in astrophysics. With appropriate sets of parameters, models of galaxy formation can reproduce, for instance, the luminosity and mass distributions of today's galaxies and the cosmic star formation rate (SFR) history since the epoch of reionization. However, many of the most fundamental processes in the model are not well understood, especially down to galactic scales, where the current frontier questions in galaxy evolution lie. Central among these issues is the empirical link between galaxy assembly and supermassive black hole (MBH) accretion and growth. Advancing our understanding of this symbiotic relationship requires a complete census of the first generation of AGNs at cosmic dawn as well as a spatially-resolved study of individual galaxies at the peak of their assembly, $1 < z < 3$, to map their SF and MBH accretion activities (i.e., active galactic nuclei; AGN). Fundamental breakthroughs in these areas thus require a sub-arcsecond resolution, extinction-independent tracer of *both* AGN and SF.

Centimetric radio continuum observations uniquely meet these observational demands. Deep, high-resolution continuum surveys with current and next-generation facilities will therefore play an essential role in advancing the current galaxy formation and evolution paradigm in the decades to come. In addition to tracing AGN and SF activity in an extinction-free manner, centimetric radio continuum observations of AGN and SF emission are also relatively stable in time. While other AGN indicators such as hard X-ray emission or emission lines can fluctuate rapidly over timescales of days to months (Hickox et al. 2014), giving only an instantaneous indication of the level of activity, radio emission has a synchrotron timescale of $10^6 - 10^7$ years (Beck & Krause 2005) to serve as a beacon localizing the AGN. Obviously, a prerequisite to utilizing these characteristics is to confirm the AGN origin of the radio emission, which, by nature, traces both AGN and star formation (SF) activities. Thanks to the Atacama Large Millimeter/submillimeter Array (ALMA), this is now possible out to $z \sim 10$ with the help of the negative K-correction. As a result, we are reaching the start of an era when centimetric radio continuum can be utilized to the fullest extent to study MBH growth.

2. Capturing obscured AGN at $z \gtrsim 6$

Most of the stars today reside in galactic spheroids, whose properties are tightly tied to the MBHs at their centers, implying that the accretion activity onto MBHs leaves a lasting imprint on the evolution of their host galaxies (e.g. Kormendy & Ho 2013; Heckman & Best 2014). Directly studying the origin of this relationship requires identifying typical active galactic nuclei (AGNs) out to the reionization era. However, spectroscopically-confirmed AGNs at $z \gtrsim 6$ are limited to luminous quasars; the search for AGNs in typical galaxies at $z = 6 - 8$ through individual X-ray detections and stacking analyses has yet to be successful, suggesting that the current approaches may systematically be missing the typical population of AGNs.

Luminous AGNs have been found out to $z = 7.5$ with $M_{\rm BH} \sim 10^9$ $M_\odot$ (Bañados et al. 2018). Such extreme objects are rare (only two with spectroscopic confirmation at $z > 7$ so far), yet provide crucial evidence that MBH can grow rapidly up to massive size within a Gyr after the Big Bang. If the Bañados et al. quasar is at the bright-end of the quasar luminosity function, it remains a question whether more typical MBHs are growing rapidly elsewhere during this epoch. Typical, actively growing MBHs at $z > 6$ appear to be beyond the present observational capabilities: none of the spectroscopically confirmed $z = 6 - 8$ galaxies in the Hubble Ultra-Deep Field (HUDF) are detected in the individual or stacked *Chandra* 4 and 7 Ms images (Giallongo et al. 2015; Luo et al. 2017). Treister et al. (2013) postulate that these galaxies may not contain MBH, that MBH are not growing despite their large sSFR, or that MBHs are growing elsewhere in lower-mass or obscured galaxies not identified by the current *Hubble* and *Chandra* observations. This missing typical population of AGNs could have important implications on the cosmic accretion history, feedback on the intergalactic medium, reionization, and to our understanding of how MBHs and galactic bulges coevolved.

If the typical sites of MBH growth in the early universe are indeed in low mass galaxies, the current optical, IR, and X-ray indicators will have difficulties identifying them. They will be too faint in the optical/near-IR, contain too little dust to power mid-IR emission, and emit at too low of a luminosity for direct X-ray detection at high redshift (also not identified in large numbers in other bands to enable X-ray stacking). On the other hand, early MBHs could be accreting in a different mode that confers on them the observed rapid growth (e.g., Volonteri et al. 2015), but that the radiation is trapped (Coughlin & Begelman 2014) and conceals them from current survey approaches. In either case, centimetric radio observations have the potential to identify them because of the symbiotic nature of the accretion onto MBH and the resulting relativistic jets that are a signpost of AGNs in the radio (e.g., Begelman et al. 1984). Radio observations are also extinction-free and have recently become sensitive enough to find typical AGNs at $z \gg 4$ with the advent of the JVLA. This is therefore a potentially groundbreaking means to identify typical AGNs at high z.

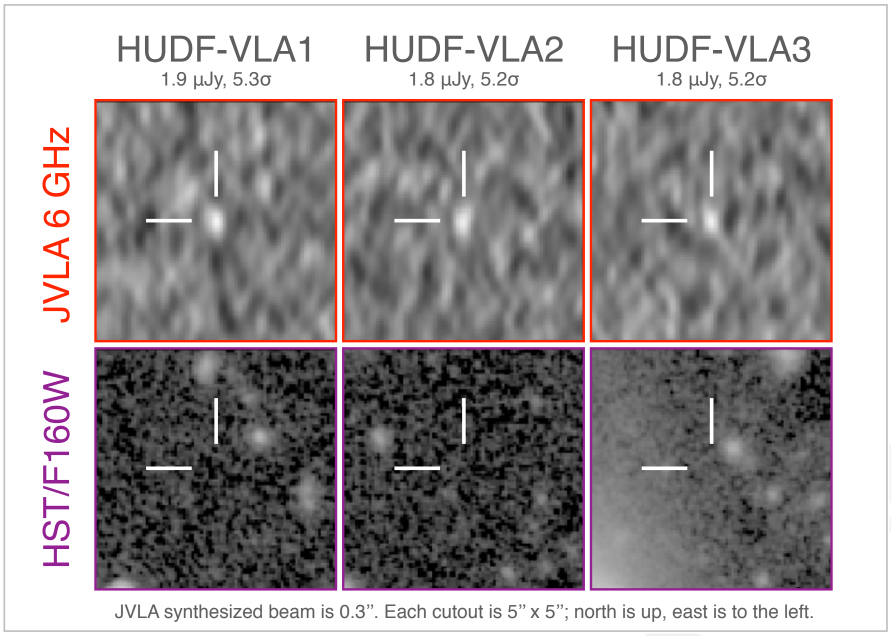

Figure 1. The $\geqslant 5\sigma$ sources in the HUDF JVLA 6 GHz survey with absolutely no counterparts in any other bands (*Hubble* 1.6 μm shown here). An object has to be at $z \gtrsim 5$ in order to evade detection in ultra-deep *Hubble, Spitzer*, and ground-based imaging sensitivity of the HUDF. There are no sources in the negative map at this significance — it is extremely unlikely that these are noise peaks.

Recently, Rujopakarn et al. (2016) has conducted a sensitive single-pointing survey of the HUDF using the JVLA at 6 GHz (0.3 μJy beam^{-1} rms). They have found that 99% of radio sources detected above 5σ have optical or near-IR counterparts. The remaining 1% – three sources within the central 100$''$ of the primary beam – are of great interest (Figure 1). They are extremely unlikely to be noise peaks because the noise distribution from the source-free area is well-fitted by a Gaussian and there are no sources in the inverted map above 5σ in the same area. They are also persistent over the two year period to acquire 177 hours of JVLA observations, effectively ruling out the possibilities of transient or non-astrophysical artifacts. To evade detection in a field with such a deep suite of ground and space-based imaging, reaching 30.5 mag (5σ) at 1 μm, an object must either be at moderate redshifts, $z \sim 1-3$, but extremely dust-obscured, which is ruled out by the lack of detections with *Spitzer* and ALMA (the 1.3 mm deep field; Dunlop et al. 2017); or have low M_* (e.g., 10^7-10^8 $M_\odot$, which will be an interesting class of AGN in itself); or they must be at higher z of $z \gtrsim 5-6$.

Characterization of these high-z radio AGN candidates has proven to be extremely challenging for current facilities. An example is a candidate shown in Figure 2 from the pilot survey of Rujopakarn et al. (2016). In this case, a faint *Spitzer*/IRAC counterpart is found, but the non-detection in deep *Hubble* and ground-based near-IR images effectively ruled out hosts with $M_* \gtrsim 10^8$ $M_\odot$ at $z \lesssim 4$. This radio source was followed-up with the X-Shooter instrument (simultaneous UV, optical, and near-IR spectroscopy) on the ESO Very Large Telescope for 6 hours to search for a Lyα line to confirm the

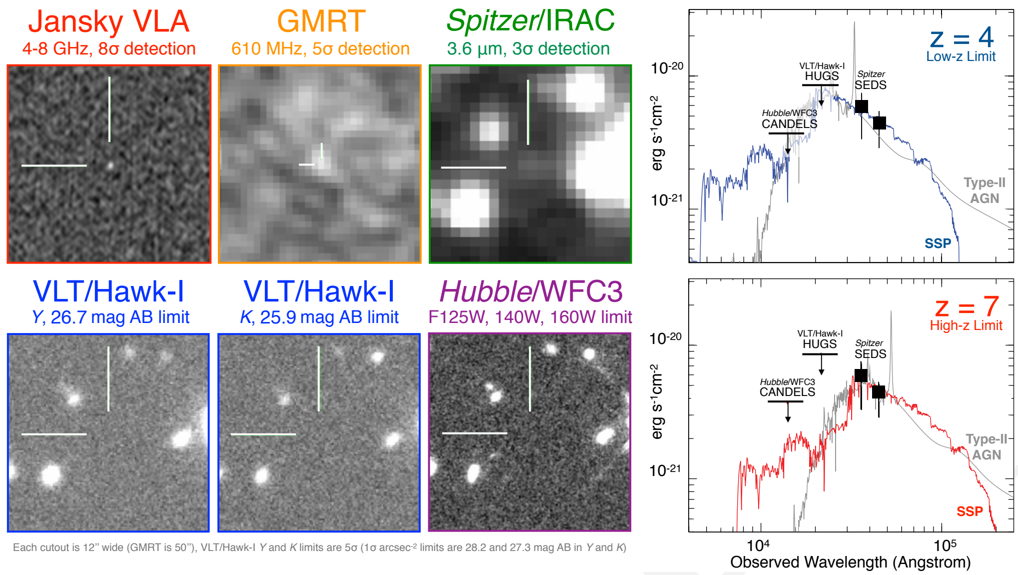

Figure 2. A high-z AGN candidate detected in the pilot survey of Rujopakarn et al. (2016) that is only detected in the VLA and an ultra-deep follow-up imaging with the GMRT and *Spitzer*/IRAC, but not any other bands; the most probable redshift is $z \sim 4 - 7$. Follow-up spectroscopy with the ESO VLT/X-Shooter with 6-hours integration finds no Lyα, typical for $z > 6$ candidates, highlighting the necessity for next-generation facilities, e.g., *JWST*, to study these populations.

redshift. No line was detected, suggesting that this could be a case of the low Lyα detection rate at $z \gtrsim 6.5$, where the reionization is not yet completed (Schenker et al. 2014). Their characterization is beyond the capability of current optical/IR observatories and will require next-generation facilities, e.g., *JWST*.

A survey with the ngVLA carried out in a similar manner to the VLA Sky Survey (VLASS) would be significantly more efficient due to the wider field of view of the 18m dishes and higher collecting area compared to the VLA. An all-sky survey with the same total observing time as VLASS (≈6000 hours) could be ≈10 times deeper, thereby capturing this potentially new AGN populations only detectable in the radio.

3. Witnessing MBH–bulge coevolution at $z \sim 2$

Despite the multiple lines of evidence showing a link between galaxy assembly and MBH growth, there is no consensus on the causality of this relationship. Direct links on a global scale between a MBH accretion rate (BHAR) and the star formation rate (SFR) of its host are elusive. Although the two processes appear to be correlated, this result may only reflect that both depend on the stellar mass of the host galaxy (Xu et al. 2015; Stanley et al. 2017). For local galaxies, there is evidence for *localized* enhanced SF close to an AGN, related to the BHAR (e.g., Diamond-Stanic & Rieke 2012). Improving our understanding of this link at higher redshifts requires higher resolution imaging to determine whether the sites of MBHs are also associated with the most vigorous SF.

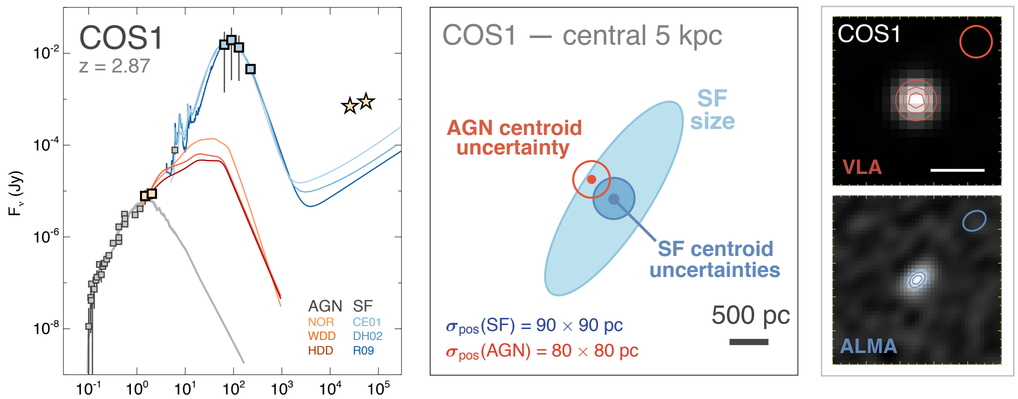

Figure 3. A new technique to accurately pinpoint the sites of intense SF and MBH growth at $z \sim 2$. Left: strong radio excess over the level associated with SFR is AGN-dominated, whereas the submillimeter emission captured by ALMA is virtually free of the AGN emission and hence trace the distribution of SF. Middle: Using this technique, Rujopakarn et al. (2018) found AGNs to occur within the compact regions of intense SF. Right: Accurate localization of SF and AGN are enabled by sub-arcsec ALMA and JVLA observations. Postage stamps are $4'' \times 4''$; the synthesized beam size is shown in the respective image.

Yet, such images have until very recently been impossible at $z \sim 2$, at the peak of both SFR and BHAR and thus potentially the formative era for the current relation. The commonly used tracers of AGN do not have the required resolution, e.g., the most sensitive *Chandra* X-ray observations of the Chandra Deep-Field South (Luo et al. 2017) has $\sim 1''$ resolution (8 kpc at $z = 3$). The potentially extreme $A_V \gtrsim 100$ mag near the center of rapidly star-forming galaxies at this epoch found by Simpson et al. (2017) requires an extinction-independent SF tracer such as far IR, but resolutions of only $\sim 5''$, i.e., a few tens of kpc, are available.

High-resolution centimetric radio imaging, with the help of ALMA, once again can make a significant breakthrough. The JVLA provides sub-arcsecond imaging that can penetrate dust to trace synchrotron emission associated with SF as well as emission from any AGN core and jets. The submillimeter continuum at, e.g., 870 μm traces the cold dust emission associated with SF. This emission is virtually free of AGN contribution because the IR spectra of AGN tori plummet rapidly longward of 40 μm (Lyu & Rieke 2017). Likewise, extrapolating the radio slopes from ~1 GHz to the ALMA band shows that the non-thermal emission from all but the most radio-loud AGNs is likely to be 2 – 3 orders of magnitude fainter than the thermal dust emission of their hosts. Any galaxy where the radio emission is enhanced to well above the level implied by the far-IR/radio correlation for SF galaxies presents a robust radio AGN signature (Figure 3). In these galaxies with strong radio enhancement, JVLA traces AGN and ALMA traces nearly pure SF, so sub-arcsecond JVLA and ALMA images can localize — at sub-kpc resolution — the sites of SF relative to the MBH in active galaxies.

Central to this technique is that (1) at $z \sim 2$, AGNs commonly have strong radio sources, unresolved at sub-arcsec resolution (cf. parsec-scale cores and jets; Zensus 1997); (2) at GHz rest frequencies, the central radio emission within a sub-arcsec beam accurately pinpoints the AGN core (Nagar et al. 2002; Pushkarev & Kovalev 2012); (3) the uncertainty of the centroid position, $\sigma_{\rm pos}$, of a radio or submillimeter source is $\sigma_{\rm pos} \approx \theta_{\rm beam}/(2 \times {\rm S/N})$, where $\theta_{\rm beam}$ is the synthesized beam size and S/N is the peak signal-to-noise ratio (Condon 1997). For example, a 10σ point source observed with a $0\farcs15$ beam can be localized to about 8 milliarcsecond (mas); and, lastly (4) the astrometric references of the JVLA and ALMA are tied to their respective phase calibrator positions, which are in turn tied to the International Coordinate Reference Frame (ICRF) to within $\lesssim$ 10 mas. That is, the astrometry of JVLA and ALMA are tied to the common reference frame and can be directly compared.

Rujopakarn et al. (2018) demonstrated this technique in three objects with $\geqslant 5\times$ radio excess over the level predicted by the far-IR/radio correlation, and with the ALMA observations resolving the sub/millimeter emission. In all three galaxies, the AGNs are located within the $\lesssim$ 1 kpc regions of gas-rich, heavily obscured, intense nuclear SF (Figure 3). If the star-formation and AGN-driven outflows that may be present (e.g., Mullaney et al. 2013) do not completely disrupt the cold gas supply, and both types of activity proceed for the duration of their host's typical stellar mass doubling time of $\simeq$ 0.2 Gyr, then the newly formed stellar mass within the central kpc will be of order 10^{11} $M_\odot$. Likewise, if the MBH is allowed to accrete at a rate predicted by the correlation between SFR and the average BHAR relation (e.g., Chen et al. 2013) for the same duration, the accreted MBH mass will be $10^{6.7} - 10^{7.8}$ $M_\odot$, similar to those found in local massive galactic bulges. That is, the ongoing episode of SF and MBH growth in these galaxies is potentially capable of producing bulge stellar masses and MBH masses on the local scaling relations. This is consistent with a picture of *in situ* galactic bulge and MBH growth, and may represent the dominant process regulating the bulge–MBH relationship through which all massive galaxies may pass.

The milliarcsecond resolution of ngVLA will push the localization accuracy of the AGN to sub-milliarcsecond regime using this technique. Most importantly, it will resolve the morphologies of these sub-kpc jets at $z \sim 2$ to understand their role in regulating the assembly of the bulge (Nyland et al. 2018). Because there is no local counterparts of gas-rich bulge-forming galaxies, ngVLA will be the only avenue to provide theorists and simulators with constraints on the nature of typical jet feedbacks at the peak of galaxy assembly.

References

Bañados, E., Venemans, B. P., Mazzucchelli, C., Farina, E. P., Walter, F., Wang, F., Decarli, R., Stern, D., Fan, X., Davies, F. B., Hennawi, J. F., Simcoe, R. A., Turner, M. L., Rix, H.-W., Yang, J., Kelson, D. D., Rudie, G. C., & Winters, J. M. 2018, Nat, 553, 473. 1712.01860

Beck, R., & Krause, M. 2005, Astronomische Nachrichten, 326, 414. astro-ph/0507367

Begelman, M. C., Blandford, R. D., & Rees, M. J. 1984, Reviews of Modern Physics, 56, 255

Chen, C.-T. J., Hickox, R. C., Alberts, S., Brodwin, M., Jones, C., Murray, S. S., Alexander, D. M., Assef, R. J., Brown, M. J. I., Dey, A., Forman, W. R., Gorjian, V., Goulding, A. D., Le Floc'h, E., Jannuzi, B. T., Mullaney, J. R., & Pope, A. 2013, ApJ, 773, 3. 1306.1227

Condon, J. J. 1997, PASP, 109, 166

Coughlin, E. R., & Begelman, M. C. 2014, ApJ, 781, 82. 1312.5314

Diamond-Stanic, A. M., & Rieke, G. H. 2012, ApJ, 746, 168. 1106.3565

Dunlop, J. S., McLure, R. J., Biggs, A. D., Geach, J. E., Michałowski, M. J., Ivison, R. J., Rujopakarn, W., van Kampen, E., Kirkpatrick, A., Pope, A., Scott, D., Swinbank, A. M., Targett, T. A., Aretxaga, I., Austermann, J. E., Best, P. N., Bruce, V. A., Chapin, E. L., Charlot, S., Cirasuolo, M., Coppin, K., Ellis, R. S., Finkelstein, S. L., Hayward, C. C., Hughes, D. H., Ibar, E., Jagannathan, P., Khochfar, S., Koprowski, M. P., Narayanan, D., Nyland, K., Papovich, C., Peacock, J. A., Rieke, G. H., Robertson, B., Vernstrom, T., Werf, P. P. v. d., Wilson, G. W., & Yun, M. 2017, MNRAS, 466, 861. 1606.00227

Giallongo, E., Grazian, A., Fiore, F., Fontana, A., Pentericci, L., Vanzella, E., Dickinson, M., Kocevski, D., Castellano, M., Cristiani, S., Ferguson, H., Finkelstein, S., Grogin, N., Hathi, N., Koekemoer, A. M., Newman, J. A., & Salvato, M. 2015, A&A, 578, A83. 1502.02562

Heckman, T. M., & Best, P. N. 2014, ARA&A, 52, 589. 1403.4620

Hickox, R. C., Mullaney, J. R., Alexander, D. M., Chen, C.-T. J., Civano, F. M., Goulding, A. D., & Hainline, K. N. 2014, ApJ, 782, 9. 1306.3218

Kormendy, J., & Ho, L. C. 2013, ARA&A, 51, 511. 1304.7762

Luo, B., Brandt, W. N., Xue, Y. Q., Lehmer, B., Alexander, D. M., Bauer, F. E., Vito, F., Yang, G., Basu-Zych, A. R., Comastri, A., Gilli, R., Gu, Q.-S., Hornschemeier, A. E., Koekemoer, A., Liu, T., Mainieri, V., Paolillo, M., Ranalli, P., Rosati, P., Schneider, D. P., Shemmer, O., Smail, I., Sun, M., Tozzi, P., Vignali, C., & Wang, J.-X. 2017, ApJS, 228, 2. 1611.03501

Lyu, J., & Rieke, G. H. 2017, ApJ, 841, 76. 1704.06987

Mullaney, J. R., Alexander, D. M., Fine, S., Goulding, A. D., Harrison, C. M., & Hickox, R. C. 2013, MNRAS, 433, 622. 1305.0263

Nagar, N. M., Falcke, H., Wilson, A. S., & Ulvestad, J. S. 2002, A&A, 392, 53. astro-ph/0207176

Nyland, K., Harwood, J. J., Mukherjee, D., Jagannathan, P., Rujopakarn, W., Emonts, B., Alatalo, K., Bicknell, G., Davis, T. A., Greene, J., Kimball, A., Lacy, M., Lonsdale, C., Lonsdale, C., Maksym, W. P., Molnar, D., Morabito, L., Murphy, E., Patil, P., Prandoni, I., Sargent, M., & Vlahakis, C. 2018, ArXiv e-prints. 1803.02357

Pushkarev, A. B., & Kovalev, Y. Y. 2012, A&A, 544, A34. 1205.5559

Rujopakarn, W., Dunlop, J. S., Rieke, G. H., Ivison, R. J., Cibinel, A., Nyland, K., Jagannathan, P., Silverman, J. D., Alexander, D. M., Biggs, A. D., Bhatnagar, S., Ballantyne, D. R., Dickinson, M., Elbaz, D., Geach, J. E., Hayward, C. C., Kirkpatrick, A., McLure, R. J., Michałowski, M. J., Miller, N. A., Narayanan, D., Owen, F. N., Pannella, M., Papovich, C., Pope, A., Rau, U., Robertson, B. E., Scott, D., Swinbank, A. M., van der Werf, P., van Kampen, E., Weiner, B. J., & Windhorst, R. A. 2016, ApJ, 833, 12. 1607.07710

Rujopakarn, W., Nyland, K., Rieke, G. H., Barro, G., Elbaz, D., Ivison, R. J., Jagannathan, P., Silverman, J. D., Smolčić, V., & Wang, T. 2018, ApJ, 854, L4. 1801.07072

Schenker, M. A., Ellis, R. S., Konidaris, N. P., & Stark, D. P. 2014, ApJ, 795, 20. 1404.4632

Simpson, J. M., Smail, I., Swinbank, A. M., Ivison, R. J., Dunlop, J. S., Geach, J. E., Almaini, O., Arumugam, V., Bremer, M. N., Chen, C.-C., Conselice, C., Coppin, K. E. K., Farrah, D., Ibar, E., Hartley, W. G., Ma, C. J., Michałowski, M. J., Scott, D., Spaans, M., Thomson, A. P., & van der Werf, P. P. 2017, ApJ, 839, 58. 1611.03084

Stanley, F., Alexander, D. M., Harrison, C. M., Rosario, D. J., Wang, L., Aird, J. A., Bourne, N., Dunne, L., Dye, S., Eales, S., Knudsen, K. K., Michałowski, M. J., Valiante, E., De Zotti, G., Furlanetto, C., Ivison, R., Maddox, S., & Smith, M. W. L. 2017, MNRAS, 472, 2221. 1707.05334

Treister, E., Schawinski, K., Volonteri, M., & Natarajan, P. 2013, ApJ, 778, 130. 1310.2249

Volonteri, M., Silk, J., & Dubus, G. 2015, ApJ, 804, 148. 1401.3513

Xu, L., Rieke, G. H., Egami, E., Haines, C. P., Pereira, M. J., & Smith, G. P. 2015, ApJ, 808, 159. 1508.02453

Zensus, J. A. 1997, ARA&A, 35, 607

Science with a Next-Generation Very Large Array
ASP Conference Series, Monograph 7
Eric J. Murphy, ed.

DRAFT EDITION

From Megaparsecs To Milliparsecs: Galaxy Evolution & Supermassive Black Holes with NANOGrav and the ngVLA

Stephen R. Taylor[1,2] and Joseph Simon,[2,1]
[1]*Theoretical AstroPhysics Including Relativity (TAPIR) Group, MC 350-17, California Institute of Technology, Pasadena 91125, CA, USA;* `srtaylor@caltech.edu.edu`

[2]*Jet Propulsion Laboratory, California Institute of Technology, 4800 Oak Grove Drive, Pasadena 91109, CA, USA;* `joseph.j.simon@jpl.nasa.gov`

1. Scientific Goals

Within the current paradigm of hierarchical cosmological structure formation, galaxy growth occurs through a continuous process of gas and dark matter accretion, interspersed with major and minor mergers (e.g Blumenthal et al. 1984). The fact that most massive galaxies are expected to harbor a supermassive black hole (SMBH) (Kormendy & Richstone 1995; Magorrian et al. 1998) has led to the understanding that central SMBHs share a common evolutionary history with their host galaxies. The prevalence of major mergers and the rate of gas accretion, both of which can contribute to the growth of SMBH and galaxy alike, are, as of yet, poorly constrained across cosmic time. One avenue for understanding the relative roles of these mechanisms is the study of post-merger galaxies, which are expected to harbor a "dual" SMBH system composed of the two black holes from each of the merging galaxies. Understanding the dynamical evolution of SMBH binaries in the rich physical environment of post-merger galactic environments is key to solving the puzzles of how SMBHs and galaxies co-evolve, how SMBHs grow over cosmic time, and how (or even if) the final stages of SMBH mergers take place in galaxy centers.

Precision timing of Galactic millisecond pulsars over the last decade has allowed the North American Nanohertz Observatory for Gravitational Waves (NANOGrav, and other collaborations around the globe) to use Arecibo, GBT, and VLA observations to forge a network of kiloparsec-spaced "clocks" that can respond to transiting nanohertz gravitational waves (GWs) through induced Doppler shifts of radio-pulse arrival rates. The dominant source of these nanohertz GWs is likely to be a population of SMBH binaries that are formed naturally in post-merger galaxies. The SMBHs from each galaxy will sink to the center of the common merger remnant through interactions with the galactic gas, stars and dark matter, and eventually become gravitationally bound as binaries (Begelman et al. 1980). Through continued interaction with the environment, the binaries' orbits will tighten and GW emission will become an increasingly dominant factor in their continued evolution. After sufficiently strong environmental interactions the binaries will eventually reach milliparsec orbital separation, at which point their GWs will be emitted in the Pulsar Timing Array (PTA) band at roughly nanohertz frequencies.

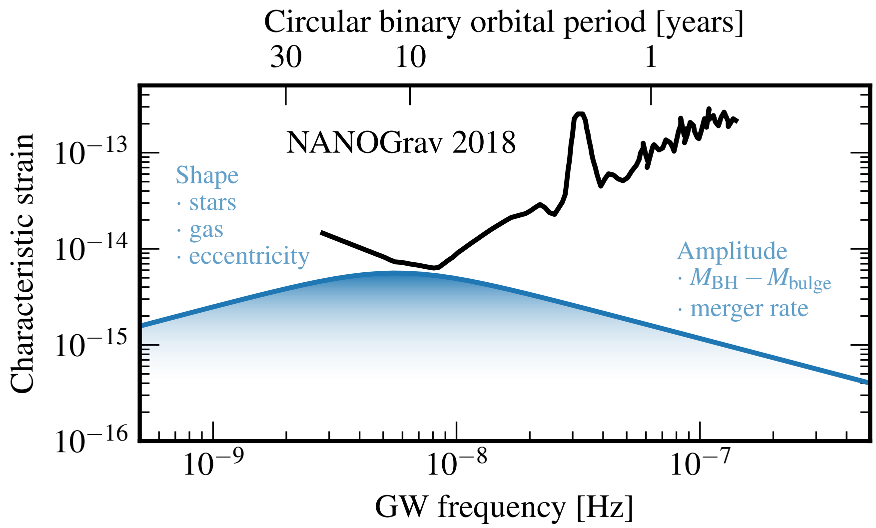

Figure 1. An illustration of the various astrophysical factors affecting the shape and amplitude of the characteristic strain spectrum of GWs emitted by a population of inspiraling supermassive black-hole binaries. This is contrasted against the per-frequency sensitivity of NANOGrav's most recent dataset, consisting of 45 millisecond pulsars with precision timing over an 11-year timescale. The spike at a frequency of 1 yr^{-1} corresponds to a loss in PTA sensitivity due to fitting each pulsar's position.

NANOGrav seeks to understand the evolution of galaxies and massive black-holes through cosmic time, as well as the dynamics of massive black-hole binaries formed through galaxy mergers. These goals intersect with the ngVLA science case in various ways; the most pertinent being:

- **Detection of a stochastic background of GWs from inspiraling SMBH binary systems**, thus proving that dynamical interactions in galactic centers can mitigate the "final parsec problem" of SMBH evolution, allowing SMBHs to merge in galaxy centers. *The ngVLA has a goal resolution of 30 mas, equivalent to* ~ 300 *pc at* $z \sim 1$*, which is sufficient to distinguish dual AGN and convert observed fractions of dual/multiple AGN into SMBH merger rates. These rate estimates can inform future NANOGrav observing strategies.*
- **Spectral characterization of the GW strain signal** which will lead to an inference of the dynamical processes influencing SMBH binaries at sub-parsec scales. The dominant process is expected to be scattering of stars on orbits that intersect the central galactic regions, or interaction with a viscous circumbinary disk. *If intercontinental VLBI capabilities are added to the ngVLA, it will achieve ~pc-scale resolution of central galactic regions out to* $z \sim 0.1$*. This will allow a large statistical sample of SMBH binary separations to be collected, thereby informing whether binaries stall at ~pc separations, or are driven efficiently inward.*
- **Constrain the scaling relationships between galactic bulge properties and central SMBHs** (Ferrarese & Merritt 2000; Gebhardt et al. 2000), thereby illumi-

nating the symbiotic evolution between the two, and shedding light on the growth of galaxies/SMBHs through cosmic time. *The ngVLA will be able to resolve the influence radius of* $10^9 M_\odot$ *supermassive black holes out to* $z \sim 0.1$, *drastically improving mass estimates that may lead to revisions of the* $M_{\rm BH} - M_{\rm bulge}$ *relationship.*

- **Understanding how accretion of gas onto SMBHs in the galactic center is related to the inflow of gas at larger scales**. There is some question of whether accretion of material from a circumbinary disk is an important mechanism of SMBH binary hardening, given that the resident massive galaxies should in general be gas poor. But this is highly uncertain. *ngVLA observations of gas reservoirs and inflow at larger scales, as well as gas dynamics in the innermost galaxy regions, will provide crucial constraints on gaseous accretion onto a central SMBH binary.*

2. SMBH Dynamical Evolution In Post-merger Galaxies

The dynamical evolution of SMBH binaries in post-merger galaxies is complex, involving a series of physical processes handing off to the next at ever smaller scales as the SMBHs become gravitationally bound, then tighten to milliparsec separations. We now describe the series of physical processes within post-merger galaxies that drive SMBHs to become gravitationally bound, and then to evolve as a binary into the nanohertz-emitting regime where PTAs are sensitive. At each stage, we comment on how ngVLA goals and observations interface with NANOGrav requirements.

2.1. Dynamical friction

When massive galaxies merge together, their resident SMBHs sink to the center of the resulting galactic remnant through *dynamical friction* (Merritt & Milosavljević 2005). This is the consequence of many weak and long-range gravitational scattering events within the surrounding stellar, gas, and dark matter distributions, creating a drag that causes the SMBHs to decelerate and transfer energy to the ambient media (Chandrasekhar 1943). For systems with extreme mass ratios ($\lesssim 10^{-2}$) or very low total masses, dynamical friction may not be effective at forming a bound binary from the two SMBH within a Hubble time. In this case the pair might become "stalled" at larger separations, with one of the two SMBH left to wander the galaxy at ~ kpc separations (Dvorkin & Barausse 2017). It is possible that a non-negligible fraction of galaxies may have such wandering SMBH, some of which may be observable as offset-AGN.

- If the ngVLA is expanded with intercontinental VLBI-like capabilities, the improvement in angular resolution over existing instruments will allow for direct imaging of systems that may contain off-set AGN to extend to much higher redshifts (Casey et al. 2015), thereby potentially gathering a large enough statistical sample to test this stalling hypothesis.

2.2. Stellar loss-cone scattering

At parsec separations, dynamical friction hands off to individual 3-body scattering events between stars in the galactic core and the SMBH binary (Begelman et al. 1980). Stars slingshot off the binary, which can extract orbital energy from the system

(Mikkola & Valtonen 1992; Quinlan 1996). However, only stars in centrophilic orbits with very low angular momentum have trajectories which bring them deep enough into the galactic center to interact with the binary. The region of stellar-orbit phase space that is occupied by these types of stars is known as the “loss cone" (LC) (Frank & Rees 1976). Stars which extract energy form the binary in a scattering event tend to be ejected from the core, depleting the LC. As with dynamical friction at larger scales, binaries can also stall here, at parsec scales, due to inefficiency of the LC-refilling —a phenomenon referred to as the “final parsec problem" (Milosavljević & Merritt 2003). Generally, binaries which don’t reach sub-parsec separations will be unable to merge via GW emission within a Hubble time (McWilliams et al. 2014).

Various mechanisms have been explored to see whether the LC can be efficiently refilled or populated to ensure continuous hardening of the binary down to milliparsec separations. In general, any form of bulge morphological triaxiality will ensure a continually-refilled LC that can mitigate the final-parsec problem (Vasiliev & Merritt 2013). Isolated galaxies often exhibit triaxiality, and given that the SMBH binaries of interest are the result of galactic mergers, triaxiality and general asymmetries can be expected as a natural post-merger by-product. Also, post-merger galaxies often harbor large, dense molecular clouds that can be channeled into the galactic center, acting as a perturber for the stellar distribution that will refill the LC (Young & Scoville 1991), or even directly hardening the binary (Goicovic et al. 2017).

- Current instruments cannot directly resolve molecular gas clouds within post-merger galaxies. However, the ngVLA will provide the sub-parsec resolution that is necessary to image these gas clouds (Bolatto et al. 2017). This will provide a much-needed causal link explaining how the LC can remain filled in different kinds of post-merger galaxies.

2.3. Viscous circumbinary disk interaction

At centiparsec to milliparsec separations, viscous angular momentum exchange to a gaseous circumbinary disk may play an important role in hardening the binary (Begelman et al. 1980; Kocsis & Sesana 2011). This influence will depend on the details of the dissipative physics of the disk. The simplest model is that of a coplanar prograde α-disk (Shakura & Sunyaev 1973), where the binary torques the disk and carves out a cavity where no gas flows. The individual SMBHs may be surrounded by smaller “mini-disks”. More complex disk structures are possible, such as the existence of several physically-distinct regions (Shapiro & Teukolsky 1986). Additionally, high-density disks (equivalently: high-accretion rates) may provide rapid hardening, but are potentially unstable. Furthermore, hardening rates will change as the system passes through different types of migration based on the interaction between the secondary SMBH and the disk — at larger separations the secondary SMBH is driven along with the gas flow, whereas when the mass enclosed by the binary orbit becomes comparable to the secondary SMBH the system is driven by binary dynamics.

- All of these complicated processes are happening on scales that are beyond the reach of current observational instruments. The ngVLA may have the capability to resolve the cold gas reservoirs feeding these disks and the subsequent AGN (Nyland et al. 2018).

2.4. Gravitational-wave inspiral

The emission of gravitational radiation will always dominate binary orbital evolution at the smallest separation scales ($\lesssim$ milliparsec). This is when the binary has decoupled from the galactic environment and can be considered as an isolated physical system. In this case, the dissipation of orbital energy will depend only on the constituent SMBH masses, the orbital semi-major axis, and the binary's eccentricity.

- This stage is below the angular resolution scale of the ngVLA, and will require PTA observations of nanohertz GWs to complete the picture of SMBH dynamical evolution.

3. Anticipated Complementary Results

NANOGrav's key goal is the detection and characterization of GWs at nanohertz frequencies, with the target being a population of inspiraling SMBH binaries. The stochastic gravitational wave background (GWB) signal produced by a population of inspiraling SMBH binaries can be described by its characteristic-strain spectrum, $h_c(f)$. The strain budget at different frequencies depends on various cosmological and astrophysical factors (Sesana et al. 2004), which are summarized in Figure 1 and in the following. In the simple case of a population of circular binaries whose orbital evolution is driven entirely by the emission of GWs, $h_c(f) \propto f^{-2/3}$.

Interaction of a binary with its surrounding galactic stellar distribution, as described in Section 2.2, will lead to low-frequency attenuation of the characteristic strain spectrum of GWs (i.e. a spectral turnover). This can be separated into two distinct effects: (1) the direct coupling leads to a faster reduction in the orbital separation than GW-driven inspiral, such that the amount of time spent by each binary at low frequencies is reduced; (2) extraction of angular momentum by stellar slingshots can excite eccentricity, which leads to faster GW-driven inspiral, and (again) lower residence time at low frequencies. The excitation of binary eccentricity by interaction with stars will further attenuate the strain spectrum at low frequencies, leading to an even sharper turnover (e.g. Taylor et al. 2017). Coupling of a viscous circumbinary disk with a SMBH binary, as discussed in Section 2.3, will also lead to attenuation of the characteristic strain spectrum of GWs through both direct coupling, and excitation of eccentricity.

3.1. Detection of stochastic background

NANOGrav expects to detect the nanohertz GWB within the next 2-3 years (Taylor et al. 2016). This initial detection will likely be of a long-timescale stochastic process, present in all pulsars and correlated between them with a signature unique to GWs. But it is unlikely that the shape of the spectrum will be very well constrained. Nevertheless, detection alone is sufficient to provide the first direct evidence that the final parsec problem of massive black-hole evolution is mitigated, and even with poorly constrained parameters, there will be many models of post-merger galactic environments that will be ruled out.

3.2. Spectral characterization of background

Over the next decade, NANOGrav's sensitivity will improve to the stage at which the slope of the GW strain spectrum will be well constrained. This will allow for robust inference of the dominant dynamical process for SMBH binary evolution. However, the entire population will consist of a mixture of galaxy types and dynamical environmental processes. Thus, it will only be through the combination of NANOGrav data with models built from the in-depth surveys of galactic cores, like those the ngVLA will conduct, that a complete understanding of the conditions under which the final parsec problem is mitigated will be gained.

3.3. Constraining the scaling relationships between galaxies and central SMBHs

NANOGrav limits on the stochastic GWB can already be expressed directly as limits on various model parameters, and the scaling relationship between galactic bulge properties and central SMBH masses has been shown to be one of the most important model parameters (Simon & Burke-Spolaor 2016; Arzoumanian et al. 2018). In the coming years, NANOGrav will place tight constraints on the galaxy-SMBH scaling relationship, specifically for SMBHs in post-major-merger galaxies. As with constraints on the strain-spectrum slope, these constraints on the scaling relation can only be properly used to make a clear statement about galaxy growth when combined with electromagnetic observations of the associated galactic bulges. To this end, the ngVLA's proposed capabilities will allow resolution down to the influence radius of $10^9 M_\odot$ SMBHs out to $z \sim 0.1$, which is more than sufficient to characterize properties of galactic bulges and to measure the SMBH mass.

3.4. Accretion onto SMBH

NANOGrav's spectral characterization of the GWB signal will illuminate the important dynamical processes that harden SMBH binaries to milliparsec separations. This will allow a measurement of various astrophysical parameters, such as the mass density of loss-cone stars in galactic centers, binary eccentricities, and SMBH accretion rates. Inference of the latter will of course depend on the assumed disk dynamics, but will ultimately describe the relevance of gas dynamics are in this overall picture of SMBH dynamical evolution. It may be the case that the kinds of SMBHs that we are looking for reside in gas-poor massive galaxies, in which case stellar scattering will control the evolution at sub-parsec separations until GW-driven inspiral begins to dominate. We currently lack sufficient observational constraints on circumbinary disk dynamics to inform our intuition of its importance. The ngVLA will measure the accretion and build-up of H1 gas in galactic outskirts, track gas inflow to central regions, and (with expanded VLBI capabilities) be able to resolve down to the ~pc scale out to $z \sim 0.1$. It will therefore give crucial insight into the importance of gas dynamics in SMBH evolution.

4. Summary & Synergies

Pulsar-timing arrays (such as NANOGrav) will detect the ensemble gravitational-wave signal from many inspiraling supermassive black-hole binaries throughout the Universe within the next $3 - 7$ years (Taylor et al. 2016). The statistical properties of this signal will reflect the dynamical history of these supermassive black-holes as they evolve to form a bound system and reach milliparsec orbital separations. NANOGrav will constrain the environments of supermassive black-hole binaries (Taylor et al. 2017) through detailed studies of the gravitational-wave strain spectrum in the nanohertz band. The ngVLA has a goal resolution of 30 mas, equivalent to $\sim$ 300 pc at $z \sim 1$. This resolution is sufficient to distinguish dual AGN, allowing estimates of SMBH merger rates to be formed that can act as prior constraints for PTA analysis. Furthermore, if intercontinental VLBI capabilities are added to the ngVLA it will achieve ~pc-scale resolution out to $z \sim 0.1$, allowing a large measured sample of SMBH binary separations to inform whether binaries stall at ~pc separations or are driven efficiently to the sub-pc regime by dynamical interactions. Intercontinental VLBA will also allow the influence radius of supermassive black-holes to be resolved, which will drastically improve mass estimation and thus the fidelity of derived $M_{\rm BH} - M_{\rm bulge}$ relationships. Finally, ngVLA observations of galactic gas reservoirs, large-scale inflows, and gas dynamics in central galactic regions will provide crucial insight into the physics of SMBH binary accretion processes.

There are several current and future facilities that will complement the ngVLA in the aforementioned areas. These include the *Atacama Large Millimeter/submillimeter Array* (ALMA)[1], whose angular resolution at 230 GHz with baseline length of 15 km is 15 mas, which is comparable to the ngVLA's goal resolution of 30 mas at 40 GHz with a baseline length of 180 km (Casey et al. 2015). Likewise, the ngVLA should have similar angular resolution to adaptive-optics corrected images from the *Giant Magellan Telescope* (GMT)[2], *Thirty Meter Telescope* (TMT)[3], and the *Extremely Large Telescope* (ELT)[4]. This range of complementarity in angular resolution will allow for validation and comparison studies of sub-kiloparsec galaxy scales out to $z \sim 1$, which is sufficient to distinguish dual AGN for the purpose of estimating SMBH binary merger rates. On the other hand, the SKA[5] is expected to operate concurrently with the ngVLA, but its point-source sensitivity will be only be half that of the ngVLA in their frequency-overlap band (Casey et al. 2015). Similarly, JWST[6] will operate at similar wavelengths to GMT/TMT/ELT, but have lower angular resolution than those instruments and the ngVLA.

NANOGrav gravitational-wave analysis, in concert with observations by the ngVLA and complementary facilities, will paint a multi-messenger portrait of galaxy evolution and the dynamics of the most massive black-holes in the Universe.

Acknowledgments. The NANOGrav project receives support from NSF Physics Frontier Center award number 1430284. SRT acknowledges support from the NANOGrav Physics Frontier Center. JS acknowledge support from the JPL RTD program. Some of this research was undertaken at the Jet Propulsion Laboratory, California Institute of Technology, under a contract with the National Aeronautics and Space Administration.

[1] http://www.eso.org/public/usa/teles-instr/alma

[2] https://www.gmto.org

[3] https://www.tmt.org

[4] https://www.eso.org/public/usa/teles-instr/elt

[5] https://www.skatelescope.org

[6] https://www.jwst.nasa.gov

References

Arzoumanian, Z., Baker, P. T., Brazier, A., Burke-Spolaor, S., Chamberlin, S. J., Chatterjee, S., Christy, B., Cordes, J. M., Cornish, N. J., Crawford, F., Thankful Cromartie, H., Crowter, K., DeCesar, M., Demorest, P. B., Dolch, T., Ellis, J. A., Ferdman, R. D., Ferrara, E., Folkner, W. M., Fonseca, E., Garver-Daniels, N., Gentile, P. A., Haas, R., Hazboun, J. S., Huerta, E. A., Islo, K., Jones, G., Jones, M. L., Kaplan, D. L., Kaspi, V. M., Lam, M. T., Lazio, T. J. W., Levin, L., Lommen, A. N., Lorimer, D. R., Luo, J., Lynch, R. S., Madison, D. R., McLaughlin, M. A., McWilliams, S. T., Mingarelli, C. M. F., Ng, C., Nice, D. J., Park, R. S., Pennucci, T. T., Pol, N. S., Ransom, S. M., Ray, P. S., Rasskazov, A., Siemens, X., Simon, J., Spiewak, R., Stairs, I. H., Stinebring, D. R., Stovall, K., Swiggum, J., Taylor, S. R., Vallisneri, M., van Haasteren, R., Vigeland, S., Zhu, W. W., & The NANOGrav Collaboration 2018, ApJ, 859, 47. 1801.02617

Begelman, M. C., Blandford, R. D., & Rees, M. J. 1980, Nat, 287, 307

Blumenthal, G. R., Faber, S. M., Primack, J. R., & Rees, M. J. 1984, Nat, 311, 517

Bolatto, A. D., Chatterjee, S., Casey, C. M., Chomiuk, L., de Pater, I., Dickinson, M., Di Francesco, J., Hallinan, G., Isella, A., Kohno, K., Kulkarni, S. R., Lang, C., Lazio, T. J. W., Leroy, A. K., Loinard, L., Maccarone, T. J., Matthews, B. C., Osten, R. A., Reid, M. J., Riechers, D., Sakai, N., Walter, F., & Wilner, D. 2017, ArXiv e-prints. 1711.09960

Casey, C. M., Hodge, J. A., Lacy, M., Hales, C. A., Barger, A., Narayanan, D., Carilli, C., Alatalo, K., da Cunha, E., Emonts, B., Ivison, R., Kimball, A., Kohno, K., Murphy, E., Riechers, D., Sargent, M., & Walter, F. 2015, NRAO Next Generation Very Large Array Memos Series. 1510.06411, URL http://library.nrao.edu/ngvla.shtml

Chandrasekhar, S. 1943, ApJ, 97, 255

Dvorkin, I., & Barausse, E. 2017, MNRAS, 470, 4547. 1702.06964

Ferrarese, L., & Merritt, D. 2000, ApJ, 539, L9. astro-ph/0006053

Frank, J., & Rees, M. J. 1976, Monthly Notices of the Royal Astronomical Society, 176, 633

Gebhardt, K., Bender, R., Bower, G., Dressler, A., Faber, S. M., Filippenko, A. V., Green, R., Grillmair, C., Ho, L. C., Kormendy, J., Lauer, T. R., Magorrian, J., Pinkney, J., Richstone, D., & Tremaine, S. 2000, ApJ, 539, L13. astro-ph/0006289

Goicovic, F. G., Sesana, A., Cuadra, J., & Stasyszyn, F. 2017, MNRAS, 472, 514. 1602.01966

Kocsis, B., & Sesana, A. 2011, MNRAS, 411, 1467. 1002.0584

Kormendy, J., & Richstone, D. 1995, ARA&A, 33, 581

Magorrian, J., Tremaine, S., Richstone, D., Bender, R., Bower, G., Dressler, A., Faber, S. M., Gebhardt, K., Green, R., Grillmair, C., Kormendy, J., & Lauer, T. 1998, AJ, 115, 2285. astro-ph/9708072

McWilliams, S. T., Ostriker, J. P., & Pretorius, F. 2014, ApJ, 789, 156. 1211.5377

Merritt, D., & Milosavljević, M. 2005, Living Reviews in Relativity, 8. astro-ph/0410364

Mikkola, S., & Valtonen, M. J. 1992, MNRAS, 259, 115

Milosavljević, M., & Merritt, D. 2003, in The Astrophysics of Gravitational Wave Sources, edited by J. M. Centrella, vol. 686 of American Institute of Physics Conference Series, 201. astro-ph/0212270

Nyland, K., Harwood, J. J., Mukherjee, D., Jagannathan, P., Rujopakarn, W., Emonts, B., Alatalo, K., Bicknell, G., Davis, T. A., Greene, J., Kimball, A., Lacy, M., Lonsdale, C., Lonsdale, C., Maksym, W. P., Molnar, D., Morabito, L., Murphy, E., Patil, P., Prandoni, I., Sargent, M., & Vlahakis, C. 2018, ArXiv e-prints. 1803.02357

Quinlan, G. D. 1996, New Astronomy, 1, 35. astro-ph/9601092

Sesana, A., Haardt, F., Madau, P., & Volonteri, M. 2004, ApJ, 611, 623. astro-ph/0401543

Shakura, N. I., & Sunyaev, R. A. 1973, A&A, 24, 337

Shapiro, S. L., & Teukolsky, S. A. 1986, Black Holes, White Dwarfs and Neutron Stars: The Physics of Compact Objects (John Wiley & Sons)

Simon, J., & Burke-Spolaor, S. 2016, ApJ, 826, 11. 1603.06577

Taylor, S. R., Simon, J., & Sampson, L. 2017, Physical Review Letters, 118, 181102. 1612.02817

Taylor, S. R., Vallisneri, M., Ellis, J. A., Mingarelli, C. M. F., Lazio, T. J. W., & van Haasteren, R. 2016, ApJ, 819, L6. 1511.05564
Vasiliev, E., & Merritt, D. 2013, ApJ, 774, 87. 1301.3150
Young, J. S., & Scoville, N. Z. 1991, ARA&A, 29, 581

Part VIII

The Formation and Evolution of Black Holes in the Era of Multi-Messenger Astronomy:

Science with a Next-Generation Very Large Array
ASP Conference Series, Monograph 7
Eric J. Murphy, ed.

DRAFT EDITION

Supermassive Black Hole Pairs and Binaries

Sarah Burke-Spolaor[1,2], Laura Blecha[3], Tamara Bogdanović[4], Julia M. Comerford[5], Joseph Lazio[6], Xin Liu[7], Thomas J. Maccarone[8], Dominic Pesce[9,10], Yue Shen[7], and Greg Taylor[11]

[1] *Department of Physics and Astronomy, West Virginia University, Morgantown WV 26505, USA;* `sarah.spolaor@mail.wvu.edu`

[2] *Center for Gravitational Waves and Cosmology, West Virginia University, Morgantown WV 26501, USA*

[3] *Department of Physics, University of Florida, Gainesville, FL 32611, USA;* `lblecha@ufl.edu`

[4] *Center for Relativistic Astrophysics, Georgia Institute of Technology, Atlanta, GA 30332, USA;* `tamarab@gatech.edu`

[5] *Department of Astrophysical and Planetary Sciences, University of Colorado, Boulder, CO 80309, USA;* `Julie.Comerford@colorado.edu`

[6] *Jet Propulsion Laboratory, California Institute of Technology, Pasadena CA, 91109, USA*

[7] *Department of Astronomy, University of Illinois at Urbana-Champaign, Urbana, IL 61801, USA;* `xinliuxl@illinois.edu`, `shenyue@illinois.edu`

[8] *Department of Physics & Astronomy, Texas Tech University, Lubbock, TX 79409-1051, USA*

[9] *Department of Astronomy, University of Virginia, 530 McCormick Road, Charlottesville, VA 22904, USA*

[10] *National Radio Astronomy Observatory, 520 Edgemont Road, Charlottesville, VA 22903, USA;* `dpesce@virginia.edu`

[11] *Department of Physics and Astronomy, University of New Mexico, Albuquerque, NM 87131, USA;* `gbtaylor@unm.edu`

1. The Importance and Impact of Binary Supermassive Black Hole Observations

The ngVLA will be a powerful probe of dual and binary supermassive black holes (SMBHs), performing detailed studies of their population and evolution, and enabling powerful multi-messenger science when combined with gravitational-wave detection. The ngVLA will enable such studies by an unprecedented combination of sensitivity, frequency coverage, and particularly if equipped with long baselines, essentially unparalleled angular resolution.

Dual ($\lesssim 10$ kpc separation) and binary ($\lesssim 10$ pc separation) SMBH systems can form during major galaxy mergers. Figure 1 illustrates the formation and evolution of double SMBH systems, from the initial stages of a merger of galaxies to the emission of gravitational waves to an SMBH merger (Begelman et al. 1980). When one or both SMBHs power an active galactic nucleus, multi-wavelength emission can directly mark the presence and locations of the SMBHs. Jets produced by these active nuclei will generate radio emission. Because jet cores closely trace the location of a SMBH, and because of the extended lifetime of synchrotron jet observability, radio observations both at high resolution and of larger-scale jet structures provide excellent tools to trace the current and past dynamics of SMBHs in a merging system.

SMBH pairs confidently mark ongoing galaxy mergers and imminent SMBH coalescences, and are therefore a strong probe of redshift-dependent merger rates, occupation fractions of dual SMBHs in galaxies, and post-merger dynamical evolution. If we determine the rate and environments of systems containing two or more widely separated active galactic nuclei (AGN), we can explore merger-induced activity of nuclei and susbequent SMBH growth. These dual AGN probe the critical regime during which the black holes and their associated galactic-scale stellar cores are virialized (e.g., within ~10 kpc black hole separation). During this phase, both star formation and AGN activity peak during galaxy mergers, according to cosmological simulations (Blecha et al. 2013). Having a sample of dual AGN is key to testing predictions from simulations, such as whether the most luminous AGN are preferentially triggered in mergers and whether there is a time-lag between star formation triggering and AGN triggering in mergers (Hopkins 2012; Hopkins et al. 2014).

A systematic survey of dual and binary SMBHs also allows a direct prediction of the projected gravitational wave signals in the low and very low frequency regime of gravitational radiation. Both pulsar timing arrays (PTAs) and future space-based laser interferometers have binary SMBHs as a key target. They may detect both "discrete" individual targets, and a stochastic background of small-orbit SMBH binaries.

The ngVLA will also be coming online at a time when PTAs like the North American Nanohertz Observatory for Gravitational Waves (NANOGrav) expects to have already detected a number of discrete binary SMBHs (e.g., Mingarelli et al. 2017; Kelley et al. 2017b). LISA is expected to directly constrain SMBH binary coalescence rates soon after its launch (Klein et al. 2016; Amaro-Seoane et al. 2017). Gravitational-wave and multi-messenger astronomy with SMBHs will thus be a leading pursuit of the ngVLA era. Particularly with long (VLBI) baselines, ngVLA will have the potential to identify the hosts of emitting gravitational-wave systems, enabling broad-scoped science that includes:

- Precise orbital tracking of binary SMBHs via parsec-scale jet morphology and core tracking (Bansal et al. 2017).
- Use of SMBHs as a standard ruler (D'Orazio & Loeb 2017).
- Measurement of merger-induced accretion rates and imaging of small-scale AGN feedback (Müller-Sánchez et al. 2015)
- Detailed multi-wavelength and multi-messenger studies of circumbinary disk evolution and binary inspiral timescales (e.g., Kelley et al. 2017a).
- Calibration of SMBH-host relations up to moderate/high redshifts via direct SMBHB mass measurements (host identification breaks the distance/mass degeneracy encountered in PTA discrete source detection).

In the remainder of this chapter, we describe the various approaches that can be used to identify SMBH pairs with the ngVLA (Sec. 2), compare those with past searches

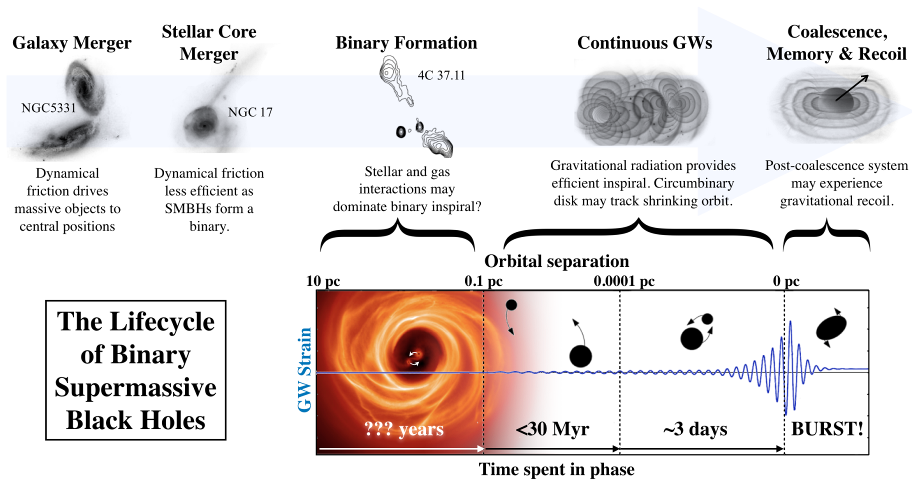

Figure 1. Figure from Burke-Spolaor et al. (2018), summarizing the binary SMBH life-cycle. A major unknown in binary evolution theory is the efficiency of inspiral from ~10 pc down to ~0.1 pc separations, after which the binary can coalesce efficiently due to gravitational waves. The ngVLA will discover widely separated binaries, and depending on its long-baseline sensitivity, could discover targets detectable by pulsar timing arrays (PTAs). PTAs such as NANOGrav can detect supermassive ($> 10^8$ $M_\odot$) binaries within ~0.1 pc separation (second panel in the lower figure). On rare occasion, PTAs may detect the permanent space-time deformation (GW memory) caused by a binary's coalescence (Favata 2009). LISA will detect lower-mass binaries, up to $\sim 10^7$ $M_\odot$, in the weeks or months leading up to coalescence. Image credits: Galaxies, Hubble/STSci; 4C37.11, Rodriguez et al. (2006); Simulation visuals, C. Henze/NASA; Circumbinary accretion disk, C. Cuadra.

in Sec. 3, and discuss synergies with multi-wavelength observations in Sec. 4. Finally, Sec. 3 lays out several example ngVLA studies and their general requirements for success.

2. Identifying Paired SMBHs with Radio Emission

The ngVLA could be used to conduct surveys for SMBH pairs, follow up candidates identified in other surveys, or both. Either way, in order to reveal dual or binary SMBH candidates with the ngVLA, a few identification methods are available. ngVLA can identify pairs through studies of morphology, spectra, and/or time-dependence of the bulk relativistic flow of particles from the SMBHs.

2.1. Direct Core Imaging

Radio imaging of multiple self-absorbed synchrotron cores in the ~1–50 GHz frequency range is one of the most direct routes to identify dual SMBHs. It is exceedingly rare to find bright multiple flat-spectrum objects within close proximity (e.g., Rodriguez et al. 2006; Burke-Spolaor 2011). The radio "core" that is seen in SMBHs represents the shock front near the base of the radio jet, which is compact and in a region of considerable optical depth. These can show a flat spectrum (with spectral index $\alpha \gtrsim -0.5$, where $S \propto f^{\alpha}$) up to moderate GHz frequencies (e.g., Blandford & Königl 1979). This technique relies on detecting more than one flat-spectrum, compact radio source within a common merger host. Confident confirmation of the nature of such detections requires

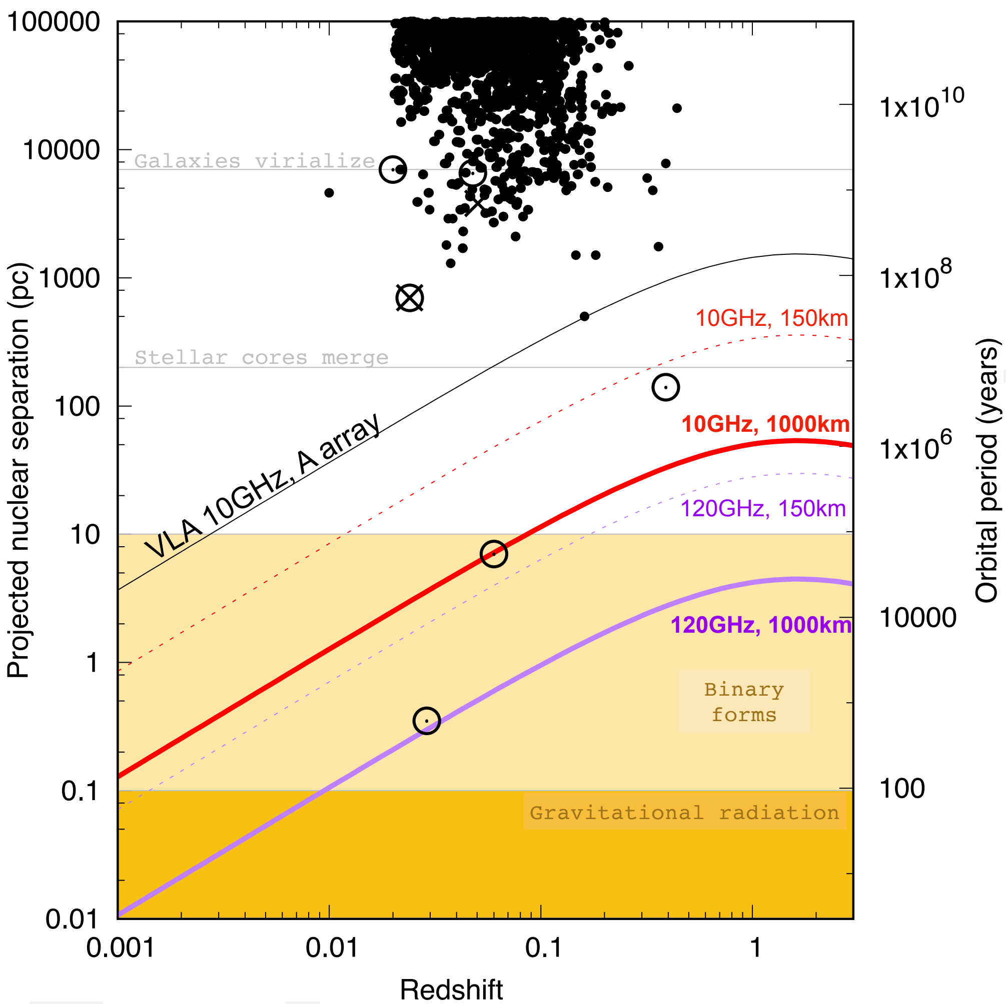

Figure 2. The observed population of candidate AGN pairs to date compared with the resolution of the ngVLA. Each point represents a dual AGN discovered via radio (X), X-ray (circles), or optical/near-IR (dots; from Liu et al. 2011). Approximate lines for critical stages in binary formation and evolution are marked as horizontal lines. The red, green, and purple curves indicate the resolution limit of 10 GHz, 50 GHz, and 120 GHz center observing bands, respectively; for each observing set-up, one cannot resolve a binary orbit below that line. The dashed curves show the resolution limit of 150 km baselines, while the solid curves show a nominal 1000 km extended-baseline array. The ngVLA with a VLBI expansion can resolve, and hence directly image and identify, double supermassive black holes at sub-10 pc separations. Longer baselines and higher frequencies have the potential to resolve multi-messenger SMBH binaries in the nearby Universe (indicated by the curves that cross the dark yellow region).

modelling of broad-band continuum spectra, high-resolution morphological modelling, and ideally long-term studies of proper motion. For instance, in the object 4C37.11 (Fig. 1), there are two cores at a projected separation of 7 pc that remain compact down to sub-mas resolutions, with larger-scale diffuse emission that support the interpretation of the two knots as distinct, but gravitationally interacting, SMBHs. Long-term astrometric observations of this object have led to the first tentative "orbital tracking" for a resolved binary, although its orbital period is fairly long at $\sim 10^4$ yr (Bansal et al. 2017).

Figure 2 shows a census of known and candidate resolved (imaged) dual SMBHs. Uniquely, radio identifications have probed separations within a few hundred parsecs: the radius of a typical galactic stellar bulge (Merritt & Milosavljević 2005). Double black hole systems with separations smaller than a few tens of parsecs are *direct precursors* to the gravitational-wave emitters detectable by PTAs and space-based laser interferometers, so are of utmost interest to the target science outlined in Section 1. There is only one confident binary in this range (Rodriguez et al. 2006), and only a scant list of candidates (Deane et al. 2014; Kharb et al. 2017).

Binary SMBHs are relatively rare, and performing a complete blind search for dual radio cores requires relatively high dynamic range and thorough u, v coverage at high resolution. Present facilities have aspects of these but not all. While the VLA has excellent sensitivity and u, v coverage, it lacks sufficient resolution to discover close pairs. While current long-baseline facilities have excellent resolution, they lack the snapshot sensitivity and u, v coverage to thoroughly probe cores (e.g., Deller & Middelberg 2014). The ngVLA has a unique potential to reach a balance between these factors (Bansal et al. in prep).

2.2. Jet Morphology

Identification of dual AGN via large-scale jet morphology is somewhat fraught because of the difficulty in discerning external vs. internal influences on the jet(s). Dual AGN emitting on long time scales can produce quadruple jets (Fig. 3), and binary interactions can result in precessing jets that produce large-scale S-shaped radio jet morphologies. Parabolic SMBH-SMBH encounters and binary coalescences can rapidly reorient a jet, potentially producing X-shaped morphologies (Merritt & Ekers 2002). Previous large-scale radio surveys (e.g.,, NVSS, FIRST) have had a strong output of candidate binary or post-merger SMBHs identified through their large-scale jet morphologies. Recent surveys of such radio jet morphologies include 87 X-shaped radio jets found with the VLA (Roberts et al. 2018). However, past studies have revealed that many such morphologies can be described by backwards-flows of expelled jet material caused by fluid dynamics, rather than originating from a dual system (Saripalli & Subrahmanyan 2009).

Still, some (as shown in Fig. 3) have been demonstrated either conclusively or extensively as candidate genuine dual AGN. Broad searches for such features require low-surface-brightness sensitivity coupled with resolution.

Large-scale periodic knots along radio jets have also been hypothesized to be periodic accretion episodes fueled by a binary; however, these are difficult to distinguish from flow instabilities (Godfrey et al. 2012).

2.3. Variability in Morphology or Flux

Some radio quasars show light curves that appear to be periodic or sinusoidal. At high spatial resolutions, some jets have morphological variability: e. g. 1928+738 has jets that trace out helical patterns as a function of time (Figure 3; Roos et al. 1993). A

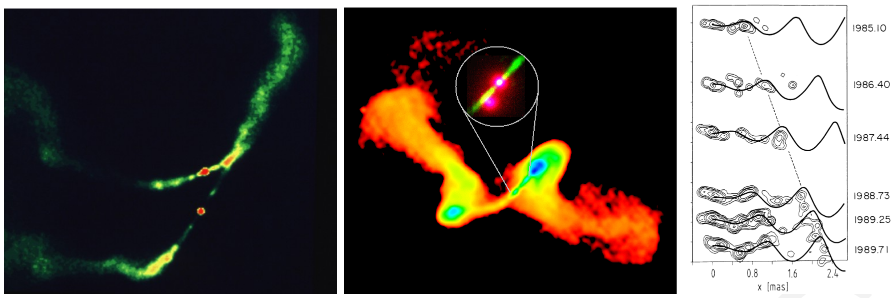

Figure 3. Three examples of candidate dual AGN identified through their static or time-dependent radio jet morphology (Sections 2.2, 2.3). *Left:* 3C 75, the dual cores of which have a 7 kpc projected separation and exhibits large-scale jet structures that have misaligned but correlated morphology. (Credit: NRAO/AUI; F. N. Owen, C. P. O'Dea, M. Inoue, & J. Eilek). *Center:* NGC 326, which has an X-shaped structure that inspired its dual nucleus interpretation. The cores were confirmed at other wavelengths, as shown. (Credit: NRAO/AUI; STScI [inset]). *Right:* The helical jet of 1928+738 shows a 2.9-year cycle (Roos et al. 1993).

common interpretation of both of these effects is that an accreting, jet-producing black hole has a jet axis whose angle is being modified by a secondary, orbiting SMBH. Confident identification of a periodicity in a light curve requires long-term variability monitoring (over more than a few cycles) to ensure that the observed variability is genuinely cyclical, and not simply the detection of a red noise process (Vaughan et al. 2016; Charisi et al. 2018). Thus, light curve variability programs require a long-term time investment for candidate binary identification.

As with the tracking of 4C37.11 (Bansal et al. 2017), in an ideal case we will be able to track the orbital movements of one or two distinct cores. However, making the simple but suitable assumption that binaries are circular and obey Kepler's third law, their approximate largest physical separation scales with binary period as $a \propto P^{2/3}$. This means that the majority of resolvable binaries will have orbital periods well beyond human lifetimes. Tracking the orbital motion will only be possible for long baselines, and for the massive compact systems at low redshifts. With long-baseline (~10,000 km) arrays, such observations will be possible for $10^9 M_\odot$ radio-emitting binaries with few parsec separations out to $z \sim 0.1$ on timescales of a few years. This clearly underscores the importance of a VLBI option for the ngVLA. If ngVLA baselines are limited to 300 km, then the timescales for resolving orbital properties will increase by a factor of 200, essentially making the ngVLA unsuitable for such studies despite its terrific snapshot sensitivity.

2.4. Maser Dynamics

Long-baseline observations of masers have been instrumental in finding SMBH masses and analyzing accretion disk dynamics (e.g., Miyoshi et al. 1995, Braatz et al. 2010, Kuo et al. 2013, Gao et al. 2016). Deviations from Keplerian motion in the maser rotation curves can indicate that the potential is not that of a point source (e.g., Kuo et al. 2011), and they can therefore be sensitive to close SMBH binaries (i.e., orbital separations of roughly ~0.01–0.1 pc).

For wider SMBH binaries (~1–100 pc separation), the maser rotation curve is not expected to be substantially different from Keplerian. In this case, one can compare the barycenter velocity derived from the maser rotation curve (which unambiguously traces the SMBH velocity) to that of the galaxy on large scales (~10's of kpc, traced using stellar or HI dynamics). Significant differences between these two velocities are then indicative of binary or recoiling SMBHs, although a measurement of a velocity offset cannot by itself distinguish between the two possibilities (Pesce et al. 2018, submitted to ApJ).

3. Current Radio Searches and Limitations

In the past, most radio-identified candidate binary SMBHs have mainly been found serendipitously. A few concerted efforts have attempted to survey directly for binary SMBHs. Here we discuss these, their successes, and limitations.

A number of blind or semi-blind searches have been made for dual radio cores, which as described in Sec. 2.1 is most easily realized through spectral imaging to search for multiple compact, flat-spectrum radio components. Burke-Spolaor (2011) searched all available historical data from the Very Long Baseline Array with dual-frequency imaging; despite the large sample size (~3200 AGN), this search was limited primarily by sensitivity. The VIPS survey of radio cores (Helmboldt et al. 2007) originally discovered 4C37.11 as an extended flat-spectrum object; this source was later evidenced to be a binary SMBH (Rodriguez et al. 2006). Tremblay et al. (2016) performed multi-frequency imaging of the flux-limited ~1100 AGN included in VIPS, all of which were pre-selected to be bright and flat-spectrum. This search did not identify any new binary systems from the VIPS sample, and concluded that 15 candidates remained unconfirmed. Finally, Condon et al. (2011) performed deep observations of 834 radio-bright 2MASS galaxies, under the hypothesis that the most massive galaxies must have undergone a major merger in their history, and therefore might contain a binary or recoiling SMBH. So far from these surveys, only one resolved dual core, 4C37.11, was re-detected. On simple arguments of merger rates, inspiral timescales, and radio AGN luminosity functions, at least tens of SMBH pairs must exist within these samples; thus, it is clear that these past experiments have been limited by a combination of u, v coverage, sensitivity, dynamic range, and perhaps sample size.

4. Current Multi-wavelength Synergies and Limitations

Dual and binary SMBH signatures have been proposed in a number of wavebands (see, e.g.,, the review in Burke-Spolaor 2013), and searches pursuing those signatures have revealed a number of binary candidates. We note that in all cases SMBH binaries have been challenging to identify because of their small separation on the sky, the uncertainties related to the uniqueness of their observational signatures, and the limited baseline of monitoring campaigns. Direct radio imaging, however, can provide an excellent follow-up to explore the nature of objects identified with these signatures.

The most prolific binary search method thus far has been the use of photometric and spectroscopic optical signatures to reveal candidate SMBH binaries. We describe that work here given its relevance to upcoming synoptic sky surveys that will be contemporary to ngVLA.

Multi-wavelength (radio, optical, and X-ray) searches for SMBH systems with large separations, corresponding to early stages of galactic mergers, have so far successfully identified a number of dual and offset AGN, as shown in Fig. 3 (Komossa et al. 2003; Fu et al. 2011; Koss et al. 2011, 2016; Liu et al. 2013; Comerford et al. 2015; Barrows et al. 2016; Müller-Sánchez et al. 2015, and others).

SMBHs with even smaller (parsec and sub-parsec) separations are representative of the later stages of galactic mergers in which the two SMBHs are sufficiently close to form a gravitationally bound pair. Direct imaging using VLBI can confidently detect such a system, however requires deep observations to do so successfully. In this regard, optical surveys can help to identify a sample of SMBH binaries for VLBI followup (see Bogdanović 2015, for a review). Current studies have been exploring periodic quasar variability as a potential indicator for binary SMBH emissions; these and future surveys of this kind using synoptic instruments like PAN-STARRS and LSST will reveal many candidate binary systems ideal for follow-up with the ngVLA plus a long-baseline extension.

Current photometric surveys have already uncovered about 150 SMBH binary candidates (e.g., Valtonen et al. 2008; Graham et al. 2015; Charisi et al. 2016; Liu et al. 2016). In this approach, the quasi-periodic variability in the lightcurves of monitored quasars is interpreted as a manifestation of binary orbital motion. Because of the finite temporal extent of the surveys, most of these candidates have orbital periods of order a few years, hence would be in the regime of gravitational-radiation-dominated inspiral (Fig. 1). However, studies of this type suffer the same red-noise issues noted in Sec. 2.3. A recent, initially quite promising binary SMBH candidate from a quasar light curve, PG1302, has recently been losing traction. Additional data from the All-Sky Automated Survey for Supernovae (ASAS-SN), extending the light curve to present-day, shows that the periodicity does not persist and disfavors the binary SMBH interpretation (Liu et al. 2018). Furthermore, the upper limit placed by PTAs on the gravitational wave background largely rules out the amplitude implied by the $\sim$ 150 photometric binary candidates, implying that some significant fraction of them are unlikely to be SMBH binaries (Sesana et al. 2017). While this will lead to a downward revision in the number of photometrically identified SMBH binary candidates, it provides a nice example of the effectiveness of multi-messenger techniques, when they can be combined.

Spectroscopic searches for SMBH binaries have so far identified several dozen candidates. They rely on the detection of a velocity shift in the emission-line spectrum of an SMBH binary that arises as a consequence of the binary orbital motion (Gaskell 1983, 1996; Bogdanović et al. 2009). The main complication of this approach is that the velocity-shift signature is not unique to SMBH binaries; it may also arise from outflowing winds near the SMBH, or even from a gravitational-wave recoil kick (e.g., Popović 2012; Eracleous et al. 2012; Barth et al. 2015). To address this ambiguity, spectroscopic searches have been designed to monitor the offset of broad emission-line profiles over multiple epochs and target sources in which modulations in the offset are consistent with binary orbital motion (Bon et al. 2012, 2016; Eracleous et al. 2012; Decarli et al. 2013; Ju et al. 2013; Liu et al. 2014; Shen et al. 2013; Runnoe et al. 2015, 2017; Li et al. 2016; Wang et al. 2017). Two drawbacks of this approach however remain: (a) temporal baselines of spectroscopic campaigns cover only a fraction of the SMBH binary orbital cycle and (b) intrinsic variability of the line profiles may mimic or hide radial velocity variations, making these measurements more challenging and less deterministic (Runnoe et al. 2017).

5. Example ngVLA Studies

Dual and binary SMBH studies can be realized by a number of specific studies enabled by the ngVLA:

Blind surveys. The ngVLA can survey many sources (thousands) with high sensitivity, high dynamic range, and high two-dimensional image fidelity (i. e. relatively complete u, v coverage) in the frequency range 1–50 GHz with moderate resolution. These abilities would enable a blind survey for resolved dual cores in the $\gtrsim$few parsec separation regime. Such a survey could also reveal single, offset cores that may arise from a gravitational-wave recoil kick following a SMBH merger. Candidates can be cross-matched with future optical/near-IR or X-ray (e.g.,, Athena) surveys to measure spectra, redshifts, and disturbed host galaxy structures. While the multi-wavelength observations might not have the resolution of the ngVLA, they would provide a more complete understanding of a candidate and whether it is a genuine dual AGN, a gravitational lens, a chance projection, or even a recoiling SMBH.

Targeted surveys to test candidate binaries. Many binary SMBH candidates are likely to be identified in the coming decades by numerous instruments (including PTAs, LSST and the extremely large optical telescopes currently being planned). The ngVLA will be the premier instrument to follow up these candidates in radio, with the goal of understanding their long-term dynamics through large-scale jet morphologies (at low GHz frequencies, given sufficient sensitivity to low surface brightness emission). A VLBI component on the ngVLA will enable observation and tracking of resolved dual cores, which will truly confirm a binary and allow in-depth study of SMBH binary evolution.

Core variability. The frequency range of ngVLA makes it well-suited to observe AGN that are dominated by core emission. Past work has shown that in blind surveys at ~10 GHz, radio cores are more dominant than diffuse lobes (Massardi et al. 2011). Thus, the high sensitivity of the ngVLA at tens of GHz frequencies can permit easier time-resolved radio quasar light curve monitoring, and thus have the potential to identify more examples that might exhibit periodic activity due to variable accretion or orbital precession.

Multi-messenger searches. GW experiments can only poorly localize their detections (Ellis 2013). In concert with multi-wavelength facilities, the ngVLA could perform efficient follow-up surveys for all galaxies within a given error radius, identifying a host by looking for the signatures described above. With sufficiently high sensitivity on long baselines, the ngVLA could observe and track the orbital motions of radio cores for the most nearby GW candidates, thus enabling specific multi-messenger studies. In particular, PTAs will preferentially detect the most massive ($M_{\rm BH} \gtrsim 10^9$ M$_\odot$), nearby ($z \lesssim 0.1$) objects that are accessible to Earth-based VLBI (e.g., Kelley et al. 2017a; Mingarelli et al. 2017).

Long-baseline benefits. A VLBI component to the ngVLA has clear benefits for this field of research. A long-baseline extension to the ngVLA, where each long baseline consists of a cluster of ~5 antennas, would yield several major benefits. First, much of the imaging of double black holes is resolution-limited, meaning that going to longer baselines would immediately allow the probing of closer pairs of black holes. Second, long baselines would allow the maser experiments described in Section 2.4. Third, the clusters themselves can be used for pulsar timing when the ngVLA core is not being used as part of a VLBI project, giving access to the pulsars too far north for SKA timing.

The above studies enabled by the ngVLA will provide unique probes of SMBH binary evolution in regimes inaccessible with other methods. This includes crucial data on binaries in the truly gravitationally bound phase, such as information about their separations, inspiral timescales, luminosities and variability even when not in a rapidly-accreting "quasar" state. Moreover, studies of radio jet morphology and energetics will provide unprecedented constraints on the mechanisms by which SMBH feedback drives host evolution and contributes to the origin of the observed SMBH-galaxy correlations. In concert with complementary SMBH binary studies by PTAs and LISA,[1] the ngVLA will be a key cornerstone in the coming era of multimessenger astronomy. The synergy between these electromagnetic and gravitational-wave probes of the binary regime has the potential to unravel the full puzzle of binary SMBH evolution and its close ties to the evolution of galaxies.

Acknowledgments. SBS is supported by NSF award #1458952. SBS and TJWL are members of the NANOGrav Physics Frontiers Center, which is supported by NSF award #1430284. T.B. acknowledges support by the National Aeronautics and Space Administration under Grant No. NNX15AK84G issued through the Astrophysics Theory Program and by the Research Corporation for Science Advancement through a Cottrell Scholar Award. L.B. is supported by NSF award #1715413. D. P. acknowledges support from the NSF through the Grote Reber Fellowship Program administered by Associated Universities, Inc./National Radio Astronomy Observatory. Y.S. acknowledges support from an Alfred P. Sloan Research Fellowship and NSF grant AST-1715579. Part of this research was carried out at the Jet Propulsion Laboratory, California Institute of Technology, under a contract with the National Aeronautics and Space Administration.

References

Amaro-Seoane, P., Audley, H., Babak, S., & et al. 2017, ArXiv e-prints. 1702.00786
Bansal, K., Taylor, G. B., Peck, A. B., Zavala, R. T., & Romani, R. W. 2017, ApJ, 843, 14
Barrows, R. S., Comerford, J. M., Greene, J. E., & Pooley, D. 2016, ApJ, 829, 37. 1606.01253
Barth, A. J., Bennert, V. N., Canalizo, G., & et al. 2015, ApJS, 217, 26. 1503.01146
Begelman, M. C., Blandford, R. D., & Rees, M. J. 1980, Nat, 287, 307
Blandford, R. D., & Königl, A. 1979, ApJ, 232, 34
Blecha, L., Loeb, A., & Narayan, R. 2013, MNRAS, 429, 2594. 1201.1904
Bogdanović, T. 2015, in Gravitational Wave Astrophysics, edited by C. F. Sopuerta, vol. 40 of Astrophysics and Space Science Proceedings, 103. 1406.5193
Bogdanović, T., Eracleous, M., & Sigurdsson, S. 2009, New Astronomy reviews, 53, 113
Bon, E., Jovanović, P., Marziani, P., & et al. 2012, ApJ, 759, 118. 1209.4524
Bon, E., Zucker, S., Netzer, H., & et al. 2016, ApJS, 225, 29. 1606.04606
Braatz, J. A., Reid, M. J., Humphreys, E. M. L., Henkel, C., Condon, J. J., & Lo, K. Y. 2010, ApJ, 718, 657. 1005.1955

[1]See also the chapter on ngVLA/LISA synergies in this volume; Ravi et al.

Burke-Spolaor, S. 2011, MNRAS, 410, 2113. 1008.4382
— 2013, Classical and Quantum Gravity, 30, 224013. 1308.4408
Burke-Spolaor, S., Hazboun, J., Kelley, L., Lazio, J., Madison, D., McMann, N., Mingarelli, C., Rasskazov, A., Siemens, X., Simon, J., Smith, T., & Taylor, S. 2018, in prep.
Charisi, M., Bartos, I., Haiman, Z., & et al. 2016, MNRAS, 463, 2145. 1604.01020
Charisi, M., Haiman, Z., Schiminovich, D., & D'Orazio, D. J. 2018, MNRAS. 1801.06189
Comerford, J. M., Pooley, D., Barrows, R. S., & et al. 2015, ApJ, 806, 219. 1504.01391
Condon, J., Darling, J., Kovalev, Y. Y., & Petrov, L. 2011, ArXiv e-prints. 1110.6252
Deane, R. P., Paragi, Z., Jarvis, M. J., & et al. 2014, Nat, 511, 57
Decarli, R., Dotti, M., Fumagalli, M., & et al. 2013, MNRAS, 433, 1492. 1305.4941
Deller, A. T., & Middelberg, E. 2014, AJ, 147, 14. 1310.8191
D'Orazio, D. J., & Loeb, A. 2017, ArXiv e-prints. 1712.02362
Ellis, J. A. 2013, Classical and Quantum Gravity, 30, 224004. 1305.0835
Eracleous, M., Boroson, T. A., Halpern, J. P., & Liu, J. 2012, ApJS, 201, 23. 1106.2952
Favata, M. 2009, ApJ, 696, L159. 0902.3660
Fu, H., Zhang, Z.-Y., Assef, R. J., & et al. 2011, ApJ, 740, L44+. 1109.0008
Gao, F., Braatz, J. A., Reid, M. J., Lo, K. Y., Condon, J. J., Henkel, C., Kuo, C. Y., Impellizzeri, C. M. V., Pesce, D. W., & Zhao, W. 2016, ApJ, 817, 128. 1511.08311
Gaskell, C. M. 1983, in Liege International Astrophysical Colloquia, edited by J.-P. Swings, vol. 24, 473
— 1996, ApJ, 464, L107. astro-ph/9605185
Godfrey, L. E. H., Lovell, J. E. J., Burke-Spolaor, S., & et al. 2012, ApJ, 758, L27. 1209.4637
Graham, M. J., Djorgovski, S. G., Stern, D., & et al. 2015, MNRAS, 453, 1562. 1507.07603
Helmboldt, J. F., Taylor, G. B., Tremblay, S., & et al. 2007, ApJ, 658, 203. astro-ph/0611459
Hopkins, P. F. 2012, MNRAS, 420, L8. 1101.4230
Hopkins, P. F., Kocevski, D. D., & Bundy, K. 2014, MNRAS, 445, 823. 1309.6321
Ju, W., Greene, J. E., Rafikov, R. R., & et al. 2013, ApJ, 777, 44. 1306.4987
Kelley, L. Z., Blecha, L., & Hernquist, L. 2017a, MNRAS, 464, 3131. 1606.01900
Kelley, L. Z., Blecha, L., Hernquist, L., Sesana, A., & Taylor, S. 2017b, submitted. 1711.00075
Kharb, P., Lal, D. V., & Merritt, D. 2017, Nature Astronomy, 1, 727. 1709.06258
Klein, A., Barausse, E., Sesana, A., Petiteau, A., Berti, E., Babak, S., Gair, J., Aoudia, S., Hinder, I., Ohme, F., & Wardell, B. 2016, Phys.Rev.D, 93, 024003. 1511.05581
Komossa, S., Burwitz, V., Hasinger, G., & et al. 2003, ApJ, 582, L15. arXiv:0212099
Koss, M., Mushotzky, R., Treister, E., & et al. 2011, ApJ, 735, L42. 1106.2163
Koss, M. J., Glidden, A., Baloković, M., & et al. 2016, ApJ, 824, L4. 1708.06762
Kuo, C. Y., Braatz, J. A., Condon, J. J., Impellizzeri, C. M. V., Lo, K. Y., Zaw, I., Schenker, M., Henkel, C., Reid, M. J., & Greene, J. E. 2011, ApJ, 727, 20. 1008.2146
Kuo, C. Y., Braatz, J. A., Reid, M. J., Lo, K. Y., Condon, J. J., Impellizzeri, C. M. V., & Henkel, C. 2013, ApJ, 767, 155. 1207.7273
Li, Y.-R., Wang, J.-M., Ho, L. C., & et al. 2016, ApJ, 822, 4. 1602.05005
Liu, T., Gezari, S., Burgett, W., & et al. 2016, ApJ, 833, 6. 1609.09503
Liu, T., Gezari, S., & Miller, M. C. 2018, ArXiv e-prints. 1803.05448
Liu, X., Civano, F., Shen, Y., Green, P., Greene, J. E., & Strauss, M. A. 2013, ApJ, 762, 110
Liu, X., Shen, Y., Bian, F., Loeb, A., & Tremaine, S. 2014, ApJ, 789, 140. 1312.6694
Liu, X., Shen, Y., Strauss, M. A., & Hao, L. 2011, ApJ, 737, 101. 1104.0950
Massardi, M., Ekers, R. D., Murphy, T., & et al. 2011, MNRAS, 412, 318
Merritt, D., & Ekers, R. D. 2002, Science, 297, 1310. astro-ph/0208001
Merritt, D., & Milosavljević, M. 2005, Living Reviews in Relativity, 8. astro-ph/0410364
Mingarelli, C. M. F., Lazio, T. J. W., Sesana, A., & et al. 2017, Nature Astronomy, 1, 886
Miyoshi, M., Moran, J., Herrnstein, J., Greenhill, L., Nakai, N., Diamond, P., & Inoue, M. 1995, Nat, 373, 127
Müller-Sánchez, F., Comerford, J. M., Nevin, R., & et al. 2015, ApJ, 813, 103. 1509.04291
Popović, L. Č. 2012, New Astronomy Reviews, 56, 74. 1109.0710
Roberts, D. H., Saripalli, L., Wang, K. X., & et al. 2018, ApJ, 852, 47. 1708.02306
Rodriguez, C., Taylor, G., Zavala, R., Peck, A., Pollack, L., & Romani, R. 2006, ApJ, 646, 49

Roos, N., Kaastra, J. S., & Hummel, C. A. 1993, ApJ, 409, 130
Runnoe, J. C., Eracleous, M., Mathes, G., & et al. 2015, ApJS, 221, 7. 1509.02575
Runnoe, J. C., Eracleous, M., Pennell, A., & et al. 2017, MNRAS, 468, 1683. 1702.05465
Saripalli, L., & Subrahmanyan, R. 2009, ApJ, 695, 156. 0811.1907
Sesana, A., Haiman, Z., Kocsis, B., & Kelley, L. Z. 2017, ArXiv e-prints. 1703.10611
Shen, Y., Liu, X., Loeb, A., & Tremaine, S. 2013, ApJ, 775, 49. 1306.4330
Tremblay, S. E., Taylor, G. B., Ortiz, A. A., & et al. 2016, MNRAS, 459, 820. 1603.03094
Valtonen, M. J., Lehto, H. J., Nilsson, K., & et al. 2008, Nat, 452, 851. 0809.1280
Vaughan, S., Uttley, P., Markowitz, A. G., & et al. 2016, MNRAS, 461, 3145. 1606.02620
Wang, L., Greene, J. E., Ju, W., Rafikov, R. R., Ruan, J. J., & Schneider, D. P. 2017, ApJ, 834, 129. 1611.00039

Science with a Next-Generation Very Large Array
ASP Conference Series, Monograph 7
Eric J. Murphy, ed.

DRAFT EDITION

Compact binary mergers as traced by gravitational waves

A. Corsi[1], D. A. Frail[2], D. Lazzati[3], D. Carbone[1], E. J. Murphy[4], B. J. Owen[1], D. J. Sand[5], R. O'Shaughnessy[6]

[1]*Department of Physics and Astronomy, Texas Tech University, Box 1051, Lubbock, TX 79409, USA;* `e-mail:alessandra.corsi@ttu.edu`

[2]*National Radio Astronomy Observatory, P.O. Box O, Socorro, NM 87801, USA;*

[3]*Department of Physics, Oregon State University, 301 Weniger Hall, Corvallis, OR, 97331, USA;*

[4]*National Radio Astronomy Observatory, 520 Edgemont Rd, Charlottesville, VA 22903, USA;*

[5]*Department of Astronomy and Steward Observatory, University of Arizona, 933 N Cherry Ave, Tucson, AZ 85719, USA.*

[6]*Center for Computational Relativity and Gravitation, Rochester Institute of Technology, Rochester, NY 14623, USA.*

Abstract. In light of the recent dazzling discovery of GW170817, we discuss several new scientific opportunities that would emerge in multi-messenger time-domain astrophysics if a facility like the next generation Very Large Array (ngVLA) were to work in tandem with ground-based gravitational wave (GW) detectors. These include probing wide-angle ejecta and off-axis afterglows of neutron star (NS)-NS mergers; enabling direct size measurements of radio ejecta from NS-NS mergers; and unraveling the physics behind the progenitors of compact binary mergers via host galaxy studies at radio wavelengths. Our results show that, thanks to its unprecedented sensitivity and resolution, the ngVLA will enable transformational results in the multi-messenger exploration of the transient radio sky.

1. Introduction

Thanks to its unprecedented sensitivity and resolution, the next generation Very Large Array (ngVLA) has the potential to enable transformational results in the exploration of the dynamic radio sky (Bower et al. 2015). In light of the recent dazzling discovery of GW170817, a binary neutron star merger whose gravitational wave (GW) chirp (Abbott et al. 2017d) was accompanied by light at all wavelengths (see e.g. Abbott et al. 2017e, and references therein), here we discuss several new scientific opportunities that would emerge in multi-messenger time-domain astrophysics if a facility like the ngVLA[1] were to work in tandem with ground-based GW detectors:

1. Probing wide-angle ejecta and off-axis afterglows of neutron star (NS)-NS, and black hole (BH)-NS mergers in low density ISM via Stokes I continuum and polarization measurements;

2. Enabling direct size measurements and dynamical constraints with Very Long baseline interferometry (VLBI) of radio ejecta from NS-NS and/or BH-NS mergers;

3. Unraveling the physics behind the progenitors of BH-BH, BH-NS, and NS-NS mergers via host galaxy studies at radio wavelengths.

In what follows, we briefly describe the scientific landscape expected to be realized when the ngVLA may become operational (Section 2). Then, we discuss radio studies of NS-NS/BH-NS ejecta in Stokes I continuum, linear polarization fraction, and resolved imaging (Sections 3 and 4). We show how the ngVLA could perform resolved host galaxy studies of binary NS-NS and BH-NS mergers (Section 5). Finally, in Section 6, we summarize and conclude.

2. Multi-messenger astronomy in the post-2027 scientific landscape

During their first two observing runs (O1/O2), the advanced Laser Interferometer Gravitational wave Observatory (LIGO) and Virgo made the big leagues by detecting several BH-BH binaries (Abbott et al. 2016a,b, 2017b,c) as well as GW170817, a NS-NS merger with an electromagnetic (EM) counterpart (Abbott et al. 2017a,d,e). Thanks to these discoveries we expect that about 10 years from now, in the ngVLA era, the field of time-domain astronomy will have fully transitioned to time-domain GW astrophysics. Based on current projections, in the ngVLA era the network of ground-based GW detectors could include Virgo operating at nominal advanced sensitivity, the two advanced LIGO detectors likely in their so-called plus configuration (which foresees a factor of ~ 5 increase in event rates with respect to advanced LIGO at full sensitivity), the Kamioka Gravitational Wave Detector (KAGRA), and LIGO India. This world-wide network of detectors will be identifying potentially tens to hundreds of GW in-spirals and mergers in the local universe, with localization areas of order $\lesssim 10\,\mathrm{deg}^2$ (a factor of $\gtrsim 10$ better than today; Abbott et al. 2016c).

As demonstrated by the massive broad-band observational effort that unveiled the EM counterpart of GW170817 (see Abbott et al. 2017e, and references therein), spectroscopic and multi-wavelength observations of GW localization areas are going to be key to finding EM counterparts to GW triggers, removing potential false positives, identifying host galaxies, and constraining several key aspects of the physics of compact binary mergers. Radio and optical observations, for example, crucially complement

[1]Hereafter we assume that the ngVLA will have $\approx 10\times$ the collecting area of the Jansky VLA, operate from 1 GHz (30 cm) to 116 GHz (2.6 mm) with up to 20 GHz of bandwidth with a compact core for high surface-brightness sensitivity, and extended baselines of at least hundreds of kilometers and ultimately across the continent for high-resolution imaging (Bolatto et al. 2017).

each other: while optical emission traces the slower thermally-emitting material, radio probes the non-thermal fastest-moving ejecta. Indeed, in the case of GW170817 (Abbott et al. 2017a,d), optical/IR observations revealed a kilonova and the r-process nucleosynthesis, while the late-time radio and X-ray emissions probed a completely different component, namely, a fast ejecta observed at large angles (e.g Abbott et al. 2017a,e; Coulter et al. 2017; Evans et al. 2017; Hallinan et al. 2017; Kasliwal et al. 2017; Lazzati et al. 2017, 2018; Mooley et al. 2018; Troja et al. 2017; Valenti et al. 2017).

Hereafter, we make the reasonable assumption that by the time the ngVLA becomes operational the community will have collected statistically significant samples of various type of compact binary mergers, and that for at least some of them host galaxies will have been identified (either directly through the detection of EM counterparts, or indirectly through potential anisotropy in their spatial distribution; see e.g., Raccanelli et al. 2016, and references therein). It is in this context that the value of a PI-driven radio array such as the ngVLA, with a sensitivity and resolution matched to (or encompassing that of) other post-2027 facilities, is best understood. Here we focus on topics that make use of the superior ngVLA (+VLBI) sensitivity and resolution at frequencies in between those for which SKA1-MID ($\nu \lesssim 1$ GHz) and ALMA ($\nu \gtrsim 100$ GHz) will be the premier radio facilities.

3. Probing wide-angle ejecta and off-axis jets of NS-NS/BH-NS mergers

Broadly speaking, three major classes of radio counterparts of BH-NS/NS-NS mergers are thought to exist (e.g., Nakar & Piran 2011; van Eerten et al. 2012; Hotokezaka et al. 2016; Lazzati et al. 2017, 2018; Nakar & Piran 2018): (i) Counterparts associated with sub-relativistic merger ejecta producing radio remnants on timescales of a few years; (ii) ultra-relativistic jets that produce short gamma-ray bursts (GRBs) and (on-axis) radio afterglows in the direction of the jet (evolving on timescales of a few days); (iii) mildly-relativistic, wide-angle "cocoons", also referred to as jet "wings", whose emission evolves on timescales of weeks, and which may or may not be accompanied by the contribution of a successful but (initially) off-axis ultra-relativistic jet. A more detailed description of these various components can be found in the contribution to this science book by Nicole Lloyd-Ronning.

While the presence of fast jets that successfully break out from the merger ejecta (scenario (ii) above) is predicted by models positing NS-NS mergers as central engines of short GRBs, the temporal evolution of GW170817 radio afterglow has given evidence for the presence of emission coming from a wide-angle outflow (scenario (iii) above; Kasliwal et al. 2017; Hallinan et al. 2017; Lazzati et al. 2017; Mooley et al. 2018; Lazzati et al. 2018). The key question of whether a relativistic, short GRB-like jet also emerged successfully, but was not observed as a bright, fast-decaying afterglow in GW170817 because misaligned with our line of sight (off-axis), remains open. Answering this question is crucial to ultimately understand whether short GRBs track the NS-NS merger rate, or if instead a larger variety of ejecta outcomes is possible in these mergers, including so-called "choked" jets.

Building a large sample of NS-NS/BH-NS mergers with radio counterparts is the first step into answering the above question. To this end, we certainly need a radio array like the ngVLA: as evident from the top panel of Fig. 1, only with the ngVLA we can detect GW170817-like radio counterparts (in Stokes I continuum) up to distances

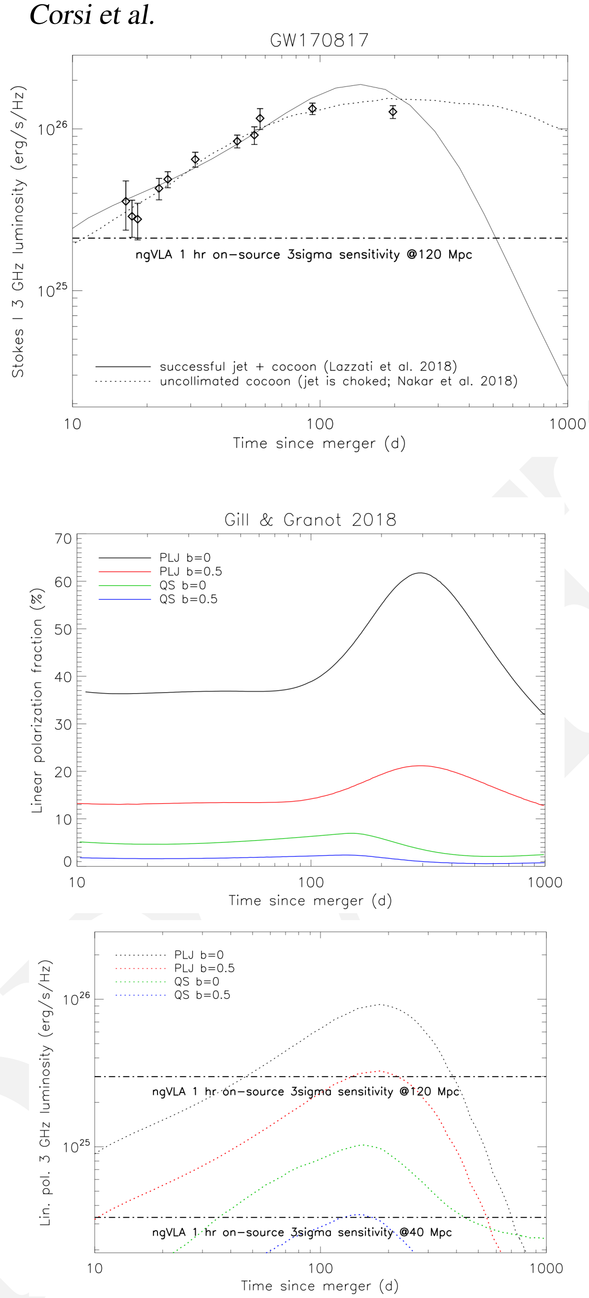

Figure 1. *TOP: GW170817 3 GHz light curve (diamonds; Dobie et al. 2018) compared with the best fit models in a successful jet plus cocoon scenario (solid line; Lazzati et al. 2018), and in a cocoon with choked jet scenario (dotted line; Nakar et al. 2018). Only with the ngVLA (rms sensitivity* $\approx 0.4\,\mu$*Jy in 1 hr at 2-3 GHz) we can probe GW170817-like radio counterparts up to the distance horizon for highly significant triple coincidence detections by LIGO and Virgo at their full sensitivty (*$d_L \approx 120\,$*Mpc,* $3\times$ *farther than GW170817, for an event rate about* $30\times$ *higher; see Abbott et al. 2016c). CENTER: Predictions by Gill & Granot (2018) for the linear polarization fraction* $\sqrt{Q^2+U^2}/I$ *of the GHz radio flux for different types of ejecta and magnetic field structures. The quasi-spherical ejecta (QS) best represents a cocoon with a choked jet; the power-law jet (PLJ) best represents the case of a successful jet with a cocoon; the parameter b describes the structure of the magnetic field: for* $b = 0$ *the field is completely in the plane of the shock, and for* $b = 0.5$ *the field component in the direction of the shock normal also contributes. See Gill & Granot (2018) for more details. BOTTOM: Best fit Stokes I continuum at 3 GHz from the top panel (solid and dotted lines), multiplied by the linear polarization fraction shown in the center panel for different ejecta and magnetic fields. The ngVLA will probe a large variety of ejecta and magnetic field structures, which are inaccessible to current radio facilities.*

comparable to the horizon for highly significant triple (LIGO+Virgo) coincidence triggers of current ground-based detectors at their full sensitivity ($d_L \approx 120$ Mpc or 3× farther than GW170817, or an event rate about 30× higher; Abbott et al. 2016c). This conclusion has been confirmed more generally in the recent study by Carbone & Corsi (2018), which shows that even considering a larger variety of possible radio afterglow outcomes from NS-NS mergers (see (i)-(iii) above), the ngVLA will be key to enabling discoveries within a volume large enough for statistically meaningful studies ($\gtrsim 10$ events per year).

While radio continuum monitoring of NS-NS merger ejecta cannot fully remove model degeneracies (see e.g. the top panel of Fig. 1 where the dotted and continuum line largely overlap until a few hundred days since merger; Nakar & Piran 2018; Lazzati et al. 2018), radio polarimetry offers the potential of providing a much stronger model discriminant (see Fig. 1 central panel, and e.g. Rossi et al. 2004; Gill & Granot 2018; Nakar et al. 2018, for further discussion). Indeed, the sensitivity of an array like the ngVLA will offer us the unprecedented opportunity of probing directly the angular and radial structure of NS-NS merger ejecta, and of their magnetic fields, via radio polarization studies (Corsi et al. 2018). As shown in the central panel of Fig. 1, a large degree of linear polarization can be considered a smoking gun for the presence of a successful misaligned jet accompanying a large angle outflow in a NS-NS merger. On the other hand, a quasi-spherical outflow that could result from a choked jet would produce linearly polarized emission at a much lower level.

As evident from the bottom panel of Fig. 1, we need the sensitivity of the ngVLA to track the temporal evolution of the linear polarization fraction of GW170817-like radio counterparts up to $d_L \sim 120$ Mpc. The degree of linear polarization can help constrain outflow structure models and, when paired with direct imaging (which can constrain the ejecta structure regardless of the details of magnetic field structure), also enable us to gain critical insight into the possible magnetic field configurations in NS-NS merger ejecta (b parameter in the central panel of Fig. 1).

4. Direct size measurement of radio ejecta from NS-NS and BH-NS mergers

Resolved imaging of the radio ejecta associated with BH-NS or NS-NS mergers, which requires VLBI techniques, represents the only direct way to map the speed distribution of merger ejecta, and distinguish e.g. collimated relativistic fireballs observed off-axis from quasi-spherical relativistic ejecta. Imaging, coupled with linear polarization studies, could break the degeneracy between outflow and magnetic field structure (see previous section and Fig. 1 central panel).

The image of a NS-NS merger ejecta will generally depend on the details of the interaction of the fastest ejecta component with with the slower, neutron-rich material, and several different outcomes are possible (see e.g. Nakar et al. 2018). However, following Lazzati et al. (2018), here we consider two extreme cases that are likely to roughly "bracket" the variety of possible outcomes: an uncollimated (spherical) relativistic ejecta whose image would appear to be ring-like - brighter near the edge and dimmer near the center (see the top-left panel of Fig. 3; see also Granot et al. 1999); and a top-hat (i.e. uniform) collimated relativistic jet whose axis is misaligned with respect to the observer (see the middle- and bottom-left panels of Fig. 2).

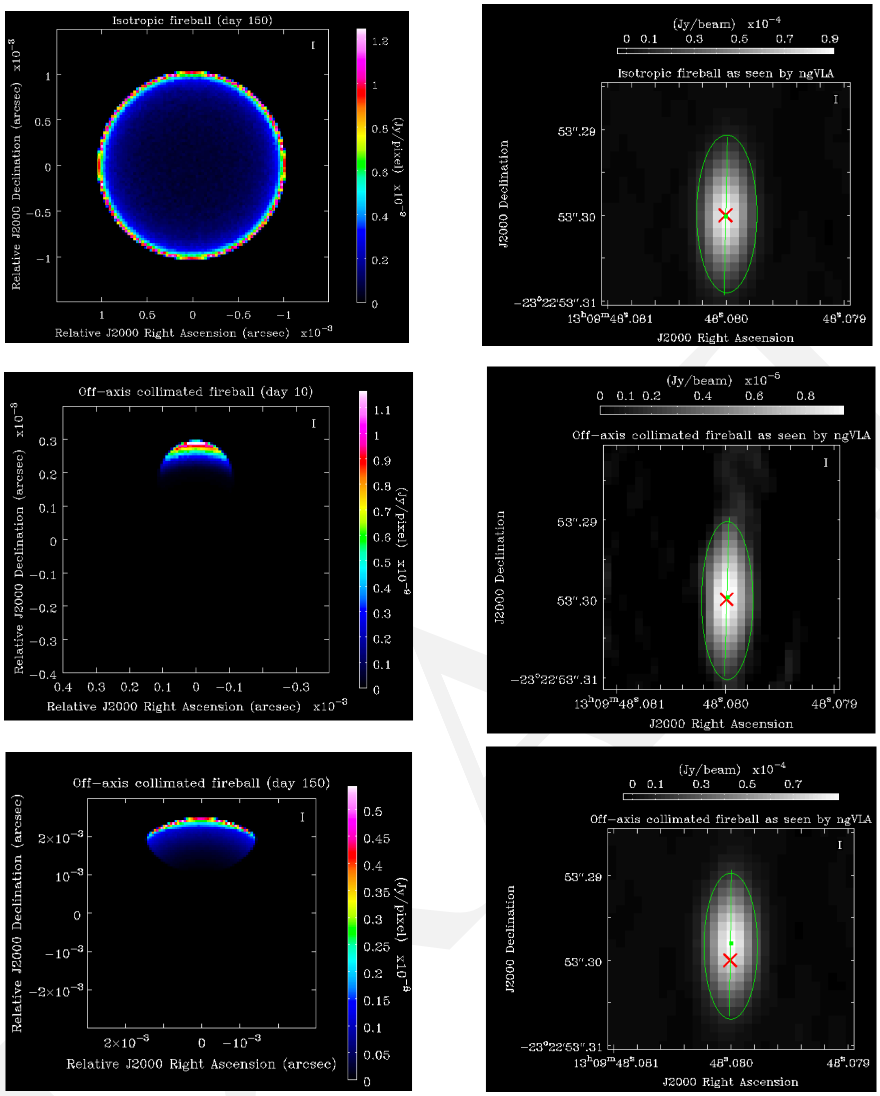

Figure 2. *TOP: Predicted image (left) and simulated observation (right) at 2.4 GHz of an isotropic NS-NS merger ejecta at day* $\approx$ 150 *since merger with isotropic energy* $E_{\rm iso}$ = 2.5×10^{49} *erg, fraction of energy in electrons of* ϵ_e = 0.03*, fraction of energy in magnetic fields of* ϵ_B = 0.0002*, expanding in an ISM of density* $n_{\rm ISM}$ = 6.8×10^{-4} *cm*$^{-3}$ *(see Lazzati et al. 2018, for more details). CENTER: Predicted image (left) and simulated observation (right) at 2.4 GHz of a top-hat collimated (*θ_j = 23 *deg) fireball from a NS-NS merger observed off-axis (*$\theta_{\rm view}$ = 39 *deg), at day* $\approx$ 10 *since merger, with* $E_{\rm iso}$ = 5.7×10^{50} *erg,* ϵ_e = 0.01, ϵ_B = 0.003, $n_{\rm ISM}$ = 3.2×10^{-4} *cm*$^{-3}$*. BOTTOM: Same as center but for an observing epoch of 150 d since merger. In all right panels we have assumed the April 2018 ngVLA-VLBA configuration (see text), 4 hr integration time at a central frequency of 2.4 GHz, 2.3 GHz bandwidth, and noise rms of* 0.2 μ*Jy (natural weighting). As evident, the off-axis collimated ejecta would appear to have an emission centroid (green dot) offset from the location of the emission centroid that one would measure at early times and/or e.g. at optical wavelengths (red cross). Moreover, for a collimated off-axis fireball the emission centroid is observed to move over time (compare the location of the green dot in the center- and bottom-right panels relative to the red cross).*

Using the April 2018 updated VLBA configuration of the ngVLA[2], we have simulated what the ngVLA would see given the emission models shown in the left panels of Fig. 2. We have assumed a 4 hr-long observation at 2.4 GHz, and an rms sensitivity of about 0.2 μJy/beam (for natural weighting). As shown in the right panels of Fig. 2, an off-axis collimated ejecta would appear to have a time-dependent emission centroid increasingly offset from the location of the counterpart that one would measure at very early times and/or e.g. at optical wavelengths (compare the time-dependent location of the green dot in the middle- and bottom-right panels relative to the fixed red cross). On the other hand, the emission centroid of an isotropic ejecta would be time-invariant and coincide with the optical location at all times (top-right panel in Fig. 2). Moreover, as shown in Fig. 3, the VLBA configuration of the ngVLA will give us enough sensitivity and resolution for mapping directly radio ejecta of NS-NS (and BH-NS) mergers as bright as GW170817 ($\approx$ 100 μJy) around $\approx$ 150 d since merger. Specifically, an analysis of the visibility as a function of baseline will distinguish off-axis collimated outflows from isotropic ones.

Table 1. *Host galaxy properties of short GRBs. Form left to right the columns are: GRB name, redshift, host galaxy (optical) SFR, effective host galaxy radius (in optical/IR), expected galaxy radio FWHM at $d_L \approx 120$ Mpc, 2.4 GHz luminosity as derived from the optical SFR (see text for more details), 2.4 GHz radio flux density at $d_L = 120$ Mpc, and derived radio brightness temperature at 2.4 GHz and 120 Mpc (see text for more details).*

GRB	z	SFR ($M_\odot$/yr)	$r_{e,z}$ ($''$)	r_e (kpc)	$FWHM_{120\,\mathrm{Mpc}}$ ($''$)	$L_{2.4\,\mathrm{GHz}}$ (erg s^{-1} Hz^{-1})	$F_{2.4\,\mathrm{GHz},120\,\mathrm{Mpc}}$ (μJy)	$T_{2.4\,\mathrm{GHz}}$ (K)
061201	0.111	0.14	1.09	2.2	4.0	1.5×10^{27}	8.8×10	1.2
070429B	0.902	1.1	0.65	5.1	9.2	1.2×10^{28}	6.9×10^{2}	1.7
070714B	0.922	0.44	0.34	2.7	4.9	4.6×10^{27}	2.8×10^{2}	2.5
070724A	0.457	2.5	0.63	3.7	6.7	2.6×10^{28}	1.6×10^{3}	7.5
071227	0.381	0.6	0.91	4.8	8.7	6.3×10^{27}	3.8×10^{2}	1.1
090510	0.903	0.3	0.93	7.3	13	3.1×10^{27}	1.9×10^{2}	0.23
090515	0.403	0.1	1.19	6.5	12	1.0×10^{27}	6.3×10	0.097
130603B	0.356	1.7	0.62	3.1	5.6	1.8×10^{28}	1.1×10^{3}	7.3

5. Resolving the host galaxies of compact binary mergers

GW observations of compact object binaries (NS-NS, BH-NS, or BH-BH) can constrain the properties of the compact object themselves, such as masses, spins, and merger rates. However, understanding their progenitors and formation channels (i.e. how do compact binary systems actually form and evolve) requires the identification of host galaxies, and more generally a detailed study of the merger environment.

A first constraint on the progenitors of compact binary mergers, and their age distribution, would be provided by the demographics of host galaxies. In fact, the distribution of merger timescales impacts the mix of early- and late-type hosts: generally speaking, the smaller the merger delay, the stronger the connection with (recent) star

[2]This includes the full 214 antennas of the reference array, plus 11 continential-scale antennas: five 18 m antennas randomly placed at the Green Bank site and individual 18 m antennas located at the existing Saint Croix, Hancock, North Liberty, Brewster, Owens Valley, Mauna Kea VLBA sites.

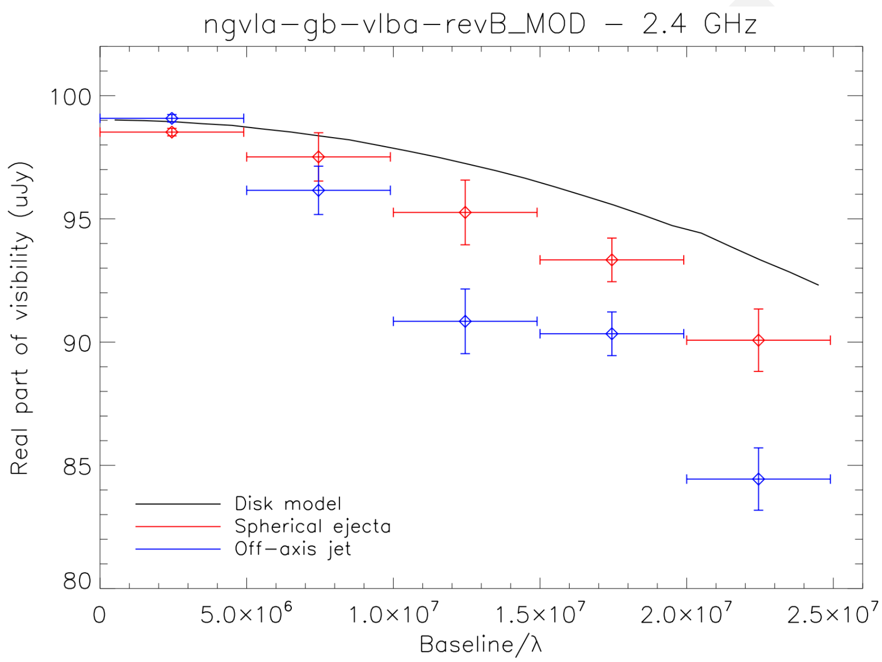

Figure 3. *Real part of the ngVLA visibility as a function of baseline for the two models shown in the top and bottom panels of Fig. 2 (isotropic and off-axis collimated fireballs at at 150 d since explosion when the 2.4 GHz flux is of order ≈ 100 μJy) compared to that of a uniform disk of 2 mas diameter and total flux of 100 μJy (comparable to the 3 GHz peak flux of GW170817). We assume the April 2018 ngVLA-VLBA configuration (see text), 4 hr integration time at a central frequency of 2.4 GHz, a nominal 2.3 GHz bandwidth, and noise rms of 0.2 μJy (natural weighting). As evident, the ngVLA can resolve and distinguish different ejecta structures.*

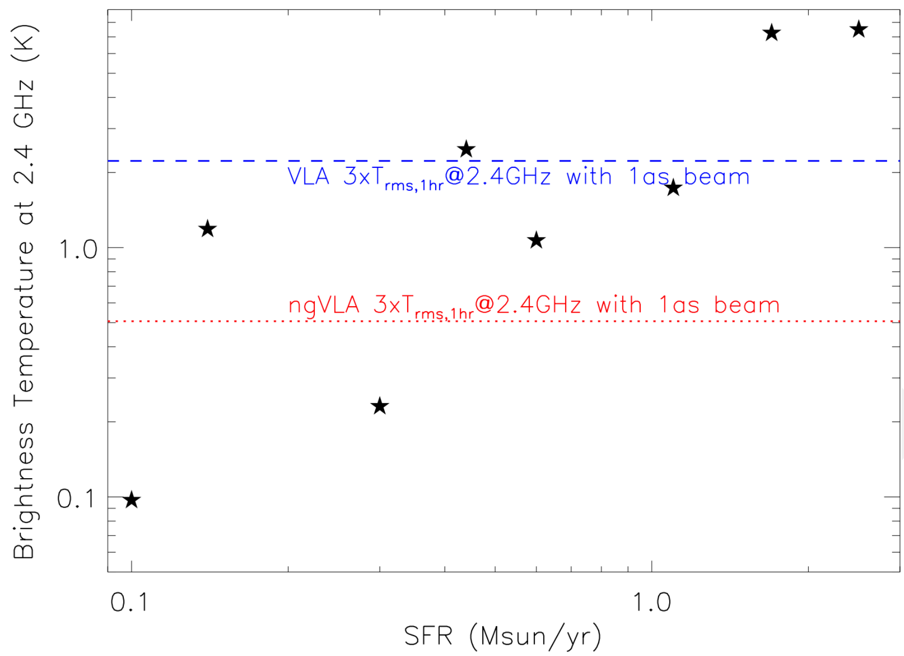

Figure 4. *Predictions for the radio brightness temperature of NS-NS and BH-NS binary merger host galaxies located at 120 Mpc. These predictions are based on our current knowledge of short GRB hosts (see Table 1). The ngVLA will reach a surface brightness sensitivity of* $\approx$ 0.1688 *K in 1 hr with* $\approx 1''$ *resolution at 2.4 GHz, thus resolving all of these hosts at* $d_L \lesssim 120$ *Mpc (red dotted line). More than half of the short GRB-like host galaxies at* $d_L \lesssim 120$ *Mpc are inaccessible to the current Jansky VLA in 1 hr (blue dashed line).*

formation (SF) rather than with stellar mass alone, and the larger the late-type fraction (e.g., Zheng & Ramirez-Ruiz 2007).

Radio continuum emission from galaxies traces the SF rate (SFR) during the last $\sim 50-100$ Myr (e.g., Murphy et al. 2011), and could thus help track the connection between mergers and recent SFR rate. In fact, due to the age-dust-metallicity degeneracy, the optical/UV emission alone is an unreliable measure of SFR in dusty galaxies. Of course, radio measurements are subject to AGN contamination. That said, radio measurements have been demonstrated to be an important complementary tool to constrain the SFR in the past, for example for short GRB hosts. Short GRB mergers are believed to be cosmological compact binary mergers containing at least one NS, so are immediately pertinent comparisons. Radio observations of the host galaxies of GRB 071227 and GRB 120804A provided clear evidence for SFRs at least an order of magnitude larger than those derived using optical data alone (Nicuesa Guelbenzu et al. 2014), suggesting either a starburst origin or an AGN contribution. The host galaxy NGC4993 of the recently detected binary NS merger GW170817, associated with the short GRB 170817A, shows a radio SFR of $\approx 0.1\,M_{\odot}$/yr, approximately 10× higher than the one estimated using the galaxy broad-band photometry, indicative of an AGN dominating the radio emission (Blanchard et al. 2017). We note that while the FIR is also an extinction free SFR tracer, ground-based extinction-free radio observations are advantageous compared to satellite-based FIR observations.

The study of sub-galactic environments (achievable via *resolved* multi-wavelength studies of the host galaxies) can be used to gain other clues to the progenitors of compact binary mergers, such as the presence or absence of a spatial association with star formation or stellar mass, and the distribution of offsets of EM counterparts with respect to their host galaxy light (which can be used to map natal kicks, e.g. Belczynski et al. 2006; Behroozi et al. 2014, and references therein).

While currently most of the cosmological short GRB host galaxies remain undetected in the radio, a sensitive array like the ngVLA will be able to resolve short GRB-like hosts within the LIGO horizon distance. To show this, in Table 1 we collected the (optical/UV) SFR and optical sizes of short GRB hosts available in the literature (Berger 2014). We use the measured SFR to calculate the expected host galaxy luminosity at 1.4 GHz via the Murphy et al. (2011) SFR-to-non-thermal radio emission calibration relation: $\left(\frac{\mathrm{SFR}_{1.4\,\mathrm{GHz}}}{M_{\odot}\mathrm{yr}^{-1}}\right) = 6.35\times10^{-29}\left(\frac{L_{1.4\,\mathrm{GHz}}}{\mathrm{erg\,s^{-1}Hz^{-1}}}\right)$. To estimate the corresponding luminosity at ≈ 2.4 GHz (the central frequency of the ngVLA lowest frequency band), we extrapolate from the 1.4 GHz luminosity using a spectral index of ≈ -0.75 (as appropriate for non-thermal galaxy emission). Since radio emission from local galaxies is observed to be more concentrated than in the optical (Condon et al. 2002; Murphy et al. 2017), we then use the effective galaxy radius r_e from optical/IR observations as FWHM size of the galaxy at radio wavelengths (Fong & Berger 2013), and calculate the brightness temperature as: $T = 1.36\frac{\lambda^2}{\theta^2}S$, where λ is the observed wavelength in cm, θ is the FWHM radio size in arcsec, and S is the flux density in mJy at the considered wavelength ($\lambda \approx 12.5$ cm for observations at 2.4 GHz). Our results are plotted in Fig. 4. The ngVLA will reach a surface brightness sensitivity of ≈ 0.1688 K in 1 hr with $\approx 1''$ resolution at 2.4 GHz, thus resolving most of these hosts at $d_L \lesssim 120$ Mpc. The current Jansky VLA in its A configuration would offer a comparable resolution of $\approx 1''$ at 2.4 GHz, but with a worse surface brightness sensitivity in 1 hr of ≈ 0.742 K. More than half of the host galaxies in Fig. 4 have a brightness temperature $\lesssim 3\times0.742\,\mathrm{K} \approx 2.2$ K, thus the ngVLA is likely to greatly enlarge the sample of resolvable short GRB-like host galaxies.

6. Summary and conclusion

We have investigated three new scientific opportunities that would emerge in time-domain astrophysics if a facility like the ngVLA were to work in tandem with ground-based GW detectors, and shown that:

1. The ngVLA, thanks to its superior sensitivity, will substantially extend the reach of the current Jansky VLA for discovering and characterizing radio afterglows of NS-NS/BH-NS mergers, and their linear polarization fractions, to distances 3× as large (for which event rates are a factor of ~ 30× larger);

2. The ngVLA+VLBA, thanks to its superior sensitivity at the longest baselines, can enable direct size measurements of radio afterglows from NS-NS and/or BH-

NS mergers, probe directly the dynamics of merger ejecta and, when VLBI is paired with linear polarization studies, constrain the magnetic field structure;

3. The ngVLA, thanks to its improved surface brightness sensitivity at lower frequencies, can also enable resolved studies of NS-NS and/or BH-NS mergers host galaxies within distances of $\approx 120\,\mathrm{Mpc}$.

Acknowledgments. A.C. thanks Chris Carilli and Remy Indebetouw for helping with ngVLA simulations in CASA. A.C. and D.C. acknowledge support form NSF CAREER award #1455090. The NRAO is a facility of the National Science Foundation operated under cooperative agreement by Associated Universities, Inc.

References

Abbott, B. P., Abbott, R., Abbott, T. D., et al. (LIGO Scientific Collaboration and Virgo Collaboration) 2016a, Phys. Rev. Lett., 116, 241103
Abbott, B. P., Abbott, R., Abbott, T. D., et al. 2016b, Phys. Rev. Lett., 116, 061102
— 2016c, Living Reviews in Relativity, 19, 1
— 2017a, ApJL, 848, L13. 1710.05834
— 2017b, Phys. Rev. Lett., 118, 221101
— 2017c, Phys. Rev. Lett., 119, 141101
— 2017d, Phys. Rev. Lett., 119, 161101. 1710.05832
— 2017e, ApJL, 848, L12. 1710.05833
Behroozi, P. S., Ramirez-Ruiz, E., & Fryer, C. L. 2014, ApJ, 792, 123. 1401.7986
Belczynski, K., Perna, R., Bulik, T., Kalogera, V., Ivanova, N., & Lamb, D. Q. 2006, ApJ, 648, 1110. astro-ph/0601458
Berger, E. 2014, ARA&A, 52, 43. 1311.2603
Blanchard, P. K., Berger, E., Fong, W., Nicholl, M., Leja, J., Conroy, C., Alexander, K. D., Margutti, R., Williams, P. K. G., Doctor, Z., Chornock, R., Villar, V. A., Cowperthwaite, P. S., Annis, J., Brout, D., Brown, D. A., Chen, H.-Y., Eftekhari, T., Frieman, J. A., Holz, D. E., Metzger, B. D., Rest, A., Sako, M., & Soares-Santos, M. 2017, ApJ, 848, L22. 1710.05458
Bolatto, A., et al. 2017, ngVLA Memo Series, 19
Bower, G. C., et al. 2015, ngVLA Memo Series, 9
Carbone, D., & Corsi, A. 2018, ApJ, submitted
Condon, J. J., Cotton, W. D., & Broderick, J. J. 2002, AJ, 124, 675
Corsi, A., Hallinan, G. W., Lazzati, D., Mooley, K. P., Murphy, E. J., Frail, D. A., Carbone, D., Kaplan, D. L., Murphy, T., Kulkarni, S. R., & Hotokezaka, K. 2018, ArXiv e-prints. 1806.03136
Coulter, D. A., Foley, R. J., Kilpatrick, C. D., Drout, M. R., Piro, A. L., Shappee, B. J., Siebert, M. R., Simon, J. D., Ulloa, N., Kasen, D., Madore, B. F., Murguia-Berthier, A., Pan, Y.-C., Prochaska, J. X., Ramirez-Ruiz, E., Rest, A., & Rojas-Bravo, C. 2017, ArXiv e-prints. 1710.05452
Dobie, D., Kaplan, D. L., Murphy, T., Lenc, E., Mooley, K. P., Lynch, C., Corsi, A., Frail, D., Kasliwal, M., & Hallinan, G. 2018, ArXiv e-prints. 1803.06853
Evans, P. A., Cenko, S. B., Kennea, J. A., Emery, S. W. K., Kuin, N. P. M., Korobkin, O., Wollaeger, R. T., Fryer, C. L., Madsen, K. K., Harrison, F. A., Xu, Y., Nakar, E., Hotokezaka, K., Lien, A., Campana, S., Oates, S. R., Troja, E., Breeveld, A. A., Marshall, F. E., Barthelmy, S. D., Beardmore, A. P., Burrows, D. N., Cusumano, G., D'Ai, A., D'Avanzo, P., D'Elia, V., de Pasquale, M., Even, W. P., Fontes, C. J., Forster, K., Garcia, J., Giommi, P., Grefenstette, B., Gronwall, C., Hartmann, D. H., Heida, M., Hungerford, A. L., Kasliwal, M. M., Krimm, H. A., Levan, A. J., Malesani, D., Melandri, A., Miyasaka, H., Nousek, J. A., O'Brien, P. T., Osborne, J. P., Pagani, C., Page, K. L., Palmer, D. M., Perri, M., Pike, S., Racusin, J. L., Rosswog, S., Siegel, M. H.,

Sakamoto, T., Sbarufatti, B., Tagliaferri, G., Tanvir, N. R., & Tohuvavohu, A. 2017, ArXiv e-prints. 1710.05437
Fong, W., & Berger, E. 2013, ApJ, 776, 18
Gill, R., & Granot, J. 2018, ArXiv e-prints. 1803.05892
Granot, J., Piran, T., & Sari, R. 1999, ApJ, 513, 679. astro-ph/9806192
Hallinan, G., Corsi, A., Mooley, K. P., Hotokezaka, K., Nakar, E., Kasliwal, M. M., Kaplan, D. L., Frail, D. A., Myers, S. T., Murphy, T., De, K., Dobie, D., Allison, J. R., Bannister, K. W., Bhalerao, V., Chandra, P., Clarke, T. E., Giacintucci, S., Ho, A. Y. Q., Horesh, A., Kassim, N. E., Kulkarni, S. R., Lenc, E., Lockman, F. J., Lynch, C., Nichols, D., Nissanke, S., Palliyaguru, N., Peters, W. M., Piran, T., Rana, J., Sadler, E. M., & Singer, L. P. 2017, Science, 358, 1579. 1710.05435
Hotokezaka, K., Nissanke, S., Hallinan, G., Lazio, T. J. W., Nakar, E., & Piran, T. 2016, ApJ, 831, 190. 1605.09395
Kasliwal, M. M., Nakar, E., Singer, L. P., Kaplan, D. L., Cook, D. O., Van Sistine, A., Lau, R. M., Fremling, C., Gottlieb, O., Jencson, J. E., Adams, S. M., Feindt, U., Hotokezaka, K., Ghosh, S., Perley, D. A., Yu, P.-C., Piran, T., Allison, J. R., Anupama, G. C., Balasubramanian, A., Bannister, K. W., Bally, J., Barnes, J., Barway, S., Bellm, E., Bhalerao, V., Bhattacharya, D., Blagorodnova, N., Bloom, J. S., Brady, P. R., Cannella, C., Chatterjee, D., Cenko, S. B., Cobb, B. E., Copperwheat, C., Corsi, A., De, K., Dobie, D., Emery, S. W. K., Evans, P. A., Fox, O. D., Frail, D. A., Frohmaier, C., Goobar, A., Hallinan, G., Harrison, F., Helou, G., Hinderer, T., Ho, A. Y. Q., Horesh, A., Ip, W.-H., Itoh, R., Kasen, D., Kim, H., Kuin, N. P. M., Kupfer, T., Lynch, C., Madsen, K., Mazzali, P. A., Miller, A. A., Mooley, K., Murphy, T., Ngeow, C.-C., Nichols, D., Nissanke, S., Nugent, P., Ofek, E. O., Qi, H., Quimby, R. M., Rosswog, S., Rusu, F., Sadler, E. M., Schmidt, P., Sollerman, J., Steele, I., Williamson, A. R., Xu, Y., Yan, L., Yatsu, Y., Zhang, C., & Zhao, W. 2017, Science, 358, 1559. 1710.05436
Lazzati, D., Deich, A., Morsony, B. J., & Workman, J. C. 2017, MNRAS, 471, 1652. 1610.01157
Lazzati, D., Perna, R., Morsony, B. J., López-Cámara, D., Cantiello, M., Ciolfi, R., giacomazzo, B., & Workman, J. C. 2018, ArXiv e-prints. 1712.03237
Mooley, K. P., Nakar, E., Hotokezaka, K., Hallinan, G., Corsi, A., Frail, D. A., Horesh, A., Murphy, T., Lenc, E., Kaplan, D. L., de, K., Dobie, D., Chandra, P., Deller, A., Gottlieb, O., Kasliwal, M. M., Kulkarni, S. R., Myers, S. T., Nissanke, S., Piran, T., Lynch, C., Bhalerao, V., Bourke, S., Bannister, K. W., & Singer, L. P. 2018, Nature, 554, 207. 1711.11573
Murphy, E. J., Condon, J. J., Schinnerer, E., Kennicutt, R. C., Calzetti, D., Armus, L., Helou, G., Turner, J. L., Aniano, G., Beirão, P., Bolatto, A. D., Brandl, B. R., Croxall, K. V., Dale, D. A., Donovan Meyer, J. L., Draine, B. T., Engelbracht, C., Hunt, L. K., Hao, C.-N., Koda, J., Roussel, H., Skibba, R., & Smith, J.-D. T. 2011, ApJ, 737, 67. 1105.4877
Murphy, E. J., Momjian, E., Condon, J. J., Chary, R.-R., Dickinson, M., Inami, H., Taylor, A. R., & Weiner, B. J. 2017, ApJ, 839, 35. 1702.06963
Nakar, E., Gottlieb, O., Piran, T., Kasliwal, M. M., & Hallinan, G. 2018, ArXiv e-prints. 1803.07595
Nakar, E., & Piran, T. 2011, Nat, 478, 82. 1102.1020
— 2018, ArXiv e-prints. 1801.09712
Nicuesa Guelbenzu, A., Klose, S., Michaowski, M., et al. 2014, ApJ, 789, 45
Raccanelli, A., Kovetz, E. D., Bird, S., Cholis, I., & Muñoz, J. B. 2016, Phys.Rev.D, 94, 023516. 1605.01405
Rossi, E. M., Lazzati, D., Salmonson, J. D., & Ghisellini, G. 2004, MNRAS, 354, 86. astro-ph/0401124
Troja, E., Piro, L., van Eerten, H., Wollaeger, R. T., Im, M., Fox, O. D., Butler, N. R., Cenko, S. B., Sakamoto, T., Fryer, C. L., Ricci, R., Lien, A., Ryan, R. E., Korobkin, O., Lee, S.-K., Burgess, J. M., Lee, W. H., Watson, A. M., Choi, C., Covino, S., D'Avanzo, P., Fontes, C. J., González, J. B., Khandrika, H. G., Kim, J., Kim, S.-L., Lee, C.-U., Lee, H. M., Kutyrev, A., Lim, G., Sánchez-Ramírez, R., Veilleux, S., Wieringa, M. H., &

Yoon, Y. 2017, Nat, 551, 71. 1710.05433
Valenti, S., David, Sand, J., Yang, S., Cappellaro, E., Tartaglia, L., Corsi, A., Jha, S. W., Reichart, D. E., Haislip, J., & Kouprianov, V. 2017, ApJ, 848, L24. 1710.05854
van Eerten, H., van der Horst, A., & MacFadyen, A. 2012, ApJ, 749, 44. 1110.5089
Zheng, Z., & Ramirez-Ruiz, E. 2007, ApJ, 665, 1220. astro-ph/0601622

Science with a Next-Generation Very Large Array
ASP Conference Series, Monograph 7
Eric J. Murphy, ed.

DRAFT EDITION

Radio Emission from Short Gamma-ray Bursts in the Multi-messenger Era

Nicole Lloyd-Ronning[1,2]
[1]*Los Alamos National Lab, Los Alamos, NM, USA 87545;* [2]*University of New Mexico, Los Alamos* `lloyd-ronning@lanl.gov`

Abstract. We examine the expected radio emission from short GRBs detectable by the ngVLA, guided by the observed distributions of their afterglow parameters. We give estimates for the peak emission from both the forward and reverse shock, as well as the late-time off-axis jet emission. In the context of neutron star merger model for short GRBs, we also estimate the radio emission from the dynamical ejecta of these double neutron star systems. The latter two quasi-spherical radio emission components are particularly important given the advent of gravitational wave (GW) detections of binary compact object mergers. We discuss how the ngVLA has potential to shed light on the physics behind short GRBs, and estimate the fraction of GRBs detectable in the radio that may be coincident with a GW signal from a neutron star (NS) merger.

1. Introduction

The most robust model for short gamma-ray bursts (sGRBs) is the merger of two compact objects, such as two neutrons stars (NS-NS) or a neutron star and a black hole (NS-BH). The timescales and energetics involved in the merger have always made these systems plausible progenitors for sGRBs (Eichler et al. 1989; Narayan et al. 1992), but other clues including the location of these bursts in their host galaxies, the lack of associated supernovae, and the observed sGRB rates have provided convincing evidence that these bursts are associated with the older stellar populations expected of compact objects (Rosswog & Ramirez-Ruiz 2003; Fox et al. 2005; Soderberg et al. 2006a; Lee & Ramirez-Ruiz 2007; Berger et al. 2009; Kocevski et al. 2010; Leibler & Berger 2010; Fong et al. 2010; Berger 2010; Fong et al. 2013, 2014). The recent detection of gravitational waves from a neutron star merger (Abbott et al. 2017) and the associated short gamma-ray burst (Abbott et al. 2017b) have provided the smoking-gun evidence that at least some sGRB progenitors result from binary neutron star mergers.

There has been a concerted effort to follow up short GRBs with the goal of detecting the afterglow and potentially learning more about this class of gamma-ray bursts (for a review, see Berger (2014)). To date, about 93%, 84%,, and 58% of sGRBs have been followed up in the X-ray, optical, and radio respectively (Fong et al. 2015). Of these follow-up efforts, 74% have an X-ray afterglow, 34% have been seen in the optical, and only 7% in the radio.

Radio emission in particular has been suggested as a useful tool to help elucidate sGRBs (Nakar & Piran 2011; Metzger & Berger 2012; Berger 2014; Hotokezaka et al. 2016; Resmi 2017). In the classic fireball model (Meszaros & Rees 1997; Sari, Piran, & Narayan 1998), the afterglow emission comes from synchrotron radiation from the forward (and sometimes reverse) shock of the blast wave; the radio component tends to peak at later times, farther from the central engine, more clearly probing the circumstellar environment of the progenitor (compared to the optical and X-ray occurring at earlier times, closer to the cataclysmic event). In addition, the radio afterglow can in principle be detected when the jet has decelerated (so that the radiation is not strongly beamed), and be detected even when the observer is not aligned with the axis of the GRB jet (Levinson et al. 2002; Totani & Panaitescu 2002), or potentially (if there is enough baryon contamination) from a hot cocoon surrounding the merger site (Ramirez-Ruiz et al. 2002; Murguia-Berthier et al. 2014; Lazzati et al. 2016). Finally, models of compact object mergers predict a significant amount of mass tidally ejected during the merger process (Rosswog 2005; Oechslin et al. 2007; Korobkin et al. 2012) which can radiate in several ways, including via shocks with the external medium (Nakar & Piran 2011). These latter two emission scenarios are particularly exciting as they are potential electromagnetic counterparts (and hence carry additional important information) to a gravitational wave signal from a double neutron star (DNS) merger event.

The ngVLA - with its broadband frequency coverage and superb sensitivity - is the ideal instrument to study the radio emission components of sGRBs. In particular, the ngVLA frequency range of 1.2 to 116 GHz is a prime bandpass for catching the early radio reverse shock emission, early-time self-absorbed forward shock emission, later-time optically thin forward shock and off-axis jet emission. As we discuss below, discerning these emission components is the key to constraining the physical parameters that determine the emission of a compact object merger.

2. Radio Emission Components from Compact Object Mergers

In the standard picture of a relativistic external blast wave, the onset of the afterglow occurs around the deceleration time - i.e. when the blast wave has swept up enough external material to begin to decelerate $t_{dec} \propto (E/n)^{1/3}\Gamma^{-8/3}$ (Blandford & McKee 1976). Assuming the emission mechanism is primarily synchrotron radiation one can calculate the characteristic synchrotron break frequencies at this time, depending on the global and microphysical parameters of the burst. These characteristic frequencies are ν_a, the synchrotron self-absorption frequency, ν_m, the frequency corresponding to the "minimum" (characteristic) electron energy, and ν_c, the frequency corresponding to the energy at which an electron loses most of its energy to radiation

These expressions are given in Table 2 of Granot & Sari (2002) for both a constant density and wind medium.

In general, $\nu_a < \nu_m < \nu_c$ for the forward shock component. We can - in the context of this model - calculate how the frequencies evolve with time and when they enter the radio band. For optically thin emission, ν_m is usually the most relevant - i.e. the flux is brightest at this frequency and it should dominate the spectrum in the radio band (here, we focus on optically thin emission keeping in mind this provides upper limits to what we should detect in the radio band, although see the brief discussion of the effects of self-absorption below). The cooling frequency ν_c generally stays well above the radio band for an extended time (this may in any case be an oversimplification of the acceleration and cooling processes - see e.g. Lloyd & Petrosian (2000) for a discussion on how realistic continual acceleration of particles eliminates this characteristic frequency). For the reverse shock, the minimum electron frequency is roughly $\nu_{m,RS} \approx \nu_m/\Gamma^2$ (assuming the fraction of energy in the magnetic field is roughly the same for the forward and reverse shock, as explained below), and thus peaks in the radio at earlier times than the forward shock. We discuss the radio emission from the different components of a compact object merger below.

2.1. Jet Forward Shock

For a constant density medium, we consider the peak flux at ν_m when it enters the radio band. This frequency is given by:

$$\nu_m = 10^{15}\ \mathrm{Hz} \cdot \left\{3.73(p - 0.67)(1 + z)^{1/2}\epsilon_e^2\epsilon_B^{1/2}E_{52}^{1/2}t_{days}^{-3/2}\right\} \tag{1}$$

where p is the electron energy power-law index, z is the redshift, ϵ_e is the fraction of energy in the electrons, ϵ_B is the fraction of energy in the magnetic field, E_{52} is the isotropic equivalent energy normalized to 10^{52} ergs and t_{days} is the time normalized to a day. Notice this expression is particularly sensitive to the fraction of energy in the electrons.

The peak flux at this frequency is given by:

$$f_p(\nu_m) = 9930\ \mu\mathrm{Jy} \cdot \left\{(p + 0.14)(1 + z)\epsilon_B^{1/2}n^{1/2}E_{52}d_{L28}^{-2}\right\} \tag{2}$$

2.2. Jet Reverse Shock

There have been many studies of the reverse shock from a relativistic blast wave (e.g., Meszaros & Rees (1997); Sari & Piran (1999); Kobayashi (2000); Zhang et al. (2003); Kobayashi & Zhang (2003); Zou et al. (2005) and references therein), and the early-time radio flare observation of GRB 990123 has been attributed to the reverse shock (Kulkarni, Frail & Sari 1999; Nakar & Piran 2005). In addition, Soderberg & Ramirez-Ruiz (2003) examined the expected strength of the reverse shock in six long GRBs, and were able to constrain the hydrodynamic evolution and bulk Lorentz factors of these bursts from this component.

As pointed out by these references and others, the evolution of the flux and break frequencies in the reverse shock depends on whether the blast wave is Newtonian or relativistic (among other factors), which in turn is related to the shell thickness Δ estimated from the observed prompt gamma-ray burst duration T by $\Delta \sim cT/(1+z)$. For a thick shell, $\Delta > l/2\Gamma^{8/3}$, where l is the Sedov length in an ISM medium $\equiv (3E/4\pi n m_p c^2)^{1/3}$, the reverse shock has time to become relativistic and the standard Blandford-McKee solution applies. For a thin shell, the reverse shock remains Newtonian and the Lorentz factor of this shock evolves as $\Gamma_{RS} \sim r^{-g}$, with $g \sim 2$ (Kobayashi 2000). Short bursts with $T < 1s$ are likely in the thin shell - and therefore Newtonian - regime. However, we note that for a range of g values, the time evolution of the flux and characteristic frequencies are fairly similar between the relativistic and Newtonian regimes.

Generally speaking, because of the higher mass density in the shell, the peak flux in the reverse shock $f_{p,RS}$ will be higher by a factor of Γ relative to the forward shock,

$$f_{p,RS} \approx \Gamma f_{p,FS} \tag{3}$$

but the minimum electron frequency in the reverse shock $\nu_{m,RS}$ will be lower by a factor of Γ^2,

$$\nu_{m,RS} \approx \nu_{m,FS}/\Gamma^2 \tag{4}$$

assuming the forward and reverse shock have the same fraction of energy in the magnetic field (not necessarily a well-justified assumption). At early times, when this emission is brightest, this frequency falls right in the range of the ngVLA bandpass for typical sGRB parameters; the ngVLA gives us the opportunity for the first time to catch the peak of this reverse shock emission, breaking the degeneracies among the various parameters that determine sGRB emission.

2.2.1. Self-absorbed Reverse Shock

At radio wavelengths, synchrotron self-absorption should be considered - under certain conditions lower energy photons are self-absorbed, and the flux is suppressed. Self-absorption may be particularly relevant in the region of reverse shock, where the density is higher relative to the forward shock region. Resmi & Zhang (2016) calculated the relevance of the self-absorption frequency and flux in the reverse shock, before and after shock crossing. For later time radio emission, we consider the frequencies and fluxes after the shock crosses the thin shell (but see their Appendix A.1 for expressions in all ranges of parameter space).
Roughly, at the high radio frequencies we are considering here, the flux at the time of the peak can be obtained from equation 30 of Resmi & Zhang (2016):

$$f_{p,RS} = f_{p,RS,\nu_m}(\nu_{a,RS}/\nu_{m,RS})^{-\beta} \tag{5}$$

where $\beta = (p-1)/2$.
The reverse shock flux is suppressed at a minimum by factors ranging from about 0.3 to 0.01. We emphasize again, therefore, that our estimates are upper limits to the emission from the reverse shock.

2.3. Jet Off-axis Emission

Because GRB outflows are relativistic, off-axis emission is highly suppressed due to the relativistic beaming of the radiation. However, once the Lorentz factor decreases to a value on the order of the inverse of the viewing angle of the observer, $\Gamma \sim 1/\theta_v$, the flux is similar to an on-axis observer (Rhoads (1997); Granot et al. (2002); See also Figures 7 and 8 of Granot & van der Horst (2014)).

As a simple estimate of the peak of the off-axis emission, we calculate the flux at a time when the blast wave is no longer relativistic, so that the radiation is no longer relativistically beamed and is detectable to an observer well off-axis. This time - which occurs after the jet break time - is also an upper limit to the time of detection of the unbeamed flux. The blast wave becomes non-relativistic around $\sim$ 1 yr $(E_{52}/n)^{1/3}$ (Piran 2004); at this time, ν_m is usually well below the typical observed radio band. Hence, to estimate the radio emission we need the flux above ν_m at a time when the blast wave has decelerated enough to become non-relativistic. Using Frail, Waxman, Kulkarni (2000), the flux at 8.46GHz at the non-relativistic transition is:

$$\begin{aligned} F_{\nu>\nu_m} = 1635\ \mu\mathrm{Jy}\ \{&(1+z)\epsilon_e\epsilon_B^{3/4}n^{3/4}E_{52}(t/t_{NR})^{3(1-p)/2+3/5} \\ &d_{L28}^{-2}(\nu/8.46\ \mathrm{GHz})^{(1-p)/2}(\theta_j/0.1)^2\} \end{aligned} \tag{6}$$

where θ_j is the physical opening angle of the jet. Note there are many ways to model off-axis emission (see, e.g. Nakar, Piran, & Granot (2002), Soderberg et al. (2006b), Waxman (2004), Oren et al. (2004)), depending on the underlying assumptions of the behavior of the jet. This emission - the magnitude and time of the of the peak flux in particular - depends of course on the observer viewing angle (for a recent estimation of radio flux dependence on viewing angle, see Carbone & Corsi (2018)). We emphasize again that we have taken the very conservative estimate of the flux at a time when the blast wave is non-relativistic, and the emission is isotropic and observable to viewers at all angles.

2.4. Tidal or Dynamical Ejecta

In addition to emission from the jet component, there is also emission from mass either dynamically ejected or from winds during the merger process (Rosswog et al. 1999; Ruffert & Janka 2001; Yamamoto, Shibata, & Taniguchi 2008; Rezzolla et al. 2010). This mass (typically in the range from $\sim 0.01 - .1 M_{\odot}$) is ejected with a velocity $\beta_i = v/c \sim 0.1$ (Nakar & Piran 2011), and can shock with the external medium, emitting in the radio band. We note that some simulations have found higher values for the tidal ejecta velocity, $\sim 0.2c - 0.3c$, (e.g. Radice et al. (2016)), which will increase the values of the peak flux; however, this value depends strongly on the equation of state of the neutron star, and a definitive value for the ejecta velocity from neutron star mergers is far from settled (for a brief discussion of this issue, see Metzger (2017)). We note importantly that the bulk of the ejecta mass (which likely came from the wind component of the merger) from GW170817 was fit with a velocity of $0.08c$ (Troja et al. 2017).

If the observed frequency is above the minimum electron frequency ν_m and the self-absorption frequency ν_a - both expected to be less than around 1GHz for canonical values of energies and densities for mergers - then the flux will peak at a time (Nakar & Piran 2011; Nakar, Piran, & Rosswog 2013):

$$t_{dec} \approx 300 \text{ days } E_{51}^{1/3} n^{-1/3} \beta_i^{-5/3} \tag{7}$$

Where $t_{dec} = R_{dec}/c\beta_i$ is the deceleration time (when the ejecta has swept up mass comparable to its own at a radius R_{dec}; after t_{dec}, the flow decelerates in Sedov-Taylor flow $\beta \approx \beta_i (R/R_{dec})^{-3/2}$).

The peak of the specific flux occurs at t_{dec} and is given by (Nakar & Piran 2011):

$$F_{\nu > \nu_m} \approx 4012\, \mu\text{Jy } E_{52} n^{\frac{p+1}{4}} \epsilon_B^{\frac{p+1}{4}} \epsilon_e^{p-1} \beta_i^{\frac{5p-7}{2}} d_{28}^{-2} \left(\frac{\nu_{obs}}{8.46GHz}\right)^{-\frac{p-1}{2}} \tag{8}$$

Note our change of units compared to Nakar & Piran (2011) and Berger (2014), that ϵ_B and ϵ_e are the absolute, non-normalized values, and ν_{obs} is the observed frequency normalized to 8.46 GHz.

3. Predicted Radio Emission from a Compact Merger

Figure 1 shows the predicted radio flux at 8.46 GHz from the forward shock (blue circles), reverse shock (red stars), off-axis emission (green squares), and tidal ejecta (light blue diamonds) for different models, described in the figure caption. For the top panels of Figure 1, we drew each of the physical GRB parameters from a Gaussian distribution with a normalized mean of 1, except for the electron energy power-law index which was fixed at $p = 2.3$, and - in the case of the tidal ejecta component - an ejecta velocity of $\beta_i = 0.1$. We used a mean density of 0.1 cm^{-3}, a mean energy of

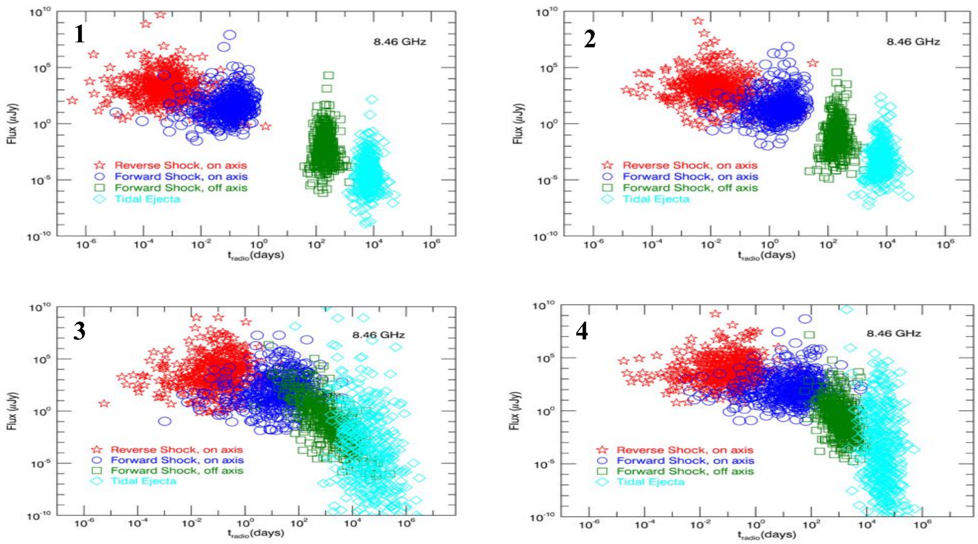

Figure 1. **Top Left, Model 1:** Flux as a function of time using densities from a distribution centered around 0.1 cm^{-3}, a mean energy of $E = 10^{50} erg$, a mean Lorentz factor of 50, a mean redshift of 0.3, a fixed value of $p = 2.3$, and ϵ_e and ϵ_B drawn from a Gaussian with a mean of 0.01. For the tidal ejecta component, we assumed an ejecta velocity $\beta_i = 0.1$. **Top Right, Model 2:** Same as Model 1 in left panel, but with ϵ_e and ϵ_B drawn from a Gaussian with a mean of 0.1 and 0.01 respectively. **Bottom Left, Model 3:** Flux as a function of time using distributions of parameters mimicking those from the multi-wavelength fits of Fong et al. (2015). Densities are from a distribution centered around 0.005 cm^{-3} with a large spread ($\sim$ 2.5 orders of magnitude), a mean energy of $E = 10^{51} erg$, a mean redshift of 0.5, a mean value of $p = 2.43$. The parameters ϵ_e and ϵ_B are both drawn from a Gaussian with a mean of 0.1. The Lorentz factor employed is $\Gamma = 50$. **Bottom Right, Model 4:** Same as Model 3, but with less spread in the density distribution (a standard deviation of 1.25 orders of magnitude as opposed to 2.5 orders of magnitude).

$E = 10^{50} erg$, a mean Lorentz factor of 50, and a mean redshift of 0.3. The averages of the parameters ϵ_e and ϵ_B varied from 0.1 to 0.01. These plots show that the variation in GRB parameters can give a wide range of flux values.

For the bottom panels in Figure 1, we plot the predicted radio fluxes, where spectral parameters were taken from distributions that mimic the observed or fitted distributions from Fong et al. (2015). The difference between these two bottom panels is the choice of standard deviation of the density distribution in log space (2.5 and 1.5 for the left and right panels respectively). Again, there is a large distribution in flux from the various emission components for our choice of spectral parameters. In principle, we may be able to distinguish these components from the time at which they peak in the radio. This is relatively well delineated, with the reverse shock peaking earliest, then the forward shock, off-axis emission and finally, the dynamical ejecta component. As is always the case with gamma-ray bursts, the more multi-band temporal and spectral information we can obtain for each burst, the better chance we have of putting constraints on their emission and therefore underlying spectral parameters. In particular, multi-wavelength observations will help us constrain the characteristic frequencies (and their corresponding fluxes) of the spectrum, helping to break some of the degeneracy between various physical GRB parameters. In addition to this, however, there is a real need from a theoretical standpoint to better understand the microphysics of relativistic shocks (through, for example, long timescale particle-in-cell simulations) and place tighter constraints on the electron energy index p, as well as the parameters ϵ_e and ϵ_B, both of which can in principle take on a wide range of values (spanning orders of magnitude) and contribute to large uncertainty in the expected flux.

3.1. Prospects for "Orphan" Components, and EM Detections Coincident with aLIGO

Because the off-axis and tidal ejecta components are quasi-isotropic, we can ask what fraction of these components we might detect in the radio, if the GRB jet is not directed toward us (such that the prompt gamma-ray signal is not detected). With the successful detection of gravitational waves from astrophysical events (Abbott et al. 2016), and in particular the detection of gravitational waves and electromagnetic emission from GW170817 Abbott et al. (2017), we have definitively entered a new era of multi-messenger astronomy.

The left panel of Figure 2 shows the fraction of GRBs with tidal ejecta (dotted lines) and off-axis components (solid lines) that fall above a conservative limit of $100\mu Jy$ out to a redshift $z \sim .15$ (relevant to aLIGO's design sensitivity in detecting a GW signal from a DNS). We show curves for models 2, 3 and 4 in Figure 1, under the assumption that we have full time coverage (i.e. that we are pointing our telescopes at the GRB at the time of the peak). We find that for the models that mimic the observed/fitted sGRB parameters from Fong et al. (2015), we expect to detect the quasi-isotropic radio emission component in $\sim 10-20\%$ of events that occur at distances to which aLIGO will be (at design specification) sensitive to NS mergers ($\sim 100 Mpc$). Note that at the distance of GW170817 (40 Mpc or z=0.009783), we expect to detect the off-axis radio component from the sGRB jet and it appears that this component was indeed detected (Alexander et al. 2017b). The right panel of Figure 2 shows this fraction multiplied by a fiducial sGRB differential redshift distribution, modeled after the solid line in Figure 4 of Guetta & Piran (2006) - a distribution of redshift that peaks at about $z = 0.5$ and falls off gradually to zero by $z \sim 2$. The left and right panels of Figure 3 are similar to Figure 2, but extended to a redshift of 2. See the chapter by Corsi et al. in this volume for further discussion of coincident gravitational and electromagnetic waves from compact binary mergers.

4. The Future of sGRBs with ngVLA

The ngVLA - with its broad spectral range and sensitivity - will allow us for the first time to better discriminate between different components of sGRB emission and elucidate the physics behind these fascinating events.

We can get additional important information on short gamma-ray bursts if there is rapid follow-up (< 1 day) in the radio - this will give the best chance of detecting the reverse shock emission component, and the ngVLA may afford us this opportunity. The circumburst density must also be low enough to allow for a slow-cooling reverse shock (as mentioned in Laskar et al. (2013, 2016)), but such densities are expected for compact object binary progenitors of sGRBs.

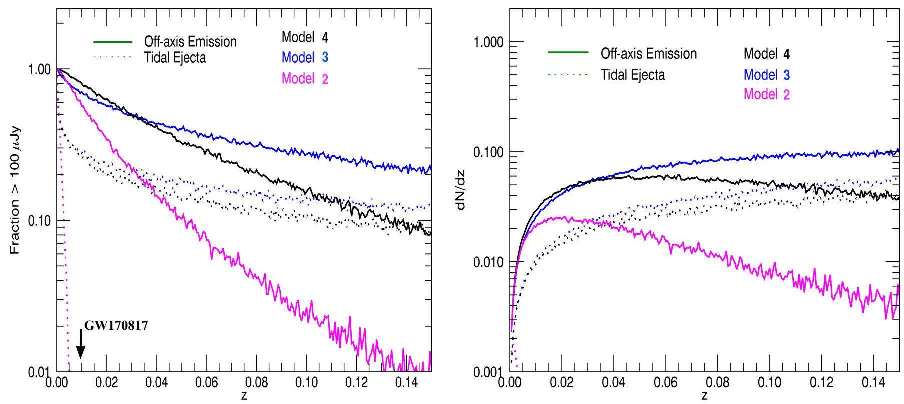

Figure 2. **Left panel:** Fraction of GRBs with off-axis emission (solid lines) and tidal ejecta emission (dotted lines) above $100\mu Jy$ at low redshifts (relevant to the sensitivity of aLIGO in detecting gravitational waves from neutron star mergers), for models 2 - 4 described in Figure 1). **Right panel:** The fraction from the left panel multiplied by the sGRB differential distribution as a function of z. Details on the distribution used are described in the text. Note we have marked the distance of the neutron star merger/gamma-ray burst GW170817 for reference.

The detectable radio components to DNS or NS-BH or mergers are not necessarily easy to distinguish given the observed range of sGRB physical parameters (in other words, the distributions of sGRB parameters based on afterglow fits give a wide spread in their radio flux values). However, detecting the time of the peak of each emission component is perhaps the biggest distinguishing factor (see Figure 1), and spectral information constraining the peak flux of each component is crucial. The ngVLA's wider spectral coverage will be crucial in separating these components.

The fraction of sGRBs with an off-axis "orphan" component detectable in the radio (at late times when the blast wave is non-relativistic and the emission is no longer beamed) and potentially coincident with a gravitational wave signal from a DNS merger is ~ 0.1 at distances to which aLIGO would be sensitive to such a signal. This statement is of course model dependent. However, for a reasonable set of models based on the Fong et al. (2015) fits to sGRB afterglow data, *we expect to detect the quasi-isotropic radio emission for about* 10% *(for the tidal ejecta emission) and up to* 20% *(for the off-axis emission) of sGRBs at a redshift of* $z \sim 0.15$. For shorter distances (e.g. the distance of GW170817 of 40 Mpc or z=0.009783), there is a very high probability to detect the radio emission from the off-axis jet component for most fiducial models. At larger distances, the detectable fraction of these quasi-isotropic components falls off significantly.

The radio emission is a key piece of the puzzle in understanding GRB emission and combining ngVLA observations with additional multi-wavelength follow-up will allow us to constrain the underlying physics of the outflow producing short gamma-ray bursts. Efforts in this vein are particularly timely in light potential additional detections by aLIGO of gravitational wave emission from a double neutron star merger. A better understanding of the various components of electromagnetic emission from these

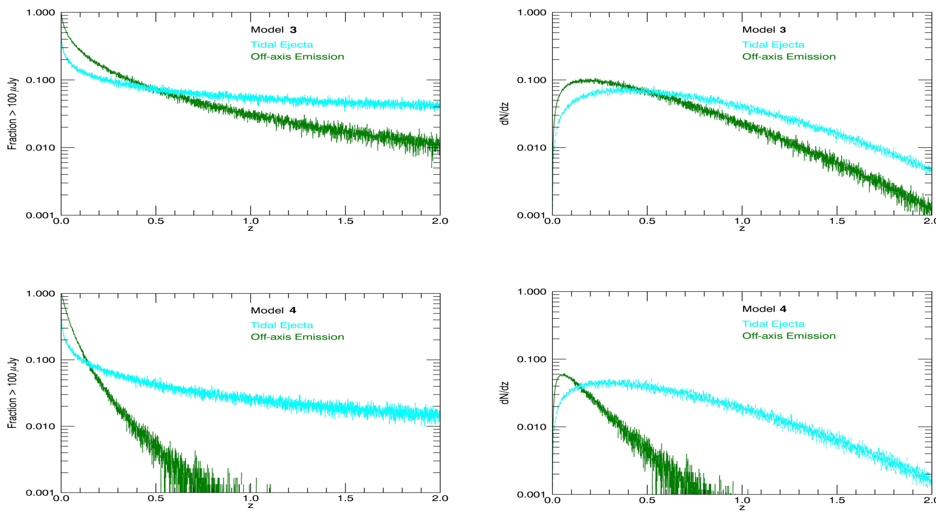

Figure 3. **Left panels:** Fraction of GRBs with off-axis emission (green) and tidal ejecta emission (cyan) above $100\mu Jy$ as a function of redshift, for the Models 3 (top) and 4 (bottom) described in Figure 1. **Right panels:** The fraction from the left panels multiplied by the sGRB differential distribution as a function of z. Details on the distribution used are described in the text.

objects will provide a more complete picture of these systems and ultimately help us understand their role in the context of stellar evolution in the universe.

Acknowledgments. We thank Dieter Hartmann, Chris Fryer and Brandon Wiggins for discussions related to this work. Work at LANL was done under the auspices of the National Nuclear Security Administration of the US Department of Energy at Los Alamos National Laboratory LA-UR-17-24900

References

Abbott, B.P., et al. 2016, Phys. Rev. Lett, 116, 6
Abbott, B.P., et al. 2017, ApJ, 848, L43
Abbott, B.P., et al. 2017, ApJ, 848, L13
Alexander, K.D., et al. 2017, ApJ, 848, L21
Berger, E. , Cenko, S.B, Fox, D.B., & Cucchiara, A. 2009, ApJ, 704, 877
Berger, E. 2010, ApJ, 722, 1946
Berger, E. 2014, ARA&A, 52, 43
Blandford, R.D. & McKee, C.F. 1976, Phys.Fluids, 19, 1130
Carbone, D. & Corsi, A. 2018, arXiv 1801.02361
Eichler, D., Livio, M., Piran, T., & Schramm, D. N. 1989, Nature, 240, 126
Fong, W., Berger, E., & Fox, D.B., 2010, ApJ, 708, 9
Fong, W., et al. 2013, ApJ, 769, 56
Fong, W., et al. 2014, ApJ, 780, 118
Fong, W., Berger, E., Margutti, R., & Zauderer B.A., 2015, ApJ, 815, 102
Fox, D.B., et al. 2005, Nature, 437, 845
Frail, D.A., Waxman E., Kulkarni, S.R., 2000, ApJ, 537, 191
Granot, J. & Sari, R. 2002, ApJ, 568, 820
Granot, J., Panaitescu, A., Kumar, P. & Woosley, S. 2002,
Granot, J. & van der Horst, A.J. 2014, PASA, 31, 8

Guetta, D. & Piran, T. 2006, A&A, 453, 823
Hotokezaka, K. et al. 2016, ApJ, 831, 190
Kobayashi, S.2000, ApJ, 545, 807
Kobayashi, S. & Zhang, B. 2003, ApJ, 597, 455
Kocevski, D., et al. 2010, MNRAS, 404, 963
Kopac, D. 2015, ApJ, 806, 179
Korobkin, O., Rosswog, S., Arcones, A., Winteler, C. 2012, MNRAS, 426, 1940
Kulkarni, S., Frail, D.A. & Sari, R. 1999, ApJ, 522, L97
Laskar, T. et al. 2013, ApJ, 776, 119
Laskar, T. et al. 2016, ApJ, submitted, arXiv1606.08873
Lazzati, D. et al. 2016, MNRAS, submitted, arXiv1610.01157
Lee, W.H. & Ramirez-Ruiz, E. 2007 NJPh, 9, 17
Leibler, C.N. & Berger, E. 2010, ApJ, 725, 1202
Levinson, A., Ofek, E. O., Waxman, E., Gal-Yam, A. 2002, ApJ, 576, 923
Lloyd, N.M. & Petrosian, V. 2000, ApJ, 543, 722
Meszaros, P. & Rees, M.J. 1997, ApJ, 476, 231
Metzger, B.D. & Berger, E. 2012, ApJ, 746, 48
Metzger, B.D. 2017, arXiv 1710.05931
Murguia-Berthier, A., et al. 2014, ApJ, 788, L8
Nakar, E. & Piran, T. 2005, ApJ, 619, L147
Nakar, E. & Piran, T. 2011, Nature, 478, 82
Nakar, E., Piran, T. & Granot, J. 2002, ApJ, 579, 699
Nakar, E., Piran, T. & Rosswog, S. 2013, MNRAS, 430, 2121
Narayan, R., Paczynski, B., & Piran, T. 1992, ApJ, 395, L83
Oechslin, R., Janka, H.-T., & Marek, M. 2007, A&A, 467, 395
Oren, Y., Nakar, E., & Piran, T. 2004, MNRAS, 353, L35
Piran, T. 2004, RvMP, 76, 1143
Radice, D., et al. 2016, MNRAS, 460, 3255
Ramirez-Ruiz, E., Celotti, A., Rees, M.J. 2002, MNRAS, 337, 1349
Resmi, L. & Zhang, B. 2016, ApJ, 825, 48
Resmi, L. 2017 JApA, 38, 56
Rezzolla, L., Baiotii, L., Giacomazzo, B., Link, D., Font, J.A. 2010, Classical Quantum Gravity, 27, 114105
Rhoads, J.E. 1997, ApJ, 478, L1
Rosswog, S., et al. 1999, A&A, 341, 499
Rosswog, S. & Ramirez-Ruiz, E. 2003, MNRAS, 343, L36
Rosswog, S. 2005, ApJ, 634, 1202
Ruffert, M. & Janka, H.-T. 2001, A& A 380, 544
Sari,R. & Piran, T. 1999, ApJ, 520, 641
Sari,R., Piran, T., & Narayan, R. 1998, ApJ, 497, L17
Soderberg, A. et al. 2006, ApJ, 638, 930
Soderberg, A. & Ramirez-Ruiz, E. 2003, MNRAS, 345, 854
Soderberg, A. et al. 2006, ApJ, 650, 261
Totani, T. & Panaitescu, A. 2002, ApJ, 576, 120
Troja, E. et al. 2107, Nature, in press
Waxman, E. 2004, ApJ, 602, 886
Yamamoto, T., Shibata, M. & Taniguchi, K. 2008, Phys. Rev. D. 78, 064054
Zhang, B., Kobayashi, S. & Meszaros, P. 2003, ApJ, 595, 950
Zou, Y.C, Wu, X.F. & Dai, Z.G. 2005, MNRAS, 363, 93

Science with a Next-Generation Very Large Array
ASP Conference Series, Monograph 7
Eric J. Murphy, ed.

DRAFT EDITION

Revealing the Galactic Population of BHs

Thomas J. Maccarone,[1] Laura Chomiuk,[2] James Miller-Jones,[3] Greg Sivakoff,[4] & Jay Strader[2]

[1]*Texas Tech University, Lubbock, TX, USA;* Thomas.Maccarone@ttu.edu

[2]*Michigan State University, East Lansing, MI, USA;* chomiuk@pa.msu.edu , strader@pa.msu.edu

[3]*Curtin University, Perth, WA, Australia* james.miller-jones@curtin.edu.au

[4]*University of Alberta, Edmonton, Alberta, Canada* sivakoff@ualberta.ca

1. Description of the problem

The ngVLA will illuminate the formation processes of BHs (BHs) in close binaries through high angular resolution, high sensitivity radio observations. A multi-epoch Galactic survey with the ngVLA will answer key questions like: How many binaries host BHs? What kinds of cosmic cataclysms produce BHs? How do BHs end up in close systems with other compact objects, in order to merge and produce gravitational waves?

Such a survey is timely, as we currently stand at the dawn of gravitational wave astrophysics. In recent years, we have seen the discoveries of stellar-mass BH-BH binaries merging, as well as one double neutron star merger (Abbott et al. 2016, 2017) . While LIGO demonstrates the existence of inspiraling BH binaries (and can measures key parameters like mass and spin for these objects), understanding the origin of these systems requires information that can only come from electromagnetic studies of BH binary progenitors. Key questions remain about whether these objects form via standard binary stellar evolution (e.g. Belczynski et al. 2007), triple star evolution (e.g., Rodriguez & Antonini 2018), chemically homogeneous binary evolution (de Mink et al. 2009), or dynamically in globular clusters (e.g. Miller & Hamilton 2002). The rates of these mergers are dependent on a variety of poorly constrained parameters, including, but not limited to common envelope efficiency, BH natal kicks distributions, and the range of masses of BHs in binaries. Understanding the populations of BHs in binaries in our own Galaxy will yield crucial constraints on all of these.

Furthermore, the same data that will yield the measurements needed to understand double compact object mergers will give vital insights into how the supernovae themselves explode. We currently know of only ≈20 dynamically confirmed stellar-mass BHs in our Milky Way. The known objects have mostly been discovered via bright X-ray outbursts, and then followed up spectroscopically in quiescence. This selection function creates a strong bias toward systems with long orbital periods (e.g. Arur & Maccarone 2018) Building a sample of accreting BHs in quiescence through a sensitive radio survey will yield a sample with much better understood selection effects. The ngVLA can build such a sample, with suffiicient sensitivity to detect quiescent BH X-ray binaries over a large volume of our Galaxy, and sufficient resolution to measure proper motions and thereby filter out background extragalactic contaminants.

2. Scientific importance and Astronomical Impact

The total number of accreting stellar-mass BHs in our Galaxy is wildly unconstrained, potentially ranging from $100 - 10^8$ (Tetarenko et al. 2016), with clear dynamical signatures of about 20 (Casares & Jonker 2014) and about 60 strong candidates (Corral-Santana et al. 2016). Arguments based on the metal enrichment of the Galaxy suggest that there should be $\sim 10^8 - 10^9$ stellar-mass BHs in the Galaxy (e.g. Samland 1998), and this number is consistent with the upper limits from microlensing searches (e.g. Wyrzykowski et al. 2016). Typically 1–2 new stellar-mass black holes in outburst are discovered per year, and almost all of the known stellar-mass BHs are on the near side of the Milky Way Galaxy. These facts, plus modelling of selection effects suggest that the total number of BH low-mass X-ray binaries is likely to be a few thousand or more (Arur & Maccarone 2018).

The number with high mass donor stars is even more uncertain, in part because wind-fed systems may evade discovery because they do not host X-ray outbursts (see e.g Tetarenko et al. 2016). There may, in fact, be a population of systems very similar to the canonical high mass X-ray binary BH system Cygnus X-1, except with wider separations so that they have lower accretion rates and X-ray luminosities. These systems are poor bets to be discovered in X-ray and optical/IR surveys because of the broad similarities between their expected appearance and the expected appearance of generic massive stars. However, they should be readily distinguished at radio wavelengths by their spectral index; the flat radio spectra produced by an accreting BH's jets will contrast with the optically-thick thermal spectrum expected for a massive star:

An improved understanding of the population size of accreting BHs in the Milky Way will place strong constraints on some of the largest open questions in stellar astrophysics today. It will be a crucial constraint on the efficiency of common envelope evolution in close binary systems (e.g. Ivanova & Chaichenets 2011). It will also constrain the strength of kicks granted to BHs in their natal supernovae.

The amplitude of BH kicks can illuminate the primary channel of stellar-mass BH formation. It has been speculated that BHs may form from a prompt collapse of the entire massive star at the end if its lifetime or, alternatively, from fallback accretion on to a neutron star. The latter case should apply a much stronger natal kick to the BH at the time of formation, both because of the temporary presence of the neutron star (e.g. Kalogera 1996) and the symmetric mass loss from a moving object in a binary (Blaauw 1961). Measurement of BH kicks is also important for determining if LIGO BH binaries are produced through normal binary evolution or dynamical interaction (i.e., in dense star clusters). The gravitational waveform reveals the misalignment of spin—of the black holes relative to one another, and relative to the orbital plane. Dynamically formed binaries should have an approximately random distribution of spin orientations, while binaries formed through binary evolution should have some preference for aligned spins—unless very large kicks take place (REF). It is thus vital to determine whether typical BH kicks are large enough to misalign BH spins substantially from their orbital planes in order to understand how robustly misaligned spins indicate a globular cluster formation scenario. The scale heights of black holes and neutron stars in current samples seem to be quite similar (Repetto & Nelemans 2015).

However, there does seem to be at least one case, Cygnus X-1, where the applied kick appears quite small (Wong et al. 2012). An ngVLA survey for accreting BHs will constrain BH kicks in two ways—by measuring the number of BHs in close binaries in our Galaxy, and by directly measuring their proper motions.

We can also place constraints on the formation of LIGO BH mergers by comparing the BH populations in the Galactic field with those in dense stellar environments (globular clusters, Galactic center), and estimating the relative importance of binary and dynamical channels for forming close BH binaries. At the present time, there are some strong radio-selected BH candidates in globular clusters (e.g. Strader et al. 2012; Chomiuk et al. 2013). Both new detections and confirmations of existing candidates' membership can be made via astrometry.

A larger, more representative sample of black holes will enable a high-quality measurement of the BH mass distribution, and thereby constrain some of the most poorly understood aspects of supernova explosions. In particular for core-collapse supernovae, there is still no consensus about why the explosions actually take place, with the leading models being a standing accretion shock instability and the Rayleigh-Taylor instability (e.g. Belczynski et al. 2012 and references within). Because the process takes place while a thick envelope covers the stellar core, and the supernova light curves and spectra are largely sensitive only to the total energy input and the mass of the envelope, other approaches to understanding the events are vital. In principle, gravitational waves and neutrinos provide information at the time of explosion, but these are only detectable at the time of explosion and within small horizon volumes. The compact remnants of supernovae are therefore the best observational clues as to the processes driving supernovae—and specifically, the distribution of the masses of the compact stellar remnants is very information-rich. Belczynski et al. (2012) argue that models in which the explosion proceeds on a timescale of less than about 0.2 seconds after the core collapse will produce a substantial gap in masses between the heaviest neutron stars and the lightest BHs, while explosions which happen on timescales of order 0.5 seconds or more will lead to a continuous distribution of compact object masses. At the present time, there appears to be such a gap when the mass distribution is modelled as the sum of Gaussians (Özel et al. 2010; Farr et al. 2011), but other functional forms for the mass distribution allow a continuous range of masses (Farr et al. 2011).

The present size of the BH mass sample is simply not sufficient to establish firmly whether there is a mass gap. Furthermore, some biases in our estimates of the inclination angles of the binaries may be partially or fully responsible for the apparent presence of this mass gap (Kreidberg et al. 2012). Astrometric wobble measurements of even a few binaries would provide gold-standard calibration for ellipsoidal modulation measurements, and would be possible with high sensitivity, high frequency VLBI measurements (see also the article by Reid & Loinard in this volume). With the identification of a substantial population of accreting BHs, we will have in hand an ideal sample for follow-up observations enabled by both the ngVLA itself along with other multi-wavelength facilities available in the next decades. This larger sample will also be unbiased, sampling the full population of accreting stellar-mass black holes to enable a measurement of the BH mass function and the amplitude of BH natal kicks.

3. Anticipated results

The ngVLA can detect accreting stellar-mass BHs over a large volume of our Galaxy, and distinguish them from interlopers. An astrometric survey would quickly yield the ability to separate background AGN from foreground X-ray binaries while simultaneously giving good measurements of their proper motions. Numerous other classes of Galactic sources will also be present in a deep, wide astrometric survey, and the combination of the radio properties with other multi-wavelength data sets will not only allow identification of which objects are stellar-mass BHs in binaries, but also will allow characterization of these other populations. We expect to detect bright flare stars, cataclysmic variables, planetary nebulae, and pulsars (most of which should identifiable based on radio spectra, radio variability, angular extent of radio emission or obvious associations with bright foreground stars), and also neutron star X-ray binaries, transitional millisecond pulsars and colliding wind binaries (which may require more careful follow-up work). A particularly interesting class of other objects that could be found in such a survey is isolated black holes accreting from the interstellar medium (Maccarone 2005; Fender, Maccarone & Heywood 2013).

The radio survey could be conducted in a reasonable exposure time, since objects like the radio-faintest known X-ray binaries (e.g. A0620-00 & XTE J1118+480 – Gallo et al. 2006; Gallo et al. 2014) could be detected in about 6 minutes at 6σ at a distance of 2-4 kpc with the proposed ngVLA sensitivity. BHs accreting at higher rates, like V404 Cyg in quiescence, are a factor of ~ 15 more luminous (Miller-Jones et al. 2009) and can be observed well past the distance of the Galactic Center. We thus expect to be able to detect $\sim 10\%$ of the short period BH X-ray binaries in a 10 square degree survey region near the Galactic Center. This region contains about 10% of the stellar mass of the Galaxy, meaning that we would expect to detect at least 1% of the total number of short period BH X-ray binaries in the Milky Way, and the majority of the long period, V404 Cyg-like BH X-ray binaries. We thus expect that ~ 100 new BH X-ray binaries should be discovered in this proposed survey, based on population estimates from X-ray studies (e.g. Arur & Maccarone 2018), and perhaps much larger numbers based on the surprising discovery of a single strong BH candidate with a parallax placing it in front of M15 (Tetarenko et al. 2016). We emphasize further that this proposed program would require a modest amount of time, ado a broad range of additional science, and be easily extendable over time both by extending the field of view and making deeper observations.

At a distance of 8 kpc, with 10 mas resolution (requiring significant collecting area on baselines of at least 1000 km), an uncertainty on proper motion of 20 km/s would result from a nominal two-year time baseline for 6σ detections. Thus the uncertainty will be much less than the typical stellar velocity dispersion in the Solar neighborhood, so only a small fraction of objects should be expected to have small enough proper motions to be confused with background AGN, and this fraction should decrease further if the majority of systems form with strong natal kicks.

Having long baselines (of approximately 1000 km or more) is thus crucial in order to allow sufficiently precise proper motion measurements to make the proper motions diagnostics sufficient both for ruling out background AGN sources, and allowing the measurements to yield useful information about natal kicks. While the proper motion uncertainty increases for sources behind the Galactic Center, if such sources follow the Galactic rotation curve, they will have space velocities of about 400 km/sec because of the rotation relative to the Earth's motion, so even sources at such distances, if bright enough to be detectable, should show measureable proper motions, even in the absence of natal kicks.

4. Limitations of current astronomical instrumentation

Current long baseline arrays are simply not sensitive enough to meet our science goals. It would require 23 hours per pointing to reach our per-epoch sensitivity goal with the LBO—a factor of 4000 longer than with the ngVLA, and to cover 10 square degrees at 6 GHz would require about 640 pointings, so that it would take about 7 years at 6 hours per day to conduct this survey. The European long baseline facilities are too far north to do this work effectively (e.g. e-Merlin sees the Galactic Center region as a maximum elevation of 7 degrees). The VLBA also runs into some problems with source scattering in the most scattered parts of the sky so that only a small fraction of its baselines become useful in such regions.

While the *Gaia* mission holds some promise for identifying BHs in very wide binaries from their astrometric wobble (Barstow et al. 2014; Mashian & Loeb 2017), it will struggle to obtain results on the optically faint quiescent binaries in the crowded, dust-extinguished region of the Galactic Bulge. This dense and populous region is essential for understanding the Galactic BH population and how its characteristics depend on density. Furthermore, the orbital period range probed by *Gaia* through astrometric wobble is much longer than the orbital period range probed by detecting accreting systems – if *Gaia* does discover many stellar mass BHs as wobblers, this information is complementary to what radio observations could discover. Only about 10% of the strong candidate BH X-ray binaries known are bright enough optically for *Gaia* to detect them, despite the strong biases in existing samples toward nearby, unreddened objects.

5. Connection to unique ngVLA capabilities

The long baselines (~1000 km) and high resolution of the ngVLA are critical to this astrometric survey. In addition, relatively high frequencies (> 4 GHz) are necessary to obtain good image quality in the Galactic Plane and the Galactic Bulge, as low frequencies will be affected by scattering. A broad range of baselines is needed for these studies in order that even in the most confused regions, like those in Cygnus and those very close to the Galactic Center, good angular resolution is possible without over-resolving heavily scatter-broadened sources.

5.1. Benefits to this science from a more extended configuration

In addition, continental and global baselines would be of tremendous interest for follow-up of many of the sources discovered through an astrometric survey. Most of the known X-ray binaries are too faint optically for *Gaia* to provide parallax distances. Absolute astrometry with the *James Webb Space Telescope* is expected to be limited to about 0.5 milliarcsecond, even at arbitrarily large signal to noise, meaning that geometric parallax distances will be limited to about 1 kiloparsec. As a result, the best geometric parallax distances for these sources will come from radio data, rather than from optical data. Follow-up could be done with only antennae on the outer part of the array, plus either VLBA stations, or newer longer baseline ngVLA dishes. While the follow-up would require more time per target, it could be done at higher frequencies to improve positional accuracy in a given integration time and mitigate the effects of scattering, and it could be done only for the sources of interest. It would make an excellent usage of the portion of the array that would not be needed when most of the core antennae are being used for low surface brightness extended source projects. To do this follow-up though, a sample of X-ray binaries with known radio brightness must first be collected.

6. Experimental layout

We plan to observe in the band covering 4–12 GHz, as a compromise between field of view, resolution, and sensitivity (we expect the spectra of accreting BHs to be flat, $S_\nu \propto \nu^0$). We estimate that the required sensitivity of each epoch of the survey is 0.8 μJy beam^{-1} (achievable in 6 minutes on source). We require at least three visits covering the survey area, in order to obtain high-quality proper motion measurements. We anticipate achieving an image resolution of $\sim$10 mas by working at medium frequency with 1000 km baselines.

By covering 10 sq. deg. of the Galactic bulge, we will survey the BH population over a substantial fraction of the Galaxy and span a range of environments, including the dense central regions and star-forming regions and the Galactic field. We estimate that each epoch will require 100 hours on source, implying that the entire survey can be carried out in 300 hours.

After doing preliminary classification of the radio sources based solely on their radio properties, the AGN, pulsars, planetary nebulae, cataclysmic variables and isolated massive stars should have been filtered out of the data sample.

Many of these other classes of Galactic stellar radio sources will be interesting in their own rights. Remaining after filtering will be various classes of BH and neutron star X-ray binaries, active binaries and colliding wind binaries. For these, multi-wavelength follow-ups will be necessary. The active binaries will be the most challenging class of contaminant of the X-ray binary population, but the bulk of these should be identifiable from circular polarization for relatively high signal-to-noise sources. For fainter sources radio/X-ray ratios, which will be high enough to be X-ray binaries only in flaring states, will be useful, since the source are highly unlikely to be flaring in all epochs.

7. Complementarity with searches at other wavelengths

Non-simultaneous coordination with the WFIRST microlensing planet search fields will provide high cadence infrared data and thereby ellipsoidal modulation measurements to estimate orbital periods and inclination angles for many of the objects.[1] BH mass estimates can be obtained using optical/IR spectroscopy to measure the width of emission lines, in conjunction with the Casares (2016) relation. A healthy diverse portfolio of optical/IR telescopes spanning diameters, 4–30m, would be ideal for the spectroscopic follow-up, but it is likely that once the sources of interest are identified

[1]Because of the very large number of W UMa stars, using the WFIRST data alone is unlikely to produce good catalogs of BH and neutron star candidates.

that most should be bright enough that the Casares relation or some infrared equivalent will be suitable for estimating the radial velocity amplitude from emission lines.

Proposed future X-ray missions such as eROSITA and Athena (which are scheduled to proceed), and Lynx and STAR-X can be expected to deliver substantial populations of faint candidate X-ray binaries, interspersed with large numbers of members of other X-ray source classes. Because large fractions of these will be radio sources as well, particularly at the sensitivity levels we discuss here, the relatively uncrowded radio data, which will carry with them proper motion infomation, will help sort out the identification of these sources.

8. Additional astrometric stellar-mass BH science

Apart from the value of a large, dedicated Galactic survey, the ngVLA, especially with long baselines, would be vital for a variety of other stellar-mass BH science. In particular, with μJy sensitivity on 5000 km baselines, at 40 GHz would allow for geometric parallax distance measurements for most of these same stellar-mass BHs the survey would find, and for many accreting neutron stars, even in heavily scattered regions. Doing this requires, at bare minimum, retaining the current VLBA stations and upgrading their receivers to make them part of the ngVLA, but exposure times a factor of 5 shorter can be obtained for the same precision by putting about 10% of the collecting area on baselines longer than 1000 km.

We can anticipate that there would be about 300 baselines from the New Mexico core to the 10 VLBA antennae, so that the sensitivity would be about 5.5 times worse than the ngVLA's overall sensitivity for VLBI experiments. Putting 10% of the collecting area on longer baselines would improve the sensitivity by a factor of about 2.6, reducing the exposure time needed for such projects by a factor of about 5, and making the long baseline sensitivity only about a factor of 2 worse than the overall sensitivity.

In the case with no new collecting area beyond 1000 km, follow-up measurements to obtain parallax distances would require about 30 times the total exposure needed to detect the sources, and five epochs would be needed to make reliable parallax measurements. Since the survey observations are expected to be only 6 minutes each, this would require 15 hours per object, so that if 100 BHs were detected, this would become a 1500 hour project at most. In practice, many of the source will be significantly brighter than the detection limit, and some of the foreground objects may have detections from Gaia as well. If 10% of the collecting area were on long baselines, this survey could be done in about 1/5 the time, or, in approximately the same amount of time using the long baselines alone, and with somewhat better astrometric precision since a larger fraction of the collecting area would be at baselines longer than the baselines to New Mexico. With 0.2 masec resolution, and 6 σ detections, and assuming good phase calibration, one could expect parallax measurements accurate to about 15% for sources at the Galactic Center distance, and the accuracy would improve linearly with both signal to noise, and decreasing distance.

9. A next stage, more ambitious plan for detecting more sources

The plan outlined above shows that with 300 hours of ngVLA time, one would be able to do some important first order work on understanding the populations of X-ray binaries. It is important to consider, though, that this survey would discover $\sim$ 100 BH binaries, and would only reach Galactic Center distances for the brightest ones. To build a sample of many hundreds of BH binaries, one could easily expand this survey through a combination of deeper observations on the same part of the sky, and coverage of a wider swath of the Galactic Plane. Since observations within 1 degree of the Galactic Plane will reach a height of 500 pc only at the furthest reaches of the Galaxy, we can expect that increasing the exposure time will increase the number of sources roughly linearly, since the volume included will scale as $t^{3/4}$, and until the most numerous source classes can be reached at the distance of the Galactic Center, the space density of sources should be rising with increased distance. Thus to reach a number of $\sim$ 1000 sources, we could conduct a survey which detects objects like A0620-00 at the distance of the Galactic Center, which would require quadrupling the exposure times for one epoch.

References

Abbott, B. P., et al. 2016, PRL, 6, 041015
Abbott, B. P., et al. 2017, PRL, 119, 161101
Arur K., Maccarone T.J., 2018, MNRAS, 474, 69
Barstow M., et al., 2014, "White paper: Gaia and the end states of stellar evolution", arXiv/1407.6163
Belczynski K., Taam R.E., Kalogera V., Rasio F.A., Bulik T., 2007, ApJ, 662, 504
Belczynski K., Wiktorowicz G., Fryer C.L., Holz D.E., Kalogera V., 2012, ApJ, 757, 91
Blaauw A., 1961, BAN, 15, 265
Casares, J. & Jonker P.G., 2014, SSRv, 182, 223
Chomiuk L., Strader J., Maccarone T.J., Miller-Jones J.C.A., Heinke C. Noyola E., Seth A.C., Ransom S., 2013, ApJ, 777, 69
Corral-Santana J.M., Casares J., Muñoz-Darias T., Bauer F.E., Martínez-Pais I.G., Russell D.M., 2016, A&A, 587, 61
de Mink S., Cantiello M., Langer N., Pols O.R., Brott I., Yoon S.-C., 2009, A&A, 497, 243
Farr W., Sravan N., Cantrell A., Kreidberg L., Bailyn C.D., Mandel I., Kalogera V., 2011, ApJ, 741, 103
Fender R.P., Maccarone T.J., Heywood I., 2013, MNRAS, 430, 1538
Gallo E., Fender R.P., Miller-Jones J.C.A., Merloni A., Jonker P.G., Heinz S., Maccarone T.J., van der Klis M., 2006, MNRAS, 370, 1351
Gallo E., et al., 2014, MNRAS, 445, 290
Ivanova N., Chaichenets S., 2011, ApJ, 731L, 36
Kalogera V., 1996, ApJ, 471, 352
Maccarone T.J., 2005, MNRAS, 360L, 30
Mashian N., Loeb A., 2017, MNRAS, 470, 2611
Miller M.C., Hamilton D.P., 2002, MNRAS, 330, 232
Özel F., Psaltis D., Narayan R., McClintock J.E., 2010, ApJ, 725, 1918
Reid M.J., McClintock J.E., Narayan R., Gou L., Remillard R.A., Orosz J.A., 2011, ApJ, 742, 83
Repetto S., Nelemans G., 2015, MNRAS, 453, 3341
Reynolds C.S., 2014, SSRv, 183, 277
Rodriguez, C. L. & Antonini, F. 2018, arXiv 1805.08212
Samland M., 1998, ApJ, 496, 155
Strader J., Chomiuk L., Maccarone T.J., Miller-Jones J.C.A., Seth A.C., 2012, Nature, 490, 71
Tetarenko B.E., et al., 2016, ApJ, 825, 10
Wong T.-W., Valsecchi F., Fragos T., Kalogera V., 2012, ApJ, 747, 111
Wyrzykowski, L., et al., 2016, MNRAS, 458, 3012
Zhang S., Cui W., Chen W., 1997, ApJ, 482, L155

Science with a Next-Generation Very Large Array
ASP Conference Series, Monograph 7
Eric J. Murphy, ed.

DRAFT EDITION

Local Constraints on Supermassive Black Hole Seeds from a Next Generation Very Large Array

Richard M. Plotkin[1] and Amy E. Reines[2]

[1]*International Centre for Radio Astronomy Research - Curtin University, GPO Box U1987, Perth, WA 6845, Australia;* `richard.plotkin@curtin.edu.au`

[2]*Department of Physics, Montana State University, Bozeman, MT 59717, USA;* `amy.reines@montana.edu`

Abstract. Determining the mechanisms that formed and grew the first supermassive black holes is one of top priorities in extragalactic astrophysics. Observational clues can be inferred from the demographics of massive black holes (in the ten thousand - million Solar mass range) in nearby low-mass galaxies. This chapter of the next generation Very Large Array (ngVLA) Science Book describes how an ngVLA can play a prominent role in developing large samples of weakly accreting active galactic nuclei in low-mass galaxies (out to nearly 1 Gpc), which will help constrain the types of objects that originally seeded the growth of supermassive black holes.

1. Introduction

Determining the formation mechanism(s) of the first black holes is one of the highest priority research areas in extragalactic astrophysics today. In this chapter we describe how a next generation Very Large Array (ngVLA) will provide key new constraints on the types of objects that originally "seeded" the growth of supermassive black holes. In particular, when combined with other multiwavelength probes, an ngVLA will be a crucial player in performing population studies of black holes in the $10^4 \lesssim M_{\rm BH} \lesssim 10^6\,M_\odot$ range, objects that we will refer to as massive black holes (mBHs).

Radio observations provide a window into one of the most energetically important components of accreting black holes, their relativistic jets. Jets can carry large amounts of mechanical power away from a black hole accretion disk, making them one of the primary channels through which black holes can influence their large-scale (kpc) environments (e.g., Fabian 2012). As strong synchrotron emitters, jets release large amounts of radiative power in the radio waveband. Thus, jetted radio emission can serve as a signpost that signals the presence of an accreting black hole. With its order of magnitude improvement in sensitivity and exquisite spatial resolution, an ngVLA will be a powerful machine for identifying and studying accreting mBHs. Combining ngVLA radio signatures with radiation at other wavebands (e.g., X-ray spectral and timing studies, high spatial-resolution infrared/optical spectroscopy and imaging, etc.) will provide a significantly improved understanding on the local mBH population, on accretion processes onto mBHs, and on how black hole growth was seeded in the early Universe.

2. The First Black Holes

The existence of high-redshift quasars powered by $\sim 10^9\,M_\odot$ black holes at $z \gtrsim 7$ suggests that the first black hole seeds were 'heavy', with masses $M_{\rm BH} \sim 10^5\,M_\odot$ (which could have formed from the direct collapse of large clouds of gas, e.g., Loeb & Rasio 1994; Begelman et al. 2006). Otherwise, $10^9\,M_\odot$ black holes could not have grown so massive only 700 Myr after the Big Bang (assuming growth through Eddington limited accretion, e.g., Mortlock et al. 2011; Bañados et al. 2018). However, whether or not $10^5\,M_\odot$ seeds are the exception or the rule remains uncertain, and it is possible that some fraction of black holes could have been seeded with lighter objects in the $\sim 10^2\,M_\odot$ range (i.e., remnants from Population III stars, e.g,. Haiman & Loeb 2001; Madau & Rees 2001; Madau et al. 2014).

While observations of high-redshift quasars provide important constraints and boundary conditions, it is not feasible with current facilities to directly observe black holes as small as $10^5\,M_\odot$ in the very high-redshift Universe (Volonteri & Reines 2016). To study low-mass black holes, we instead rely on clues that are embedded within black hole populations found in nearby galaxies. In particular, the fraction of galaxies hosting a nuclear black hole (as a function of galaxy stellar mass) and black hole/host galaxy scaling relations at low masses provide local diagnostics on the seed black hole population (see, e.g., Volonteri 2010; Greene 2012; Reines & Comastri 2016; Mezcua 2017 for reviews).

2.1. Low-mass Black Holes in Nearby Dwarf Galaxies

Because of their relatively quiet evolutionary histories, and the ability for supernova feedback to stunt black hole growth, we do not expect black holes in nearby dwarf galaxies[1] to have grown much within a Hubble time (e.g., Dubois et al. 2015; Habouzit et al. 2017). In turn, characterizing mBHs in dwarf galaxies provides a powerful lever arm for constraining the seed black hole population (e.g., Volonteri & Natarajan 2009; van Wassenhove et al. 2010; Bellovary et al. 2011). In the past decade we have witnessed an explosion in sample sizes of mBHs in dwarf galaxies, growing from a handful of isolated cases 10-15 years ago (e.g., Filippenko & Ho 2003; Barth et al. 2004), to now homogeneously selected samples reaching $\sim 10^2$ objects in dwarfs (e.g., Reines et al. 2013; Mezcua et al. 2018) and other low-mass galaxies (e.g., Greene & Ho 2004, 2007; Dong et al. 2012). mBHs in dwarf galaxies typically have masses in the $10^4 - 10^6\,M_\odot$ range, with the smallest mBH discovered so far residing in the dwarf galaxy RGG 118, weighing in at only $5 \times 10^4\,M_\odot$ (Baldassare et al. 2015).

Discovering mBHs in dwarf galaxies relies on exploiting radiative signatures from accreting mBHs (see Reines & Comastri 2016 for a recent review). That is, we are sensitive only to mBHs that happen to be shining as active galactic nuclei (AGN). Arguably the most efficient discovery method so far has been based on optical signatures using emission line diagnostics (utlizing data from large-scale spectroscopic surveys; Reines et al. 2013).[2] Optical selection, however, is biased toward AGN with low extinction that are accreting relatively rapidly ($L_{\rm bol}/L_{\rm Edd} > 0.1$).

---

[1]Following Reines et al. (2013), we define dwarf galaxies as having stellar masses $M_\star < 3 \times 10^9\,M_\odot$, which is comparable to the Large Magellanic Cloud.

[2]Infrared searches have also yielded large sample sizes, although see Hainline et al. (2016) for a discussion on the purity of infrared selected samples.

Low-mass AGN can also be found through X-ray surveys (e.g., Kamizasa et al. 2012; Schramm et al. 2013; Lemons et al. 2015; Mezcua et al. 2016, 2018), although X-ray selection is biased against highly obscured systems. Also, a practical limitation with (current) X-ray surveys is that economically surveying large areas of sky generally requires single-epoch X-ray 'snapshots' with our most sensitive facilities. These types of X-ray observations rarely provide enough photons to pursue high signal-to-noise spectroscopic or timing studies. Without spectral and timing information, current X-ray facilities are not usually capable (on their own) of differentiating between accreting mBHs and luminous X-ray binary systems in cases with X-ray luminosities $L_X \lesssim 10^{40}\mathrm{erg\,s^{-1}}$, except for in a handful of bright systems with long X-ray exposure times, or in some cases with a sufficient number of epochs to monitor variability.

3. Revealing Low-mass AGN with an ngVLA

Some of the current practical limitations to pursuing large population studies can be overcome by exploiting jetted radio emission from accreting mBHs. Radio observations have already discovered a few mBHs in dwarfs (Reines et al. 2011, 2014), and a new survey of dwarf galaxies with the Jansky Very Large Array (VLA) is revealing many new candidates (Reines et al. in prep). As described below, once radio facilities start reaching ngVLA sensitivities, mBH AGN selection can become efficient through combined multiwavelength efforts.

At low Eddington ratios ($<10^{-2}\,L_{\rm Edd}$), all AGN are believed to launch compact, partially self-absorbed synchrotron jets that will appear point-like even at ngVLA resolutions (Blandford & Königl 1979; Ho 2008). In this weak accretion regime, the ratio of radio:X-ray luminosity scales in a predictable way with the mass of the accreting black hole according to the fundamental plane of black hole activity, $\log L_{\rm R} = 0.6\log L_{\rm X} + 0.78\log M_{\rm BH} + 7.33$ (e.g., Merloni et al. 2003; Falcke et al. 2004; Plotkin et al. 2012), where $L_{\rm R}$ is at 5 GHz, $L_{\rm X}$ is from 2-10 keV, and $M_{\rm BH}$ is in Solar units.

Since radio jets are expected to be ubiquitous at low accretion rates, a radio survey can be effective at recovering populations of mBH candidates if undertaken with a sensitive enough telescope. Advantages of a radio survey include:

- targeting mBHs in a weak accretion regime will recover objects missed by optical surveys (where the latter rely on diagnostics that are expected to be present mostly at higher accretion rates). Note that for any sensible luminosity function, the majority of AGN accrete at low Eddington ratios;

- jetted radio emission will be detectable from highly absorbed AGN, thereby allowing radio selection to uncover some objects that would be missed by complementary X-ray and/or optical approaches;

- at Mpc distances, contamination in the radio waveband from X-ray binary systems should be negligible. Except, we note that at ngVLA sensitivities ($5\sigma_{\rm rms} \approx 1\,\mu$Jy), it is plausible to (rarely) detect emission from transient radio flares produced by accreting stellar mass black holes out to ≈30 Mpc.[3]

---

[3]We estimate this limit by scaling an extreme 20 Jy radio flare from the Galactic black hole X-ray binary Cyg X-3 (Corbel et al. 2012).

We note that, in this low-luminosity regime, radio surveys will have to contend with radio emission from star formation (i.e., free-free emission in H II regions) and from supernova remnants. However, jetted radio emission from weakly accreting mBHs will be compact and unresolved at Mpc distances. Thus, with long ngVLA baselines ($\sim 10^3$ km), point-like radio emission would be a strong indicator of a viable AGN candidate (e.g., Reines & Deller 2012).

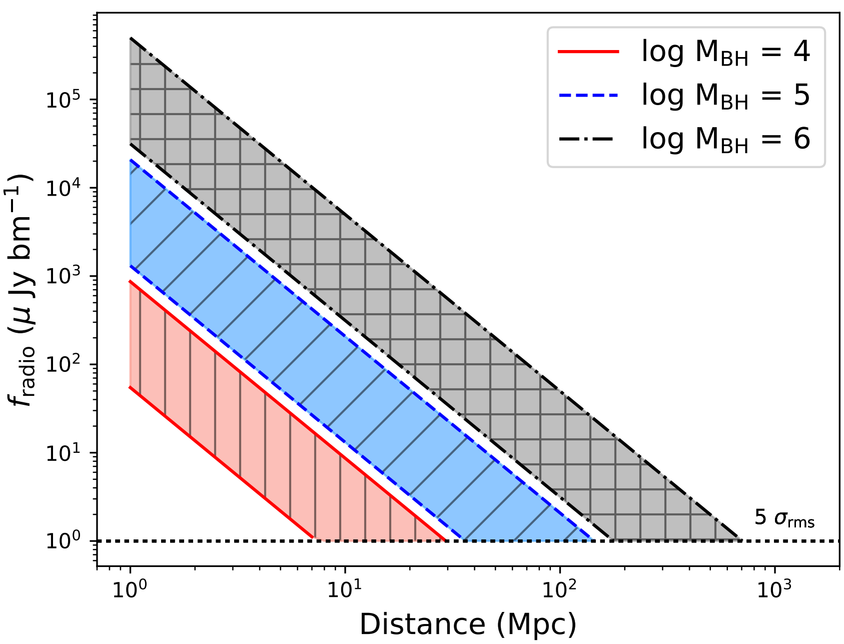

Figure 1. Distances to which an ngVLA could detect compact radio emission from an accreting mBH with 1 hour integrations, if the mBH falls on the fundamental plane of black hole activity (Merloni et al. 2003), and if the mBH has a 2-10 keV X-ray flux $F_X > 10^{-15}$ erg s^{-1} cm^{-2}. The red shaded region bounded by red solid lines illustrates the expected radio flux density (at 8 GHz) for a $10^4\ M_\odot$ mBH accreting between $10^{-5} < L_X < 10^{-3}\ L_{\rm Edd}$; the blue shaded region (bounded by dashed lines) and the grey shaded region (bounded by dashed-dotted lines) illustrate the same for a 10^5 and $10^6\ M_\odot$ mBH, respectively. $5\sigma_{\rm rms}$ radio detection limits for an ngVLA and for the VLA are shown as dashed and dotted lines, respectively (both assuming 1 hour on source). An ngVLA could detect relatively massive mBHs out to nearly 1 Gpc, and it could detect mBHs as small as $10^4\ M_\odot$ at the distance of the Virgo cluster of galaxies ($\sim$16.4 Mpc). Note that the Merloni et al. (2003) fundamental plane has an intrinsic scatter of 0.88 dex in radio luminosity, which is not included in this figure.

In Figure 1 we show the radio flux densities expected at 8 GHz for $10^{-5} < L_X/L_{\rm Edd} < 10^{-3}$ AGNs powered by 10^4 (red swath), 10^5 (blue swatch) and $10^6\ M_\odot$

(grey swath) mBHs as a function of distance.[4] We also show the current VLA $5\sigma_{\rm rms}$ detection limit (dotted horizontal line) and an ngVLA $5\sigma_{\rm rms}$ detection limit (dashed horizontal line) assuming 1 hour integrations. The shaded regions require 2-10 keV X-ray fluxes $F_{\rm X} > 10^{-15}$ erg s^{-1} cm^{-2} to illustrate the types of AGN that can be accessed with an ngVLA combined with an X-ray facility like *Chandra*. An ngVLA would be able to detect relatively massive mBHs ($10^6\,M_\odot$) out to nearly 1 Gpc (almost a factor of four farther than accessible by the current VLA within reasonable exposure times). Excitingly, an ngVLA could detect jetted radio emission from $10^4\,M_\odot$ mBHs accreting at $L_{\rm X} \gtrsim 10^{-4}\,L_{\rm Edd}$, or $10^5\,M_\odot$ mBHs at $\gtrsim 10^{-6}\,L_{\rm Edd}$, at the distance of the Virgo cluster (16.4 Mpc; corresponding to 2-10 keV X-ray fluxes $F_{\rm X} \gtrsim 4\times10^{-15}$ and $\gtrsim 4\times10^{-16}$ erg s^{-1} cm^{-2}, respectively), which we expand on in Section 5.

4. Jet Physics and Mass Scaling

We describe in the next section one way in which revealing new samples of mBHs through an ngVLA would observationally constrain the masses of black hole seeds. In this section, we stress that more sensitive radio observations would also allow studies on the physics of jets in the low-accretion rate and low-mass regime. For example, the sensitivity of an ngVLA would open up economic time-domain studies for bright sources, and its wideband frequency capabilities would allow radio spectral studies (up to 10^2 GHz) for an unprecedented large sample of mBHs (which might even allow detailed decomposition of mBH radio jets from radio emission produced by star formation for the brightest objects). An ngVLA would help constrain the role of AGN feedback in dwarf galaxies and at low accretion rates in the so-called ‘kinetic’ feedback mode (e.g., Xie et al. 2017; Dashyan et al. 2018). By populating observations of extragalactic jets launched by black holes in the $10^4 - 10^6 M_{\rm BH}$ range, an ngVLA would also provide empirical constraints to drive studies on the scalability of black hole accretion and jet launching, through comparisons of mBHs to more massive black holes ($\gtrsim 10^6\,M_\odot$) at the centers of large galaxies, and to lower-mass stellar black holes ($\sim 10\,M_\odot$) in X-ray binary systems.

5. Multiwavelength Studies of Black Hole Seeds

5.1. Multiwavelength Coordination

Constraining black hole seeds through AGN in dwarf galaxies is a multiwavelength endeavor, and it is not a problem that can be tackled looking within only a single band of the electromagnetic spectrum. However, in a multiwavelength context, we expect a radio facility like the ngVLA to play a prominent role. For example, as discussed earlier, optical selection so far has proved to be effective at higher Eddington ratios ($\gtrsim 0.1 L_{\rm Edd}$), but optical surveys largely miss the types of weakly accreting objects for which combined radio/X-ray searches are optimal. It is not obvious whether (in the near future) large high-spatial resolution optical telescopes will outperform radio surveys in the weak accretion regime: weakly accreting AGN do not always have obvious

[4] We note that we expect all AGN accreting at $\lesssim 10^{-2}\,L_{\rm Edd}$ to emit compact radio emission. We adopt the range $10^{-5} - 10^{-3}\,L_{\rm Edd}$ in Figure 1 simply for illustrative purposes, to keep the figure from appearing too cluttered.

optical counterparts in dwarf galaxies (e.g., Reines et al. 2011, 2014), and optical AGN diagnostics, like broad emission lines and narrow high-excitation lines, are expected to become substantially weaker at lower Eddington ratios (e.g., Padovani et al. 2017, and references therein). Thus, efficient optical selection of weakly accreting mBHs would require routine detections of low-excitation narrow AGN emission lines, a method that is possible in principle but has not yet revealed large numbers of AGN candidates in dwarf galaxies. Combining radio and optical samples will therefore reveal AGN over a wider range of Eddington ratios than can be recovered individually.

It is challenging for current (and near-future) X-ray facilities to economically survey large numbers of dwarf galaxies, especially with sufficient sensitivity to unambiguously control for contamination from X-ray binaries. Advantages of an ngVLA are that it can *efficiently* reach useful sensitivities in relatively short (<1 hour) exposures, and contamination from X-ray binaries will be rare for nearby galaxies, and negligible at $\gtrsim$30 Mpc. Furthermore, with its long baselines, contamination from star formation can be minimised by selecting only point-like radio emission.

Radio-selected AGN candidates would then await confirmation by other telescopes, including high spatial-resolution X-ray facilities like the *Chandra X-ray Observatory* or the *Athena X-ray Observatory* (Figure 1 demonstrates the discovery space that is currently feasible via *Chandra* followup to ngVLA AGN candidates). Some of the X-ray brighter systems (e.g., $F_X \gtrsim 10^{-13}$ erg s^{-1} cm^{-2}) will also appear in future all sky surveys (e.g., eROSITA on the *Spectrum-Roentgen-Gamma* satellite). Excitingly, high spatial-resolution infrared spectroscopy, e.g., with the *James Webb Space Telescope (JWST)*, will provide crucial line diagnostics to confirm weakly accreting and/or optically obscured AGN (e.g., Satyapal et al. 2009; Inami et al. 2013; Cann et al. 2018).

5.2. Local Constraints on Black Hole Growth

Identifying AGN in dwarf galaxies is still a young field observationally. The progression of connecting observations of mBHs to theoretical models of seed black hole formation will require continuing to systematically assemble even larger samples over the next decades. As an example, consider the AGN Multiwavelength Survey of Early-Type Galaxies (AMUSE; Gallo et al. 2008; Miller et al. 2012), which performed a *Chandra* X-ray survey of 100 early-type galaxies in the Virgo cluster and 100 non-cluster galaxies at comparable distances to Virgo. By considering the fraction of nuclear X-ray detections within the 200 object AMUSE sample, Miller et al. (2015) provide a framework demonstrating how black hole occupation (and seed formation) can be constrained through local observations of weakly accreting AGN. They place a limit that >20% of local low-mass galaxies ($M_\star < 10^{10} M_\odot$) are occupied by an mBH, and they cannot rule out full occupation. Amongst the results from Miller et al. (2015) we note:

- their 200 object sample is not large enough to place stringent constraints on occupation (although see their Figure 4 for how uncertainties improve with sample size);

- with the types of X-ray sensitivities achievable if aiming to pursue $N \sim 10^2$ sample sizes, contamination from X-ray binaries is an important systematic to be controlled for.

Despite the above, we stress that quantitative methods are already fully developed by Miller et al. (2015), who demonstrate that local calculations of the occupation fraction are in reach. An ngVLA would help improve sample sizes, and it would help provide confidence that contamination from X-ray binaries is negligible.

Since one expects full occupation at the high galaxy (stellar) mass end regardless of the seed black hole mass distribution, diagnosing the seed formation channels will require focusing on lower-mass galaxies (Miller et al. 2015). A typical *Chandra* X-ray exposure time utilized by the AMUSE survey at the distance of Virgo was $\sim$1.4 h, which allowed identification of a $10^5\,M_\odot$ mBH accreting at nearly $10^{-5}\,L_{\rm Edd}$ (a regime that is just barely accessible with the current VLA; see Figure 1). With a comparable or shorter time investment on an ngVLA (depending on overheads), radio observations could identify a $10^5\,M_\odot$ mBH accreting an order of magnitude more weakly ($10^{-6}\,L_{\rm Edd}$), which would clearly improve the sample size the corresponding X-ray flux would be $\approx 4\times10^{-16}$ erg s^{-1} cm^{-2}, which is feasible given that only a subset of objects would be so faint). Thus, identification of AGN in dwarf galaxies (at ngVLA sensitivites) can be expected to place significantly improved constraints on the local black hole occupation fraction and mBH mass distribution, thereby helping to place observational constraints on the population of objects that seeded the growth of black holes in the early Universe.

References

Bañados, E., Venemans, B. P., Mazzucchelli, C., Farina, E. P., Walter, F., Wang, F., Decarli, R., Stern, D., Fan, X., Davies, F. B., Hennawi, J. F., Simcoe, R. A., Turner, M. L., Rix, H.-W., Yang, J., Kelson, D. D., Rudie, G. C., & Winters, J. M. 2018, Nat, 553, 473. 1712.01860

Baldassare, V. F., Reines, A. E., Gallo, E., & Greene, J. E. 2015, ApJ, 809, L14. 1506.07531

Barth, A. J., Ho, L. C., Rutledge, R. E., & Sargent, W. L. W. 2004, ApJ, 607, 90. astro-ph/0402110

Begelman, M. C., Volonteri, M., & Rees, M. J. 2006, MNRAS, 370, 289. astro-ph/0602363

Bellovary, J., Volonteri, M., Governato, F., Shen, S., Quinn, T., & Wadsley, J. 2011, ApJ, 742, 13. 1104.3858

Blandford, R. D., & Königl, A. 1979, ApJ, 232, 34

Cann, J. M., Satyapal, S., Abel, N. P., Ricci, C., Secrest, N. J., Blecha, L., & Gliozzi, M. 2018, ArXiv e-prints. 1805.09351

Corbel, S., Dubus, G., Tomsick, J. A., Szostek, A., Corbet, R. H. D., Miller-Jones, J. C. A., Richards, J. L., Pooley, G., Trushkin, S., Dubois, R., Hill, A. B., Kerr, M., Max-Moerbeck, W., Readhead, A. C. S., Bodaghee, A., Tudose, V., Parent, D., Wilms, J., & Pottschmidt, K. 2012, MNRAS, 421, 2947. 1201.3356

Dashyan, G., Silk, J., Mamon, G. A., Dubois, Y., & Hartwig, T. 2018, MNRAS, 473, 5698. 1710.05900

Dong, X.-B., Ho, L. C., Yuan, W., Wang, T.-G., Fan, X., Zhou, H., & Jiang, N. 2012, ApJ, 755, 167. 1206.3843

Dubois, Y., Volonteri, M., Silk, J., Devriendt, J., Slyz, A., & Teyssier, R. 2015, MNRAS, 452, 1502. 1504.00018

Fabian, A. C. 2012, ARA&A, 50, 455. 1204.4114

Falcke, H., Körding, E., & Markoff, S. 2004, A&A, 414, 895. astro-ph/0305335

Filippenko, A. V., & Ho, L. C. 2003, ApJ, 588, L13. astro-ph/0303429

Gallo, E., Treu, T., Jacob, J., Woo, J.-H., Marshall, P. J., & Antonucci, R. 2008, ApJ, 680, 154. 0711.2073

Greene, J. E. 2012, Nature Communications, 3, 1304. 1211.7082

Greene, J. E., & Ho, L. C. 2004, ApJ, 610, 722. astro-ph/0404110

— 2007, ApJ, 670, 92. 0707.2617

Habouzit, M., Volonteri, M., & Dubois, Y. 2017, MNRAS, 468, 3935. 1605.09394

Haiman, Z., & Loeb, A. 2001, ApJ, 552, 459. astro-ph/0011529
Hainline, K. N., Reines, A. E., Greene, J. E., & Stern, D. 2016, ApJ, 832, 119. 1609.06721
Ho, L. C. 2008, ARA&A, 46, 475. 0803.2268
Inami, H., Armus, L., Charmandaris, V., Groves, B., Kewley, L., Petric, A., Stierwalt, S., Díaz-Santos, T., Surace, J., Rich, J., Haan, S., Howell, J., Evans, A. S., Mazzarella, J., Marshall, J., Appleton, P., Lord, S., Spoon, H., Frayer, D., Matsuhara, H., & Veilleux, S. 2013, ApJ, 777, 156. 1309.4788
Kamizasa, N., Terashima, Y., & Awaki, H. 2012, ApJ, 751, 39. 1205.2772
Lemons, S. M., Reines, A. E., Plotkin, R. M., Gallo, E., & Greene, J. E. 2015, ApJ, 805, 12. 1502.06958
Loeb, A., & Rasio, F. A. 1994, ApJ, 432, 52. astro-ph/9401026
Madau, P., Haardt, F., & Dotti, M. 2014, ApJ, 784, L38. 1402.6995
Madau, P., & Rees, M. J. 2001, ApJ, 551, L27. astro-ph/0101223
Merloni, A., Heinz, S., & di Matteo, T. 2003, MNRAS, 345, 1057. astro-ph/0305261
Mezcua, M. 2017, International Journal of Modern Physics D, 26, 1730021. 1705.09667
Mezcua, M., Civano, F., Fabbiano, G., Miyaji, T., & Marchesi, S. 2016, ApJ, 817, 20. 1511.05844
Mezcua, M., Civano, F., Marchesi, S., Suh, H., Fabbiano, G., & Volonteri, M. 2018, MNRAS. 1802.01567
Miller, B., Gallo, E., Treu, T., & Woo, J.-H. 2012, ApJ, 747, 57. 1112.3985
Miller, B. P., Gallo, E., Greene, J. E., Kelly, B. C., Treu, T., Woo, J.-H., & Baldassare, V. 2015, ApJ, 799, 98. 1403.4246
Mortlock, D. J., Warren, S. J., Venemans, B. P., Patel, M., Hewett, P. C., McMahon, R. G., Simpson, C., Theuns, T., Gonzáles-Solares, E. A., Adamson, A., Dye, S., Hambly, N. C., Hirst, P., Irwin, M. J., Kuiper, E., Lawrence, A., & Röttgering, H. J. A. 2011, Nat, 474, 616. 1106.6088
Padovani, P., Alexander, D. M., Assef, R. J., De Marco, B., Giommi, P., Hickox, R. C., Richards, G. T., Smolčić, V., Hatziminaoglou, E., Mainieri, V., & Salvato, M. 2017, A&A Rev., 25, 2. 1707.07134
Plotkin, R. M., Markoff, S., Kelly, B. C., Körding, E., & Anderson, S. F. 2012, MNRAS, 419, 267. 1105.3211
Reines, A. E., & Comastri, A. 2016, PASA, 33, e054. 1609.03562
Reines, A. E., & Deller, A. T. 2012, ApJ, 750, L24. 1204.1970
Reines, A. E., Greene, J. E., & Geha, M. 2013, ApJ, 775, 116. 1308.0328
Reines, A. E., Plotkin, R. M., Russell, T. D., Mezcua, M., Condon, J. J., Sivakoff, G. R., & Johnson, K. E. 2014, ApJ, 787, L30. 1405.0278
Reines, A. E., Sivakoff, G. R., Johnson, K. E., & Brogan, C. L. 2011, Nat, 470, 66. 1101.1309
Satyapal, S., Böker, T., Mcalpine, W., Gliozzi, M., Abel, N. P., & Heckman, T. 2009, ApJ, 704, 439. 0908.1820
Schramm, M., Silverman, J. D., Greene, J. E., Brandt, W. N., Luo, B., Xue, Y. Q., Capak, P., Kakazu, Y., Kartaltepe, J., & Mainieri, V. 2013, ApJ, 773, 150. 1305.3826
van Wassenhove, S., Volonteri, M., Walker, M. G., & Gair, J. R. 2010, MNRAS, 408, 1139. 1001.5451
Volonteri, M. 2010, A&A Rev., 18, 279. 1003.4404
Volonteri, M., & Natarajan, P. 2009, MNRAS, 400, 1911. 0903.2262
Volonteri, M., & Reines, A. E. 2016, ApJ, 820, L6. 1602.05711
Xie, F.-G., Yuan, F., & Ho, L. C. 2017, ApJ, 844, 42. 1705.05037

Science with a Next-Generation Very Large Array
ASP Conference Series, Monograph 7
Eric J. Murphy, ed.

DRAFT EDITION

Tidal Disruption Events

Sjoert van Velzen[1], Geoffrey C. Bower[2], and Brian D. Metzger[3]
[1]*New York University, New York, NY 10003, USA;* sjoert@nyu.edu

[2]*Academia Sinica Institute of Astronomy and Astrophysics, Hilo, HI 96720, USA*

[3]*Columbia Astrophysics Laboratory, New York, NY 10027, USA*

Abstract. The tidal disruption and subsequent accretion of a star by a supermassive black hole can be used as a laboratory to study the physics of relativistic jets. The ngVLA is the only planned instrument that can both discover and characterize a large number of these short-lived radio sources. In particular the high-frequency capabilities of the ngVLA enable this important leap forward. Multi-frequency radio follow-up observations (3-100 GHz) of tidal disruption events found in optical or X-ray surveys will provide a measurement of the jet efficiency as a function of black hole spin, thus enabling a direct test of the prediction that relativistic jets require high spin. Hundreds tidal disruption jets will be discovered in a blind ngVLA survey for radio transients. By including VLBI observations we can resolve some of these sources, obtaining a robust measurement of the jet launch date and the magnetic field strength. From the thermal emission of the tidal disruption flare we can measure the accretion rate at this launch date, thus providing another unique opportunity to identify the conditions that lead to jet production.

1. Introduction: thermal and non-thermal emission

A rare glimpse into the properties of normally quiescent massive black holes is afforded when a star passes sufficiently close that it is torn apart by the black hole's tidal gravitational field (Hills 1975). The process of disruption leaves a significant fraction of the shredded star gravitationally bound to the black hole (Rees 1988; Evans & Kochanek 1989) and this stellar debris has been predicted to power a thermal flare at optical, UV, and X-ray wavelengths. Over a dozen such thermal tidal disruption flare (TDF) candidates have now identified (Komossa 2015; van Velzen 2018 and references therein). Based on the current detection rate in optical surveys, we expect that the Large Synoptic Survey Telescope (LSST) will yield thousands of thermal TDFs per year (Gezari et al. 2009; van Velzen et al. 2011).

Radio follow-up observations of thermal TDFs have mostly yielded non-detections (Bower et al. 2013; van Velzen et al. 2013; Arcavi et al. 2014). Only two low-redshift thermal TDFs ($z < 0.02$) have been detected in radio follow-up observations (van Velzen et al. 2016; Alexander et al. 2016, 2017). The origin of this radio emission is debated, both a jet (van Velzen et al. 2011), a disk-wind (Alexander et al. 2016), or unbound stellar debris (Krolik et al. 2016) have been proposed. For one event (ASASSN-14li; Holoien et al. 2016), the detection of a cross-correlation between the X-ray and

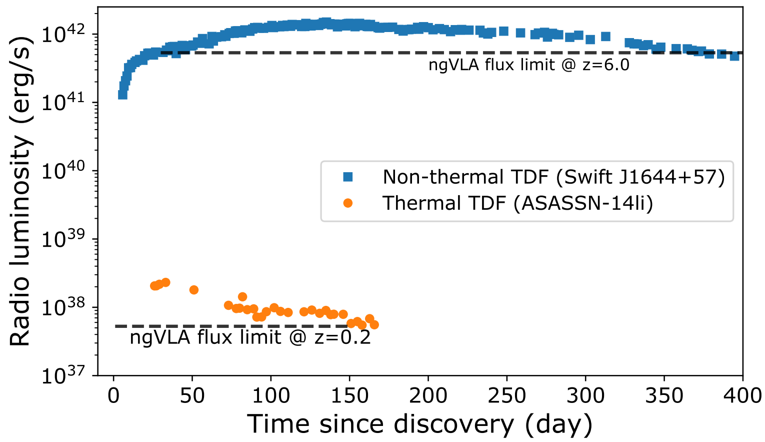

Figure 1. Radio light curve (15 GHz) of two archetype radio-emitting TDFs. The dashed line indicates a 5σ detection threshold of a potential ngVLA transient survey using 10 minute snapshots at 8 GHz (Band 2) to a reach an image rms of 1 μJy/beam. If most thermal TDFs are accompanied by radio emission similar to ASASSN-14li, a blind ngVLA survey covering 300 deg^2 should detect $\sim$ 10 of these events per year, the expected detection rate of events similar to Swift J1644+57 is an order of magnitude higher.

radio light curves provides evidence that the radio emission is produced internal to a moderately relativistic jet (Pasham & van Velzen 2018).

While most known TDFs are dominated by thermal emission, a second class of events is discovered via non-thermal γ-ray emission. The most famous example in this class is Swift J1644+57 (Bloom et al. 2011; Levan et al. 2011; Burrows et al. 2011; Zauderer et al. 2011). This source was characterized by powerful ($\nu L_\nu \sim 10^{47}$ erg s^{-1}) hard X-ray emission. The long duration of Swift J1644+57 and a position coincident with the nucleus of a previously quiescent galaxy led to the conclusion that it was powered by rapid accretion onto the central black hole following a stellar disruption. The rapid X-ray variability suggested an origin internal to a jet that is relativistically beaming its radiation along our line of sight, similar to the blazar geometry of normal active galactic nuclei (Bloom et al. 2011).

Swift J1644+57 was also characterized by luminous synchrotron radio emission, that brightened gradually over the course of several months (Berger et al. 2012; Zauderer et al. 2013), as shown in Figure 1. This radio emission resulted from the shock interaction between the stellar tidal disruption jet and the external gas surrounding the black hole (Giannios & Metzger 2011), similar to a gamma-ray burst afterglow. Two more jetted tidal disruption events with similar X-ray and radio properties to Swift J1644+57 have been found (Cenko et al. 2012; Pasham et al. 2015; Brown et al. 2015).

2. Using tidal disruption events to study the physics of jet launching

When a central object gathers mass through an accretion disk, jets are ubiquitous. Jets transport energy away from the disk, thus greatly enhancing the scale at which the accreting object (neutron star, black hole, or protostar) can influence its environment. As discussed in detail in earlier chapters of this book, jets from supermassive black holes can provide strong negative feedback onto their host galaxy. However, adding jet mode feedback to cosmological galaxy simulations (e.g., Vogelsberger et al. 2014) requires a key ingredient that is currently missing: the jet duty cycle and lifetime. If powerful, long-lived jets can only be produced for a small fraction of active galactic nuclei (AGN), jet feedback will be limited to the sub-class of galaxies that host these black holes. On the other hand, AGN may experience multiple cycles of jet production, implying a higher efficiency of inter-galaxy jet feedback. These two scenarios, long-lived versus intermittent jets, broadly correspond to two opposing theories of jet production: the spin paradigm and the accretion paradigm.

In the spin paradigm, jets are powered by the rotational energy of the black hole, which can be tapped using the magnetic field lines that thread the black hole horizon (Blandford & Znajek 1977). Only rapidly spinning black holes are observed to be radio loud. Alternatively, the low number of radio-loud quasars (e.g., Kellermann et al. 1989) can be explained by intermittent jet production due to a state change of the accretion disk (Falcke et al. 2004; Körding et al. 2006). This accretion-paradigm is motivated by observations of stellar mass black holes in X-ray binaries, where jet production triggered by a state change of the accretion disk can be observed directly (Fender, Belloni, & Gallo 2004).

The current body of observations of AGN is not sufficient to solve the problem of jet launching because state changes of these systems are nearly[1] impossible to observe directly due to the long timescales associated with the feeding of AGN. A tidal disruption event provides an opportunity to observe jets from supermassive black holes in real time. Since the fallback rate onto the black hole changes from super-Eddington to sub-Eddington in a few months to years, we may expect jet production due to state changes of the accretion disk (Giannios & Metzger 2011; van Velzen et al. 2011). However our current radio observations of tidal disruption are not yet sufficient to make unambiguous inference on jet production. First of all, the number of radio-detected sources is very small. Second, the nature of radio emission from thermal TDFs is unclear. And third, the event rate of the non-thermal TDFs with powerful jets is unknown.

The ngVLA will overcome all these limitations at once. A key element that makes this possible is the increased sensitivity at high-frequency ($\nu > 3$ GHz). Due to synchrotron self-absorption, TDF jets—like most synchrotron-powered transients—are very faint at low radio frequencies. Only when the source grows large enough, it becomes bright at $\nu \sim 1$ GHz. But at this large size, the typical timescale of the radio emission long (~ 1 yr); since this timescale is similar to the cadence of most surveys, the amplitude of most synchrotron transients observed at low frequencies is small. Finally, with the high angular resolution of the ngVLA(+VLBI) we can resolve radio emission from TDFs and thus watch these newborn jets grow with time.

[1]The so-called changing look AGN (e.g., LaMassa et al. 2015) could present an exception to normal AGN variability (Graham et al. 2017) and can be used to study the jet-disk connection over ~ 10 yr timescales (e.g., Koay et al. 2016)

In the next two subsections we discuss how the ngVLA can revolutionize TDF research using two different modes of observation: follow-up and discovery.

2.1. Follow-up of TDFs with the ngVLA

Radio follow-up observations with current facilities have only yielded detections for low-redshift TDFs ($z < 0.05$). Current optical surveys for thermal TDF are nearly complete for these nearby events, finding about one per year. While the LSST and other optical or X-ray surveys will increase the detection rate of thermal TDFs to thousands per year, the majority of these will be far too distant to be detectable with Jansky VLA follow-up observations. This implies the detection rate of radio-emitting thermal TDFs will fall behind the overall detection rate of TDFs.

A tenfold increase to the sensitivity of the Jansky VLA will push the maximum redshift for detection (within 10 min of integration time per source) of radio emission from thermal TDFs to $z = 0.2$. The order of magnitude increase to the detection rate will enable measurements of the incidence of radio emission as a function of host galaxy properties. Most importantly, we can measure the jet production efficiency as a function of black hole spin. Disruptions by black holes more massive than $10^8\,M_\odot$ are visible only when the black hole is spinning (Stone et al. 2018). Such events are rare, but the first TDF candidate from a black hole above this critical mass was recently detected (Dong et al. 2016; Leloudas et al. 2016; Margutti et al. 2017; Krühler et al. 2018). To conclude, ngVLA follow-up observations of thermal TDFs will yield a measurement of the radio luminosity as a function of black hole spin, thus providing a crucial test of the spin paradigm of jet production.

2.2. Discovery of TDFs in blind ngVLA surveys

Thanks to their high luminosity, radio emission from non-thermal TDF jets (such as Swift J1644+57) can be detected by current radio surveys well into the dawn of galaxy formation (Metzger, Williams, & Berger 2015). As demonstrated in van Velzen et al. (2013), the detection rate of these events in surveys for radio transients can be estimated using the observed light curve of Swift J1644+57. This estimate requires the volumetric event rate, which can in turn be estimated from the observed rate of on-axis tidal disruption jets ($\sim 10^{-2}\,\mathrm{Gpc}^{-3}\mathrm{yr}^{-1}$, based on the *Swift* data; Brown et al. 2015; Levan et al. 2016) and applying a beaming correction (δ) to obtain the isotropic rate. The beaming correction can both be estimated from the requirement that the intrinsic X-ray luminosity should not exceed the Eddington limit, or by modeling the radio light curves. Both of these approaches yield $\delta \sim 10^2$, hence the volumetric rate of events similar to Swift J1644+57 can be estimated to be $\sim 1\,\mathrm{Gpc}^{-3}\mathrm{yr}^{-1}$.

Using a model to predict the off-axis light curve of events similar to Swift J1644+57, the resulting detection rate of off-axis TDF jets in VLASS is about 10 per year. However the cadence of the VLASS is low ($\approx$ 16 months), hence most sources will be detected after maximum light. The cadence of surveys at $\approx$ 1 GHz by SKA precursors, such as VAST (Murphy et al. 2013) and ThunderKAT (Fender et al. 2017), is higher. The detection rate for off-axis TDF jets in these surveys is also about 10 per year (Metzger et al. 2015). However, due to the very shallow amplitude of the 1 GHz light curves, the identification of these events using only SKA data will be difficult; coordinated observations at higher frequencies (X-ray or optical) will be required (Donnarumma & Rossi 2015; Donnarumma et al. 2015). Follow-up observations of SKA-discovered TDFs with the VLA or ALMA are difficult because the emission at these higher radio frequencies fades within months to weeks, while the emission at 1 GHz is delayed by about a year. Therefore most TDFs candidates found in SKA surveys will have monochromatic radio light curves.

The high frequency capabilities for the ngVLA will enable both the discovery *and* characterization of TDFs in blind radio surveys. Using observations from 3 to 100 GHz, we can measure the total energy of the jet and estimate the expansion velocity. By comparing the event rate from this blind radio survey to observed rate of TDFs found by *Swift* we obtaind the beaming factor (δ). The detection of a low beaming factor will imply a super-Eddington luminosity for the hard X-ray, as suggested in some models of Swift J1644+57 (Kara et al. 2016). Scaling from estimates by Metzger et al. (2015) for the number of TDFs in VLASS (using 10^4 deg^2 at an rms of 0.1 mJy/beam), we can expect $\sim 10^2$ event per year for a ngVLA transient survey in band 1 (3 GHz).

For some low-redshift TDFs with powerful jets we can resolve the new radio source. With ngVLA observations in band 4 ($\approx$ 30 GHz, yielding a maximum resolutoin of a few mas) we can likely resolve jets similar to Swift J1644+57 at $z < 0.1$ within one year after launch. The number of detections at this redshift is low ($<$ 1 per year); including VLBI to the ngVLA would signficantly increase the detection rate. Resolving a newly created jet presents a unique oppurtunity, allowing a measurement of the magnetic field of the radio-emitting region without using the equipartition assumption (e.g., Falcke et al. 1999). Furthermore, by extrapolating the source size measurements backwards in time, we obtain the launch date of the jet. This launch date can be compared to the light curve of the TDF disk emission, providing a direct test of the prediction that jet launching requires super-Eddington accretion rates (e.g., Tchekhovskoy et al. 2014).

Comparing the rate of tidal disruption jets detected in ngVLA surveys to the rate of TDFs detected by their thermal disk emission (in X-ray or optical surveys) we obtain the jet efficiency (i.e., the fraction of disruptions that lead to jets). Using multi-frequency radio light curves we can measure jet efficiency as a function of the total jet energy. Within the accretion paradigm we would expect that the efficiency is constant because the jet energy reflects the amount of stellar debris that was accreted. If, on the other hand, jets are powered by spin, we would expect a few TDFs with a total jet energy that exceeds the rest-mass energy of the accreted debris.

In this chapter we focused on using radio observations of TDFs to constrain models of jet formation. Yet the radio light curves of these sources can also be used as tools to measure the gas density in nuclei of their host galaxies (Zauderer et al. 2011; Berger et al. 2012; Generozov et al. 2017; Eftekhari et al. 2018). Since we can detect sources similar to Swift J1644+57 to very high redshifts (Fig. 1), we can use ngVLA observations to probe the environments of black holes in the earliest stages of their growth.

References

Alexander, K. D., Berger, E., Guillochon, J., Zauderer, B. A., & Williams, P. K. G. 2016, ApJ, 819, L25
Alexander, K. D., Wieringa, M. H., Berger, E., Saxton, R. D., & Komossa, S. 2017, ApJ, 837, 153
Arcavi, I., Gal-Yam, A., Sullivan, M., et al. 2014, ApJ, 793, 38
Berger, E., Zauderer, A., Pooley, G. G., et al. 2012, ApJ, 748, 36
Blandford, R. D., & Znajek, R. L. 1977, MNRAS, 179, 433
Bloom, J. S., Giannios, D., Metzger, B. D., et al. 2011, Science, 333, 203

Bower, G. C., Metzger, B. D., Cenko, S. B., Silverman, J. M., & Bloom, J. S. 2013, ApJ, 763, 84

Brown, G. C., Levan, A. J., Stanway, E. R., et al. 2015, MNRAS, 452, 4297

Burrows, D. N., Kennea, J. A., Ghisellini, G., et al. 2011, Nat, 476, 421

Cenko, S. B., Bloom, J. S., Kulkarni, S. R., et al. 2012, MNRAS, 420, 2684

Dong, S., Shappee, B. J., Prieto, J. L., et al. 2016, Science, 351, 257

Donnarumma, I., & Rossi, E. M. 2015, ApJ, 803, 36

Donnarumma, I., Rossi, E. M., Fender, R., et al. 2015, Advancing Astrophysics with the Square Kilometre Array (AASKA14), 54

Eftekhari, T., Berger, E., Zauderer, B. A., Margutti, R., & Alexander, K. D. 2018, ApJ, 854, 86

Evans, C. R., & Kochanek, C. S. 1989, ApJ, 346, L13

Falcke, H., Körding, E., & Markoff, S. 2004, A&A, 414, 895

Falcke, H., Bower, G. C., Lobanov, A. P., et al. 1999, ApJ, 514, L17

Fender, R., Woudt, P., Armstrong, R., et al. 2017, 1711.04132

Fender, R. P., Belloni, T. M., & Gallo, E. 2004, MNRAS, 355, 1105

Generozov, A., Mimica, P., Metzger, B. D., et al. 2017, MNRAS, 464, 2481

Gezari, S., Heckman, T., Cenko, S. B., et al. 2009, ApJ, 698, 1367

Giannios, D., & Metzger, B. D. 2011, MNRAS, 416, 2102

Graham, M. J., Djorgovski, S. G., Drake, A. J., et al. 2017, MNRAS, 470, 4112

Hills, J. G. 1975, Nat, 254, 295

Holoien, T. W.-S., Kochanek, C. S., Prieto, J. L., et al. 2016, MNRAS, 455, 2918

Kara, E., Miller, J. M., Reynolds, C., & Dai, L. 2016, Nat, 535, 388

Kellermann, K. I., Sramek, R., Schmidt, M., Shaffer, D. B., & Green, R. 1989, AJ, 98, 1195

Koay, J. Y., Vestergaard, M., Bignall, H. E., Reynolds, C., & Peterson, B. M. 2016, MNRAS, 460, 304

Komossa, S. 2015, Journal of High Energy Astrophysics, 7, 148

Körding, E. G., Jester, S., & Fender, R. 2006, MNRAS, 372, 1366

Krolik, J., Piran, T., Svirski, G., & Cheng, R. M. 2016, ApJ, 827, 127

Krühler, T., Fraser, M., Leloudas, G., et al. 2018, A&A, 610, A14

LaMassa, S. M., Cales, S., Moran, E. C., et al. 2015, ApJ, 800, 144

Leloudas, G., Fraser, M., Stone, N. C., et al. 2016, Nature Astronomy, 1, 0002

Levan, A. J., Tanvir, N. R., Cenko, S. B., et al. 2011, Science, 333, 199

Levan, A. J., Tanvir, N. R., Brown, G. C., et al. 2016, ApJ, 819, 51

Margutti, R., Metzger, B. D., Chornock, R., et al. 2017, ApJ, 836, 25

Metzger, B. D., Williams, P. K. G., & Berger, E. 2015, ApJ, 806, 224

Murphy, T., Chatterjee, S., Kaplan, D. L., et al. 2013, 30, 6

Pasham, D. R., & van Velzen, S. 2018, ApJ, 856, 14

Pasham, D. R., Cenko, S. B., Levan, A. J., et al. 2015, ApJ, 805, 68

Rees, M. J. 1988, Nat, 333, 523

Stone, N. C., Kesden, M., Cheng, R. M., & Velzen, S. v. 2018, arXiv:1801.10180v1

Tchekhovskoy, A., Metzger, B. D., Giannios, D., & Kelley, L. Z. 2014, MNRAS, 437, 2744

van Velzen, S. 2018, ApJ, 852, 72

van Velzen, S., Frail, D. A., Körding, E., & Falcke, H. 2013, A&A, 552, A5

van Velzen, S., Körding, E., & Falcke, H. 2011, MNRAS, 417, L51

van Velzen, S., Farrar, G. R., Gezari, S., et al. 2011, ApJ, 741, 73

van Velzen, S., Anderson, G. E., Stone, N. C., et al. 2016, Science, 351, 62

Vogelsberger, M., Genel, S., Springel, V., et al. 2014, Nat, 509, 177

Zauderer, B. A., Berger, E., Margutti, R., et al. 2013, ApJ, 767, 152

Zauderer, B. A., Berger, E., Soderberg, A. M., et al. 2011, Nat, 476, 425

Science with a Next-Generation Very Large Array
ASP Conference Series, Monograph 7
Eric J. Murphy, ed.

DRAFT EDITION

Intermediate-Mass Black Holes in Globular Cluster Systems

J. M. Wrobel,[1] J. C. A. Miller-Jones,[2] K. E. Nyland,[3] and T. J. Maccarone[4]
[1]*National Radio Astronomy Observatory, P.O. Box O, Socorro, NM 87801, USA;* jwrobel@nrao.edu

[2]*International Centre for Radio Astronomy Research, Curtin University, GPO Box U1987, Perth, WA 6845, Australia;* james.miller-jones@curtin.edu.au

[3]*National Radio Astronomy Observatory, Charlottesville, VA 22903, USA;* knyland@nrao.edu

[4]*Department of Physics and Astronomy, Texas Tech University, Box 41051, Lubbock, TX 79409-1051, USA;* thomas.maccarone@ttu.edu

Abstract. Using the Next Generation Very Large Array (ngVLA), we will make a comprehensive inventory of intermediate-mass black holes (IMBHs) in hundreds of globular cluster systems out to a distance of 25 Mpc. IMBHs have masses $M_{IMBH} \sim 100 - 100,000\ M_\odot$. Finding them in globular clusters would validate a formation channel for seed black holes in the early universe and inform event predictions for gravitational wave facilities. Reaching a large number of globular clusters is key, as Fragione et al. (2018) predict that only a few percent will have retained their gravitational-wave fostering IMBHs.

1. Scientific Motivation

Theory suggests that globular clusters (GCs) of stars can host intermediate-mass black holes (IMBHs) with masses $M_{IMBH} \sim 100 - 100,000\ M_\odot$ (Miller & Hamilton 2002; Gurkan et al. 2004; Portegies Zwart et al. 2004; Giersz et al. 2015; Mezcua 2017). Finding IMBHs in GCs would validate a formation channel for seed black holes (BHs) in the early universe (e.g., Volonteri 2010; Sakurai et al. 2017); populate the mass gap between the well-understood stellar-mass BHs and the well-studied supermassive BHs (e.g., Kormendy & Ho 2013; Tetarenko et al. 2016a); and test if scaling relations between stellar systems and their central BHs extend into poorly-explored mass regimes (e.g., Graham & Scott 2015). Also, the GC system of a typical galaxy contains several hundred GCs (Harris 2016). Thus studying such a system could constrain the mass spectrum of IMBHs in its GCs and, related, the ability of its GCs to retain their IMBHs and foster gravitational wave (GW) events (e.g., Holley-Bockelmann et al. 2008; Fragione et al. 2018). These properties could vary from galaxy to galaxy, so many GC systems should be studied. Importantly, a GC system with a low fraction of IMBHs at present could be linked to a high rate of GW events in the past.

To search for IMBHs in GCs, one looks for evidence that the IMBHs are affecting the properties of their GC hosts. For GCs in the Local Group, a common approach is to use optical or infrared data to look for the dynamical signatures of IMBHs on the orbits of stars in the GCs. Such sphere-of-influence studies have a contentious history (e.g., Baumgardt 2017; Mezcua 2017, and references therein), even leading to differing IMBH masses when using the orbits of stars or of radio pulsars in the same GC (e.g., Gieles et al. 2017; Perera et al. 2017). Having 3-dimensional velocity fields should improve the dynamical searches (Drukier & Bailyn 2003). Still, they are fundamentally limited by shot noise due the small number of orbits influenced (e.g., van der Marel 2013). The dynamical searches are also susceptible to measuring high concentrations of stellar remnants rather than an IMBH (e.g., den Brok et al. 2014).

An independent approach that bypasses these issues is to look for the accretion signatures of IMBHs in GCs (Maccarone 2016, and references therein). This approach leverages on decades of studies of the signatures of accretion onto both stellar-mass and supermassive BHs (Fender & Munoz-Darias 2016, and references therein). Here, we apply a synchrotron radio model to search for the signatures of low rates of accretion onto IMBHs in entire GC systems. The model was developed for GCs in the Local Group (Maccarone 2004; Maccarone & Servillat 2008, 2010; Strader et al. 2012) and is summarized in Section 2. We have used the US National Science Foundation's Karl G. Jansky Very Large Array (VLA; Perley et al. 2011) to demonstrate the feasibility of a radio search for IMBHs in one nearby GC system (Wrobel et al. 2016) and summarize that effort in Section 3. In Section 4 we demonstrate the breakthrough role that the Next Generation VLA (ngVLA; Selina & Murphy 2017) will have in searching for IMBHs in hundreds of GC systems hosted in nearby galaxies. We close, in Section 5, by linking these searches to related studies using facilities contemporary with the ngVLA.

2. Synchrotron Radio Model

We invoke a semi-empirical model to predict the mass of an IMBH that, if accreting slowly from the tenuous gas supplied by evolving stars, is consistent with the synchrotron radio luminosity of a GC (Strader et al. 2012, and references therein). Following Strader et al. (2012), we assume gas-capture at 3% of the Bondi rate (Pellegrini 2005; Merloni & Heinz 2007) for gas at a density of 0.2 particles cm^{-3} as measured by Freire et al. (2001), and at a constant temperature of 10,000 K as justified by Scott & Rose (1975). We also assume that accretion proceeds at less than 2% of the Eddington rate, thus involving an advection-dominated accretion flow with a predictable, persistent X-ray luminosity. (An IMBH accreting at higher than 2% of the Eddington rate would enter an X-ray-luminous state (Maccarone 2003) and be easily detectable in existing surveys. But no such X-ray sources exist in Galactic GCs.) We then use the empirical fundamental-plane of BH activity (Merloni et al. 2003; Falcke et al. 2004; Plotkin et al. 2012) to predict the synchrotron radio luminosity. The radio emission is expected to be persistent, flat-spectrum, jet-like but spatially unresolved, and located near the dynamical center of the GC.

From parameter uncertainties, Strader et al. (2012) estimate that the IMBH mass associated with a given radio luminosity could be in error by 0.39 dex, thus a factor of 2.5. To improve the robustness of such masses, one could fold in more recent data, especially regarding the highly uncertain gas-capture parameter. It could also be profitable to examine the model's underlying framework. For example, guided by Scott & Rose (1975), the model assumes that the classic Bondi flow toward a point mass, the IMBH, is isothermal. Yet the classic Bondi accretion rate would be lower if the flow could be argued to be adiabatic (Pellegrini 2005; Perera et al. 2017). On the other hand,

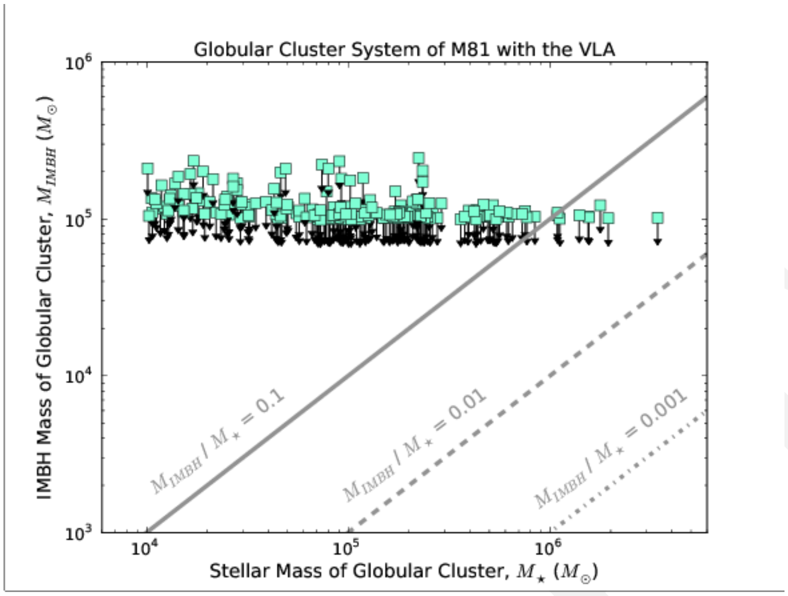

Figure 1. 3σ upper limits to the mass of the IMBH, M_{IMBH}, according to the Strader et al. (2012) model, as a function of the stellar mass, $M_\star$, for probable GCs in M81 (Wrobel et al. 2016). The grey diagonal lines of constant $M_{IMBH}/M_\star$ convey fiducial ratios of IMBH mass to stellar mass.

models for an isothermal flow toward an IMBH embedded in a realistic GC potential appear to achieve higher accretion rates than classic Bondi flows that are isothermal (Pepe & Pellizza 2013).

3. Globular Cluster System of M81 with the VLA

We searched for the radiative signatures of IMBH accretion from 206 probable GCs in M81 (Wrobel et al. 2016), a spiral galaxy at a distance of 3.63 Mpc (Freedman et al. 1994). Forty percent of the probable GCs are spectroscopically confirmed, with the balance deemed to be good GC candidates (Nantais et al. 2011). Our search used a four-pointing VLA mosaic at a wavelength of 5.5 cm and a spatial resolution of 1.5 arcsec (26.4 pc). It achieved 3σ upper limits of $3\times(4.3-51)$ μJy for point sources in individual GCs, depending on their location in the mosaic. Weighted-mean image stacks yielded 3σ upper limits of 3×0.43 μJy for all GCs and 3×0.74 μJy for the 49 GCs with stellar masses $M_\star \gtrsim 200,000 M_\odot$ based on the Nantais et al. (2011) photometry. We applied the Strader et al. (2012) synchrotron model to predict the IMBH mass, M_{IMBH}, consistent with a given luminosity at 5.5 cm. Figure 1 shows upper limits on M_{IMBH} and $M_\star$ for the individual GCs.

For 7 GCs in M81 the ratios of their IMBH masses to stellar masses, $M_{IMBH}/M_\star$, appear to be less than 0.03-0.09. These upper limits are competitive with the value of 0.02 for the five-times-closer G1, the only extragalactic GC with an IMBH inferred by spatially resolving its sphere of influence on cluster stars (Gebhardt et al. 2005). (Note, though, that G1's X-ray and radio properties suggest a ratio of less than 0.01 (Miller-Jones et al. 2012).) Also, the M81 stacks correspond to mean IMBH masses of less than 42,000 $M_\odot$ for all GCs and less than 51,000 $M_\odot$ for the 49 GCs with high stellar masses. The VLA is thus making inroads into the difficult-to-observe regime of IMBHs in extragalactic GCs. Further significant progress demands deeper radio observations of individual GCs in M81 and in other nearby GC systems. Such efforts will admittedly have poorer mass sensitivities than possible for individual Galactic GCs (e.g., Strader et al. 2012). But an extragalactic observation can capture many GCs and its mass sensitivity can be improved by stacking those GCs.

4. Globular Cluster Systems with the ngVLA

We consider using Band 3 of the ngVLA (Selina & Murphy 2017) to examine globular cluster systems in the local universe. Band 3 has a central frequency of 17 GHz and a bandwidth of 8.4 GHz. We approximate its central wavelength as 2 cm. The Harris et al. (2013) compilation of GC systems involves 422 galaxies. The distribution of the galaxies' distances shows two peaks. A minor peak contains tens of galaxies with distances out to 10 Mpc. A major peak contains hundreds of galaxies with distances between 10 and 25 Mpc. A typical galaxy's GC system holds several hundred GCs spread over an effective diameter of a few tens of kpcs (Harris 2016; Kartha et al. 2016). Notably, the major peak in distance contains tens of thousands of GCs in total. Figure 2 shows a potentially rich GC system at 23 Mpc (Brodie et al. 2014).

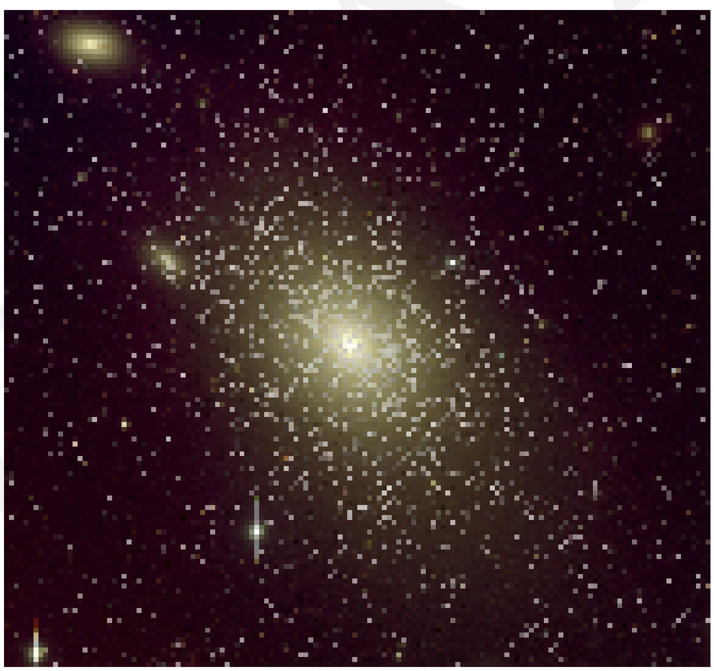

Figure 2. GC system of the early-type galaxy NGC 4365 at a distance of 23 Mpc. The small circles mark the GC candidates in the inner 18 arcmin × 17 arcmin of a *gri* Suprime-Cam image. 1 arcmin = 6.7 kpc. From Brodie et al. (2014).

We applied the Strader et al. (2012) synchrotron model to predict the luminosity at 2 cm as a function of the mass, M_{IMBH}, of a putative IMBH in a GC. The associated point-source flux densities, S_{2cm}, were then derived for GCs at distances of 10 and

25 Mpc. In Figure 3, the sloping lines show how to convert from S_{2cm} to M_{IMBH} for the two distances, while the vertical lines show 3σ detections with the ngVLA, assuming tapered and robust weighting, with integrations of 1, 10 and 100 hours (Selina & Murphy 2017). At higher signal-to-noise ratios, the wide frequency coverage could test the flat-spectrum prediction, as well as raise flags about steep-spectrum contaminants.

At 10 Mpc the synchrotron model predicts a flux density of S_{2cm} = 0.35 μJy from an IMBH of 83,000 $M_\odot$. The ngVLA can make a 3σ detection with a 10-hour integration and a tapered, robustly-weighted resolution of 100 mas (5 pc). This resolution matches the half-starlight diameter of a GC (Brodie & Strader 2006). From Selina & Murphy (2017), the field of view (FOV) of the ngVLA is a circle of diameter 3.4 arcmin (10 kpc) at full width half maximum. Most of a GC system can therefore be encompassed in a few FOVs. Each FOV can simultaneously capture many GCs. Undetected GCs can also be stacked. A stacking performance as for M81 (Section 3) can improve the IMBH mass sensitivity by a factor of two. At 25 Mpc the synchrotron model predicts a flux density of S_{2cm} = 0.35 μJy from an IMBH of 163,000 $M_\odot$. The ngVLA can make a 3σ detection with a 10-hour integration, localize the source to the GC, and encompass most of the GC system in a few FOVs. Each FOV can simultaneously capture many GCs. Stacking can also be done, and is expected to reach the mass sensitivity mentioned above for an individual GC at 10 Mpc.

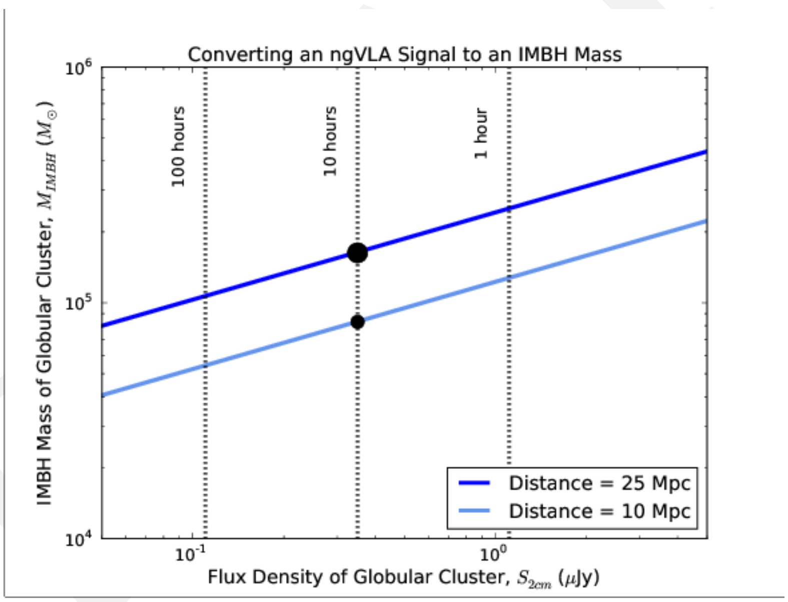

Figure 3. ngVLA signals, S_{2cm}, from IMBH masses, M_{IMBH}, in GCs at distances of 10 and 25 Mpc, according to the Strader et al. (2012) model. The small and big black dots highlight 3σ mass sensitivities at 10 and 25 Mpc, respectively, after 10 hours on target. Hundreds of GC systems have distances between 10 and 25 Mpc, and hold tens of thousands of GCs in total. Reaching large numbers of GCs is key, as Fragione et al. (2018) predict that only a few percent will have retained their IMBHs.

Regarding possible radio contaminants in extragalactic GCs, guidance comes from radio studies of X-ray binaries in the Galaxy and M31. Dozens of persistent radio emitters are known in the Galaxy, and their range of radio luminosities suggests negligible contamination beyond the Local Group (e.g., Tetarenko et al. 2016b). One radio-flaring

X-ray binary has been identified in M31 (Middleton et al. 2013). A radio analog of it could be detected out to 25 Mpc, but it would fade after a few months so not be mistaken for a persistent emitter. Three Galactic X-ray binaries have similarly strong radio emission. In two cases this is likely related to massive donar stars, absent from GCs. The third case, GRS 1915+105, is an unusually long-lived transient that is both radio and X-ray bright (Fender & Belloni 2004). An analog of GRS 1915+105 would be detectable at both wavelengths out to 25 Mpc, but the fundamental plane of BH activity would unmask it as a stellar-mass BH. Also, when searching tens of thousands of GCs, we should beware of possible radio contamination from background source populations. Simulated source counts near 2 cm suggest that star forming galaxies will dominate at μJy levels (Wilman et al. 2008). But such galaxies have steep specta and finite sizes, so will not be mistaken for IMBHs that have flat spectra and are point-like.

In summary, with its sensitivity, bandwidth, spatial resolution, and FOV, the ngVLA at 2 cm will efficiently probe IMBH masses in hundreds of GC systems out to a distance of 25 Mpc.

5. The ngVLA and Its Contemporary Facilities in the 2030s

Gravitational Wave Facilities. Fragione et al. (2018) explored the fate of primordial GCs, each born with a central IMBH. They modelled the evolution of the GCs in their host galaxy, and of the IMBHs undergoing successive, GW-producing mergers with stellar-mass BHs in the GCs. For primordial GCs that survived to the present day, they found that a few percent retained their IMBHs and the balance lost their IMBH when a GW recoil ejected it from the GC host. Once ejected, the IMBHs are no longer able to foster GW events. They used these results to predict GW event rates for the *Laser Interferometer Space Antenna* (*LISA*; Amaro-Seoane et al. 2017) and Europe's Einstein Telescope (Hild et al. 2011). The rates for the latter facility also apply to the US's similarly-scoped Cosmic Explorer (Abbott et al. 2016). IMBHs with masses between 1000 and 10,000 $M_\odot$ yielded mergers at rates that could be detected by all three GW facilities. IMBHs with masses $\gtrsim 10,000\ M_\odot$ yielded mergers at rates that could be detected only by *LISA*. If the ngVLA searches do not find the expected mix of IMBHs in GC systems, it could challenge the framework underlying the GW predictions. ngVLA searches for point-like emission from IMBHs would be easy to conduct during Early Science, notionally starting in 2028. Guided by such early ngVLA results, Fragione et al. (2018) could revisit their GW predictions.

Electromagnetic Wave Facilities. A key science driver for extremely large telescopes (ELTs) in the 30-m class is to measure, at a distance of 10 Mpc, a BH mass as low as 100,000 $M_\odot$ by spatially resolving its sphere of influence in its GC host (Do et al. 2014). For example, if the Infrared Imaging Spectrometer (IRIS) [1] on the Thirty Meter Telescope (TMT) can achieve the diffraction limit of 18 mas at 2 μm, then this approach will yield a sample of IMBHs in GCs out to a distance of 10 Mpc. A sphere-of-influence study with IRIS must be done one GC at a time, a shortcoming that makes it expensive to inventory the range of IMBH masses in a galaxy's GC system. The TMT's Infrared Multi-object Spectrometer (IRMS) [2] in spectroscopy mode will have a

[1] `https://www.tmt.org/page/science-instruments`

[2] `https://www.tmt.org/page/science-instruments`

FOV of 2.0 arcmin $\times$ 0.6 arcmin. This being a tenth of the ngVLA FOV, a sphere-of-influence study with IRMS would require ten pointings to cover one ngVLA pointing. Regardless of the situation at 10 Mpc, the ELT approach cannot reach the hundreds of GC systems with distances between 10 and 25 Mpc.

The *Chandra* X-ray mission and its proposed successors, *Lynx* [3] and the *Advanced X-ray Imaging Satellite* [4], feature spatial resolutions of 300 to 500 mas. These will suffice to roughly localize X-ray sources to GCs out to a distance of 25 Mpc. But an X-ray–only search for the accretion signatures of IMBHs in GCs will be hindered by confusion from X-ray binaries in GCs (e.g., Joseph et al. 2017). Specifically, X-ray–only detections of GCs cannot discriminate between X-ray binaries and IMBHs. Fortunately, the empirical fundamental-plane of BH activity (Merloni et al. 2003; Falcke et al. 2004; Plotkin et al. 2012) implies that the persistent radio emission from IMBHs is expected to be several hundred times greater than that from X-ray binaries. Thus ngVLA imaging can be used to separate X-ray detections into bins for X-ray binaries and for IMBHs. X-ray binaries are known to be time-variable in both the radio and X-ray bands, so this radio–X-ray synergy would be strengthened by simultaneous observations with the ngVLA and the X-ray mission.

The deployment baseline of SKA1-Mid (Dewdney et al. 2015; Borjesson 2017) will offer a spatial resolution of 57 mas at 3.3 cm with uniform weighting. This resolution suffices to search for the accretion signatures of IMBHs in GCs with declinations south of 10 degrees. But as only 67 SKA1-Mid antennas will be available at 3.3 cm, the effective collecting area of that telescope will only be about that of the current VLA, which is insufficient for our purposes.

Many of the GC systems in Harris et al. (2013) will need further optical imaging before finding charts are available for all of their GCs. Such images can mostly be acquired with current ground-based telescopes in the 4-m class (e.g., Hargis & Rhode 2014) or 8-m class (e.g., Brodie et al. 2014). But for some particularly confused regions, it may be necessary to obtain images from space-based telescopes. For example, the Near Infrared Camera on the *James Webb Space Telescope* will offer spatial resolutions of 80 and 160 mas in its short- and long-wavelength channels, respectively [5].

Acknowledgments. The National Radio Astronomy Observatory is a facility of the National Science Foundation, operated under cooperative agreement by Associated Universities, Inc.

References

Abbott, B. P., et al. 2016, arXiv:1607.08697
Amaro-Seoane, P., et al. 2017, Laser Interferometer Space Antenna, arXiv:1702.00786
Baumgardt, H. 2017, MNRAS, 464, 2174
Borjesson, L. 2017, Notes from the Chair of the SKA Board from the meeting of 718-192017
Brodie, J. P., & Strader, J. 2006, ARA&A, 44, 193
Brodie, J. P., Romanowsky, A. J., Strader, J., et al. 2014, ApJ, 796, 52

---

[3] `http://cxc.harvard.edu/cdo/cxo2lynx2017/index.html`

[4] `http://axis.astro.umd.edu`

[5] `https://jwst.stsci.edu/files/live/sites/jwst/files/home/instrumentation/technical\documents/jwst-pocket-guide.pdf`

Dewdney, P., Turner, W., Braun, R. 2015, SKA-TEL-SKO-0000308
den Brok, M., van de Ven, G., van den Bosch, R., & Watkins, L. 2014, MNRAS, 438, 487
Do, T., Wright, S., Barth, A. J., et al. 2014, AJ, 147, 93
Drukier, G. A., & Bailyn, C. D. 2003, ApJ, 597, L125
Falcke, H., Kording, E., & Markoff, S. 2004, A&A, 414, 895
Fender, R., & Belloni, T. 2004, ARA&A, 42, 317
Fender, R., & Munoz-Darias, T. 2016, in Astrophysical Black Holes, Lecture Notes in Physics, Volume 905, eds. F. Haardt et al. (Springer International Publishing: Switzerland), 65
Fragione, G., Ginsburg, I., & Kocsis, B. 2018, ApJ, 856, 92
Freedman, W. L., Hughes, S. M., Madore, B. F., et al. 1994, ApJ, 427, 628
Freire, P. C., Kramer, M., Lyne, A. G., et al. 2001, ApJ, 557, L105
Gebhardt, K., Rich, R. M., & Ho, L. C. 2005, ApJ, 634, 1093
Gieles, M., Balbinot, E., Yaaqib, R. I. S. M., et al. 2017, MNRAS, 473, 4832
Giersz, M., Leigh, N., Hypki, A. Lutzgendorf, N., & Askar, A. 2015, MNRAS, 454, 315
Graham, A. W., & Scott, N. 2015, ApJ, 798, 54
Gurkan, M. A., Freitag, M., & Rasio, F. A. 2004, ApJ, 604, 632
Hargis, J. R., & Rhode, K. L. 2014, ApJ, 796, 62
Harris, W. E., Harris, G. L., & Alessi, M. 2013, ApJ, 772, 82
Harris, W. E. 2016, AJ, 151, 102
Hild, S., et al. 2011, Class. Quantum Grav., 2011, 28, 094813
Holley-Bockelmann, K., Gültekin, K., Shoemaker, D., & Yunes, N. 2008, ApJ, 686, 829
Joseph, T. D., Maccarone, T. J., Kraft, R.P., & Sivakoff, G. R. 2017, MNRAS, 470, 4133
Kartha, S. S., Forbes, D. A., Alabi, A. B., et al. 2016, MNRAS, 458, 105
Kormendy, J., & Ho, L. C. 2013 ARA&A, 51, 511
Maccarone, T. J. 2003, å, 409, 697
Maccarone, T. J. 2004, MNRAS, 351, 1049
Maccarone, T. J., & Servillat, M. 2008, MNRAS, 389, 379
Maccarone, T. J., & Servillat, M. 2010, MNRAS, 408, 2511
Maccarone, T. J. 2016, Mem. S. A. It., 87, 559
Merloni, A., Heinz, S., & DiMatteo, T. 2003, MNRAS, 345, 1057
Merloni, A., & Heinz, S. 2007, MNRAS, 381, 589
Mezcua, M. 2017, Int. J. Mod. Phys. D, 26, 1730021
Middleton, M. J., Miller-Jones, J. C. A., Markoff, S., et al. 2013, Nat, 493, 187
Miller, M. C., & Hamilton, D. P. 2002, MNRAS, 330, 232
Miller-Jones, J. C. A., Wrobel, J. M., Sivakoff, G. R., et al. 2012, ApJ, 755, L1
Nantais, J. B., Huchra, J. P., Zezas, A., Gazeas, K., & Strader, J. 2011, AJ, 142, 183
Pellegrini, S. 2005, ApJ, 624, 155
Pepe, C., & Pellizza, L. J. 2013, MNRAS, 430, 2789
Perera, B. B. P., Stappers, B. W., Lyne, A. G., et al. 2017, MNRAS, 468, 2114
Perley, R. A., Chandler, C. C., Butler, B. J., & Wrobel, J. M. 2011, ApJ, 739, L1
Plotkin, R. M., Markoff, S., Kelly, B. C., Koerding, E., & Anderson, S. F. 2012, MNRAS, 419, 267
Portegies Zwart, S. F., Baumgardt, H., Hut, P., Makino, J., & McMillian, S. L. W. 2004, Nat, 428, 724
Sakurai, Y., Yoshida, N., Fujii, M. S., & Hirano, S. 2017, MNRAS, 472, 1677
Scott, E. H., & Rose, W. K. 1975, ApJ, 197, 147
Selina, R. & Murphy, E. 2017, Next Generation Very Large Array Memo No. 17, ngVLA Reference Design Development & Performance Estimates
Strader, J., Chomiuk, L., Maccarone, T. J., et al. 2012, ApJ, 750, L27
Tetarenko, B. E., Sivakoff, G. R., Heinke C. O., & Gladstone, J. C. 2016a, ApJS, 222, 15
Tetarenko, B. E., Bahramian, A., Arnason, R. M., et al. 2016b, ApJ, 825, 10
van der Marel, R. 2013, SnowPAC 2013 - Black Hole Fingerprints: Dynamics, Disruptions and Demographics
Volonteri, M. 2010, Astron. Astrophys. Rev., 18, 279
Wilman, R. J., Miller, L., Jarvis, M. J., et al. 2008, MNRAS, 388, 1335

Wrobel, J. M., Miller-Jones, J. C. A., & Middleton, M. J. 2016, AJ, 152, 22

Part IX

Pulsars in the Galactic Center:

Science with a Next-Generation Very Large Array
ASP Conference Series, Monograph 7
Eric J. Murphy, ed.

DRAFT EDITION

Galactic Center Pulsars with the ngVLA

Geoffrey C. Bower[1], Shami Chatterjee[2], Jim Cordes[2], Paul Demorest[3], Julia S. Deneva[4], Jason Dexter[5], Michael Kramer[6], Joseph Lazio[7], Scott Ransom[8], Lijing Shao[6], Norbert Wex[6], Robert Wharton[6]
[1]*Academia Sinica Institute of Astronomy and Astrophysics, Hilo, HI 96720, USA;* gbower@asiaa.sinica.edu.tw

[2]*Department of Astronomy, Cornell University, Ithaca, NY 14853, USA;* shami@astro.cornell.edu, cordes@astro.cornell.edu

[3]*NRAO, Socorro, NM, 87801, USA* pdemores@nrao.edu

[4]*George Mason University, resident at the Naval Research Laboratory, Washington, DC 20575, USA;* iulia.deneva.ctr@nrl.navy.mil

[5]*Max Planck Institute for Extraterrestrial Physics, Garching, Germany;* jdexter@mpe.mpg.de

[6]*Max-Planck-Institut für Radioastronomie, Auf dem Hügel 69, D-53121 Bonn, Germany;* mkramer@mpifr-bonn.mpg.de, lshao@mpifr-bonn.mpg.de, wex@mpifr-bonn.mpg.de, wharton@mpifr-bonn.mpg.de

[7]*Jet Propulsion Laboratory, California Institute of Technology, CA 91109, USA* Joseph.Lazio@jpl.nasa.gov

[8]*NRAO, Charlottesville, VA 22903, USA;* sransom@nrao.edu

Abstract. Pulsars in the Galactic Center (GC) are important probes of General Relativity, star formation, stellar dynamics, stellar evolution, and the interstellar medium. Despite years of searching, only a handful of pulsars in the central 0.5° are known. The high-frequency sensitivity of ngVLA will open a new window for discovery and characterization of pulsars in the GC. A pulsar in orbit around the GC black hole, Sgr A*, will provide an unprecedented probe of black hole physics and General Relativity.

1. Scientific Goals

Currently, only six pulsars in the central 30′ of the Galaxy have been detected. The most spectacular of these, J1745−2900, is a transient magnetar located only 0.1 pc in projection from Sgr A*. This small number stands in sharp contrast to predictions for the number of pulsars based on the rapid star formation rate and high density of young massive stars that can serve as pulsar progenitors. Numerous searches at a wide range of wavelengths have been carried out.

Until recently, the standard explanation for the absence of pulsars was the presence of hyperstrong interstellar scattering that smeared pulses over a timescale of $> 10^2$ s at low frequencies. Higher frequency searches reduced scattering effects but suffered from lower sensitivity due to the typical steep spectrum of pulsars. The discovery of J1745−2900 in 2013, however, suggested that scattering effects from the hyperstrong screen cannot fully account for the absence of detected pulsars, leading to the "missing pulsar" problem. Possible solutions to the absence of observed pulsars include more complex scattering models, stellar population synthesis arguments, and mechanisms for the suppression of the pulsar emission mechanism.

The population of millisecond pulsars (MSPs), which are the most prized targets for dynamical studies, has not been probed at all by existing observations. Even with the much reduced scattering strength inferred by J1745−2900, nearly all MSPs would remain undetected by existing surveys through a combination of time smearing and low flux density. ngVLA Galactic Center (GC) pulsar surveys will probe both the slow pulsar and MSP populations.

The ngVLA will make dramatic changes to our understanding of the GC pulsar population and potentially lead to the discovery of a pulsar in a short-period bound orbit to Sgr A*. This will come primarily through the factor of 10 improvement in sensitivity at high frequencies that the ngVLA promises.

Specific science goals are

- Searching for and Timing a Pulsar Bound to Sgr A*: It has been demonstrated that pulsars orbiting Sgr A* will be superb probes for studying the properties of the central supermassive black hole. It is sufficient to find and time a normal, slowly rotating pulsar in a reasonable orbit, in order to measure the mass of Sgr A* with a precision of $1M_{\odot}$(!), to test the cosmic censorship conjecture to a precision of about 0.1% and to test the no-hair theorem to a precision of 1%. These tests are possible even with a rather modest timing precision of 100 μs due to the large mass of Sgr A* and the measurement of relativistic and classical spin-orbit coupling, including the detection of frame-dragging.

- Searching for and Characterizing the GC Pulsar Population: Finding GC pulsars will not only lead to unique studies of the General Relativistic description of black holes, but we also gain invaluable information about the GC region itself: the characteristic age distribution of the discovered pulsars will give insight into the star formation history; MSPs can be used as accelerometers to probe the local gravitational potential; the measured dispersion and scattering measures (and their variability) would allow us to probe the distribution, clumpiness and other properties of the central interstellar medium; this includes measurements of the central magnetic field using Faraday rotation. Proper motions of young pulsars can be used to point back to regions of recent star formation and/or supernova remnants. Broadly, we define the GC pulsar population to be that which falls within the Central Molecular Zone (diameter ~ 250 pc).

- Characterizing the Scattering Environment: Interstellar scattering prevents detection of pulsars at low frequencies. This scattering appears to be strongly variable as a function of position towards the GC. Observations of low frequency masers, extragalactic background sources, as well as known pulsars can characterize the scattering screen and provide insights into the window function for pulsar detection.

The proximity of the Galactic Center and the power of the ngVLA combine to provide an unprecedented and unique opportunity to study the environment of a galactic nucleus through pulsars.

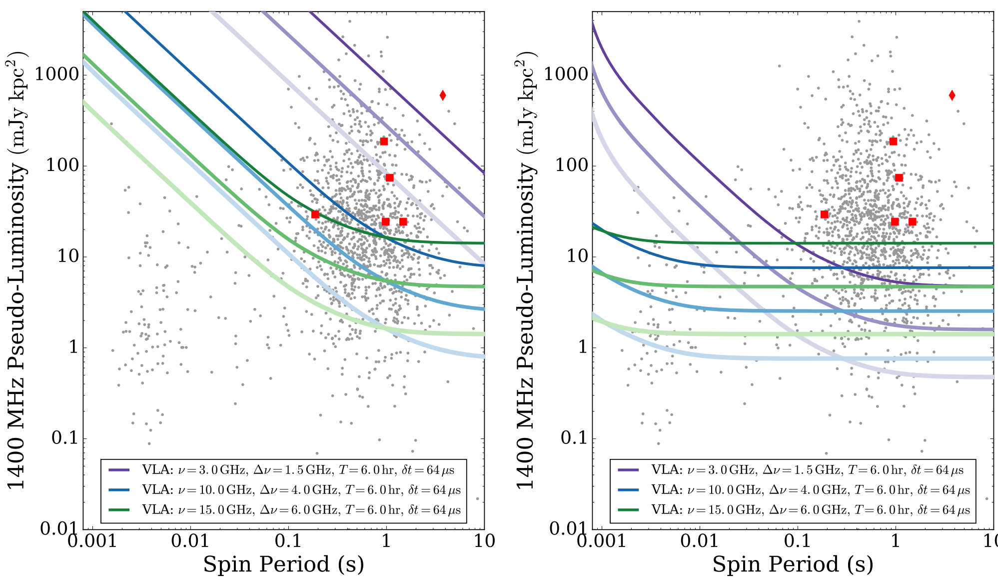

Figure 1. Field and GC pulsars (grey dots and red symbols, respectively) in period-pseudo-luminosity space for hyperstrong scattering (left) and magnetar-like scattering (right). The red diamond indicates the GC magnetar J1745−2900. Curves indicate sensitivity of the 1, 3, and 10× the VLA at three frequencies (darker to lighter curves). Sensitivity curves include nominal VLA and ngVLA system performance and scaling for average pulsar spectral index.

2. Pulsar Searching in the GC

Numerous searches for GC pulsars have been carried out over a wide range of frequencies. Prior to 2013, these searches had led to the detection of only five pulsars in the central 0.5° (e.g., Kramer et al. 2000; Johnston et al. 2006; Deneva et al. 2009; Macquart et al. 2010; Siemion et al. 2013; Eatough et al. 2013b). Theoretical expectations based on the high star formation rate and the density of high mass stars in the central molecular zone suggest that there should be hundreds or thousands of detectable pulsars within this region (Pfahl & Loeb 2004). In particular, the immediate environment of the Sgr A* contains a 10^5 $M_\odot$ cluster of massive stars with ages ∼ 4 Myr–8 Myr bound to the black hole, which are possible progenitors to neutron stars and pulsars (Blum et al. 2003; Pfuhl et al. 2011).

The strong interstellar scattering towards the GC may account for the absence of detected pulsars, especially at low radio frequencies. Turbulent electrons along the line of sight will produce angular broadening of sources in the image domain and temporal broadening of sources in the time domain. The temporal scattering scales for a thin scattering screen is related to the angular broadening by the following equation:

$$\tau_s = 6.3\ \mathrm{s}\ \times \left(\frac{D}{8.5\mathrm{kpc}}\right)\left(\frac{\theta_s}{1.3\ \mathrm{arcsec}}\right)^2 \left(\frac{D}{\Delta} - 1\right)\nu^{-4}, \quad (1)$$

where $D = 8.3 \pm 0.3$ kpc (Genzel et al. 2010) is the distance to the GC, Δ is the distance from the GC to the scattering medium, and ν is the observing frequency in GHz

(Cordes & Lazio 1997). The observed angular diameter θ_s is extrapolated to a frequency of 1 GHz using a scaling of ν^{-2}. For Kolmogorov turbulence with an inner scale $r_{in} > b_{max}$, we expect $\theta_s \propto \nu^{-2}$ and $\tau_s \propto \nu^{-4}$. Several pieces of evidence demonstrate that scattering may be important in the GC. Sgr A* itself is observed to show substantial angular broadening, as are OH masers and some extragalactic background sources. These pieces of evidence have been used to argue for a hyperstrong scattering screen that is located within the central few hundred parsecs of the GC (Lazio & Cordes 1998b). If the source to screen distance is small, an observed angular broadening implies a large temporal broadening. In the case of the hyperstrong model, $\tau_s \gtrsim 10^3$ s at 1 GHz, sufficient to make even slow pulsars undetectable up to $\sim$ 10 GHz.

The discovery and characterization of the GC magnetar J1745−2900 has indicated that the hyperstrong scattering model cannot hold for all of the GC (Eatough et al. 2013a; Spitler et al. 2014; Bower et al. 2014). The GC magnetar, with $P = 3.76$ s is detected to frequencies as low as $\sim$ 1 GHz, with a characteristic $\tau_s = 1.3$ s at 1 GHz. The GC magnetar also shows angular broadening identical to that of Sgr A*. Together, these results imply a source to screen distance of order 6 kpc, well outside of the GC, and the ability to readily detect pulsars in the GC at frequencies of a few GHz. It remains unclear whether the magnetar-like scattering screen describes all of the GC region or may be patchy. Characterization of the other GC pulsars show distances to the scattering screen $\lesssim 2$ kpc (Dexter et al. 2017). Other environmental effects may also alter the neutron star population in the GC (Dexter & O'Leary 2014).

In the case of both hyperstrong and magnetar-like scattering, there is still a substantial benefit in reduction of scattering that is achieved by going to higher frequencies. This benefit has to be offset against the steep spectral index of both slow pulsars and MSPs and decreasing sensitivity of many search telescopes with increasing frequency. The average slow pulsar has a spectral index of $\alpha \approx -1.4$ (Bates et al. 2013) although some objects including magnetars have flat spectra to very high frequencies (Torne et al. 2017).

Figure 1 shows the distribution of known field pulsars along with sensitivity curves for the VLA and the ngVLA at a range of frequencies and for hyperstrong and magnetar-like scattering. These curves reveal that for magnetar-like scattering the ngVLA will have sensitivity to discover the majority of field pulsars at the GC and a significant fraction of MSPs. In the more challenging case of hyperstrong scattering, the high frequency ngVLA is essential for obtaining sensitivity to slow pulsars.

3. Constraints on Black Hole Parameters

In order to estimate the impact of ngVLA on timing of a pulsar around Sgr A* and testing the no-hair theorem, we have extended the work by Wex & Kopeikin (1999) and Liu et al. (2012). We have set up a numerical integration scheme for orbits around Sgr A*, using MCMC parameter estimation code; we extract the parameter uncertainties and covariances. Figure 2 shows estimates of the uncertainty in black hole mass, spin, and quadrupole moment for a set of pulsar orbits timed with the VLA and the ngVLA. Results for a more complete set of orbits will be presented in a future publication (Shao et al., in prep.). Effectively, the precision on these parameters in this regime scales directly with increased collecting area.

The parameter constraints are governed primarily by the rms time of arrival (TOA) residuals, $\sigma_{\rm TOA}$. For given intrinsic pulsar emission properties and scattering proper-

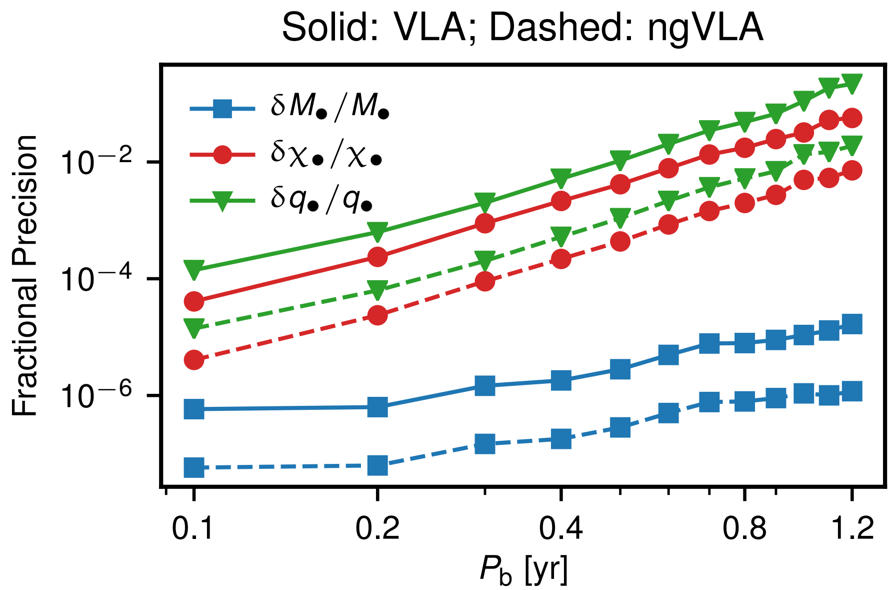

Figure 2. Constraints on black hole parameters from timing observations of a pulsar in a bound orbit for the VLA (solid lines) and for the ngVLA (dashed lines). Constraints are given for black hole mass ($M_\bullet$), spin ($\chi_\bullet$), and quadrupole ($q_\bullet$). These constraints were calculated for a $P = 0.5$ s pulsar with orbital eccentricity $e = 0.8$ and timing residuals of $\sigma_{\rm TOA} = 1$ ms and 0.1 ms for the VLA and ngVLA, respectively. Simulations include weekly observations over a 5 yr interval.

ties, $\sigma_{\rm TOA}$ scales inversely with collecting area. Figure 3 shows estimates of the timing error for two scattering models (hyperstrong and magnetar) as a function of frequency for the VLA, ngVLA with 107 antennas, and ngVLA with 214 antennas.

General Relativistic effects are best measured in systems where the observational duration is greater than the orbital period, but constraints on General Relativity and BH properties can still be obtained for longer period systems. We consider the case of a pulsar with a 15 yr period observed over a 5 yr interval during pericenter. The BH mass can be constrained with ngVLA to an accuracy $\sim 10^{-5}$. Lense-Thirring precession parameters will be found with an signal-to-noise ratio between 10 and 1000, depending on the details of orbit and the observations. At large radii, perturbations to the pulsar orbit through stellar interactions will limit the accuracy with which General Relativity constraints can be made. Next generation adaptive optics on large optical telescopes imaging the stellar cluster may enable modeling of these perturbations.

Another limitation of current GC pulsar searches is the insensitivity to a large fraction of binary pulsars. The minimum detectable pulsar pseudo-luminosity ($L = S d^2$) for a pulsar survey scales roughly as

$$L_{\rm min} \propto d^{-2} G^{-1} T_{\rm obs}^{-1/2} \tag{2}$$

where d is distance, G is the telescope gain, and $T_{\rm obs}$ is the observing time. Because the GC is so far away, GC searches have typically observed for as long as possible ($\approx$ 6 hr at the VLA). While this increases the sensitivity to faint isolated pulsars, it can also reduce the effectiveness of typical binary pulsar search methods. For example, the acceleration

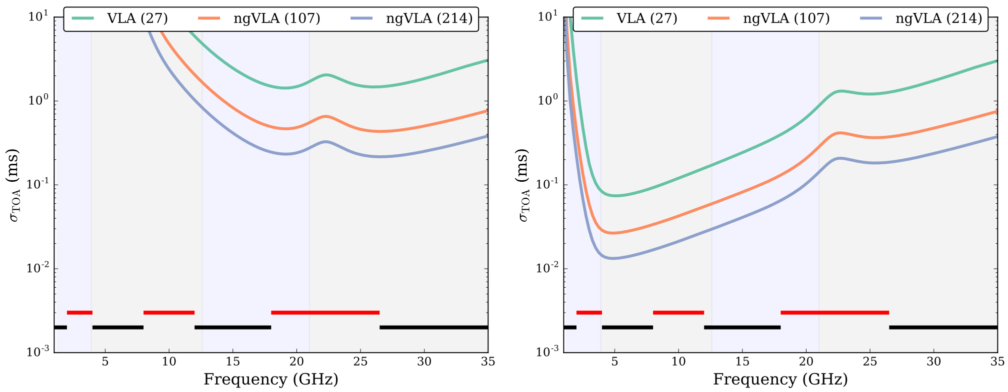

Figure 3. TOA residuals for a $P = 0.5$ s pulsar with a 10 ms pulsar width, using an integration time of 4 hr and a bandwidth of 1 GHz. The residuals are shown for hyperstrong scattering with $\tau = 2300$ s at 1 GHz (*left*) and for a level of scattering comparable to the magnetar J1745−2900, with $\tau = 1.3$ s at 1 GHz (*right*).

search technique is only effective for orbital periods with $P_{\mathrm{orb}} \gtrsim 10T_{\mathrm{obs}}$ (Johnston & Kulkarni 1991; Ransom et al. 2003). A VLA GC pulsar search that observes for 6 hr would be most sensitive to binary pulsars with orbits longer than about 60 hr, which includes only about 50% of known pulsar binaries (and only 30% of binaries in globular clusters).

The increased sensitivity of the ngVLA means that flux density limits achieved by the VLA can be reached in much shorter observing times, thus allowing for the possibility of detecting much shorter period binary pulsars. For $(G_{\mathrm{ng}}/G_{\mathrm{VLA}}) = 5$, the ngVLA could reach the same flux density limit as a 6 hr VLA observation in only $T_{\mathrm{ng}} = T_{\mathrm{VLA}}/\sqrt{5} \approx 15$ min. In this shorter observing span, an acceleration search could be used to find pulsars with orbits as short as 2.5 hr, which would include about 95% of all known pulsar binaries.

Long baseline astrometry of the pulsar relative to Sgr A* can also contribute to parameter constraints for long-period systems. For the case of 100 μas astrometric error (Bower et al. 2015), we can measure the orientation of the pulsar orbit in the sky, i.e., the longitude of the ascending node with sufficient precision to improve General Relativistic constraints.

4. Other Probes of Black Hole Physics and the Uniqueness of ngVLA

There are a number of experiments currently seeking to characterize Sgr A*, the properties of the SMBH, and General Relativity. These include the Event Horizon Telescope (EHT) and its millimeter wavelength imaging of Sgr A* and large optical telescope campaigns to measure stellar orbits near Sgr A*. ngVLA timing of a pulsar in a bound orbit compares favorably against these techniques and provides important complementary information (Psaltis et al. 2016).

EHT constraints will primarily arise from modeling the static and time-domain images of the immediate region surrounding Sgr A* out to a radius of $\sim 10R_{\mathrm{S}}$ (Broderick et al. 2014). General Relativity and BH properties introduce image distortions that can be translated into parameter constraints. These measurements, however, must be interpreted in light of the complex astrophysics of accretion, jet launching, and particle acceleration in the vicinity of the BH. Simulations have shown that EHT results will be able to measure the BH mass, spin, and quadrupole moment.

Stellar astrometry with existing and future large optical telescopes has the potential to measure orbital precession. Current constraints on the black hole mass from stellar orbits have an accuracy of order 10% (e.g., Genzel et al. 2010) and future measurements with existing facilities are projected to improve on these results substantially (Waisberg et al. 2018). The closest star, S2, has a period of 15 yr and is currently going through periastron passage. Improved instruments may discover fainter stars in shorter orbits leading to greater precision. Sub-milliarcsecond astrometry provides a length-scale precision that is orders of magnitude less precise than millisecond-accuracy pulsar timing, leading to complementary but correspondingly less accurate BH and General Relativity parameter constraints.

5. The Accretion Flow, ISM, and Stars

Pulsed emission provides a powerful probe of the plasma and magnetic field along the line of sight through a variety of measurements. The dispersion measure (DM) gives the total electron column density. The rotation measure (RM) gives the integrated line of sight magnetic field and electron density. The scattering measure (SM) characterizes turbulent plasma, which is typically localized to individual regions along the line of sight.

A short period pulsar will orbit inside of the Bondi radius ($\sim 10^5 R_S$; $P \sim 10^3$ yr) of Sgr A*. Polarimetry of Sgr A* and the magnetar J1745−2900 has shown that a substantial fraction of the observed Sgr A* RM originates from the accretion flow on scales between 10 R_S and 10^5 R_S, providing strong constraints on the accretion rate and the nature of the radiatively inefficient accretion flow (Bower et al. 2003; Marrone et al. 2007). A pulsar in an eccentric orbit would provide a measure of the radial profile of the accretion flow, inaccessible to any other technique.

On larger angular scales, a collection of GC pulsars would provide multiple probes of the interstellar medium (ISM) in the GC region (Schnitzeler et al. 2016). With a sufficient density of pulsars, the ngVLA can map out magnetized and ionized structures throughout the central molecular zone. Astrometry of these pulsars can provide origins of individual pulsars in known SNR or young stellar clusters.

ngVLA pulsar studies will complement ngVLA and SKA studies of the GC ISM through other means. The scattering medium has been studied in the past through imaging of stellar masers and extragalactic background sources (van Langevelde & Diamond 1991; van Langevelde et al. 1992; Frail et al. 1994; Lazio & Cordes 1998a). Sensitivity and angular resolution constraints have limited observations, however, to a small number of sight lines. The ngVLA will provide the sensitivity and resolution to measure the angular sizes of a wide range of maser species and a large number of background sources and map out the spatial variations of the scattering towards the inner degree of the GC. This will provide important insight into both the source of scattering and characterization of the scattering that can lead to optimization of pulsar searches.

6. Implications for Array Design

A number of elements of the array design are constrained by our scientific goals.

- Correlator and beamformer requirements: Searches for pulsars will make use of beamforming capabilities as well as high-time resolution imaging with the correlator. Different regimes of the search space will be optimized through tradeoffs in field of view and bandwidth. Timing observations will rely primarily on wide-band receivers and beamformer backends.
- Effect of the various receiver options on GC searches: Pulsar searching requires high instantaneous sensitivity that cannot always be traded off against greater integration time. High frequency ($\sim$ 30 GHz) sensitivity is likely to be required to avoid the effects of scattering for detection of MSPs.
- Effect of array configuration on GC searches: Searching and imaging primarily require a compact configuration. Timing observations can be obtained with beamforming of extended configurations but these will introduce challenges in calibration and availability due to weather. Characterization of the scattering environment and pulsar astrometry will require $>$ 1000 km baselines to resolve compact sources and achieve sub-milliarcsecond positional accuracy.

7. Summary

The order of magnitude increase in high frequency sensitivity that the ngVLA provides will be essential for the discovery and characterization of pulsars in the Galactic Center, the nearest and best studied galactic nucleus. Characterization of the population within the Central Molecular Zone will give new insights into the ISM and stellar populations of one of the most dynamic regions in the Galaxy. Discovery of a pulsar in orbit around Sgr A* will provide an unprecedented opportunity for fundamental physics in the environment of a black hole.

Acknowledgments. SC, JMC, PD, JL, and SR are members of the NANOGrav Physics Frontier Center, which is supported by the National Science Foundation award 1430284. MK, LS, NW, and RW acknowledge financial support by the European Research Council (ERC) for the ERC Synergy Grant BlackHoleCam under contract no. 610058. JSD acknowledges support by NASA under grant DPR S–15633–Y. Part of this research was carried out at the Jet Propulsion Laboratory, California Institute of Technology, under a contract with the National Aeronautics and Space Administration.

References

Bates, S. D., Lorimer, D. R., & Verbiest, J. P. W. 2013, MNRAS, 431, 1352. 1302.2053

Blum, R. D., Ramírez, S. V., Sellgren, K., & Olsen, K. 2003, ApJ, 597, 323. astro-ph/0307291

Bower, G. C., Deller, A., Demorest, P., Brunthaler, A., Eatough, R., Falcke, H., Kramer, M., Lee, K. J., & Spitler, L. 2014, ApJ, 780, L2. 1309.4672

Bower, G. C., Deller, A., Demorest, P., Brunthaler, A., Falcke, H., Moscibrodzka, M., O'Leary, R. M., Eatough, R. P., Kramer, M., Lee, K. J., Spitler, L., Desvignes, G., Rushton, A. P., Doeleman, S., & Reid, M. J. 2015, ApJ, 798, 120. 1411.0399

Bower, G. C., Wright, M. C. H., Falcke, H., & Backer, D. C. 2003, ApJ, 588, 331
Broderick, A. E., Johannsen, T., Loeb, A., & Psaltis, D. 2014, ApJ, 784, 7. 1311.5564
Cordes, J. M., & Lazio, T. J. W. 1997, ApJ, 475, 557. arXiv:astro-ph/9608028
Deneva, J. S., Cordes, J. M., & Lazio, T. J. W. 2009, ApJ, 702, L177. 0908.1331
Dexter, J., Deller, A., Bower, G. C., Demorest, P., Kramer, M., Stappers, B. W., Lyne, A. G., Kerr, M., Spitler, L. G., Psaltis, D., Johnson, M., & Narayan, R. 2017, MNRAS, 471, 3563. 1707.03842
Dexter, J., & O'Leary, R. M. 2014, ApJ, 783, L7. 1310.7022
Eatough, R. P., Falcke, H., Karuppusamy, R., Lee, K. J., Champion, D. J., Keane, E. F., Desvignes, G., Schnitzeler, D. H. F. M., Spitler, L. G., Kramer, M., Klein, B., Bassa, C., Bower, G. C., Brunthaler, A., Cognard, I., Deller, A. T., Demorest, P. B., Freire, P. C. C., Kraus, A., Lyne, A. G., Noutsos, A., Stappers, B., & Wex, N. 2013a, Nat, 501, 391. 1308.3147
Eatough, R. P., Kramer, M., Klein, B., Karuppusamy, R., Champion, D. J., Freire, P. C. C., Wex, N., & Liu, K. 2013b, in IAU Symposium, vol. 291 of IAU Symposium, 382. 1210.3770
Frail, D. A., Diamond, P. J., Cordes, J. M., & van Langevelde, H. J. 1994, ApJ, 427, L43. astro-ph/9402018
Genzel, R., Eisenhauer, F., & Gillessen, S. 2010, Reviews of Modern Physics, 82, 3121. 1006.0064
Johnston, H. M., & Kulkarni, S. R. 1991, ApJ, 368, 504
Johnston, S., Kramer, M., Lorimer, D. R., Lyne, A. G., McLaughlin, M., Klein, B., & Manchester, R. N. 2006, MNRAS, 373, L6. arXiv:astro-ph/0606465
Kramer, M., Klein, B., Lorimer, D., Müller, P., Jessner, A., & Wielebinski, R. 2000, in IAU Colloq. 177: Pulsar Astronomy - 2000 and Beyond, edited by M. Kramer, N. Wex, & R. Wielebinski, vol. 202 of Astronomical Society of the Pacific Conference Series, 37. arXiv:astro-ph/0002117
Lazio, T. J. W., & Cordes, J. M. 1998a, ApJS, 118, 201. URL http://adsabs.harvard.edu/cgi-bin/nph-bib_query?bibcode=1998ApJS..118..201L&db_key=AST
— 1998b, ApJ, 505, 715. URL http://adsabs.harvard.edu/cgi-bin/nph-bib_query?bibcode=1998ApJ...505..715L&db_key=AST
Liu, K., Wex, N., Kramer, M., Cordes, J. M., & Lazio, T. J. W. 2012, ApJ, 747, 1. 1112.2151
Macquart, J.-P., Kanekar, N., Frail, D. A., & Ransom, S. M. 2010, ApJ, 715, 939. 1004.1643
Marrone, D. P., Moran, J. M., Zhao, J.-H., & Rao, R. 2007, ApJ, 654, L57. arXiv:astro-ph/0611791
Pfahl, E., & Loeb, A. 2004, ApJ, 615, 253. arXiv:astro-ph/0309744
Pfuhl, O., Fritz, T. K., Zilka, M., Maness, H., Eisenhauer, F., Genzel, R., Gillessen, S., Ott, T., Dodds-Eden, K., & Sternberg, A. 2011, ApJ, 741, 108. 1110.1633
Psaltis, D., Wex, N., & Kramer, M. 2016, ApJ, 818, 121. 1510.00394
Ransom, S. M., Cordes, J. M., & Eikenberry, S. S. 2003, ApJ, 589, 911. arXiv:astro-ph/0210010
Schnitzeler, D. H. F. M., Eatough, R. P., Ferrière, K., Kramer, M., Lee, K. J., Noutsos, A., & Shannon, R. M. 2016, MNRAS, 459, 3005. 1604.05322
Siemion, A., Bailes, M., Bower, G., Chennamangalam, J., Cordes, J., Demorest, P., Deneva, J., Desvignes, G., Ford, J., Frail, D., Jones, G., Kramer, M., Lazio, J., Lorimer, D., McLaughlin, M., Ransom, S., Roshi, A., Wagner, M., Werthimer, D., & Wharton, R. 2013, in IAU Symposium, vol. 291 of IAU Symposium, 57
Spitler, L. G., Lee, K. J., Eatough, R. P., Kramer, M., Karuppusamy, R., Bassa, C. G., Cognard, I., Desvignes, G., Lyne, A. G., Stappers, B. W., Bower, G. C., Cordes, J. M., Champion, D. J., & Falcke, H. 2014, ApJ, 780, L3. 1309.4673
Torne, P., Desvignes, G., Eatough, R. P., Karuppusamy, R., Paubert, G., Kramer, M., Cognard, I., Champion, D. J., & Spitler, L. G. 2017, MNRAS, 465, 242. 1610.07616
van Langevelde, H. J., & Diamond, P. J. 1991, MNRAS, 249, 7P
van Langevelde, H. J., Frail, D. A., Cordes, J. M., & Diamond, P. J. 1992, ApJ, 396, 686
Waisberg, I., Dexter, J., Gillessen, S., Pfuhl, O., Eisenhauer, F., Plewa, P. M., Bauböck, M., Jimenez-Rosales, A., Habibi, M., Ott, T., von Fellenberg, S., Gao, F., Widmann, F., &

Genzel, R. 2018, MNRAS. 1802.08198
Wex, N., & Kopeikin, S. M. 1999, ApJ, 514, 388. astro-ph/9811052

Science with a Next-Generation Very Large Array
ASP Conference Series, Monograph 7
Eric J. Murphy, ed.

DRAFT EDITION

Science with Pulsar Timing Arrays and the ngVLA

The North American Nanohertz Observatory for Gravitational Waves Collaboration

info@nanograv.org

1. Summary

Pulsar timing arrays (PTAs) can be used to detect and study gravitational waves in the nanohertz band (i.e., wavelengths of order light-years). This requires high-precision, decades-long data sets from sensitive, instrumentally stable telescopes. NANOGrav and its collaborators in the International Pulsar Timing Array consortium are on the verge of the first detection of the stochastic background produced by supermassive binary black holes, which form via the mergers of massive galaxies. By providing Northern hemisphere sky coverage with exquisite sensitivity and higher frequency coverage compared to the SKA, the ngVLA will be a fundamental component in the next phase of nanohertz GW astrophysics, enabling detailed characterization of the stochastic background and the detection of individual sources contributing to the background, as well as detections of (or stringent constraints on) cosmic strings and other exotica. Here we summarize the scientific goals of PTAs and the technical requirements for the ngVLA to play a significant role in the characterization of the nanohertz gravitational wave universe.

2. Introduction: Science with Pulsar Timing Arrays

The recent detections of binary black hole (Abbott et al. 2016) and binary neutron star (Abbott et al. 2017) mergers by the LIGO-Virgo collaboration provide spectacular confirmation of the existence of gravitational waves (GWs) at frequencies of a few hundred hertz. These discoveries have measured the speed of gravity to phenomenal precision, determined the origin of half of the elements of the periodic table, and probed relativistic explosions, as well as changing our understanding of stellar evolution and binary interactions.

GWs at nanohertz frequencies—with wavelengths on the order of light-years—can be detected by a pulsar timing array (PTA), where a collection of stable millisecond pulsars (MSPs) is timed over a period of years to decades. These low-frequency GWs produce pulse arrival-time perturbations that are *spatially correlated* with a quadrupolar pattern on the sky (e.g., Hellings & Downs 1983), enabling the identification of a GW signal against a background of other effects including pulsar timing noise, stochastic pulse propagation in the interstellar and interplanetary media, and uncertainties in the position of the solar system barycenter. The most promising sources of GWs at nanohertz frequencies are supermassive black hole binaries (SMBHBs). Our current understanding of the formation of galaxies and the history of mass assembly in the universe requires the mergers of galaxies and, very probably, mergers of the supermassive black holes they host. Figure 1 shows the SMBHB life-cycle. A detection of the stochastic background of GW emission produced by the mergers of SMBHBs is imminent. The next step is studying individual binary systems through multimessenger probes. By allowing the flexible allocation of collecting area to time pulsars of interest on a sustained and regular basis, the ngVLA will contribute significantly to the sensitivity of PTAs. Since all-sky coverage is essential, the ngVLA complements the Southern hemisphere coverage of the planned SKA. Further, as we show below, the optimal frequencies for timing distant, high dispersion measure pulsars are significantly higher than 1 GHz, making the ngVLA an ideal instrument for the expanding PTAs of the future.

In addition, through sky imaging techniques, the ngVLA may uncover widely separated SMBHBs, and depending on its long-baseline sensitivity, could discover targets that are simultaneously emitting gravitational waves in the PTA band. This would make the ngVLA a premier multi-messenger astronomy facility *on its own*. Thus, it is possible that ngVLA could be a leading facility in the detection and study of binary SMBHs. It may contribute unique information to the full characterization of SMBH evolution that will be performed by current and future observatories such as LISA, LSST, ELT-class facilities, and the North American Nanohertz Observatory for Gravitational Waves (NANOGrav).

3. Current State of the Art and Scientific Impact

NANOGrav is a collaboration of astronomers using the world's most sensitive pulsar timing facilities (the Arecibo Observatory and the Green Bank Telescope) to monitor several tens of millisecond pulsars: we are expanding and improving a Galactic-scale detector for low-frequency GWs. NANOGrav's recent 11-year data release (Arzoumanian et al. 2018b) has allowed stringent limits to be placed on the stochastic background of GWs from SMBHB mergers (Arzoumanian et al. 2018a), as well as meaningful constraints on more speculative source classes such as primordial GWs and cosmic strings that can form during phase transitions in the early Universe.

At present NANOGrav both competes and collaborates with its international partners, the European PTA and the Parkes PTA. As new telescopes (such as FAST and CHIME) come on line, we expect that collaboration under the umbrella of the International Pulsar Timing Array (IPTA) will play a more significant role. The leadership role of NANOGrav depends on continued access to telescope facilities for pulsar timing, along with new instrumentation that enables improvement in the sensitivity to gravitational waves.

In the next decade, we expect that the stochastic GW background will be successfully detected, either by NANOGrav or as an IPTA effort. The scientific focus will then shift to the precise spectral characterization of the stochastic GW background, measurement of its anisotropy, detection of continuous waves and bursts with memory from individual GW sources, joint observations of their electromagnetic counterparts, as well as constraints on the predictions from more exotic physics. This will help address pressing questions in the joint evolution of supermassive black holes and their host galaxies (see NANOGrav Astrophysics Working Group et al. 2018 for more details).

For instance, galaxy merger rates, SMBH-host co-evolution, dynamical relaxation timescales including the potential that SMBHBs may stall at wide separations, can all affect the amplitude scaling of the GW background. The GW background spec-

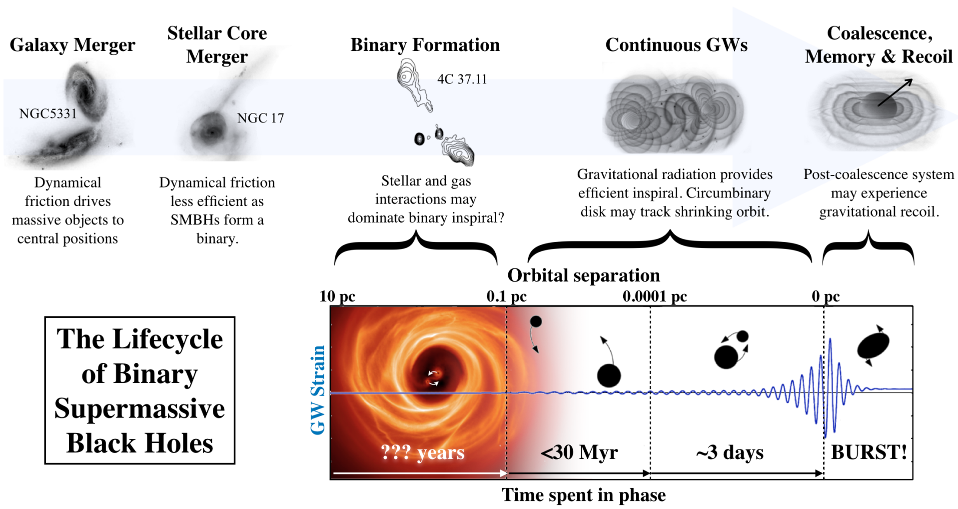

Figure 1. Plot of the binary SMBH life-cycle, adapted from NANOGrav Astrophysics Working Group et al. (2018). A significant unknown in binary evolution theory is the efficiency of inspiral from ~10 pc down to ~0.1 pc separations–the "final parsec" problem–after which the binary can coalesce efficiently due to gravitational wave emission. Through sky imaging techniques, the ngVLA itself may discover widely separated binaries, and depending on its long-baseline sensitivity, could discover targets that are detectable by PTAs. Separately, the ngVLA could contribute to the sensitivity of PTAs, allowing the detection of GW emission from the same systems. PTAs such as NANOGrav can detect supermassive ($> 10^8$ $M_\odot$) black hole binaries within ~0.1 pc separation (second panel in the lower figure). On rare occasion, PTAs may detect the permanent space-time deformation (GW memory) caused by a binary's coalescence (Favata 2009). Image credits: Galaxies, Hubble/STScI; 4C37.11, Rodriguez et al. (2006); Simulation visuals, C. Henze/NASA; Circumbinary accretion disk, C. Cuadra.

trum might be detected with a shallow slope at frequencies $\lesssim$10 nHz if SMBHBs have strong interactions with their environments (stars and gas) during the late stages of orbital evolution. PTA constraints on or measurement of the background's amplitude and spectral shape can inform all of the above astrophysical uncertainties about the ensemble SMBHB population. A detection of the SMBHB background would provide the first comprehensive proof of the consensus view that SMBHs reside in most or all massive galaxies. Moving past global characterizations, constraints on the background anisotropy may highlight actively interacting galaxy clusters or large-scale cosmic features.

Beyond the detection of the stochastic background, PTAs will reveal individually-resolvable continuous-wave sources as massive and nearby systems can be disentangled from the background. These detections will provide the most direct probe of the early-inspiral stage of a SMBHB, and can provide measurements of the binary's position, phase, and an entangled estimate of chirp mass and luminosity distance ($\mathcal{M}/D_{\rm L}$). If the host of a continuous-wave source can be identified with electromagnetic data, the mass/distance degeneracy can be broken by a redshift measurement; furthermore, this will enable a "calibration" of black hole mass/host galaxy relations at intermediate redshifts by the precise measurement of the central mass in these galaxies. If detected, the pulsar term can permit temporal aperture synthesis, also allowing $\mathcal{M}$ and $D_{\rm L}$ to be disentangled. Evolution of the waveform over PTA experimental durations is unlikely for SMBHBs; however, this would also disentangle the $\mathcal{M}/D_{\rm L}$ term.

In our roadmap for the next 15 to 20 years, the ngVLA will provide Northern hemisphere coverage for PTAs with superb sensitivity and be a fundamental component of the multi-telescope program needed for nanohertz GW science that will be conducted by NANOGrav and the IPTA.

Figure 2 shows our GW sensitivity goal with the ngVLA in terms of the gravitational wave strain versus frequency. The top curve shows the sky-averaged 95% upper limits for the NANOGrav 11-yr data set (our most current data set). The bottom two curves (sky-averaged and best sky-location 95% upper limit curves) are computed from observation simulations that assume a continuation of our current observing program followed by 10 years of ngVLA observations. The black points show the brightest 10 sources in 500 simulations of the SMBHB population in the universe. Depending on the details of the simulation parameters, an average of 5-10 SMBHB lie above the upper limit curve for our best sky location using the ngVLA. This estimate is also in broad agreement with Mingarelli et al. (2017), who base their predictions on local massive galaxies.

Figure 3 shows the improvement in our detection range with the ngVLA in terms of the luminosity distance as a function of the supermassive black hole binary total mass for two of our most sensitive frequencies. In the range of supermassive black hole binary masses relevant for pulsar timing arrays, the luminosity distance (our astrophysical reach) improves by over an order of magnitude. This increases the volume of the universe that is being probed for individual systems of nanohertz GW emission by a factor of over 1000.

Below we detail the improvements necessary to increase the sensitivity of our GW PTA detectors to achieve the scientific goals described here, and outline a future observational program. These improvements are then translated into a summary of the technical and usage requirements for the ngVLA to play a leading role in PTA science.

4. Improving Nanohertz GW Detectors

The key features of the ngVLA that are relevant to PTAs are its high sensitivity, Northern hemisphere sky-coverage, broad spectral coverage, and the ability to multiplex its sensitivity into subarrays. The last is a game-changing advantage over large single-dish telescopes. We discuss two of the more important advances possible with the ngVLA below.

4.1. Subarrays and the Fight Against Jitter

The subarray capability of the ngVLA is particularly important because, unlike traditional imaging observations, pulsar timing observations do not allow sensitivity to be traded against integration time without constraints. Pulsar timing involves time-tagging of pulse profiles obtained by averaging large numbers ($N \sim 10^5$ to 10^6) of individual pulses. While such averages are highly stable, the amplitude and pulse-phase jitter of individual pulses causes small deviations of the average shape, which translate into arrival time errors $\propto N^{-1/2}$, as illustrated in Figure 4.

Pulse jitter therefore sets a floor on the minimum number of pulses that must be averaged to achieve a specified arrival-time precision for the millisecond pulsars whose

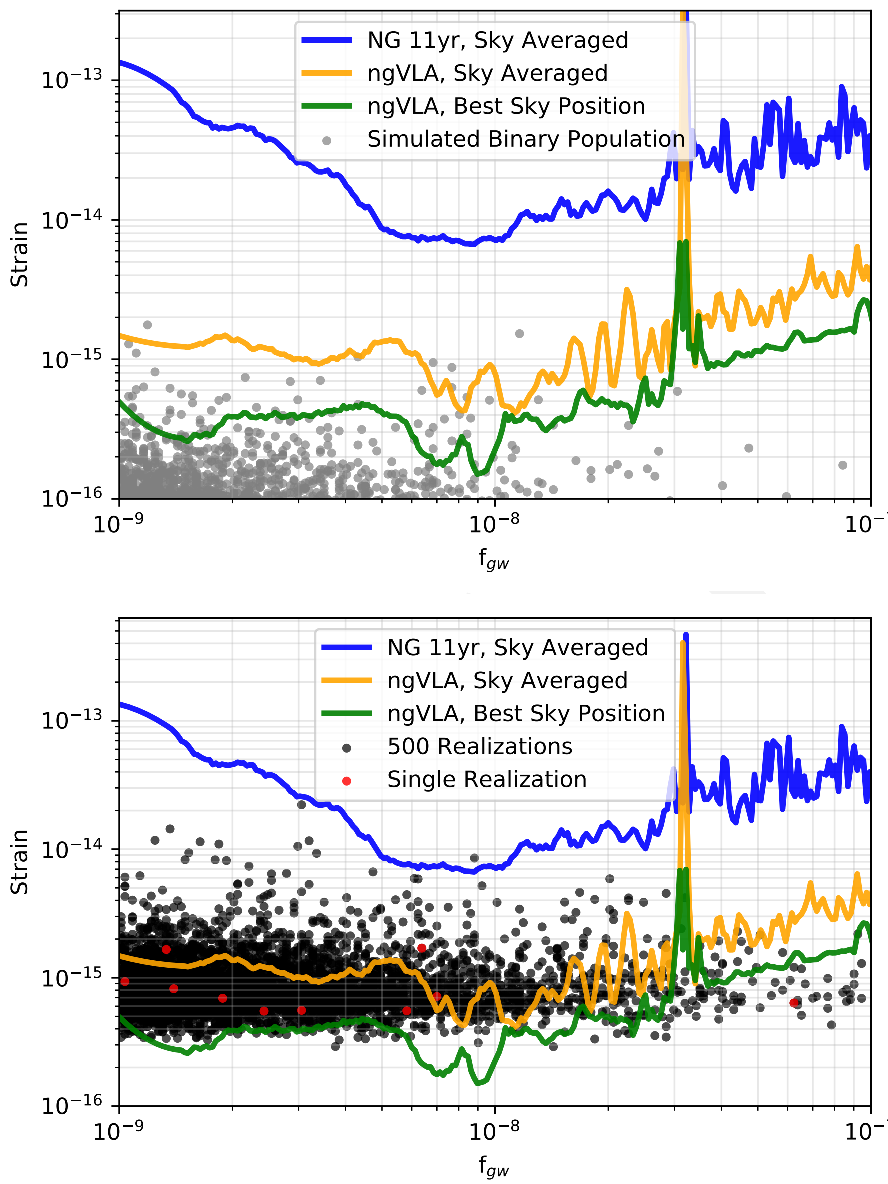

Figure 2. Plot of current sensitivity and sensitivity improvements for simulated observations using the ngVLA. In each panel, the top (blue) curve shows the current sky-averaged NANOGrav 11-yr 95% upper limits. The bottom curves show the sky-averaged (orange) and best sky location (green) 95% upper limits for simulated observations that assume a continuation of our current observing program followed by 10 years of ngVLA observations. **Upper panel:** The gray points show a single simulation of the supermassive binary black hole population, the majority of which lie below our sensitivity limits. **Lower panel:** The black points show the brightest 10 sources (only) in each of 500 simulations of the supermassive binary black hole population. Red points show the brightest 10 sources in one of these simulations.

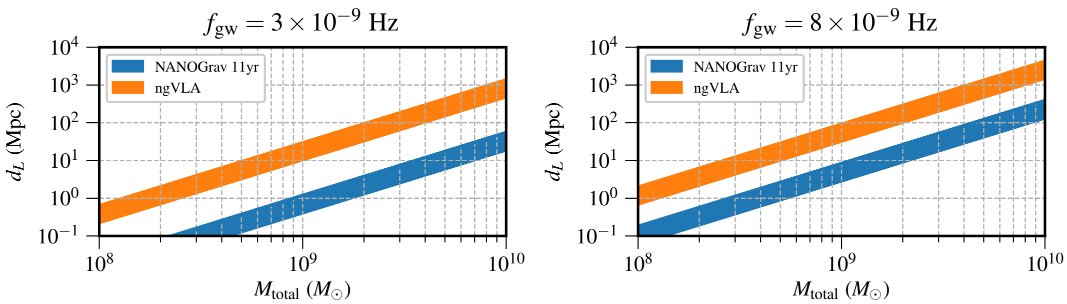

Figure 3. Plot of the luminosity distance versus the supermassive binary black hole total mass for our most current observations (the NANOGrav 11-yr data set, blue) and simulated ngVLA observations (orange). The luminosity distance (our astrophysical reach) increases by over an order of magnitude over all mass ranges.

arrival time errors are dominated by jitter (rather than signal-to-noise ratio considerations). For those objects, the required integration time does not decrease with increased telescope sensitivity. For faint pulsars where radiometer noise currently dominates timing errors, increased sensitivity can improve their arrival time estimation precision and in some cases they will then be jitter dominated. Therefore the full sensitivity of the ngVLA can be used to improve the timing errors of weaker MSPs, while brighter MSPs lend themselves to observations with subarrays large enough so that the arrival times are jitter dominated, thus optimizing pulsar timing throughput with the ngVLA.

4.2. Frequency Coverage and the Fight Against the ISM

The ionized interstellar medium causes chromatic perturbations of arrival times that must be removed using multifrequency observations at frequencies that are optimized for each MSP. Currently, there is not much flexibility in the choice of observing bands used for timing measurements, implying that there are significant opportunities for improving arrival times and the sensitivity to GWs with future instrumentation and at the ngVLA.

Pulsars are typically brighter at lower frequencies ($S_\nu \propto \nu^\alpha$; $\alpha \sim -1.6$) but considerations of receiver and sky background noise along with interstellar effects drive the range of observation frequencies (0.4 to 2 GHz) currently used by NANOGrav at Arecibo and the GBT. Typically, a given MSP is observed at both a low frequency (typically < 1 GHz) and a high frequency (> 1 GHz) in order to fit for the dispersion measure (DM), which corresponds to the integrated line-of-sight electron column density ($\mathrm{DM} \equiv \int_0^s n_e \, ds$). For the very high precision timing required for PTAs, the time variability of the DM requires contemporaneous measurements over a wide frequency range at each observation epoch.

The optimization of pulsar timing observations with respect to radio observing bands has been investigated in detail by Lam et al. (2017), leading to the conclusion that MSP timing can be improved significantly by using higher frequencies and larger bandwidths. As shown in Figure 5, higher frequencies and larger bandwidths can produce higher precision time-of-arrival (TOA) measurements than currently achieved. The effect is especially pronounced for pulsars at higher DMs, where propagation effects are increasingly important (Figure 5, right panel). As the NANOGrav PTA expands, newer

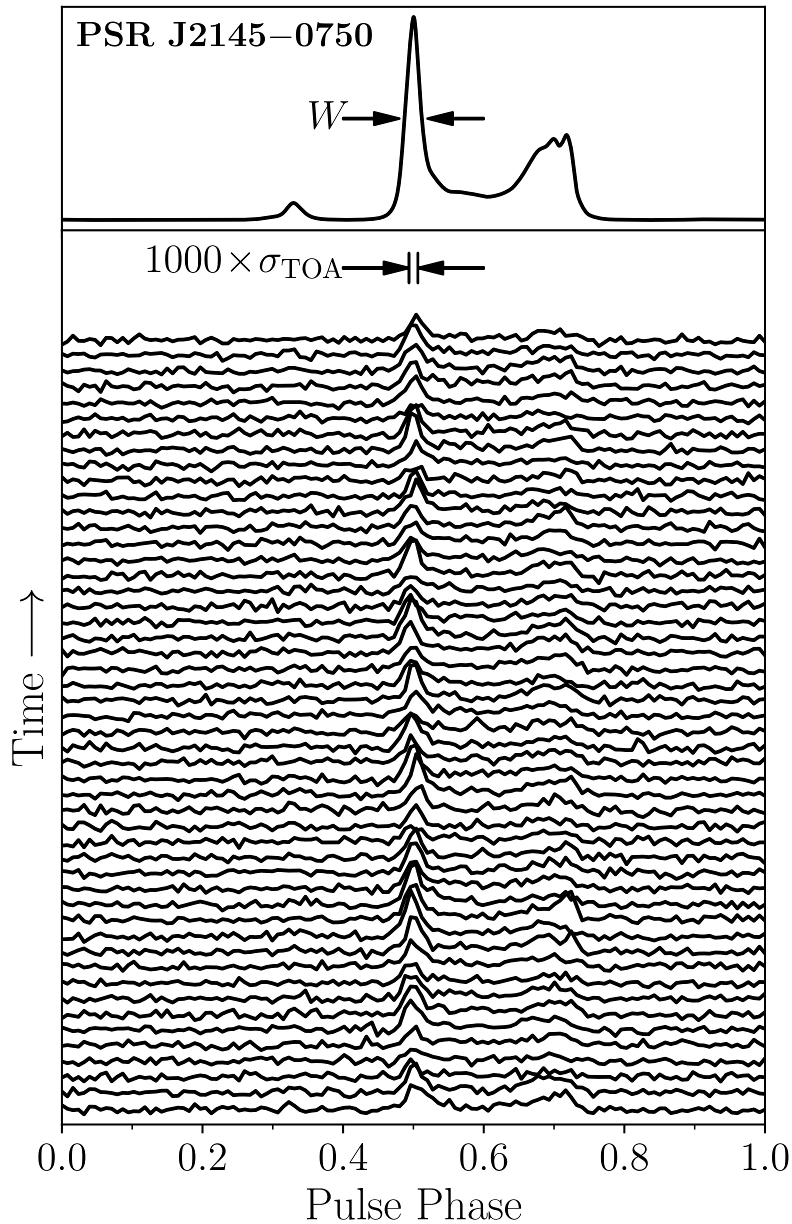

Figure 4. Pulse profiles for PSR J2145−0750, a 16.05 ms pulsar, at 820 MHz. The long-term average profile is shown at the top. The waterfall plot consists of a sequence of 10-pulse average profiles, illustrating the effect of pulse jitter, which reduces with the (number of pulses)$^{-1/2}$. The attained TOA precision $\sigma_{\mathrm{TOA}} \sim 0.1\ \mu$s, much smaller than the pulse width $W \sim 395\ \mu$s. High-sensitivity, broad-bandwidth observations with the ngVLA can reduce the arrival-time uncertainties drastically for many of our pulsars, allowing for improved GW characterization in the future.

pulsar discoveries are likely to be fainter and more distant, so higher sensitivities and higher frequencies will become critical over time. However, access to frequencies down to 1–1.5 GHz remains essential; we note that with wide enough available bandwidths, dual-frequency observations may no longer be required for DM estimation, leading to large gains in efficiency.

These requirements can be addressed using the ngVLA's continuous frequency coverage in the overall $\sim$ 1 to 10 GHz range of interest for PTAs.

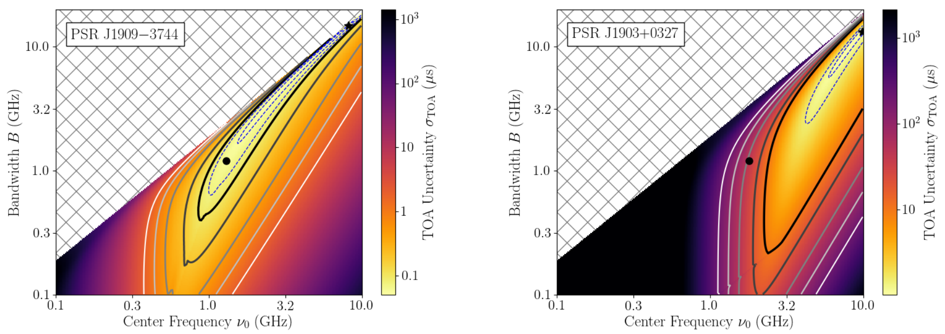

Figure 5. The uncertainty in pulse time of arrival measurements as a function of observing center frequency and bandwidth for two millisecond pulsars currently being observed by NANOGrav, adapted from our work in Lam et al. (2017). **Left:** PSR J1909–3744, which is one of the best-timed pulsars. Solid contours indicate TOA uncertainties of 2, 1, 0.5, 0.2, and 0.1 μs, in order of increasing darkness and thickness. The minimum TOA uncertainty (black star) is $\sigma_{\rm TOA}(\nu_0 = 8.1~\text{GHz}, B = 14.8~\text{GHz}) = 50$ ns and the estimate given the current frequency coverage (black circle) is $\sigma_{\rm TOA}(\nu_0 = 1.3~\text{GHz}, B = 1.2~\text{GHz}) = 59$ ns. The two dashed blue contours represent a 10% and 50% increase above the minimum $\sigma_{\rm TOA}$. **Right:** PSR J1903+0327, which is the pulsar with the highest dispersion measure (297.52 pc cm^{-3}) currently observed by NANOGrav. Contours indicate TOA uncertainties of 200, 100, 50, 20, and 10 μs, in order of increasing darkness and thickness. The minimum TOA uncertainty (black star) is $\sigma_{\rm TOA}(\nu_0 = 9.8~\text{GHz}, B = 13.2~\text{GHz}) = 1.0~\mu$s and the estimate given the current frequency coverage (black circle) is $\sigma_{\rm TOA}(\nu_0 = 1.8~\text{GHz}, B = 1.2~\text{GHz}) = 44.0~\mu$s. Higher observing frequencies with larger bandwidths potentially allow significant improvements in timing precision.

5. Observational Program

The current NANOGrav timing program (Arzoumanian et al. 2018b) uses integration times of 0.25–0.5 hr per pulsar at Arecibo and Green Bank with cadences of weekly (for the best pulsars) to once every three weeks, and allocating similar integration times with a selected fraction of the ngVLA collecting area offers more flexibility and higher efficiency compared to steering the entire collecting area of a large single dish to a sequence of pulsar timing targets.

Thus we envisage two usage modes of the ngVLA for PTA observations: (1) A sole-user mode, where the array is used in full on a single object or with up to $\sim$ 5 subarrays, each observing a pulsar of interest; or (2) A shared-user mode, where a single phased subarray $\gtrsim$20% of the ngVLA collecting area (i.e., comparable to the current GBT or more), depending on the pulsar flux density, is used to observe a single pulsar. As an aside, we note that sub-arraying reduces the net computational load, since baselines are not correlated across sub-arrays. Thus, as long as the correlator resources can be flexibly re-deployed, no extra computation resources will be required for shared-user or multi-target phased sub-array operation.

Frequency and Bandwidth: As described above, frequency agility in the overall 1 to 10 GHz range is needed.

Observing Cadence: NANOGrav currently observes ~70 pulsars, with each pulsar in the array being observed (approximately) every three weeks. Beyond the detection of the stochastic GW background, the future PTA scientific program requires both an increasing number of pulsars in the array and an improved observing cadence.

A straw-man future observing program might involve ~200 pulsars distributed over the sky. If each pulsar can be timed with a 20% sub-array of the ngVLA for ~0.5 hr every week, the total NANOGrav observing program may require ~20 hr/week of the full array. However, such estimates require two important caveats. (1) The PTA observing program needs to be sustained for years—see, e.g., our recent data release spanning 11 years (Arzoumanian et al. 2018b). (2) As the PTA expands, future pulsar additions to the array may be disproportionately fainter, requiring larger integration times. Instead, it appears more likely that NANOGrav will rely on the ngVLA to time the most critical and faintest pulsars, with the remainder being timed at partner facilities.

Pulsar Searching: The PTA requirements for the ngVLA described here do *not* include the capability of blind, full field-of-view pulsar searches, which impose enormous computational loads. However, sensitivity to GWs increases with the number of pulsars, and requires a distribution of sources all over the sky for a good GW detector response function. It is likely that the discovery of new pulsars will be dominated by single dish telescopes and by hybrid methods, where multi-wavelength imaging is used to identify candidate compact sources that are then searched for pulsations. (A pulsar that is suitable for timing as part of a PTA will be easily identified as a compact source in radio sky survey images, or potentially via a high-energy counterpart.)

Complementarity with the SKA: In contrast to the ngVLA, pulsar searching will be part of the core scientific mission of the planned SKA, and it will detect new pulsars to be timed as part of the future PTA. However, the varied scientific demands on the SKA imply that it is unlikely to accommodate regular pulsar timing observations at the required cadence for an all-sky PTA with a large number of pulsars. The ngVLA program described here will provide unique Northern hemisphere coverage, as well as the high frequencies needed to optimally observe distant, high-DM pulsars, as shown in Figure 5. We expect to continue our current practice of cross-observing of the best few pulsars (e.g., PSR J1909−3744 is currently observed by Australian, European, and North American telescopes) in order to address systematics and build a robust, fully-integrated international timing program.

Multi-messenger Coverage: Elsewhere in this volume, chapters by Taylor and Simon (“From Megaparsecs To Milliparsecs: Galaxy Evolution and Supermassive Black Holes with NANOGrav and the ngVLA”) and Burke-Spolaor et al. (“Supermassive Black Hole Pairs and Binaries”) discuss the complementary capabilities of the ngVLA to not only contribute to the detection of GWs, but to observe the radio signatures of the selfsame targets. This capability potentially makes the ngVLA a comprehensive facility for multi-messenger studies of binary SMBHs by itself. In addition, the next generation of Extremely Large Telescopes and space-based optical/infrared and high energy surveys will reveal electromagnetic counterparts to the SMBHB population probed by PTA observations.

6. Technical Requirements for PTA Observations with the ngVLA

Given the more general programmatic issues described above, here we summarize the technical requirements for the ngVLA in order to enable PTA observations. We note that at present, none of these requirements represents a "tall pole" or driver for the ngVLA specifications.

Phased Sub-Arrays: Multiple independent sub-arrays are required, up to ∼10, with each sub-array providing an independent phased array beam. It is preferable if each sub-array can maintain phase coherence over the duration of a pulsar timing observation, possibly using real-time self-calibration strategies with in-field calibrator sources.

Frequency coverage and Bandwidth: As described above and investigated further in Lam et al. (2017), wide-band frequency coverage is required and coverage down to 1–1.5 GHz is essential. We note that some pulsars with large and time-variable DMs may be suited to simultaneous dual-band observations using two independent sub-arrays, a capability of the ngVLA that is simply not available at any single-dish facility.

Correlator and Computation needs: Correlator specifications for pulsar observations are described in an ngVLA memo by Demorest et al., but in broad outline, phased array beams that can be sampled at 50 μs with 0.5 MHz channels are sufficient for PTA requirements. The output of the phased array beam will be coherently de-dispersed (i.e., a digital filter will be applied to remove the known average pulse dispersion as a function of frequency) in real time, before sampling. Given that cross-correlation for imaging will not be routinely required (and in any case, dishes observing different fields will never be correlated against each other), PTA observations using sub-arrays will be far less computationally challenging than full field-of-view, full-resolution imaging observations.

Polarization Calibration: Emission from millisecond pulsars is typically polarized, with linear polarizations at the few–50% level (e.g., Yan et al. 2011). The phased array beams will thus require polarization calibration (and more importantly, polarization stability) at the 5–10% level, preferably better.

Clock Stability: The long-term clock stability requirement for pulsar timing observations is currently met by tying observatory masers to GPS time. On the short term, clock stability requirements for pulsar timing are exceeded by the requirements for high-frequency VLBI.

Data Management and Curation: PTA observations are a long-term enterprise, and the scientific value of the data set increases with time baseline as wider ranges of GW frequencies are probed to higher sensitivities. NRAO has an exemplary track record of incorporating infrastructure for data management over decade-long timescales at the VLA, but pulsar observations (e.g. at the GBT) have typically not been included in these plans. For the ngVLA, the volume of PTA observations is expected to be dwarfed by full-field visibility storage requirements, and a long term archival and curation plan is both essential and straightforward.

7. Conclusions

PTAs have the potential to open a new window on the gravitational wave spectrum, probing nanohertz emission from the supermassive binary black hole mergers that accompany mass assembly in the universe, as well as other, more exotic, sources. Due to its exquisite sensitivity and northern hemisphere sky-coverage, the ngVLA will play a key role in PTA observations as long as certain key requirements are met: most importantly, independently phased sub-arrays and frequency coverage down to 1–1.5 GHz. None of the requirements or constraints pose a significant obstacle given the existing specifications of the ngVLA.

Acknowledgments. The NANOGrav Physics Frontiers Center is supported by the National Science Foundation award number 1430284.

References

Abbott, B. P., Abbott, R., Abbott, T. D., Abernathy, M. R., Acernese, F., Ackley, K., Adams, C., Adams, T., Addesso, P., Adhikari, R. X., et al. 2016, Physical Review Letters, 116, 061102. `1602.03837`

Abbott, B. P., Abbott, R., Abbott, T. D., Acernese, F., Ackley, K., Adams, C., Adams, T., Addesso, P., Adhikari, R. X., Adya, V. B., et al. 2017, Physical Review Letters, 119, 161101. `1710.05832`

Arzoumanian, Z., Baker, P. T., Brazier, A., Burke-Spolaor, S., Chamberlin, S. J., Chatterjee, S., Christy, B., Cordes, J. M., Cornish, N. J., Crawford, F., Thankful Cromartie, H., Crowter, K., DeCesar, M., Demorest, P. B., Dolch, T., Ellis, J. A., Ferdman, R. D., Ferrara, E., Folkner, W. M., Fonseca, E., Garver-Daniels, N., Gentile, P. A., Haas, R., Hazboun, J. S., Huerta, E. A., Islo, K., Jones, G., Jones, M. L., Kaplan, D. L., Kaspi, V. M., Lam, M. T., Lazio, T. J. W., Levin, L., Lommen, A. N., Lorimer, D. R., Luo, J., Lynch, R. S., Madison, D. R., McLaughlin, M. A., McWilliams, S. T., Mingarelli, C. M. F., Ng, C., Nice, D. J., Park, R. S., Pennucci, T. T., Pol, N. S., Ransom, S. M., Ray, P. S., Rasskazov, A., Siemens, X., Simon, J., Spiewak, R., Stairs, I. H., Stinebring, D. R., Stovall, K., Swiggum, J., Taylor, S. R., Vallisneri, M., van Haasteren, R., Vigeland, S., Zhu, W. W., & The NANOGrav Collaboration 2018a, ApJ, 859, 47. `1801.02617`

Arzoumanian, Z., Brazier, A., Burke-Spolaor, S., Chamberlin, S., Chatterjee, S., Christy, B., Cordes, J. M., Cornish, N. J., Crawford, F., Thankful Cromartie, H., Crowter, K., DeCesar, M. E., Demorest, P. B., Dolch, T., Ellis, J. A., Ferdman, R. D., Ferrara, E. C., Fonseca, E., Garver-Daniels, N., Gentile, P. A., Halmrast, D., Huerta, E. A., Jenet, F. A., Jessup, C., Jones, G., Jones, M. L., Kaplan, D. L., Lam, M. T., Lazio, T. J. W., Levin, L., Lommen, A., Lorimer, D. R., Luo, J., Lynch, R. S., Madison, D., Matthews, A. M., McLaughlin, M. A., McWilliams, S. T., Mingarelli, C., Ng, C., Nice, D. J., Pennucci, T. T., Ransom, S. M., Ray, P. S., Siemens, X., Simon, J., Spiewak, R., Stairs, I. H., Stinebring, D. R., Stovall, K., Swiggum, J. K., Taylor, S. R., Vallisneri, M., van Haasteren, R., Vigeland, S. J., Zhu, W., & The NANOGrav Collaboration 2018b, ApJS, 235, 37. `1801.01837`

Favata, M. 2009, ApJ, 696, L159. `0902.3660`

Hellings, R. W., & Downs, G. S. 1983, ApJ, 265, L39

Lam, M. T., McLaughlin, M. A., Cordes, J. M., Chatterjee, S., & Lazio, T. J. W. 2017, ApJ, submitted. 1710.02272

Mingarelli, C. M. F., Lazio, T. J. W., Sesana, A., Greene, J. E., Ellis, J. A., Ma, C.-P., Croft, S., Burke-Spolaor, S., & Taylor, S. R. 2017, Nature Astronomy, 1, 886. 1708.03491

NANOGrav Astrophysics Working Group, et al. 2018, in prep.

Rodriguez, C., Taylor, G. B., Zavala, R. T., Peck, A. B., Pollack, L. K., & Romani, R. W. 2006, ApJ, 646, 49. astro-ph/0604042

Yan, W. M., Manchester, R. N., van Straten, W., Reynolds, J. E., Hobbs, G., Wang, N., Bailes, M., Bhat, N. D. R., Burke-Spolaor, S., Champion, D. J., Coles, W. A., Hotan, A. W., Khoo, J., Oslowski, S., Sarkissian, J. M., Verbiest, J. P. W., & Yardley, D. R. B. 2011, MNRAS, 414, 2087. 1102.2274

Part X

Cosmology:

Weak gravitational lensing with CO galaxies

Philip Bull
Radio Astronomy Laboratory, University of California Berkeley, Berkeley, CA 94720, USA; philbull@berkeley.edu

Ian Harrison
Jodrell Bank Centre for Astrophysics, School of Physics & Astronomy, The University of Manchester, Manchester M13 9PL, UK;
ian.harrison-2@manchester.ac.uk

Eric Huff
Jet Propulsion Laboratory, California Institute of Technology, 4800 Oak Grove Drive, Pasadena, California, USA; Eric.M.Huff@jpl.nasa.gov

Abstract. Optical weak lensing surveys have become a powerful tool for precision cosmology, but remain subject to systematic effects that can severely bias cosmological parameter estimates if not carefully removed. We discuss the possibility of performing complementary weak lensing surveys at radio/microwave frequencies, using detections of CO-emitting galaxies with resolved continuum images from ngVLA. This method has completely different systematic uncertainties to optical weak lensing shear measurements (e.g. in terms of blending, PSF, and redshift uncertainties), and can provide additional information to help disentangle intrinsic alignments from the cosmological shear signal. A combined analysis of optical and CO galaxy lensing surveys would therefore provide an extremely stringent validation of highly-sensitive future surveys with Euclid, LSST, and WFIRST, definitively rejecting biases due to residual systematic effects. A lensing survey on ngVLA would also provide valuable spectral (kinematic) and polarimetric information, which can be used to develop novel cosmological analyses that are not currently possible in the optical.

1. Introduction and scientific motivation

As light travels from distant galaxies, it is distorted by the gravitational pull of matter that it encounters along the way. While some light rays pass close enough to dense concentrations of matter to be strongly lensed, producing arcs and multiple images, the majority of rays are only slightly affected. This weak gravitational lensing effect can be measured in a number of ways, but the most common is to look for lensing shear, which causes coherent correlations in the ellipticity of galaxies over angular scales of a few arcminutes or larger (Bartelmann & Schneider 2001; Munshi et al. 2008; Hoekstra & Jain 2008; Kilbinger 2015; Mandelbaum 2017). This has motivated the development of a slew of large galaxy surveys, predominantly in the optical, that seek to measure the shapes of many tens or even hundreds of millions of galaxies across cosmic time in order to characterize the statistical properties of the weak lensing 'shear' signal.

Weak lensing has rapidly developed into one of the pillars of observational cosmology. This is due in large part to its extremely high information content – the lensing signal not only encodes information about the total matter distribution (including cold dark matter and baryons) along the line of sight, but also the growth rate of large-scale structure and the geometry of space (Van Waerbeke et al. 1999; Jain & Taylor 2003). These quantities are instrumental in attempts to understand some of the biggest problems in cosmology and fundamental physics, such as the nature of cosmic acceleration and the Cosmological Constant problem, and the nature of gravity on extremely large distance scales. Lensing can also be used to understand the connection between galaxies and the dark matter structures that they are embedded in (Hoekstra et al. 2004; Sheldon et al. 2004).

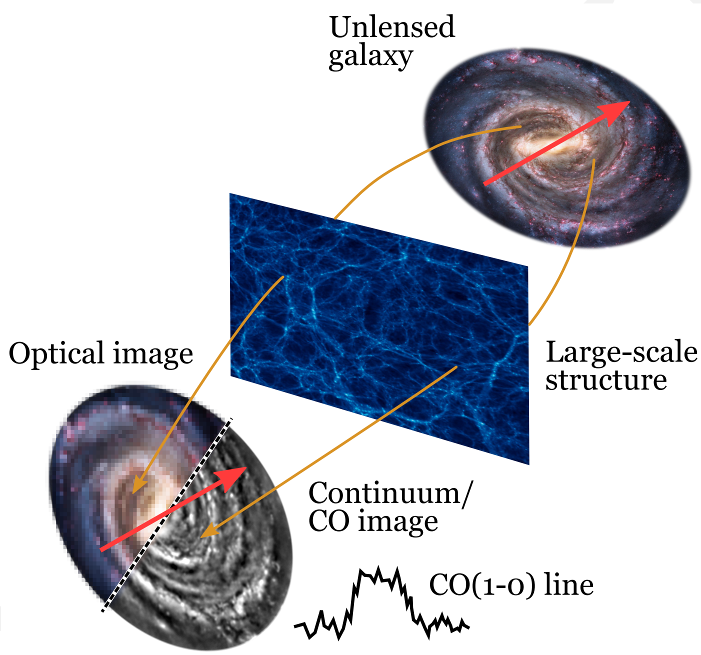

Figure 1. Illustration showing the weak gravitational lensing of CO galaxies. Light rays (orange lines) are bent and sheared as they pass through the large-scale structure, resulting in a distortion of the observed shape of the galaxy. The galaxy can be imaged in multiple bands, including optical and radio continuum/CO line emission. The advantage of the CO/radio continuum strategy advocated here is that it preserves redshift information through detection of the CO(1–0) line, and has different PSF characteristics from the optical. The fact that lensing leaves the polarization angle unaffected (red arrows) can also be used to reduce shape noise and solve for the intrinsic alignment effect. (Composite image. Credit: P. Bull/NASA/S. Gottlober/MultiDark.)

This information does not come easily however. Weak lensing observations remain some of the most challenging in all of astronomy, with precise control over myriad instrumental and astrophysical systematics required to even detect the effect, let alone measure its statistical properties with the sub-percent precision required to beat down errors on cosmological parameters. Despite a series of enhancements in analysis techniques (e.g. Kaiser et al. 1995; Bernstein & Jarvis 2002; Miller et al. 2007; Huff

& Mandelbaum 2017), low-level systematics can still remain in the data, subtly biasing the resulting cosmological constraints (Heavens et al. 2000; Hirata & Seljak 2003; Huterer et al. 2006; Massey et al. 2013; Mandelbaum 2017).

The development of a rigorous and independent cross-check of the optical weak lensing signal is therefore of vital importance – without it, the unprecedented precision of flagship datasets such as the LSST lensing sample could be undermined. Radio weak lensing (Fig. 1) represents a highly promising solution to this problem (Chang et al. 2004; Brown 2012; Patel 2016; Camera et al. 2017) – the galaxy shape measurement process is fundamentally different in the radio, owing to the almost-deterministic nature of synthesized beams, the lack of atmospheric seeing effects, and differences in galaxy morphologies between the radio and optical (Patel et al. 2010; Tunbridge et al. 2016). As such, many weak lensing systematics are expected to be strongly suppressed by radio-optical cross-correlations (Demetroullas & Brown 2016). A consistent picture between the radio and optical cross- and auto-power spectra would also be strong evidence that systematics are under control, and could therefore thoroughly validate the weak lensing methodology.

In addition to providing a cross-check on optical surveys, radio surveys also open up several exciting possibilities to measure extra information about the lensing galaxy sample that would be difficult, if not impossible, to obtain in the optical. Spectroscopic redshifts can be measured for large fractions of the sample for example, an extremely costly exercise in the optical. As well as removing photometric redshift calibration as a key source of uncertainty, this would allow more information to be recovered from the lensing signal in the radial direction, potentially significantly improving constraints on some cosmological parameters. Polarization information can also be readily obtained in the radio, allowing the intrinsic orientations of galaxies to be inferred – again removing an important source of systematic error (intrinsic alignments).

In this chapter, we examine the possibility of measuring the weak lensing shear signal from a large sample of CO-emitting galaxies in several spectroscopic redshift bins across a substantial sky area and redshift range. This requires a survey of a large number of moderately-resolved CO-emitting galaxies. The galaxy shapes can be measured using continuum emission integrated over a few wide channels in each band, while the galaxy redshifts will be determined from spectroscopic detections of the CO(1-0) line. The resulting shear catalog can be cross-correlated with optical catalogs to greatly reduce the impact of systematics. We also discuss some of the novel analysis techniques that are enabled by radio observations, including polarization-based measurements of intrinsic alignments, and kinematic lensing using resolved spectral lines.

2. Systematics mitigation with radio-optical cross-correlations

Cosmological constraints from weak lensing surveys require the creation of a shear map on the sky. The spatially varying shear γ must be estimated from the shapes of individual galaxies which sample the shear field, and is typically done using a simple (often weighted) average over galaxies in a sky patch small enough such that the shear is constant within the patch. Because weak lensing causes such a small change in the ellipticity of an individual galaxy, even small systematic biases in the estimation of its shape can quickly overwhelm the cosmological signal and cause significant errors in e.g. measuring the dark energy equation of state. For a linear model of bias on shear $\gamma_{\rm meas} = (1+m)\gamma_{\rm true} + c$ it is necessary for $m < \mathcal{O}(10^{-2})$ and $c < \mathcal{O}(10^{-3})$ for Stage

III surveys such as DES and SKA1 and $m < O(10^{-3})$ and $c < O(10^{-4})$ for Stage IV surveys such as LSST and SKA2 (Amara & Refregier 2008).

Weak lensing with interferometers at radio wavelengths provides a unique opportunity to mitigate many of these systematics. Cosmological constraints are typically derived by taking two-point statistics of shear maps; if these power spectra are made by cross-correlating radio and optical shear maps, wavelength-dependent systematics either disappear or can be calibrated out (see Camera et al. 2017). Some of the most important systematics for optical surveys are as follows:

PSF systematics. Estimating γ from galaxy shapes requires deconvolution of the shape of the Point Spread Function (PSF) from each individual source. For ground-based optical surveys, atmospheric seeing produces a PSF which spatially varies in a non-deterministic way. Significant efforts are put into PSF reconstruction and strategies for precise and accurate deconvolution. Even for space-based surveys, challenges remain due to instabilities in the optical systems, non-trivial color dependence of the PSF, and effects within the CCD (Mandelbaum 2015).

In contrast, interferometer dirty beams may be seen as a stable and highly deterministic forward model, allowing for either precise determination of galaxy shapes in images or directly in the *uv* plane. Even if shape measurement systematics remain, they will be highly uncorrelated with those from optical surveys, meaning systematic uncertainties from PSF removal should be highly suppressed in radio-optical cross-correlations.

Blended (confused) sources. A substantial fraction of the galaxies detected in deep optical surveys like LSST are expected to be overlapping on the sky. Such 'blended' sources can be hard to identify, especially when the resolution limits imposed by atmospheric seeing are taken into account. Unidentified blends mostly add random noise to the measured shear signal, as the blended galaxies should have no preferred orientation. This source of noise can be removed simply by removing the blended sources (if they can be identified), although this can substantially reduce the effective number density of galaxies in the sample. More problematic is the effect of blends on photometric redshift estimation; trying to fit a photometric redshift to two sources at very different redshifts can result in catastrophic failure of the photo-z algorithm, which can ultimately cause biases in cosmological parameter estimates (Samuroff et al. 2018). The high angular resolution afforded by the long baselines of ngVLA may be useful in at least identifying blended sources for some of the galaxies in overlapping optical surveys from continuum images, while the degree of blending/confusion in the radio survey will only depend on instrumental resolution (since the atmospheric seeing is a much smaller effect). The availability of CO line redshifts will also help mitigate catastrophic photometric redshift errors caused by blends. The extent to which ngVLA data is useful for identifying blends in optical data will depend on the final array layout and depth of the survey, but if suitable optimizations are made, the impact could be considerable – especially if photo-z estimation algorithms are unable to reduce their sensitivity to blends.

Intrinsic alignments. The simple average estimator for γ relies on the assumption that galaxy shapes were uncorrelated before lensing (i.e. in the absence of lensing, the average ellipticity should be zero). However, the realities of galaxy formation processes mean that this is not true in the real Universe. Failing to account for these intrinsic galaxy alignments may bias cosmological parameter estimation by many standard deviations (Troxel & Ishak 2014). By measuring both the lensed total intensity galaxy position angle and a quantity which is not affected by lensing, such as polarization position angle (Brown & Battye 2011) or spatially-resolved kinematics (Morales 2006), intrinsic alignments can be mapped and accounted for in the lensing analysis. Being able to account for this directly has significant advantages over current strategies applied in optical weak lensing surveys, which typically involve either removing data (seriously degrading cosmological constraints) or the application of poorly-motivated models for the intrinsic alignment signal. Such a map of intrinsic alignments would not only be useful for an ngVLA weak lensing survey itself, but could also be used to model the intrinsic alignments within optical surveys (if the same galaxy populations are being probed).

3. Limitations of current astronomical instrumentation

While pathfinder weak lensing observations have been made with existing radio facilities (e.g. Chang et al. 2004; Patel et al. 2010), they are far from achieving parity with optical surveys – by any metric. The current state of the art is SuperCLASS[1], a ~ 1.75 deg^2 survey on e-MERLIN and JVLA that targets several Abell clusters with overlapping Subaru imaging. While these instruments have comparatively slow survey speeds, somewhat sparse *uv* coverage (even when combined), and operate in a band ($\sim 1.4 - 1.5$ GHz) that lacks emission lines suitable for providing redshift information, SuperCLASS is nevertheless useful as a way of proving the radio weak lensing method and providing a testing ground for future techniques.

The Square Kilometre Array (SKA) and its precursors MeerKAT and ASKAP have better sensitivity and much denser *uv* coverage, making imaging and shape measurement much easier. The precursors lack sufficiently long baselines that are needed to resolve higher-redshift continuum galaxies however, and so the first large-area radio weak lensing survey will probably have to wait until SKA1 comes online. A $\sim 5,000$ deg^2 continuum survey on SKA1-MID Band 2 (950 – 1750 MHz) is expected to be competitive with the Dark Energy Survey (Brown et al. 2015; Harrison et al. 2016), and a fraction of the detected galaxies will have 21cm line detections and therefore redshifts. Unless they can be cross-matched with optical galaxies (with spectroscopic or photometric redshifts), the large fraction of sources without a 21cm detection will have effectively no redshift information, resulting in what would effectively be a 2D lensing survey (containing significantly less information about cosmological evolution).

As discussed in the previous section, optical surveys also have some inherent limitations when it comes to measuring the weak lensing signal, mostly centered around uncertainties in the shape, stability, and frequency-dependence of the point spread function, and a lack of knowledge about the intrinsic shapes of the galaxies. A number of these can be mitigated by some features of ngVLA and radio weak lensing observations more generally, as we discuss in the next section.

[1] `http://www.e-merlin.ac.uk/legacy/projects/superclass.html`

4. Connection to unique ngVLA capabilities

The ngVLA will have a unique combination of spectral/spatial resolution and wide bandwidth, allowing it to detect large numbers of semi-resolved galaxies in both continuum and CO line emission at low and intermediate redshifts. Other radio weak lensing surveys have been proposed, for example using the SKA at lower frequencies ($\sim$ 1.5 GHz), but these mostly lack redshift information except for a small fraction of sources that also have a detectable 21cm line. A CO galaxy sample would also be better matched to the LSST and DES samples than a 21cm sample, as it will preferentially contain normal star-forming galaxies that will make up the bulk of the optical samples. The higher angular resolution of ngVLA will also reduce the occurrence of blended/confused sources, which are a significant source of noise in lensing measurements (Samuroff et al. 2018).

ngVLA will also be able to operate in fundamentally different survey modes from optical experiments. A major advantage over optical telescopes is the ease with which polarized observations can be made. Weak lensing leaves the polarization angle of a galaxy unchanged. Since polarization traces the disk, this can be used to measure the intrinsic orientation of the galaxy, i.e. its orientation before it was sheared. As discussed in Section 2, this helps to mitigate the effects of intrinsic alignments, which are correlations in the ellipticities of galaxies caused by non-lensing effects like tidal shears that are a significant nuisance effect for weak lensing cosmology (e.g. Joachimi et al. 2015).

The high spectral resolution of ngVLA can be used to similar effect. If the CO lines of some subset of galaxies can be spectrally resolved, one can obtain highly complementary information about their circular velocity. As in the polarized case, this can be used to infer the intrinsic ellipticity and thus greatly suppress shape noise (Morales 2006). If a significant decrease in shape noise can be achieved, the number density of galaxies required to obtain a high SNR detection of the lensing signal can also be greatly reduced, making ngVLA a much more efficient weak lensing survey instrument without the need to substantially alter its design.

5. Measurement technique and experimental layout

In this section, we give a high-level overview of how a CO weak lensing survey could be carried out in practice. Two measurements are required per galaxy:

(a). The galaxy's shape (ellipticity), which can be obtained with high signal-to-noise through imaging of the continuum emission;

(b). A spectroscopic determination of its redshift through a detection of the CO (1-0; 115.2712 GHz) line.

The first measurement requires that the target galaxies be sufficiently resolved that their ellipticities can be measured. This suggests a target resolution of $\sim$1" for galaxies at $z \sim 1$ (see Fig. 2). A wide instantaneous bandwidth is preferred to maximize continuum SNR, ideally breaking up the full available bandwidth into a handful of wide channels to allow for the correction of frequency-dependent beam effects. Note that the galaxies need only be semi-resolved in order to measure their ellipticities accurately enough. Beam smearing effects will be important when measuring the shape of the galaxy, hence

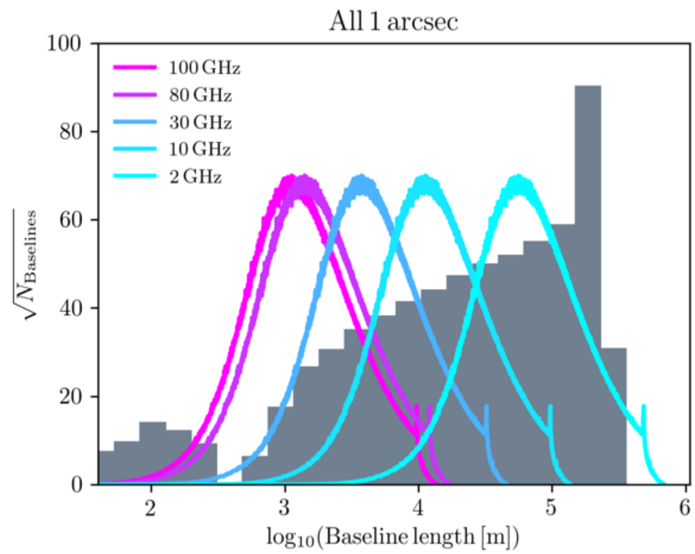

Figure 2. Comparison of the angular resolution of ngVLA to the angular scales affected by the cosmic shear signal, as a function of frequency band (redshift). The colored curves show the (normalized) shear signal for different observed CO(1–0) line frequencies. They were calculated by taking a representative field of view populated with galaxies, smoothed to 1 arcsec resolution, applying an appropriate level of weak lensing shear, and then calculating the power spectrum of the difference between the sheared and unsheared images (note the Nyquist artefact in the tails). The gray histogram is the orientation-averaged ngVLA baseline distribution, assuming the Conway array layout.

the need to break up the band into smaller chunks; the PSF must be known very accurately, including its frequency dependence, and time-variation of the PSF should also be strongly controlled. An accurate flux density calibration is not strictly required, except to apply cuts to select certain galaxy sub-populations. Imaging may not be strictly necessary if visibility-space shape measurement methods can be used (Chang & Refregier 2002; Patel et al. 2014; Rivi et al. 2016), although this will require gridded visibilities to be stored (Harrison & Brown 2015).

The second measurement requires just enough spectral resolution to identify and measure the redshifted CO line integrated over the solid angle of the galaxy. In the simplest case, there is no requirement to accurately measure the line flux, line width, or other spectroscopic properties, so a low-SNR line detection is sufficient. Depending on typical linewidths, the spectral resolution required will likely be a few hundred km/s.

The SNR of the weak lensing measurement strongly depends on the number density of sources for which shapes can be measured, as well as the spatial volume that can be surveyed. A minimal proof of concept survey would need to target a few hundred square degrees with source number densities of order a few per sq. arcmin. An ideal survey for studying lensing systematics would be matched to the WFIRST footprint (~2,200 sq. deg.), with a high source number density ($\sim 60-70$ per sq. arcmin). An ideal cosmological survey would cover a large fraction of the Euclid or LSST footprints (~15,000 sq. deg.) with 20-30 sources per sq. arcmin. Lower number densities could be sustained with the addition of spectroscopic redshift information, which compensates by providing access to radial Fourier modes that LSST and other photometric surveys effectively discard. A continuum-only weak lensing survey would also be possible, negating the need to carry out measurement (b), but is unlikely to be competitive with optical surveys with photometric redshifts.

An alternative to increasing the source number density is to measure (c) the polarization angle of the galaxies; or (d) accurately measure their linewidths. These would allow the methods described in Section 4 to be used to recover the intrinsic galaxy shapes/alignment, thus significantly cancelling important noise sources such as shape noise and intrinsic alignments. Carrying out these much more detailed measurements would likely necessitate a much smaller survey area, with greater depth per pointing. The trade-offs between these different survey modes will need to be explored within the context of a realistic model of the (polarized) luminosity, size, and circular velocity distribution of CO galaxies.

Finally, a significant hurdle is the small field of view of ngVLA, which substantially reduces its survey speed. The ~ 1 deg primary beam of SKA gives it a significant advantage in this respect. Array designs that increase the field of view of ngVLA and optimize its baseline distribution for sensitivity at ~ 1 arcsec scales (c.f. Fig. 2) are therefore highly desirable for this science case. Examples of how to achieve this might include reducing dish sizes and adopting a more compact layout with a denser core, perhaps in the context of a 'hybrid' design with a dense core of small dishes at the center and larger dishes spread out to longer baseline lengths. An advantage of such a design is that the core and outer sets of dishes could be operated independently if desired, allowing large surveys and high-resolution pointed observations to be performed concurrently.

6. Complementarity

While a radio weak lensing survey performed with ngVLA on its own would be a interesting and potentially valuable cosmological test, the power of performing such a survey lies firmly in the ability to jointly analyze it with an overlapping optical survey. The cross-correlation of a radio weak lensing sample with contemporary optical datasets (e.g. from LSST, WFIRST, and Euclid) would provide an extremely robust validation of the weak lensing methodology that so much of the observational cosmology program will rely upon in the next decade. This represents an immensely valuable synergy with practically all of the large cosmological survey instruments planned for the beyond-2025 timeframe, and would represent the "last word" in the interpretation of weak lensing data.

This science case also complements and extends the radio weak lensing science case of the SKA to higher frequencies, higher spatial resolutions, and arguably a more appropriate sample for optical cross-correlations, as well as providing high-value spectroscopic redshift information, and the ability to use novel techniques such as kinematic lensing and intrinsic alignment removal with polarization. Additionally, the large sample of galaxies that would be obtained in performing a radio weak lensing survey would clearly be valuable for a wide array of astrophysical applications too, such as studies of galaxy formation and evolution, and galaxy structure and dynamics (if spectrally resolved/polarized observations are prioritized), providing a further connection to future NASA flagship missions such as the Origins Space Telescope and LUVOIR.

Acknowledgments. We are grateful to J. Lazio for useful discussions.

References

Amara, A. & Refregier, A. MNRAS **391** 228 (2008).
Bartelmann, M. & Schneider, P. Phys. Rept. **340**, 291 (2001).
Bernstein, G. M. & Jarvis, M. Astron. J. **123**, 583 (2002).
Brown, M. L., & Battye, R. A. MNRAS, 410, 2057 (2011).
Brown, M. L. arXiv:1206.4437 (2012).
Brown, M. L. et al. [JVLA Collaboration]. arXiv:1312.5618 (2013).
Brown, M. L. et al. PoS AASKA **14**, 023 (2015).
Camera, S., Harrison, I., Bonaldi, A. & Brown, M. L. MNRAS **464**, 4, 4747 (2017).
Chang, T.-C., & Refregier, A. ApJ, 570, 447 (2002).
Chang, T. C., Refregier, A. & Helfand, D. J., Astrophys. J. **617**, 794 (2004).
Demetroullas, C. & Brown, M. L. MNRAS **456** 3, 3100 (2016).
Harrison, I., & Brown, M. L. arXiv:1507.06639 (2015).
Harrison, I., Camera, S., Zuntz, J., & Brown, M. L. MNRAS **463**, 3574 (2016).
Heavens, A., Refregier, A. & Heymans, C. Mon. Not. Roy. Astron. Soc. **319**, 649 (2000).
Hirata, C. M. & Seljak, U. Mon. Not. Roy. Astron. Soc. **343**, 459 (2003).
Hoekstra, H., Yee, H. K. C. & Gladders, M. D. Astrophys. J. **606**, 67 (2004).
Hoekstra, H. & Jain, B. Ann. Rev. Nucl. Part. Sci. **58**, 99 (2008).
Huff, E. M., Krause, E., Eifler, T., George, M. R. & Schlegel, D. arXiv:1311.1489 (2013).
Huff, E. & Mandelbaum, R. arXiv:1702.02600.
Huterer, D., Takada, M., Bernstein, G. & Jain, B. Mon. Not. Roy. Astron. Soc. **366**, 101 (2006).
Jain, B. & Taylor, A. Phys. Rev. Lett. **91**, 141302 (2003).
Joachimi, B. et al. Space Sci. Rev. **193** 1, 1 (2015).
Kaiser, N., Squires, G. & Broadhurst, T. J. Astrophys. J. **449**, 460 (1995).
Kilbinger, M. Rept. Prog. Phys. **78**, 086901 (2015).
Mandelbaum, R. JINST **10** 05, C05017 (2015).
Mandelbaum, R. arXiv:1710.03235 (2017).
Massey, R., Hoekstra, H., Kitching, T., et al. MNRAS, 429, 661 (2013).
Miller, L., Kitching, T. D., Heymans, C., et al. MNRAS **382**, 315 (2007).
Morales, M. F. Astrophys. J. **650**, L21 (2006).
Munshi, D., Valageas, P., Van Waerbeke, L. & Heavens, A. Phys. Rept. **462**, 67 (2008).
Patel, P., Bacon, D. J., Beswick, R. J. et al. MNRAS, 401, 2572 (2010).
Patel, P., Abdalla, F. B., Bacon, D. J., et al. MNRAS, 444, 2893 (2014).
Patel, P. arXiv:1602.07482 (2016).
Rivi, M., Miller, L., Makhathini, S., & Abdalla, F. B. MNRAS, 463, 1881 (2016).
Samuroff, S., Bridle, S. L., Zuntz, J., et al. MNRAS, 475, 4524 (2018).
Sheldon, E. S. et al. [SDSS Collaboration], Astron. J. **127**, 2544 (2004).
Troxel, M. A. & Ishak, M. Phys. Rept. **558** 1 (2014).
Tunbridge, B., Harrison, I. & Brown, M. L. MNRAS **463**, 3, 3339 (2016).
Van Waerbeke, L., Bernardeau, F. & Mellier, Y. Astron. Astrophys. **342**, 15 (1999).

Extragalactic Proper Motions: Gravitational Waves and Cosmology

Jeremy Darling[1], Alexandra Truebenbach[1], and Jennie Paine[1]

[1]*Center for Astrophysics and Space Astronomy, Department of Astrophysical and Planetary Sciences, University of Colorado, 389 UCB, Boulder, CO 80309-0389, USA*

1. Background

The universe is dynamic, as we know from cosmological redshifts induced by the Hubble expansion, but astronomers tend to treat extragalactic objects as fixed in the sky with fixed apparent velocities. If measured with enough precision, however, nothing is constant: all objects will change their redshifts and positions at a rate of order $H_0 \simeq 7 \times 10^{-11}$ yr^{-1} $\simeq 15$ μarcsec yr^{-1}. The secular redshift drift caused by a non-constant expansion (Sandage 1962) is of order 0.3 cm s^{-1} yr^{-1} at $z \simeq 1$ and may be measured by optical telescopes using the Lyα forest or by radio telescopes using H 1 21 cm or molecular absorption lines (Loeb 1998; Darling 2012). Proper motions of extragalactic objects may be caused by peculiar motions induced by large scale structure (Darling 2013), by primordial gravitational waves (e.g., Pyne et al. 1996; Gwinn et al. 1997; Book & Flanagan 2011; Darling et al. 2018), by the recession of fixed objects such as the baryon acoustic oscillation, or by anisotropic expansion (Fontanini et al. 2009; Quercellini et al. 2009; Titov 2009; Darling 2014).

Observer-induced proper motions are also possible: these include the secular aberration drift caused by acceleration of the solar system barycenter about the Galactic Center (e.g., Bastian 1995; Eubanks et al. 1995), observations from a rotating reference frame, and secular extragalactic parallax caused by motion with respect to the cosmic microwave background (CMB; Ding & Croft 2009).

Proper motions depict a discretely sampled vector field on the celestial sphere. In order to detect and characterize correlated motions, it is natural to describe vector fields using vector spherical harmonics (VSH), which are the vector equivalent of the scalar spherical harmonics used to describe signals such as the CMB temperature pattern, the geoid, or equipotentials (Mignard & Klioner 2012). VSH are characterized by their degree ℓ and order m, and resemble electromagnetic fields. They can therefore be separated into curl-free (E-mode) and divergenceless (B-mode) vector fields that are typically connected to distinct physical phenomena. The general method for characterizing a correlated proper motion field is to fit VSH to the observed proper motions and to calculate the power in and significance of each degree ℓ for each mode.

2. Expected (and Possible) Signals

Table 1 summarizes the expected and possible global extragalactic proper motion signals. This summary is likely to be incomplete. Here we provide a brief description of each physical or observer-induced effect, and Section 3 discusses the impact the ngVLA might have on detecting or constraining these phenomena.

2.1. Secular Aberration Drift

Aberration of light is caused by the finite speed of light and the motion of the observer with respect to a light source. The resulting deflection of light scales as $\vec{v}/c$. If the observer accelerates, then the aberration exhibits a secular drift, and objects appear to stream in the direction of the acceleration vector. The solar system barycenter accelerates at roughly 0.7 cm s^{-1} yr^{-1} as the Sun orbits the Galactic Center, resulting in an apparent ~5 μarcsec yr^{-1} E-mode dipole converging on the Galactic Center (Figure 1). This has been detected in the proper motions of radio sources, first by Titov et al. (2011), using *a priori* knowledge of the expected effect for data trimming, and recently without priors by Truebenbach & Darling (2017). Titov & Krásná (2018) has further developed the VLBI-specific methodology for extracting this signal.

2.2. Secular Parallax

The CMB shows a temperature dipole of 3.4 mK, which is caused by the motion of the solar system barycenter with respect to the CMB rest frame (e.g., Hinshaw et al. 2009). This amounts to a relative motion of 369 ± 0.9 km s^{-1} or 78 AU yr^{-1}. This motion will induce a maximum secular parallax of 78 μarcsec yr^{-1} Mpc^{-1}: nearby galaxies in directions perpendicular to the CMB poles will show a reflex motion opposite our motion when compared to distant galaxies. Precise proper motion measurements of galaxies within ~20 Mpc will allow a statistical detection of the distance-dependent E-mode dipole caused by secular parallax. When referenced to this average dipole, it will be possible to detect the peculiar motions of individual galaxies as well as their geometric distances. Secular parallax may provide a distance ladder-free method for measuring distances in the local universe.

2.3. Rotation

As observers in a rotating reference frame, we have traditionally used quasars to define a fixed, non-rotating reference frame in order to measure and monitor the rotation of the Earth (e.g., McCarthy & Petit 2004). We thus have no means to detect non-terrestrial rotation that has an axis close to polar, but it is possible to detect or constrain rotation about axes that are not aligned with the polar axis. While the question of a rotating universe can be nettlesome to contemplate and violates our assumption of cosmological isotropy, one can nonetheless make precise, sub-μarcsec yr^{-1} measurements of the effect because it would manifest as a B-mode dipole in the proper motion vector field.

2.4. Anisotropic Expansion

In an isotropically expanding universe, objects move radially away from every observer (modulo small peculiar motions due to local density perturbations; see Section 2.6), so there will be no global correlated proper motions caused by isotropic Hubble expansion. However, anisotropic expansion would cause objects to stream across the sky toward the directions of fastest expansion and away from directions of slowest expansion. Assuming a simple triaxial anisotropy, one can show that the resulting celestial proper motion pattern can be completely described by an E-mode VSH quadrupole

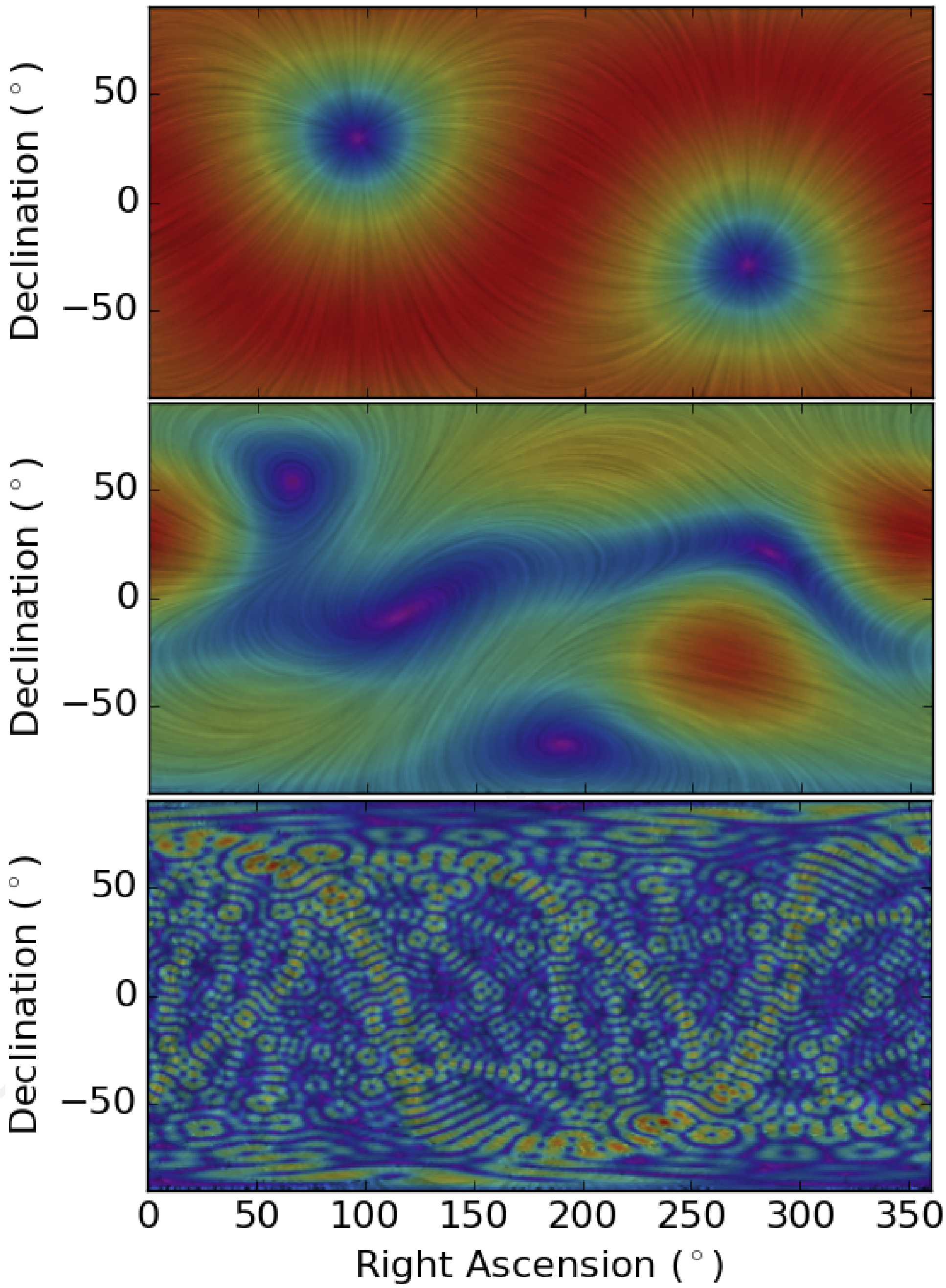

Figure 1. All-sky stream plots. Streamlines indicate the vector field direction, and the colors indicate the vector amplitude, from violet (zero) to red (maximum). Top: Secular aberration drift dipole detected by (Truebenbach & Darling 2017). Middle: Randomly generated gravitational wave stream plot, after Darling et al. (2018). Bottom: Randomly generated BAO streamlines.

(Darling 2014). Fitting a curl-free quadrupole to a proper motion field can therefore measure or constrain the (an)isotropy of the Hubble expansion without *a priori* knowledge of H_0. We can express the Hubble constant in terms of an angular rate, $H_0 \simeq 15\,\mu$arcsec yr^{-1}, which means that a 10% anisotropy would produce a quadrupole with amplitude 1.5 μarcsec yr^{-1}.

2.5. Gravitational Waves

Stochastic gravitational waves deflect light rays in a quadrupolar (and higher ℓ) pattern with equal power in the E- and B-modes (Figure 1; Pyne et al. 1996; Gwinn et al. 1997; Book & Flanagan 2011). The gravitational waves that will produce extragalactic proper motions lie in the frequency range 10^{-18} Hz $< f <$ 10^{-8} Hz (H_0 to 0.3 yr^{-1}), which overlaps the pulsar timing and CMB polarization regimes, but uniquely covers about seven orders of magnitude of frequency space between the two methods (Darling et al. 2018). The cosmic energy density of gravitational waves Ω_{GW} can be related to the proper motion variance as

$$\Omega_{\rm GW} \sim \langle \mu^2 \rangle / H_0^2 \tag{1}$$

and to the quadrupolar power P_2 as

$$\Omega_{\rm GW} = \frac{6}{5}\,\frac{1}{4\pi}\,\frac{P_2}{H_\circ^2} = 0.00042\,\frac{P_2}{(1\;\mu\text{as yr}^{-1})^2}\,h_{70}^{-2} \tag{2}$$

(Gwinn et al. 1997; Book & Flanagan 2011; Darling et al. 2018). Measuring or constraining the proper motion quadrupole power can therefore detect or place limits on primordial gravitational waves in a unique portion of the gravitational wave spectrum.

2.6. Large Scale Structure

The mass density distribution of large-scale structure reflects the mass power spectrum, the shape and evolution of which relies on cosmological parameters. The transverse peculiar motions of extragalactic objects can be used to measure the density perturbations from large-scale structure without a reliance on precise distance measurements. While line-of-sight velocity studies use distances to differentiate Hubble expansion from peculiar velocity, peculiar motions across the line-of-sight are separable from Hubble expansion because no proper motion will occur in a homogeneous expansion (Nusser et al. 2012; Darling 2013). Thus, one can employ pairs of galaxies as "cosmic rulers" to measure the real-time change in the apparent size of the rulers caused by the cosmic expansion and to detect structures that have decoupled from the Hubble flow (Darling 2013).

Given the definition of angular diameter distance, $\theta = \ell/D_A$, where a "ruler" of proper length ℓ subtends small angle θ at angular diameter distance D_A, cosmic expansion and a changing ℓ can produce an observed fractional rate of change in θ:

$$\frac{\Delta\theta/\Delta t_\circ}{\sin\theta} \equiv \frac{\dot\theta}{\sin\theta} = \frac{-\dot D_A}{D_A} + \frac{\dot\ell}{\ell} = \frac{-H(z)}{1+z} + \frac{\dot\ell}{\ell} \tag{3}$$

where $H(z) = H_\circ\sqrt{\Omega_{M,\circ}(1+z)^3 + \Omega_\Lambda}$ in a flat universe, $\Delta t_\circ$ is the observer's time increment, $\dot\theta$ is the *relative* proper motion, and $\dot\ell$ is the observed change in proper length, $\Delta\ell/\Delta t_\circ$, related to the physical (rest-frame) transverse velocity as $v_\perp = \dot\ell\,(1+z)$.

If ℓ is not a gravitationally influenced structure and grows with the expansion, then $\dot\ell/\ell = H(z)/1+z$, exactly canceling the first term in Eqn. (3). In this case, $\dot\theta = 0$, and there is no proper motion for objects co-moving with an isotropically expanding universe, as expected. If ℓ is decoupled from the expansion, however, then for most reasonable gravitational motions, $\dot{\ell}/\ell$ is a minor modification to the expansion contribution to $\dot{\theta}/\theta$ because the expansion, except for small redshifts or small structures, dominates (Darling 2013). The deviation of $\dot{\theta}/\theta$ from the null signal of pure Hubble expansion can be used to probe the mass distribution of large-scale structure and, thus, to test the shape of the mass power spectrum without a dependence on precise distance measurements or a "distance ladder."

2.7. Baryon Acoustic Oscillation Evolution

The baryon acoustic oscillation (BAO) is a standard ruler arising from pre-CMB density fluctuations, which can be observed as an overdensity of galaxies on the scale of ~150 comoving Mpc (Eisenstein et al. 2005). At redshift $z = 0.5$, the BAO scale subtends $\theta_{BAO} = 4.5°$, which is equivalent to VSH degree $\ell \sim 40$. Taking the time derivative, we obtain an expression for proper motion on these scales:

$$\mu_{BAO} = \frac{\Delta\theta_{BAO}}{\Delta t_\circ} \simeq -\theta_{BAO}\, H_0 \simeq -1.2\ \mu\text{as yr}^{-1}. \tag{4}$$

The BAO evolution will therefore manifest as a convergent E-mode signal around $\ell \sim 40$ (Figure 1). To first order, the BAO scale depends on the expansion rate $H(z)$ and the angular diameter distance $D_A(z)$ at the observed redshift, but the rate of change of this standard ruler is dominated by its recession ("receding objects appear to shrink") and depends to first order on $H_0/D_A(z)$. Detection of this effect relies critically on the sky density of sources, which must adequately sample angular scales smaller than 4.5°.

Table 1. Global Correlated Proper Motion Signals

Effect	ℓ	Mode	Amplitude (μarcsec yr^{-1})	Recent Measurement (μarcsec yr^{-1})	Ref	*Gaia* (Predicted)	ngVLA (Predicted)	Prev. Work
Secular Aberration Drift	1	E	$\sim$5	5.2 ± 0.2	1	10σ	50σ	2,3,4,5
Secular Parallax	1	E	78 Mpc^{-1}	...	...	$\sim 10\sigma$	$\sim 10\sigma$ (1)	6
Rotation	1	B	Unknown	0.45 ± 0.27	7	$< 0.5\ \mu$as yr^{-1}	$< 0.1\ \mu$as yr^{-1} (2)	2,5,7
Anisotropic Expansion	2	E	Unknown	$< 7\%$	8	$< 3\%$	$< 0.7\%$	8,9,10,11
Gravitational Waves	≥ 2	E+B	Unknown	$\Omega_{GW} < 6.4 \times 10^{-3}$	7	$\Omega_{GW} < 4 \times 10^{-4}$	$\Omega_{GW} < 10^{-5}$	1,7,12,13,14,15,16
Large Scale Structure	$\gtrsim 5$	E	-15 to $+5$	8.3 ± 14.9	17	10σ	$\sim 20\sigma$ (3)	17,18
BAO Evolution	$\sim$40	E	-1.2 at $z = 0.5$	...	...	4σ	$\sim 10\sigma$ (4)	...

Notes: 1 – Detection of the secular parallax is limited by the number of compact radio sources that can (and would) be monitored in the local volume. 2 – ngVLA observations will only be sensitive to rotation axes that are not aligned with the Earth's rotation axis. 3 – Detection of peculiar velocities associated with large scale structure will depend on the number of close pairs of radio sources. 4 – Detection of the BAO evolution signal will depend strongly on the sky density of proper motion measurements.

Previous work references: 1 – Titov & Krásná (2018) 2 - Titov et al. (2011); 3 – Xu et al. (2012); 4 – Titov & Lambert (2013); 5 – Truebenbach & Darling (2017); 6 – Ding & Croft (2009); 7 – Darling et al. (2018); 8 – Darling (2014); 9 – Chang & Lin (2015); 10 – Bengaly (2016); 11 – Paine et al. (2018); 12 – Braginsky et al. (1990); 13 – Pyne et al. (1996); 14 – Kaiser & Jaffe (1997); 15 – Gwinn et al. (1997); 16 – Book & Flanagan (2011); 17 – Darling (2013); 18 – Truebenbach, A., 2018, ApJ, in prep.

3. ngVLA Science

The ngVLA can detect or constrain all of these phenomena and improve upon many of the expected *Gaia* measurements. Table 1 lists the various proper motion signals, their VSH modes, the expected amplitude of the signal (if known), a recent measurement (if any), and predictions for *Gaia* and the ngVLA. We make the following assumptions about a ngVLA astrometry program:

- A sample of 10,000 objects
- Astrometric observations spanning 10 years
- VLBA-level astrometric precision: ± 10 μas yr^{-1} per object

Implicit in these assumptions are VLBA-sized baselines with roughly ten times the current VLBA collecting area. We further assume that radio jets will pose the same challenges as are found in the current VLBA data. In practice, we simply scale current VLBA-based observations — which include the added intrinsic proper motion "noise" contribution from relativistic jets — by N or $\sqrt{N}$, as appropriate, to the expected ngVLA sample. The proposed sample is roughly ten times larger than current VLBA geodetic monitoring samples, but an increased collecting area would enable the ngVLA (or a long-baseline subarray) to monitor the expanded sample without increasing the observing time commitment. The ngVLA sample would leverage the current VLBA sample and the radio-loud *Gaia* AGN, providing super-decade time baselines for a significant subset of objects.

The proposed observations will enable global detection of correlated signals of ~ 0.1 μas yr^{-1}, which is $\sim 0.7\%$ of H_0. For most of the phenomena described in Section 2, the ngVLA would significantly improve on previous work, including the expected *Gaia* performance. While the ngVLA sample size will be a factor of ~ 50 smaller than the *Gaia* sample, the per-source astrometry will be a factor of ~ 20–50 times better. We therefore predict that ngVLA observations will substantially improve on *Gaia* global correlated proper motion measurements in most cases. The proposed ngVLA program may not perform as well as our expectations for *Gaia* for measurements requiring fine angular sampling (BAO evolution) or dense volumetric sampling (secular parallax). This is due to the overall physical paucity of compact radio sources compared to optical sources across the sky and in the very nearby universe.

4. Conclusions

The outlook for extragalactic proper motions using the ngVLA is promising, and in most cases it can surpass the expected performance of *Gaia*, despite the added challenge of the intrinsic proper motion caused by radio jets. In particular, the proposed ngVLA astrometry program would provide exquisite precision on the Solar motion in the Galaxy and place the strongest constraints to date on the isotropy of the Hubble expansion in the epoch of dark energy and on the primordial gravitational wave background over roughly 10 decades in frequency.

Acknowledgments. The authors acknowledge support from the NSF grant AST-1411605 and the NASA grant 14-ATP14-0086.

References

Bastian, U. 1995, in ESA Special Publication, Vol. 379, Future Possibilities for Astrometry in Space, ed. M. A. C. Perryman & F. van Leeuwen, 99
Bengaly, C. A. P., Jr. 2016, JCAP, 4, 036
Book, L. G. & Flanagan, É. É. 2011, Phys. Rev. D, 83, 024024
Bower, G. C., Demorest, P., Braatz, J., et al. 2015, ArXiv e-prints, arXiv:1510.06432
Braginsky, V. B., Kardashev, N. S., Polnarev, A. G., & Novikov, I. D. 1990, Nuovo Cimento B, 105, 1141
Chang, Z., & Lin, H.-N. 2015, MNRAS, 446, 2952
Darling, J. 2012, ApJ, 761, L26
Darling, J. 2013, ApJ, 777, L21
Darling, J. 2014, MNRAS, 442, L66
Darling, J., Truebenbach, A., & Paine, J. 2018, ApJ, submitted
Ding, F., & Croft, R. A. C. 2009, MNRAS, 397, 1739
Eisenstein, D. J., Zehavi, I., David W. Hogg, D. W., et al. 2005, ApJ, 633, 560
Eubanks, T. M., Matsakis, D. N., Josties, F. J., et al. 1995, in IAU Symposium, Vol. 166, Astronomical and Astrophysical Objectives of Sub-Milliarcsecond Optical Astrometry, ed. E. Hog & P. K. Seidelmann, 283
Fontanini, M., West, E. J., & Trodden, M. 2009, Phys. Rev. D, 80, 123515
Gwinn, C. R., Eubanks, T. M., Pyne, T., Birkinshaw, M., & Matsakis, D. N. 1997, ApJ, 485, 87
Hinshaw, G., Weiland, J.L., Hill, R.S., et al. 2009, ApJS, 180, 225
Kaiser, N. & Jaffe, A. 1997, ApJ, 484, 545
Loeb, A. 1998, ApJ, 499, L111
McCarthy, D. D., & Petit, G. 2004, IERS Technical Note, 32
Mignard, F. & Klioner, S. 2012, A&A, 547, A59
Nusser, A., Branchini, E., & Davis, M. 2012, ApJ, 755, 58
Paine, J., Darling, J., & Truebenbach, A. 2018, ApJS, submitted
Pyne, T., Gwinn, C. R., Birkinshaw, M., Eubanks, T. M., & Matsakis, D. N. 1996, ApJ, 465, 566
Quercellini, C., Quartin, M., & Amendola, L. 2009, Phys.Rev.Lett, 102, 151302
Sandage, A. 1962, ApJ, 136, 319
Titov, O. 2009, in Proc. 19th European VLBI for Geodesy and Astrometry (EVGA) Working Meeting, ed. G. Bourda, et al., 14
Titov, O., Lambert, S. B., & Gontier, A.-M. 2011, A&A, 529, A91
Titov, O., & Lambert, S. 2013, A&A, 559, A95
Titov, O., & Krásná, H. 2018, A&A, in press
Truebenbach, A. E., & Darling, J. 2017, ApJS, 233, 3
Xu, M. H., Wang, G. L., & Zhao, M. 2012, A&A, 544, A135